

2007

Late Jurassic to Early Cretaceous stable isotope and geochemical records from the northern high latitudes: implications for palaeoclimate

NUNN, ELIZABETH VICTORIA

<http://hdl.handle.net/10026.1/1760>

<http://dx.doi.org/10.24382/3859>

University of Plymouth

All content in PEARL is protected by copyright law. Author manuscripts are made available in accordance with publisher policies. Please cite only the published version using the details provided on the item record or document. In the absence of an open licence (e.g. Creative Commons), permissions for further reuse of content should be sought from the publisher or author.

**LATE JURASSIC TO EARLY CRETACEOUS STABLE
ISOTOPE AND GEOCHEMICAL RECORDS FROM THE
NORTHERN HIGH LATITUDES: IMPLICATIONS FOR
PALAEOCLIMATE**

by

ELIZABETH VICTORIA NUNN

A thesis submitted to the University of Plymouth
in partial fulfilment for the degree of

DOCTOR OF PHILOSOPHY

School of Earth Ocean & Environmental Sciences
Faculty of Science

March 2007

University of Plymouth Library	
Item no.	9007 666715
Shelfmark	THESIS 551.60901

NUN .

ABSTRACT

Elizabeth Nunn

Late Jurassic to Early Cretaceous Stable Isotope and Geochemical Records from the Northern High Latitudes: Implications for Palaeoclimate

The Jurassic and Cretaceous periods are widely accepted as being dominated by greenhouse conditions with elevated CO₂ levels and warm polar regions. Although much compelling evidence to support this idea of global warmth exists, some recent studies propose that the greenhouse climate may at times have been punctuated by sub-freezing polar conditions and the presence of limited polar ice. The evidence, however, is somewhat equivocal and is both spatially and temporally limited with much of this research until now being concentrated in mid- to low latitudes, despite it being generally accepted that global climate is defined to a significant degree by prevailing conditions at the poles. Existing data are also often plagued by poor sampling resolutions and dubious diagenetic histories.

This research presents the first extensive stable isotope and geochemical investigation of well-preserved belemnite rostra from the Callovian-Hauterivian Boreal Realm. Belemnites of the genera *Cylindroteuthis*, *Pachyteuthis*, *Acroteuthis*, *Lagonibelus* and occasionally *Belemnopsis* were investigated. Preservation was assessed using Backscattered Scanning Electron Microscopy, Cathodoluminescence, carbonate staining and trace element techniques. Organic carbon isotope analysis of fossilised wood was also undertaken where possible. Material from Staffin Bay, Isle of Skye, and Helmsdale, Sutherland, Scotland; the Izhma River, Timan-Pechora Basin, Russia; the Boyarka River, Yenisei-Khatanga Basin, Siberia; and Festningen and Janusfjellet, Svalbard was analysed.

The carbon isotope data record relatively positive values in the Oxfordian, followed by a gradual shift towards more negative values through the Kimmeridgian and into the Volgian/Tithonian. A distinct Late Valanginian positive carbon isotope excursion is identified in both the marine carbonate and terrestrial organic carbon records from the Izhma and Boyarka rivers. The excursion occurs at a time of relatively low sea level in Russia and Siberia. The exposure and erosion of lowland areas and restricted ocean circulation (and therefore enhanced stratification) associated with a period of sea-level lowstand may account for increased rates of organic carbon burial. The Late Valanginian positive carbon isotope excursion is coeval with a distinct cooling in the Russian Izhma River succession. This could be explained by a fall in atmospheric CO₂ concentration and a subsequent drop in temperature as the result of significant burial of sediments rich in organic carbon. Further evidence for cold conditions during the Valanginian interval comes from glendonites and dropstones, which were identified on Svalbard.

High latitude warmth is most likely the norm for the Late Jurassic and Early Cretaceous interval, although this warmth is likely to have been punctuated by cold conditions providing the opportunity for the development of at least a seasonal cover of polar ice. The oxygen isotope data record the occurrence of cold episodes during the Lower Oxfordian *Cordatum* Zone, the mid-Ryazanian *Kochi-Analogus* zones and the Upper Valanginian *Bidichotomus* Zone. Palaeotemperatures as low as 2°C were calculated, providing strong evidence for the existence of cold polar conditions at these times. Ultimately, climatic instability is probably the key characteristic of this greenhouse interval.

TABLE OF CONTENTS

ABSTRACT.....	I
TABLE OF CONTENTS	II
LIST OF FIGURES.....	V
LIST OF TABLES.....	VII
LIST OF PLATES	VII
ACKNOWLEDGEMENTS	IX
AUTHOR'S DECLARATION.....	X
1. INTRODUCTION	1
1.1. Rationale.....	1
1.2. Locations.....	4
1.3. Aims & Objectives	6
1.4. Thesis Structure	7
2. THE LATE JURASSIC AND EARLY CRETACEOUS	8
2.1. Biostratigraphy	8
2.1.1. Boreal-Tethyan Correlation	9
2.2. Palaeogeography	13
2.2.1. Arctic Palaeogeography & Palaeoceanography	15
2.3. Palaeoclimate.....	18
2.3.1. Evidence for a Warm, Equable Climate	18
2.3.2. Evidence for Cold Polar Regions	22
3. BELEMNITES.....	27
3.1. Systematic Position	27
3.2. The Belemnite Animal	28
3.2.1. Belemnite Morphology	29
3.2.2. Belemnite Palaeoecology	31
3.3. Belemnite Palaeobiogeography	34
3.3.1. Boreal Realm.....	35
3.3.2. Tethyan Realm	36
3.3.3. Austral Realm	37
3.4. Belemnites as Palaeoclimate Indicators	38
4. METHODOLOGY	42

4.1. Selection of Sites	42
4.2. Field Techniques	43
4.2.1. Graphic Sedimentary Logs.....	44
4.2.2. Sample Collection	44
4.3. Laboratory Techniques	45
4.3.1. Rationale	45
4.3.2. Optical Techniques	52
4.3.3. Trace Element Analysis	56
4.3.4. Carbonate Stable Isotope Analysis.....	57
4.3.5. Organic Carbon Analysis	58
4.3.6. Total Organic Carbon (TOC)	59
4.3.7. Rock-Eval Pyrolysis.....	60
4.3.8. Storage of Material.....	60
 5. STAFFIN BAY, ISLE OF SKYE, SCOTLAND	 61
5.1. Location & Site Description	61
5.2. Geological Setting	62
5.3. Sampling & Methodology.....	67
5.4. Results.....	69
5.5. Discussion	77
5.5.1. Stable Isotope, Geochemical & Taxonomic Records.....	77
5.5.2. The Oxygen Isotope Record & Palaeotemperature Implications	77
5.5.3. The Elemental Records & Palaeotemperature Implications.....	81
5.5.4. The Terrestrial Carbon Isotope Record.....	85
5.5.5. The Marine Carbon Isotope Record	87
5.5.6. The Carbon Isotope Records & Ocean-Atmosphere Correlation.....	88
5.5.7. Callovian-Kimmeridgian Marine & Terrestrial Isotopic Records.....	89
5.6. Conclusions.....	93
 6. HELMSDALE, SUTHERLAND, SCOTLAND	 98
6.1. Location & Site Description	98
6.2. Geological Setting	99
6.3. Sampling & Methodology.....	104
6.4. Results.....	106
6.5. Discussion	110
6.5.1. Stable Isotope, Geochemical & Taxonomic Records.....	110
6.5.2. The Oxygen Isotope Record & Palaeotemperature Implications	110
6.5.3. The Elemental Records & Palaeotemperature Implications.....	111
6.5.4. The Carbon Isotope Record	115
6.5.5. Kimmeridgian Stable Isotope Records.....	116
6.5.6. Correlation of the Helmsdale & Staffin Bay Isotope Records	119
6.6. Conclusions.....	122
 7. BOYARKA RIVER, YENISEI-KHATANGA BASIN, SIBERIA	 127
7.1. Location & Site Description	127
7.2. Geological Setting	128

7.3. Sampling & Methodology.....	132
7.4. Results.....	134
7.5. Discussion	139
7.5.1. Stable Isotope, Geochemical & Taxonomic Records.....	139
7.5.2. The Oxygen Isotope Record & Palaeotemperature Implications	140
7.5.3. The Elemental Records & Palaeotemperature Implications.....	143
7.5.4. The Terrestrial Carbon Isotope Record.....	145
7.5.5. The Marine Carbon Isotope Record.....	147
7.5.6. The Carbon Isotope Records & Ocean-Atmosphere Correlation.....	148
7.5.7. Ryazanian-Hauterivian Marine & Terrestrial Isotopic Records.....	150
7.6. Conclusions.....	154
 8. IZHMA RIVER, TIMAN-PECHORA BASIN, RUSSIA.....	 161
8.1. Location & Site Description	161
8.2. Geological Setting	162
8.3. Sampling & Methodology.....	167
8.4. Results.....	168
8.5. Discussion	171
8.5.1. Stable Isotope, Geochemical & Taxonomic Records.....	171
8.5.2. The Oxygen Isotope Record & Palaeotemperature Implications	174
8.5.3. The Elemental Records & Palaeotemperature Implications.....	175
8.5.4. The Carbon Isotope Record	177
8.5.5. Volgian-Hauterivian Stable Isotope Records	178
8.6. Conclusions.....	182
 9. FESTNINGEN & JANUSFJELLET, SVALBARD	 187
9.1. Location & Site Description	187
9.2. Geological Setting	189
9.3. Sampling & Methodology.....	195
9.4. Results.....	196
9.5. Discussion	199
9.5.1. Sedimentary Indicators of Palaeoclimate - Glendonites	199
9.5.2. Sedimentary Indicators of Palaeoclimate - Outsized Clasts.....	201
9.5.3. Stable Isotope, Geochemical & Taxonomic Records.....	204
9.5.4. The Oxygen Isotope Record & Palaeotemperature Implications	204
9.5.5. The Elemental Records & Palaeotemperature Implications.....	207
9.5.6. The Carbon Isotope Record	211
9.5.7. Ryazanian-Valanginian Stable Isotope Records	212
9.6. Conclusions.....	213
 10. DISCUSSION	 218
10.1. Evaluating Belemnites as Palaeoenvironmental Indicators	218
10.1.1. Preservation.....	218
10.1.2. Natural Variability in Belemnite Records.....	220
10.1.3. Oxygen Isotopes.....	226
10.1.4. Elemental/Ca Ratios.....	229

10.1.5. Carbon Isotopes.....	234
10.2. Late Jurassic - Early Cretaceous Global Palaeoenvironment.....	237
10.2.1 Boreal Realm Data	237
10.2.2. Global Palaeoenvironmental Studies.....	242
11. CONCLUSIONS	251
11.1. Summary of Site Specific Investigations.....	251
11.1.1. Staffin Bay, Isle of Skye, Scotland	251
11.1.2. Helmsdale, Sutherland, Scotland	252
11.1.3. Boyarka River, Yenisei-Khatanga Basin, Siberia	252
11.1.4. Izhma River, Timan-Pechora Basin, Russia.....	253
11.1.5. Festningen & Janusfjellet, Svalbard.....	253
11.2. Wider Implications of Research	254
11.2.1. Belemnites as Palaeoenvironmental Indicators	254
11.2.2. Late Jurassic - Early Cretaceous Global Palaeoenvironment	255
11.3. Future Work.....	256
REFERENCES.....	259
APPENDIX 1. SYSTEMATIC PALAEONTOLOGY	335
A1.1. Introduction.....	336
A1.2. Systematic Descriptions.....	338
APPENDIX 2. DATA TABLES : BELEMNITES.....	415
APPENDIX 3. DATA TABLES : ORGANICS.....	429

LIST OF FIGURES

Figure 1.1. Atmospheric CO ₂ through the Phanerozoic.....	1
Figure 1.2. Distribution of potentially glacially derived sediments and glendonites through the Mesozoic	2
Figure 1.3. Present day circumpolar view of the Northern hemisphere.....	4
Figure 1.4. Temporal distribution of the locations investigated as part of this study.	5
Figure 2.1a. Tethyan-Boreal (British and Russian) correlation of the Middle-Upper Jurassic period.....	10
Figure 2.1b. Tethyan-Boreal (British and Russian) correlation of the Lower Cretaceous period.....	11
Figure 2.2. Callovian palaeogeography map	13
Figure 2.3. Hauterivian palaeogeography map	14
Figure 2.4. Late Jurassic palaeogeography of the Arctic region.....	15
Figure 3.1. Belemnite morphology	30
Figure 3.2. Hauterivian palaeobiogeography.....	35
Figure 4.1. Volgian circumpolar map	43
Figure 4.2. Key to sedimentary log symbols used in this study.....	44
Figure 5.1. Location map of Staffin Bay	61
Figure 5.2. Broad foreshore exposure typical of the Staffin Bay coast.....	62
Figure 5.3. Mid-Jurassic (Bathonian) Scottish palaeogeography.....	63
Figure 5.4. Stratigraphic chart of the Staffin Bay section	65
Figure 5.5. Relatively abundant belemnites in a mudrock.....	68
Figure 5.6. Cross-plot of $\delta^{18}\text{O}$ and $\delta^{13}\text{C}$ values from belemnites from Staffin Bay.....	70
Figure 5.7. Cross-plots of $\delta^{18}\text{O}$ against Fe and Mn.....	71

Figure 5.8. Cross-plots of $\delta^{18}\text{O}$ against El/Ca	72
Figure 5.9. El/Ca ratios from the Callovian-Lower Kimmeridgian at Staffin Bay	73
Figure 5.10. $\delta^{13}\text{C}_{\text{org}}$, $\delta^{13}\text{C}_{\text{carb}}$ and $\delta^{18}\text{O}_{\text{carb}}$ records from the Callovian-Lower Kimmeridgian succession at Staffin Bay	74
Figure 5.11. TOC record from the Callovian-Lower Kimmeridgian succession at Staffin Bay	75
Figure 5.12. Van Krevlan diagram showing the origin of organic matter analysed from the Callovian-Lower Kimmeridgian Staffin Bay succession	76
Figure 5.13. Palaeotemperatures calculated from Mg/Ca data	79
Figure 5.14. Temperature-salinity plot for the Staffin Bay data	81
Figure 5.15. Callovian-Lower Kimmeridgian $\delta^{13}\text{C}$ correlation between a composite Tethyan $\delta^{13}\text{C}_{\text{carb}}$ curve and the $\delta^{13}\text{C}_{\text{carb}}$ and $\delta^{13}\text{C}_{\text{org}}$ curves from Staffin Bay	92
Figure 6.1. Location map of the Sutherland coastal region	98
Figure 6.2. Foreshore exposure typical of the area around the Helmsdale coast	99
Figure 6.3. Late Jurassic palaeogeography	100
Figure 6.4. Stratigraphic chart for the Middle-Upper Jurassic of the Brora-Helmsdale region	101
Figure 6.5. Typical preservation of Helmsdale belemnites	105
Figure 6.6. Cross-plots of $\delta^{18}\text{O}$ against Fe and Mn	106
Figure 6.7. $\delta^{13}\text{C}$ and $\delta^{18}\text{O}$ records from the Kimmeridgian succession at Helmsdale and Eathie	108
Figure 6.8. Cross-plot of $\delta^{18}\text{O}$ and $\delta^{13}\text{C}$ values from belemnites from Helmsdale, Eathie and Brora	109
Figure 6.9. Cross-plots of $\delta^{18}\text{O}$ against El/Ca	112
Figure 6.10. El/Ca ratios from the Kimmeridgian succession at Helmsdale and Eathie	114
Figure 6.11. Kimmeridgian palaeogeography map showing published belemnite derived palaeotemperatures for this time period	116
Figure 6.12. Kimmeridgian $\delta^{13}\text{C}$ correlation between a composite Tethyan $\delta^{13}\text{C}_{\text{bulk}}$ curve and the $\delta^{13}\text{C}$ curve from Helmsdale	118
Figure 6.13. Composite Callovian-Kimmeridgian $\delta^{13}\text{C}$ and $\delta^{18}\text{O}$ records from northern Scotland	121
Figure 7.1. Location map of the Boyarka River	127
Figure 7.2. River-side cliff, exposure typical of the Boyarka River	128
Figure 7.3. Simplified geological map of the Yenisei-Khatanga Basin and surrounding areas	129
Figure 7.4. Sedimentary log and photographs of the Boyarka River succession	130
Figure 7.5. Photographs of belemnites and macroscopic wood from the Boyarka River succession	133
Figure 7.6. Cross-plots of $\delta^{18}\text{O}$ against Fe and Mn	134
Figure 7.7. $\delta^{13}\text{C}_{\text{org}}$, $\delta^{13}\text{C}_{\text{carb}}$, and $\delta^{18}\text{O}_{\text{carb}}$ records from the Ryazanian-Lower Hauterivian Boyarka River succession	136
Figure 7.8. Cross-plot of $\delta^{18}\text{O}$ and $\delta^{13}\text{C}$ values from belemnites from the Boyarka River succession	137
Figure 7.9. El/Ca ratios from the Ryazanian-Lower Hauterivian succession at the Boyarka River	138
Figure 7.10. Close-up of the Ryazanian <i>Kochi-Analogus</i> zones, Boyarka River	139
Figure 7.11. Temperature-salinity plot for the Boyarka River data	142
Figure 7.12. Cross-plots of $\delta^{18}\text{O}$ against El/Ca for the Boyarka River belemnites	144
Figure 7.13. Valanginian-Hauterivian $\delta^{13}\text{C}$ correlation between the Boyarka River succession $\delta^{13}\text{C}_{\text{org}}$ curve and the Crimea, and the $\delta^{13}\text{C}_{\text{carb}}$ curve and a composite Tethyan bulk $\delta^{13}\text{C}$ curve	151
Figure 8.1. Location map of the Izhma River	161
Figure 8.2. River-side cliff, exposure typical of the Izhma River	162
Figure 8.3. Simplified map of the Timan-Pechora Basin and surrounding areas	163
Figure 8.4. Sedimentary log and photographs of the Izhma River succession	166
Figure 8.5. Photographs of belemnites from the Izhma River succession	168
Figure 8.6. Cross-plots of $\delta^{18}\text{O}$ against Fe and Mn	169
Figure 8.7. Cross-plot of Mn and Fe	170
Figure 8.8. Cross-plot of $\delta^{18}\text{O}$ and $\delta^{13}\text{C}$	170
Figure 8.9. $\delta^{13}\text{C}$ and $\delta^{18}\text{O}_{\text{carb}}$ records from the Callovian-Lower Hauterivian Izhma River succession	172
Figure 8.10. El/Ca records from the Callovian-Lower Hauterivian Izhma River succession, Russia	173
Figure 8.11. Cross-plots of $\delta^{18}\text{O}$ against El/Ca	176
Figure 8.12. Ryazanian-Hauterivian $\delta^{13}\text{C}$ and $\delta^{18}\text{O}$ correlation between the Izhma River succession and the Boyarka River succession	181
Figure 9.1. Location map of Svalbard	187
Figure 9.2. Low coastal cliff typical of the Festningen exposure	188
Figure 9.3. Typical exposure at Janusfjellet	188
Figure 9.4. Simplified palaeogeographic map of the Arctic region	189
Figure 9.5. Summary of events and facies in the Late Jurassic and Early Cretaceous history of Svalbard ..	190
Figure 9.6. Stratigraphic chart for principal lithostratigraphic units of the Middle Jurassic to Early Cretaceous of Svalbard	192

Figure 9.7. Typical preservation of Svalbard belemnites.....	196
Figure 9.8. Cross-plot of Fe and Mn for belemnites from Svalbard.....	197
Figure 9.9. Cross-plot of $\delta^{18}\text{O}$ and $\delta^{13}\text{C}$	198
Figure 9.10. Glendonites from the Rurikfjellet Formation at Janusfjellet and Festningen	199
Figure 9.11. Outsized clast	202
Figure 9.12. $\delta^{13}\text{C}$ and $\delta^{18}\text{O}$ records from the Upper Valanginian succession at Festningen	205
Figure 9.13. $\delta^{13}\text{C}$ and $\delta^{18}\text{O}$ records from the Ryazanian-Upper Valanginian succession at Janusfjellet	206
Figure 9.14. Cross-plots of $\delta^{18}\text{O}$ and El/Ca	208
Figure 9.15. El/Ca ratios from the Upper Valanginian succession at Festningen	209
Figure 9.16. El/Ca ratios from the Ryazanian-Upper Valanginian succession at Janusfjellet	210
Figure 9.17. Valanginian palaeogeography map showing published belemnite derived palaeotemperatures for this time period.....	212
Figure 10.1. Cross plots of $\delta^{18}\text{O}$ and $\delta^{13}\text{C}$ offsets observed from coeval belemnites.....	224
Figure 10.2. Calculated palaeotemperatures and relative $\delta^{18}\text{O}_{\text{seawater}}$ values for the Callovian-Hauterivian Izhma River succession, Russia.	233
Figure 10.3. Callovian-Hauterivian compilation of $\delta^{13}\text{C}_{\text{carb}}$ and $\delta^{18}\text{O}_{\text{carb}}$ data.....	238
Figure 10.4a. Callovian-Hauterivian compilation of $\delta^{13}\text{C}_{\text{carb}}$ data derived from this study and compared with published data.....	239
Figure 10.4b. Callovian-Hauterivian compilation of $\delta^{18}\text{O}_{\text{carb}}$ data derived from this study and compared with published data.....	240
Figure 10.5. Latitudinal changes in $\delta^{18}\text{O}_{\text{seawater}}$ in warm climates	245
Figure 10.6. Calculated average palaeotemperatures for the Oxfordian and Valanginian periods	246
Figure A1.1. Morphological terms employed in the systematic descriptions of belemnite rostra	337
Figure A1.2. Stratigraphical and geographical ranges of the belemnite species recorded in this study.....	374

LIST OF TABLES

Table 10.1. Table showing genus-level differences in stable isotope and geochemical measurements from coeval belemnites	222
Table 10.2. Table showing ontogenetic differences in stable isotope and geochemical measurements from coeval belemnites.	223
Table 10.3. Compilation of published Late Jurassic-Early Cretaceous $\delta^{18}\text{O}$ and palaeotemperature data ...	243
Table A2. Data tables: Belemnites.....	415
Table A3. Data tables: Organics.....	429

LIST OF PLATES

Plate 1. Staffin Bay, Isle of Skye, Scotland. CL.....	95
Plate 2. Staffin Bay, Isle of Skye, Scotland. BSEM	96
Plate 3. Staffin Bay, Isle of Skye, Scotland. Carbonate Staining	97
Plate 4. Helmsdale, Sutherland, Scotland. CL	124
Plate 5. Helmsdale, Sutherland, Scotland. BSEM	125
Plate 6. Helmsdale, Sutherland, Scotland. Carbonate Staining.....	126
Plate 7. Boyarka River, Yenisei-Khatanga Basin, Siberia. CL	156
Plate 8. Boyarka River, Yenisei-Khatanga Basin, Siberia. BSEM	157
Plate 9. Boyarka River, Yenisei-Khatanga Basin, Siberia. Carbonate Staining.....	158
Plate 10. Boyarka River, Yenisei-Khatanga Basin, Siberia. Wood.....	159
Plate 11. Boyarka River, Yenisei-Khatanga Basin, Siberia. Wood.....	160
Plate 12. Izhma River, Timan-Pechora Basin, Russia. CL.....	184
Plate 13. Izhma River, Timan-Pechora Basin, Russia. BSEM.....	185
Plate 14. Izhma River, Timan-Pechora Basin, Russia. Carbonate Staining	186
Plate 15. Festningen & Janusfjellet, Svalbard. CL.....	215
Plate 16. Festningen & Janusfjellet, Svalbard. BSEM.....	216
Plate 17. Festningen & Janusfjellet, Svalbard. Carbonat Staining.....	217
Plates A1. Belemnite Taxonomy	377
Plates A2. Belemnite Taxonomy	379

Plates A3. Belemnite Taxonomy	381
Plates A4. Belemnite Taxonomy	384
Plates A5. Belemnite Taxonomy	387
Plates A6. Belemnite Taxonomy	389
Plates A7. Belemnite Taxonomy	391
Plates A8. Belemnite Taxonomy	393
Plates A9. Belemnite Taxonomy	395
Plates A10. Belemnite Taxonomy	397
Plates A11. Belemnite Taxonomy	399
Plates A12. Belemnite Taxonomy	401
Plates A13. Belemnite Taxonomy	403
Plates A14. Belemnite Taxonomy	405
Plates A15. Belemnite Taxonomy	407
Plates A16. Belemnite Taxonomy	410
Plates A17. Belemnite Taxonomy	414

ACKNOWLEDGEMENTS

I would like to thank my supervisors, Gregory Price and Malcolm Hart for all of their help, advice and support throughout my time at Plymouth. In addition I am very grateful to Kevin Page for his help and advice on anything and everything relating to palaeontology or biostratigraphy and also to Jörg Mutterlose at Ruhr-Universität Bochum for his crash-course on belemnite identification.

My thanks also go to my fieldwork colleagues; Greg, Kevin, Jörg, Evgenij Baraboshkin, Sergey Gavrilov and others. I am indebted to Maggie Grimbly, Rob Harvey, Sally Madgwick, Kev Solman, Peter Bond, Paul Sutton and countless others at the University of Plymouth for their technical assistance. I would also like to thank Duncan Pirrie at Camborne School of Mines (for his assistance with cathodoluminescence microscopy), Melanie Leng and others at NIGL, Keyworth (for their assistance with the Staffin Bay isotope analyses), Jacqui Duffett at Royal Holloway (for her help with trace element analysis), Thierry Adatte at the University of Neuchâtel, Switzerland (for Rock-Eval Pyrolysis) and Darren Gröcke at McMaster University, Canada (for conducting the Boyorka River organic carbon isotope analysis). I am also grateful to all of the Geology staff and many of the Geology and Geography PhD students at Plymouth (in particular Jodie, Katie, Becky, Jenny, Claire and Ben) for their continuing advice and support.

The University of Plymouth, British Federation of Women Graduates, Palaeontological Association, International Association of Sedimentologists and the British Sedimentological Research Group provided funds in support of this project. I am grateful to them all. In addition, elements of the fieldwork and lab work could not have been undertaken without further grants awarded to Gregory Price from the Natural Environmental Research Council and National Geographic.

Finally, on a more personal note I would like to my mum, dad and brother for their constant support and encouragement, and Mark, who has kept me sane these past few years. Thank you.

AUTHOR'S DECLARATION

At no time during the registration for the degree of Doctor of Philosophy has the author been registered for any other University award without prior agreement of the Graduate Committee.

This study was financed with the aid of a studentship from the University of Plymouth.

A programme of advanced study was undertaken, which included training in palaeontological, isotopic and geochemical analytical techniques.

Relevant scientific seminars and conferences, both national and international were regularly attended at which work was often presented and external institutions were visited for consultation purposes.

Publications (or presentation of other forms of creative and performing work):

- Price, G. D., & Nunn, E. V. A Sedimentological and Isotopic evaluation of a high latitude Jurassic - Early Cretaceous succession from Svalbard. BSRG AGM, Aberdeen (Dec 2006).
- Price, G. D., & Nunn, E. V. Early Cretaceous Isotope Records from the Arctic. EGU General Assembly, Vienna, Austria (Apr 2006).
- Nunn, E. V., Price, G. D., Hart, M. B., Page, K. N. & Leng, M. J. A Callovian - Kimmeridgian Organic Carbon-Isotope Record from Staffin Bay, Isle of Skye. BSRG AGM, Durham (Dec 2005).
- Nunn, E. V. & Price, G. D. Late Jurassic and Early Cretaceous of the Northern High Latitudes. BSRG AGM, Durham (Dec 2005). Poster.
- Nunn, E. V., Price, G. D., Hart, M. B. & Baraboshkin, E. J. Isotopic Signals from Ryazanian - Hauterivian Arctic Belemnites of the Boyarka River, Northern Central Siberia. 7th International Symposium on the Cretaceous, Neuchâtel, Switzerland (Sep 2005).
- Price, G. D., Nunn, E. V., Baraboshkin, E. J. & Mutterlose, J. Isotopic Signals from Early Cretaceous Subpolar Belemnites, Siberia. 7th International Symposium on the Cretaceous, Neuchâtel, Switzerland (Sep 2005). Poster.
- Price, G. D., Rogov, M. & Nunn, E. V. Assessing the Evidence for a Late Jurassic (Oxfordian - Kimmeridgian) Icehouse to Greenhouse Transition. BSRG AGM, Manchester (Dec 2004).

External Contacts:

- Melanie Leng, NERC Isotope Geosciences Laboratory.
- Jörg Mutterlose, Ruhr-Universität Bochum.
- Duncan Pirrie, Camborne School of Mines.
- Jacqui Duffett, Royal Holloway.
- Thierry Adatte, University of Neuchâtel.

Word count of main body of thesis: 57,106

Signed 

Date 23/03/07

1. INTRODUCTION

1.1. Rationale

The Jurassic and Cretaceous periods are widely accepted as being a time of warm equable climates with a low global temperature gradient (e.g., Frakes, 1979; Barron, 1983; Huber *et al.*, 1995), elevated CO₂ levels (e.g., Barron *et al.*, 1983; Weissert & Lini, 1991; Francis & Frakes, 1993; Berner, 1994; Bice & Norris, 2002; Dromart *et al.*, 2003a; Royer *et al.*, 2004) and warm polar regions (e.g., Poulsen *et al.*, 1999; Spicer *et al.*, 2002; Tarduno *et al.*, 1998; Jenkyns *et al.*, 2004). The general assumption has been that this period of extreme warmth is primarily the result of elevated concentrations of atmospheric CO₂ (Fig. 1.1). This presents an interesting idea, namely that the Jurassic and Cretaceous 'greenhouse' period could be considered as a potential analogue for future climatic change providing it was better understood.

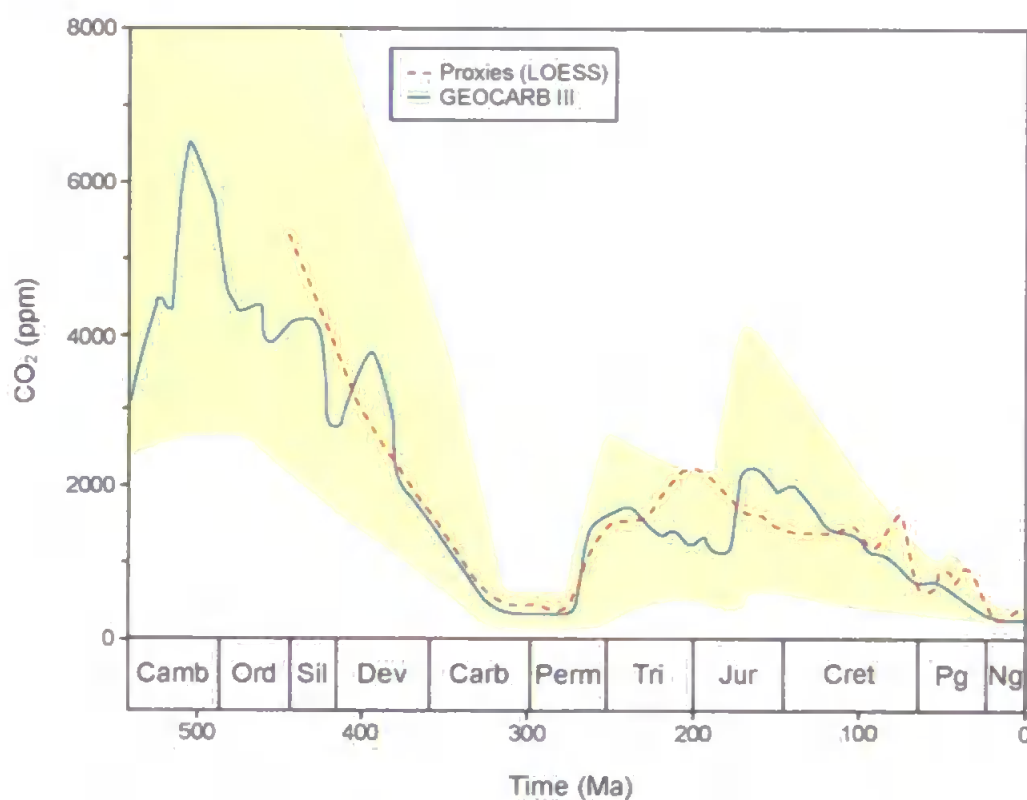


Figure 1.1 Atmospheric CO₂ through the Phanerozoic. The LOESS record is a compilation of published proxies (e.g., palaeosols, stomata, phytoplankton, boron, liverworts) produced by Royer (2006). The GEOCARB III record is derived from a geochemical model (Berner & Kothavala, 2001). Diagram adapted after Royer (2006).

The assumption that warm equable climates existed throughout the Jurassic and Cretaceous has recently been contested by newer research suggesting that the greenhouse climate may at times have been punctuated by sub-freezing polar conditions and the presence of limited polar ice. Such evidence includes the presence of potentially glacially derived sediments and minerals (Fig. 1.2) (e.g., Woolfe & Francis, 1991; Frakes & Krassay, 1992; Francis & Frakes, 1993; De Lurio & Frakes, 1999; Price, 1999; Alley & Frakes, 2003), observations from global sea level curves (e.g., Stoll & Schrag, 1996, 2000; Dromart *et al.*, 2003a; Miller *et al.*, 2003, 2005) and isotopic studies (e.g., Pirrie & Marshall, 1990; Ditchfield *et al.*, 1994; Pirrie *et al.*, 1995; Ditchfield, 1997; van de Schootbrugge *et al.*, 2000; Puc  at *et al.*, 2003; Price & Mutterlose, 2004).

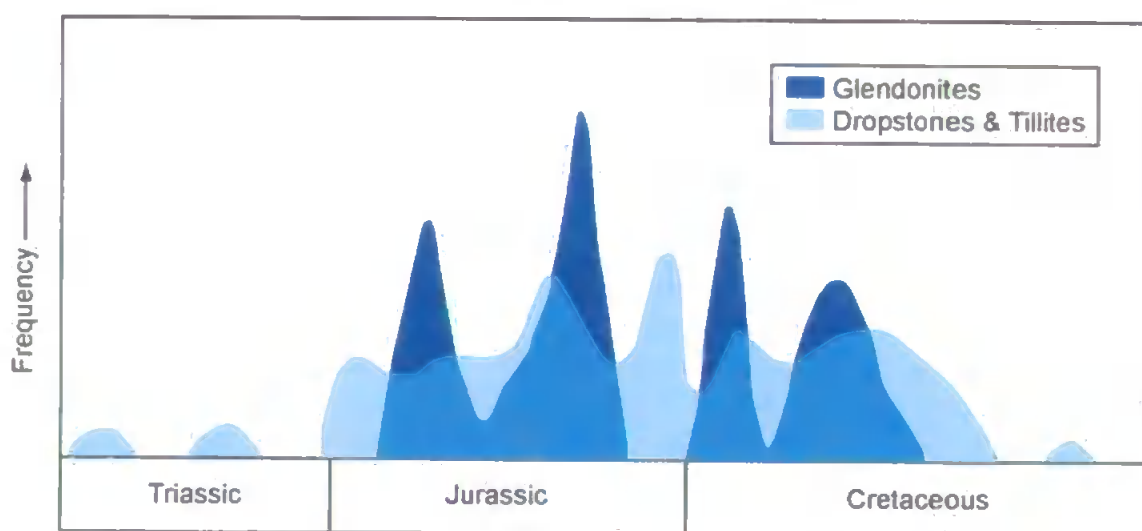


Figure 1.2 Distribution of potentially glacially derived sediments and glendonites through the Mesozoic. Diagram adapted after Price (1999).

The evidence for cool polar conditions, however, is still somewhat equivocal since much of the existing research has been carried out at a poor sampling resolution (in the high latitudes) or in the mid- to low latitudes or in the southern high latitudes of Antarctica, South America, Australia and New Zealand. There has been very little research undertaken in the Arctic region, which prevents a thorough understanding of this issue. It is generally accepted that global climate is defined to a significant degree by the prevailing conditions at the poles (e.g., Jenkyns *et al.*, 2004) and it is therefore essential to collect

robust data from the northern high latitudes in order to accurately reconstruct palaeoclimatic conditions.

In September 2004, the first scientific drilling expedition to the central Arctic Ocean was completed. Integrated Ocean Drilling Program (IODP) Expedition 302, the Arctic Coring Expedition (ACEX) recovered sediment cores, of Late Cretaceous to Holocene age, from the Lomonosov Ridge, 250 km from the North Pole. In their IODP proposal Backman *et al.* (2002) highlighted the importance of the Arctic Ocean in driving climate change. They stated that:

“The Arctic Ocean and its marginal seas play a fundamental role in the global ocean/climate system. The dense cold bottom waters of most of the world's oceans, which originate in the Nordic seas, strongly influence global thermohaline circulation, driving world climate. The permanent Arctic sea-ice cover has a tremendous influence on the Earth's albedo and the distribution of fresh water. It varies both seasonally and over longer time periods and thus has a direct influence on global heat distribution and climate. While understanding the history of the Arctic Ocean is critical for any climate, ocean-circulation or tectonic model that would be truly global, the logistical difficulties associated with the work in this remote and harsh region have prevented us from gathering the critical data needed to document the role of this key region in the development and maintenance of the global climate system.”

Backman *et al.* (2002) ultimately recognised that a lack of knowledge about the influence of the Arctic Ocean on the development and maintenance of climatic extremes creates a fundamental gap in our ability to understand and model global environmental change.

This study will therefore investigate the Late Jurassic and Early Cretaceous northern high latitudes with regards to palaeoclimate. The Late Jurassic-Early Cretaceous

time interval has been chosen firstly, because only limited investigation has been carried out on this interval (most of the previously published palaeoclimate studies considering this issue prefer to concentrate on the Late Cretaceous) and secondly because several authors have indicated that sub-freezing polar conditions may be present throughout this interval, most notably during the Callovian-Oxfordian (e.g., Dromart *et al.*, 2003a, b; Lécuyer *et al.*, 2003), the Tithonian/Volgian (e.g., Price, 1999; Schudack, 1999) and the Valanginian (e.g., Price, 1999; Pucéat *et al.*, 2003; Kessels *et al.*, 2006) periods. Stable isotope and geochemical proxies (in conjunction with other observations) will be used to examine the Late Jurassic-Early Cretaceous Arctic palaeoclimate due to the high resolution data that these techniques can provide.

1.2. Locations



Figure 1.3 Present day view of the Northern hemisphere showing the locations investigated as part this study.

In order to contribute to the current debate about the existence of cold polar conditions during the Jurassic and Cretaceous greenhouse climate, five northern high latitude locations were considered (Fig. 1.3). The sites selected for this research ranged from Early Callovian to Early Hauterivian in age and were situated at Arctic or sub-Arctic palaeolatitudes during this time interval. There is a considerable degree of temporal overlap between the locations, which is essential for the accurate correlation of data between the different field sites (Fig. 1.4). Further information about each location is given in the respective chapters.

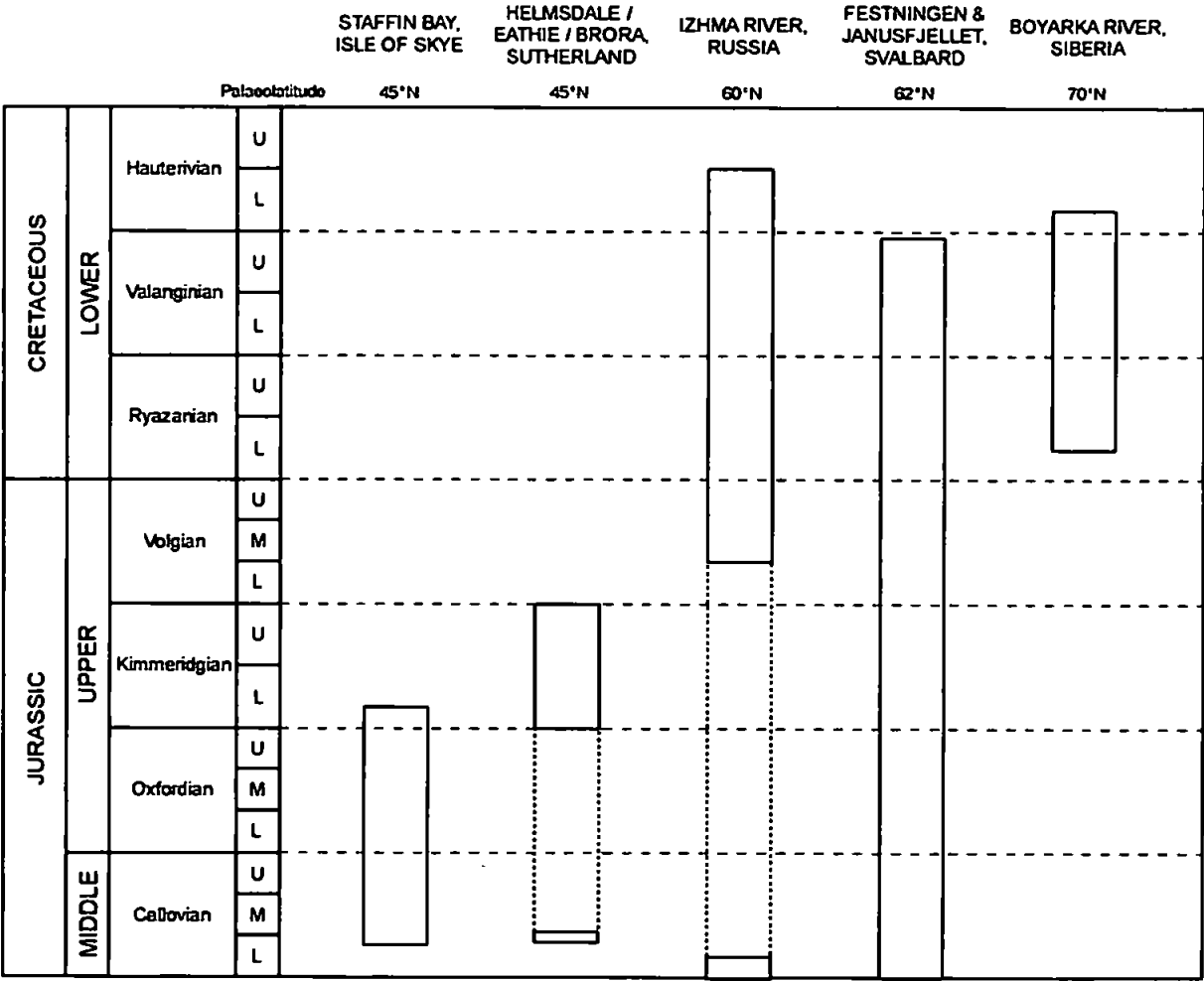


Figure 1.4 Temporal distribution of the locations investigated as part of this study. The timescale is illustrated is the Boreal (Russian) timescale.

1.3. Aims & Objectives

The major aim of this research is to investigate the nature of Late Jurassic and Early Cretaceous northern high latitude climates, principally via stable isotope and geochemical proxies as derived from belemnites and fossilised wood.

In order to achieve this aim the following objectives must be accomplished:

- To undertake high resolution sedimentary logging and systematic bed-by-bed sampling of belemnites and, where possible, fossilised wood fragments/wood debris from five biostratigraphically constrained localities within the Upper Jurassic and Lower Cretaceous of the Boreal Realm (see Chapter 2).
- To assess the level of preservation and effects of diagenesis on belemnite specimens.
- To provide stable isotope ($\delta^{18}\text{O}$ and $\delta^{13}\text{C}$) and trace element records (Fe, Mn, Ca, Mg, Sr, Na and Li) from belemnite rostra from each of the five locations.
- To produce palaeotemperature estimates for each of the localities based on $\delta^{18}\text{O}$ data.
- To investigate ocean-atmosphere links using marine (belemnite carbonate) and terrestrial (wood) records from coeval successions (Isle of Skye, Scotland and Boyarka River, Siberia).
- To provide organic geochemical analysis of fossilised wood from the Isle of Skye and Boyarka River (e.g., $\delta^{13}\text{C}_{\text{org}}$, TOC and Rock-Eval pyrolysis).
- To evaluate the use of belemnites, stable isotopes and elemental/Ca ratios as palaeoclimate indicators.
- To provide a critical analysis of palaeoenvironmental conditions in the Late Jurassic and Early Cretaceous northern high latitudes.

1.4. Thesis Structure

Chapters 2 and 3 of this thesis present background information that is critical to the current study. An overview of Late Jurassic and Early Cretaceous biostratigraphy and palaeogeography is presented in Chapter 2 with particular reference to the Arctic region. Also discussed in Chapter 2 are the key elements of the aforementioned palaeoclimate debate. In Chapter 3, an introduction to belemnites is given. This chapter provides a summary of the current state of knowledge with regards to this extinct group of organisms and ultimately focuses on the use of belemnites as palaeoclimate indicators. Together these chapters present the context in which the current study should be considered. A comprehensive review of methodology is given in Chapter 4, where each of the techniques utilised in this study are examined.

Chapters 5-9 present the full range of data obtained from each of the field sites investigated as part of this study (Staffin Bay, Helmsdale, Boyarka River, Izhma River, Festningen/Janusfjellet). Stable isotope and geochemical data are presented alongside detailed sedimentological and biostratigraphical information. The data are then interpreted in terms of palaeoclimate, with an emphasis on palaeotemperature and carbon cycling.

Chapter 10 expands upon earlier discussions and examines a number of broader themes relating to this thesis. The nature of Late Jurassic-Early Cretaceous climates in the northern high latitudes is discussed and a number of issues arising from the methodologies utilised and results obtained are explored. Finally, Chapter 11 presents the conclusions drawn from this work, acknowledges the limitations of the work and makes recommendations for future investigation.

2. THE LATE JURASSIC AND EARLY CRETACEOUS

2.1. Biostratigraphy

The Jurassic and Cretaceous periods have traditionally been correlated and subdivided on the basis of ammonite zones (e.g., d'Orbigny, 1842-51; Oppel, 1856-8; Arkell, 1933, 1956; Cope *et al.*, 1980a, b; Cox, 2001a), with the bases of most stages corresponding to the base of an ammonite zone (Ogg, 2004a). This biostratigraphic system was adopted due to the abundance of ammonite fossils from these periods (Harland *et al.*, 1990) as well as historical precedence.

A number of additional fossil groups have also been used for Jurassic-Cretaceous biostratigraphical purposes. These include brachiopods (e.g., Prossorovskaya, 1993; Garcia & Dromart, 1997; Cresta *et al.*, 2001), bivalves (e.g., Sha & Fürsich, 1993; Cresta *et al.*, 2001), belemnites (e.g., Meledina *et al.*, 1998), foraminifera (e.g., Dave & Chatterjee, 1996; Moss & Finch, 1997; Kabal & Tasli, 2003; Nagy & Seidenkrantz, 2003), ostracods (e.g., Boomer, 1994; Cresta *et al.*, 2001; Coimbra *et al.*, 2002), calcareous nannofossils (e.g., Moss & Finch, 1997; Halasova, 1999; Marino *et al.*, 2004), dinoflagellates (e.g., Poulsen, 1992), charophytes (e.g., Feist *et al.*, 1995) and palynomorphs (e.g., Mahmoud *et al.*, 1999; Cresta *et al.*, 2001; Coimbra *et al.*, 2002), although many of these taxa are often used on a local rather than a global scale.

The use of ammonites to construct a global biostratigraphic system poses a significant problem however, due to the marked provinciality displayed by ammonites throughout the Mesozoic (e.g., Arkell, 1956; Imlay, 1965; Casey, 1971; Hallam, 1971, 1975; Fürsich & Sykes, 1997; Page, 1996). During the Jurassic and most of the Cretaceous ammonites occupied three distinct realms, the Boreal Realm, the Tethyan Realm and the Austral Realm, the boundaries and extent of which changed considerably through time (Page, 1996). Such provincialism prevents the development of a truly global biostratigraphic scheme for this time, since different ammonite zones will characterise

different palaeogeographical regions (most significantly the Boreal and Tethyan Realms) making high-resolution correlation between these different realms difficult, but by no means impossible (Ogg, 2004a).

The major method of correlation is a biostratigraphic one (since the global system is based on ammonite zones) although additional techniques have also been employed. These include, for example, magnetostratigraphy (e.g., Housa *et al.*, 1999; Llanos & Riccardi, 2000; Hoedemaeker & Herngreen, 2003; Hounslow *et al.*, 2004; Speranza *et al.*, 2005; Grabowski & Pszczolkowski, 2006), strontium isotope stratigraphy (e.g., Jones *et al.*, 1994a, b; Crame *et al.*, 1999; Jenkyns *et al.*, 2002; Waltham & Gröcke, 2006) and carbon isotope stratigraphy (e.g., Jenkyns *et al.*, 2002; Padden *et al.*, 2002; Rey & Delgado, 2002, 2005).

2.1.1. Boreal-Tethyan Correlation

Many of the stratotypes for the Late Jurassic and Early Cretaceous stages and substages are situated within western European (Tethyan) basins (Zakharov, 1997; Ogg *et al.*, 2004). For example, the proposed Global Boundary Stratotype Sections and Points (GSSP's) recognised by the International Commission on Stratigraphy for the bases of the Oxfordian, Tithonian, Valanginian, Hauterivian, Barremian and Aptian stages, are all from the UK, France, Italy or Spain (Ogg, 2004b).

The differentiation of marine faunas has resulted in the development of a separate biostratigraphic scheme for the Boreal Realm that includes different stages and ammonite zones to those recognised in the Tethyan regions. In particular, the Jurassic-Cretaceous boundary has a plethora of regional terms and, for example, is represented by the Tithonian-Berriasian boundary in the Tethyan Realm and by the Portlandian-Ryazanian boundary or Volgian-Ryazanian boundary in the Boreal British or Boreal Russian Realms respectively (Sey & Kalacheva, 1999).

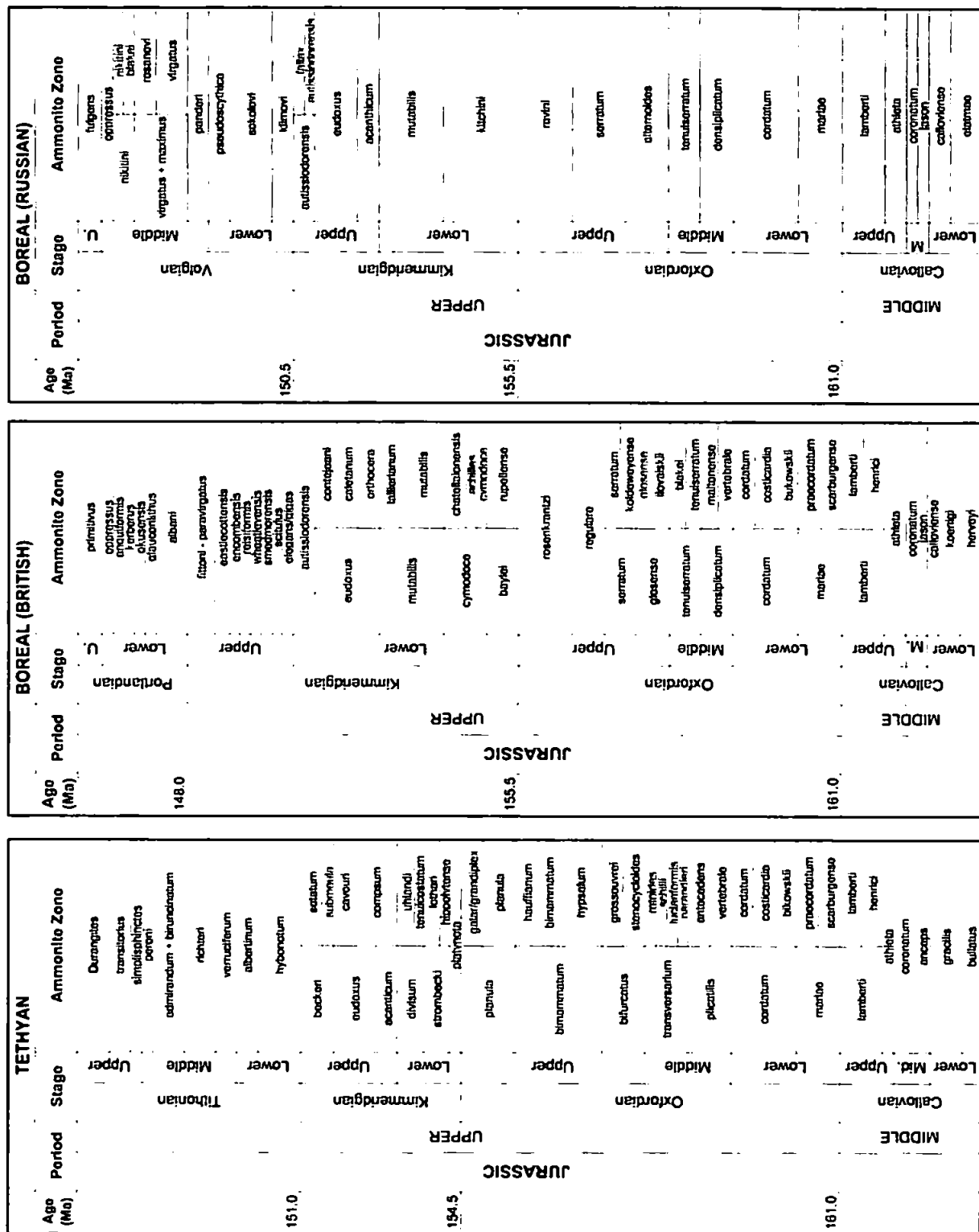
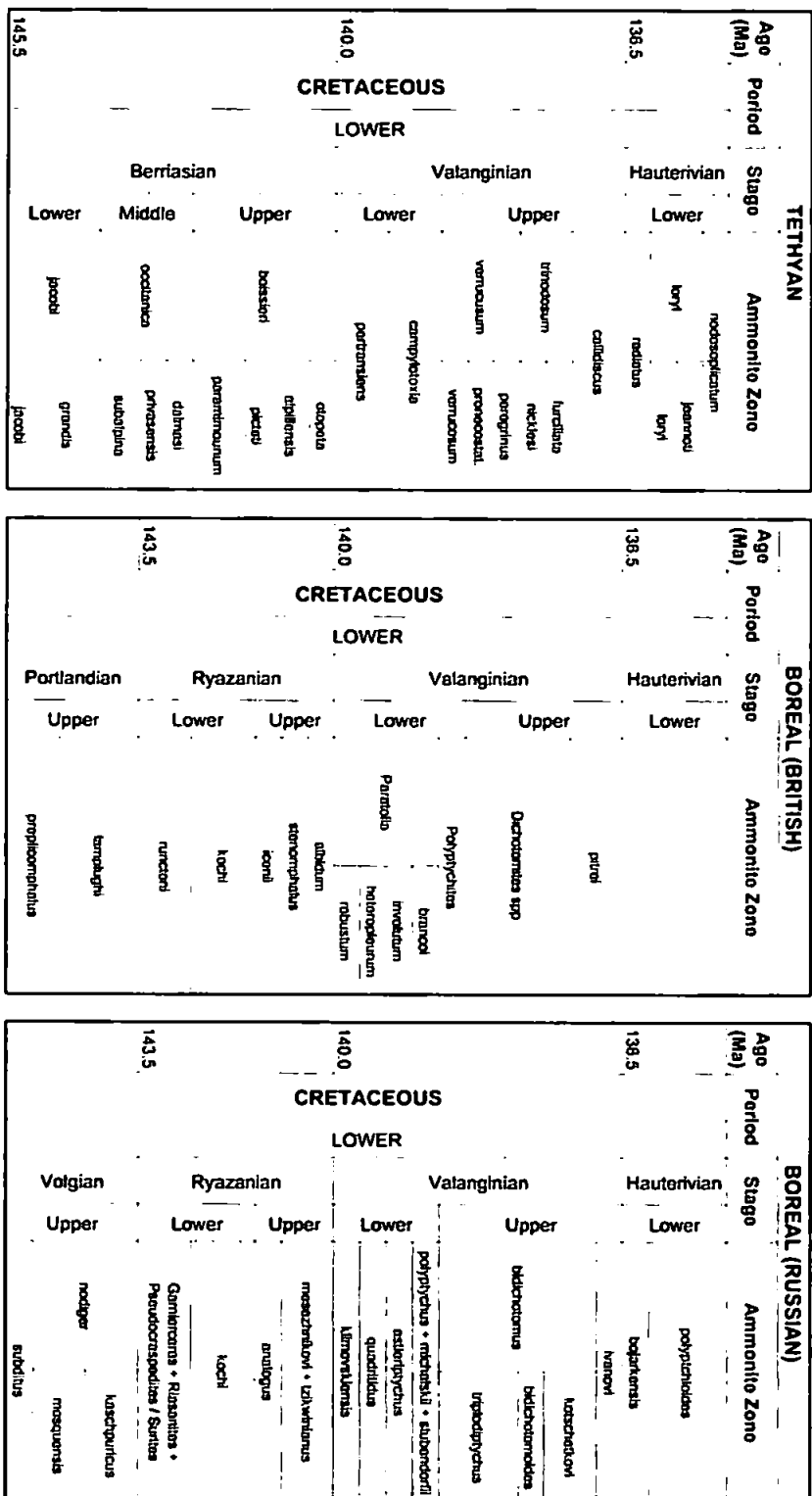


Figure 2.1a Tethyan-Boreal (British and Russian) correlation of the Middle-Upper Jurassic period (after Ogg, 2004a; Ogg *et al.*, 2004, with additions from Sahagian *et al.*, 1996; Baraboshkin, 2004; Pearce *et al.*, 2005 (and references therein)).

Figure 2.1b Tethyan-Boreal (British and Russian) correlation of the Lower Cretaceous period (after Ogg, 2004a; Ogg *et al.*, 2004, with additions from Sahagian *et al.*, 1996; Baraboshkin, 2004; Pearce *et al.*, 2005 (and references therein)).



The Boreal-Tethyan correlation of zonal biostratigraphic scales is particularly important and has been attempted by several authors (e.g., Sey & Kalacheva, 1997, 1999; Zakharov *et al.*, 1997; Baraboshkin, 1999, 2002, 2004; Ogg *et al.*, 2004). In order to attempt such correlation, it is necessary to either employ for example, chemostratigraphic or magnetostratigraphic techniques or to identify localities with a mixed Tethyan-Boreal fauna (e.g., the Russian platform, northern Caucasus, Mangyshlak (western Kazakhstan), the Crimea and Poland) (Sey & Kalacheva, 1997, 1999). The presence of a mixed ammonite fauna is obviously desirable, however correlations have also been attempted where Tethyan ammonites are associated with the Boreal bivalve, *Buchia* (e.g., California, Oregon and western Canada) (Jeletzky, 1984; Zeiss, 1986; Hoedemaeker, 1987; Sey & Kalacheva, 1997, 1999). It is also worth noting that there is some considerable variability, in terms of ammonite zonation, between different Boreal Zonal schemes. British, Russian Platform and Siberian schemes, for example, are not always consistent, although attempts to correlate these different schemes have been made (e.g., Zakharov *et al.*, 1997; Baraboshkin, 1999, 2002; Ogg *et al.*, 2004).

The Jurassic and Cretaceous Boreal-Tethyan correlations (Fig. 2.1a & b) used for this research were compiled primarily from the work of Ogg (2004a) and Ogg *et al.* (2004), with additions from Sahagian *et al.* (1996), Baraboshkin (2004) and Pearce *et al.* (2005) (and references therein). Wherever possible the most appropriate timescale was used for each of the sites investigated here. For example, the Boreal (Russian) timescale was used for the Izhma River and Boyarka River successions, whilst the Boreal (British) timescale was used for the Staffin Bay succession. At Helmsdale, the Boreal (British) timescale (as illustrated in Fig. 2.1a) was also used with the *autissioderensis-paravirgatus* ammonite zones regarded as belonging to the Upper Kimmeridgian (as per the BGS Helmsdale sheet S103EC). It should be noted however, that the use of the Upper Kimmeridgian in this sense is now commonly considered to be redundant, with this

interval generally renamed as the Tithonian following the Tethyan nomenclature; although other alternative stage names have also been proposed (e.g., the Bolonian (Ogg, 2004a)).

2.2. Palaeogeography

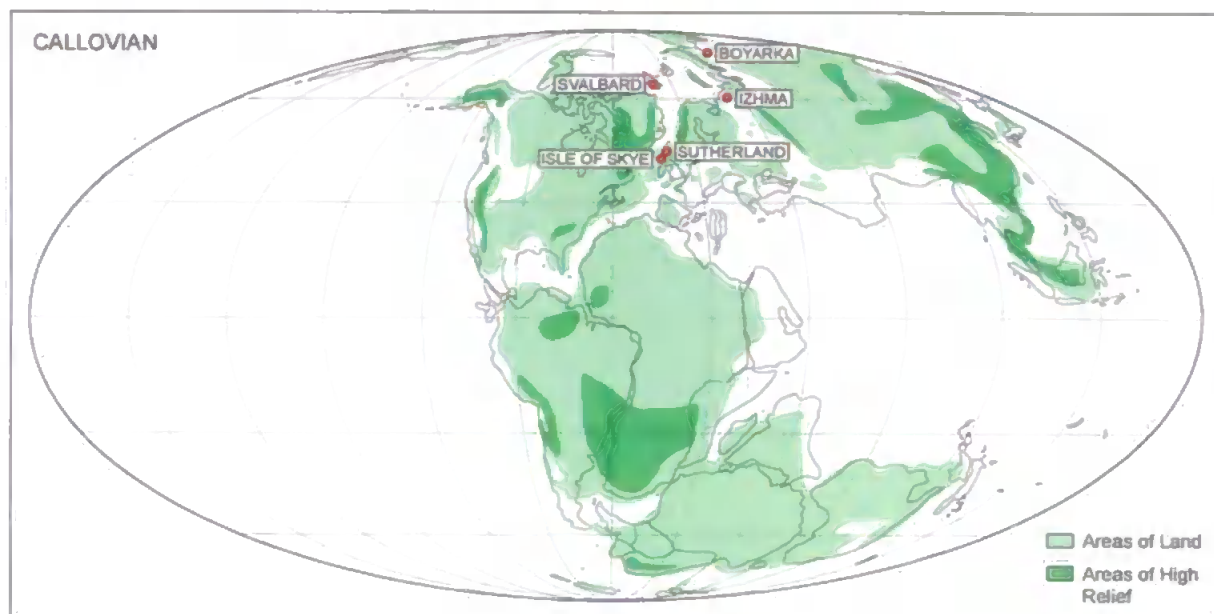


Figure 2.2 Callovian palaeogeography map. The sites investigated in this study are shown. Map adapted after Smith *et al.* (1994).

The break-up of the supercontinent Pangaea began in the Early to mid-Jurassic (Fig. 2.2) with the opening of the Central Atlantic Ocean and continued into the Early Cretaceous (Fig. 2.3) (Irving, 1983; Scotese, 1991; Golonka & Bocharova, 2000; Veevers, 2004; Page 2005). Two key mechanisms have been postulated as being the origin of this break-up, namely, mantle plume activity (e.g., Leitch *et al.*, 1998; Golonka & Bocharova, 2000; Janney & Castillo, 2001) and lithospheric stress (e.g., Scotese, 1991; McHone, 2000). It has been argued that the large volumes of melt associated with the Central Atlantic Magmatic Province (CAMP) and the geochemical signature of the earliest Atlantic crust could only be produced by plume activity, whilst advocates of a non-plume origin have argued that the geochemical diversity of CAMP magmas indicates a lithospheric origin (Beutel *et al.*, 2005).

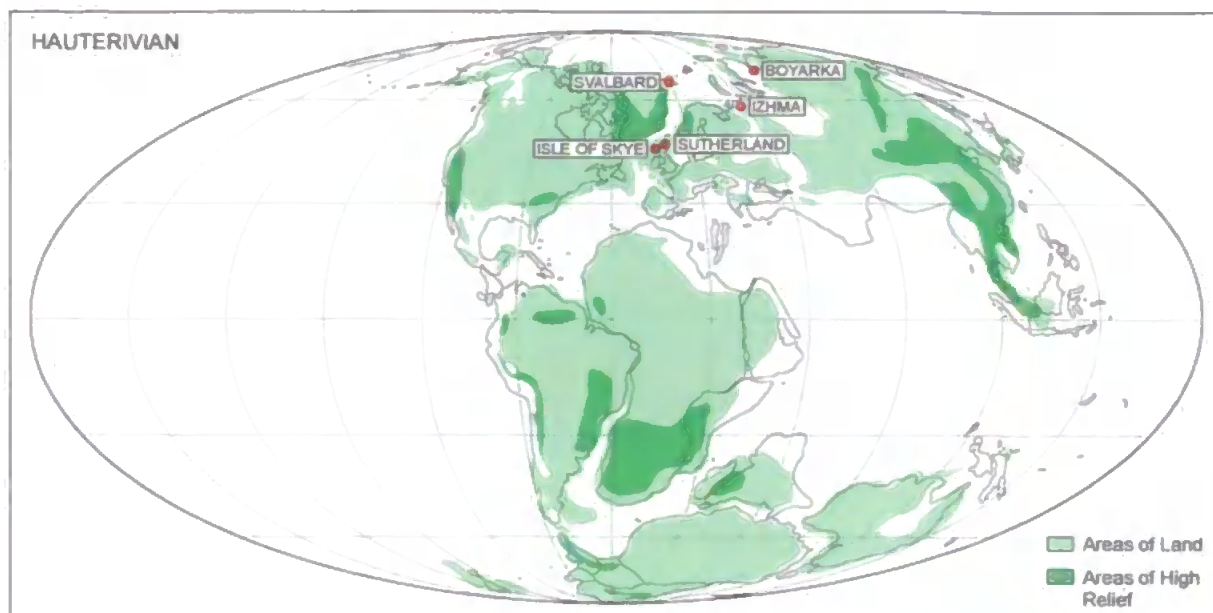


Figure 2.3 Hauterivian palaeogeography map. The sites investigated in this study are shown. Map adapted after Smith *et al.* (1994).

In the Middle Jurassic, Atlantic spreading continued and by the Late Jurassic, the North Atlantic and western Tethys had opened significantly (Irving, 1983), with the Central Atlantic Ocean reaching a width of ~500 km (Veevers, 2004). During this time, the Laurasian continents (North America, North China, Siberia and Eurasia) rifted away from the still intact Gondwana (Africa, South America, India, Australia, Antarctica) (MacLeod, 2005) and the two discrete supercontinents were separated by a continuous equatorial seaway through which surface ocean currents could flow (Skelton, 2003).

Rifting in the South Atlantic and the separation of India from Africa and from Antarctica/Australia, began in the Valanginian-Barremian (Irving, 1983; Veevers *et al.*, 1985; Scotese, 1991) splitting Gondwana first into two distinct parts (South America-Africa and India-Antarctica-Australia) (MacLeod, 2005) and by the Albian (at ~100 Ma) into five dispersed continents (Veevers, 2004). Connections between the newly developed oceans were generally narrow and shallow, which had significant implications for ocean circulation, poleward heat transport and global climate (Skelton, 2003). Continental fragmentation and drift continued throughout the Cretaceous, until the mid-Tertiary, when the main elements of modern physical geology emerged (Irving, 1983).

2.2.1. Arctic Palaeogeography & Palaeoceanography

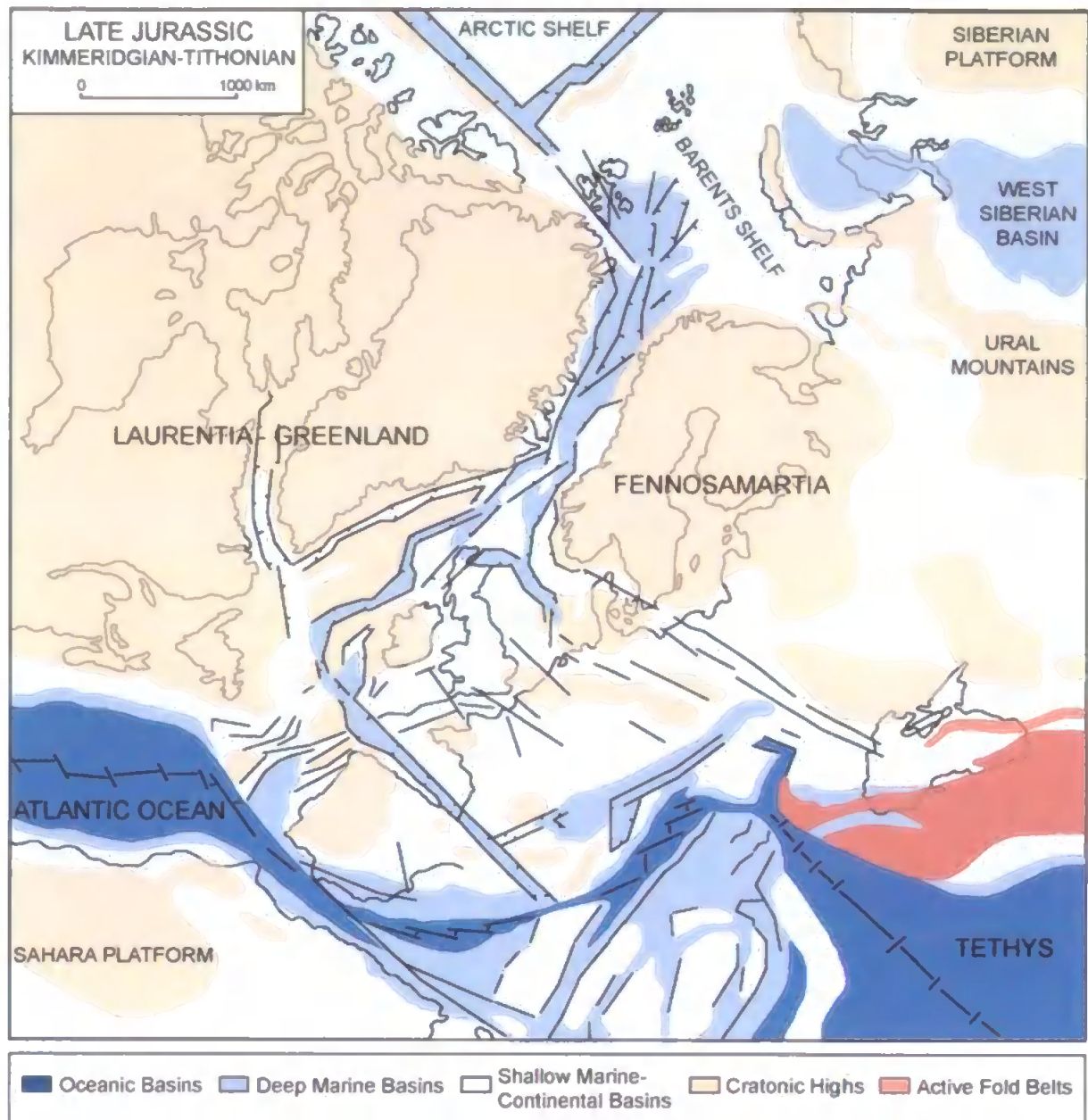


Figure 2.4 Late Jurassic palaeogeography of the Arctic region. Adapted after Ziegler (1990).

Throughout the Jurassic and earliest Cretaceous, Arctic palaeogeography and palaeoceanography were controlled principally by the break-up of Pangaea and the opening of the Arctic-North Atlantic rift (Fig. 2.4). From the earliest Jurassic a connection between the Tethys and Arctic seas was established via a series of major marine transgressions across the Arctic-North Atlantic rift system and by the end of the Early Jurassic, epi-continental seas covered much of Western and Central Europe (Ziegler, 1990;

Doré, 1991). The development and uplift of the North Sea rift dome in the Middle Jurassic created a barrier between the Tethys and Arctic seas as a consequence of the silting-up and choking of the connecting seaways (Ziegler, 1990; Doré, 1991). This barrier was a major contributing factor to the pronounced provinciality displayed by marine faunas at this time (e.g., Arkell, 1956; Imlay, 1965; Stevens, 1967; Hallam, 1975; Doyle, 1987; Mutterlose, 1988, 1998). The North Sea rift dome collapsed during the Callovian to Volgian (Ziegler, 1990). At this time, a strong transgressive regime continued and crustal extension intensified throughout the Arctic-North Atlantic rift to re-open the Tethys-Arctic connection via a system of interconnected straits and seas (Ziegler, 1990; Doré, 1991; Bjerrum *et al.*, 2001). These conditions continued into the Early Cretaceous, although tectonic activity increased at the Jurassic-Cretaceous boundary (Ziegler, 1990) and a series of structural highs developed, which controlled faunal provinciality through the construction of land barriers in the European-Arctic seaway (Doré, 1991).

The deposition of organic-rich black shales is widespread in the Late Jurassic and Early Cretaceous, giving rise to extensive oil and gas accumulations across the circum-Arctic region (Ziegler, 1990; Doré, 1991; Langrock *et al.*, 2003; Mutterlose *et al.*, 2003; Langrock & Stein, 2004). Economically viable accumulations of such petroleum source rocks are known from West Siberia, the Barents Shelf, mid-Norway and the North Sea Basin (Doré, 1991). An increase in the preservation potential of organic carbon can be caused by several different mechanisms, such as anoxic bottom waters, high primary production, reduced clastic input and rapid burial (Demaison & Moore, 1980; Stein *et al.*, 1986; Meyers, 1997; Langrock *et al.*, 2003).

Late Jurassic and Early Cretaceous black shale formation in the Norwegian-Greenland seaway has been attributed to suboxic to anoxic bottom water conditions in restricted shallow marine basins as the result of a sea-level low stand (e.g., Ziegler, 1990; Mutterlose *et al.*, 2003; Langrock *et al.*, 2003). Langrock & Stein (2004) suggest that in addition to formation in anoxic or stagnant conditions, black shales from this region were

also deposited in highly-productive environments resulting from coastal upwelling. Macquaker & Keller (2005) consider organic-rich mudstone sedimentation from the Lower Cretaceous of Alaska to be attributed to high organic productivity related to episodic and rapid sedimentation rather than bottom water anoxia or upwelling. Doré (1991) concluded that organic-rich shale deposition was the result of multiple local mechanisms operating concurrently during the Late Jurassic and Early Cretaceous (e.g., a strong transgressive regime, extensional tectonics, reduced clastic input and the globally warm and equable climate), which together created an environment prone to stagnation and organic productivity in some basins. This trend was terminated post-Berriasian as the result of palaeoceanographic changes creating new ocean margins in the Canada Basin and Rockall Trough (Doré, 1991).

During the Early Cretaceous the Canadian Basin of the Arctic Ocean began to open (Ziegler, 1990; Hay *et al.*, 1999) and the extensive rifting history of the Rockall Trough culminated in a spreading event (Doré, 1991). At the same time the narrow Greenland-Norwegian Seaway (at the north of the Arctic-North Atlantic rift) reached a length of 1500-2000 m and a width of ~300 km (Gradstein *et al.*, 1999; Mutterlose *et al.*, 2003). The rotational opening of the Canadian Basin may have provided a connection between the Arctic Basin and the Pacific Ocean, possibly along a narrow, deep passage to the South Anyui Basin (Hay *et al.*, 1999; Mutterlose *et al.*, 2003), although this passage may have been blocked by a land bridge so that there was no deep water connection between the Arctic Basin and the world ocean at this time (Mutterlose *et al.*, 2003). In the mid-Cretaceous, tectonic activity gradually abated in Central and Western Europe (Ziegler, 1990). A major marine transgression in the Aptian-Albian submerged the structural highs created by Late Jurassic to Early Cretaceous tectonics and formed an open seaway from southern England to the Barents Sea, so that by the mid-Albian faunal connections from Svalbard to the Mediterranean had been fully established (Doré, 1991). Arctic-North Atlantic plate reorganisation continued from the Late Mesozoic until the Late Eocene-

Neogene post-Alpine plate reorganisation, which led to the present-day continent assembly and configuration of the Arctic Ocean (Ziegler, 1990).

2.3. Palaeoclimate

As mentioned previously the Jurassic and Cretaceous periods are commonly considered as a time of warm, equable global climates (e.g., Frakes, 1979; Hallam, 1981, 1985, 1993). High mean annual temperatures, a low global temperature gradient (and subsequently weak climatic zonation) and warm polar regions are commonly hypothesised for this period (e.g., Frakes, 1979; Hallam, 1981; Barron, 1983).

A number of studies have, however, suggested that during this period a more variable climate with seasonally low ocean temperatures and limited polar ice caps would have been present (e.g., Francis & Frakes, 1993; Ditchfield, 1997; Price, 1999; Price & Mutterlose, 2004; Kessels *et al.*, 2006).

2.3.1. Evidence for a Warm, Equable Climate

There is much compelling evidence to support the concept of a warm, equable, ice-free climate during the Jurassic and Cretaceous periods. In the past, the reported absence of glacial deposits has been considered as sufficient evidence for a greenhouse world (e.g., Hallam, 1985). Some of the more convincing recent evidence is discussed below and includes information about CO₂ levels, polar forests and plant phenology, polar faunas, General Circulation Models (GCM's), stable isotopes and the new TEX₈₆ temperature proxy. It should be noted that much of this research has been conducted on the Cretaceous period.

The general assumption is that this greenhouse climate was related to high atmospheric concentrations of carbon dioxide (e.g., Barron *et al.*, 1993; Weissert & Lini, 1991; Francis & Frakes, 1993; Dromart *et al.*, 2003a; Royer *et al.*, 2004), with recent estimates for Jurassic and mid-Cretaceous CO₂ levels in the range of 1200 to 3000 ppm

(approximately 4-10 times modern pre-industrial values) (Dromart *et al.*, 2003a) and >4000 ppm (Bice & Norris, 2002) respectively. Additional factors of climatic significance may be the galactic cosmic ray flux (e.g., Shaviv & Veizer, 2003; Wallmann, 2004) and palaeogeography (e.g., Barron & Washington, 1982; Barron, 1983).

Perhaps the most compelling evidence of Jurassic and Cretaceous polar warmth is the abundance of fossil forest localities recorded from both poles (<85° palaeolatitude) throughout the Mesozoic (Spicer & Parish, 1986). The poleward limit of present day forest vegetation is 59°N - 72°N in the northern hemisphere and 55°S in the southern hemisphere (Falcon-Lang *et al.*, 2001). Cretaceous fossil forests have been recorded from high palaeolatitudes in Alaska (e.g., Herman & Spicer, 1997), Northern Russia (e.g., Spicer *et al.*, 2002), New Zealand (e.g., Kennedy *et al.*, 2002), Australia (e.g., Dettmann *et al.*, 1992) and Antarctica (e.g., Cantrill & Nichols, 1996; Falcon-Lang *et al.*, 2001; Falcon-Lang & Cantrill, 2001). In the northern hemisphere these forests tended to be dominated by deciduous vegetation and in the southern hemisphere by evergreen vegetation (Falcon-Lang & Cantrill, 2001; Brentnall *et al.*, 2005).

Plants are not mobile after germination and, therefore, strongly reflect the physical environment in which they lived (Spicer & Corfield, 1992). Analysis of fossil leaf phenology (e.g., Falcon-Lang & Cantrill, 2001), including physiognomy (e.g., Herman & Spicer, 1996, 1997; Spicer *et al.*, 2002), the analysis of growth rings or anatomical characters in trunk woods (e.g., Creber & Chaloner, 1985; Francis & Poole, 2002) and comparison with nearest living relatives (e.g., Chaloner & Creber, 1990) have yielded palaeotemperature information indicating that the Cretaceous poles were relatively warm. For example, Spicer *et al.* (2002) calculated a mean annual temperature of $13.0 \pm 1.8^{\circ}\text{C}$ and a cold month mean temperature of $5.5 \pm 3.3^{\circ}\text{C}$ for northeastern Russia during the mid-Cretaceous.

The extensive distribution of fossil fauna at high latitudes is also considered to be evidence for warmer polar climates in the past. The first record of polar dinosaurs is

believed to be that of Lapparent (1960) who discovered *Iguanodon* footprints on Svalbard. Since then, dinosaurs, mosasaurs, plesiosaurs, ichthyosaurs, champosaurs and crocodilians have all been recorded from Mesozoic polar regions (e.g., Huber, 1998; Markwick, 1998; Tarduno *et al.*, 1998; Rich *et al.*, 2002; Buffetaut, 2004; Kear, 2006). Many authors interpret such finds as providing confirmation that polar regions were warm rather than near freezing. Tarduno *et al.* (1998), for example, estimate a mean annual temperature of $>14^{\circ}\text{C}$ for the Late Cretaceous based on the presence of champosaurs in the Canadian Arctic. Poleward habitat expansion of marine thermophilic organisms (rudistid bivalves, gastropods, larger foraminifera and coral reefs) has also been observed and further supports the idea of Cretaceous polar warmth (Kauffman, 1973; Gordon, 1973; Habicht, 1979; Lloyd, 1982; Huber *et al.*, 1995). It is worth noting, however, that Markwick (1998) considers the periodic absence of crocodilians from high latitudes in the Late Cretaceous as an indicator of cooling in these regions at these times and that Kear (2006) suggests that Early Cretaceous plesiosaur and ichthyosaur taxa may have possessed adaptations to enable them to cope with low temperatures (e.g., elevated metabolic levels or annual migration).

GCM's have been used to provide both qualitative and quantitative evaluation of Jurassic and Cretaceous climates. Such models have generally supported the concept of Mesozoic warmth in the mid- to low latitudes (e.g., Moore *et al.*, 1992; Barron *et al.*, 1995; Price *et al.*, 1997; Poulsen *et al.*, 1999) although the nature of high latitude climates is more equivocal. Barron *et al.* (1995) conducted a series of GCM simulations of mid-Cretaceous climate. Their model simulation, which best matched observations, recorded a globally averaged sea surface temperature of 6.2°C above present-day levels. Barron *et al.* (1995) suggest that this value is at the lowest end of estimates for Cretaceous warmth.

There is an abundance of stable isotope data consistent with a warm, equable greenhouse climate dominating the Jurassic and Cretaceous periods (e.g., Stevens & Clayton, 1971; Barron, 1983; Huber *et al.*, 1995; Clarke & Jenkyns, 1999; Poulsen *et al.*,

1999; Wilson & Norris, 2001; Norris *et al.*, 2002; Wilson *et al.*, 2002), although much of the available data concentrates on the mid- to Late Cretaceous. Barron (1983) estimated sea surface temperatures in the range of 27-32°C for equatorial regions in the Albian-Cenomanian based on planktonic foraminifera. This is consistent with the data of Wilson *et al.* (2002), who estimated equatorial sea surface temperatures of 30-33°C for the Turonian using glassy foraminiferal calcite and the data of Clarke & Jenkyns (1999), who estimated low-latitude temperatures of >33°C for the mid-Cretaceous generated from calcareous fine-fraction and bulk sediments from the Exmouth Plateau.

Huber *et al.* (1995) investigated foraminiferal data from the southern high latitudes to provide evidence of a reduced latitudinal temperature gradient for the mid- to Late Cretaceous. They record palaeotemperatures of 17-23°C from the Albian to Cenomanian and <33°C in the Turonian, although they acknowledge that such values seem “excessively warm” for palaeolatitudes of 56-60°S. Further evidence consistent with mid-Cretaceous high-latitude warmth was reported by Poulsen *et al.* (1999) who recorded palaeotemperatures of approximately 18-20°C in the southern high-latitudes (Falkland Plateau and southeast Indian Ocean at ~58-62°S). These values were derived from the $\delta^{18}\text{O}$ ratios of foraminiferal calcite. The $\delta^{18}\text{O}$ values however, were inconsistent with the model predictions of the same study (Poulsen *et al.*, 1999), which for the same sites predicted palaeotemperatures ranging from 7-11°C. It should be noted that for all of the above palaeotemperature estimates there is an estimate of $\delta^{18}\text{O}_{\text{seawater}}$. This can be highly variable and is a potential unknown that must be acknowledged (and is discussed later).

Shouten *et al.* (2002) developed a new organic palaeothermometer, TEX₈₆, which is based on the composition of lipids in the membranes of crenarchaeota (floating marine micro-organisms) and is independent of salinity or nutrient availability (Schouten *et al.*, 2002). Using the TEX₈₆ proxy, low latitude palaeotemperatures of ~30-36°C for the mid-Cretaceous were calculated from the Shatsky Rise (Dumitrescu *et al.*, 2006). In addition, Jenkyns *et al.* (2004) calculated an average sea surface temperature of ~ 15°C for the

Arctic Ocean in the Late Cretaceous and extrapolated a temperature in excess of 20°C for polar waters during the mid-Cretaceous. Such palaeotemperatures are however, significantly higher than many previous calculations and the technique has yet to be fully evaluated. Sluijs *et al.* (2006) applied the TEX₈₆ proxy to Arctic Ocean sediments deposited at the Paleocene/Eocene Thermal Maximum and recognised that the TEX₈₆ record was probably skewed towards summer temperatures, since the export of lipids to the sea floor coincides with high phytoplankton productivity and hence the Cretaceous estimates may represent extreme summer values.

2.3.2. Evidence for Cold Polar Regions

The Mesozoic Era almost certainly represents the longest period of warmth during the Phanerozoic. Nevertheless, this period of warmth would have been punctuated by oscillations in climate, which may or may not have been of sufficient magnitude and duration to produce cooling and the formation of polar ice (Price, 1999). Whilst many authors argue that this is unlikely, or at the least highly equivocal (e.g., Rowley & Markwick, 1992), there is much compelling evidence to the contrary (e.g., Moore *et al.*, 1992; Sellwood *et al.*, 1994; Pirrie *et al.*, 1995; Stoll & Schrag, 1996; De Lurio & Frakes, 1999; Price, 1999; Gale *et al.*, 2002; Alley & Frakes, 2003; Dromart *et al.*, 2003a; Miller *et al.*, 2003, 2005). The evidence presented below includes data from stable isotopes, GCM's, sea-level curves and from glacially derived sediments and minerals.

Much of the isotopic evidence for warm, equable Jurassic and Cretaceous climates has been based on climatic data derived from the mid- to low palaeolatitudes (Ditchfield, 1997; Price & Mutterlose, 2004), introducing a potential bias when considering higher latitude conditions. Even in studies conducted in the mid to low latitudes however, cooling episodes have been observed during the Cretaceous greenhouse climate (e.g., Stoll & Schrag, 2000; Miller *et al.*, 2003, 2005). Puc  at *et al.* (2003) investigated Tethyan marine waters using the oxygen isotope composition of fish tooth enamel. They were able to

distinguish three major cooling events at the million-year scale: at the Berriasian-Valanginian boundary; during the earliest Late Valanginian; and during the earliest Aptian. Such data are supported by other studies, for example, van de Schootbrugge *et al.* (2000), which identifies progressively cooler temperatures from the late Valanginian to early Hauterivian in southeastern France.

Where studies of high latitude sites have been undertaken, the isotopic data often record palaeotemperature values that are significantly cooler than might be expected based on mid- to low latitude estimates (e.g., Barrera *et al.*, 1987; Pirrie & Marshall, 1990; Ditchfield *et al.*, 1994; Sellwood *et al.*, 1994; Pirrie *et al.*, 1995; Ditchfield, 1997; Price & Mutterlose, 2004). It is possible, that studies recording very warm temperatures for the high-latitude regions may be recording a diagenetic component, since partial recrystallisation will generally lower $\delta^{18}\text{O}$ values and, therefore, generate overestimates of palaeotemperature (Schrug *et al.*, 1992). Price *et al.* (1996) argue that this may account for the “intuitively unlikely” temperatures proposed by Huber *et al.* (1995) for the mid- to Late Cretaceous southern high-latitudes (<33°C).

Ditchfield *et al.* (1994) conducted an oxygen isotope study of molluscan macrofossils in Antarctica. They concluded that mean temperatures of almost 0°C may have occurred at the South Pole from the mid-Cretaceous and that elevated high latitude terrains were probably glaciated. Price & Mutterlose (2004) calculated minimum palaeotemperatures of 2°C derived from belemnites from the late Valanginian to early Hauterivian in the Yatria River, Western Siberia. This is consistent with the data of Polyak *et al.* (2003) whose stable isotope measurements of modern benthic foraminifera in the Kara and Pechora seas record an annual range of temperatures from -1 to +12°C. Cretaceous isotopic data have also been derived from foraminifera, for example, Sellwood *et al.* (1994) produced a poleward extrapolation of planktonic foraminiferal data to give an estimate of mid-Cretaceous latitudinal variations in mean annual temperature. Their model

suggested that palaeotemperatures could reach sub-freezing values at both poles during this time.

Several GCM simulations have predicted the presence of sub-freezing conditions and limited polar ice at the Jurassic and Cretaceous poles. Moore *et al.* (1992) considered two simulations of the Kimmeridgian/Tithonian palaeoclimate with differing CO₂ levels (280 and 1200 ppm). Each simulation predicted the presence of sea-ice, although the amount of sea-ice was significantly reduced in the 1200 ppm simulation. Valdes *et al.* (1995) also used a GCM to predict the presence of ice during the Late Jurassic. Their data indicate the presence of a modest, but significant Antarctic ice-cap, which they suggest would have disappeared at times of maximum seasonal forcing. Mid-Cretaceous greenhouse and icehouse climates were modelled by Price *et al.* (1998). Their icehouse simulation predicts small permanent ice-caps at both poles during this time.

Further evidence for the presence of ice sheets during the Jurassic and Cretaceous can be found in records of rapid sea level change. Stoll & Schrag (1996) use strontium data from the Berriasian and Valanginian to suggest that global sea level fluctuated by ~50 m over 200,000 to 500,000 years and that such geologically rapid fluctuations indicated the existence of an Antarctic ice sheet at this time. This hypothesis is supported by the authors oxygen isotope measurements, which suggested that these rapid sea level changes were indeed caused by the growth of continental ice sheets. Dromart *et al.* (2003a) provide a detailed record of northern hemisphere sea surface temperatures for the Middle to Late Jurassic transition that record a severe cooling event coincident with an abrupt global-scale sea level fall. Such data could indicate a period of ice sheet formation, which the authors suggest may have developed over the mountainous regions of far-east Russia. A further sea level study of the Late Cretaceous shows large and rapid sea level changes occurring on a global scale, which are also interpreted as having a glacio-eustatic control (Miller *et al.*, 2003). Miller *et al.* (2003, 2005) comment that the only alternative to a glacio-eustatic mechanism would be something that is as yet undefined since other potential mechanisms

(e.g., water storage in lakes, groundwater, deepwater changes or sea ice) cannot explain such large and rapid sea level changes.

Tillites, dropstones and glendonites are often considered to be evidence of glacial conditions. Deposits with affinities to glacial tillites have been described from the Jurassic and Cretaceous of Russia, Siberia, Eastern Europe, Antarctica, South America and Australia (e.g., Epshteyn, 1978; Chumakov, 1981a, b; Woolfe & Francis, 1991; Price, 1999; Huber *et al.*, 2001; Alley & Frakes, 2003). However, the glacial nature of such deposits is often disputed and alternative mechanisms of origin are commonly proposed. For example, Oberbeck *et al.* (1993) and Rampino (1994) suggest that meteoric impacts could produce tillite-like deposits.

Potential dropstones have been described from the Jurassic and Cretaceous of Europe and Australia (e.g., Pickton, 1981; Jeans *et al.*, 1991; Frakes & Krassay, 1992; Francis & Frakes, 1993; Price, 1999). Such deposits are commonly considered to be the result of ice-rafting, although, it should be noted that Bennett & Doyle (1996) and Bennett *et al.* (1996) argue that caution should be exercised when interpreting dropstone evidence, because there are many agents besides icebergs by which dropstones may be transported (e.g., seaweed, kelp, driftwood).

Glendonites are star shaped calcite pseudomorphs after the metastable mineral ikaite that are commonly taken to reflect deposition in cold subaqueous conditions (Francis & Frakes, 1993; Sellwood & Price, 1994; De Lurio & Frakes, 1999). Cretaceous glendonites have been identified from Svalbard (Kemper, 1983), Australia (De Lurio & Frakes, 1999; Alley & Frakes, 2003) and Canada (Kemper & Schmitz, 1975, 1981). De Lurio & Frakes (1999) investigated glendonites from the Lower Cretaceous Bulldog Shale in Australia and concluded that the presence of glendonites at this site indicated a gradual warming of waters from near-freezing temperatures to temperatures above 5-8°C.

A well argued overview of this debate is presented by Price (1999). He evaluates published evidence for Mesozoic ice and cool temperatures from around the world. Based

on such evidence he suggests that several cold or sub-freezing periods can be identified in the polar regions, namely, during the (?)Pliensbachian, Bajocian-Bathonian, Tithonian/Volgian, Valanginian and Aptian. Price (1999) concludes that although high latitude warmth is the norm throughout the Mesozoic, the occurrence of limited polar ice at times is not a myth but a reality.

3. BELEMNITES

3.1. Systematic Position

The Belemnoidea (Hyatt, 1884) are a superorder of the Coleoidea, a monophyletic group of cephalopod molluscs characterised primarily by their possession of an internal (endocochleate) shell (Doyle *et al.*, 1994; House, 1998). The Belemnoidea first appeared in the Early Devonian (Engeser & Bandel, 1988; Doyle, 1990a), possibly in response to the diversification of fish at the time (Young *et al.*, 1998) and finally became extinct at the Cretaceous/Tertiary boundary (Engeser & Bandel, 1988).

Autapomorphies (the characteristics defining a taxon) of the Belemnoidea are the closing organic membrane of the phragmocone, the 5-layered conotheca (the outer wall of the phragmocone), and the presence of arm hooks on ten subequal arms (Engeser & Bandel, 1988; Engeser, 1990). These characters are widely accepted, although some have yet to be demonstrated in certain groups.

The Belemnoidea can be subdivided into the orders Aulacocerida (Middle Carboniferous - Early Jurassic), Belemnitida (Early Jurassic - end-Cretaceous) and Diplobelida (Late Jurassic - mid-Cretaceous), based primarily on their body chamber characteristics (Doyle *et al.*, 1994; Doyle & Shakides, 2004). The Order Belemnitida (Zittel, 1895) is the one to which the true 'belemnites' belong. The classification of the Belemnitida shown below is based on that of Doyle *et al.* (1994). Information beyond family level is not given.

In addition to the suborders Belemnitina and Belemnopseina (as included here), other suborders have also been included in various Belemnitida classifications (e.g., Diplobelina (Jeletzky, 1966; Mutterlose, 1988) and Belemnotheutididina (Doyle *et al.*, 1994)), however the taxonomic positions of such suborders are often disputed, with some authors preferring to create new orders for such problematic groups. As such, only those

suborders universally recognised (Belemnitina and Belemnopseina) have been included here.

The major distinction between the Belemnitina and Belemnopseina is in the ventral groove. The Belemnitina display apical furrows, whilst the Belemnopseina possess alveolar grooves (Mutterlose, 1988).

Class CEPHALOPODA Cuvier, 1794

Subclass COLEOIDEA Bather, 1888

Superorder BELEMNOIDEA Hyatt, 1884

Order BELEMNITIDA Zittel, 1895

Suborder BELEMNITINA Zittel, 1895

Family PASSALOTEUTHIDIDAE Naef, 1922

Family SALPINGOTEUTHIDIDAE Doyle, 1992a

Family HASTITIDAE Naef, 1922

Family CYLINDROTEUTHIDIDAE Stolley, 1919

Family OXYTEUTHIDIDAE Stolley, 1919

Suborder BELEMNOPSEINA Jeletzky, 1965

Family BELEMNOPSEIDAE Naef, 1922

Family DICOELITIDAE Saks and Nal'nyaeva, 1967

Family PSEUDODICOELITIDAE Saks and Nal'nyaeva, 1967

Family DUVALIIDAE Pavlow, 1914

Family BELEMNITELLIDAE Pavlow, 1914

Family DIMITOBELIDAE Whitehouse, 1924

3.2. The Belemnite Animal

The discussion presented below provides a general overview of belemnite morphology, palaeoecology and palaeobiogeography, as well as an overview of the use of

belemnites in palaeoclimate studies. It is worth considering, however, that with regards to belemnite morphology and palaeoecology one model may not fit all.

3.2.1. Belemnite Morphology

The belemnite animal can perhaps best be described as a marine squid-like cephalopod (e.g., Bandel & Spaeth, 1988; Cox & Doyle, 1996; Clarkson, 1998), similar in appearance to the extant squid *Loligo* (Bandel & Spaeth, 1988). Modern squids possess a flexible, unmineralised internal shell called a gladius, which is composed of chitin (Donovan & Toll, 1988). Unlike most modern squid however, belemnites possessed a hard (calcified) internal skeleton (Kear *et al.*, 1995; Cox & Doyle, 1996). The only extant coleoid families which also possess mineralised tissue are the Sepiidae and Spirulidae (Kear *et al.*, 1995), which have retained a primitive phragmocone (Young *et al.*, 1998). The Sepiidae and Spirulidae are, therefore, commonly considered to be the closest analogue for the extinct order Belemnitida.

The hard internal skeleton of the belemnite animal is known as a rostrum (and is also commonly referred to as a guard, although this has an invalid functional connotation (Doyle & Kelly, 1988; Doyle, 1990a)). The rostrum is composed of low-magnesium calcite (Hudson & Anderson, 1989; Sælen, 1989; Doyle & Bennett, 1995) and is consequently readily preserved in the fossil record (as discussed later).

Early belemnite studies interpreted concentric rings exhibited within the rostrum as primary seasonal growth bands (e.g., Bøggild, 1930; Müller-Stoll, 1936; Urey *et al.*, 1951; Spaeth *et al.*, 1971) and the observed variations in oxygen isotope ratios between the bands were, therefore, interpreted as seasonal variations in temperature (Urey *et al.*, 1951). Longinelli (1969) however, hypothesised that diagenetic processes may have simulated seasonal temperature variations, since it was apparent that radial variations in oxygen isotope composition could be observed in belemnites that had undergone considerable diagenetic alteration (whilst such oscillations, if a primary feature, should be obscured by

diagenesis). Modern studies suggest (although not conclusively) that this pattern of concentric rings was probably the result of organic matter decay (Rosales *et al.*, 2004a). It is believed that belemnite rostra were originally composed of radial crystals of low-magnesium calcite, which were porous and contained variable amounts of organic matter that would have decayed post-mortem to create void space that was later infilled by secondary calcite (e.g., Sælen, 1989; Sælen & Karstang, 1989; Podlaha *et al.*, 1998; Rosales *et al.*, 2004a).

The rostrum is the largest and most posterior section of the belemnite shell (Fig. 3.1). It is cylindric in form, tapers to a point posteriorly and is indented by a conical cavity (the alveolus) at the anterior end (Clarkson, 1998). The phragmocone is an aragonitic, thin-walled and chambered part of the shell situated within, and projecting out of the alveolus (Sælen, 1989; Clarkson, 1998). A slender siphuncle threads through the phragmocone septa at the ventral margin (Clarkson, 1998). The final (and most anterior) component of the belemnite shell is the pro-ostracum. This is a long, flat, tongue-shaped extension of the phragmocone, which projects forwards and presumably covered the anterior part of the body (Clarkson, 1998). These three major components of the belemnite shell were wholly internal, with the complete structure surrounded by soft tissue.

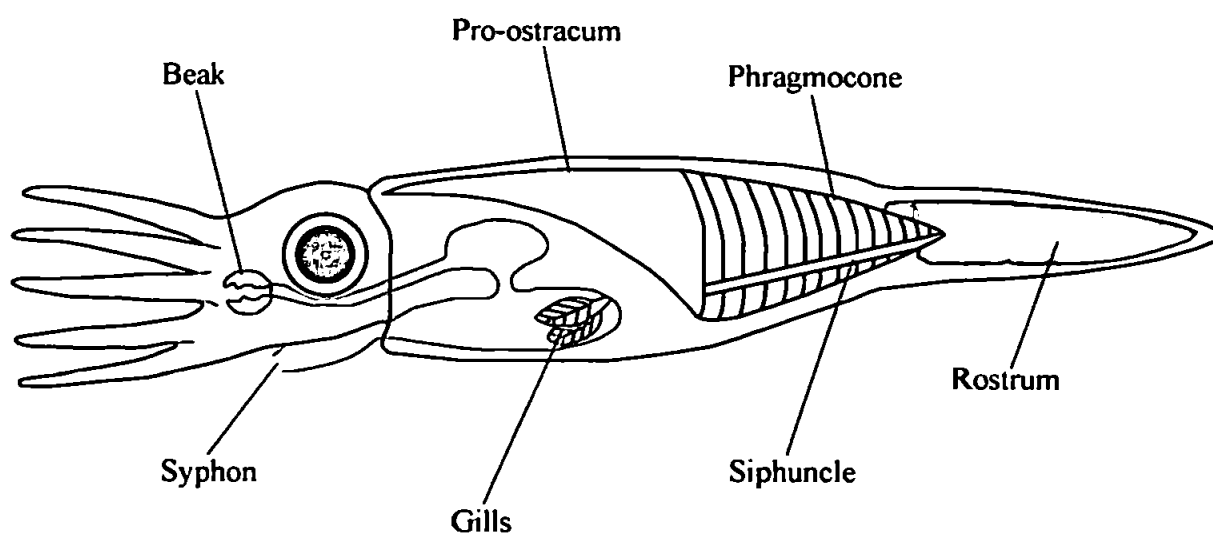


Figure 3.1 Belemnite morphology. A reconstruction of a living belemnite showing the internal skeleton. Adapted after Eyden (2003).

The preservation of belemnite soft body parts is extremely rare, although four belemnite specimens with soft parts, ink sacs and hooks preserved have been described from the Early Jurassic Posidonia Shale of South Germany (Reitner & Urlichs, 1983; Riegraf & Hauff, 1983; Engeser & Clarke, 1988). These specimens show the outline of the mantle and head, arms with double rows of hooks, but no fins (Hewitt *et al.*, 1999). No clear records of belemnite fins have ever been discovered, although fins are frequently included in reconstructions (Young *et al.*, 1998). For hydrodynamic reasons it seems likely that small manoeuvrable fins would have been present (probably attached at the sides, where lateral grooves can be seen in the rostrum), as in other coleoids (Monks *et al.*, 1996; Hewitt *et al.*, 1999).

Belemnites are believed to have had 10 subequal arms, each equipped with 30-50 pairs of normal sized hooks (Engeser & Bandel, 1988; Engeser & Clarke, 1988). Of the four belemnites described from the Posidonia Shale, one had a very large 'onychite' hook at the base of the arm crown, which has been interpreted as a sexual modification, probably of the male belemnite (Engeser & Clarke, 1988). The possibility of sexual dimorphism in belemnites was first proposed by d'Orbigny (1842) and has since been mentioned by numerous authors, for example Phillips (1867), Lissajous (1925), Roger (1952), Waterston (1952), Delattre (1956), Stevens (1965a), and Doyle (1985). The presence of dimorphic characters in ammonites (e.g., Makowski, 1963; Calloman, 1963; Palframan, 1966) and extant cephalopods (e.g., Westermann, 1969) has been widely accepted and it therefore seems reasonable to expect some degree of dimorphism in belemnites (Doyle, 1985).

3.2.2. Belemnite Palaeoecology

Belemnites, like modern squid, were nektonic organisms (Stevens, 1963; Spaeth *et al.*, 1971; Bandel & Spaeth, 1988; Anderson *et al.*, 1994; Doyle *et al.*, 1997; Rosales *et al.*, 2004a). Today, squid inhabit a diverse range of marine environments, including, the pelagic zones of shallow estuaries, continental shelves and open oceans, as well as the deep

sea, and polar oceans (Pörtner & Zielinski, 1998). This might suggest that belemnites also inhabited a comparable range of environments.

Hewitt *et al.* (1999) suggest that belemnites would have swum in a horizontal position similar to that of modern *Loligo*, although the method for achieving this horizontal poise is debated (e.g., Monks *et al.*, 1996; Hewitt *et al.*, 1999). Belemnites were presumably active pelagic swimmers, although there is also evidence to suggest that some may have been nektonic (Bandel & Spaeth, 1988; Anderson *et al.*, 1994; Martill *et al.*, 1994). A disparity in the oxygen isotope derived palaeotemperatures of belemnites and ammonites has long been recognised (e.g., Tan *et al.*, 1970), and indicates that these nektonic organisms preferred to inhabit different positions in the water column. For example, Tan *et al.* (1970) observed a depletion of 1.0 to 1.6 ‰ in the oxygen isotope values of ammonites compared with associated belemnites, which they interpreted as ammonites inhabiting warmer, near-surface or near-shore waters than belemnites. Anderson *et al.* (1994) and Wierzbowski & Joachimski (2006) also record a lower range of palaeotemperatures for belemnites than for ammonites. These lower temperatures are often indistinguishable from those derived from benthic bivalves (Anderson *et al.*, 1994) or oysters (Wierzbowski & Joachimski, 2006) of the same succession, which the authors interpret as belemnites inhabiting colder, deeper waters than the ammonites, which inhabited the warmer surface waters. This interpretation is supported by other authors (e.g., Martill *et al.*, 1994; Price & Sellwood, 1994; van de Schootbrugge *et al.*, 2000).

Analysis of concave septa in extant and fossil cephalopods can provide an estimate of the mechanical limits of coleoid shells to water depth. Westermann (1973) estimated that the Belemnitida would have inhabited rather shallow waters, with a maximum depth range of 50-200 m. The exception to this being *Cylindroteuthis*, which could potentially have descended to a maximum depth of 400 m. The notion that belemnites were restricted to shallow shelf waters is supported by the abundance of fossilised belemnite rostra in shallow marine deposits (e.g., Podlaha *et al.*, 1998).

It is now commonly accepted that belemnites lived in neritic (probably near-shore to mid-shelf) environments rather than in the open ocean (Christensen, 1976; Wignall & Hallam, 1991; Monks *et al.*, 1996; Rosales *et al.*, 2004a). The observed diversity in the habitats of modern squid however (e.g., Pörtner & Zielinski, 1998), may suggest that belemnites potentially inhabited different sub-habitats (which could be reflected in isotopic values). It has been hypothesised that although active swimmers, belemnites could have been restricted to shelf areas by their prey, which were themselves confined to the shelves (Stevens, 1963).

By analogy with extant squid it has been deduced that belemnites were carnivorous, hunting small fish and crustaceans (Bandel & Spaeth, 1988). Belemnites themselves were preyed upon by bony fish, sharks and marine reptiles (e.g., ichthyosaurs) (Cox & Doyle, 1996). Evidence for such predation has been identified in the form of tooth marks in belemnite rostra (Hölder, 1973; Hewitt, 1980) or healed rostra (Abel, 1916), as well as the presence of rostra (Bandel & Spaeth, 1988; Pollard, 1990; Cox & Doyle, 1996) and belemnite arm hooks (Martill, 1996) in the stomach contents of well preserved sharks and ichthyosaurs. Fossilised ichthyosaur vomit has even been discovered, with the regurgitated belemnites displaying signs of acid etching, presumably from the ichthyosaurs digestive juices (Doyle, 2002). The presence of an ink sac in exceptionally preserved specimens indicates that belemnites would have been able to expel a cloud of ink as a defensive mechanism when under attack (Bandel & Spaeth, 1988; Cox & Doyle, 1996).

Mass accumulations of belemnite rostra ('belemnite battlefields') are common in the Mesozoic fossil record (e.g., Quenstedt, 1856; Frebold, 1957; Taylor *et al.*, 1979; Jarvis, 1980; Ager, 1988; Doyle & Macdonald, 1993). This might suggest that like the majority of living coleoids, belemnites tended to form schools, particularly for feeding and spawning (Doyle & Macdonald, 1993). Post-spawning mortality has been recorded from almost all extant coleoid groups (Mangold, 1987) and has been extensively investigated in neritic squid populations (e.g., Fields, 1965; Mangold, 1987). Such a mechanism could

easily account for the occurrence of belemnite battlefields, where the population is composed only of adult individuals of a single species (e.g., Doyle & Macdonald, 1993).

3.3. Belemnite Palaeobiogeography

Since the now classic study of Neumayr (1883) it has been recognised that many Jurassic marine faunas do not have a cosmopolitan distribution (Hallam, 1975; Fürsich & Sykes, 1977). Such provinciality has been well summarised by several authors (e.g., Arkell, 1956; Imlay, 1965; Stevens, 1967).

Belemnite provinciality developed in the Early Jurassic (Doyle, 1987) and from the Late Jurassic to Early Cretaceous belemnites occupied three distinct faunal realms (Fig. 3.2): the Boreal Realm (Russia, northern Europe, Greenland and North America) dominated by the suborder Belemnitina, which is often informally divided into the Boreal-Atlantic and Boreal-Arctic Provinces; the Tethyan Realm (southern and central Europe, East Africa, Madagascar, Antarctica, South America, Australasia and India) dominated by the suborder Belemnopseina and informally divided into the Mediterranean and Indo-Pacific Provinces; and the Austral Realm (Madagascar, Patagonia, New Zealand), dominated by the family Dimitobelidae (Stevens, 1963, 1971, 1973a, b; Doyle, 1987; Mutterlose, 1988, 1998). These realms persisted until the Aptian, when the Tethyan and Boreal Realms were homogenised by cosmopolitan taxa and a bipolar distribution of belemnites developed resulting in a Tethyan-Boreal Realm and an Austral Realm (Stevens, 1973b; Mutterlose, 1988, 1998; Doyle, 1992b).

The boundaries of these realms changed through time and migration between the realms was rare. The causes of this provinciality have been widely debated (e.g., Stevens, 1963, 1965b, 1973a, b; Fürsich & Sykes, 1977, Doyle, 1987) and include climate control, temperature or salinity gradients, environmental stability and physical or physiological barriers. The dominance of certain belemnite genera in the different realms has been

comprehensively described by a number of authors (e.g., Stevens, 1963, 1973a, b, Mutterlose *et al.*, 1983; Mutterlose, 1988, 1998; Doyle, 1987, 1992b).

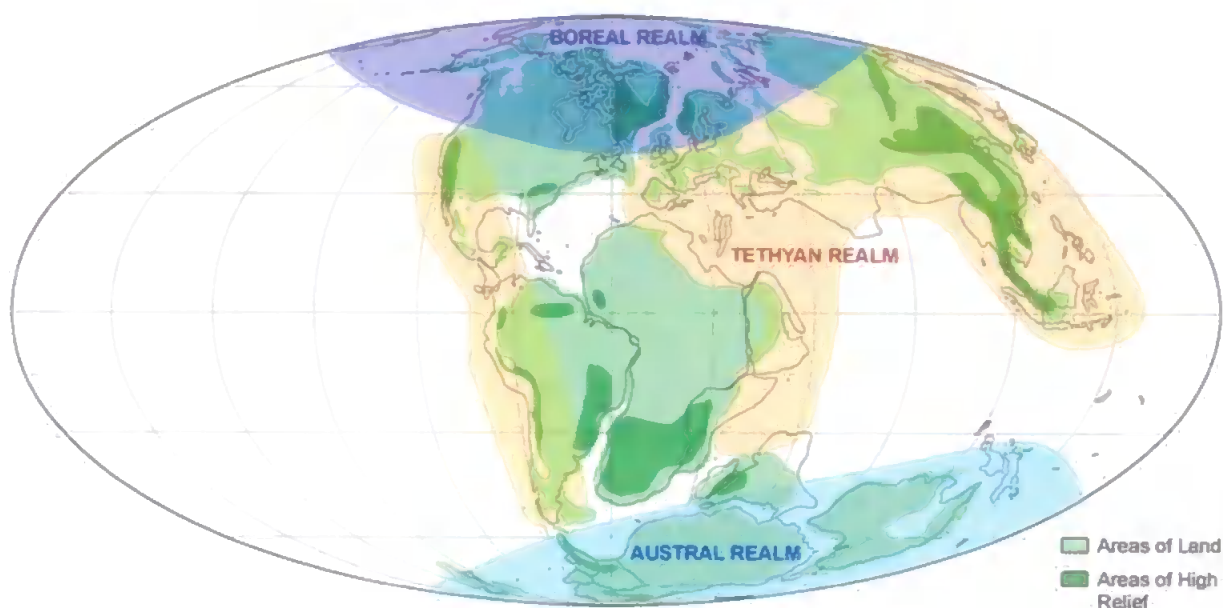


Figure 3.2 Hauterivian palaeobiogeography. The three distinct belemnite Realms are shown. Palaeogeographic map adapted after Smith *et al.* (1994) with additional palaeobiogeographic data from Stevens (1971, 1973b) and Doyle (1987).

3.3.1. Boreal Realm

In the Pliensbachian, Boreal-Tethyan provinciality can be distinguished in certain ammonite families (Howarth, 1973; Hallam, 1975). It is not until the Toarcian, however, that such provinciality can be confirmed in belemnites (Doyle, 1987). In the Toarcian belemnites colonised Siberia, Svalbard and North America for the first time (Doyle *et al.*, 1997) with fauna dominated by endemic genera (Saks & Nal'nyaeva, 1970, 1975; Doyle *et al.*, 1997).

From the late mid-Jurassic the family *Cylindroteuthidae* became dominant in the Boreal Realm, after their first appearance in the Bajocian-Bathonian interval (Doyle, 1987). At this time the realm was characterised by the genera *Cylindroteuthis* and *Pachyteuthis*. *Pachyteuthis* evolved in the Arctic Basin from the Bajocian onwards and therefore dominated the Boreal-Arctic Province, whilst the Boreal-Atlantic Province was dominated by *Cylindroteuthis* (Mutterlose, 1988). Both genera were extremely common throughout the Boreal regions, with specimens found in sediments from Svalbard, North

Russia and East Greenland (Doyle, 1987). However, in the Kimmeridgian *Cylindroteuthis* and *Lagonibelus* migrated into the Boreal-Arctic Province so that by the Early Cretaceous the Boreal-Atlantic Province was characterised by the cylindroteuthid genus *Acroteuthis* (which appeared in the Volgian), although *Cylindroteuthis* and *Pachyteuthis* were still common in places (e.g., Doyle, 1987; Mutterlose, 1988).

In the Late Berriasian (and into the Early Valanginian) *Acroteuthis* assumed dominance in both the Boreal-Atlantic and Boreal-Arctic Provinces (Stevens, 1973b). This dominance continued until the Early Hauterivian, when the Tethyan genus *Hibolithes* invaded the Boreal Realm and largely displaced *Acroteuthis* in the Boreal-Atlantic Province (Doyle, 1987). In the Barremian the differentiation of the Boreal Realm cannot be recognised and by the Albian, a distinct Boreal assemblage no longer exists (Mutterlose, 1988).

The Boreal family Cylindroteuthidae remained restricted to the Boreal Realm throughout the Late Jurassic and Early Cretaceous, despite the presence of conditions suitable for incursions of Tethyan taxa during parts of the Early Cretaceous (Mutterlose, 1998).

3.3.2. Tethyan Realm

During the Early Jurassic, belemnite evolution was centred in Europe, with migration somehow prevented until the Late Pliensbachian (Stevens, 1973a). Belemnites became widespread for the first time in the Toarcian, with diversity increasing significantly in the Late Toarcian (Doyle *et al.*, 1997).

From the mid-Jurassic the Tethyan Realm was characterised by the belemnopseid genera *Hibolithes* and *Belemnopsis* (Stevens, 1963; Doyle, 1987, 1992b; Mutterlose, 1988, 1998; Doyle *et al.*, 1997). *Belemnopsis* first appeared in the Mediterranean region during the Toarcian and in the Aalenian *Belemnopsis* migrated to the north and south (Mutterlose, 1988). *Hibolithes* gradually replaced *Belemnopsis* in the Mediterranean region throughout

the Callovian, to become the dominant Mediterranean genus by the Oxfordian (at which time European-type belemnites still dominated the Tethyan seaway) (Stevens, 1973a). From the Oxfordian, the Tethyan Realm faunas became differentiated into Mediterranean (with rare *Belemnopsis*) and Indo-Pacific Provinces (dominated by endemic *Belemnopsis* species) (Stevens, 1971, 1973a; Mutterlose, 1988).

The belemnopseid taxa continued their dominance of the Tethyan Realm into the Early Cretaceous. In the Valanginian of Europe, species of *Hibolithes*, *Duvalia* and *Conobelus* evolved and migrated along the Tethyan seaway, whilst the Indo-Pacific Province largely disappeared (Stevens, 1973b). During the Valanginian and Hauterivian, the Tethyan genus *Hibolithes* was able to penetrate the Boreal Realm and co-exist with cylindroteuthids, for example in the Pechora Basin, Svalbard and California (Doyle, 1987). The Aptian Tethyan Realm was characterised by *Mesohibolites*, *Neohibolites* and *Parahibolites* (Stevens, 1963, 1973b; Mutterlose, 1988).

The Tethyan Realm finally disappeared after the Early Cenomanian with the extinction of Belemnitidae genera *Neohibolites* and *Parahibolites* and for the remainder of the Cretaceous only Austral Realm and (homogenised) Tethyan-Boreal Realm faunas can be differentiated (Stevens, 1963, 1973b; Doyle, 1992b).

3.3.3. Austral Realm

The anti-Boreal (Austral) Realm first developed during the Kimmeridgian-Tithonian in waters with earlier Jurassic Tethyan affinities and became firmly established after the Hauterivian (Stevens, 1973a, b). Throughout the Kimmeridgian and Tithonian, Indo-Pacific Province belemnites (*Belemnopsis*, *Hibolithes*, *Duvalia*, *Conobelus*) occupied much of the Southern hemisphere, extending to approximately 75°S. At this time an endemic form of *Belemnopsis* evolved in Madagascar and Patagonia that is believed to be the precursor of the Austral Realm genera (Stevens, 1973a).

The Dimitobelidae, which eventually dominated the Austral Realm, populated the Indo-Pacific and western Antarctic regions from the Aptian onwards, leading Stevens (1965) to differentiate them as part of an Indo-Pacific Realm, although Stevens (1973a, b) recognised that their later association with other Cretaceous Austral taxa, suggested that they should instead be assigned to an Austral Realm. From the Early Cenomanian the Austral Realm belemnites became restricted to Australasia and Antarctica (Stevens, 1973b; Doyle, 1992b).

3.4. Belemnites as Palaeoclimate Indicators

Urey (1947) was the first to hypothesise the correlation between temperature and $\delta^{18}\text{O}$ variations as recorded in primary calcite. This was later confirmed by Epstein *et al.* (1953). Since that time belemnites have been considered to be one of the most eminently suitable fossil groups for palaeotemperature determinations (Spaeth *et al.*, 1971), because they have arguably the highest potential to preserve an original isotopic signal (Marshall, 1992). Belemnite rostra are constructed of low-magnesium calcite (Sælen, 1989), which is relatively insoluble in surface environments (compared with high-magnesium calcite or aragonite, which are metastable) and is therefore unlikely to undergo significant pervasive alteration (Marshall, 1992). It is worth noting that evidence for a belemnite species with an aragonitic rostrum has been presented (Bandel & Kulicki, 1988). There is also evidence for the incorporation of small amounts of phosphate in the carbonate rostrum (Longinelli *et al.*, 2002, 2003). Some modern marine organisms (e.g., *Sepia*) precipitate small amounts of phosphate (<0.5 %) in their carbonate shells, with such precipitation in isotopic equilibrium with the carbonate and ambient seawater (Bettencourt & Guerra, 1999; Longinelli *et al.*, 2003).

Belemnites are largely facies independent and have a wide geographic range (from the Toarcian until their extinction at the end-Cretaceous) (Doyle and Bennett, 1995). Consequently belemnites are relatively abundant in the fossil record, and can therefore be

used for accurate comparisons of palaeotemperatures on considerable spatial and temporal scales. This is important because different organisms can give different palaeotemperature results from the same locations, e.g., belemnites and ammonites (Tan *et al.*, 1970; Anderson *et al.*, 1994), and belemnites and planktonic foraminifera (Huber *et al.*, 1995; Price *et al.*, 1996; Huber & Hodell, 1996). Belemnites appear to record cooler palaeotemperatures than known shallow water taxa (Lowenstam & Epstein, 1954; Pirrie & Marshall, 1990; Ditchfield *et al.*, 1994), supporting the notion that belemnites inhabited intermediate to benthic water depths. Today, belemnite-derived palaeotemperatures are thought to potentially represent minimum estimates of sea-surface temperatures at high latitudes (Price *et al.*, 1996), as vertical ocean temperature gradients in shallow, high latitude regions will be minimal (Barrera *et al.*, 1987; Price *et al.*, 1996).

As an extinct group of organisms, belemnites provide several complicating factors when being considered for palaeoenvironmental analysis, since it is impossible to observe their life cycle and habitat. Being nektonic animals, it is possible that their habitat changed with ontogeny, perhaps as the result of migration, either laterally or vertically in the water column. Significant lateral migration appears unlikely, given the distinct provinciality exhibited by belemnites (e.g., Stevens, 1963, 1973a, b; Mutterlose *et al.*, 1983; Doyle, 1987, 1992b, 1997; Mutterlose, 1988, 1998). However, short-range lateral and vertical migration within a biogeographic province seems probable. Such behaviour would almost certainly produce an isotopic shift in shell composition, and shells can therefore be expected to preserve an average record of temperature for the areas in which the individual animal lived and secreted its shell (Spaeth *et al.*, 1971).

Another factor to be considered is that belemnite shell precipitation may involve a 'vital effect'. This occurs when an organism does not secrete its shell in equilibrium with its environment, a process that is known from several marine organisms, most notably echinoderms (Spaeth *et al.*, 1971) and corals (Hudson & Anderson, 1989). Modern cephalopods however, are known to secrete their shells very close to equilibrium with

seawater (Taylor & Ward, 1983; Morrison & Brand, 1986; Rosales *et al.*, 2004a; Rexfort & Mutterlose, 2006). More specifically, the oxygen isotope composition of extant molluscan shells appears to be in equilibrium with ambient seawater, whilst for the carbon isotope, disequilibrium precipitation often prevails, with shells being less enriched in ^{13}C than might be predicted (Wefer and Berger, 1991; Klein *et al.*, 1996; Bettencourt & Guerra, 1999; Geist *et al.*, 2005). Wefer & Berger (1991) attribute this to the presence of a larger pool of oxygen (i.e., water) compared with carbon (i.e., dissolved inorganic carbon, mostly bicarbonate) available for shell formation. The observed offset in the carbon isotope data is often attributed to a contribution from metabolic or kinetic carbon (e.g., Tanaka *et al.*, 1986; Klein *et al.*, 1996; Geist *et al.*, 2005).

Such isotopic disequilibrium has been observed in the cephalopod genera *Sepia*, *Spirula*, *Argonauta* and *Nautilus* (Rexfort & Mutterlose, 2006). Rexfort & Mutterlose (2006) studied stable isotope records from *Sepia officinalis* as an analogy for belemnites. They concluded that the oxygen isotope composition of *Sepia* was in equilibrium with the surrounding seawater and therefore, reflected ambient temperature. However, for the carbon isotope signal a biofractionation control was possible, although it was acknowledged that no direct conclusions could be drawn from their dataset. Wefer & Berger (1991) recorded lighter than expected carbon isotope values in the earliest portion of the calcareous shells. This, however, has been interpreted as the result of embryonic precipitation of the earliest septa within the egg (Eichler & Ristedt, 1966; Cochran *et al.*, 1981; Taylor & Ward, 1983; Wefer & Berger, 1991). Belemnite rostra can, therefore, be considered to record both carbon and oxygen isotope changes in ambient seawater, and be used for palaeoclimatic analysis, providing care is taken with the use of juvenile specimens or early ontogenetic elements of the rostra. It is also important to note that no major seasonal or taxonomic differences in fractionation have yet been confirmed (Sælen *et al.*, 1996; Podlaha *et al.*, 1998; Rosales *et al.*, 2004a), although McArthur *et al.* (2004) suggest

that differences in fractionation or habitat may potentially produce a disparity in stable isotope values for different belemnite species.

Finally, it is important to ensure that the calcite being analysed has not been post-depositionally altered to corrupt the primary isotopic composition. Methods of identifying diagenesis are described and evaluated by Sælen (1989) and include scanning-electron microscopy, cathode-luminescence microscopy, blue-light fluorescence microscopy, staining of thin sections (using Dickson's (1955, 1966) methodology), and x-ray diffractometry. Furthermore, trace element geochemistry, in particular the analysis for Mn and Fe can be used to screen for diagenesis (see Chapter 4), as Fe and Mn are commonly associated with diagenetic cements (Veizer *et al.*, 1983). Once a belemnite has been ascertained to be unaltered (or only altered in easily removable sections of the specimen) it can be analysed with confidence.

4. METHODOLOGY

4.1. Selection of Sites

The purpose of this research is primarily to investigate northern high latitude climates during the Late Jurassic and Early Cretaceous. In order to explore this, it was necessary to consider a range of field locations. Those selected for this study were: Staffin Bay, Isle of Skye, Scotland; Helmsdale, Sutherland, Scotland; Izhma River, Timan-Pechora Basin, Russia; Boyarka River, Yenisei-Khatanga Basin, Northern Central Siberia; and Festningen and Janusfjellet, Svalbard. Each of the sites selected was situated within the Boreal Realm of the Late Jurassic - Early Cretaceous, with the sites deliberately chosen to provide a significant spatial and temporal distribution of data.

In terms of spatial distribution (Fig. 4.1), the sites ranged from palaeolatitudes of ~ 45°N (Isle of Skye and Sutherland) at the periphery of the Boreal Realm to ~ 70°N (Boyarka River), well within the palaeogeographic Arctic Circle (according to Smith *et al.*, 1994). The sites are also well distributed throughout the eastern circumpolar region.

The ages of the sections varied from Callovian (Middle Jurassic) in Staffin Bay, Brora (Sutherland), the Izhma River, Festningen and Janusfjellet to Hauterivian (Early Cretaceous) in the Izhma and Boyarka Rivers (Fig. 1.4). Whilst this distribution of age was important, it was also essential to ensure that there would be a considerable degree of temporal overlap between the different locations. This overlap is crucial for the correlation of data between the different field sites.

Additional factors that were considered when selecting these sites were faunal content, available biostratigraphic information and logistics. Most importantly, it was vital that the section was known to contain relatively abundant and well preserved belemnites. In addition, it had to be possible to date the section accurately (in terms of ammonite biostratigraphy). This was ensured by choosing sections where a detailed biostratigraphy already existed, or where a fairly accurate estimate of age was known by co-workers and

could be determined after a short period in the field. In this case the presence of abundant ammonites was also required, in order to constrain the section biostratigraphically.

The field sites selected for this study (Staffin Bay, Isle of Skye, Scotland; Helmsdale, Sutherland, Scotland; Boyarka River, Northern Central Siberia; and Festningen and Janusfjellet, Svalbard) were chosen using the criteria outlined above. An additional site that satisfied the aforementioned criteria was also included in this study but did not require fieldwork (Izhma River, Russia). The material obtained from this site was collected by Dr Gregory Price (University of Plymouth) in the summer of 2003.



Figure 4.1 Volgian circumpolar map. The extent of the Boreal (blue) and Tethyan (brown) belemnite Realms are shown and the sites investigated in this study are highlighted. Map adapted after Smith *et al.*, (1981) with additional data from Doyle (1987) and Stevens (1973a).

4.2. Field Techniques

Field data were collected during two major field seasons: in the spring/summer of 2004; and the spring/summer of 2005. UK based field work (e.g., Isle of Skye and

Sutherland) was conducted during the spring time, whilst Arctic field work (e.g., Siberia and Svalbard) was carried out during the summer months.

4.2.1. Graphic Sedimentary Logs

At each individual field location a sedimentary log was drawn. Features such as lithology, sedimentary characteristics and fossil content were noted, as well as the positions from which samples were obtained. It should be noted that the extent of the outcrops varied significantly between locations. For a guide to the log symbols used see Figure 4.2.



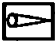





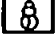






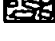

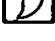
	Claystone/Mudstone		Planar Lamination		Belemnite
	Siltstone		Cross Bedding		Bivalve
	Sandstone		Concretion		Gastropod
	Limestone		Glendonite		Ammonite
	Conglomerate		Dropstone		Crinoid
	Boulder Bed		Wood		Coral

Figure 4.2 Key to sedimentary log symbols used in this study.

4.2.2. Sample Collection

The primary focus of the sample collection for this research was on belemnites. At each site, belemnite rostra were collected bed-by-bed from wherever possible. Multiple samples were taken from stratigraphic horizons where belemnites were abundant, with care being taken to select representative samples and, therefore, avoid any selection bias. Occasionally other elements of the faunal assemblages were collected either by myself or co-workers: e.g., ammonites were collected by Dr Kevin Page (University of Plymouth) from the Isle of Skye and Svalbard and Prof. Evgenij Baraboshkin (Moscow State University) from the Izhma River, Russia and Boyarka River, Siberia. Such samples were collected primarily for their use in biostratigraphy.

In addition to the belemnite sampling, bulk sediment and fossil wood samples were also collected (from the Isle of Skye and Boyarka River respectively). The mudrock sediments of Staffin Bay, Isle of Skye are known to contain microscopic wood debris (Pearce *et al.*, 2005). The bulk sediment samples were collected frequently (although not regularly) at an average interval spacing of ~ 70 cm. The macrofossil wood samples were also collected frequently but irregularly (here, as a consequence of the limited presence of wood in certain sections of the outcrop). These samples were collected at intervals of ~ 1m.

4.3. Laboratory Techniques

4.3.1. Rationale

The laboratory techniques outlined below were carefully selected for inclusion in this study. Each of the techniques has been repeatedly tested (in an appropriate context) through years of published, peer-reviewed research.

Optical Techniques

The photographic techniques employed either provided a record of representative specimens (prior to isotopic or geochemical analysis) or when used in combination with other techniques provided an assessment of sample preservation. Photography was undertaken principally on belemnite specimens, but also on wood samples.

Representative photographs of belemnite specimens were taken after the application of a thin coating of ammonium chloride (e.g., Doyle & Kelly, 1988). The use of such coating prevents preservational features obscuring morphological characteristics and therefore produces photographs that are suitable for taxonomic comparisons.

Additional optical techniques were employed on a number of belemnite rostra in order to identify areas of diagenetic alteration, for example, representative specimens were

photographed under cathodoluminescence (CL) and backscattered scanning electron microscopy (BSEM) conditions, and after carbonate staining (Dickson, 1965, 1966). Perhaps the most commonly used of these optical techniques (if used in isolation) is cathodoluminescence (e.g., McArthur *et al.*, 2000; O'Neill *et al.*, 2003; Rosales *et al.*, 2004a; Koleva-Rekalova & Metodiev, 2005). However, more often, a range of these techniques is used in combination in order to ensure that any and all alteration can be identified (e.g., Sælen, 1989; Podlaha *et al.*, 1998; Veizer *et al.*, 1999; Gröcke *et al.*, 2003; McArthur *et al.*, 2004; Price & Mutterlose, 2004).

Finally, photography was also performed on representative samples of well preserved macroscopic wood fragments. Photographs were taken using a scanning electron microscope (SEM), a technique which is popular for such samples as it permits an evaluation of preservation (e.g., Gröcke *et al.*, 2005; Pearce *et al.*, 2005).

Trace Element Techniques

Trace element analysis was undertaken for two primary reasons, firstly to identify the presence of diagenesis (undertaken in addition to the optical techniques) and secondly, to complement the stable isotope analysis of palaeoclimate. Investigations of extant molluscan species indicate that the concentrations of Fe and Mn incorporated into the mollusc shell are relatively low in recent populations. Milliman (1974) recorded values of Fe and Mn from recent *Sepia* (cuttlefish) shells (possibly the closest modern analogue of the extinct belemnite) as 32 ppm and 4 ppm respectively. These data are supported by more recent studies such as that of Miramand & Bentley (1992), which recorded average values of 42 ± 8 ppm for Fe and 2 ± 0.4 ppm for Mn from modern *Sepia* collected from the French coast of the English Channel. Miramand *et al.* (2006) also recorded Fe values from the cuttlebone of mature adults of the species *Sepia officinalis*. They recorded average values of 25 ± 2 ppm for Fe but did not measure Mn. In a study of the extant limpet *Patella aspera*, Cravo *et al.* (2002) recorded Fe and Mn concentrations in shells collected

from Portugal. They recorded average values of 35.8 ppm and 29.9 ppm for Fe and Mn respectively, although the maximum Fe and Mn values were 70.5 and 130.5 ppm respectively. Such data suggest that relatively low Fe and Mn concentrations should be present in well-preserved belemnite rostra and authors commonly accept that values of <150 ppm Fe and <100 ppm Mn are representative of well preserved individuals (e.g., Pirrie & Marshall, 1990; Podlaha *et al.*, 1998; Price & Mutterlose, 2004).

Post-depositional repartitioning of trace elements during diagenesis typically causes the depletion of Sr, Mg, Na and Ba and the enrichment of Mn, Fe and Zn (among other elements) in low magnesium calcite (Veizer, 1983, 1999; Brand, 1989; Podlaha *et al.*, 1998). Diagenetic effects can normally be identified via trace element analysis (particularly of Fe and Mn), although it should be noted that alteration can take place in the absence of Fe and Mn, for instance, under oxidising conditions (Marshall, 1992; Jones *et al.*, 1994b). Nevertheless, trace element analysis is a technique that is commonly used to identify diagenetic alteration in belemnites and other carbonates since high concentrations of Fe and Mn virtually guarantee the presence of diagenetic calcite (e.g., Brand & Veizer, 1980; Ditchfield *et al.*, 1994; Jones *et al.*, 1994b; Price & Sellwood, 1997; Gröcke *et al.*, 2003; Price & Mutterlose, 2004). This technique was used here, together with the optical techniques outlined above, to ensure that the presence of any diagenetic alteration could be constrained.

Isotopic and trace element analysis of well preserved belemnite calcite have been used extensively to investigate (mainly Jurassic) seawater chemistry (e.g., Jenkyns *et al.*, 2002; Bailey *et al.*, 2003; McArthur *et al.*, 2004; Rosales *et al.*, 2004a). The trace element ratios Mg/Ca, Sr/Ca, Na/Ca and Li/Ca have been used here to assess changes in the environmental conditions of seawater (e.g., temperature and salinity). Mg/Ca and Sr/Ca ratios in biogenic calcite are commonly measured in order to investigate environmental conditions (e.g., Klein *et al.*, 1996, 1996; Bailey *et al.*, 2003; McArthur *et al.*, 2004; Rosales *et al.*, 2004a, b, 2006), although Na/Ca (e.g., Bailey *et al.*, 2003) and Li/Ca (e.g.,

Hall & Chan, 2001; Bailey *et al.*, 2003) are less commonly utilised. Convention is followed here by expressing these values as mmol/mol (Mg/Ca, Sr/Ca, Na/Ca) or $\mu\text{mol/mol}$ (Li/Ca) (e.g., McArthur *et al.* 2000; Bailey *et al.*, 2003; Rosales *et al.*, 2004a, 2004b). Arguably the most useful of these ratios is Mg/Ca, which has been shown to vary mainly with water temperature (e.g., Klein *et al.*, 1996; Wei *et al.*, 2000; Lear *et al.*, 2002; Steuber & Rauch, 2005) and to be affected only to an extremely limited degree by salinity (e.g., Yasamanov, 1981; Klein *et al.*, 1997; Rosales *et al.*, 2004a). It can therefore potentially be used as a salinity-independent (unlike $\delta^{18}\text{O}$) palaeotemperature proxy (Rosales *et al.*, 2004a).

McArthur *et al.* (2000) and Bailey *et al.* (2003) have recently investigated this relationship in belemnites, where they identified a marked correspondence between elemental composition (Mg/Ca, Sr/Ca, Na/Ca) and $\delta^{18}\text{O}$, suggesting that Mg/Ca (although, perhaps not Sr/Ca or Na/Ca) can be used as a palaeotemperature proxy. This technique (together with the $\delta^{18}\text{O}$ technique) will be explored fully in this study, by using the Mg/Ca palaeotemperature equation of Klein *et al.* (1996), which was developed for extant bivalves. It remains impossible however to calculate absolute palaeotemperatures from Mg/Ca ratios (or $\delta^{18}\text{O}$ values) as belemnites are an extinct group, and therefore the response of such proxies to water temperature cannot be observed experimentally (Rosales *et al.*, 2004a).

Carbonate Stable Isotope Techniques

Since the earliest days of isotope analysis when it was first observed that the precipitation of the ^{18}O -isotope in calcite was related to temperature (Urey, 1948) and that this provided the means to reconstruct palaeoclimates (Epstein *et al.*, 1953), belemnites have been considered as remarkably suitable organisms for such investigations (e.g., Urey *et al.*, 1951; Bowen, 1961a, b; Longinelli, 1969; Anderson *et al.*, 1994; Podlaha *et al.*, 1998; Bailey *et al.*, 2003; Voigt *et al.*, 2003; Wierzbowski, 2004). Plausible estimates of

palaeotemperature have been determined from belemnites, after taking into account the ecology, diagenesis and the isotopic composition of seawater (e.g., Pirrie & Marshall, 1990; Podlaha *et al.*, 1998; Price *et al.*, 2000; Hesselbo *et al.*, 2000). Belemnite derived oxygen isotope data were therefore produced for this research and palaeotemperatures were calculated using the equation of Anderson & Arthur (1983) for molluscan calcite.

There are however, limitations to using $\delta^{18}\text{O}$ data to calculate palaeotemperatures. These are that the isotopic composition (which can be related to salinity) of the water from which the calcite was precipitated cannot be measured directly. The Anderson & Arthur (1983) formula requires an estimate of the isotopic composition of seawater to be made. In the Jurassic/Cretaceous greenhouse world this is generally assumed to be -1 ‰ SMOW (e.g., Pirrie & Marshall, 1990; Marshall, 1992; Sælen *et al.*, 1996; Price & Sellwood, 1997; Podlaha *et al.*, 1998; Price & Mutterlose, 2004; Rosales *et al.*, 2004a). This value however, is dependent on the amount of water stored as glacial ice (Rosales *et al.*, 2004a) and the $\delta^{18}\text{O}_{\text{seawater}}$ composition can vary by as much as 1.5 ‰ between high and low latitudes in the modern open ocean (Broecker, 1989).

Local variation in $\delta^{18}\text{O}_{\text{seawater}}$ (related to salinity) is also influenced by the input of fresh-water runoff (which is depleted in ^{18}O) into the system. This will produce more negative $\delta^{18}\text{O}_{\text{seawater}}$ values than would otherwise be expected and the $\delta^{18}\text{O}$ data will therefore overestimate palaeotemperatures (Klein *et al.*, 1996). The impact of salinity on seawater temperature however, can be determined by using Mg/Ca data (e.g., Klein *et al.*, 1996; Rosales *et al.*, 2004a; Immenhauser *et al.*, 2005). The use of Mg/Ca ratios is discussed above.

Carbon isotope data were simultaneously produced and provide additional information about carbon cycling, chemostratigraphy and palaeoclimatic change (although 'vital' effects (as mentioned earlier) also need to be considered). Carbon and oxygen isotope records are commonly considered together in order to provide a detailed assessment of palaeoclimate (e.g., Weissert, 1989; van de Schootbrugge *et al.*, 2000;

Wierzbowski, 2002; Gröcke *et al.*, 2003; Price & Mutterlose, 2004). Insights to be gained from the inclusion of carbon isotope data include information relating to palaeoceanography, palaeoatmospheres (e.g., atmospheric CO₂ concentrations and methane release), weathering and carbon burial.

Organic Carbon Techniques

Carbon isotope values derived from terrestrial organic matter have been successfully used to investigate the coupling of marine and terrestrial carbon cycles throughout geological time (providing comparison is possible with marine curves), as well as providing palaeoenvironmental information (e.g., Bocherens *et al.*, 1993; Gröcke, 1998; Jahren *et al.*, 2001; Hesselbo *et al.*, 2003; Gröcke *et al.*, 2005). Gröcke *et al.* (1999) suggest that the magnitude of carbon isotope excursions as recorded in wood is considerably greater than in coeval pelagic carbonate. Detailed terrestrial carbon isotope records are virtually non-existent throughout much of the Mesozoic (Hesselbo *et al.*, 2003) and records from successions containing both marine carbonate and terrestrial organic carbon values have yet to be recorded, due to the rarity of suitable sedimentary successions in the geological record. Two such successions however, have been identified and investigated here. The terrestrial components are represented either by macroscopic fossilised wood fragments or by microscopic wood debris and the marine carbonate component by belemnites.

Modern terrestrial plants demonstrate considerable variability in $\delta^{13}\text{C}$ values between different species, individuals of the same species and within an individual (Robinson & Hesselbo, 2004). Today plants can be divided into C₃, C₄ and CAM groups based on their different photosynthetic systems (Bocherens *et al.*, 1993). Almost all Mesozoic plants can be classified as C₃ plants however, which are predominantly temperate shrubs, trees and some grasses (Bocherens *et al.*, 1993; Gröcke, 1998). Cretaceous floras, therefore, occupied one distinct photosynthetic pathway, which will

reduce the variability of carbon isotope values within the palaeo-ecosystem (Robinson & Hesselbo, 2004).

Modern C₃ plants demonstrate significant variability of carbon isotope composition ($< \pm 4 \text{ ‰}$) between leaves, branches, twigs, and late and early wood (Leavitt & Long, 1991; Loader *et al.*, 1995; Schleser, 1999). It is therefore important to restrict analyses to specific plant elements where possible. Carbon isotope ratios in modern plants may also be affected by environmental conditions such as varying salinity, temperature, light, water supply and local ρCO_2 (Gröcke, 1998). Diagenesis of fossil plant matter will also affect the $\delta^{13}\text{C}$ values. The preservation potential of plant tissue varies between constituent parts of the plant, for example, lignin and lipids are the most resistant parts to diagenesis and carbohydrates, the least resistant (Gröcke, 1998; Robinson & Hesselbo, 2004). Lipids and lignin are therefore depleted in ^{13}C relative to the whole plant whilst carbohydrates are more enriched (Hedges *et al.*, 1985; Bocherens *et al.*, 1993; Gröcke, 1998). Fossil coal and plants are reported to be enriched in ^{13}C by $\sim 3 \text{ ‰}$ compared to modern $\delta^{13}\text{C}_{\text{plant}}$ values (Gröcke, 1998; Robinson & Hesselbo, 2004), although the preservational state of fossil wood (e.g., coal or charcoal) does not appear to produce a systematic difference in $\delta^{13}\text{C}$ values (Hesselbo *et al.*, 2003; Robinson & Hesselbo, 2004; Gröcke *et al.*, 2005; Pearce *et al.*, 2005).

Similar problems are also inherent to the bulk-rock technique for analysing microscopic wood debris. Gröcke *et al.* (2005) describe the three key problems. These are that firstly, not every sample is assessed for the percentage of marine versus terrestrial organic matter (see Rock-Eval pyrolysis below), secondly, the terrestrial organic matter may be sourced from different floral components and finally, the terrestrial organic matter may be sourced from different environments (Gröcke *et al.*, 2005). Despite such potential for carbon isotope variability, $\delta^{13}\text{C}_{\text{org}}$ values can be used to indicate long-term shifts in the composition of atmospheric carbon (e.g., Robinson & Hesselbo, 2004; Gröcke *et al.*, 2005; Pearce *et al.*, 2005).

Total Organic Carbon (TOC) analysis was performed on samples of microscopic wood debris to ensure that enough organic matter was present for $\delta^{13}\text{C}_{\text{org}}$ analysis. TOC content can also provide additional information about palaeoproductivity, organic matter preservation and sediment dilution (e.g., Lallier-Vergès *et al.*, 1993; van Kaam-Peters *et al.*, 1998; Tribovillard *et al.*, 2001; Tyson, 2004).

Rock-Eval pyrolysis coupled with published palynology (e.g., Riding & Thomas, 1997; Hesketh & Underhill, 2002) was also performed in order to confirm the chemical composition of kerogen present in the microscopic wood samples and therefore, the source of organic matter (e.g., Espitalié *et al.*, 1985; Peters, 1986; Langford & Blanc-Valleron, 1990; Tyson, 2004). According to Espitalié *et al.*, (1985) Type I kerogen is predominantly lacustrine in origin, Type II kerogen is marine in origin and Type III, continental.

4.3.2. Optical Techniques

The optical techniques outlined below were undertaken on representative samples of either belemnites or wood. The techniques used to assess diagenesis in belemnites (CL, BSEM and carbonate staining) were carried out on 100 (approximately 1 in 5) of the samples measured for stable isotopes and trace element geochemistry. These samples were analysed in order to provide an independent check on the trace element results, which were conducted on all 586 of the belemnite samples.

The same 100 specimens were each analysed using CL, BSEM and carbonate staining, as all three techniques provide information at a different magnification and together, the limitations of each individual technique can be eliminated. For example, when using the CL technique on highly ferroan calcite, there will be limited or no luminescence (as Fe^{2+} is the main quencher of luminescence in calcite (Miller, 1988)). This absence of luminescence could be wrongly interpreted as indicating that there has been no diagenetic alteration in the sample. However, when the same sample is subjected to carbonate staining, it will display a purple-blue colouration, indicating that the sample

has a high Fe concentration (Dickson, 1966) and has in fact, been subject to very severe diagenetic alteration.

Ammonium Chloride Technique

This technique was used to photograph representative examples of the belemnite species considered here. Prior to photographing, the specimens were cleaned, repaired (using a standard superglue) and taxonomically identified. The samples were then coated in a fine film of ammonium chloride. This was produced by putting ammonium chloride powder into a glass puffer and heating it over a Bunsen burner to produce a vapour that was then blown onto the specimens. The specimens were then photographed in black and white using a Nikon Coolpix 4500 digital camera. The ammonium chloride coating produced a smooth final image, where morphological details were not obscured by preservational features. After a short period of time the vapour evaporated from the specimens, leaving them uncontaminated for isotopic and geochemical investigation. In total, 99 belemnites were photographed using this technique, each from at least two different perspectives (ventral outline, right profile, and where suitable transverse/alveolar section).

Cathodoluminescence (CL)

Cathodoluminescence microscopy was used to evaluate if a belemnite had been diagenetically altered, as primary biogenic carbonate is thought to be non-luminescent (Czerniakowski *et al.*, 1984; Popp *et al.*, 1986; Sælen, 1989; Sælen & Karstang, 1989). Luminescence occurs where the diagenetic product Mn is present, as Mn^{2+} is the main activator of luminescence in calcite, whilst (as noted above) Fe^{2+} is the main quencher (Miller, 1988). Areas that have been diagenetically altered will, therefore, show luminescence, providing that the amount of Fe does not dramatically exceed the amount of Mn.

Polished thin-sections of the belemnite rostra were produced, with the cross-sections cut horizontally through the rostrum (wherever possible this horizontal slice was taken from alongside the isotope/geochemical sample). Thin sections were made on a Logitech LP30 production lapping and optical polishing machine and then polished on a Buehler Petropol polishing system with a 12" lapping plate using Buehler aluminium oxide powder (0.3 micron) on a Texmet 1000 polishing cloth.

The CL analysis was performed using a CITL CL MK3A Luminoscope at the Camborne School of Mines (CSM), University of Exeter, in Cornwall. The thin sections were placed in a vacuum sealed specimen chamber, under an electron gun emitting a cathode ray (with a gun current of $\sim 450 \mu\text{A}$ and a gun voltage of $\sim 10 \text{ kV}$). The specimens were viewed through an attached petrographic microscope and photographed. In total, 100 belemnites were analysed in this way.

Backscattered Scanning Electron Microscopy (BSEM)

Backscattered scanning electron microscopy (BSEM) was also used to assess the presence of diagenesis in the belemnite rostra. The efficiency of backscattered electrons reflected from the flat surface of a specimen is dependant on the chemistry of that surface (Trewin, 1988). The reflection coefficient increases as the atomic number increases, causing a brighter image where the atomic number is higher (Thornton, 1968). The presence of diagenetic products in calcite can therefore be identified, as calcite containing the common diagenetic products Fe and Mn will have a higher atomic number than unaltered calcite, and will therefore show as brighter areas in a BSEM image.

The rostra were sliced and polished (first with a lapping wheel, then with decreasing sizes of carborundum powder (starting at 600 microns) and finally aluminium oxide powder (0.3 microns)) to produce a smooth and highly polished surface. The belemnite slice was then washed in a sonic bath, mounted on a SEM stub and placed, uncoated in a JEOL 5600 scanning electron microscope housed at the University of

Plymouth. The samples were then photographed under low vacuum conditions using a back scattered electron detector (accelerating voltage 15kV, spot size 38) to show the atomic number contrast on the polished surface. This method of analysis was conducted on the same belemnites that were subject to CL microscopy (100 belemnites in total). Whilst both techniques identify diagenetically altered regions in the rostrum, they do so at significantly different magnifications.

Scanning Electron Microscopy (SEM)

Scanning electron microscopy (SEM) was used to examine fossil plant material from the Ryazanian-Hauterivian of the Boyarka River, Siberia. All 184 samples were identified as charcoal, charcoal-coal or coal using a binocular microscope. Approximately 20 representative samples (e.g., of charcoal, charcoal-coal and coal) were then mounted on stubs and sputter coated with gold for SEM analysis. The University of Plymouth's JEOL 5600 SEM was used (in high vacuum mode with an accelerating voltage of 15kV and a spot size of 25).

Carbonate Staining

Carbonate staining was undertaken on 100 belemnites in order to identify the areas of the rostrum prone to diagenetic alteration. The technique used follows that described by Dickson (1965, 1966) for use on thin sections, where the section surface is first etched with dilute hydrochloric acid (HCl), then stained with an alizarin red-S and potassium ferricyanide mixture (3 parts : 2 parts), and finally stained with alizarin red-S to intensify the colour differentiation. This is a highly selective technique, with colouration confined sharply to crystal boundaries (Allman & Lawrence, 1972). Calcites stained using this method will display a very pale pink-red colouration, whilst ferroan calcites, show mauve-purple-royal blue colouration (Dickson, 1965).

The polished thin sections of belemnite rostra made for CL microscopy were first photographed under the CL microscope, and then stained by emersion of the section in the following sequence: dilute HCl (15 seconds), deionised water (10 seconds), alizarin red-S and potassium ferricyanide mixture (45 seconds), alizarin red-S (15 seconds), deionised water (10 seconds), deionised water (10 seconds). The thin sections were then quickly dried before being photographed under a low-powered binocular microscope using a Nikon Coolpix 4500 digital camera.

4.3.3. Trace Element Analysis

In total 586 samples were analysed (with duplicate samples taken from approximately 1 in 6 belemnite specimens to evaluate the consistency of both trace elements and stable isotope values within the rostrum). Trace element analysis of every sample was undertaken prior to stable isotope analysis. This provided screening for diagenesis, so that severely altered specimens could be excluded from further analysis. This technique was performed on every sample to ensure that there was a constant and accurate, quantitative measure of preservation for every belemnite sample. The trace element work was complimented by optical techniques (conducted on representative samples) that were used to double-check the trace element data.

The carbonate subsamples were digested in 20% nitric acid (HNO_3) (~100 mg in 10 ml) and analysed by Inductively Coupled Plasma-Atomic Emission Spectrometer (ICP-AES) using a Perkin Elmer Optima 3300RL ICP-AES system (with autosampler) at the NERC ICP facility, Department of Geology at Royal Holloway, University of London. Each sample was analysed for Ca, Na, Mg, K, Fe, Al, B, Ba, Li, Mn, Pb, Sr, Ti and Zn, with values given in ppm.

4.3.4. Carbonate Stable Isotope Analysis

Prior to isotopic analysis the areas of the belemnite rostrum most susceptible to diagenesis were removed. These areas were identified using several of the techniques described in this chapter: Cathodoluminescence (CL), Backscattered Scanning Electron Microscopy (BSEM) and carbonate staining (following the technique of Dickson (1965, 1966)). Those areas most prone to diagenetic alteration are the rostrum margin, the apical line and any cracks or prominent growth bands. Such areas were removed using a circular saw and lapping wheel. The remains were then washed in de-ionised water and fragmented, before being picked under a binocular microscope to ensure that only the most well preserved fragments were selected for analysis. The selected fragments were ground into a fine homogenous powder using an agate pestle and mortar, and a subsample was removed for trace element analysis. A similar method of preparation has been used by several authors in an attempt to homogenise any intra-specimen geochemical variation (e.g., McArthur *et al.*, 2000, 2004; Bailey *et al.*, 2003).

Stable isotope data were generated using a Multiflow (GV Instruments, UK) automated carbonate preparation module with Gilson 222XL autosampler, interfaced with an Isoprime isotope ratio mass spectrometer (GV Instruments, UK), at the University of Plymouth, UK and on a VG Optima mass spectrometer at the NERC Isotope Geosciences Laboratory (NIGL), Keyworth, UK. A small set of representative samples were analysed on both instruments to ensure reproducibility (and to allow correlation of data from the different institutions). The mean difference in values from replicate analysis was 0.28‰ and 0.09‰ for oxygen and carbon respectively. For oxygen, this value is outside of the reproducibility of each instrument (see below), however, such variability is to be expected as a belemnite sample will never be completely homogenous due to the variability occurring across a belemnite rostrum.

The Isoprime isotope ratio mass spectrometer analysed triplicate injections from each vile, with liberated CO₂ (from carbonate reaction with phosphoric acid) measured

against reference CO₂ (research grade, BOC Special Gases). The VG Optima mass spectrometer measured CO₂ liberated from water vapour under vacuum, after the carbonate had reacted with anhydrous phosphoric acid *in vacuo* overnight at a constant 25°C.

The measurements from both institutions were standardised using within-run laboratory standards and calibrated with the internationally recognised NBS19 standard using the daily correction method. Values were expressed using the standard delta (δ) notation as a per mil (‰) deviation from the Vienna Pee Dee Belemnite (V-PDB) standard. Replicate analyses for each instrument gave a reproducibility of $<\pm 0.1\text{‰}$ for both oxygen and carbon isotope ratios.

4.3.5. Organic Carbon Analysis

Bulk Sediment Samples (Microscopic Wood Debris)

Carbon isotope measurements were made on a total of 207 bulk sediment samples from Staffin Bay, Isle of Skye. For each sample approximately 1-2 g of powdered sediment was covered with 200 ml of 5% hydrochloric acid (HCl). The samples were left overnight until all the carbonate had reacted and then rinsed thoroughly with de-ionised water (3 overnight 500 ml washes). Samples were then oven dried at 40-50 °C until a constant weight. The resulting samples were then re-powdered, weighed (between 10-30 mg) and placed in tin capsules for combustion. Analyses were performed by combustion in a Carlo Erba NA1500 (series 1) elemental analyser at NIGL, Keyworth. The resulting gas samples were subsequently measured for carbon isotope ratios by an on-line VG TripleTrap and Optima dual-inlet mass spectrometer. Carbon isotope ratios were measured using within-run laboratory standards (BROC 1) and calibrated against NBS-19 and NBS-22. Values were expressed in delta (δ) notation against the international, V-PDB standard. All results were accurate to within $\pm 0.3\text{‰}$.

Macrofossil Wood Samples

A total of 184 individual wood samples were analysed for carbon isotope ratios from the Boyarka River, Siberia. Samples were divided (where enough material was present) to allow a portion of the sample to be archived. The rest of the sample was prepared for analysis using a preparation technique similar to that described previously. Samples were treated with 5% HCl to remove any carbonate material and then washed with de-ionised water. The samples were then oven dried at 40-50 °C before being powdered with an agate pestle and mortar.

The samples were analysed by Dr Darren Gröcke at McMaster University, Ontario, Canada, where samples were weighed, combusted in an elemental analyser and the resulting gas purified and passed through a SIRA II Series 2 dual-inlet isotope-ratio mass-spectrometer for isotopic analysis. Carbon isotope ratios were measured against an international standard (NBS-21). Analytical reproducibility using this method was better than $\pm 0.1\%$.

4.3.6. Total Organic Carbon (TOC)

In total 103 bulk sediment samples from Staffin Bay, Isle of Skye were analysed for Total Organic Carbon (TOC). Sediment samples were crushed, oven dried at 40-50 °C (until a constant weight) and ground to produce a fine homogenised powder.

TOC was then measured using two different techniques (to ensure accuracy a selection of samples were analysed using both methods). The first technique (which was used to analyse approximately 3 out of 4 of the samples) was the industry standard, high-temperature catalytic oxidation (HTCO) technique. This was conducted on a Primacs SLC Carbon Analyzer at the University of Plymouth. Samples were weighed (~ 100 mg) into a small crucible and covered with quartz wool before being combusted at a high temperature to release carbon, giving a measurable Total Carbon (TC) value. A separate sample was weighed (~ 100 mg) into a glass test tube and mixed with a small amount of deionised

water. This was combusted at a low temperature with acid to release the Inorganic Carbon (IC). The Total Organic Carbon was then calculated as $\text{TOC} = \text{TC} - \text{IC}$. The second technique (which was used to measure 50 sediment samples) is described below, as TOC was also measured as a component of Rock-Eval pyrolysis. All TOC values are given as wt % TOC.

4.3.7. Rock-Eval Pyrolysis

Rock-Eval pyrolysis was performed on 50 bulk sediment samples from the Isle of Skye in order to determine the source of organic matter within the sediments. The samples selected for analysis were distributed fairly evenly throughout the Staffin Bay succession, although particular attention was paid to sections of the $\delta^{13}\text{C}_{\text{org}}$ curve where minor fluctuations could have been caused by changes in the source of organic carbon. Samples were prepared according to the same technique described above for TOC analysis. The samples were then analysed with a Rock-Eval 6, at the University of Neuchâtel, Switzerland. Values for TOC, Hydrogen Index (HI) and Oxygen Index (OI) were obtained.

4.3.8. Storage of Material

All of the materials used during this research are currently stored in the School of Earth, Ocean and Environmental Sciences at the University of Plymouth, UK.

5. STAFFIN BAY, ISLE OF SKYE, SCOTLAND

5.1. Location & Site Description

The Isle of Skye lies to the northwest of the Scottish mainland at a latitude of approximately 57°N. Staffin Bay is situated on the northeast coast of Skye, on the Trotternish peninsula, approximately 30 km north of the main town of Portree.



Figure 5.1 Location map of Staffin Bay, Isle of Skye, Scotland. (A) Location of Staffin Bay. (B) Relative positions of each of the sites visited on the Staffin Bay coast.

Ten different sites were examined along a ~2.5 km stretch of the Staffin Bay coast between Digg and Kildorais (Fig. 5.1). These sites were predominantly broad foreshore exposures (Fig. 5.2), often accessible only at low tide and intermittently covered with boulders and seaweed, with such cover varying seasonally as the result of weather conditions and beach processes. Occasional low cliff exposures located near to the shore line were also studied.

The Staffin Bay composite section extends from the Middle Callovian (*Koenigi* Zone) to the Early Kimmeridgian (*Cymodoce* Zone) and provides an almost complete record of sedimentation during this time.



Figure 5.2 Broad foreshore exposure typical of the Staffin Bay coast, Isle of Skye, Scotland. Dunans Clay Member of the Staffin Shale Formation (location SK1 - see Fig. 5.1).

5.2. Geological Setting

During the Jurassic period, Scotland was situated at a palaeolatitude of approximately 45°N (Smith *et al.*, 1994). The Jurassic rocks of the Hebrides occur in tilted fault blocks within a major half graben, probably formed during the early extensional phases of the evolution of the Central and North Atlantic Oceans (Morton & Hudson, 1995). The Hebrides Basin (Fig. 5.3) is itself a complex half-graben that was gently subsiding throughout Jurassic time (Riding & Thomas, 1997; Hesselbo & Coc, 2000; Hudson & Trewin, 2002) and was just one of a system of basins on the North Atlantic margins that extended as far north as Greenland and Svalbard (Tankard & Balkwill, 1989;

Ziegler, 1990; Morton & Hudson, 1995). The basin is bounded to the west by the Minch Fault Zone, just east of the Outer Hebrides (Brewer & Smythe, 1984; Stein, 1988; Hudson & Trewin, 2002), whilst to the east, the margin is unfaulted (Morton & Hudson, 1995; Hudson & Trewin, 2002). The basin is commonly subdivided into two; the Hebrides (Little Minch) sub-basin and the Inner Hebrides sub-basin (Riding & Thomas, 1997; Hesselbo & Coe, 2000; Hudson & Trewin, 2002). It has been proposed that activity along major onshore faults linked the development of the Hebrides Basin with coeval development in the Moray Firth Basin in the northeastern North Sea (see Chapter 6) (Underhill, 1991; Wignall & Pickering, 1993; Hesselbo & Coe, 2000).

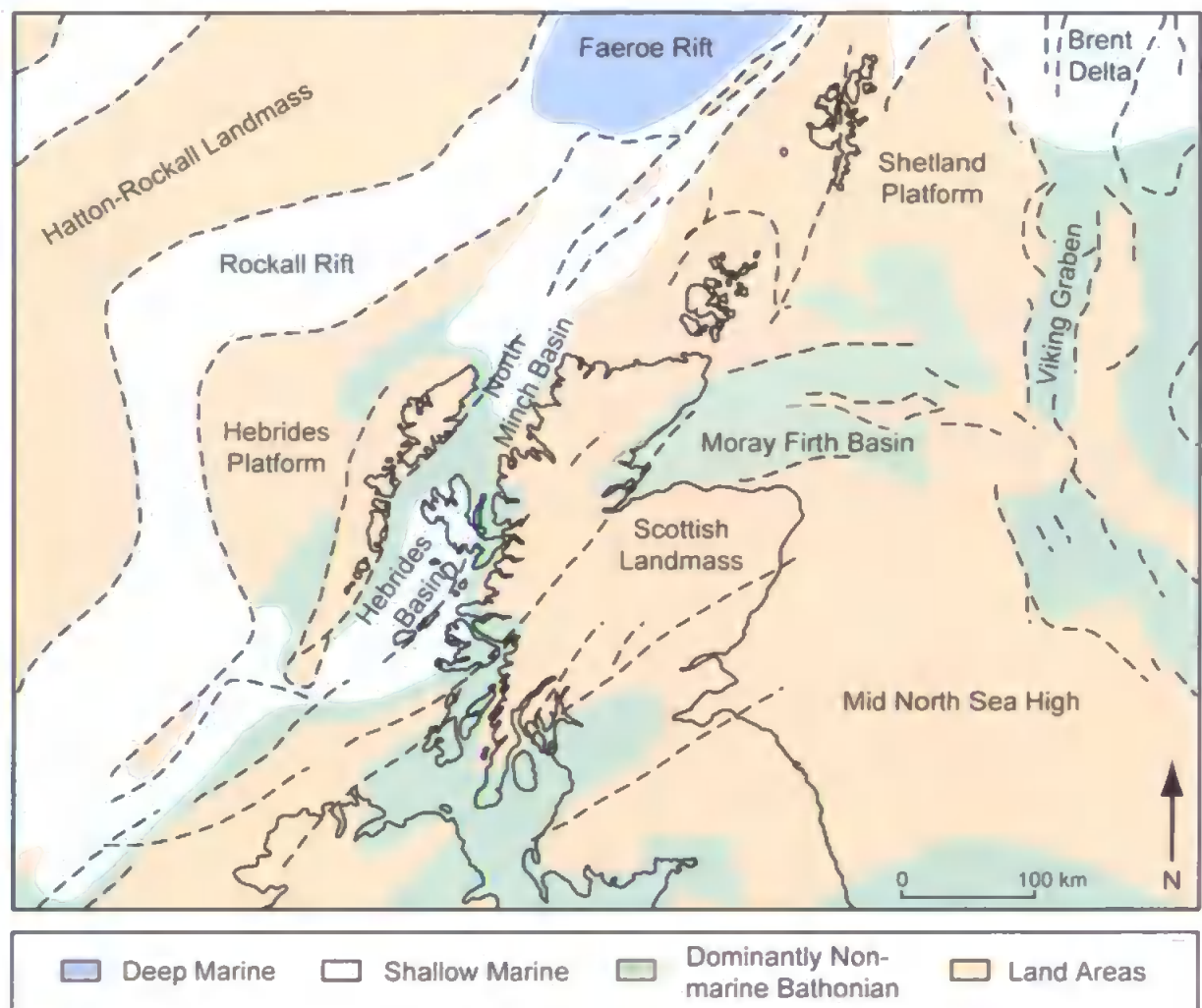


Figure 5.3 Mid-Jurassic (Bathonian) Scottish palaeogeography. Adapted after Hudson & Trewin (2002).

The Jurassic period is characterised by an overall eustatic rise in sea level (Haq *et al.*, 1987), causing widespread transgression in the Early and Late Jurassic, although, the

Middle Jurassic was marked by a relative sea level fall (Fyfe *et al.*, 1993). During the transgressive phases of the Early and Late Jurassic, deposition in the Hebrides Basin occurred predominantly in shallow-marine environments (Fyfe *et al.*, 1993).

The Mesozoic sediments of the Hebrides Basin thicken westwards as a result of faulting of the Precambrian/Palaeozoic basement (Riding & Thomas, 1997). The Jurassic succession reaches a maximum thickness of ~1000 m and is commonly overlain by basaltic lava flows from the Palaeogene Thulean Igneous Province (Morton & Parson, 1988; Riding & Thomas, 1997). Many of the successions in the Hebrides Basin have been affected by thermal alteration, although, this is not the case near Staffin (Thrasher, 1992; Bishop & Abbott, 1995; Morton & Hudson, 1995; Pearce *et al.*, 2005).

The Staffin Bay section on the Isle of Skye is one of the most stratigraphically complete Oxfordian sections in Europe (Sykes & Callomon, 1979; Morton & Hudson, 1995; Matyja *et al.*, 2004; Pearce *et al.*, 2005). It is of great importance for Upper Jurassic stratigraphy in the Boreal Realm because it contains the type localities for several of the Boreal Middle and Upper Oxfordian Zones and Subzones established by Sykes and Callomon (1979). It is also a proposed GSSP for the Oxfordian-Kimmeridgian boundary (Wierzbowski *et al.*, 2006).

The sedimentation at Staffin appears to have been continuous from the Callovian and through into the Kimmeridgian (Wright, 2001). The strata are comprised of the Staffin Bay Formation (Hudson, 1962) and the Staffin Shale Formation (Turner, 1966) (Fig. 5.4). The Staffin Bay Formation is Lower Callovian in age (*Herveyi* to *Koenigi* zones) and the Staffin Shale Formation is Middle Callovian to Lower Kimmeridgian (*Jason* to *Cymodoce* zones). The outcrops at Staffin Bay are the most accessible, extensive and fossiliferous outcrops of these formations (Morton & Hudson, 1995).

Comprehensive descriptions of the Staffin Bay and Staffin Shale Formations are given by Morton & Hudson (1995). The Staffin Bay Formation is divided into the Upper *Ostrea* Member (*Herveyi* Zone) and the Belemnite Sands Member (*Koenigi* Zone). The

Upper Ostrea Member is composed of dark grey shales with shell beds. The shell beds are generally of low but fluctuating diversity and are dominated by bivalves (Anderson & Cox, 1948; Morton & Hudson, 1995). Deposition occurred in a non-fully marine environment, most likely a coastal lagoon (Morton & Hudson, 1995). Such an interpretation is supported by palynological evidence, which is consistent with a restricted, inshore and brackish depositional environment (Riding & Thomas, 1997).

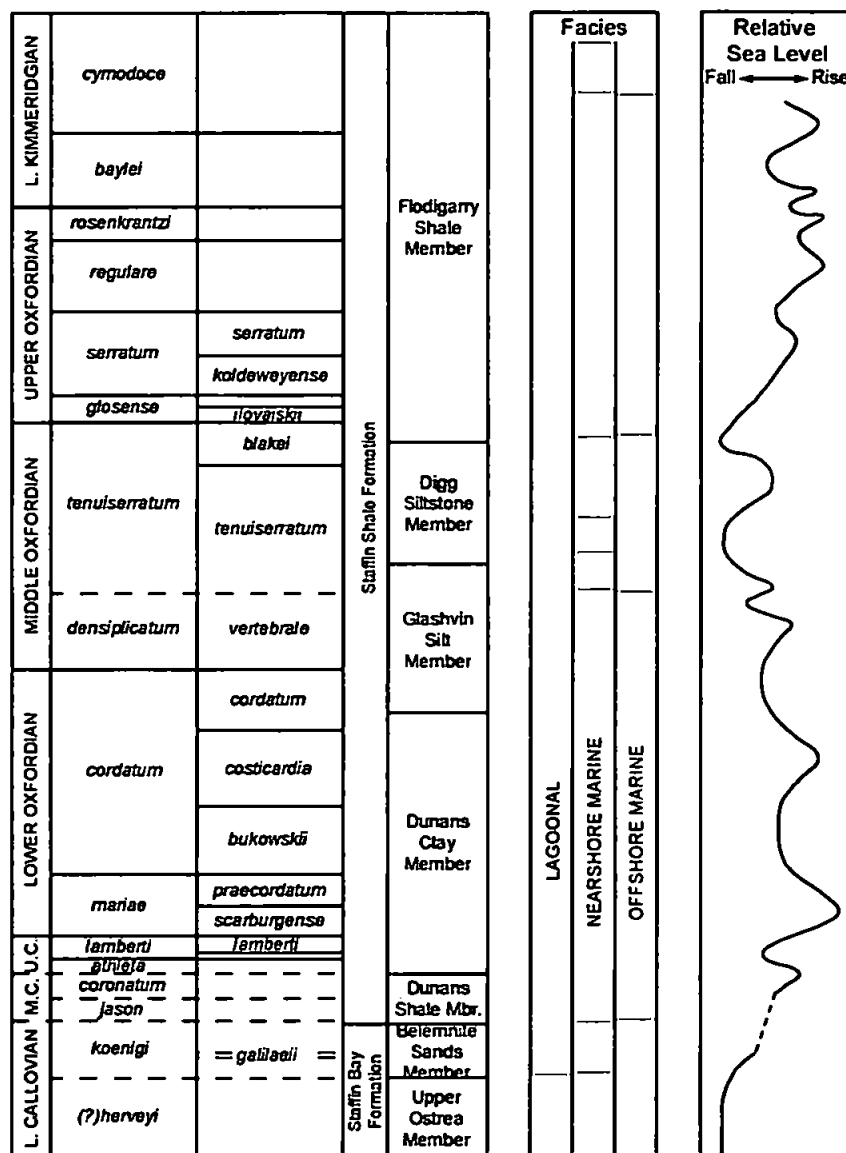


Figure 5. 4 Stratigraphic chart of the Staffin Bay section. Facies association and relative sea level are also shown. Figure adapted after Hesselbo & Coe (2000).

The Belemnite Sands Member is made up principally of siltstones and sandstones with a more varied and more marine fauna of bivalves and belemnites (Anderson & Cox, 1948; Anderson & Dunham, 1966; Morton & Hudson, 1995; Riding & Thomas, 1997).

Belemnites are common in the glauconitic beds towards the top of the member (Riding & Thomas, 1997). Morton & Hudson (1995) interpret this member as an offshore sandy bar migrating across the coastal lagoons.

The Staffin Shale Formation is dominated by mudrocks deposited in a generally offshore marine environment (Pearce *et al.*, 2005) and is broadly equivalent to the better known English Jurassic, Oxford Clay Formation, Corallian Group and Kimmeridge Clay Formation (Hesselbo & Coe, 2000). The Dunans Shale Member (*Jason* to *Coronatum* zones), Dunans Clay Member (*Athleta* to *Cordatum* zones), Glashvin Silt Member (*Cordatum* to *Tenuiserratum* zones), Digg Siltstone Member (*Tenuiserratum* Zone) and Flodigarry Shale Member (*Tenuiserratum* to *Cymodoce* zones) make up the Staffin Shale Formation (Fig. 5.4).

The dark, laminated, bituminous shales of the Dunans Shale Member are very distinct from the coarse sandstones of the Belemnite Sands Member beneath (Morton & Hudson, 1995). The bituminous shales are interspersed with thin, silty, glauconitic layers (Sykes, 1975) and belemnites are common throughout. The lack of benthos suggests a period of anoxic sea floor deposition (Fisher & Hudson, 1987), with silty, glauconitic layers representing occasional oxic perturbations (Morton & Hudson, 1995).

Sykes (1975) described the Dunans Clay Member (Fig. 5.2) as being dominated by grey-green clays with some siltstones (occasionally with visible woody debris). Both ammonites and belemnites are often abundant but the bivalve fauna is limited. Deposition probably occurred in dominantly well-oxygenated conditions (Morton & Hudson, 1995).

A gradual coarsening upwards trend, from the Dunans Clay to Digg Siltstone Member, coupled with an increase in carbonate content from the Glashvin Silt Member is described by Pearce *et al.* (2005). The Glashvin Silt Member is dominated by dark grey carbonaceous silts, with a diverse bivalve fauna (with large bivalves (*Pinna*, *Cucullaea*, *Pleuromya* and *Pholadomya*) often in life position) and some sandstones with lignite debris (Morton & Hudson, 1995; Wright, 2001). The depositional environment was probably

similar to that of the Dunans Clay Member but somewhat shallower (Morton & Hudson, 1995).

The Digg Siltstone Member is composed predominantly of light grey sandy silts with some fine sandstone beds and darker grey silts (Wright, 2001). The lithologies are coarser and lighter than those of the Glashvin Silt Member and probably represent a shallowing sequence, with deposition of this member occurring near to the fair-weather wave base (Morton & Hudson, 1995).

Dark grey, slightly bituminous, shaly clays are the principal lithology of the Flodigarry Shale Member (Wright, 1989, 2001; Morton & Hudson, 1995) (Fig. 5.5). Glauconitic silts and muds are present at the base and mark a major change of facies from the Digg Siltstone Member (Morton & Hudson, 1995; Pearce *et al.*, 2005). The Flodigarry Shale Member is particularly fossiliferous, with abundant belemnites, ammonites and bivalves (Morton & Hudson, 1995). Pearce *et al.* (2005) interpret the occurrence of glauconitic mudstones at the base of the member as representing a return to higher sea levels from the upper *Tenuiserratum* Zone.

5.3. Sampling & Methodology

The ten different sites examined in the Staffin Bay area provided an almost complete succession from the Upper Callovian - Lower Kimmeridgian. In total, 241 horizons were sampled from the Staffin Bay section. This included 174 belemnite horizons (each horizon often containing multiple specimens) and 216 sediment horizons (with such sediment containing microscopic wood debris). Wherever possible both belemnite and sediment samples were collected from the same horizon (Fig. 5.5).

The preservation of belemnite rostra was evaluated through trace element and stable isotopic analysis, backscattered scanning electron microscopy (BSEM), cathodoluminescence (CL) and carbonate staining (following the technique of Dickson (1965, 1966)). The areas most susceptible to diagenesis were removed prior to isotopic

and geochemical analysis. Samples were analysed for carbon and oxygen isotopes, with subsamples taken for trace element analysis (Fe, Mn, Ca, Sr, Mg, Na and Li). The stable isotope data was compared with a small amount of data generated by Wierzbowski (2004) for the upper part of the Staffin section. This helped ensure the reproducibility of the data.



Figure 5.5 Relatively abundant belemnites in a mudrock (suitable for sampling) containing microscopic wood debris. Flodigarry Shale Member of the Staffin Shale Formation (location SK6).

Stable isotope data were generated on a VG Optima mass spectrometer at the NERC Isotope Geosciences Laboratory (NIGL), Keyworth, UK. Samples for trace element data were digested in 20% nitric acid (HNO_3) and analysed by Inductively Coupled Plasma-Atomic Emission Spectrometer (ICP-AES) using a Perkin Elmer Optima 3300RL ICP-AES system (with autosampler) at the NERC ICP facility, Department of Geology, Royal Holloway, University of London.

Bulk sediment samples (containing microscopic wood debris) were covered with 5% hydrochloric acid (HCl) then rinsed with deionised water, oven dried and powdered with an agate pestle and mortar. Carbon isotope analysis was performed by combustion in

a Carlo Erba NA1500 (series 1) elemental analyser at NIGL, Keyworth. The resulting gas samples were subsequently measured for carbon isotope ratios by an on-line VG TripleTrap and Optima dual-inlet mass spectrometer. A representative selection of samples (67 in total) were also analysed for Total Organic Carbon (TOC) on a Primacs SLC Carbon Analyzer at the University of Plymouth. An additional 50 samples were also analysed by Rock-Eval Pyrolysis (which includes a measurement for TOC) on a Rock-Eval 6, at the University of Neuchâtel, Switzerland. For a full description of the methodology used see Chapter 4.

5.4. Results

The isotopic compositions derived from belemnite carbonate were determined using well-preserved rostra of the genera *Cylindroteuthis*, *Pachyteuthis* (Boreal Realm genera) and occasionally *Belemnopsis* (a typically Tethyan genus). There appears to be no major discrepancy between the isotope values derived from the different belemnite genera (Fig. 5.6). The belemnites sampled from this region were predominantly composed of honey-coloured translucent calcite. Several specimens displayed areas of intense endolithic borings on the margins, which were removed prior to analysis. Carbonate staining, CL and BSEM analysis (Plates 1-3) was conducted on 40 out of 206 specimens and indicated that the belemnite margins were often Fe-rich, with some pyrite replacement and sparite infilling of borings. Such features were identified by mauve-blue colouration after carbonate staining, pale grey to white colouration under BSEM and luminescence under CL conditions. Such areas were removed prior to subsampling because even subtle diagenetic alteration can have an isotopic effect.

The determined elemental abundances of the belemnite rostra were as follows: Fe 0-2134 ppm, mean 68 ppm; Mn 1-305 ppm, mean 24 ppm; Mg 539-4220 ppm, mean 1045 ppm; Sr 766-1232 ppm, mean 953 ppm and Ca 28 % - 33 %, mean 30 %. Low Mn (<100 ppm) and Fe (<150 ppm) values were recorded for most of the belemnites. Relatively low

Mn and Fe concentrations can be assumed to reflect well preserved shell material, since such concentrations have been measured from modern molluscs (e.g., Pirrie & Marshall, 1990; Podlaha *et al.*, 1998; Price & Mutterlose, 2004). Trace element data (Fe and Mn) were plotted against $\delta^{18}\text{O}$ to constrain any diagenetic alteration (Fig. 5.7). The higher amounts of Fe and Mn and occasional negative $\delta^{18}\text{O}$ outliers are regarded as an artefact of diagenesis. The lack of correlation between the values, however, suggests minimal post-depositional alteration. Those samples with higher concentrations were considered likely to have undergone diagenetic alteration and were excluded from any further analysis (24 samples in total).

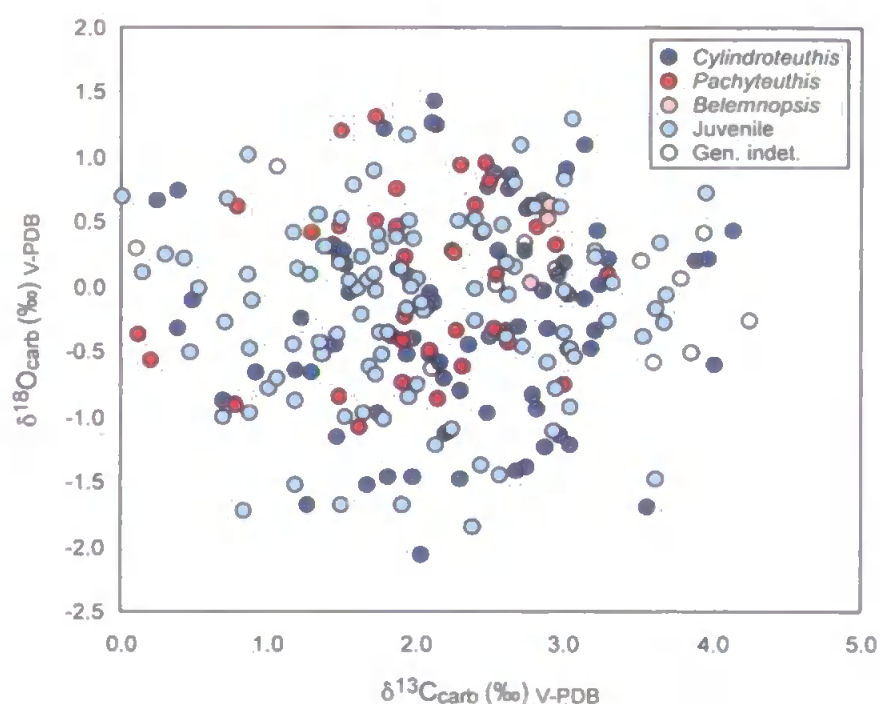


Figure 5.6. Cross-plot of $\delta^{18}\text{O}$ and $\delta^{13}\text{C}$ values derived from belemnites from Staffin Bay, Isle of Skye, Scotland.

The Mg/Ca ratios vary from 3.08 to 14.22 mmol/mol. A plot of $\delta^{18}\text{O}$ vs. Mg/Ca shows no significant correlation (Fig. 5.8). The Mg/Ca trend (Fig. 5.9) shows minimum values in the Middle Oxfordian *Densiplicatum* Zone (as low as 3.14 mmol/mol) and in the Lower Kimmeridgian *Cymodoce* Zone (as low as 3.08 mmol/mol). The Sr/Ca ratios range from 1.13 to 1.80 mmol/mol. The Sr/Ca trend (Fig. 5.9) shows a general increase in values

from the Lower Oxfordian to the Lower Kimmeridgian. A cross-plot of $\delta^{18}\text{O}$ vs. Sr/Ca reveals a negative correlation, although covariance is poor (Fig. 5.8). Neither the Na/Ca nor Li/Ca ratios show a significant covariance with $\delta^{18}\text{O}$ (Fig. 5.8). Na/Ca ratios range from 4.01 to 11.00 mmol/mol and Li/Ca ratios from 7.08 to 113.24 $\mu\text{mol/mol}$.

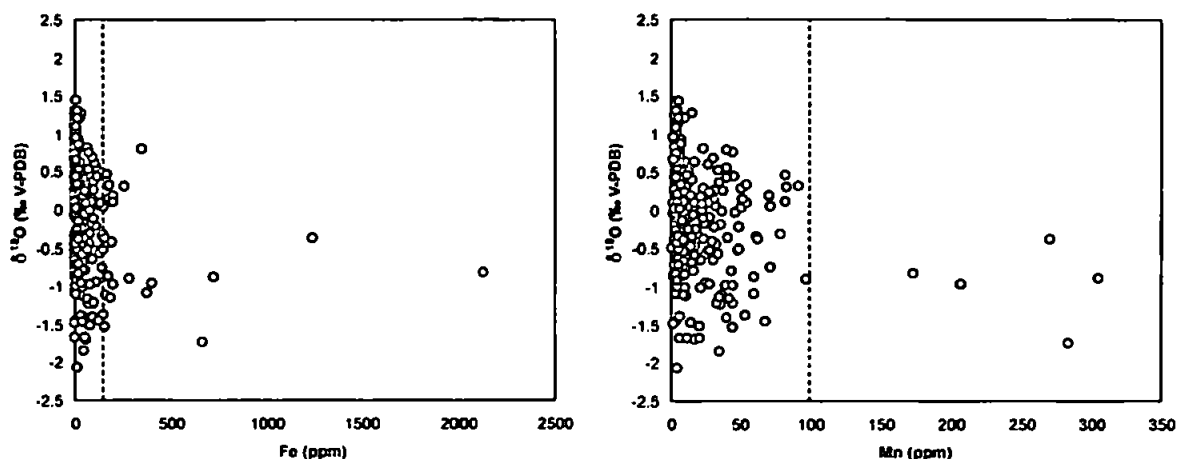


Figure 5.7 Cross-plots of $\delta^{18}\text{O}$ against Fe (left) and Mn (right). The dashed line illustrates the cut off values for well preserved samples.

The oxygen and carbon isotope values derived from well preserved belemnite rostra range from -2.07 to 1.43 ‰ and from 0.01 to 4.26 ‰ respectively (Fig. 5.10). Both the oxygen and carbon isotope values show a considerable degree of scatter, although, long-term trends can still be recognised. The oxygen isotope ratios decrease very gradually throughout the succession from values of between -0.76 to 1.43 ‰ in the Middle Callovian to Lower Oxfordian to values of -1.85 to 0.73 ‰ in the Lower Kimmeridgian.

The carbon isotope ratios also decrease gradually throughout the succession. The Middle Callovian values are in the range of c. 2.0-3.0 ‰, compared with values in the range of c. 0.5-1.5 ‰ in the Lower Kimmeridgian. There is a brief, but distinct negative carbon isotope excursion at the *Cordatum-Densiplicatum* Zone boundary (with a peak negative value of 0.01 ‰). This excursion is followed by a return to pre-excursion values, which is followed by drop in values from c. 3.0 ‰ to c. 0.5 ‰ at the *Tenuiserratum-Glosense* Zone (Middle-Upper Oxfordian) boundary. The Upper Oxfordian and Lower Kimmeridgian carbon isotope record generally fluctuates between c. 0.0 and 2.0 ‰,

although, a brief, indistinct positive fluctuation is identified at the *Baylei-Cymodoce* boundary, with values reaching 3.57 ‰. A plot of the $\delta^{18}\text{O}$ vs. $\delta^{13}\text{C}$ data (Figs 5.6) reveals no significant correlation.

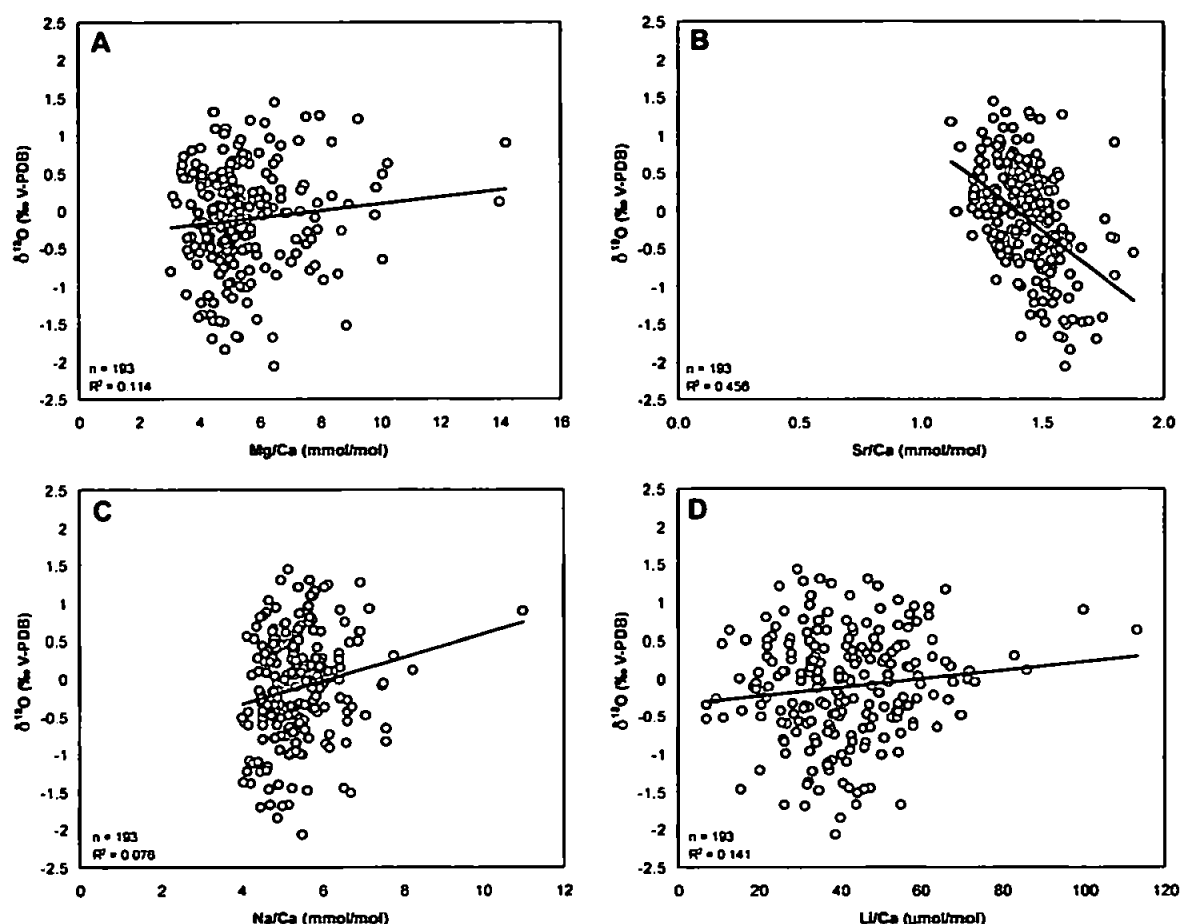


Figure 5.8 Cross-plots of $\delta^{18}\text{O}$ against (A) Mg/Ca, (B) Sr/Ca, (C) Na/Ca and (D) Li/Ca.

Total Organic Carbon (TOC) values derived from the organic wood debris range from 0.18 to 9.22 %, with values gradually increasing up the sequence, despite significant scatter (Fig. 5.11). TOC values in the Dunans Clay and Glashvin Silt members are highly variable, whilst values in the Flodigarry Shale Member are more consistent (between ~ 1 and 3 wt %). Rock-Eval pyrolysis (Fig. 5.12) indicated that the analysed material was predominantly Type III kerogen (organic matter derived from higher plants), although a small amount of Type II kerogen (derived from the marine environment) was also present. The hydrogen indices ranged from 23 to 396 HC/g TOC and from 21 to 317 $\text{CO}_2/\text{g TOC}$.

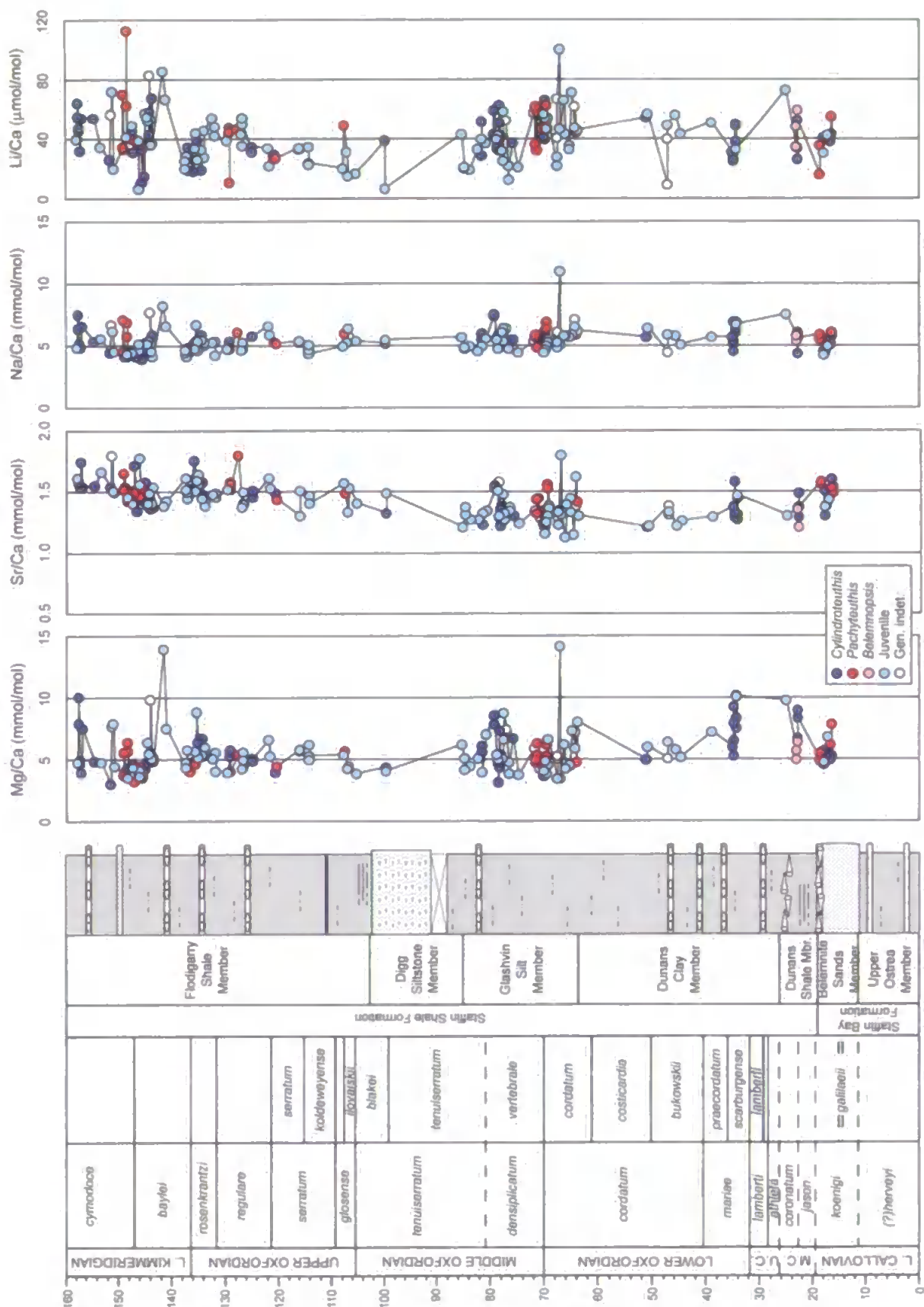


Figure 5.9. El/Ca ratios from the Callovian-Lower Kimmeridgian succession at Staffin Bay, Isle of Skye, Scotland. Boreal (British) ammonite zones and subzones illustrated. See Figure 4.2 for key to log symbols. Scale is in metres.

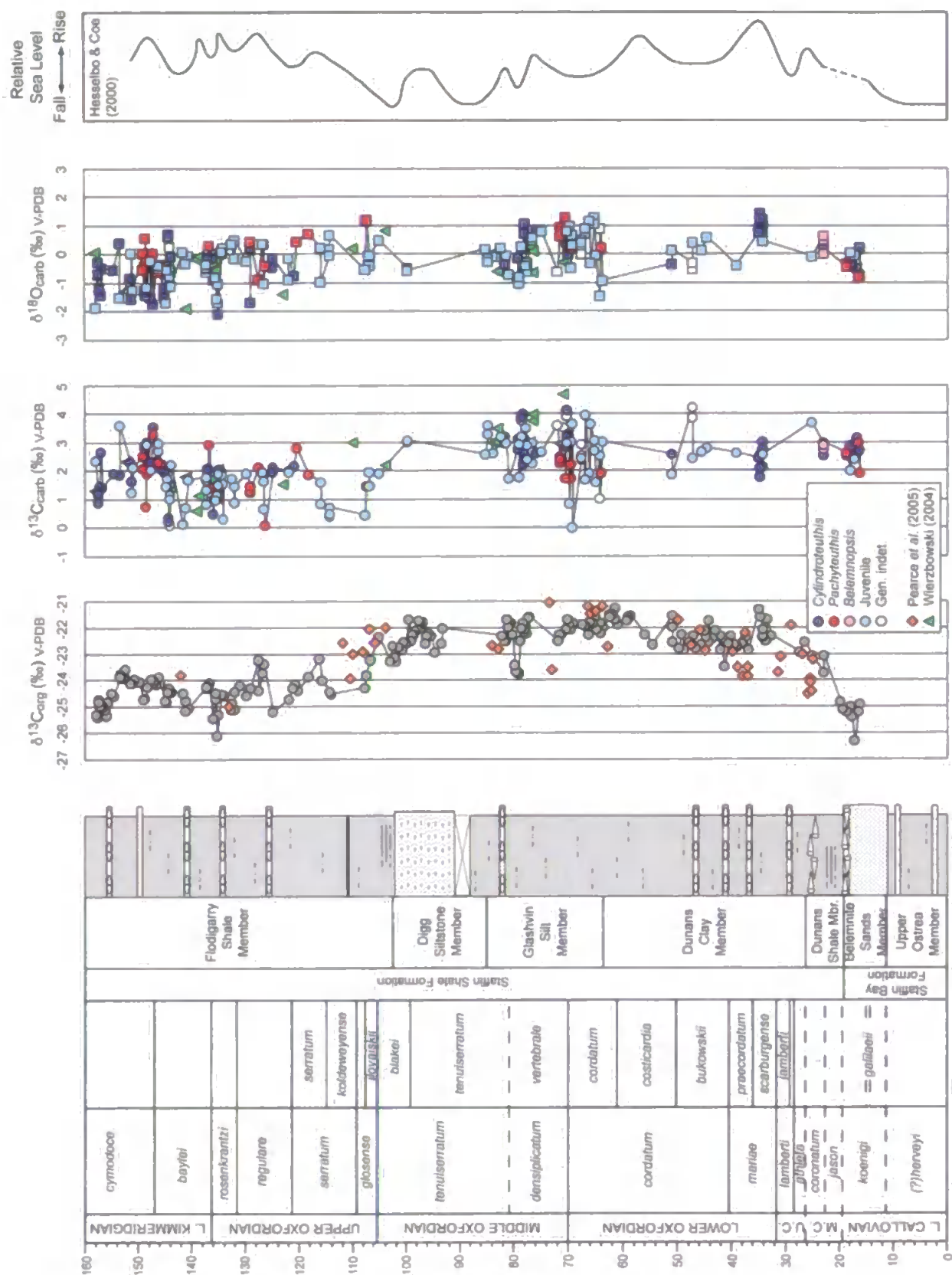


Figure 5.10 $\delta^{13}\text{C}_{\text{org}}$, $\delta^{13}\text{C}_{\text{carb}}$ and $\delta^{18}\text{O}_{\text{carb}}$ records from the Callovian-Lower Kimmeridgian succession at Staffin Bay, Isle of Skye, Scotland. Boreal (British) ammonite zones and subzones illustrated. See Figure 4.2 for key to log symbols. Scale is in metres.

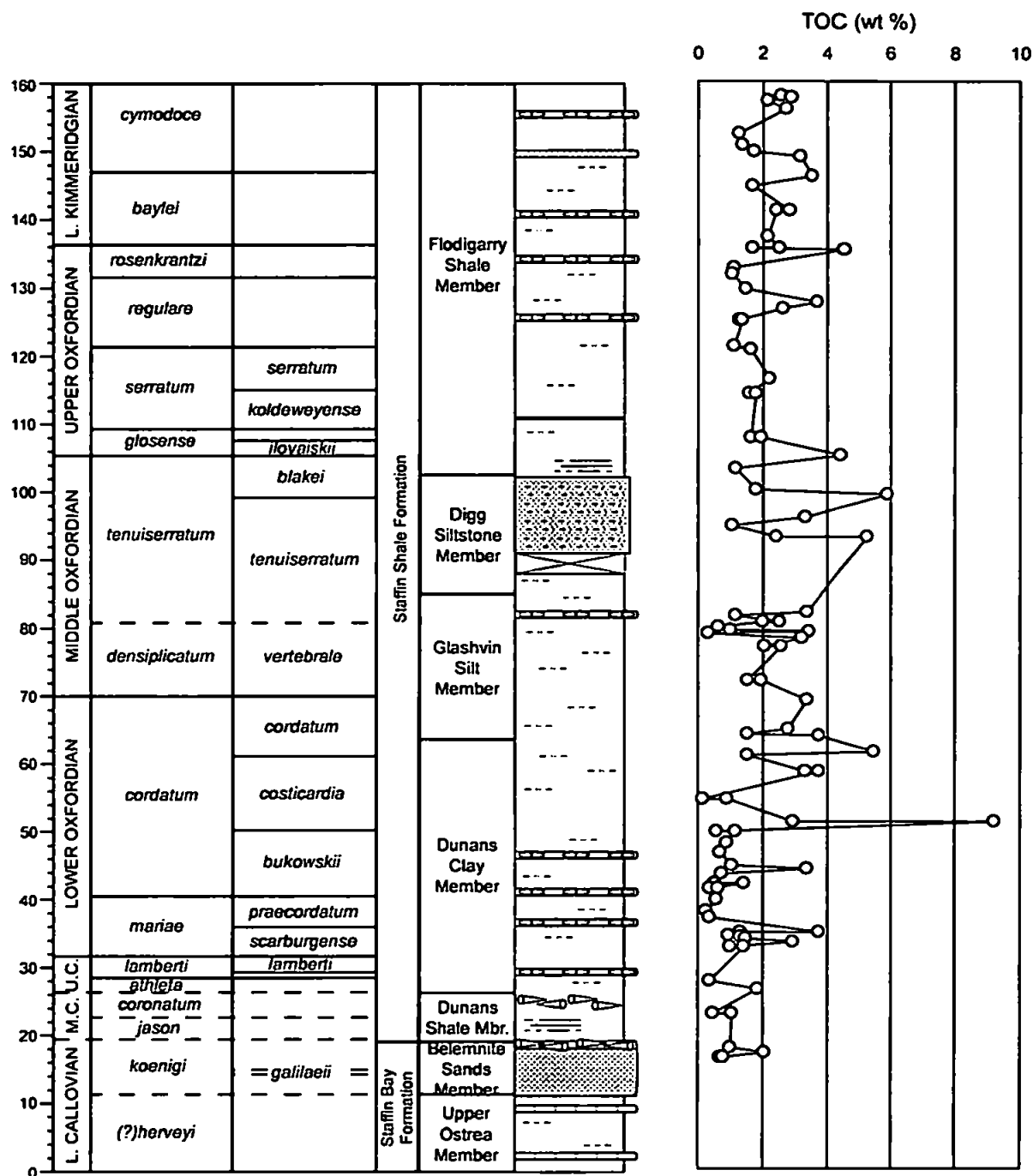


Figure 5.11 TOC record from the Callovian-Lower Kimmeridgian succession at Staffin Bay, Isle of Skye, Scotland. Boreal (British) ammonite zones and subzones illustrated. See Figure 4.2 for key to log symbols. Scale is in metres.

The fossil wood samples have an average $\delta^{13}\text{C}_{\text{org}}$ value of -23.2 ‰, with a range of -26.2 to 21.2 ‰. The organic carbon isotope data show a broad Lower to Middle Oxfordian positive carbon isotope excursion from the *Mariae* to *Tenuiserratum* Zone, with maximum values occurring in the *Cordatum* Zone (c. 21.0 ‰). This is followed by a

return to pre-excursion values continuing into the Lower Kimmeridgian *Cymodoce* Zone. There is a brief positive fluctuation in the *Cymodoce* Zone where $\delta^{13}\text{C}_{\text{org}}$ values reach -23.54 ‰). This fluctuation occurs slightly later than a similar fluctuation observed in the $\delta^{13}\text{C}_{\text{carb}}$ record, although, this is not easily identifiable given the scatter of the data. A brief negative excursion (of ~2.0 ‰) is also identified near the *Densiplicatum-Tenuiserratum* boundary. This brief negative excursion occurs approximately one ammonite zone later than negative excursion observed in the $\delta^{13}\text{C}_{\text{carb}}$ record. The $\delta^{13}\text{C}_{\text{org}}$ negative excursion was examined by Rock-Eval Pyrolysis. Five samples from the peak and shoulders of the excursion were analysed. The hydrogen indices for these samples ranged from 45 to 89 HC/g TOC and from 23 to 113 CO₂/g TOC, with each sample demonstrating a Type III origin of kerogen. This excursion is therefore not the result of a change in the source of organic matter (*cf.* Foster *et al.*, 1997).

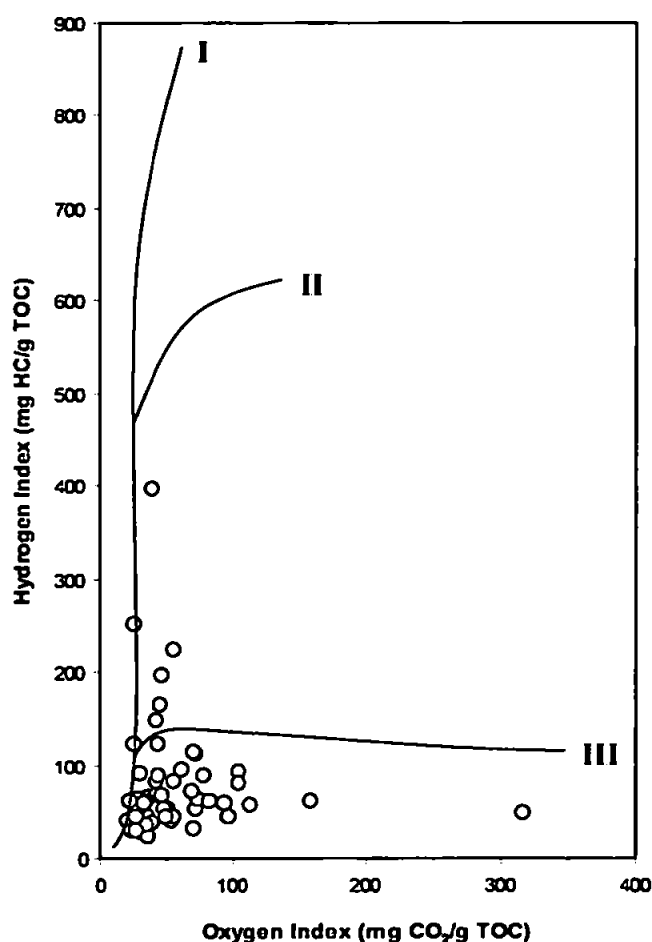


Figure 5.12 Van Krevlan diagram showing the origin of organic matter analysed from the Callovian-Lower Kimmeridgian Staffin Bay succession.

5.5. Discussion

5.5.1. Stable Isotope, Geochemical & Taxonomic Records

The stable isotope (Fig. 5.10) and *El/Ca* (Fig. 5.9) records presented here highlight the different belemnite genera from which the data were derived. This was done in order to assess the impact (if any) of genus-specific differences in isotope or trace element fractionation. The greatest degree of scatter observed from the isotope ratios was found in the genus *Cylindroteuthis* and in the juvenile specimens. This, however, could be the result of the predominance of these groups. Those groups displaying less scatter are those which are less common in the succession (e.g., *Pachyteuthis* and *Belemnopsis*), with *Pachyteuthis* displaying less scatter than the other groups in the oxygen isotope record in particular. *Belemnopsis* exhibits very little scatter in the isotope or *El/Ca* records because it was collected from only one horizon.

The *El/Ca* ratios display similar generic patterns to those observed in the stable isotope records with the juvenile group of specimens once again exhibiting the greatest scatter. In neither the isotope nor *El/Ca* records does one genus appear to be consistently more positive or negative than the others. If taxonomic differences in fractionation do exist, these data suggest that they are likely to be minor here. It is therefore highly unlikely that the trends observed here are caused solely by genus-specific effects.

5.5.2. The Oxygen Isotope Record & Palaeotemperature Implications

A long-term trend of gradually decreasing oxygen isotope values (and potentially increasing palaeotemperatures) is recorded from the Staffin Bay section. The oxygen isotope values presented here are consistent with those published by Wierzbowski (2004) from the Middle Oxfordian (*Densiplicatum* Zone) to Lower Kimmeridgian (*Cymodoce* Zone) of Staffin Bay (Fig 5.10). Wierzbowski (2004) analysed 23 belemnite specimens of the genera *Cylindroteuthis* and *Pachyteuthis* and recorded oxygen isotope values of -1.88

to 0.81 ‰ (compared with values of -2.07 to 1.20 ‰ recorded from the same time interval in this research).

There is some degree of scatter in the $\delta^{18}\text{O}$ values (<2.38 ‰, mean 0.73 ‰) recorded here from coeval belemnites. This scatter could be the result of diagenetic alteration, salinity fluctuations, generic vital effects or generic palaeoecological variability. The effect of taxonomic differences in fractionation appears to be limited here, since no major isotopic trends can be identified at the generic level (as discussed previously). Major diagenetic alteration of the specimens has also been ruled out by extensive screening. However, it is possible that subtle alteration escaped detection, although since the specimens were collected from the same location, were exposed to the same post-depositional processes and passed the same selection criteria, any such effect on the scatter of data would be very limited, as it is likely that the whole data set would have been affected and therefore the temporal trend would still be preserved even if absolute values were not.

As discussed previously (in Chapter 3) modern cephalopods are known to secrete their calcite very close to isotopic equilibrium with surrounding seawater (e.g., Taylor & Ward, 1983; Morrison & Brand, 1986; Rosales *et al.*, 2004a; Rexfort & Mutterlose, 2006) and at present no major seasonal or taxonomic differences in fractionation have been confirmed (Sælen *et al.*, 1996; Podlaha *et al.*, 1998; Rosales *et al.*, 2004a). McArthur *et al.* (2004) suggest that differences in fractionation or habitat may potentially produce a disparity in isotope values for different belemnite species, although such disparity is not observed here. The Staffin Bay oxygen isotope record is therefore considered to primarily reflect changes in environmental conditions (temperature and salinity) rather than taxonomic or diagenetic processes. It should be noted however, that since belemnites are extinct organisms it is impossible to calibrate the temperature response of $\delta^{18}\text{O}$ within the skeleton and it is therefore probably unrealistic to calculate absolute palaeotemperatures (McArthur *et al.*, 2000) from the oxygen isotope data, although the likely magnitude of

temperature change can be estimated (Bailey *et al.*, 2003). Nevertheless palaeotemperatures have been calculated here and should be considered as a guide to the potential palaeotemperatures for the region.

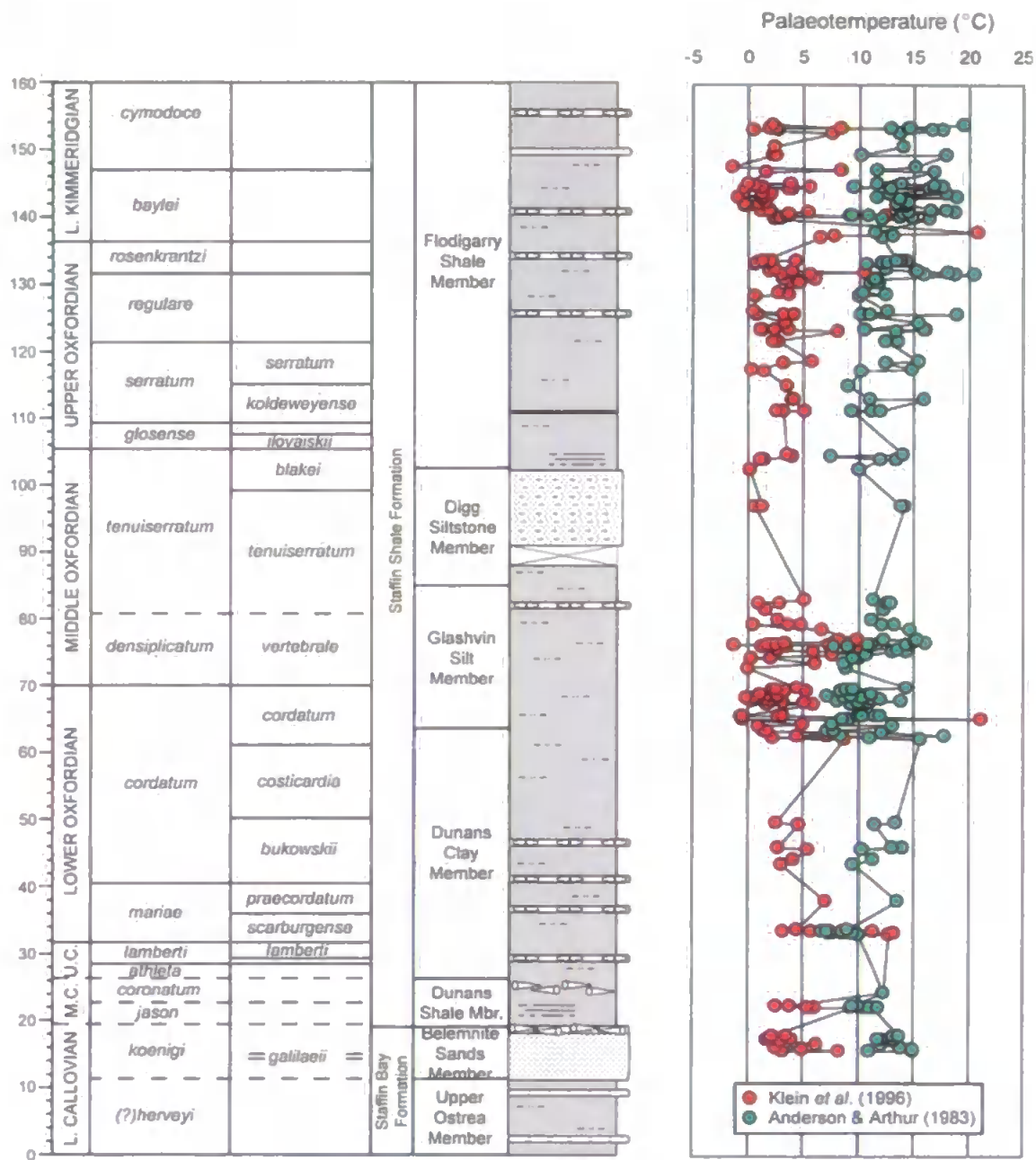


Figure 5.13 Palaeotemperatures calculated from Mg/Ca data (using the Klein *et al.*, 1996 equation) and $\delta^{18}\text{O}$ data (using the Anderson & Arthur, 1983 equation). Boreal (British) ammonite zones and subzones illustrated. See Figure 4.2 for key to log symbols. Scale is in metres.

Figure 5.13 shows seawater palaeotemperatures calculated from the $\delta^{18}\text{O}$ equation of Anderson & Arthur (1983). The isotopic composition of the water was assumed to be that of non-glacial seawater at -1 ‰ SMOW. This is consistent with previously published literature on the Jurassic period (e.g., Marshall, 1992; Sælen *et al.*, 1996; Price &

Sellwood, 1997; Podlaha *et al.*, 1998; Price & Mutterlose, 2004; Rosales *et al.*, 2004a, 2004b). The average palaeotemperature derived from the Staffin Bay belemnites was 12.4°C and the palaeotemperature range was 6.7°C to 20.6°C for the Callovian-Kimmeridgian interval. The lowest palaeotemperatures were recorded from the Lower Oxfordian *Mariae* Zone and the highest palaeotemperatures from the *Baylei* Zone of the Lower Kimmeridgian. Such values are broadly comparable with other published Oxfordian records. For example, Price & Gröcke (2002) record temperatures of 14.5 to 21.2°C from the Oxfordian-Kimmeridgian of the Falkland Plateau, Wierzbowski (2002) records values of 10.5 to 18.5°C during the Oxfordian in Central Poland and Riboulleau *et al.*, (1998) record values of 7 to 18°C from the Oxfordian of the Russian Platform.

As stated previously the Staffin Bay palaeotemperatures were calculated using a value of -1 ‰ SMOW for non-glacial seawater (following convention). Broecker *et al.* (1989) however, suggest that seawater oxygen isotope compositions can vary by as much as 1.5 ‰ between high and low latitudes as a result of evaporation, precipitation and atmospheric vapour transport. High latitude $\delta^{18}\text{O}_{\text{seawater}}$ values are lower than those of the low latitudes and have a lower salinity due primarily to the transport of isotopically depleted water vapour towards the poles. In addition, seasonal ice-melt and the proximity to landmass (and therefore the potential for riverine runoff) provide further opportunities for the input of isotopically light and low salinity waters into the high latitude system (Price & Mutterlose, 2004). Roche *et al.* (2006) modelled this phenomenon of $\delta^{18}\text{O}_{\text{seawater}}$ latitudinal distribution in past warm climates. They record surface water $\delta^{18}\text{O}_{\text{seawater}}$ values of higher than today in the equatorial region and lower than today in the high latitudes, with more pronounced differences occurring as the average climate becomes warmer. They conclude that neglecting these changes has led to an underestimation of temperature in the low latitudes and an overestimation of temperature at the poles.

The temperature-salinity plot shown in Figure 5.14 illustrates the effect that salinity can have on calculated temperature. This model was constructed by Railsback *et al.*

(1989) and Woo *et al.* (1992) with modification by Price & Mutterlose (2004). Each isopleth represents the potential range of temperature (calculated using the Anderson & Arthur (1983) equation) and salinity combinations for calcite of a known isotopic value. For example, within the model, a $\delta^{18}\text{O}$ value of 1.4 ‰ (the highest value recorded from Staffin Bay) corresponds to a palaeotemperature range of between 2.9°C (at 30 ‰ salinity) and 6.7°C (at 34 ‰ salinity) as shown by the dashed lines. The palaeotemperatures calculated using a ‘normal’ marine salinity of 34 ‰ correspond to those calculated by the Anderson & Arthur (1983) equation and a $\delta^{18}\text{O}_{\text{seawater}}$ value of -1 ‰.

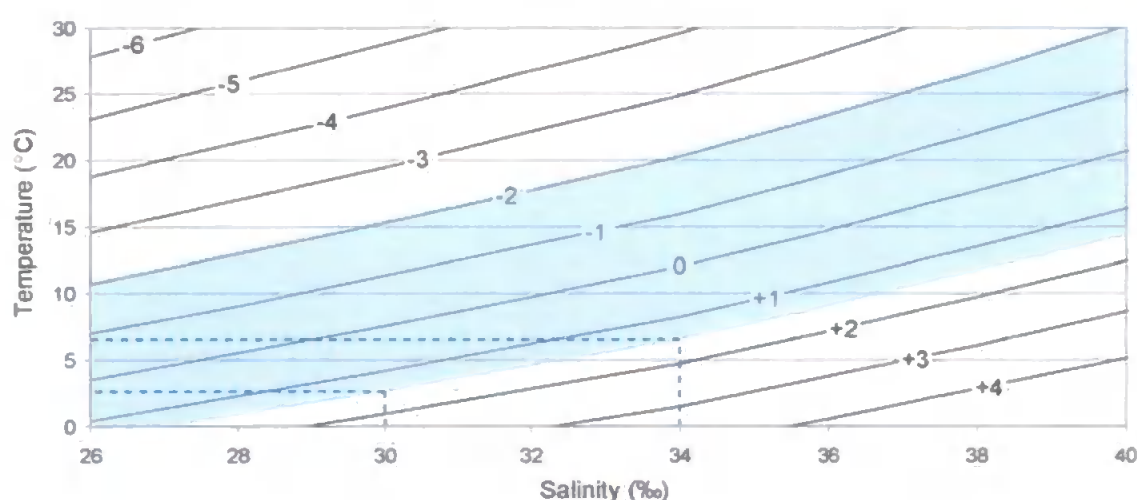


Figure 5.14 Temperature-salinity plot for the Staffin Bay data. The continuous diagonal lines are isopleths of $\delta^{18}\text{O}$ values and show the possible combination of temperature and salinity that corresponds to calcite of a given isotopic composition and for a given isotopic composition of seawater (-1 ‰). The shaded area shows the range of isotope values recorded from belemnite rostra from the Callovian-Lower Kimmeridgian succession at Staffin Bay. The dashed lines represent the values discussed in the text above.

5.5.3. The Elemental Records & Palaeotemperature Implications

Several authors have recently investigated the use of elemental ratios (e.g., Mg/Ca, Sr/Ca, Na/Ca and Li/Ca) from biogenic calcite (e.g., belemnites, foraminifera, ostracods and corals) as palaeotemperature proxies (e.g., Dwyer *et al.*, 1995; Klein *et al.*, 1996; Mitsuguchi *et al.*, 1996; Lear *et al.*, 2000, 2002; McArthur *et al.*, 2000; Wei *et al.*, 2000; Hall & Chan, 2001; Bailey *et al.*, 2003; Billups & Schrag, 2003; Rosales *et al.*, 2004a, b; Immenhauser *et al.*, 2005). It has been suggested that elemental/Ca values in belemnites may reflect only temperature, whilst $\delta^{18}\text{O}$ ratios reflect both temperature and variations in

ice-volume or salinity (McArthur *et al.*, 2000). McArthur *et al.* (2000) record a significant correlation between Sr/Ca, Na/Ca and Mg/Ca ratios with $\delta^{18}\text{O}$ and they suggest that Sr/Ca values may be the most robust elemental ratio with which to estimate palaeotemperatures. Bailey *et al.* (2003) however, concluded that their belemnite Sr/Ca records were unlikely to reflect temperature alone and that physiological factors (e.g., growth rate or metabolic effects) may also significantly influence the Sr/Ca record. As such, they suggested that Mg/Ca would provide a better palaeotemperature proxy.

Both McArthur *et al.* (2000) and Bailey *et al.* (2003) observed inverse correlations between Mg/Ca, Sr/Ca, Na/Ca and $\delta^{18}\text{O}$, with R^2 values between 0.16 and 0.69, 0.19 and 0.56, and 0.0004 and 0.45 respectively. Cross-plots of *El/Ca* against $\delta^{18}\text{O}$ for the Staffin Bay belemnites generally recorded less significant correlations, with R^2 values of 0.11 (Mg/Ca), 0.46 (Sr/Ca) and 0.18 (Na/Ca) (Fig. 5.8). Interestingly, only Sr/Ca shows a statistically significant (at the 99% confidence level) negative correlation with $\delta^{18}\text{O}$ for the Staffin Bay data, whilst neither Mg/Ca nor Na/Ca show a statistically significant correlation with $\delta^{18}\text{O}$.

Mn/Ca values were calculated for each sample and only those samples with values below 100 $\mu\text{mol/mol}$ are included here, as this is the lower limit for samples that are believed to have been altered under reducing conditions (McArthur, 1994). The elemental ratios presented here (Mg/Ca, Sr/Ca, Na/Ca and Li/Ca) show little long-term variability (Fig. 5.9), although this is also the case for the $\delta^{18}\text{O}$ record, which becomes only slightly more negative up sequence. The Mg/Ca values decrease slightly up sequence, whilst Sr/Ca values increase. The Na/Ca and Li/Ca values show no discernible long-term trend. It is difficult to fully assess the relationship between $\delta^{18}\text{O}$ and *El/Ca* ratios for the Staffin Bay section because the Callovian to Kimmeridgian interval is isotopically quite static. If instead, a major isotopic event occurred during this time the relationship between $\delta^{18}\text{O}$ and *El/Ca* would be more readily observable.

The only statistically significant correlation observed from the Staffin Bay belemnites is that between Sr/Ca and $\delta^{18}\text{O}$, where the lowest Sr/Ca values correspond with the highest $\delta^{18}\text{O}$ values. McArthur *et al.* (2000) also observed a stronger correlation between Sr/Ca and $\delta^{18}\text{O}$ than between Mg/Ca and $\delta^{18}\text{O}$, although Bailey *et al.* (2003) recorded the opposite for the same Pliensbachian-Toarcian Yorkshire succession. Studies based on extant coccoliths (Stoll *et al.*, 2002) and foraminifera (Lea *et al.*, 1999) indicate that the temperature sensitivity of Sr/Ca is approximately 10 times greater than that of Mg/Ca. However, this is not consistent with the relative changes observed here between Sr/Ca and Mg/Ca, which would indicate that these belemnite records may not reflect temperature alone. Klein *et al.* (1996) suggest that for the marine mussel *Mytilus trossulus* Sr/Ca appears to be strongly influenced by physiological factors and it is therefore possible that the Sr/Ca temperature response in belemnites is exaggerated by physiological effects.

The Mg/Ca proxy is generally considered to be the most appropriate elemental ratio with which to investigate palaeotemperature (e.g., Klein *et al.*, 1996; Lear *et al.*, 2000; Bailey *et al.*, 2003; Rosales *et al.*, 2004a, b; Immenhauser *et al.*, 2005). The Mg content of seawater is primarily controlled by the balance between fluvial supply rates and removal into biogenic carbonates and hot basalt at ocean spreading ridges (Wilkinson & Algeo, 1989). At short time scales (ammonite zones or subzones) temperature change is the most likely control on Mg/Ca ratios in biogenic carbonates (Jenkyns *et al.*, 2002). In general, low Mg/Ca ratios have been associated with cooler seawater temperatures, whilst high values are associated with warmer conditions (Rosales *et al.*, 2004b). Several authors have suggested that unlike $\delta^{18}\text{O}$, the Mg/Ca proxy is largely independent of salinity effects (e.g., Klein *et al.*, 1996; Bailey *et al.*, 2003; Rosales *et al.*, 2004a, b; Immenhauser *et al.*, 2005). This idea is supported by experimental data indicating that even a salinity decrease of 18 ‰ is only weakly reflected in Mg/Ca ratios (e.g., Naydin & Teys, 1976; Yasamanov, 1981; Klein *et al.*, 1997; Rosales *et al.*, 2004b).

For the belemnites from Staffin Bay there is no statistical correlation between Mg/Ca and $\delta^{18}\text{O}$, although the linear regression line suggests a weak positive relationship between the two values. This positive relationship is contrary to the correlation observed in modern skeletal calcite (Steuber & Rauch, 2005) and in previous belemnite studies (as mentioned previously). The absence of correlation observed here could be due to interspecies offset (as different genera were sampled), ontogenetic variations (as different regions of the rostra were sampled), metabolic activity, salinity or temperature depending on the influence of each variable on each proxy. Assuming however, that temperature is the major control on Mg/Ca ratios and that belemnites have a similar temperature sensitivity to modern biogenic calcites (as has been concluded by several of the recent studies of *El/Ca* ratios in belemnites: e.g., Bailey *et al.* (2003) and Rosales *et al.* (2004a)) it seems likely that salinity has had an effect on the $\delta^{18}\text{O}$ record. The palaeotemperatures calculated from the $\delta^{18}\text{O}$ and Mg/Ca proxies show only slight long-term variation. The $\delta^{18}\text{O}$ derived temperatures indicate a slight warming up sequence, whilst the Mg/Ca derived temperatures remain relatively static. The $\delta^{18}\text{O}$ and Mg/Ca palaeotemperatures (calculated using the Anderson & Arthur (1983) and Klein *et al.* (1996) equations respectively) show a considerable offset (Fig. 5.13), with ranges of $\delta^{18}\text{O}$ and Mg/Ca from 6.7 to 20.6 °C (average 12.4 °C) and -1.3 to 21.2 °C (average 3.8 °C) respectively. This offset is consistent with data from Klein *et al.* (1997) that recorded lower temperatures from Mg/Ca values compared with $\delta^{18}\text{O}$ values for *Mytilus trossulus*. The average discrepancy between the palaeotemperature proxies is 8.6 °C. If this temperature difference was interpreted solely as the result of salinity it would require a change in salinity from, for example, 34 to 25.2 ‰. However, a change of this magnitude seems unlikely, since it would be occurring in a shallow marine succession with an abundance of marine fauna (ammonites and belemnites) throughout as well as a diverse palynoflora indicting open marine conditions (Morton & Hudson, 1995; Riding & Thomas, 1997; Wierzbowski, 2004). An average palaeotemperature of 3.8 °C for this palaeolatitude is

intuitively unlikely, which together with the salinity changes required to achieve this suggests that the use of Mg/Ca palaeotemperature equations on belemnites (after Klein *et al.* (1996) and based on an extant bivalve species) may not be entirely appropriate. Ultimately, the use of Mg/Ca as a palaeotemperature proxy requires further evaluation.

The covariance of both Na/Ca and Li/Ca with $\delta^{18}\text{O}$ as observed here is statistically insignificant. Bailey *et al.* (2003) report weak covariance between these variables and suggest that the lack of correlation indicates that these elemental ratios are unlikely to reflect temperature variations in belemnites. This is supported by experiments on modern foraminifera (e.g., Delaney *et al.*, 1985). Hall & Chan (2001) demonstrated that for recent foraminifera Li/Ca ratios were temperature sensitive and responded in the opposite sense to Mg/Ca (with Mg/Ca ratios decreasing with falling temperatures whilst Li/Ca ratios increased). Bailey *et al.* (2003) could not confirm these observations for belemnites and suggested that Li/Ca signals were not recorded, probably as the consequence of the small size of the Li ion, which makes it likely to be quickly lost from the calcite lattice after burial.

The difficulty in interpreting the *El/Ca* ratios in terms of environmental conditions is exacerbated at Staffin Bay by the static nature of the oxygen isotope record during this time period. By considering a more dynamic time period containing more significant isotope shifts (e.g., the Valanginian - see Chapters 7 and 8) it should be possible to produce more useful data with which to assess the nature of the relationships between temperature, $\delta^{18}\text{O}$ and *El/Ca* ratios.

5.5.4. The Terrestrial Carbon Isotope Record

The organic carbon isotope ratios presented here are considered to primarily reflect changes in the terrestrial carbon isotope reservoir. The limitations and reliability of fossil wood data were discussed in Chapter 4, where it was concluded that $\delta^{13}\text{C}_{\text{org}}$ values could be used to confidently identify long-term shifts in the composition of atmospheric carbon.

The $\delta^{13}\text{C}_{\text{org}}$ data from Staffin Bay reveal a rapid change towards more positive carbon isotope values from the Lower-Middle Callovian boundary and into the Lower Oxfordian. The positive excursion has a magnitude of $\sim 5\text{‰}$ (from approximately -26.5 to -21.5‰). This excursion is coincident with a change of depositional conditions from a coastal lagoon-type environment in the Callovian to more fully marine conditions from the earliest Oxfordian. The observed shift towards more positive values in the Lower Oxfordian however, cannot be attributed to a change in the source of organic matter. This is contrary to the work of Foster *et al.* (1997), which concluded that although secular variations in $\delta^{13}\text{C}_{\text{org}}$ were present, they were often overprinted by changes in organic source or facies. The Rock-Eval data (Fig. 5.12) presented here confirm that the organic matter analysed from the Isle of Skye was predominantly derived from a terrestrial source (Type III kerogen). This is consistent with published palynological data for Staffin Bay, which record abundant palynomorphs that are dominated by gymnospermous pollen grains and associated with pteridophytic spores (Riding & Thomas, 1997). More specifically, the conifer pollen *Classopollis* and the wood genus *Cupressinoxylon* (Pearce *et al.*, 2005) have been recognised. The Rock-Eval pyrolysis identified several samples with relatively high hydrogen indices, which would suggest that a marine component is occasionally incorporated within the organic matter. Marine microplankton, most notably dinoflagellate cysts, have been recorded from throughout the Staffin Bay section (Riding & Thomas, 1997; Hesketh & Underhill, 2002). These data however, do not consistently correspond with heavier carbon isotope ratios. It is therefore assumed that the organic matter source has not significantly influenced the carbon isotope trend recorded here.

From the Lower Oxfordian the $\delta^{13}\text{C}$ values remain fairly constant, fluctuating between approximately -21 and -23‰ (values typical of terrestrial organic matter) until the Middle-Upper Oxfordian boundary, after which the carbon isotope values decrease reaching $\sim -25.5\text{‰}$ in the Lower Kimmeridgian *Cymodoce* Zone. The timing and duration of the observed $\delta^{13}\text{C}_{\text{org}}$ trend is consistent with data published by Pearce *et al.* (2005).

Pearce *et al.* (2005) analysed 37 Upper Callovian (*Athleta* Zone) to Lower Kimmeridgian (*Baylei* Zone) samples of microscopic wood debris from the Staffin Shale Formation. Microscopic wood fragments were separated from the mud matrix and crudely categorised as coal, charcoal or a combination of both, although no relationship between the state of preservation and isotope ratio was discernable. The $\delta^{13}\text{C}_{\text{org}}$ values presented here are consistent with those of Pearce *et al.* (2005) and are similar to the range expected for Cretaceous C_3 plants (-23 to -34 ‰) (Bocherens *et al.*, 1993; Gröcke, 1998; Robinson & Hesselbo, 2004; Pearce *et al.*, 2005). The coeval marine carbonate samples are offset by between 21 and 30 ‰.

5.5.5. The Marine Carbon Isotope Record

The marine $\delta^{13}\text{C}_{\text{carb}}$ record shows a distinct change from more positive values in the Lower and Middle Oxfordian (typically ~2 to 4 ‰), to more negative values from the Upper Oxfordian and into the Lower Kimmeridgian (typically ~0 to 2 ‰). This trend can be observed despite a considerable degree of scatter in the marine carbonate data. Such scatter however, is consistent with published belemnite data from other sections (e.g., Bailey *et al.*, 2003; McArthur *et al.*, 2004; Price & Mutterlose, 2004; Wierzbowski, 2004) and is most likely the result of real and natural variation. By comparison, bulk records tend to produce smoother, less noisy curves. This is the result of time averaging, which dampens natural variability and homogenisation of the constituent components. For example, a 1 mm bulk sediment sample could represent anything in the range of 100-1000 years or more, whilst a 1 mm sample of belemnite calcite probably only represents a period of months.

The belemnite derived carbon isotope values presented here are compatible with those recorded by Wierzbowski (2004) from the Middle Oxfordian (*Densiplicatum* Zone) to Lower Kimmeridgian (*Cymodoce* Zone) of Staffin Bay (Fig. 5.10). Wierzbowski (2004)

recorded carbon isotope values between 0.62 and 4.69 ‰ (compared with values of 0.11 to 4.02 ‰ recorded here for the same interval).

5.5.6. The Carbon Isotope Records & Ocean-Atmosphere Correlation

The comparison of marine with terrestrial carbon isotope stratigraphy is essential to confirm that isotopic patterns are of global origin rather than the result of local or diagenetic factors (Hesselbo *et al.*, 2003). There have been a number of recent studies that have compared marine and terrestrial carbon isotope records (e.g., Ando *et al.*, 2002, 2003; Hesselbo *et al.*, 2003; Robinson & Hesselbo, 2004; Gröcke *et al.*, 2005; Pearce *et al.*, 2005), however these studies almost always compare carbon isotope data from geographically different successions. Geological successions containing both a marine and terrestrial record suitable for isotope work are extremely rare and data from such a succession have never been published, where data were collected simultaneously. This study presents the first coeval marine and terrestrial record of this kind.

The observed offset between the Staffin Bay $\delta^{13}\text{C}_{\text{carb}}$ and $\delta^{13}\text{C}_{\text{org}}$ data is approximately ~ 25.5 ‰ on average, which is consistent with the observed offset of ~ 25 ‰ recorded by Pearce *et al.* (2005) for the same succession (their value was calculated using the carbonate data of Wierzbowski (2004)). The $\delta^{13}\text{C}_{\text{carb}}$ curve corresponds well with the $\delta^{13}\text{C}_{\text{org}}$ curve from the Lower Oxfordian and into the Kimmeridgian, which indicates a strong coupling of the ocean-atmosphere system at this time. The most positive $\delta^{13}\text{C}$ values occur during the Lower and Middle Oxfordian (*Mariae* to *Glosense* zones) where values are consistently high in both the marine and terrestrial records. A change to increasingly negative values occurs during the Upper Oxfordian *Glosense* Zone until the occurrence of a brief positive fluctuation in the Early Kimmeridgian *Cymodoce* Zone. This trend is observed in both records, which suggests that the total exchangeable carbon reservoir would have been affected. It is worth noting that the $\delta^{13}\text{C}_{\text{org}}$ data show a greater amplitude of change than the coeval $\delta^{13}\text{C}_{\text{carb}}$ data, which is in agreement with other

published Mesozoic $\delta^{13}\text{C}_{\text{wood}}$ data (e.g., Gröcke *et al.*, 1999; Robinson & Hesselbo, 2004; Pearce *et al.*, 2005).

The Callovian $\delta^{13}\text{C}_{\text{carb}}$ and $\delta^{13}\text{C}_{\text{org}}$ curves, however, do not correspond. A rapid positive excursion of approximately 4 ‰ is observed in the $\delta^{13}\text{C}_{\text{org}}$ record, whilst the $\delta^{13}\text{C}_{\text{carb}}$ values remain relatively constant. This decoupling is probably the result of a small, local event which is only recorded in either the marine or terrestrial realm, although the nature of such an event remains unclear.

5.5.7. Callovian-Kimmeridgian Marine & Terrestrial Isotopic Records

The isotopic offset between the Staffin Bay $\delta^{13}\text{C}_{\text{org}}$ and $\delta^{13}\text{C}_{\text{carb}}$ records (~25.5 ‰) is greater than that observed between $\delta^{13}\text{C}_{\text{org}}$ and $\delta^{13}\text{C}_{\text{carb}}$ values in the Oxfordian of Poland and Germany (~23 ‰) as recorded and discussed by Wierzbowski (2002, 2004) and Pearce *et al.* (2005). Wierzbowski (2004) attributes this difference in offset to isotopically heavier belemnite values as a result of ^{13}C enrichment in the Boreal Realm due to high organic matter productivity in the partly isolated Boreal seas. Since no enrichment is observed here in the $\delta^{13}\text{C}_{\text{org}}$ data (which are consistent with the sub-Tethyan Oxfordian $\delta^{13}\text{C}_{\text{wood}}$ values from Dorset (Pearce *et al.* 2005)) the observed offset must be the result of localised changes of isotopic composition in the marine carbon reservoir. This lends support to the idea that $\delta^{13}\text{C}_{\text{org}}$ data reflect a global signal influenced primarily by perturbations in the total exchangeable carbon reservoir (Pearce *et al.*, 2005).

The timing of the positive $\delta^{13}\text{C}$ excursion recorded here is similar to that recorded in previously published Callovian to Kimmeridgian $\delta^{13}\text{C}$ marine and terrestrial data. The duration of the Staffin Bay excursion is from the *Mariae* to *Tenuiserratum* zones, with the maximum occurring across the *Cordatum-Vertebrale* Subzonal boundary (using the Boreal British ammonite zonation) in both the organic and carbonate records. Pearce *et al.* (2005) also record a broad positive $\delta^{13}\text{C}_{\text{wood}}$ excursion at this time from the Staffin Bay succession, although their maximum occurs slightly later, across the *Vertebrale-*

Tenuiserratum Subzonal boundary. A broad positive $\delta^{13}\text{C}_{\text{carb}}$ excursion has also been recorded in the sub-Alpine basin of southeast France, with a maximum during the *Parandieri* Subzone (Tethyan ammonite zonation, equivalent to the Boreal British Upper *Tenuiserratum* Subzone) (Beat Louis-Schmid pers. comm.). Middle Oxfordian positive $\delta^{13}\text{C}$ excursions have also been recorded by Jenkyns (1996), Weissert & Mohr (1996), Bartolini *et al.* (1999), Wierzbowski (2002), Dromart *et al.* (2003b).

It is worth noting that although the excursion maximum observed here in the Staffin Bay data occurs earlier than in the other comparable successions, the $\delta^{13}\text{C}$ values remain relatively positive until the end of the *Tenuiserratum* Zone. Much of the discrepancy between the timing and duration of the positive excursion may be accounted for by factors such as poor sampling resolution, limited biostratigraphical data, condensed sections and missing strata in the previously published sections. The Staffin Bay data is very well constrained biostratigraphically and of a high sampling resolution, which may contribute to the elimination of some of this uncertainty.

Jenkyns (1996), Weissert & Mohr (1996) and Wierzbowski (2002) have interpreted the mid-Oxfordian positive carbon isotope excursion as the result of organic carbon burial during a eustatic sea-level rise. However, Hesselbo & Coe (2000) presented a sea level curve covering the complete Callovian to Kimmeridgian Staffin Bay succession, which led Pearce *et al.* (2005) to conclude that sea-level rise was not the primary factor to influence this $\delta^{13}\text{C}$ excursion because, according to their investigation, increasing $\delta^{13}\text{C}$ values corresponded to a relative sea-level fall. Instead, Pearce *et al.* (2005) proposed an increase in global organic carbon burial rates or an as-yet un-established mechanism to account for the excursion. Evidence for Oxfordian organic carbon burial in the form of high TOC values or organic rich deposits has been reported from Canada (Stewart *et al.*, 1992) the Arabian Peninsula and the U.S. Gulf Coast (Dromart *et al.*, 2003b). The TOC data presented here (Fig. 5.11) is relatively low (with an average value of ~2.0 wt % *cf.* ~11 wt % as reported from Canada (Stewart *et al.*, 1992)), however, this may be because the

depositional environment at this location was not favourable to organic matter preservation. The TOC data may still support the idea of increased organic carbon burial however, as a slight increase in values is seen during the Oxfordian.

Middle Oxfordian (*Transversarium* and *Bifurcatus* zones) negative carbon isotope excursions have been identified by Padden *et al.* (2001, 2002) in the Tethyan region (Switzerland and France) (Fig. 5.15). The observed excursions are relatively brief and of a high magnitude (2 ‰ in marine carbonates) leading to the suggestion that they may be associated with episodes of methane release as the excursions are of a similar magnitude and duration to the Toarcian, Aptian and Palaeocene events, which have been more firmly attributed to the dissociation of oceanic methane hydrates (Padden *et al.*, 2001). These negative excursions are not identified in the Staffin Bay data however. Small and brief negative excursions are observed in both the organic and carbonate records (~1.5 ‰), although these occur much earlier than those observed in the Tethys (in the *Vertebrale* Subzone and *Cordatum* Subzone respectively). These somewhat indistinct excursions could easily be explained by a slight fluctuation in the organic matter source (wood record) or natural variability in the data (carbonate record). It should be further noted that the negative excursion recorded in the organic carbon isotope data occurs almost immediately after the Middle Oxfordian positive $\delta^{13}\text{C}$ excursion maximum. Pearce *et al.* (2005) suggest that this relationship is compatible with the theory that a relative sea-level rise associated with the reopening of Boreal-Tethyan oceanic connections changed oceanic circulation and released methane.

Pearce *et al.* (2005) did not observe the negative carbon isotope excursions in either their Staffin Bay or Dorset datasets. They suggested that this may have been the result of an insufficient sampling resolution. However, the greatly improved sampling resolution employed here, indicates that the negative excursions observed in the Tethyan region are not occurring in this part of the Sub-Boreal Realm. This would suggest that the negative excursions identified by Padden *et al.* (2001, 2002) may not be the result of fluctuations in

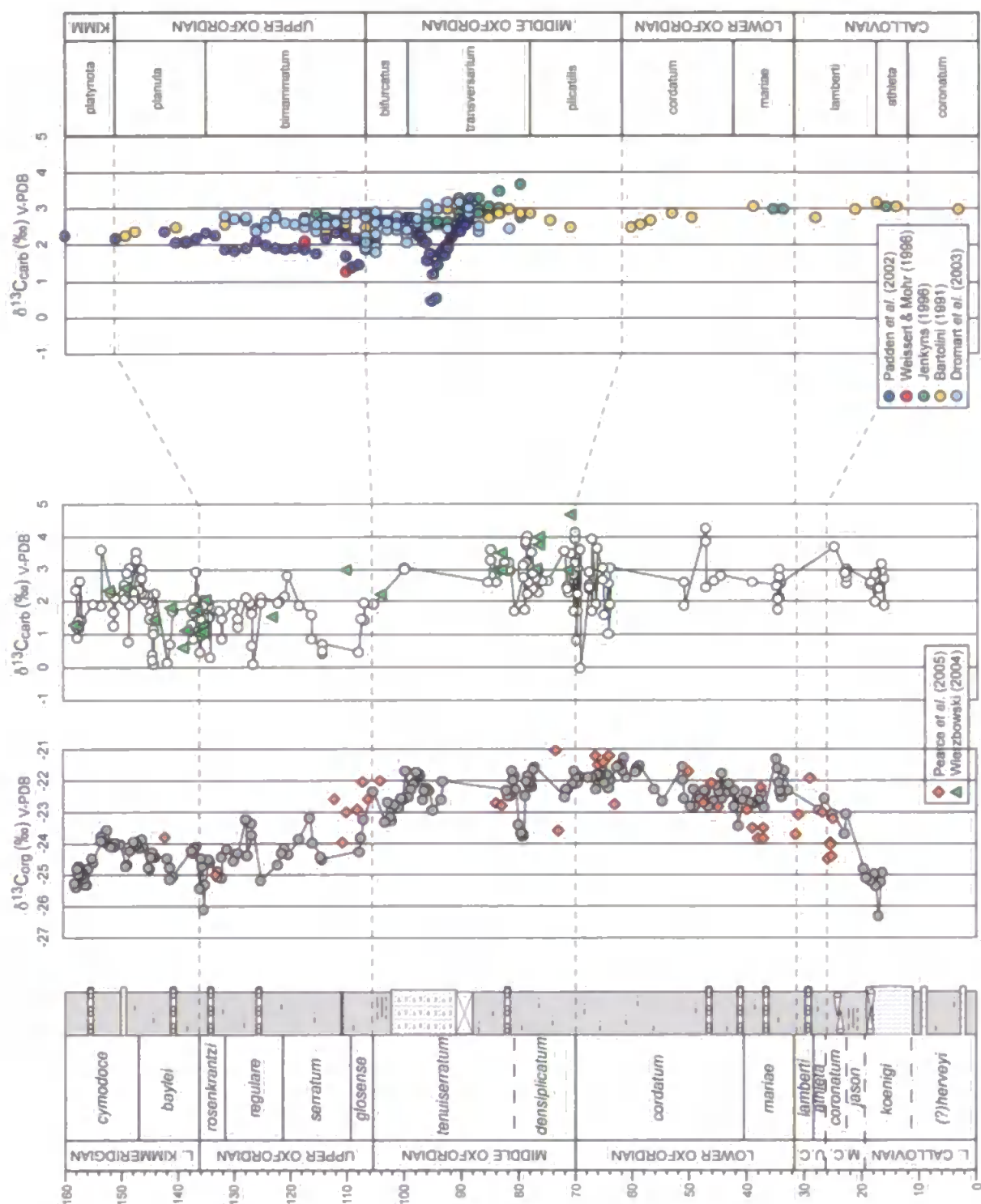


Figure 5.15 Callovian-Lower Kimmeridgian $\delta^{13}\text{C}$ correlation between a composite Tethyan $\delta^{13}\text{C}_{\text{carb}}$ curve and the $\delta^{13}\text{C}_{\text{carb}}$ and $\delta^{13}\text{C}_{\text{org}}$ curves from Staffin Bay, Isle of Skye, Scotland. The Tethyan data was collected from the following locations: Bartolini (1991) - Italy; Jenkyns (1996) - Italy; Weissert & Mohr (1996) - E. Switzerland; Padden *et al.* (2002) - S. Alps, S. Switzerland; Dromart *et al.* (2003b) - France. For Staffin Bay curve Boreal (British) ammonite zonation is illustrated and scale is in metres. See Figure 4.2 for key to log symbols. For Tethyan curve Tethyan ammonite zonation is illustrated.

the total exchangeable carbon reservoir and that perhaps the global scenario needs to be revisited.

5.6. Conclusions

- The data presented here comprise the first combined high-resolution isotope investigation of $\delta^{13}\text{C}_{\text{org}}$, $\delta^{13}\text{C}_{\text{carb}}$ and $\delta^{18}\text{O}_{\text{carb}}$ from Staffin Bay, Isle of Skye. It is also the first ever investigation of a coeval $\delta^{13}\text{C}_{\text{org}}$ and $\delta^{13}\text{C}_{\text{carb}}$ record (together with the data presented in Chapter 7), the development of which is essential to understanding ocean-atmosphere interactions.
- The average palaeotemperature derived from the Staffin Bay $\delta^{18}\text{O}$ record (using the Anderson & Arthur (1983) equation) was 12.4°C and the palaeotemperature range was 6.7°C to 20.6°C for the Callovian-Kimmeridgian interval.
- The average palaeotemperature derived from the Staffin Bay Mg/Ca record (using the Klein *et al.* (1996) equation) was 3.8°C and the palaeotemperature range was -1.3°C to 21.2°C for the Callovian-Kimmeridgian interval. This average palaeotemperature is intuitively unlikely, suggesting that the use of belemnite Mg/Ca as a palaeotemperature proxy may require further investigation.
- The $\delta^{13}\text{C}_{\text{org}}$ data record a broad Lower-Middle Oxfordian positive carbon isotope excursion of ~5 ‰. A return to pre-excursion values occurs from the Upper Oxfordian and into the Lower Kimmeridgian, although, a brief positive fluctuation is observed during the Lower Kimmeridgian *Cymodoce* Zone. This long-term trend is also observed in the $\delta^{13}\text{C}_{\text{carb}}$ data, although the magnitude of the trend is approximately half that of the $\delta^{13}\text{C}_{\text{org}}$ record (this is typical of other records). This correlation indicates a strong coupling of the ocean-atmosphere system at this time and suggests that the total exchangeable carbon reservoir was affected. Such a relationship has never before been observed from a coeval marine and terrestrial record.

- There is a possible decoupling of the ocean-atmosphere system during the Callovian. At this time a large shift of $\delta^{13}\text{C}_{\text{org}}$ values occurs, whilst $\delta^{13}\text{C}_{\text{carb}}$ values remain fairly constant. This indicates that there may have been a local influence on the marine or terrestrial realm during the Callovian period, although the nature of this influence is unclear.
- The Middle Oxfordian positive $\delta^{13}\text{C}$ excursion maximum occurs earlier in the Staffin Bay record (*Cordatum-Vertebrata* Subzonal boundary) than it does in the Tethyan records (*Tenuiserratum* Subzone). However, consistently high values are observed at Staffin Bay until the end of the *Tenuiserratum* Zone. This positive excursion is believed to be the result of an increase in global organic carbon burial rates.
- The mid-Oxfordian negative carbon isotope excursions previously identified in the Tethyan regions are not recorded in the Staffin Bay data despite the relatively high sampling resolution and good biostratigraphic control. These negative excursions have previously been attributed to methane release, however, this new data indicates that the Tethyan excursions may not represent fluctuations in the total exchangeable carbon reservoir and therefore the fidelity of the methane hypothesis should be re-evaluated.

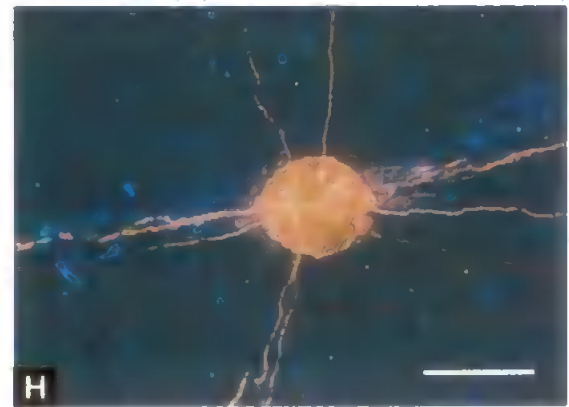
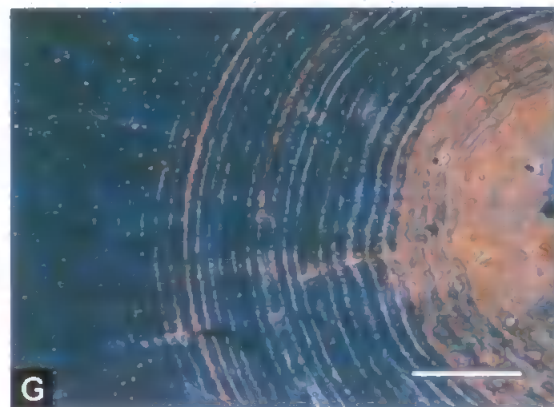
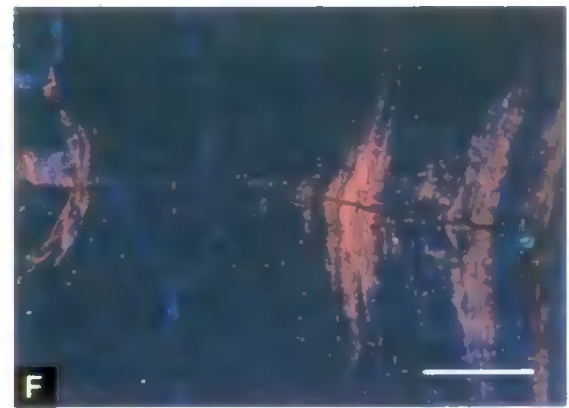
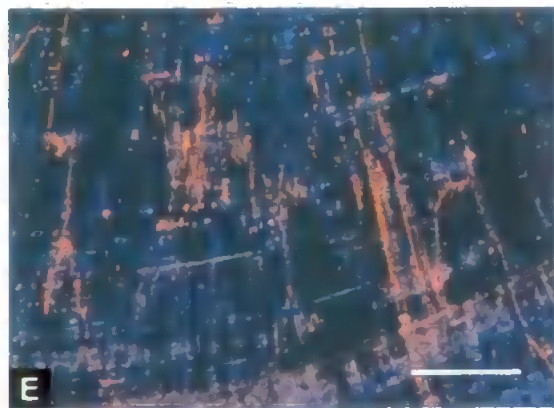
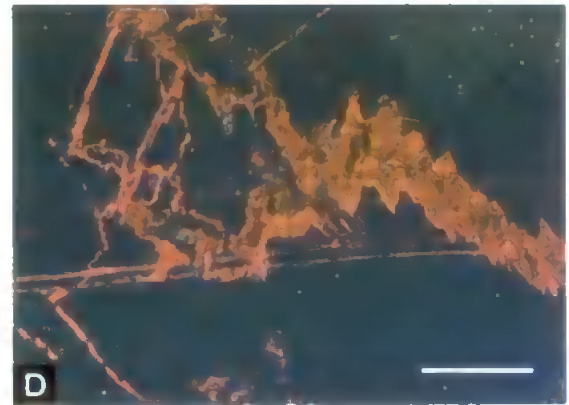
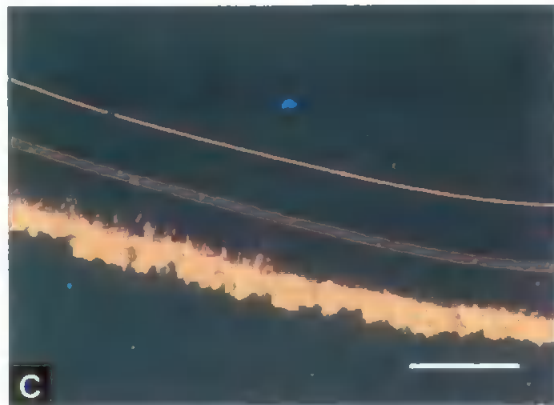
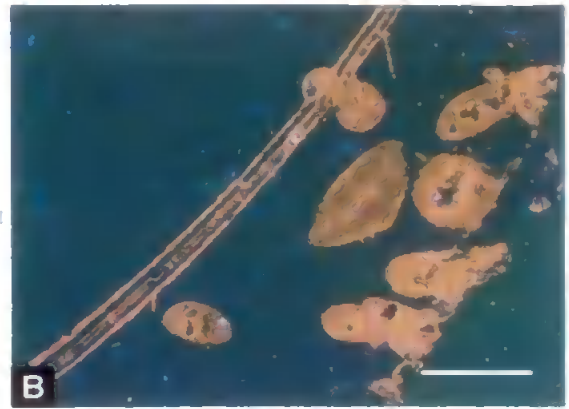
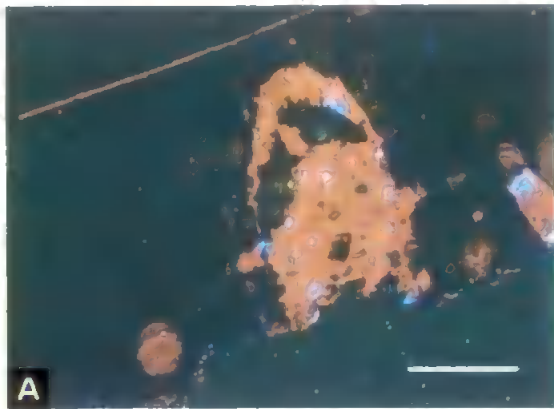


Plate 4. Cathodoluminescence images showing the state of preservation of belemnite rostra from Staffin Bay, Isle of Skye, Scotland. All scale bars represent 1 mm. (A) Borings in rostrum margin infilled with diagenetic cement. (B) Borings in rostrum margin infilled by diagenetic cement. (C) Rostrum margin and growth bands showing alteration. (D) Fractures displaying alteration. (E) Fractures and growth lines displaying alteration. (F) Fractures and growth lines displaying alteration. (G) Apical canal with sediment infilling and growth bands displaying alteration. (H) Diagenetically altered fractures emanating from the apical canal.

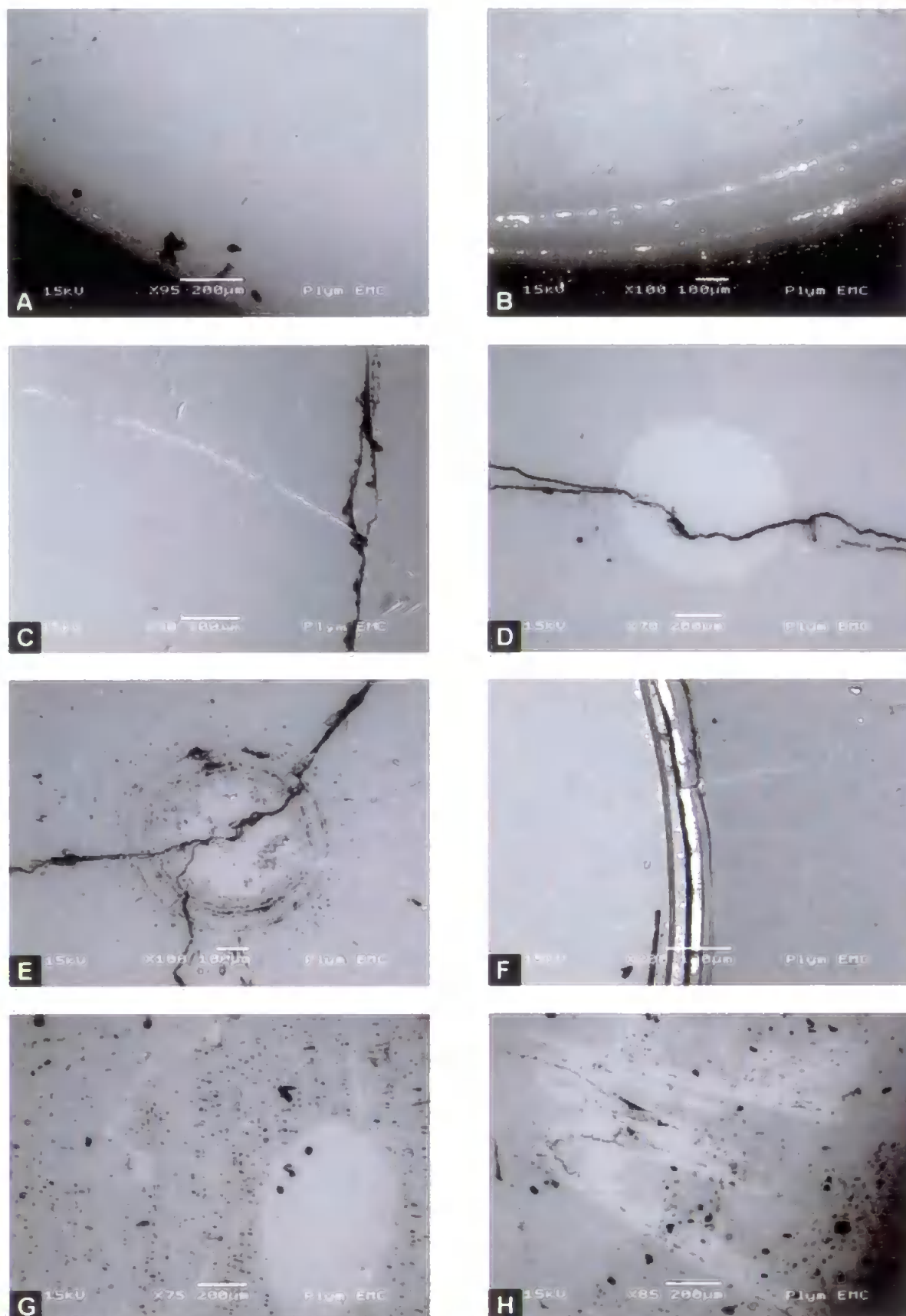


Plate 2. Backscattered SEM images showing the state of preservation of belemnite rostra from Staffin Bay, Isle of Skye. All scale bars represent lengths stated on images. (A) Well preserved calcite with some slight alteration at rostrum margin. (B) Generally well preserved calcite but with some pyrite growth along growth lines towards the rostrum margin. (C) Pyrite growth along fracture. (D) Fracture running through diagenetically altered apical canal. (E) Apical canal and surrounding growth lines displaying alteration. (F) Edge of apical canal with presence of pyrite. (G) Area of altered calcite. (H) Area of altered calcite around fractures.

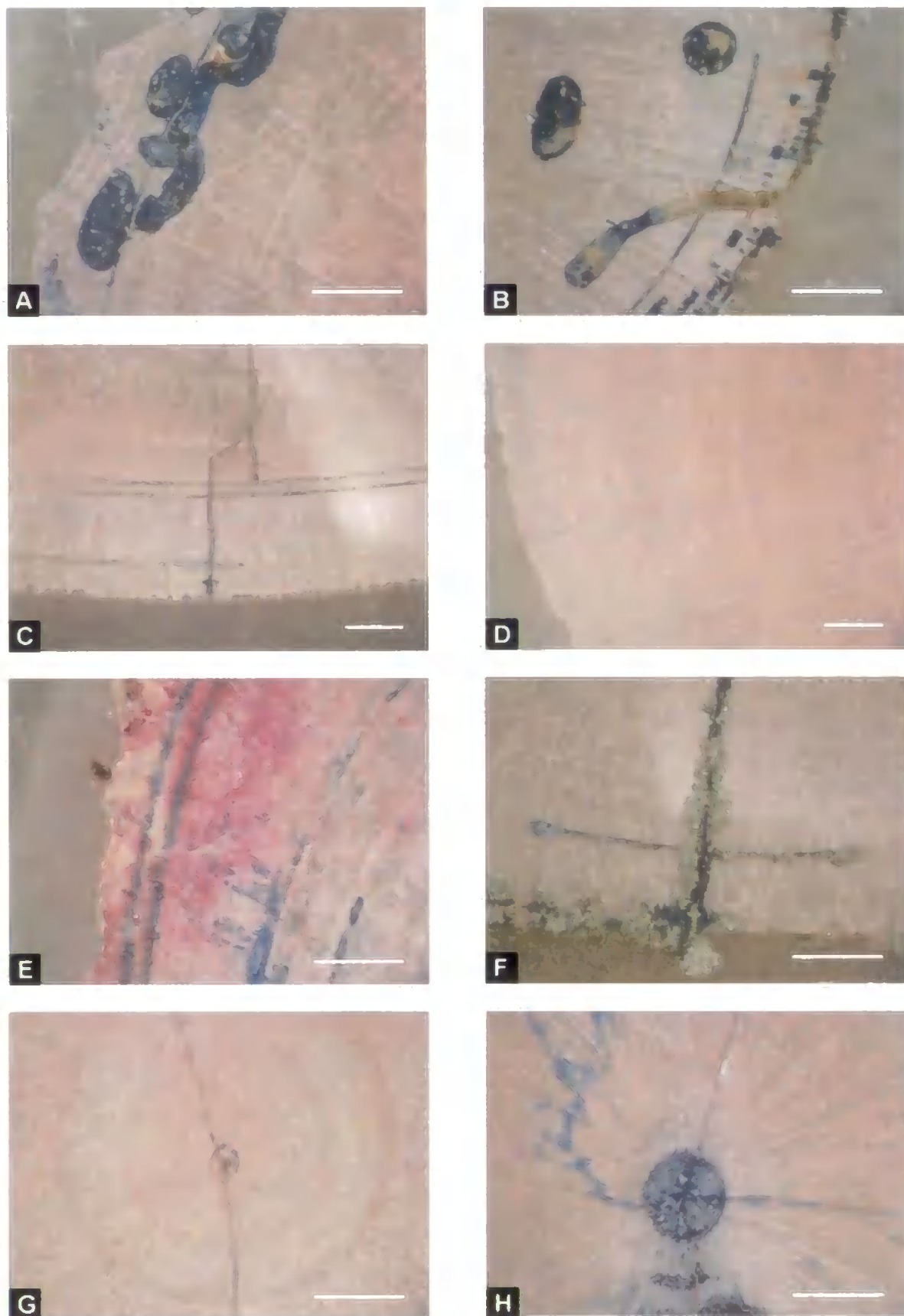


Plate 3. Carbonate stained images showing the state of preservation of belemnite rostra from Staffin Bay, Isle of Skye. All scale bars represent 1 mm. (A) Rostrum margin with borings infilled with diagenetic cement. (B) Rostrum margin with borings infilled with diagenetic cement. (C) Fractures and sections of growth lines displaying alteration, although otherwise well preserved. (D) Very well preserved calcite. No alteration present. (E) Rostrum margin showing alteration particularly along growth lines. (F) Fracture infilled with diagenetic cement and displaying pyritisation. (G) Faint fracture running through apical canal. (H) Apical canal with quartz replacement and fractures displaying alteration.

6. HELMSDALE, SUTHERLAND, SCOTLAND

6.1. Location & Site Description

Helmsdale is located on the eastern coast of Sutherland (at $\sim 58^\circ\text{N}$), on the northeast coast of the Scottish mainland near Wick (Fig. 6.1). Five sites were examined along the coastline near Helmsdale between Kintradwell and Dùn Glas. In addition a further two sites were examined; Brora, approximately 15 km south of Helmsdale and Eathie Haven, 55 km south of Helmsdale near Cromarty on the northeast tip of the Black Isle.



Figure 6.1 Location map of the Sutherland coastal region. The relative positions of Helmsdale; Brora, Eathie and Staffin (Isle of Skye) are shown (left). Also shown are the locations of the sites examined along the coast between Brora and Dùn Glas (right).

The Sutherland outcrops comprise predominantly of intermittent foreshore exposures of boulder beds, mudstones, siltstones and sandstones (Fig. 6.2). Several of the outcrops were accessible only at low tide and were covered by a mobile boulder beach and seaweed.

The Helmsdale succession provides an almost complete record of the Kimmeridgian (*sensu anglico* – see Chapter 2) *Cymodoce* to *Fittoni* ammonite zones. The Eathie section is Early Kimmeridgian (*Mutabilis* Zone) in age and the Brora section is Middle/Late Callovian in age.



Figure 6.2 Foreshore exposure typical of the area around the Helmsdale coast, Sutherland, Scotland. This photograph shows the exposure near Helmsdale Harbour (location HL5), which is part of the Portgower Boulder Beds Member.

6.2. Geological Setting

During the Jurassic Period, Scotland was situated at a palaeolatitude of approximately 45°N (Smith *et al.*, 1994). The coastal onshore Jurassic strata of northeast Scotland (e.g., at Brora, Helmsdale and Eathie) outcrop on the faulted western margin of the Inner Moray Firth Basin (Wignall & Pickering, 1993; Riding, 2005), which is part of the North Sea Basin system (Underhill, 1991) (Fig. 5.3). The Inner Moray Firth Basin was initiated in the Permian (Trewin *et al.*, 1990) and during the Mesozoic was controlled principally by two major extensional events (pre-Jurassic and Late Jurassic) (Underhill, 1991).

The basin is bounded on the north, northwest and south margins by the Wick, Helmsdale and Banff fault systems respectively (Trewin *et al.*, 1990; Underhill, 1991) and the Helmsdale and Great Glen faults separate the Helmsdale Terrace from the rest of the

basin (Wignall & Pickering, 1993) (Fig. 6.3). The Helmsdale fault was active during the Jurassic and fault controlled Kimmeridgian deposition occurred on a proximal slope to deep marine system on the downthrow side (southeast) of the fault (Pickering, 1984; Trewin *et al.*, 1990).

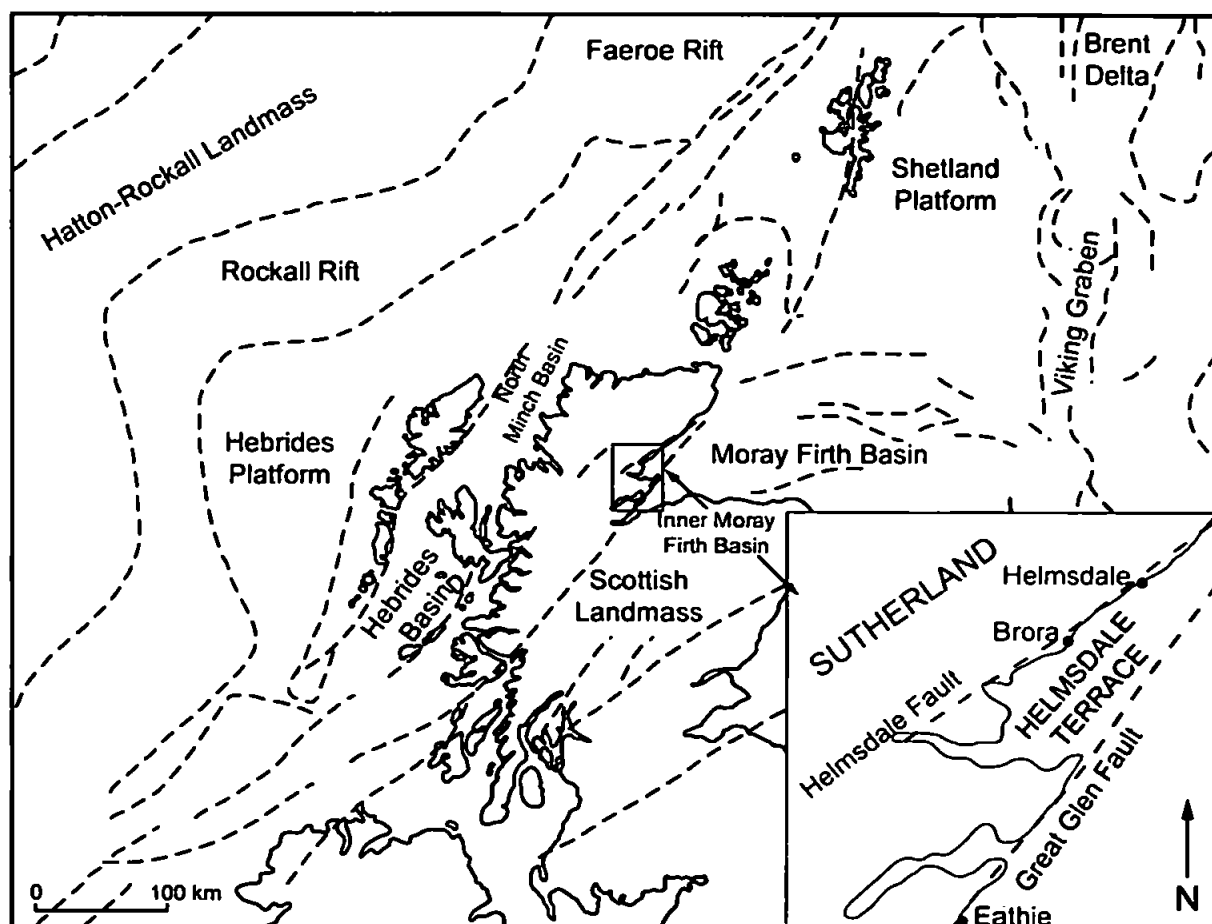


Figure 6.3 Late Jurassic palaeogeography. Inset is a locality map of the study area showing the Helmsdale Terrace and onshore outcrops of Jurassic strata. Palaeogeography map adapted after Hudson & Trewin (2002). Inset adapted after Wignall & Pickering (1993).

The basement of the Moray Firth Basin is composed of Moinian metasediments, intruded by the late Caledonian Helmsdale Granite and is unconformably overlain by Devonian Old Red Sandstone strata (Trewin *et al.*, 1990; Riding, 2005). The centre of Moray Firth deposition was situated offshore, 25 km east of Helmsdale, where the Jurassic succession reaches a thickness of ~ 2300 m (Chesher & Lawson, 1983; Riding, 2005). The most extensive and complete onshore outcrops are located on the Brora, Golspie and Dùn Glas foreshores (Riding, 2005) providing a narrow coastal strip of Jurassic outcrop bordering the margin of the Moray Firth Basin (Trewin *et al.*, 1990). The narrow outcrop

of Kimmeridgian strata in Helmsdale is the most extensive Kimmeridgian outcrop in Britain, excluding that of the Dorset coast (Cox, 2001b).

Three major formations make up the Bathonian to Upper Kimmeridgian (*sensu anglico*) strata of the Brora-Helmsdale region. These are the Bathonian-Callovian Brora Shale Formation; the Callovian-Oxfordian Clynekirkton Sandstone Formation; and the Kimmeridgian Helmsdale Boulder Beds Formation (BGS sheet S103EC, 1998) (Fig. 6.4).

UPPER JURASSIC	KIMMERIDGIAN	<i>cymodoce - fittoni</i>	HELMSDALE BOULDER BEDS FORMATION	~500m	Portgower Boulder Beds Mbr.
					Lothbeg Shale Mbr.
					Kintradwell Boulder Beds Mbr. / Allt na Cuile Sandstone Mbr.
	OXFORDIAN	<i>athleta - baylei</i>	CLYNEKIRKTON SANDSTONE FORMATION	~450m	Ardassie Limestone
					Brora-Clynesh Quarry-Fascally Ssts.
					Fascally Siltstone
	BATHONIAN - CALLOVIAN	? - <i>coronatum</i>	BRORA SHALE FORMATION	~150m	Brora Brick Clay
					Glaucinitic Sandstone
					Brora Shale
					Brora Coal
					Inverbrora Shale
					Doll Sandstone

Figure 6.4 Stratigraphic chart for the Middle-Upper Jurassic of the Brora-Helmsdale region. Data from BGS sheet S103EC, 1998.

The Brora Shale Formation (Bathonian to Middle Callovian, *Coronatum* Zone) is composed of the following units: Doll Sandstone (oldest), Inverbrora Shale, Brora Coal, Brora Shale, a Glaucinitic Sandstone and the Brora Brick Clay (youngest) (BGS sheet S103EC, 1998). The formation is exposed on the foreshore south of Brora and on the banks of the Brora River (Sykes, 1975; Trewin *et al.*, 1990; BGS sheet S103EC, 1998). It is dominated by silty to shaly mudstones, with some bioturbation (Neves & Selley, 1975; Sykes, 1975; Trewin *et al.*, 1990). The Bathonian Doll Sandstone Member at the base of

the formation is a cross-bedded sandstone containing plants and rootlets, which has been interpreted as fluvial or deltaic in origin (Hurst, 1981; Trewin *et al.*, 1990). The other units represent lagoonal conditions (the Inverbrora Shale) followed by a transgressive event (at the base of the Brora Shale Member) and subsequent marine regression (Trewin *et al.*, 1990). Belemnites are common in this formation, particularly within the Brora Shale, Glauconitic Sandstone and Brora Brick Clay members, which have a greater marine influence (Lee, 1925; Sykes, 1975; MacLennan & Trewin, 1989; Trewin *et al.*, 1990).

The Fascally Siltstone, Brora-Clynelish Quarry-Fascally Sandstone and Ardassie Limestone make up the Clynekirkton Sandstone Formation (*Athleta* to *Baylei* zones) (BGS sheet S103EC, 1998). This formation coarsens upwards slightly from bioturbated siltstones at the base (Fascally Siltstone), to fine-grained sandstones, with some rounded pebbles and trough cross-bedding towards the top of the Brora-Clynelish Quarry-Fascally Sandstone Member (Sykes, 1975; Trewin *et al.*, 1990). The ~12 m thick, Ardassie Limestone is composed of alternating calcareous sandstones and limestones, with the limestones reportedly comprised almost entirely of *Rhaxella* sponge spicules that have been replaced by calcite (Sykes, 1975; Trewin *et al.*, 1990). The sandstone facies of this formation were deposited on a coastal marine shelf during a period of marine regression, whilst the Ardassie Limestone, was deposited under transgressive conditions (Trewin *et al.*, 1990). The Clynekirkton Sandstone Formation is exposed on the foreshore near the mouth of the Brora River and along the rivers banks (Lee, 1925; Trewin *et al.*, 1990; BGS sheet S103EC, 1998). It is also exposed at Ardassie Point, just north of Brora (Lee, 1925; Trewin *et al.*, 1990; BGS sheet S103EC, 1998). Belemnites have been observed throughout the Clynekirkton Sandstone Formation (Lee, 1925; Trewin *et al.*, 1990).

The Helmsdale Boulder Beds (*Cymodoce* to *Albani* zones) include the Kintradwell Boulder Beds Member, the Allt na Cuile Sandstone Member, the Lothbeg Shale Member and the Portgower Boulder Beds Member (youngest) (BGS sheet S103EC, 1998). The Allt na Cuile Sandstone Member and the Kintradwell Boulder Beds Member are believed to be

lateral equivalents of each other, demonstrating the sedimentological variability occurring along an active fault (Trewin *et al.*, 1990). The Allt na Cuile Sandstones are medium to fine-grained and are often planar-laminated (Brookfield, 1976; Pickering, 1984; Trewin *et al.*, 1990; Wignall & Pickering, 1993). In places they are extensively veined due to their proximity to the active Helmsdale Fault (Trewin *et al.*, 1990). By comparison, the Kintradwell Boulder Beds are dominated by finely-laminated and fissile siltstones that contain rounded clasts, presumably derived from earlier Jurassic formations (Roberts, 1989; Tyson, 1989; Wignall & Pickering, 1993). Wignall & Pickering (1993) remark that perhaps the most spectacular feature of the Kintradwell Boulder Beds is the abundant evidence for syndepositional deformation. These facies are exposed on the coastal foreshore between Kintradwell and Lothbeg Point (Trewin *et al.*, 1990), although exposure is often limited by an extensive cover of seaweed. Small, isolated outcrops of the Kintradwell Boulder Beds are distributed along the coastline. The boulder beds were observed to contain relatively abundant sandstone clasts, wood debris, occasional belemnites and rare partial ammonite clasts.

Also exposed at Lothbeg point is the Lothbeg Shale Member, which overlies the Allt na Cuile Sandstone and Kintradwell Boulder Beds. It is composed of interbedded shaly mudstones, siltstones and sandstones (Trewin *et al.*, 1990; Wignall & Pickering, 1993). Again the outcrop is extensively covered by seaweed, although interbedded mudstones, siltstones and sandstones were observed, some containing slumps and folds resulting from wet sediment deformation. This unit is overlain by the Portgower Boulder Beds Member, which is exposed on the coast from Lothbeg Point to Dùn Glas, northeast of Helmsdale (Trewin *et al.*, 1990; BGS sheet S103EC, 1998). These boulder beds have been described in detail by Pickering (1984) and Wignall & Pickering (1993). The boulder beds are supported by a sandstone matrix and separated by interbedded sandstones and siltstones, some of which have been described as 'tiger-strip' facies (Pickering, 1984; Trewin *et al.*, 1990; Wignall & Pickering, 1993). The boulder bed clasts are mostly

subrounded to subangular and are typically derived from Devonian and Jurassic lithologies (Pickering, 1984; Trewin *et al.*, 1990; Wignall & Pickering, 1993). Synsedimentary wet-sediment deformation structures are common in these boulder beds (Wignall & Pickering, 1993). The exposure of the Portgower Boulder Beds Member north of Helmsdale Harbour is particularly good. The clasts within the boulder beds become more angular and chaotic up sequence and bedding becomes more difficult to discern. Belemnites are relatively abundant components in parts of the boulder bed succession and corals, gastropods, crinoids, bivalves and occasionally ammonites were also observed.

In the earliest Kimmeridgian, onset of activity along the Helmsdale Fault changed the environment of deposition from a broad, shallow marine shelf (on which the Clynekirkton Sandstone Formation was predominantly deposited) to a rapidly subsiding palaeoslope on which debris flow, rock slide and turbidity current deposition alternated with poorly oxygenated hemipelagic deposition (Pickering, 1984; Wignall & Pickering, 1993). Wignall & Pickering (1993) concluded that the deepest waters were located immediately next to the Helmsdale fault scarp, which would account for the more diverse benthic fauna observed in the lithologies at the Eathie location, representing shallower water conditions (Fig. 6.3).

6.3. Sampling & Methodology

The five main sites examined in the Helmsdale region provided samples from the Early Kimmeridgian (*Cymodoce* Zone) to latest Kimmeridgian (*Fittoni* Zone). These key sites provided an extension of the Early Kimmeridgian samples collected at Staffin Bay, Isle of Skye. In addition, the site visited in Brora (at which only 1 belemnite horizon was sampled) was Callovian in age (*Koenigi* Zone) and the site at Eathie (from which 9 belemnite horizons were sampled) was Early Kimmeridgian (*Mutabilis* Zone). In total, 58 belemnite horizons were sampled from the Sutherland region. Complete specimens were very rare from the Helmsdale region because the belemnites were generally well cemented

within the rock so that only fragments could be collected (Fig. 6.5). This was not the case at Brora or Eathie however, where more complete samples were collected from mudstones/siltstones. No sediment samples were collected from this region. Wherever possible multiple specimens were collected from the belemnite horizons. All samples were collected in June 2005.

The preservation of belemnite rostra was evaluated through trace element and stable isotopic analysis, backscattered scanning electron microscopy (BSEM), cathodoluminescence (CL) and carbonate staining (following the technique of Dickson (1965) and (1966)). The areas most susceptible to diagenesis were removed prior to isotopic and geochemical analysis. Samples were analysed for carbon and oxygen isotopes, with subsamples taken for trace element analysis (Fe, Mn, Ca, Sr, Mg, Na, Li).

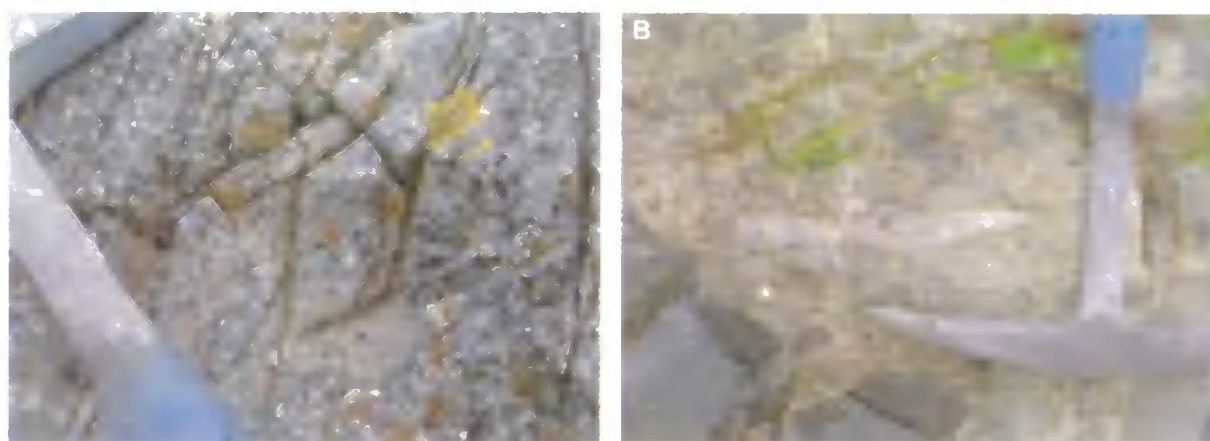


Figure 6.5 Typical preservation of Helmsdale belemnites. (A) Belemnite from the Kintradwell Boulder Beds Member on the Kintradwell coast (location HL1). (B) Belemnites from the Portgower Boulder Beds Member near Helmsdale Harbour (location HL5).

Stable isotope data were generated on a VG Optima mass spectrometer at the NERC Isotope Geosciences Laboratory (NIGL), Keyworth, UK. Trace element data were analysed by Inductively Coupled Plasma-Atomic Emission Spectrometer (ICP-AES) using a Perkin Elmer Optima 3300RL ICP-AES system (with autosampler) at the NERC ICP facility, Department of Geology at Royal Holloway, University of London. For a full description of the methodology used see Chapter 4.

6.4. Results

The belemnites sampled for this study were mostly translucent. The opportunity to conduct BSEM, CL and carbonate staining analysis on these specimens was limited due to lack of complete rostra collected. In total 11 out of 83 specimens were subject to optical analysis (Plates 4-6). Such analysis indicated that the periphery of the rostrum, the areas of the rostrum surrounding the apical canal, prominent fractures and strong growth bands were particularly susceptible to diagenetic alteration. These regions commonly appeared as pale grey-white in colour when subjected to BSEM analysis, luminescent under CL conditions and mauve-blue in colour after carbonate staining and were therefore removed prior to sampling.

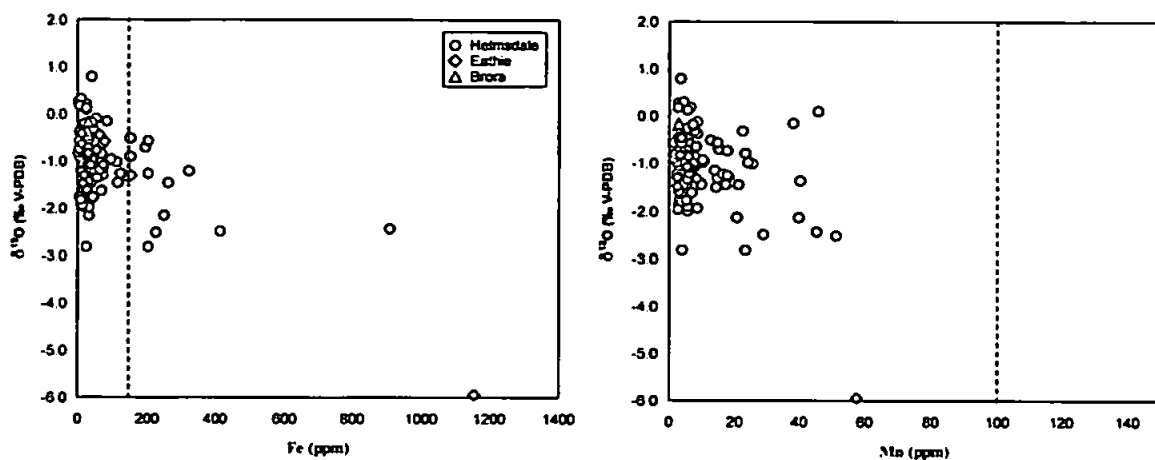


Figure 6.6 Cross-plots of $\delta^{18}\text{O}$ against Fe (left) and Mn (right). The dashed line illustrates the cut off values for well preserved samples.

The Mn and Fe concentrations of the belemnites were also determined in order to provide an additional method by which to assess their state of preservation as noted previously. The determined values of Fe and Mn from the Helmsdale belemnite rostra were 5-910 ppm, mean 78 ppm and 2-51 ppm, mean 11 ppm respectively. The Fe and Mn values for the Eathie belemnites were 26-1154 ppm, mean 142 ppm and 3-57 ppm, mean 8 ppm respectively and the values for the Brora horizon were 30-32 ppm, mean 31 ppm for Fe and a mean of 3 ppm for Mn. Low Fe and Mn values were recorded for most of the

belemnites, with a total of 17 samples rejected from this study on the basis of poor preservation. Trace element data (Fe and Mn) were plotted against $\delta^{18}\text{O}$ to constrain any diagenetic alteration (Fig. 6.6). The higher amounts of Fe and Mn and occasional negative $\delta^{18}\text{O}$ outliers are regarded as an artefact of diagenesis. The lack of correlation between the values, however, suggests minimal post-depositional alteration. Those samples with high Fe or Mn values that are considered to have possibly undergone some level of alteration were excluded from further analysis.

Additional elemental abundances derived from belemnite rostra from Helmsdale were as follows: Sr 676-1918 ppm, mean 1276 ppm, Mg 531-3280 ppm, mean 1189 ppm, Ca 22 % - 42 %, mean 30 %. Abundances for rostra from Eathie were: Sr mean 1172 ppm, Mg 1215-2971 ppm, mean 1792 ppm, Ca 30 % - 31 %, mean 30 %. For Brora the values were: Sr 905-950 ppm, mean 928 ppm, Mg 859-1194 ppm, mean 1066 ppm, Ca mean 30 %.

The oxygen and carbon isotope values of well preserved belemnites from Helmsdale range from -2.84 to 0.78 ‰ and from -2.25 to 2.82 ‰ respectively; from Eathie range from -1.60 to -0.41 ‰ and from 0.15 to 2.27 ‰ respectively; and from Brora range from -0.44 to -0.17 ‰ and 2.16 to 2.96 ‰ respectively. The Brora isotope values are similar to the isotope values derived from Callovian (*Koenigi* Zone) Isle of Skye belemnites, as noted previously. The *Koenigi* Zone is represented on the Isle of Skye by the Belemnite Sands Member (Morton & Hudson, 1995), a sandy glauconitic facies with abundant belemnites towards the top of the unit. The Brora belemnites were also sampled from a sandy, glauconitic unit (Early/Middle Callovian in age) with abundant belemnites. The mean values of $\delta^{18}\text{O}$ and $\delta^{13}\text{C}$ from the Brora belemnite rostra were -0.32 and 2.43 ‰ respectively, compared with values from the Isle of Skye of -0.33 ($\delta^{18}\text{O}$) and 2.65 ‰ ($\delta^{13}\text{C}$).

The oxygen and carbon isotope ratios from Helmsdale (*Cymodoce* to *Fittoni* zones) and Eathie (*Mutabilis* Zone) have some degree of stratigraphic overlap and so are

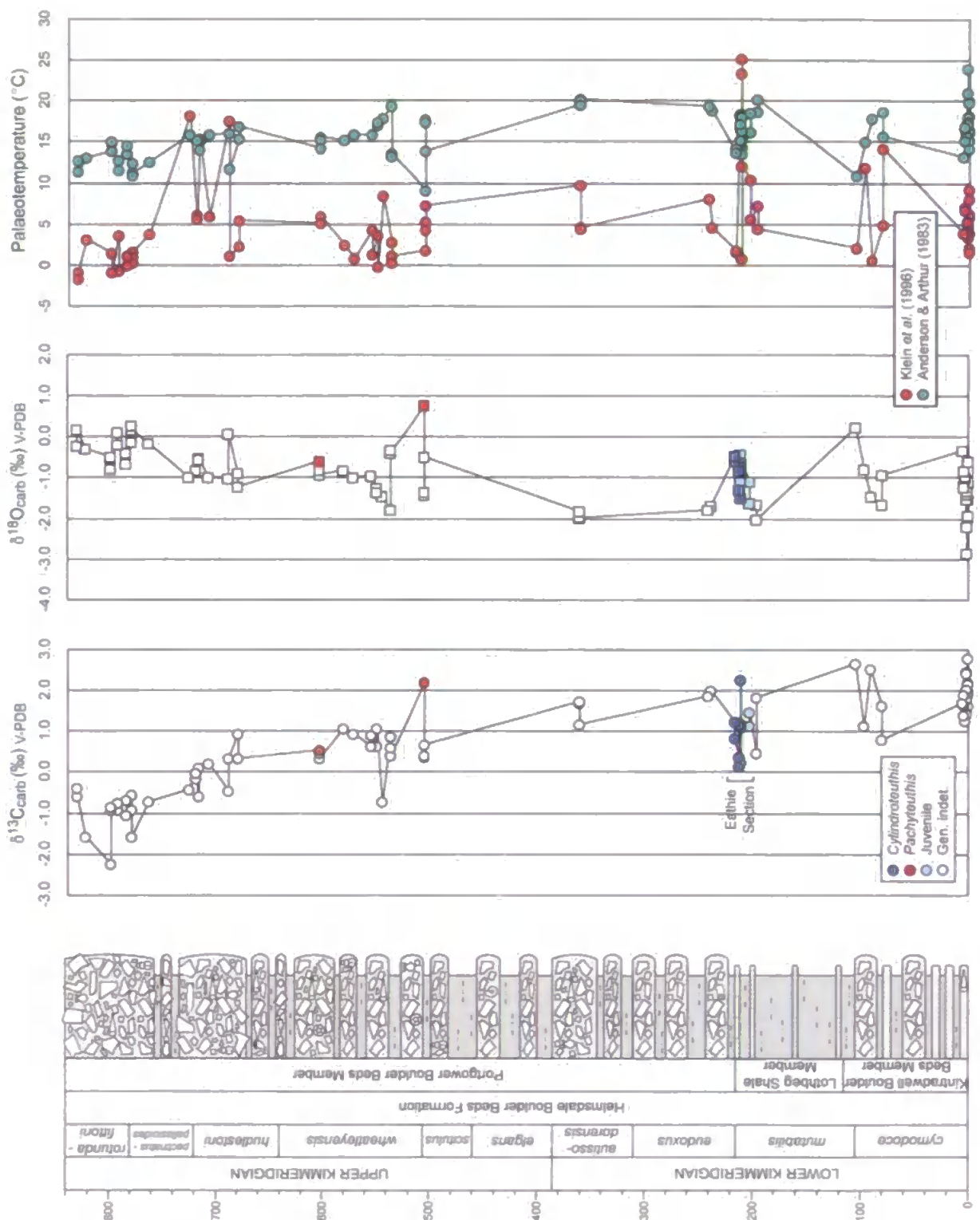


Figure 6.7 $\delta^{13}\text{C}$ and $\delta^{18}\text{O}$ records from the Kimmeridgian succession at Helmsdale and Eathie, Sutherland, Scotland. Boreal British ammonite zones are illustrated here, however, it should be noted that the Upper Kimmeridgian (*sensu anglico*) is equivalent to the Tethyan Lower-Middle Tithonian. See Figure 4.2 for key to log symbols. Scale is in metres.

combined here to provide an almost complete succession of the Kimmeridgian (*Cymodoce* to *Fittoni* zones) for northeast Scotland (Fig. 6.7). Both the oxygen and carbon ratios show short and long-term variation. The overall oxygen isotope trend is one of values becoming gradually more positive, although, shorter-term variability is superimposed on this general trend, particularly for the Early Kimmeridgian *Cymodoce* and *Mutabilis* zones, where values become first more negative (-0.58 to -2.84 ‰) before becoming more positive (-2.84 to -0.41 ‰). From the *Eudoxus* Zone, the oxygen isotope values increase more consistently from -2.00 ‰ to 0.16 ‰ in the *Fittoni* Zone. The carbon isotope ratios generally become more negative throughout the Kimmeridgian, despite some degree of scatter. Values decrease from 2.22 ‰ in the lower *Cymodoce* Zone (where the most positive values can be observed) to -2.25 ‰ in the *Fittoni* Zone (where the most negative values can be observed). Increases in $\delta^{13}\text{C}$ are mirrored by decreases in $\delta^{18}\text{O}$. This is confirmed by a cross-plot of $\delta^{18}\text{O}$ vs. $\delta^{13}\text{C}$ (Pearson's R^2 value, 0.498), which reveals a statistically significant negative correlation (at the 99% confidence level) (Fig. 6.8).

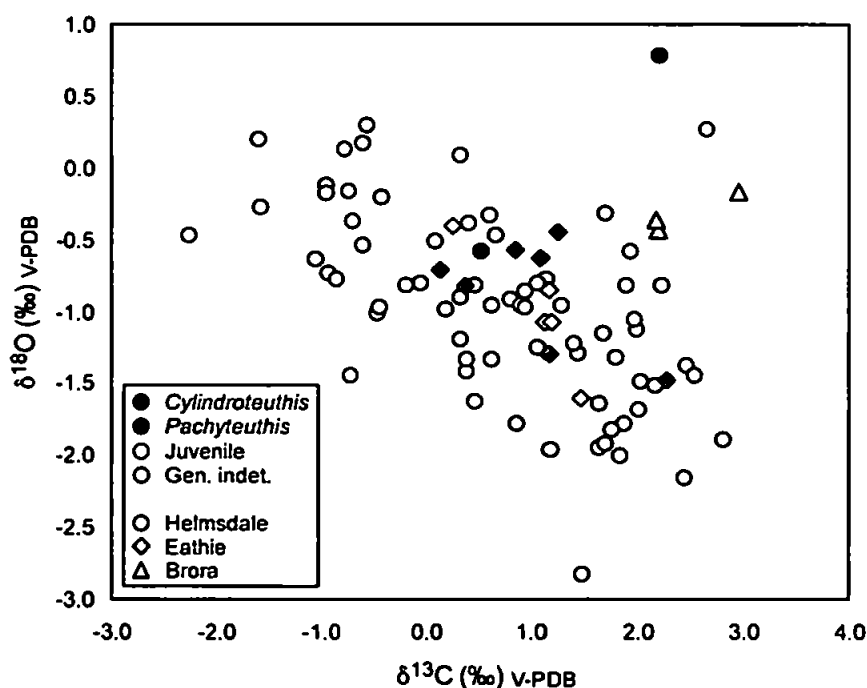


Figure 6.8 Cross-plot of $\delta^{18}\text{O}$ and $\delta^{13}\text{C}$ values from well preserved belemnites from Helmsdale, Eathie and Brora.

The belemnites sampled from these Callovian to Kimmeridgian successions were species of the boreal genera *Pachyteuthis* and *Cylindroteuthis* (although taxonomic identification was not always possible from these locations).

6.5. Discussion

6.5.1. Stable Isotope, Geochemical & Taxonomic Records

As indicated above, taxonomic identification of belemnite rostra was very difficult with specimens from the Helmsdale region. The affect of taxonomic differences on stable isotope and geochemical records is, therefore, almost impossible to assess from this location. Whilst the data available do not indicate a taxonomic influence on the isotopic and elemental records, the limited nature of the data means that such an influence cannot be ruled out.

6.5.2. The Oxygen Isotope Record & Palaeotemperature Implications

The oxygen-isotope data recorded from belemnites from the Helmsdale coast display some degree of scatter. Variation recorded from coeval belemnites ranged from 0.01 ‰ to 2.20 ‰, with an average of 0.59 ‰. This scatter could be the result of diagenetic alteration, salinity fluctuations, generic vital effects or generic palaeoecological variability as noted earlier. Major diagenetic alteration of the specimens has been ruled out by extensive screening, however, generic variations are impossible to rule out from this dataset due to the taxonomic identification problems encountered.

As discussed in Chapters 3 and 5 modern cephalopods are known to secrete their calcite very close to isotopic equilibrium with surrounding seawater (e.g., Taylor & Ward, 1983; Morrison & Brand, 1986; Rosales *et al.*, 2004a; Rexfort & Mutterlose, 2006) and at present no major seasonal or taxonomic differences in fractionation have been confirmed (Sælen *et al.*, 1996; Podlaha *et al.*, 1998; Rosales *et al.*, 2004a), although McArthur *et al.*

(2004) suggest that a small $\delta^{18}\text{O}$ offset (in the region of 0.4 ‰) may be observed between co-occurring specimens of different genera. As such, the $\delta^{18}\text{O}$ data presented here is considered primarily to reflect changes in environmental conditions. McArthur *et al.* (2000) concluded that since belemnites are extinct it is unrealistic to calculate absolute palaeotemperatures from their $\delta^{18}\text{O}$ composition. The palaeotemperatures calculated here should therefore only be regarded as a guide to the potential seawater temperatures in the region.

Palaeotemperatures calculated using the Anderson & Arthur (1983) equation are shown in Figure 6.7. The isotopic composition of the water was assumed to be that of non-glacial seawater at -1 ‰ SMOW (e.g., Marshall, 1992; Sælen *et al.*, 1996; Price & Sellwood, 1997; Podlaha *et al.*, 1998; Price & Mutterlose, 2004; Rosales *et al.*, 2004a, b). The calculated palaeotemperatures range from 9.1 to 24.0°C for the Kimmeridgian interval, with an average palaeotemperature of 15.8°C. This corresponds reasonably well with the Staffin Bay data, which record palaeotemperatures of 6.7°C to 20.6°C, with an average value of 12.4°C for the Callovian-Kimmeridgian interval. The warmest temperatures recorded from Helmsdale occur in the Lower Kimmeridgian *Cymodoce* Zone. Despite the degree of scatter present in the data a general trend of increasing $\delta^{18}\text{O}$ (and therefore decreasing temperature) is observed, particularly from the *Wheatleyensis* to *Fittoni* zones.

6.5.3. The Elemental Records & Palaeotemperature Implications

The use of combined *El/Ca* and $\delta^{18}\text{O}$ palaeotemperature investigations was discussed in Chapter 5. McArthur *et al.* (2000), Bailey *et al.* (2003) and Rosales *et al.* (2004a, b) consider *Mg/Ca* and *Sr/Ca* to be the most useful ratios with which to investigate palaeoclimate, whilst *Na/Ca* and *Li/Ca* are of more limited use. *Mg/Ca*, *Sr/Ca*, *Na/Ca* and *Li/Ca* ratios were calculated here together with *Mn/Ca* ratios, which were calculated to assess preservation, with those displaying a value exceeding 100 $\mu\text{mol/mol}$ excluded from

further analysis, since McArthur (1994) considers this to be the lower limit for samples that have experienced alteration under reducing conditions.

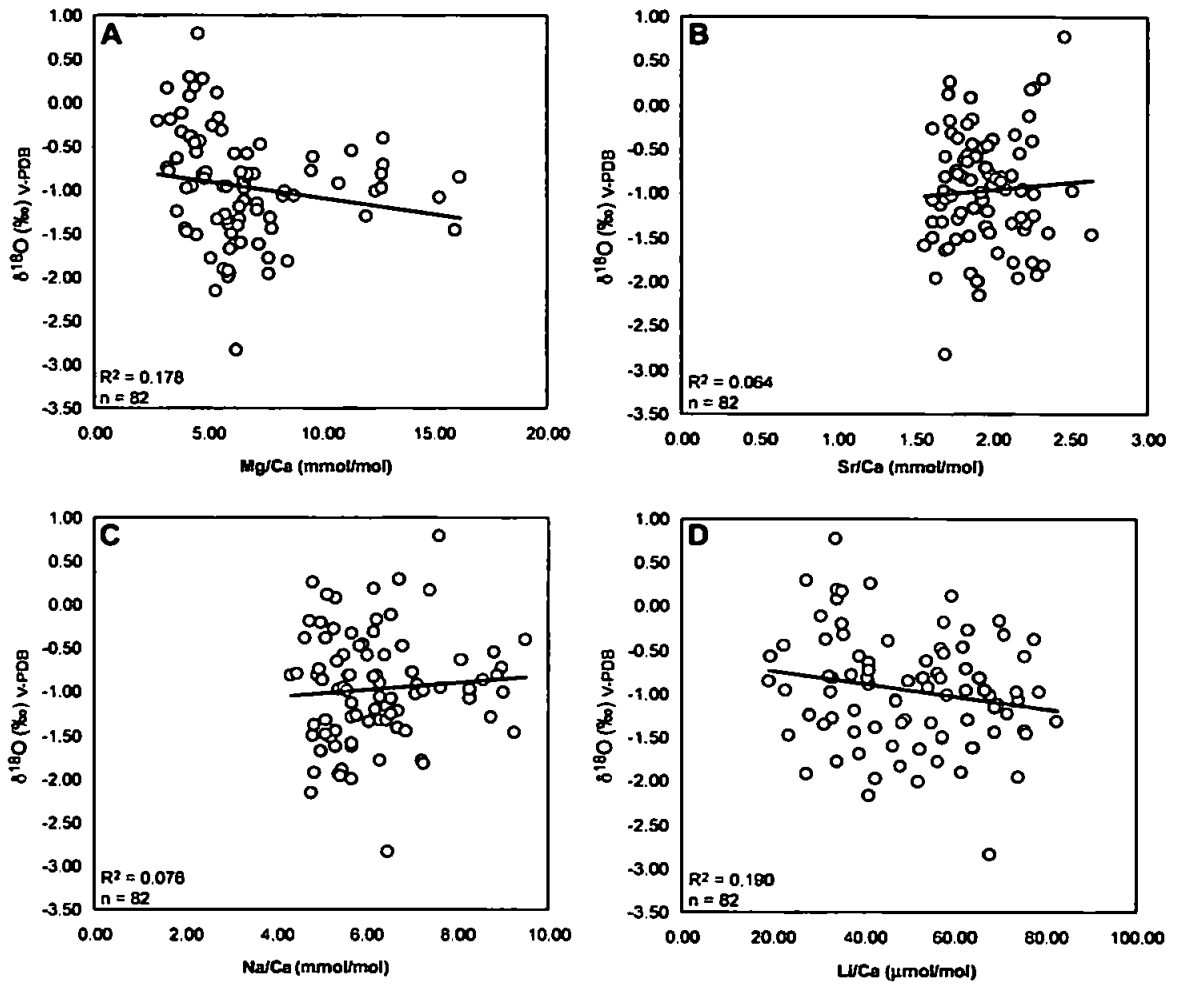


Figure 6.9 Cross-plots of $\delta^{18}\text{O}$ against (A) Mg/Ca, (B) Sr/Ca, (C) Na/Ca and (D) Li/Ca.

Cross-plots of El/Ca against $\delta^{18}\text{O}$ for the Helmsdale belemnites show no statistically significant correlations (Fig. 6.9). The maximum R^2 value recorded here was 0.190 for Li/Ca and the lowest R^2 value recorded here is between $\delta^{18}\text{O}$ and Sr/Ca, which according the McArthur *et al.* (2000) and Bailey *et al.* (2003) should be one of the strongest correlations. Mg/Ca and Sr/Ca are commonly considered to be the most appropriate El/Ca ratios with which to assess palaeotemperature and R^2 values for these ratios when plotted against $\delta^{18}\text{O}$ are commonly in the region of 0.5 (e.g., McArthur *et al.*, 2000; Bailey *et al.*, 2003). The R^2 values observed for these correlations here however are 0.178 for Mg/Ca and 0.064 for Sr/Ca. This lack of correlation could be the result of the

relatively static nature of the $\delta^{18}\text{O}$ record during the Kimmeridgian. No distinctive long-term trend is discernable for much of this period and the record displays some degree of scatter. This may go some way towards explaining the lack of covariance observed in this succession (much like the Staffin Bay succession).

There are no distinctive long-term trends in the *El/Ca* records (Fig. 6.10). The *Mg/Ca*, *Na/Ca* and *Li/Ca* records are particularly noisy, which may act to obscure a long-term trend if one were present. Some of the observed scatter may be attributed to taxon or ontogenetic variations in the biological regulation of trace elements. For example, foraminifera display an *Mg/Ca* inter-species offset of <1.5 mmol/mol (Lear *et al.*, 2002; Billups & Schrag, 2003; Rosales *et al.*, 2004a). Such processes may be superimposed on the temperature control to contribute to the scatter of the data.

Previous studies have shown that *Mg/Ca* ratios are likely to be controlled mostly by temperature (e.g., McArthur *et al.*, 2000; Bailey *et al.*, 2003; Rosales *et al.*, 2004a, b), whilst *Sr/Ca* ratios are likely to be more significantly influenced by salinity, growth rate and metabolic activity (Klein *et al.*, 1997; Rosales *et al.*, 2004a). The palaeotemperatures calculated using the Klein *et al.* (1996) equation for molluscan *Mg/Ca* ratios are shown in Figure 6.7.

The palaeotemperature range calculated from the *Mg/Ca* ratios is -1.7 to 24.7°C , with an average palaeotemperature for the Kimmeridgian of 5.0°C . The offset observed between average $\delta^{18}\text{O}$ and *Mg/Ca* derived temperatures is on average 10.8°C (compared with an offset of 8.6°C recorded from Staffin Bay). If this temperature difference was interpreted solely as the result of salinity input influencing the $\delta^{18}\text{O}$ record it would require a change in salinity from 34 ‰ (normal marine conditions) to 24.1 ‰, which seems intuitively unlikely as modern *Sepia* have only occasionally been caught in water with a salinity of down to 29 ‰ (Schäfer, 1972; Wierzbowski, 2004). A similar technique was employed by Bailey *et al.* (2003) to investigate the influence of salinity on $\delta^{18}\text{O}$ derived belemnite palaeotemperatures. Bailey *et al.* (2003) calculated a change in temperature

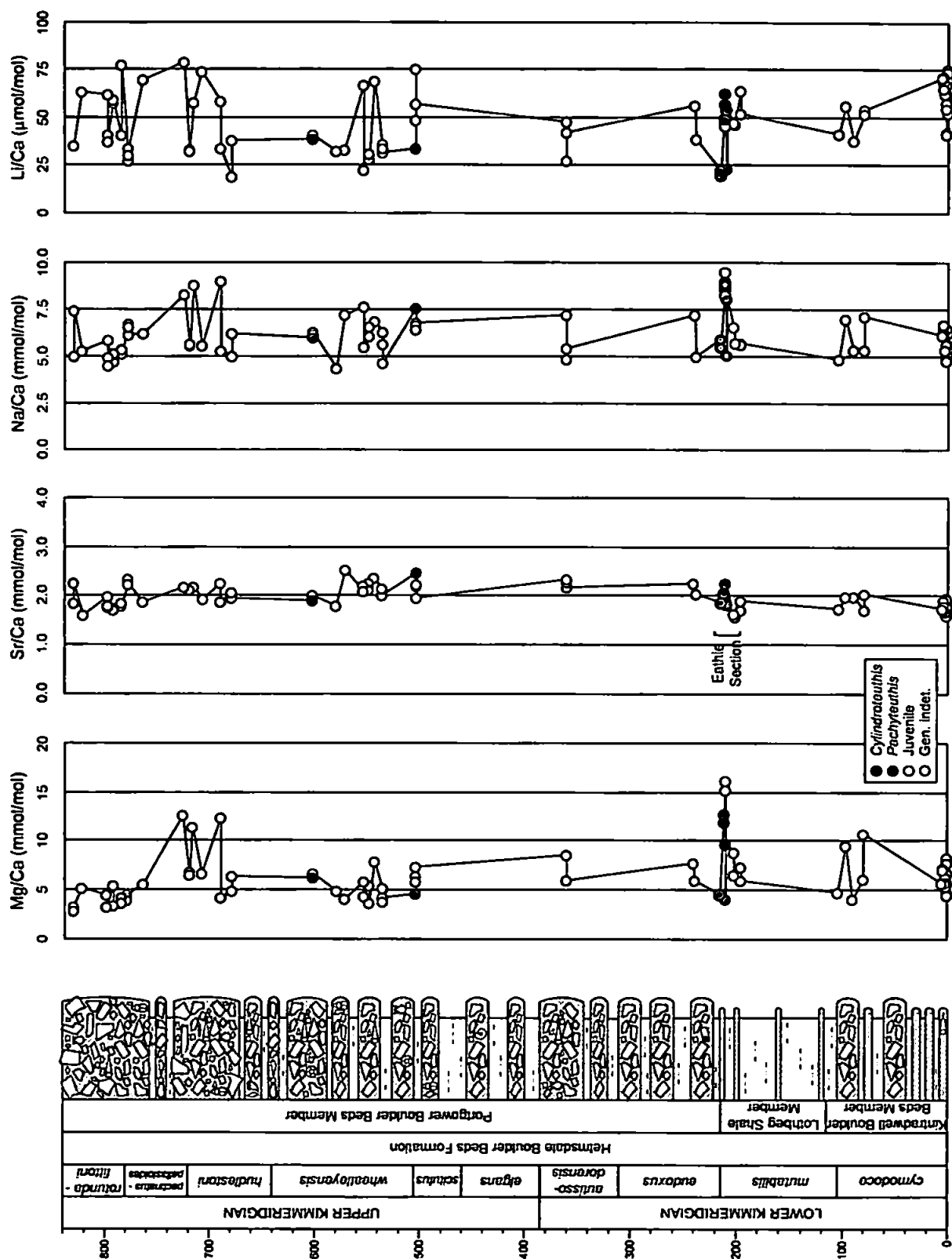


Figure 6.10 Ei/Ca ratios from the Kimmeridgian succession at Helmsdale and Eathie, Sutherland, Scotland. Boreal British ammonite zones are illustrated here, however, it should be noted that the Upper Kimmeridgian (*sensu anglico*) is equivalent to the Tethyan Lower-Middle Tithonian. See Figure 4.2 for key to log symbols. Scale is in metres.

across the Toarcian Ocean Anoxic Event (OAE) from both $\delta^{18}\text{O}$ and Mg/Ca, although their Mg/Ca temperature values were calculated using the equations of Dwyer *et al.* (1995), Elderfield & Ganssen (2000) and Lear *et al.* (2002) for foraminifera and ostracodes. They calculated a $\sim 6^\circ\text{C}$ warming, associated with a substantial freshening of seawater during the OAE event. The use of these equations seems inappropriate however, given that a mollusc-derived equation (that of Klein *et al.* (1996)) also exists.

The lowest palaeotemperatures recorded here occur during the Upper Kimmeridgian *Pectinatus* to *Fittoni* zones in both the Mg/Ca and $\delta^{18}\text{O}$ records. However, the sub-freezing temperatures calculated from the Mg/Ca ratios for this time are impossible since marine cephalopods could not live in these conditions. Immenhauser *et al.* (2005) question the validity of applying the Klein *et al.* (1996) temperature equation to fossilised skeletal calcites. They suggest that it may only be appropriate for temperatures in the range of $5\text{--}23^\circ\text{C}$ where the temperature-Mg relationship is linear and go on to suggest that the utility of Mg/Ca ratios may be limited by the ion regulating capability of the animals being considered. The data presented here lends support to the idea that the application of the Klein *et al.* (1996) palaeotemperature equation should be used with caution.

6.5.4. The Carbon Isotope Record

The marine carbonate $\delta^{13}\text{C}$ record shows a distinctive long-term trend towards more negative values throughout the Kimmeridgian (*sensu anglico*) interval (Fig. 6.7). Typical Early Kimmeridgian *Cymodoce* Zone values range between 1.3 and 2.8 ‰ compared with Late Kimmeridgian *Pectinatus*-*Fittoni* Zone values of -2.2 to -0.4 ‰. This trend is observed here despite some scatter in the belemnite data. The scatter however is consistent with that observed in other belemnite records (e.g., Bailey *et al.*, 2003; McArthur *et al.*, 2004; Rosales *et al.*, 2004a, 2006; Price & Mutterlose, 2004; Wierzbowski, 2004).

A gradual shift to more negative $\delta^{13}\text{C}$ values as observed here requires a continued input of ^{12}C to the oceanic carbon reservoir and consequently the incorporation of ^{12}C into the belemnite calcite. A decrease in $\delta^{13}\text{C}$ ratios could be caused by upwelling of cold bottom waters enriched in ^{12}C (Küspert, 1982; Price & Gröcke, 2002), methane release from the dissociation of gas hydrates (e.g., Dickens *et al.*, 1995; Padden *et al.*, 2001), volcanism (e.g., Hesselbo *et al.*, 2002), or low carbon burial rates (Weissert & Erba, 2004).

The input of isotopically light carbon observed here is possibly associated with a relative sea-level fall (Voigt & Helbrecht, 1997), during which ^{12}C could be released by the weathering, erosion and oxidation of organic-rich sediments (Voigt & Helbrecht, 1997; Price & Gröcke, 2002). A eustatic sea-level fall has been proposed for the latest Jurassic-earliest Cretaceous (e.g., Haq *et al.*, 1987; Hallam, 1992) and $^{87}\text{Sr}/^{86}\text{Sr}$ ratios rise throughout the Kimmeridgian (e.g., Jones *et al.*, 1994a; Veizer *et al.*, 1999; Jenkyns *et al.*, 2002) potentially indicating increased continental weathering, although this trend could also be attributed to decreased activity at ocean ridges (Price & Gröcke, 2002).

6.5.5. Kimmeridgian Stable Isotope Records

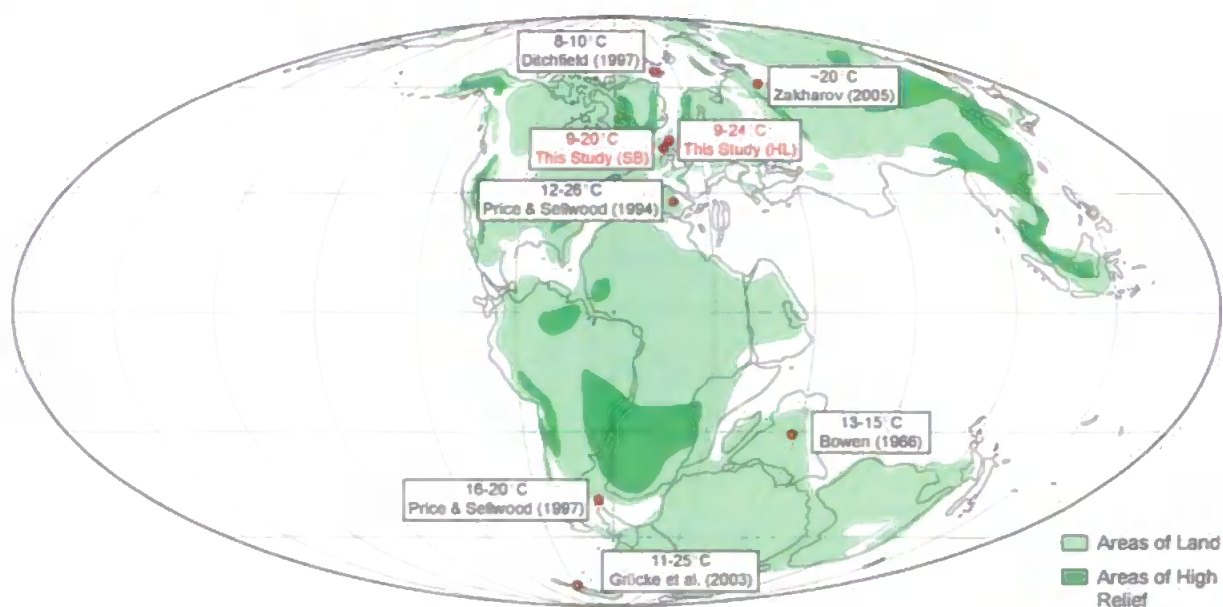


Figure 6.11 Kimmeridgian palaeogeography map showing published belemnite derived palaeotemperatures for this time period. (SB = Staffin Bay [Kimmeridgian data only]; HL = Helmsdale and Eathie).

The $\delta^{18}\text{O}$ composition of belemnite calcite from the Helmsdale coast region was considered earlier in this chapter in terms of palaeotemperature, with the Anderson & Arthur (1983) equation regarded as the most appropriate with which to perform the temperature calculations. The Kimmeridgian temperatures calculated here (9.1-24.0°C, average 15.8°C) are generally consistent with palaeotemperatures calculated from published belemnite-derived oxygen-isotope data (Fig. 6.11). The highest palaeotemperature values predicted here are consistent with those previously published, which commonly predict temperatures in excess of 20°C. The lowest values recorded here agree with the data produced by Ditchfield (1997), which is the one of the highest latitude datasets published and is the only other study to predict palaeotemperatures this low for the Kimmeridgian.

Typical belemnite derived Kimmeridgian $\delta^{13}\text{C}$ values range from -1 to 2 ‰ (Price & Gröcke, 2002; Gröcke *et al.*, 2003). The range of $\delta^{13}\text{C}$ ratios observed here however is slightly greater with values of between -1.76 and 2.96 ‰ recorded. The gradual shift (of ~5 ‰) to more negative carbon-isotope values observed here from the Helmsdale belemnites has also been recorded from other Kimmeridgian-Tithonian successions and has been shown to continue through the latest Tithonian and into the Early Berriasian (e.g., Weissert & Mohr, 1996; Weissert *et al.*, 1998; Bartolini *et al.*, 1999; Cecca *et al.*, 2001; Padden *et al.*, 2002; Price & Gröcke, 2002; Gröcke *et al.*, 2003; Weissert & Erba, 2004) (Fig. 6.12). Such $\delta^{13}\text{C}$ data have been compiled from predominantly bulk rock data from successions in Italy, Switzerland and France, although belemnite data have also been obtained from New Zealand and the Falkland Plateau (Price & Gröcke, 2002; Gröcke *et al.*, 2003). The $\delta^{13}\text{C}$ record presented here is the first high resolution record of the Kimmeridgian $\delta^{13}\text{C}$ decrease documented from a relatively high latitude in the northern hemisphere. The fact that this pattern is observed in the Tethyan region and in the northern and southern high latitudes suggests that the total carbon reservoir was affected by global conditions.

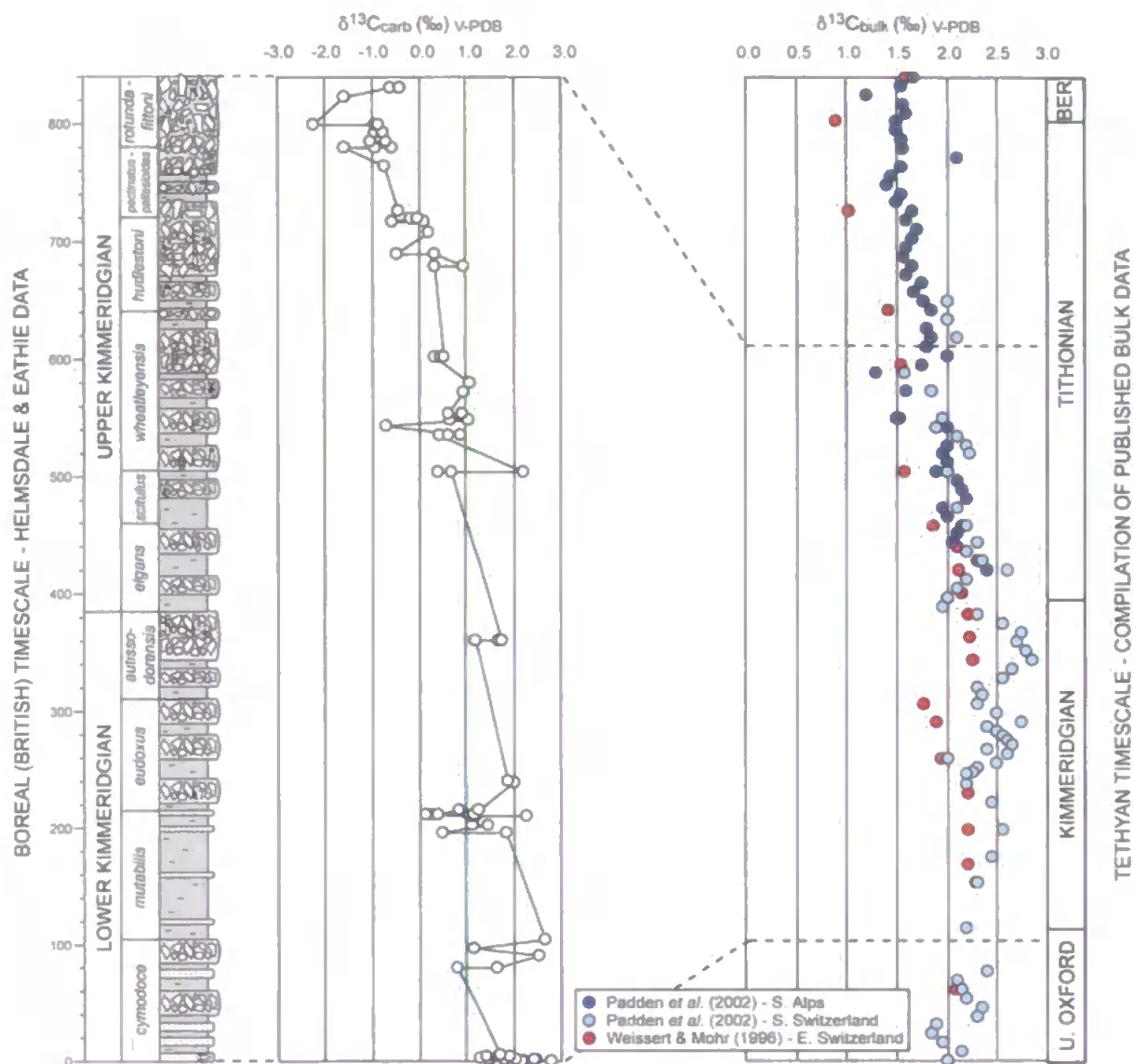


Figure 6.12 Kimmeridgian $\delta^{13}\text{C}$ correlation between a composite Tethyan $\delta^{13}\text{C}_{\text{bulk}}$ curve and the $\delta^{13}\text{C}$ curve from Helmsdale. Boreal British ammonite zones are illustrated here for the Helmsdale succession and scale is in metres. Timescale correlation is from Gradstein *et al.* (2004). See Figure 4.2 for key to log symbols.

The general decline to more negative $\delta^{13}\text{C}$ values observed during the Kimmeridgian and Tithonian has been associated with a shift from silica-rich to carbonate-rich pelagic deposition (Weissert & Channel, 1989; Padden *et al.*, 2002; Weissert & Erba, 2004). This expansion of carbonate sedimentation is believed to be the result of decreased sea floor spreading and an accompanying drop in global sea level (e.g., Haq *et al.*, 1987), which would have led to a deepening of the calcite compensation depth (CCD) (Weissert & Channel, 1989). A relative fall in sea level could result in the weathering, erosion and oxidation of newly exposed organic-rich sediments, during which ^{12}C would be released.

Such a situation creates a paradox however, since increased weathering can also be associated with increased nutrient supply rates, increased oceanic productivity and therefore a positive carbon-isotope excursion (Price & Gröcke, 2002). It is postulated that the effect of the erosion of organic-rich sediments on the $\delta^{13}\text{C}$ record at this time must be greater than the effect of increasing productivity. Substantial organic-rich deposits have been recorded from the Kimmeridgian-Tithonian, for example the Kimmeridge Clay Formation. Morgans-Bell *et al.* (2001) record very high TOC levels (up to 30 wt %) from the Kimmeridge Clay Formation in Dorset, with the highest values occurring in the *Eudoxus-Pectinatus* zones and coincident with a positive $\delta^{13}\text{C}_{\text{org}}$ excursion. The erosion of these Kimmeridge Clay deposits if exposed, could account for a significant release of ^{12}C and a negative carbon isotope excursion, although, the exposure of much older black shales is more likely. The observed decrease in $\delta^{13}\text{C}_{\text{carb}}$ values from Helmsdale in the Early Kimmeridgian however, is difficult to account for, since a synchronous increase in $\delta^{13}\text{C}_{\text{org}}$ values is observed from Dorset (Morgans-Bell *et al.*, 2001), although, this could be a local signal.

An increase in continental weathering is recorded during the Kimmeridgian-Berriasian interval, as indicated by rising $^{87}\text{Sr}/^{86}\text{Sr}$ values (e.g., Jones *et al.*, 1994a; Veizer *et al.*, 1999; Jones & Jenkyns, 2001; Jenkyns *et al.*, 2002) and would serve to increase transfer rates of alkalinity (carbonate) from the continents and into the oceans, potentially lowering atmospheric CO_2 levels (Robinson *et al.*, 2002; Weissert & Erba, 2004). Weissert & Channell (1989) suggest that the decrease in atmospheric CO_2 levels would have ultimately resulted in a decelerated hydrological cycle and therefore decreased productivity in parts of the Atlantic and Tethys Oceans.

6.5.6. Correlation of the Helmsdale & Staffin Bay Isotope Records

Helmsdale and Staffin Bay were situated at approximately the same palaeolatitude ($\sim 45^\circ\text{N}$) during the Late Jurassic (Smith *et al.*, 1994). It has been proposed that the

Hebrides Basin (in which Staffin Bay is situated) and the Moray Firth Basin (in which Helmsdale is situated) experienced coeval development as the result of activity along major onshore faults (Underhill, 1991; Wignall & Pickering, 1993; Hesselbo & Coe, 2000). As the development of these two basins was linked (i.e., the water masses were connected) it should be possible to correlate and combine the stable isotope records produced from the Helmsdale and Staffin Bay successions. The compilation of these two datasets then provides an almost complete carbonate isotope record from the Middle Callovian to Latest Kimmeridgian (*sensu anglico*) of Northern Scotland.

In order to assess the validity of this approach, isotope values from overlapping parts of the different successions were compared. These were the Lower Callovian *Koenigi* Zone and the Lower Kimmeridgian *Cymodoce* Zone deposits. The *Koenigi* Zone is represented on the Isle of Skye by the Belemnite Sands Member, a sandy glauconitic facies with abundant belemnites towards the top of the unit. In Brora, belemnites were collected from the Brora Shale Member, a sandy, glauconitic unit (Early/Middle Callovian in age) also with abundant belemnites. The mean values of $\delta^{18}\text{O}$ and $\delta^{13}\text{C}$ from the Brora belemnite rostra were -0.32 ‰ and 2.43 ‰ respectively, compared with values from Staffin Bay of -0.33 ‰ ($\delta^{18}\text{O}$) and 2.65 ‰ ($\delta^{13}\text{C}$). These values are very similar.

For the Early Kimmeridgian (*Cymodoce* Zone) the average values of $\delta^{18}\text{O}$ and $\delta^{13}\text{C}$ observed from Staffin Bay were -0.7 ‰ and 2.0 ‰ respectively. For the Helmsdale belemnites, the *Cymodoce* Zone values were -1.24 ‰ for $\delta^{18}\text{O}$ and 1.88 ‰ for $\delta^{13}\text{C}$. The greater amount of offset observed between these values (compared with those from the *Koenigi* Zone) is to be expected because the Staffin Bay values represent the lowermost *Cymodoce* Zone, whilst the Helmsdale values represent the Upper *Cymodoce* Zone. The *Koenigi* Zone correlation, however, was undertaken on belemnites from one coeval horizon and therefore the offset between the isotope values is significantly lower. The extremely close match between the *Koenigi* Zone isotope values and reasonably good match between the *Cymodoce* Zone values confirms that the Helmsdale and Staffin Bay

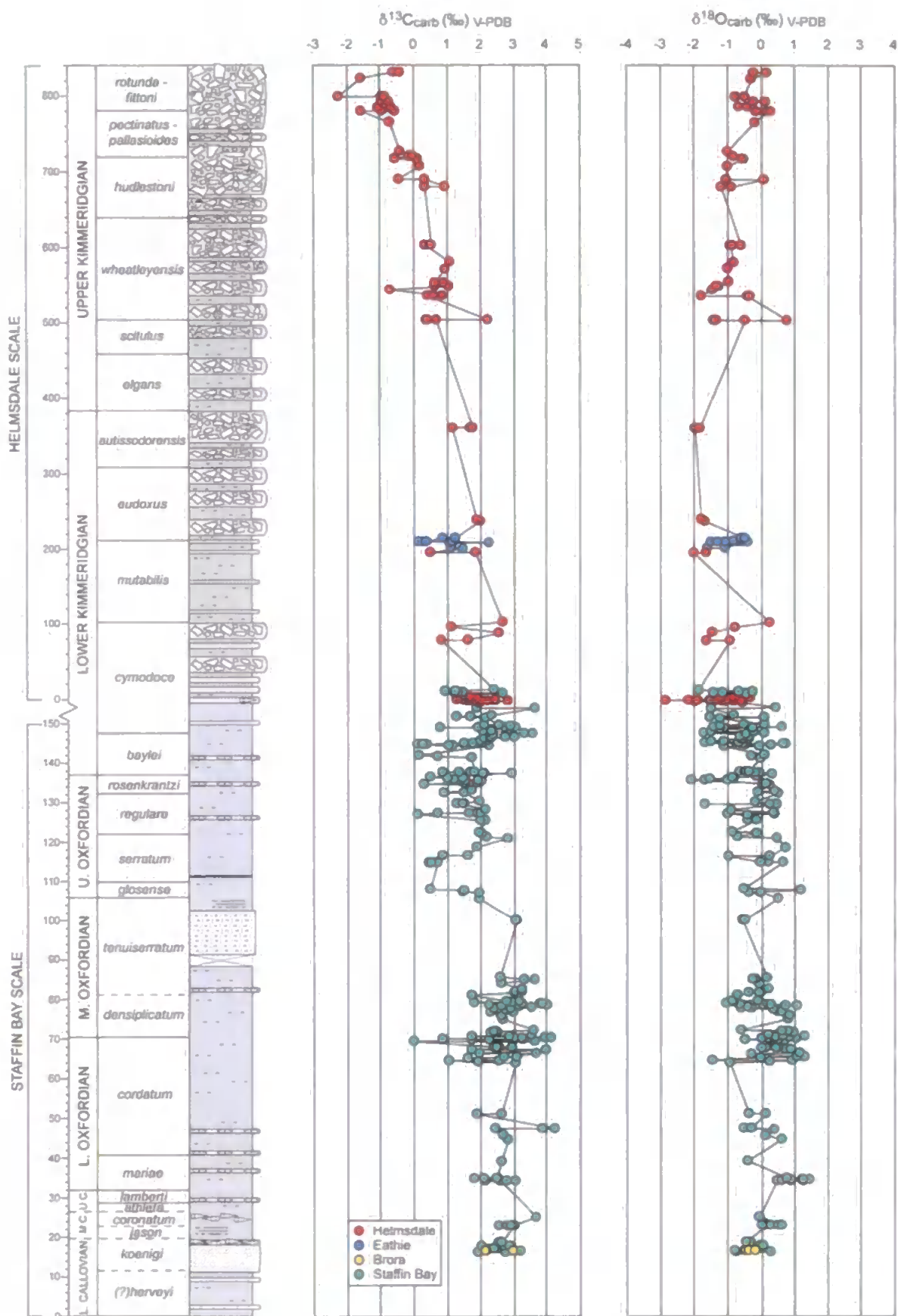


Figure 6.13 Composite Callovian-Kimmeridgian $\delta^{13}\text{C}$ and $\delta^{18}\text{O}$ records from northern Scotland (Staffin Bay, Helmsdale, Eathie and Brora). Note the change of scale between the Staffin Bay and Helmsdale sections. See Figure 4.2 for key to log symbols.

successions can be combined to produce a stable isotope record from the Middle Callovian to uppermost Kimmeridgian from this region.

The combined Helmsdale and Staffin Bay carbonate isotope data (Fig. 6.13) show a long-term $\delta^{13}\text{C}$ trend of relatively static values (on average between 2-3 ‰) through the Early and Middle Oxfordian followed by a shift to more negative values during the Late Oxfordian and into the Kimmeridgian. Despite a brief positive fluctuation in the Early Kimmeridgian (*Baylei-Cymodoce* zones) $\delta^{13}\text{C}$ values continue to decrease throughout the Kimmeridgian (to values as low as -2.25 ‰). The $\delta^{18}\text{O}$ curve shows a considerable amount of scatter, however despite this noise a very slight, gradual shift to less positive values throughout the Oxfordian and into the Early Kimmeridgian is discernable (from values of 1.43 ‰ to -2.84 ‰). From the Early to mid-Kimmeridgian a gradual return to more positive values is inferred (0.78 ‰).

6.6. Conclusions

- The data presented here comprise the first relatively high-resolution stable isotope investigation of marine biogenic carbonate (belemnites) from the Helmsdale coast, Sutherland, Scotland.
- The average palaeotemperature derived from the Helmsdale $\delta^{18}\text{O}$ record (using the Anderson & Arthur (1983) equation) was 15.8°C and the palaeotemperature range was 9.1 to 24.0°C for the Kimmeridgian interval. This corresponds well with the Callovian-Kimmeridgian palaeotemperature data derived from belemnites from the Staffin Bay succession, Isle of Skye (6.7°C to 20.6°C, average 12.4°C). The Helmsdale palaeotemperature data is also consistent with previously published literature on the Kimmeridgian-Tithonian, particularly with regards to low palaeotemperatures recorded from the northern high latitude region (e.g., Ditchfield, 1997).
- Mg/Ca derived palaeotemperature estimates range from -1.7 to 24.7°C, with an average palaeotemperature for the Kimmeridgian of 5.0°C. Records of sub-freezing

temperatures are impossible however, because marine cephalopods could not live in these conditions. This casts doubt on the use of the Klein *et al.* (1996) Mg/Ca palaeotemperature equation when applied to fossilised skeletal calcite.

- The marine carbonate $\delta^{13}\text{C}$ record shows a distinctive long-term trend towards more negative values throughout the Kimmeridgian. This input of isotopically light carbon is coincident with a relative sea-level fall during which ^{12}C would be released by the weathering, erosion and oxidation of organic-rich sediments.
- The shift to low $\delta^{13}\text{C}$ values during the Kimmeridgian is also recorded from the Tethyan region and the northern and southern hemispheres. The Helmsdale data provide the first documented record of this pattern from a northern high latitude site. The widespread occurrence of this event suggests that the total global carbon reservoir was affected.
- The Helmsdale and Staffin Bay (Chapter 5) carbonate isotope data are correlated and combined here to produce an almost complete succession from the Middle Callovian to uppermost Kimmeridgian of northern Scotland. This is possible because the Hebrides and Moray Firth Basins experience coeval development during the Late Jurassic. This is confirmed by the almost identical $\delta^{13}\text{C}$ and $\delta^{18}\text{O}$ values recorded from Lower Callovian *Koenigi* Zone belemnites from both successions.

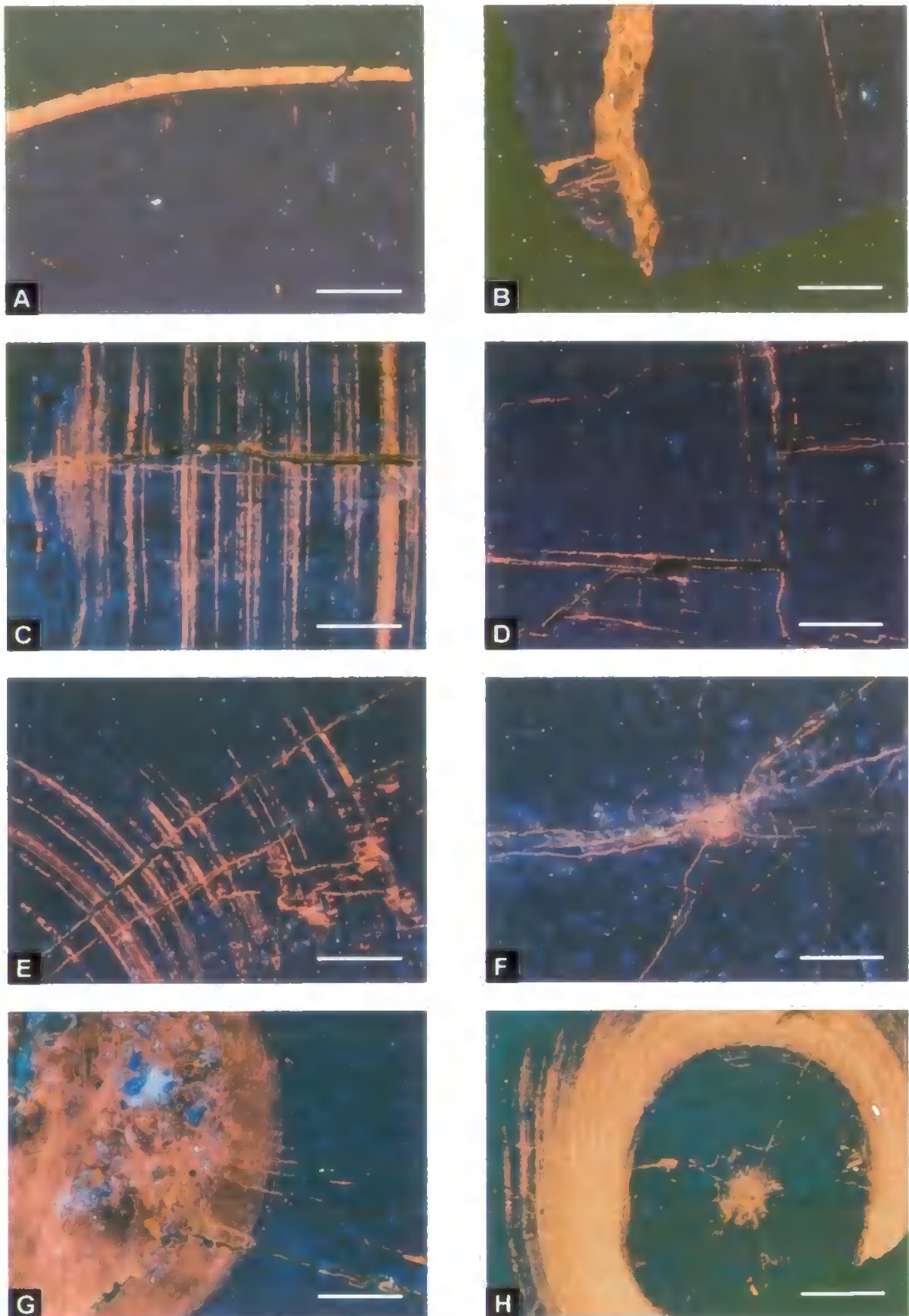


Plate 4. Cathodoluminescence images showing the state of preservation of belemnite rostra from Helmsdale, Scotland. All scale bars represent 1 mm. (A) Rostrum margin displaying alteration. (B) Fracture infilled by diagenetic cement. (C) Fracture and growth lines displaying alteration. (D) Fractures and growth lines displaying alteration. (E) Fractures and growth lines displaying alteration. (F) Fractures emanating from apical canal and showing alteration. (G) Apical canal with sediment infilling and some fine fractures. (H) Heavily altered growth bands surrounding the apical canal.



Plate 5. Backscattered SEM images showing the state of preservation of belemnite rostra from Helmsdale, Scotland. All scale bars represent lengths stated on images. (A) Well preserved calcite showing little alteration along fracture. (B) Well preserved calcite. (C) Slight alteration along growth bands. (D) Fracture running through apical canal. (E) Faint alteration around apical canal region. (F) Apical canal and surrounding growth lines displaying alteration. (G) Borings and fractures at rostrum margin. (H) Fractures showing little alteration.

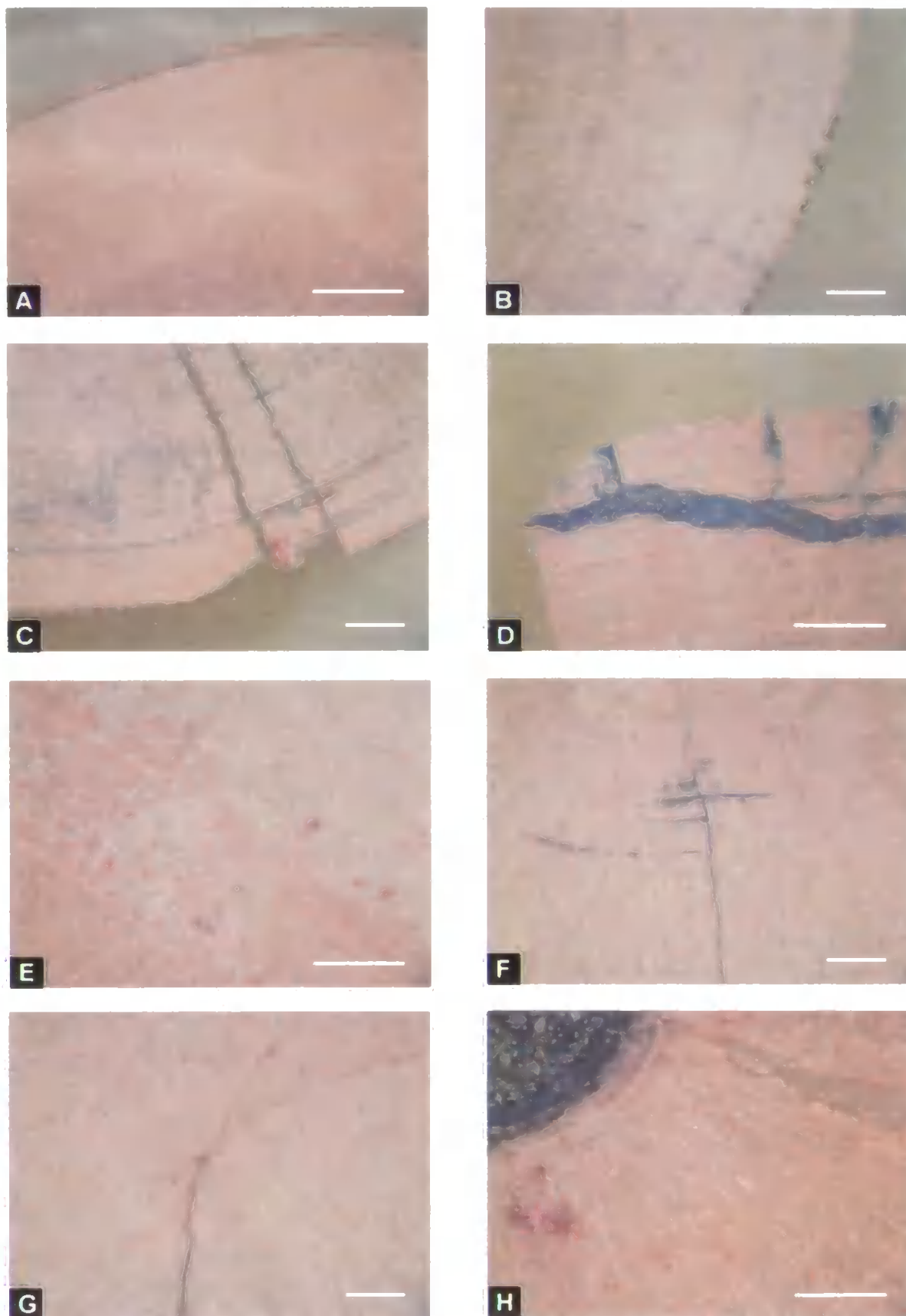


Plate 6. Carbonate stained images showing the state of preservation of belemnite rostra from Helmsdale, Scotland. All scale bars represent 1 mm. (A) Very well preserved calcite with faint alteration at margin edge. (B) Rostrum margin with some pyritisation. (C) Rostrum margin with alteration along fractures and growth lines. (D) Wide fracture infilled with diagenetic cement. (E) Generally well preserved calcite. (F) Fracture and sections of adjacent growth bands displaying alteration. (G) Fractures emanating from apical canal. (H) Apical canal with sediment infilling surrounded by some areas of alteration.

7. BOYARKA RIVER, YENISEI-KHATANGA BASIN, SIBERIA

7.1. Location & Site Description

The Boyarka River lies within the Yenisei-Khatanga Basin of northern Central Siberia, south of the Taymyr Peninsula (Fig. 7.1). The section of the river considered here is located at $\sim 70^{\circ}\text{N}$ and is approximately 300 km south of the town of Khatanga. In total five major sites were examined along a 15 km stretch of river. These sites were also the main ones visited during the study of Shulgina *et al.* (1994). The exposures were generally low river-side cliffs cut perpendicular to strike and composed predominantly of soft sands or silty-sands (Fig. 7.2).



Figure 7.1 Location map of the Boyarka River, northern Central Siberia. The location of the Boyarka River is shown (left) together with the relative positions of each of the sites examined (right).

The composite Boyarka River section is approximately 300 m thick and ranges in age from the Ryazanian (*Kochi* Zone) to the Early Valanginian (*Bojarkensis* Zone).



Figure 7.2 River-side cliff exposure typical of the Boyarka River, northern Central Siberia (location KH1-4, Upper Valanginian, *Bidichotomus* Zone).

7.2. Geological Setting

The Yenisei-Khatanga Basin is a trough on the northeastern branch of the West Siberian rift system (Khain *et al.*, 1991) (Fig. 7.3). It is bounded to the west by the West Siberian Basin, to the north by the Taymir fold belt and to the south and southeast by the East Siberian Platform (Aplonov, 1995; Vyssotski *et al.*, 2006). It is worth noting, that all of these areas are known to have been affected by the emplacement of flood basalts from the East Siberian Traps at ~250 Ma (the Permo-Triassic boundary), at which time basalts would also have extended from northeastern Siberia into the Barents and Kara seas (Vyssotski *et al.*, 2006).

During the Middle Triassic, the Yenisei-Khatanga Rift experienced a period of inversion, where compression replaced rifting, to produce inversion structures in which oil and gas zones would later accumulate (Khain *et al.*, 1991). O'Reilly *et al.* (2005) describe

the Jurassic to Cretaceous evolution of the Yenisei-Khatanga Basin. They report a period of Jurassic rifting, followed by terrane collisions in East Siberia during the Valanginian to produce the Laptev Sea and Verkhoyansk fold belts. This collision diverted continental drainage systems towards the Yenisei-Khatanga Basin, where there was a resulting influx of sedimentation until the extensional fold belt collapse of the Barremian (O'Reilly *et al.*, 2005).

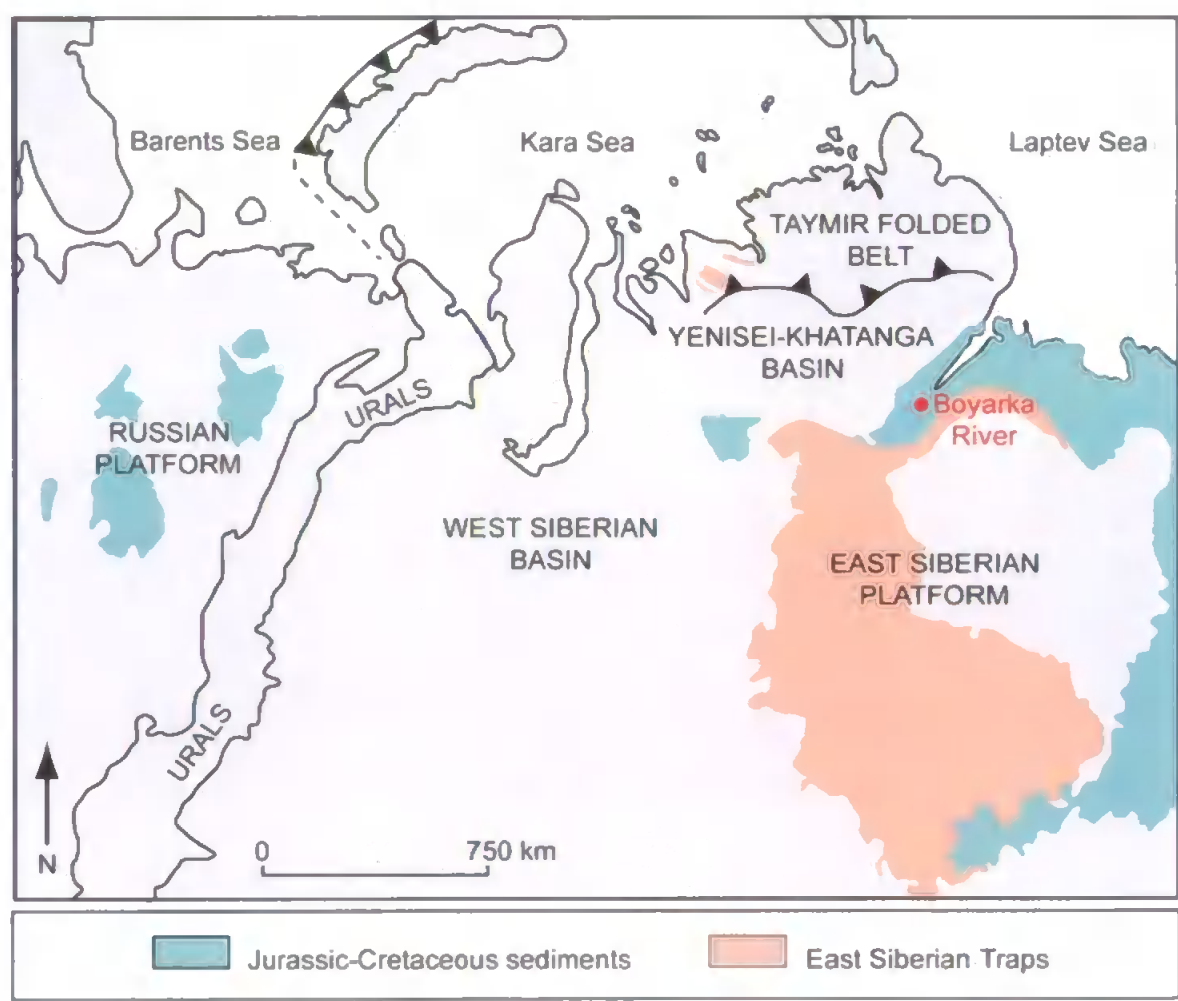


Figure 7.3 Simplified geological map of the Yenisei-Khatanga Basin and surrounding areas. Adapted after Vyssotski *et al.* (2006).

The basement of the Yenisei-Khatanga trough consists of Archean-Proterozoic igneous and metamorphic rocks similar to those of other Siberian Platform regions (Semenovich *et al.*, 1973). Jurassic to Paleogene deposits in the Yenisei-Khatanga Basin reach a thickness of 7 km (Vinogradov *et al.*, 1973), with the Jurassic to Cretaceous

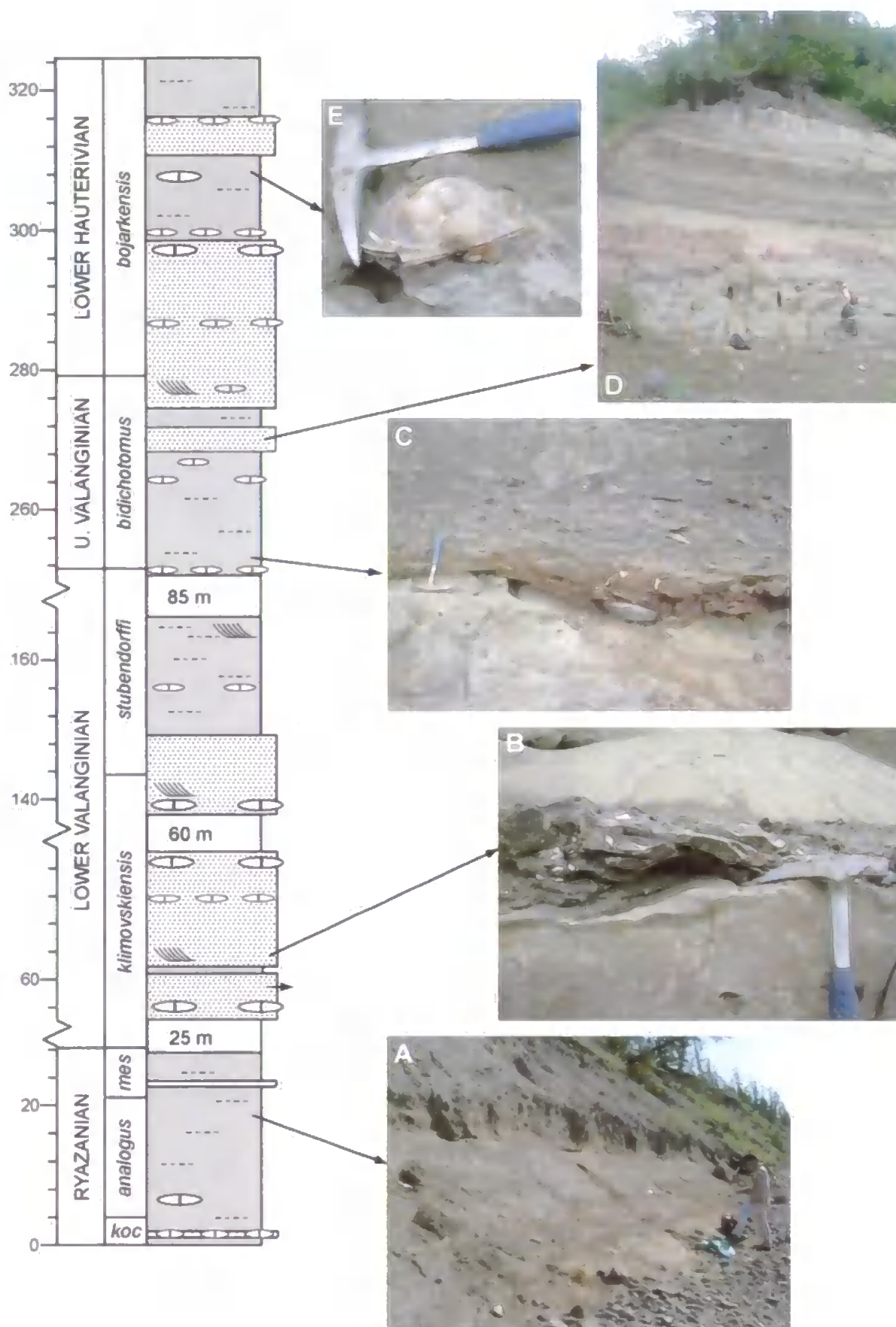


Figure 7.4 Sedimentary log and photographs of the Boyarka River succession. (A-E) described in text. Boreal (Russian) ammonite zones are illustrated. See Figure 4.2 for key to log symbols. Scale is in metres.

elements of the sedimentary epirift complex well known for their oil and gas potential (e.g., Semenovitch *et al.*, 1973; Khain *et al.*, 1991; O'Reilly *et al.*, 2005). The Lower Cretaceous Boyarka River sediments are dominated by sandstones, clays and siltstones of shallow marine origin (Fig. 7.4). Exposure is generally good where outcrops exist, however, there are large breaks in the continuity of the Ryazanian to Hauterivian sequence where no viable outcrops could be identified. The Ryazanian (*Kochi*, *Analogus* and *Meseshnikowi* ammonite zones) sediments are approximately 30 m thick and are dominated by grey silty clays with occasional concretions or limestone bands (Fig. 7.4a). There are ~10m of very poorly exposed sediments occurring during the *Analogus* Zone, however, the sediments above and below this gap appear to be the same grey silty clays. Fossilised wood fragments and belemnites are common throughout the Ryazanian.

After a break in exposure of ~25 m (estimated using dip and strike) the Lower Valanginian (*Klimovskiensis* and *Stubendorffi* zones) sediments are exposed. They are composed of approximately 120 m of sands and silts, although the exposure of the ~60m in the middle of the succession is very poor. The basal Valanginian sediments are predominantly sandstones, although occasional thin claystone beds are also present. The sandstones are green in colour and display some cross-bedding. Isolated concretions and concretionary layers are distributed throughout the succession. Large bivalve (*Mcleania*) shells are particularly common in the Lower Valanginian, either isolated or in stacks and crinoid ossicles are also present in a lower *Klimovskiensis* Zone shell bed (Fig. 7.4b). Bioturbation is common (distinct *Rhizocorallium*-like burrows are present in the *Klimovskiensis* Zone shell bed together with the crinoid ossicles) and fragments of wood and coal are distributed throughout the Lower Valanginian succession.

The Upper Valanginian (*Bidichotomus* Zone) sediments were exposed after a break in outcrop of ~90 m and are approximately 20m thick. These sediments are predominantly clayey sands or sands that are generally pale grey in colour but mottled red in places from iron-staining (Fig. 7.4c). Thin, dark grey clay layers (<3m in thickness) are

commonly interbedded with the clayey sands and sandstones. At the bases of the claystone layers small tabular concretions and belemnites are relatively common.

The Lower Hauterivian (*Bojarkensis* Zone) section continues on from the Upper Valanginian succession without a break in outcrop. The Hauterivian succession is approximately 60m thick and composed of pale grey/green sandstones and clayey sands. The sandstone units are occasionally cross-bedded and often display some degree of iron-staining giving them a mottled orange/red appearance in places (Fig. 7.4d). Large isolated concretions, although rare, do occur towards the top of the succession. Condensed clay layers with small concretions at the base (and occasional belemnites) occur relatively regularly (at an interval of ~15m) in the Hauterivian section. Large bivalves (*Mcleania*) are distributed throughout the succession (Fig. 7.4e). Beds are often locally bioturbated and fossilised wood fragments are common (including large fossilised tree branches, 50 mm in diameter) particularly towards the base of the succession.

7.3. Sampling & Methodology

The five major Boyarka River outcrops form a succession from Early Ryazanian (*Kochi* Zone) to Early Hauterivian (*Bojarkensis* Zone) in age. Samples were taken from 210 different horizons throughout this succession. This included 64 belemnite horizons (Fig. 7.5) and 150 fossilised wood horizons (Fig. 7.5). Wherever possible multiple samples were taken from a horizon. The Boyarka River was visited for a three week period in August 2004.

Once again, belemnite rostra were assessed for preservation by stable isotope and trace element analysis, backscattered scanning electron microscopy (BSEM), cathodoluminescence (CL) and carbonate staining. Areas prone to diagenesis were removed prior to isotopic and trace element analysis.



Figure 7.5 Belemnites and macroscopic wood from the Boyarka River succession. (A) Belemnite from the *Meseshnikowi* Zone (location KH17). (B) Belemnite from the *Kochi* Zone (location KH16). (C) Wood from the *Klimovskiensis* Zone (location KH13). (D) Wood from the *Bidichotomus* Zone (location KH1-4).

Stable isotope analysis was conducted on a Multiflow automated carbonate preparation module with Gilson 222XL autosampler, interfaced with an Isoprime isotope ratio mass spectrometer (GV Instruments, UK), at the University of Plymouth, UK. Trace element data were generated by Inductively Coupled Plasma-Atomic Emission Spectrometer (ICP-AES) using a Perkin Elmer Optima 3300RL ICP-AES system (with autosampler) at the NERC ICP facility, Department of Geology at Royal Holloway, University of London.

Representative macroscopic wood samples were photographed by scanning electron microscopy (SEM) on the University of Plymouth's JEOL 5600 SEM. In total 184 fossil wood samples were analysed for carbon-isotope ratios. Samples were treated with 5% HCl to remove any carbonate material and rinsed with deionised water before being oven dried and powdered with an agate pestle and mortar. Samples were analysed

by Dr Darren Gröcke at McMaster University, Ontario, Canada, where samples were measured on a SIRA II Series 2 dual-inlet isotope-ratio mass-spectrometer for isotopic analysis. For a full description of methodology see Chapter 4.

7.4. Results

The belemnites sampled from this succession were of the Boreal genera *Cylindroteuthis*, *Acroteuthis*, *Pachyteuthis* and *Lagonibelus*. Most of the belemnites were composed of translucent calcite and retained the primary concentric banding that characterise belemnite rostra. Several specimens exhibited endolithic borings around the rostrum margins. BSEM, CL and carbonate staining analysis was conducted on 14 specimens (Plates 7-9) in order to identify the areas of the rostrum that were particularly prone to diagenetic alteration (e.g., the rostrum margins, the area surrounding the apical canal, well-developed fractures and strong growth bands). Such areas tended to be Fe-rich and were sometimes subjected to partial replacement by pyrite. These areas were removed prior to sampling or were avoided.

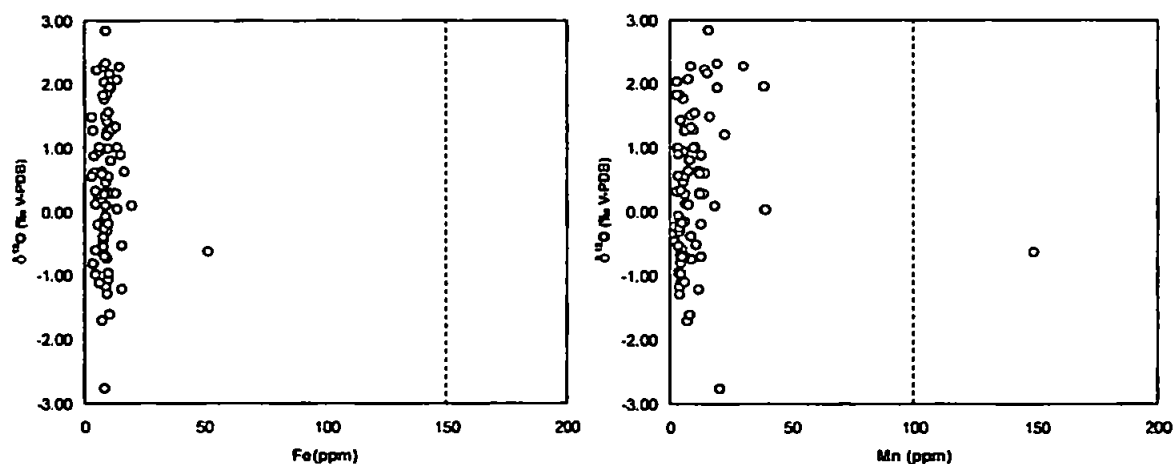


Figure 7.6 Cross-plots of $\delta^{18}\text{O}$ against Fe (left) and Mn (right). The dashed lines indicate the cut off values for well preserved samples.

The concentrations of Fe and Mn were determined to provide an additional means of assessing preservation. The Fe and Mn values derived from the Boyarka River belemnites were 3-52 ppm, mean 9 ppm (for Fe) and 2-149 ppm, mean 11 ppm (for Mn).

Fe and Mn data were plotted against $\delta^{18}\text{O}$ to constrain any diagenetic alteration (Fig. 7.6). High values of Mn or Fe and occasional outliers with regards to $\delta^{18}\text{O}$ values were regarded as an artefact of diagenetic alteration. Relatively low values of Fe (<150 ppm) and Mn (<100 ppm) were recorded from most of the Boyarka River belemnites, with only 1 sample excluded from further analysis.

Elemental abundances for additional trace elements are as follows: Sr 925-1701 ppm, mean 1187 ppm, Mg 297-1817 ppm, mean 876 ppm and Ca 28 % - 32 %, mean 30 %. The oxygen and carbon isotope values for well preserved Boyarka River belemnites range from -1.71 to 2.83 ‰ and from -1.07 to 4.24 ‰ respectively (Fig. 7.7). The oxygen isotope data from this location show a significant amount of scatter, for example the Lower Ryazanian (*Kochi* to *Analogus* zones) data show a c. 4.5 ‰ variation (from -1.71 to 2.83 ‰) compared to a c. 2.0 ‰ (from -1.07 to 0.96 ‰) variation in the concurrent carbon isotope values. The most positive oxygen isotope values are observed during the Lower Ryazanian (2.83 ‰). The carbon isotope data demonstrate an overall trend of increasing values from the Ryazanian and into the Lower Hauterivian, with a peak during the Upper Valanginian *Bidichotomus* Zone where values range from 1.68 to 4.24 ‰. After the positive carbon isotope excursion observed during the Upper Valanginian, carbon isotope values drop to a range of 1.00 to 1.72 ‰ in the Lower Hauterivian. The most negative carbon isotope values occur in the Lower Ryazanian (*Kochi* to *Analogus* zones) and are coincident with the most positive oxygen isotope values, although, a cross-plot of $\delta^{18}\text{O}$ vs. $\delta^{13}\text{C}$ reveals no statistically significant correlation (Fig. 7.8).

Macroscopic wood samples were identified as charcoal (43 samples), charcoal-coal (51 samples) or coal (61 samples) where possible and representative samples were photographed by SEM (Plates 10-11). The range of preservation did not have a significant impact on the overall long-term $\delta^{13}\text{C}_{\text{org}}$ curve (as previously demonstrated by Hesselbo *et al.*, (2003) and Gröcke *et al.*, (2005)). Identification of the wood to a generic or specific level was not undertaken. The organic carbon isotope ratios derived from these fossilised

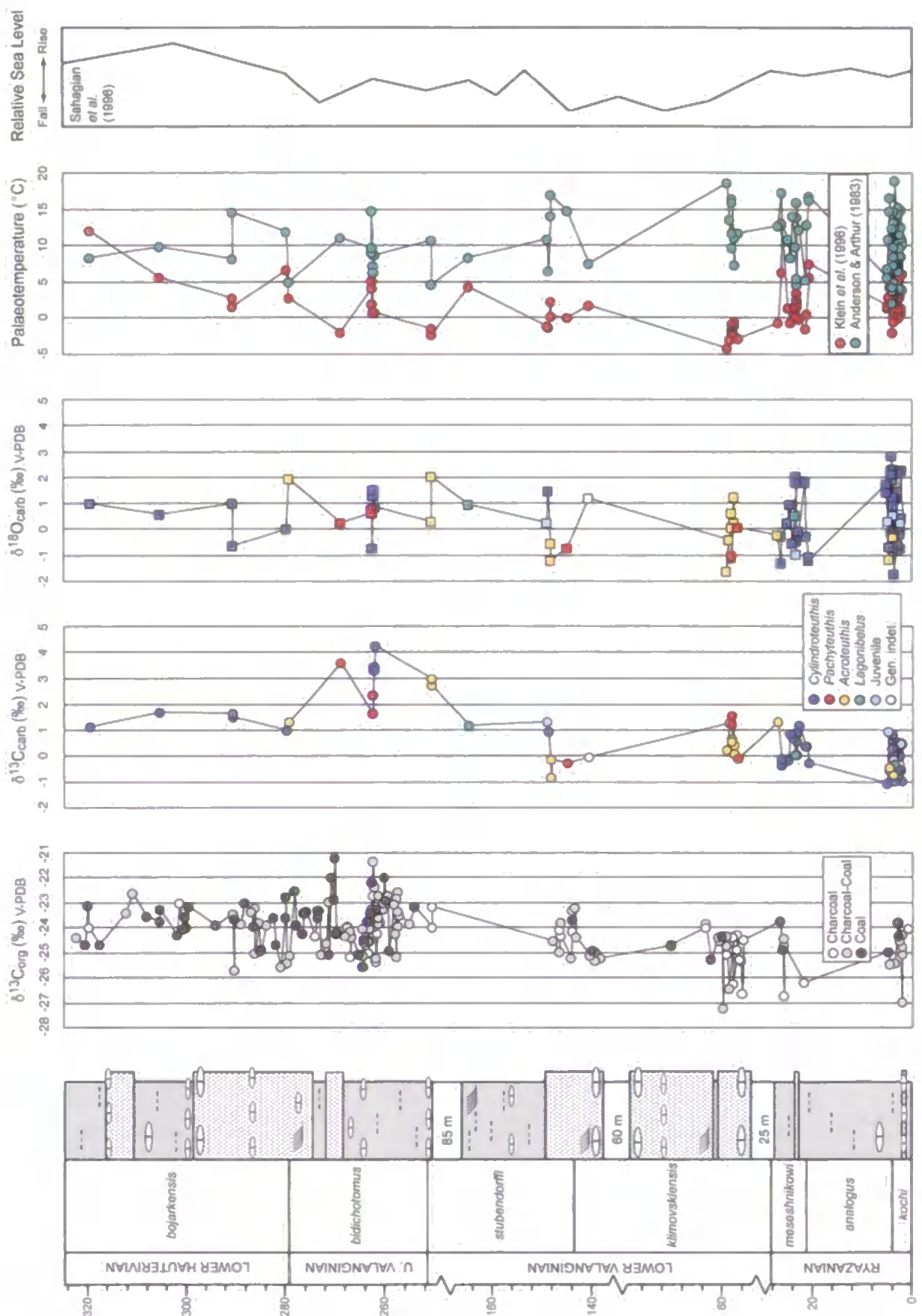


Figure 7.7 $\delta^{13}\text{C}_{\text{org}}$, $\delta^{13}\text{C}_{\text{carb}}$, and $\delta^{18}\text{O}_{\text{carb}}$ records from the Ryazanian-Lower Hauterivian Boyarka River succession, northern Central Siberia. Calculated palaeotemperatures and sea level are also shown. Boreal (Russian) ammonite zones are illustrated. See Figure 4.2 for key to log symbols. Scale is in metres.

wood samples range from -27.20 to -21.21 ‰ (Fig. 7.7). The most negative $\delta^{13}\text{C}_{\text{org}}$ values occur during the Upper Ryazanian to Lower Valanginian (*Kochi* to *Klimovskiensis* zones), with a range from -27.20 to -23.74 ‰, average -24.93 ‰. Upper Valanginian to Lower Hauterivian (*Bidichotomus* to *Bojarkensis* zones) $\delta^{13}\text{C}_{\text{org}}$ values are in the range of -25.70 to -21.21 ‰, average -23.75 ‰. These are the most positive $\delta^{13}\text{C}_{\text{org}}$ values in the succession. The $\delta^{13}\text{C}_{\text{org}}$ curve shows a long-term increase in values from the Upper Ryazanian to Lower Hauterivian, although, the increase in values is only small ($< \sim 2$ ‰). A large positive carbon isotope excursion, like that observed in the $\delta^{13}\text{C}_{\text{carb}}$ record (of ~ 4 ‰), is not identified in the $\delta^{13}\text{C}_{\text{org}}$ record. The amount of scatter present in the Boyarka river wood data is similar to that observed in previous comparable studies (e.g., Gröcke *et al.*, 1999, 2005; Robinson *et al.*, 2004).

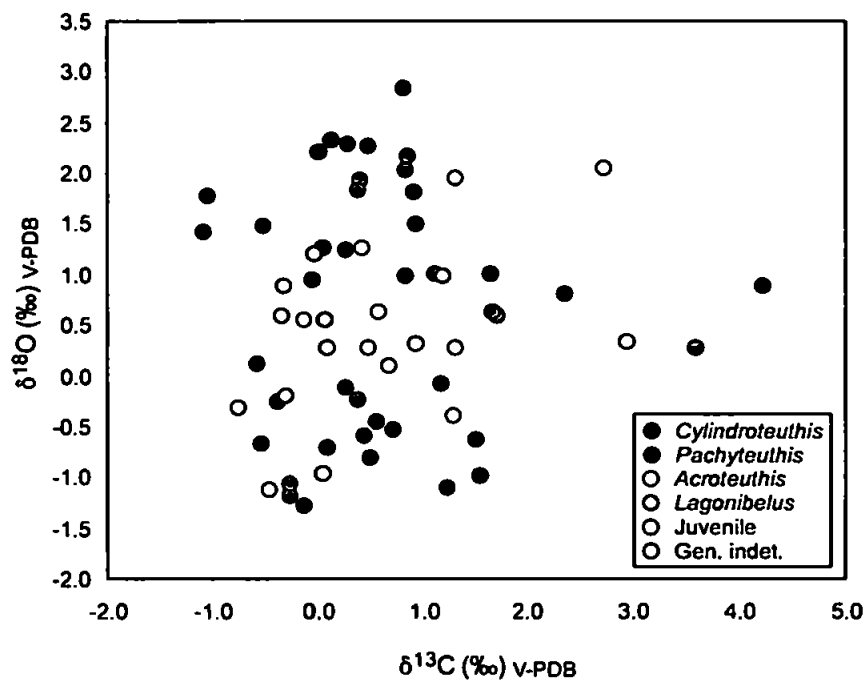


Figure 7.8 Cross-plot of $\delta^{18}\text{O}$ and $\delta^{13}\text{C}$ values derived from belemnites from the Boyarka River succession, northern Central Siberia.

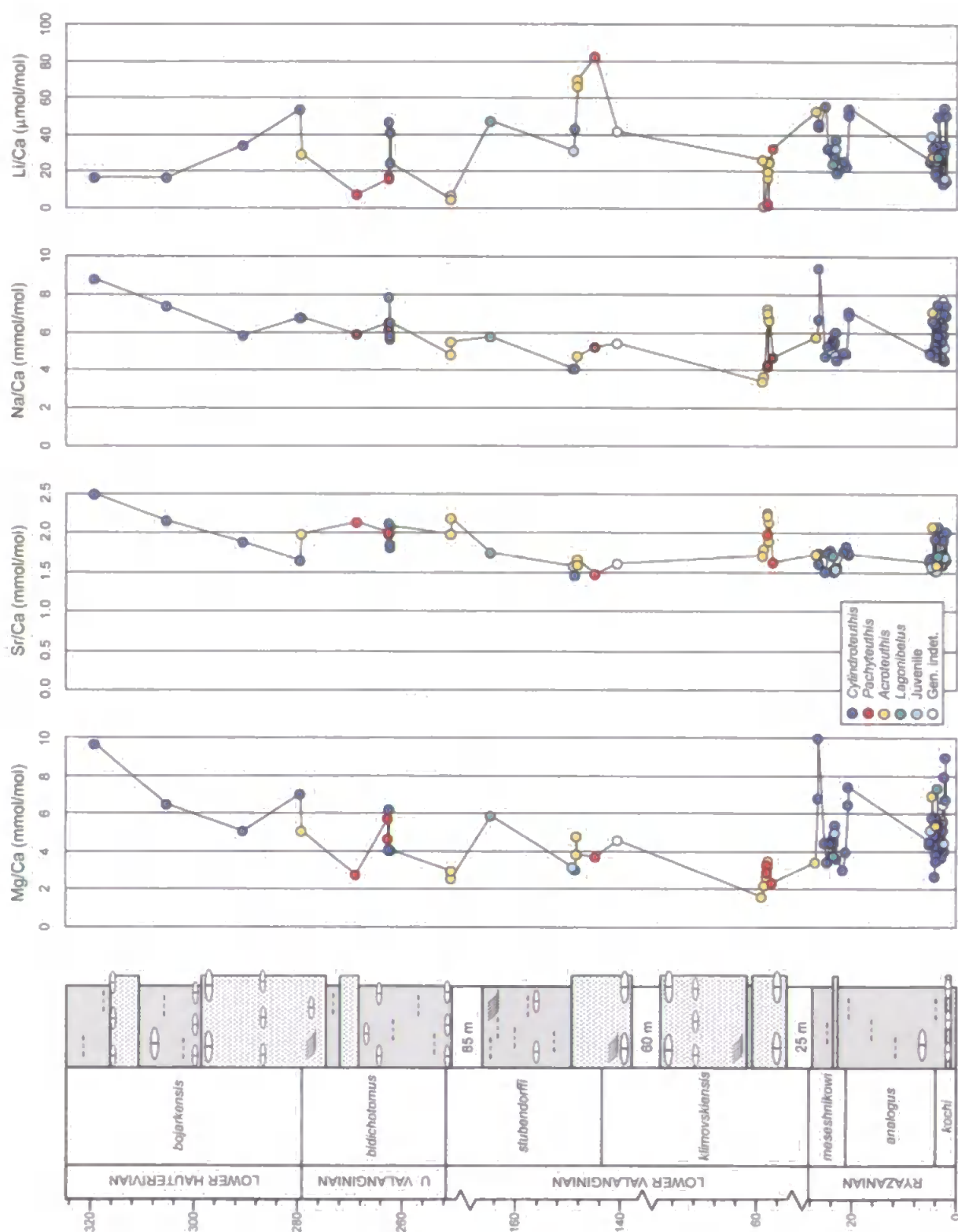


Figure 7.9 El/Ca ratios from the Ryazanian-Lower Hauterivian succession at the Boyarka River, northern Central Siberia. Boreal (Russian) ammonite zones are illustrated. See Figure 4.2 for key to log symbols. Scale is in metres.

7.5. Discussion

7.5.1. Stable Isotope, Geochemical & Taxonomic Records

McArthur *et al.* (2004) suggested that taxonomic differences may influence stable isotope (particularly oxygen) and trace element records. The data presented here, therefore, highlight the different belemnite genera (Figs 7.7 and 7.9) from which such measurements were taken in order to assess the potential influence of genus-specific differences in fractionation.

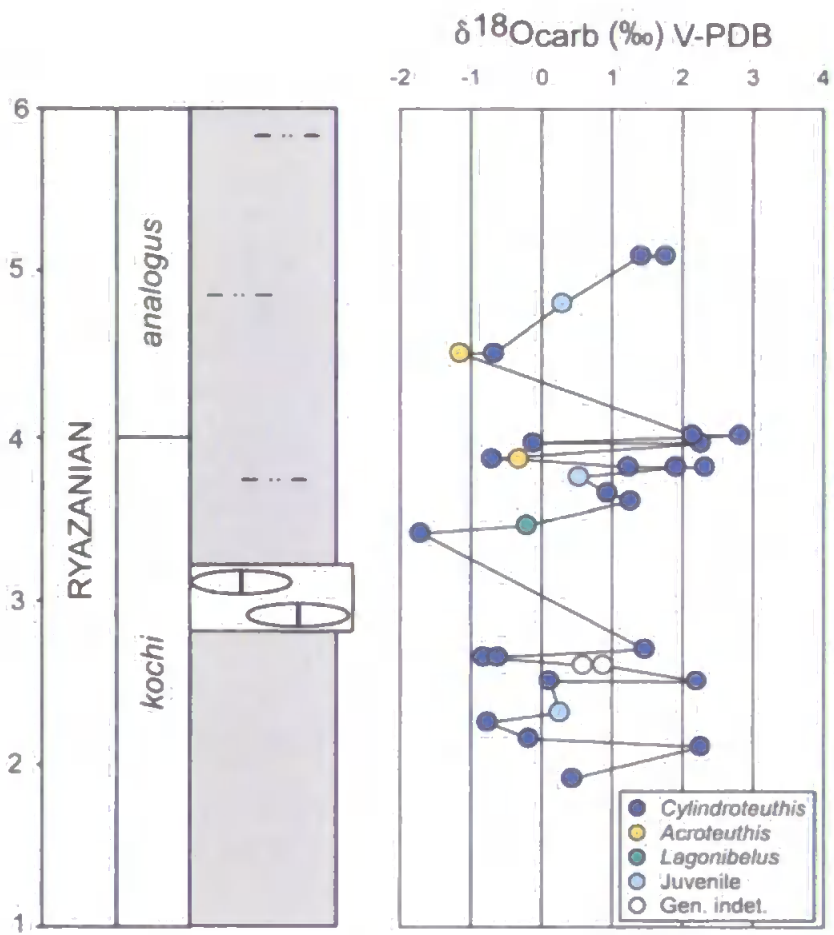


Figure 7.10 Close-up of the Ryazanian *Kochi-Analogus* zones, Boyarka River, northern Central Siberia. $\delta^{18}\text{O}$ record shown. Boreal (Russian) ammonite zones are illustrated. See Figure 4.2 for key to log symbols. Scale is in metres.

In neither the isotope nor elemental records does one genus consistently record either more negative or more positive values than any other genus, although co-occurring

belemnites of different genera are rare, making this difficult to assess with confidence. Perhaps the most striking taxonomic factor observed here is the high level of variability present in *Cylindroteuthis* specimens, particularly with regard to the $\delta^{18}\text{O}$ record. Values derived from *Cylindroteuthis* specimens almost always exceed both the highest and lowest values recorded from other genera where both occur in close proximity. The most notable example of this is in the Early Ryazanian *Kochi-Analogus* zones. The *Cylindroteuthis* $\delta^{18}\text{O}$ values for this period range from -1.71 to 2.83 ‰ compared with values of between -1.10 and 0.90 ‰ recorded from other genera (Fig. 7.10). This variability could be attributed to several factors, firstly to the abundance of *Cylindroteuthis* specimens compared to other genera, which are recording real and significant fluctuations of temperature or salinity or it could be the result of habitat and/or migration differences compared to other the genera. Interestingly, *Cylindroteuthis* is the only belemnite that is believed to have been able to withstand relatively deep water depths of down to 400m (compared to maximum water depths of 50-200m for other genera) (Westermann, 1973). The observed variability in the isotope and elemental records could, therefore, be the result of increased vertical migration within the water column compared to the other genera. This would account for the increased variability observed in the $\delta^{18}\text{O}$ record as the result of temperature fluctuations relating to water depth.

7.5.2. The Oxygen Isotope Record & Palaeotemperature Implications

The $\delta^{18}\text{O}$ record derived from belemnites of the Boyarka River displays a considerable amount of scatter. The Lower Ryazanian interval for example, shows a ~4.5 ‰ range of values (from -1.7 to 2.8 ‰). This degree of scatter is greater than would usually be expected for belemnite isotope data and is likely to be related to the shallow nature of the succession. It is also in part, probably the result of the condensed nature of the lower part of the Boyarka River succession. The succession becomes more expanded in the Valanginian and Lower Hauterivian and the scatter becomes less pronounced.

No long-term trend in the oxygen-isotope curve is discernable here, possibly as the result of the degree of scatter present in the data. The average oxygen-isotope value for the whole Lower Cretaceous succession is 0.45 ‰ and the data fluctuate about this value. Assuming that the oxygen-isotope record presented here primarily reflects changes in environmental conditions (temperature and salinity) rather than taxonomic or diagenetic processes a palaeotemperature estimate can be attempted. The problems associated with belemnite derived palaeotemperature estimates are discussed in previous chapters and so will not be repeated here, although, it must be acknowledged that any calculations presented can only be considered as a guide to the potential palaeotemperatures rather than definitive values for the region.

Figure 7.7 shows the seawater palaeotemperatures calculated using the Anderson & Arthur (1983) $\delta^{18}\text{O}$ equation. An isotopic composition of -1 ‰ SMOW was assumed for non-glacial seawater, which is consistent with previously published literature on the Cretaceous period (e.g., Pirrie & Marshall, 1990; Podlaha *et al.*, 1998; Price & Mutterlose, 2004). The average palaeotemperature calculated using $\delta^{18}\text{O}$ for the Boyarka River was 10.6°C and the palaeotemperature range was 2.1 to 19.0°C for the Ryazanian to Hauterivian interval. Both the lowest and highest palaeotemperatures occurred during the Lower Ryazanian *Kochi* to *Analogus* ammonite zones. These values are slightly higher than the modern temperature range for the region, which Polyak *et al.* (2003) estimate to be around -1 to 12°C based on foraminiferal isotope studies in the Kara and Pechora seas. Published belemnite derived palaeotemperatures for the Lower Cretaceous are consistent with those presented here. Van de Schootbrugge *et al.* (2000), for example, infer Early Valanginian temperatures of ~15°C from France and McArthur *et al.* (2004) record values of ~11°C at the base of the Hauterivian in England. Price & Mutterlose (2004) recorded a range of 7.0 to 21.4°C for the Volgian-Valanginian from the Yatria River in Siberia. The Yatria River was located at an Early Cretaceous palaeolatitude of 60-65°N (Price &

Mutterlose, 2004), which is 5-10° south of the Boyarka River. A difference in palaeotemperature of ~2.5-5.0°C between these palaeolatitudes seems reasonable.

The most positive $\delta^{18}\text{O}$ value observed here (and therefore the most likely to represent the coolest palaeotemperature) is 2.8 ‰. According to the temperature-salinity model constructed by Railsback *et al.* (1989) and Woo *et al.* (1992) with modification by Price & Mutterlose (2004) this value corresponds to a palaeotemperature of 2.1°C, when a normal marine salinity (of 34 ‰) is assumed (Fig. 7.11). However, Roche *et al.* (2006) modelled $\delta^{18}\text{O}_{\text{seawater}}$ values in past warm climates and several of their models indicated that $\delta^{18}\text{O}_{\text{sw}}$ values could reach approximately -1.5 ‰ in the Arctic (this corresponds to a salinity value of ~32 ‰). If these new values of $\delta^{18}\text{O}_{\text{sw}}$ and salinity are considered then the $\delta^{18}\text{O}$ value of 2.8 ‰ now corresponds to a palaeotemperature of 0.5°C. In order to resolve a $\delta^{18}\text{O}$ value of 2.8 ‰ for even a moderate palaeotemperature of ~10°C a marine salinity of ~41 ‰ (or a $\delta^{18}\text{O}_{\text{sw}}$ value of ~1.5 ‰) is required, either or which seems very unlikely. Such positive $\delta^{18}\text{O}$ values as observed in the Ryazanian of the Boyarka River must, therefore, correspond to very low palaeotemperatures.

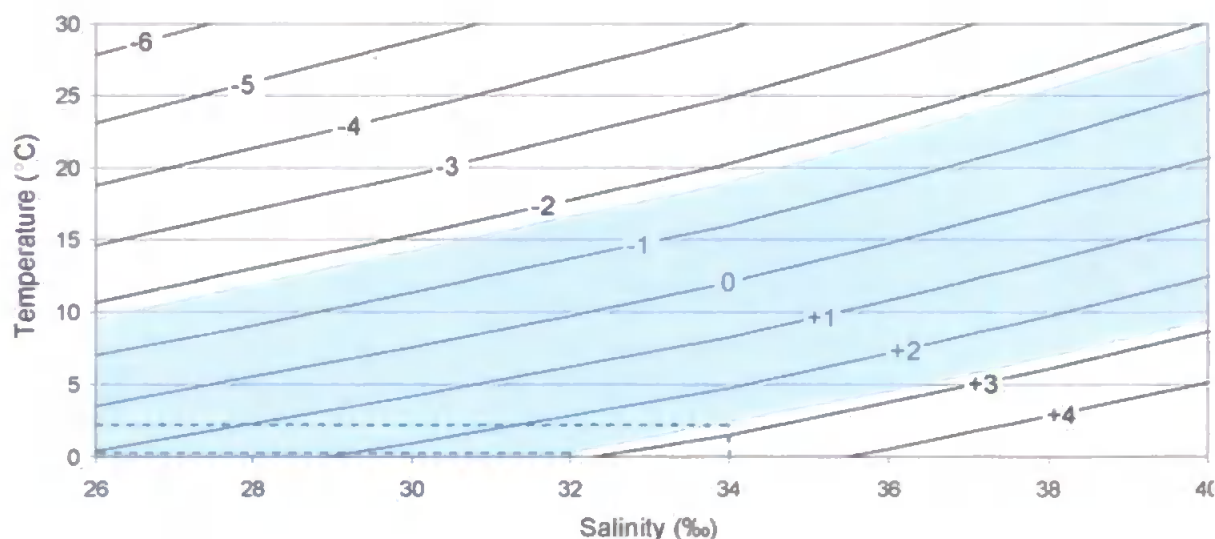


Figure 7.11 Temperature-salinity plot for the Boyarka River data. The continuous diagonal lines are isopleths of $\delta^{18}\text{O}$ values and show the possible combination of temperature and salinity that corresponds to calcite of a given isotopic composition and for a given isotopic composition of seawater (-1 ‰). The shaded area shows the range of isotope values recorded from belemnite rostra from the Ryazanian-Hauterivian succession the Boyarka River. The dashed lines represent the values discussed in the text above.

7.5.3. The Elemental Records & Palaeotemperature Implications

The rationale for, and implications of, considering El/Ca ratios together with $\delta^{18}O$ data was discussed in Chapter 5. Mg/Ca and Sr/Ca ratios are generally considered to be the key proxies with which to assess palaeoclimate, whilst Na/Ca and Li/Ca are of limited use (e.g., McArthur *et al.*, 2000; Bailey *et al.*, 2003; Rosales *et al.*, 2004a, b). Mn/Ca values were calculated for each sample and only those samples with values below 100 $\mu\text{mol/mol}$ were included here, as this is the lower limit for samples that are believed to have been altered under reducing conditions (McArthur, 1994).

The elemental ratios presented here (Mg/Ca , Sr/Ca , Na/Ca and Li/Ca) are quite noisy, however a long-term trend is apparent (Fig. 7.9). The most striking long-term trend observed here is that in the Mg/Ca record (and to a lesser degree also in the Na/Ca and Sr/Ca records). This is the relatively rapid shift to higher values during the Lower Hauterivian. This shift follows the $\delta^{13}C$ positive isotope excursion observed in both the organic and carbonate data. The El/Ca data is particularly noisy during the Ryazanian interval, probably in part, as a result of the condensed nature of the lower part of the Boyarka River succession (the same pattern is observed in the $\delta^{18}O$ data).

Cross-plots of El/Ca against $\delta^{18}O$ record very poor correlations for the Boyarka River belemnites (Fig. 7.12). This may be because the $\delta^{18}O$ record displays so much scatter. The only statistically significant correlation (at the 95% confidence level) recorded here is between Li/Ca and $\delta^{18}O$ (R^2 value, 0.253), which according to the work of Bailey *et al.* (2003) should show the least significant correlation. Both Mg/Ca and Sr/Ca display an inverse relationship with $\delta^{18}O$ as determined using a linear regression line. This is consistent with published belemnite data (e.g., McArthur *et al.*, 2000; Bailey *et al.*, 2003; Rosales *et al.*, 2004a, b) and for Mg/Ca the work of Steuber & Rauch (2005) on modern skeletal calcite.

The Mg/Ca ratio is commonly considered to be one of the most accurate palaeotemperature proxies available, primarily because, unlike $\delta^{18}O$ it is not thought to be

significantly influenced by salinity fluctuations (e.g., Klein *et al.*, 1996; Lear *et al.*, 2000; Bailey *et al.*, 2003; Rosales *et al.*, 2004a, b; Immenhauser *et al.*, 2005). The absence of correlation between Mg/Ca and $\delta^{18}\text{O}$ is therefore surprising, although this could be the result of several factors, such as, interspecies offset, ontogenetic variations, metabolic activity, salinity or temperature. Assuming however, that temperature is the major control on Mg/Ca ratios and that belemnites have a similar temperature sensitivity as modern biogenic calcites, it seems likely that salinity has had an effect on the $\delta^{18}\text{O}$ record, which is reflected by the poor correlation. The Boyarka River succession is a fully marine sequence (indicated by the abundant marine fauna, e.g., ammonites and belemnites), however the input of substantial quantities of wood suggests a very near-shore environment and fluvial, freshwater input from such a location would go some way to explaining a salinity effect on the $\delta^{18}\text{O}$ record.

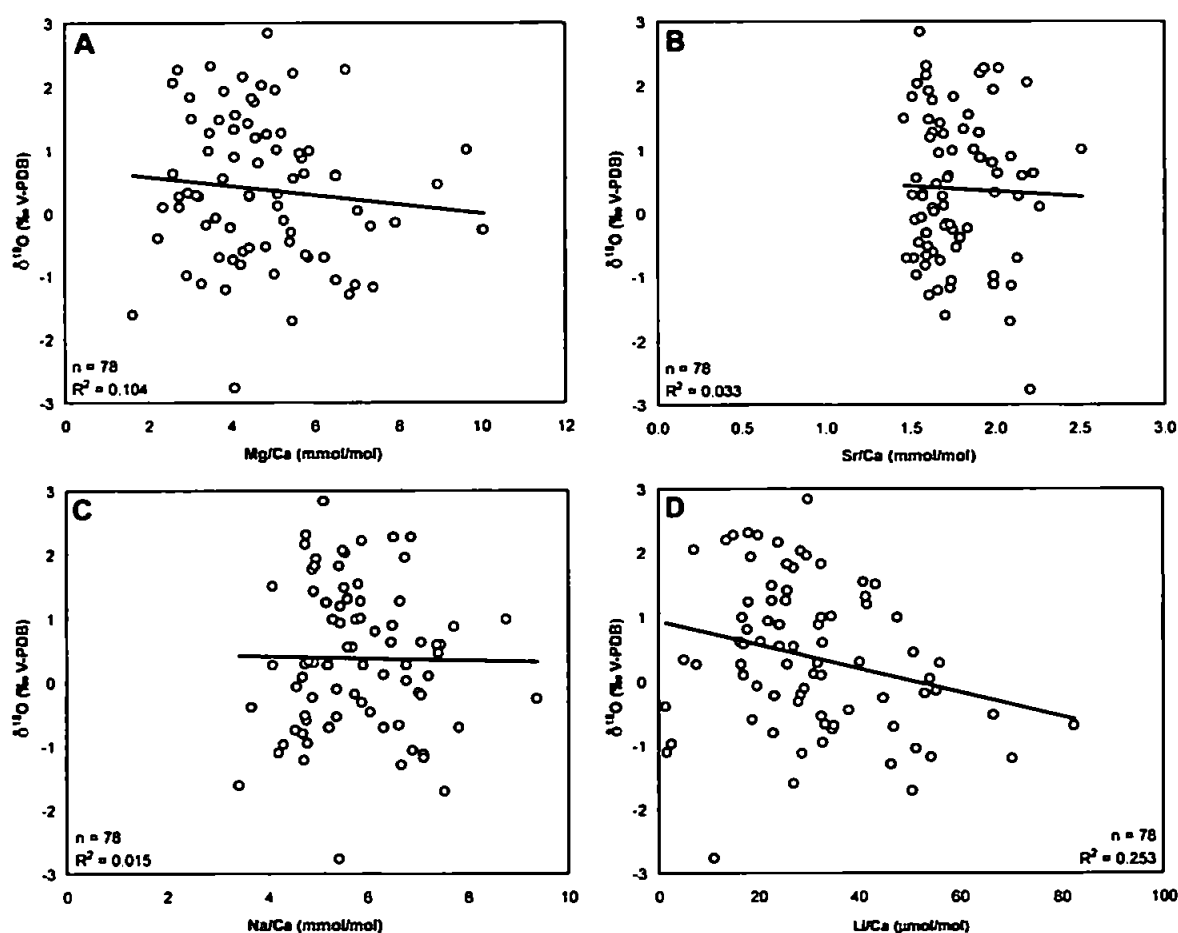


Figure 7.12 Cross-plots of $\delta^{18}\text{O}$ against (A) Mg/Ca, (B) Sr/Ca, (C) Na/Ca and (D) Li/Ca for the Boyarka River belemnites.

Palaeotemperatures were calculated from the Mg/Ca ratios using the equation of Klein *et al.*, (1996). The average Mg/Ca temperature is 2.2°C, with a range of -4.2 to 12.8°C compared to an average temperature of 10.6°C and range of 2.1 to 19.0°C as calculated from the $\delta^{18}\text{O}$ data (Fig. 7.7). The average offset between the palaeotemperature calculations is 8.4°C. Bailey *et al.* (2003) calculated the potential influence of salinity during a warming event by using estimates of Mg/Ca and $\delta^{18}\text{O}$ derived palaeotemperatures, although different Mg/Ca palaeotemperature equations were used. A similar technique was followed in Chapter 6 and will be used again here. If the 8.4°C temperature difference is interpreted solely in terms of salinity a freshening from a 'normal' marine salinity of 34 ‰ to a salinity of 25.8 ‰ is required, although, as mentioned in the previous chapter, modern *Sepia* have rarely been caught in waters with salinity values below 29 ‰ (Schäfer, 1972; Wierzbowski, 2004). An additional problem associated with the calculated palaeotemperature values and the assumption that Mg/Ca ratios represent temperature whilst $\delta^{18}\text{O}$ values are assumed to represent temperature and salinity, is that a value of -4.2°C (the lowest value calculated using Mg/Ca ratios) is impossible, since marine cephalopods could not exist in these conditions. This casts serious doubt on the use of Mg/Ca as a palaeotemperature proxy for belemnites using the Klein *et al.* (1996) palaeotemperature calibration.

7.5.4. The Terrestrial Carbon Isotope Record

The wood-derived carbon-isotope ratios presented here are considered to primarily reflect changes in the terrestrial carbon-isotope reservoir. The limitations and reliability of fossil wood data were discussed in Chapter 4, where it was concluded that $\delta^{13}\text{C}_{\text{org}}$ values could be used to confidently identify long-term shifts in the composition of atmospheric carbon. Recognisable plant fragments (e.g., charcoal and coalified material) were used to construct the organic carbon isotope record presented here rather than the bulk matter approach (as was used for Staffin Bay, Isle of Skye). The advantages of this sampling

strategy (over the bulk approach) are that only terrestrial matter is collected (not marine) and that the effects of variation in the organic matter source component or environment are minimised. The validity of this technique has been demonstrated by several Mesozoic studies (e.g., Hesselbo *et al.*, 2003; Robinson & Hesselbo, 2004; Gröcke *et al.*, 2005). The preservation of plant material ranged from charcoal to coal (see Plates 10 & 11), however this made no significant difference to the long-term $\delta^{13}\text{C}_{\text{org}}$ trend. Several previously published studies confirm the lack of influence of preservation on isotopic values (e.g., Hesselbo *et al.*, 2003; Gröcke *et al.*, 2005).

The Ryazanian-Hauterivian $\delta^{13}\text{C}_{\text{org}}$ curve from the Boyarka River succession records a positive carbon-isotope excursion with the maximum occurring in the Upper Valanginian *Bidichotomus* Zone (Fig. 7.7). The initiation of the positive isotope excursion occurs in the upper part of the Lower Valanginian *Stubendorffi* Zone, which is broadly time-equivalent to the Tethyan *Campylotoxia* Zone. Ryazanian to Lower Valanginian $\delta^{13}\text{C}_{\text{org}}$ values fluctuate between -27.2 and -23.2 ‰, whilst Upper Valanginian values reach a maximum of -21.2 ‰ (Fig. 7.7). The carbon-isotope values fall gradually across the Valanginian-Hauterivian boundary and pre-excursion values are reached (~ -25 to -23 ‰) in the Lower Hauterivian *Bojarkensis* Zone. The scatter observed in this Boyarka River record is consistent with the degree of scatter observed in previously published Mesozoic wood records (e.g., Heimhofer *et al.*, 2003; Hesselbo *et al.*, 2003; Gröcke *et al.*, 2005).

The timing and duration of the $\delta^{13}\text{C}_{\text{org}}$ positive excursion is consistent with previously published terrestrial data from the Crimea (Gröcke *et al.*, 2005). The values recorded by Gröcke *et al.* (2005) however, are ~ 3 ‰ heavier than those observed here. This may be the result of analysing different plant elements since modern C3 plants demonstrate significant variability in carbon isotope composition (< ± 4 ‰) between discrete elements (Leavitt & Long, 1991; Loader *et al.*, 1995; Schleser, 1999; Robinson & Hesselbo, 2004). In addition, lighter isotope values are commonly recorded in regions where soil moisture content is high. Heavier high latitude isotope values therefore seem

reasonable. The initiation of the excursion recorded by Gröcke *et al.* (2005) also occurs slightly later (in the Tethyan *Verrucosum* Zone) than that observed here (assuming accurate correlation). Prior to the work of Gröcke *et al.* (2005) the Upper Valanginian positive carbon isotope excursion had only been recorded in marine carbonates and marine organic matter (e.g., Lini *et al.*, 1992; Henning *et al.*, 1999; Wortmann & Weissert, 2000; Price & Mutterlose, 2004). The record presented here is the first Boreal Realm terrestrial record of this event.

7.5.5. The Marine Carbon Isotope Record

The $\delta^{13}\text{C}_{\text{carb}}$ curve shows some degree of scatter, although this is consistent with previously published belemnite data. The lowest carbon-isotope values (-1.1 ‰) occur in the Lower Ryazanian *Kochi* Zone. Values increase slightly from the Ryazanian and into the Valanginian until the rapid positive excursion initiated in the upper part of the Lower Valanginian *Stubendorffi* Zone. The positive carbon-isotope excursion is of a magnitude of approximately 3 ‰ (reaching a maximum of 4.2 ‰). A return towards pre-excursion values occurs in the Lower Hauterivian *Bojarkensis* Zone.

The Upper Valanginian positive carbon-isotope excursion recorded here in marine carbonate from the Boyarka River can be compared to data published by Price & Mutterlose (2004) from the Yatria River, Western Siberia. Price & Mutterlose (2004) also recorded the positive excursion from belemnites. They recorded the positive excursion from two sites in the Yatria River, although less positive values were observed at the excursion maximum (< 3.7 ‰) and the excursion was of a slightly smaller magnitude (< ~2 ‰). The timing and duration of the excursion was compatible with that observed here, with initiation in the upper part of the Lower Valanginian and a return to pre-excursion values into the Hauterivian.

7.5.6. The Carbon Isotope Records & Ocean-Atmosphere Correlation

As discussed in Chapter 5 the comparison of marine and terrestrial carbon isotope stratigraphy is essential to understanding perturbations in the global carbon cycle. Marine and terrestrial carbon-isotope records have been compared in a number of studies (e.g., Gröcke *et al.*, 1999, 2005; Ando *et al.*, 2002, 2003; Hesselbo *et al.*, 2003; Robinson & Hesselbo, 2004; Pearce *et al.*, 2005), however such work has almost always compared marine and terrestrial records from different successions. This presents problems in terms of accurate correlation that are often difficult to overcome. Geological successions containing terrestrial organic matter together with marine carbonate are very rare and consequently coeval marine and terrestrial records are not generally published. The Boyarka River succession however, presents this opportunity.

The observed offset between the $\delta^{13}\text{C}_{\text{org}}$ and $\delta^{13}\text{C}_{\text{carb}}$ data is approximately 25 ‰ on average. This is consistent with the average observed from the Staffin Bay, Isle of Skye data (~25.5 ‰). These values are larger than might be expected, for example, from Poland and Germany (~23 ‰) as recorded and discussed by Wierzbowski (2002, 2004) and Pearce *et al.* (2005). In Chapter 5 it was hypothesised that this difference in offset was likely to be the result of isotopically heavier belemnite values as a result of ^{13}C enrichment in the Boreal Realm, due primarily to high organic matter productivity in the partly isolated Boreal seas (Wierzbowski, 2004). The observed offset in the Boyarka River data lends further support to this hypothesis.

The initiation of the $\delta^{13}\text{C}_{\text{org}}$ and $\delta^{13}\text{C}_{\text{carb}}$ positive isotope excursions occurs simultaneously in the upper part of the Lower Valanginian *Stubendorffi* Zone. This suggests that the ocean-atmosphere system is strongly linked at this time. Previous studies of marine and terrestrial carbon isotope data have shown that the timing and duration of excursions are likely to be synchronous in terrestrial organic matter, marine organic matter and marine carbonate (e.g., Gröcke *et al.*, 1999, 2005). This can now be confirmed for terrestrial organic matter and marine carbonate by the Boyarka River data.

The $\delta^{13}\text{C}_{\text{carb}}$ excursion observed here is of a higher magnitude than that of the $\delta^{13}\text{C}_{\text{org}}$ excursion. This is quite unusual, since the magnitude of shifts in the terrestrial record is normally considerably greater than those in the respective marine record (e.g., Gröcke *et al.*, 1999; Robinson & Hesselbo, 2004; Pearce *et al.*, 2005). A classic example of this relationship is the negative carbon isotope excursion recorded at the Palaeocene Eocene Thermal Maximum (PETM), where the excursion in the terrestrial record is approximately twice the magnitude of that observed in the marine record (e.g., Bowen *et al.*, 2004, 2006). Smith *et al.* (2006) hypothesise that this may be the result of an increase in ρCO_2 concentrations at this time, causing increased warming and an increase in moisture, to which plants would respond with greater carbon isotope discrimination and ultimately an enhanced carbon isotope signature.

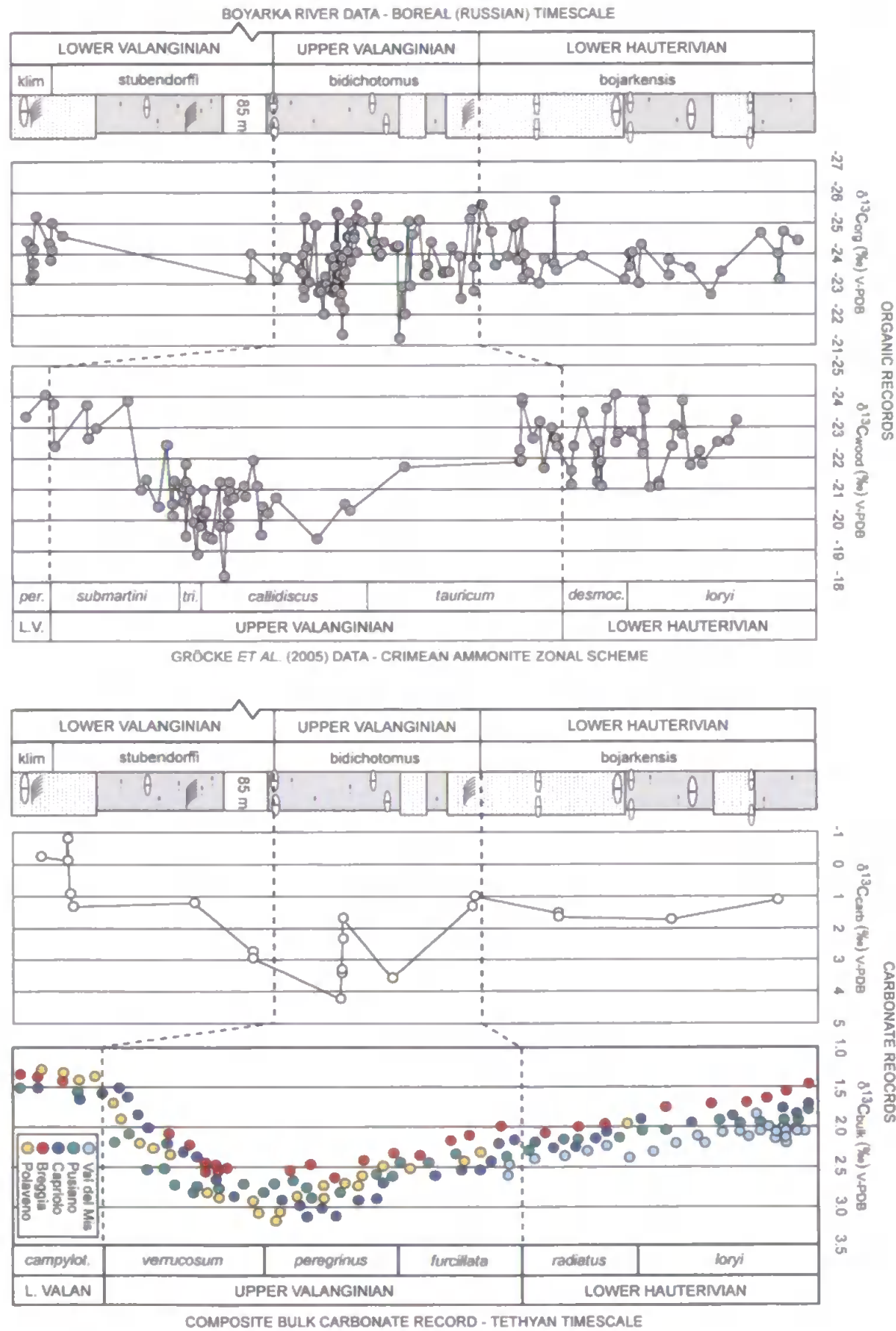
It is interesting that the inverse terrestrial-marine relationship is observed in the Boyarka River succession, which is coincident with a drop in ρCO_2 (as determined below - see section 7.5.7). Given this relationship, it is tempting to suggest that such a drop in ρCO_2 would cause plants to reduce their carbon isotope discrimination and therefore lower the magnitude of the $\delta^{13}\text{C}_{\text{org}}$ excursion. The problem with this model however, is that a fall in ρCO_2 should also result in increasing oceanic alkalinity, which would potentially reduce carbonate fractionation in the marine realm. This effect has been observed in modern foraminifera (e.g., Spero *et al.*, 1997) and would presumably also lower the rate of fractionation in Valanginian belemnites during a drop in ρCO_2 . It is possible however, that changes in ρCO_2 have a stronger or more immediate influence on the terrestrial realm, which may account for the reduced carbon isotope signature in plants but not in belemnites at this time. The usual interpretation of changes in discrimination by plants however, is that they have experienced a change in available moisture. The decrease in discrimination observed here could therefore be the result of increased water stress under drier conditions (Francesca Smith pers. comm.).

7.5.7. Ryazanian-Hauterivian Marine & Terrestrial Isotopic Records

Published marine carbonate stable isotope records for the Early Cretaceous have been constructed primarily from successions in the Tethyan region (e.g., Lini *et al.*, 1992; Weissert *et al.*, 1998; Price *et al.*, 2000; van de Schootbrugge *et al.*, 2000; Weissert & Erba, 2004), although Price & Mutterlose (2004) have also published data from a high latitude site. The overall pattern described from such research is one of decreasing $\delta^{13}\text{C}$ values across the Jurassic-Cretaceous boundary, relatively stable $\delta^{13}\text{C}$ values in the earliest Cretaceous, then a rapid mid- to Late Valanginian positive carbon-isotope excursion (occurring in the Tethyan *Campylotoxus* ammonite Zone) and a subsequent return to pre-excursion values in the Upper Valanginian and Lower Hauterivian (Price & Mutterlose, 2004) (Fig. 7.13).

The Boyarka River positive carbon-isotope excursion observed in both the $\delta^{13}\text{C}_{\text{carb}}$ and $\delta^{13}\text{C}_{\text{org}}$ records begins in the upper *Stubendorffi* zone (which is correlatable with the Tethyan *Campylotoxus* Zone). The peak of the positive $\delta^{13}\text{C}$ excursion occurs in the *Bidichotomus* Zone which corresponds well biostratigraphically with the timing of the Tethyan excursion in the *Trinodosum* and *Callidiscus* ammonite zones (e.g., van de Schootbrugge *et al.*, 2000; Weissert & Erba, 2004), however, it should be noted that much of the uppermost *Stubendorffi* Zone is missing. Lini *et al.* (1992) hypothesised that the Valanginian carbon-isotope event represented the first episode of greenhouse conditions during the Cretaceous period. This event has frequently been related to episodes of platform drowning within the Tethys (e.g., Lini *et al.*, 1992; Föllmi *et al.*, 1994; Weissert *et al.*, 1998; Wortmann & Weissert, 2000). Positive carbon isotope events are commonly attributed to increased organic carbon burial either as the result of enhanced surface water productivity or owing to enhanced preservation under reduced O_2 conditions (Weissert *et al.*, 1998; Bersezio *et al.*, 2002; Erba *et al.*, 2004; Price & Mutterlose, 2004). Van de Schootbrugge *et al.* (2000) however, highlighted the problem with this model, which is that during the Hauterivian, at least two phases of platform drowning are not associated with

Figure 7.13 Valanginian-Hauterivian $\delta^{13}\text{C}$ correlation between the Boyarka River succession $\delta^{13}\text{C}_{\text{org}}$ curve and the Crimea (based upon data from Gröcke *et al.*, 2005) and the $\delta^{13}\text{C}_{\text{carb}}$ curve and a composite Tethyan bulk $\delta^{13}\text{C}$ curve (based upon data from Lini *et al.*, 1992 and Channell *et al.*, 1993 and adapted after Gröcke *et al.*, 2005). Boreal (Russian), Crimean and Tethyan ammonite zones are illustrated. See Figure 4.2 for key to log symbols.



positive carbon-isotope excursions. Wortmann & Weissert (2000) suggested that the sea-level rise and drowning of platform carbonates corresponded to the initiation of more positive carbon-isotope values.

According to the eustatic sea-level curve of Sahagian *et al.* (1996), based on Russian platform and Siberian stratigraphy, the Upper Valanginian *Bidichotomus* Zone witnesses a brief sea-level rise coincident with the initiation of the positive carbon-isotope excursion, then a sea-level fall synchronous with the excursion maximum and followed by another rise into the Hauterivian coinciding with the return to pre-excursion values (Fig 7.7). Although the Sahagian *et al.* (1996) sea-level curve is contrary to the sea-level curve of Haq *et al.* (1987), the Valanginian section of the Sahagian *et al.* curve was constructed from data taken from the Boyarka River section itself. Positive carbon-isotope excursions may be related to regressive conditions due to an increased input of nutrients resulting from the exposure and erosion of lowland areas (Brenchley *et al.*, 1994; Gröcke *et al.*, 1999; Price & Mutterlose, 2004). Partial separation of the Boreal and Tethyan Realms during periods of sea-level lowstand could have restricted ocean circulation and enhanced stratification to promote organic carbon burial in these high latitude locations (Price & Mutterlose, 2004).

The evidence for widespread Late Valanginian marine black shales is very limited. Perhaps the best evidence comes from organic carbon-rich black shales in the Southern Alps (Bersezio *et al.*, 2002) and from the Shatsky Rise in the West Pacific (Bralower *et al.*, 2002). Price & Mutterlose (2004) suggest that the absence of widespread Valanginian black shale deposits could be due to erosion (e.g., Weissert *et al.*, 1998) or due to burial away from typical marine settings (e.g., in terrestrial environments) or away from the Tethys (e.g., at high latitudes).

The terrestrial $\delta^{13}\text{C}$ record presented here is the first Boreal Realm terrestrial record of the Upper Valanginian positive carbon-isotope event. Only one other terrestrial record of this event exists, that of Gröcke *et al.* (2005) from the Crimean Peninsula of the

southern Ukraine. Gröcke *et al.* (2005) also record the positive carbon-isotope excursion from macroscopic wood. Their excursion begins in the *Submartini* Zone (which is correlatable with the Tethyan *Verrucosum* Zone) and reaches a maximum in the Tethyan *Callidiscus* Zone. This excursion correlates well (within the limits of biostratigraphic resolution) with the carbon-isotope excursions identified in the Boyarka River and in Tethyan carbonates.

Delta-delta ($\Delta\delta = \delta^{13}\text{C}_{\text{carb}} - \delta^{13}\text{C}_{\text{org}}$) relationships observed from the paired analysis of marine carbonate and marine or terrestrial organic matter have been used as a proxy for $p\text{CO}_2$ concentrations (e.g., Weissert *et al.*, 1998; Kump & Arthur, 1999; Hasegawa *et al.*, 2003). Gröcke *et al.* (2005) calculated $\Delta\delta$ values from their $\delta^{13}\text{C}_{\text{plant}}$ data and a composite $\delta^{13}\text{C}_{\text{carb}}$ record from the Tethyan region (compiled from the work of Lini *et al.* (1992) and Channell *et al.*, (1993)). They observed a +2 ‰ shift between the Tethyan marine carbonate record and the terrestrial plant record for the Crimea, which they linked to a drop in atmospheric $p\text{CO}_2$ in the order of ~40 % and consequently to a short-term Valanginian cooling event. This was calculated following the work of several authors, which suggested that a 10 % shift in $p\text{CO}_2$ levels would result in a 0.5 ‰ change in $\delta^{13}\text{C}_{\text{org}}$ due to the alteration of photosynthetic isotopic fractionation (e.g., Körner *et al.*, 1988; Gröcke, 1998; van de Water *et al.*, 1994). An organic carbon burial event and associated positive $\delta^{13}\text{C}$ excursion would lead to this drawdown of $p\text{CO}_2$ (Gröcke *et al.*, 2005) and, potentially, acidification. The $\Delta\delta$ relationship observed from the Boyarka River dataset is consistent with that observed in the Crimea, although it is of a smaller magnitude (~1 ‰ rather than 2 ‰). The Boyarka River data therefore support the idea that the Valanginian period sees a drop in atmospheric $p\text{CO}_2$ associated with the peak of the Valanginian carbon-isotope event. Atmospheric $p\text{CO}_2$ values can also be affected by other factors however, such as volcanism, silicate weathering and deposition of calcium carbonate (Kump & Arthur, 1999; Berner & Kothavala, 2001; Gröcke *et al.*, 2005).

The idea of a Valanginian cooling event is consistent with other recently published evidence on this period (e.g., Mutterlose *et al.*, 2003; Puc  at *et al.*, 2003; Erba *et al.*, 2004; Weissert & Erba, 2004; Kessels *et al.*, 2006; McArthur *et al.*, in press). Erba *et al.* (2004) provided nannofossil and oxygen-isotope evidence for a cooling event at the $\delta^{13}\text{C}$ excursion maximum. Weissert & Erba (2004) suggest that the cooling event may have been the result of increased organic carbon burial (as reflected by the $\delta^{13}\text{C}$ positive excursion) and the resultant pumping of CO_2 from the atmosphere and into the sediment. This model is supported by oxygen-isotope data from Tethyan fish tooth enamel, which indicate a major cooling event during the earliest Late Valanginian (Puc  at *et al.*, 2003). It is further supported by a Late Valanginian boreal nannoplankton excursion in Romania (Melinte & Mutterlose, 2001) and the presence of glendonites in several Valanginian successions (e.g., Kemper, 1987; Tarduno *et al.*, 2002). Unfortunately the oxygen-isotope data from the Boyarka River succession provides somewhat inconclusive evidence with regards to palaeotemperatures. For the $\delta^{13}\text{C}$ positive excursion maximum a palaeotemperature range of 6.3 to 14.8 $^\circ\text{C}$ is recorded.

7.6. Conclusions

- The data presented here comprise the first combined high-resolution isotope investigation of $\delta^{13}\text{C}_{\text{org}}$, $\delta^{13}\text{C}_{\text{carb}}$ and $\delta^{18}\text{O}_{\text{carb}}$ from the Boyarka River, Northern Central Siberia. It is also the first ever investigation of a coeval $\delta^{13}\text{C}_{\text{org}}$ and $\delta^{13}\text{C}_{\text{carb}}$ record (together with the data presented in Chapter 5).
- The average palaeotemperature derived from the Boyarka River $\delta^{18}\text{O}$ record (using the Anderson & Arthur (1983) equation) was 10.6 $^\circ\text{C}$ and the palaeotemperature range was 2.1 to 19.0 $^\circ\text{C}$ for the Ryazanian to Hauterivian interval. This suggests that the climate may have been very variable at this time or that salinity may have had a significant influence on $\delta^{18}\text{O}$ ratios. The temperature range also indicates that the region was at

times considerably colder than previously thought, which could indicate the presence of limited polar ice.

- An Upper Valanginian positive carbon-isotope excursion is identified in both the $\delta^{13}\text{C}_{\text{org}}$ and $\delta^{13}\text{C}_{\text{carb}}$ records. The initiation of the excursion occurs simultaneously in the upper part of the Lower Valanginian *Stubendorffi* ammonite zone (broadly equivalent to the Tethyan *Campylotoxia* Zone). In both records the carbon-isotope values then decrease across the Valanginian-Hauterivian boundary and a return towards pre-excursion values occurs during the *Bojarkensis* Zone. This trend is consistent with that observed in Tethyan carbonate successions and therefore indicates a strong coupling of the ocean-atmosphere system at this time and suggests that the total exchangeable carbon reservoir was affected.
- The initiation of the positive $\delta^{13}\text{C}$ excursion is associated with a brief sea-level rise on the Russian platform, although the excursion maximum occurs during a period of overall regression. Exposure and erosion of lowland areas and restricted ocean circulation and enhanced stratification during a period of sea-level lowstand may account for increased rates of organic carbon burial.
- The Boyarka River $\Delta\delta$ values may indicate a drop in atmospheric ρCO_2 . This is likely to be the result of enhanced organic carbon burial, which could lead to a drawdown of ρCO_2 and a period of cooling in the late Valanginian.

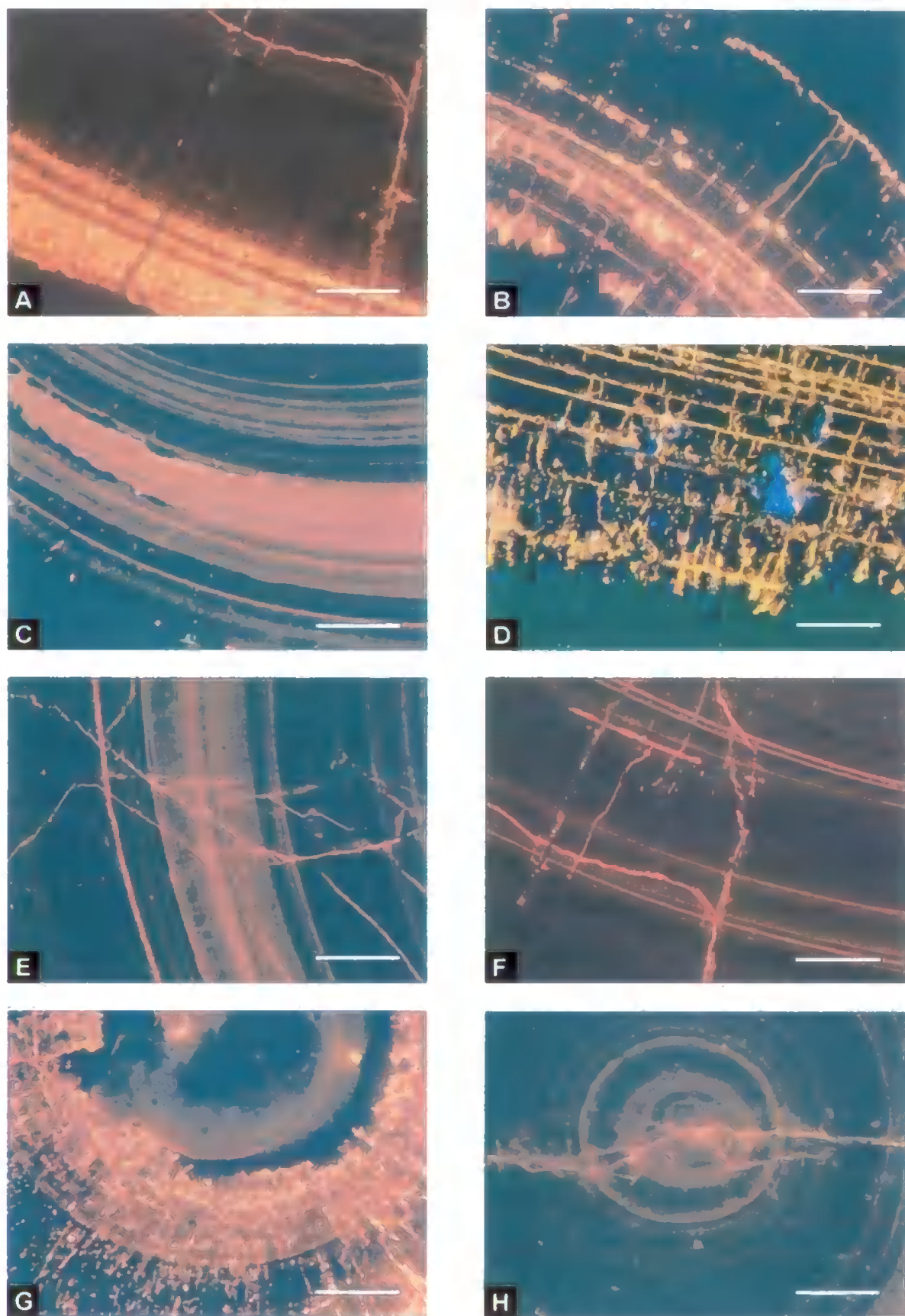


Plate 7. Cathodoluminescence images showing the state of preservation of belemnite rostra from the Boyarka River, Siberia. All scale bars represent 1 mm. (A) Rostrum margin displaying significant alteration. (B) Rostrum margin, growth bands and fractures displaying alteration. (C) Growth bands displaying significant alteration. (D) Strong alteration along the rostrum margin. (E) Fractures and growth bands displaying alteration. (F) Fractures and growth bands displaying alteration. (G) Apical canal surrounded by area displaying significant alteration. (H) Fractures emanating from and growth bands surrounding the apical canal.

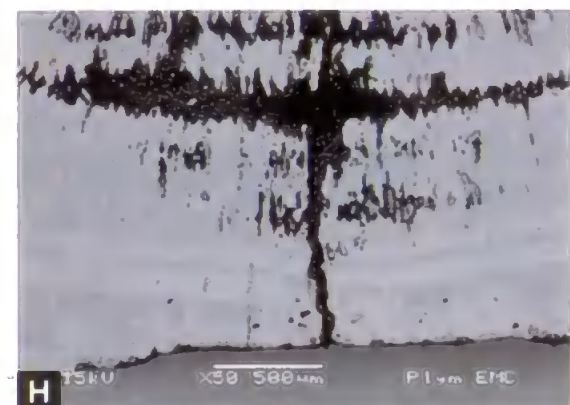
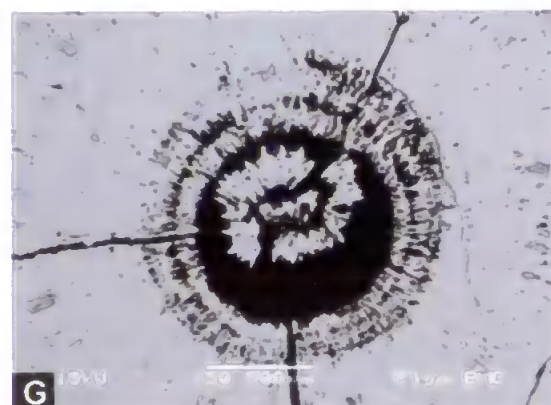
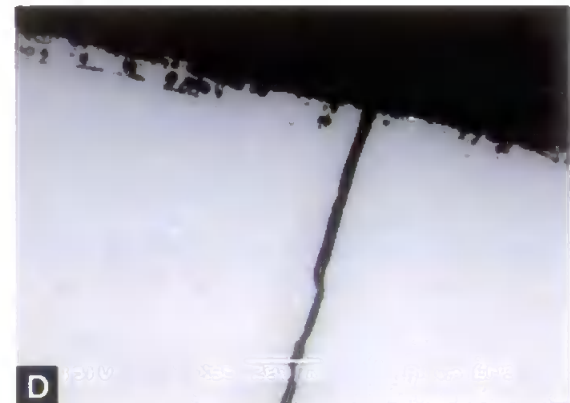
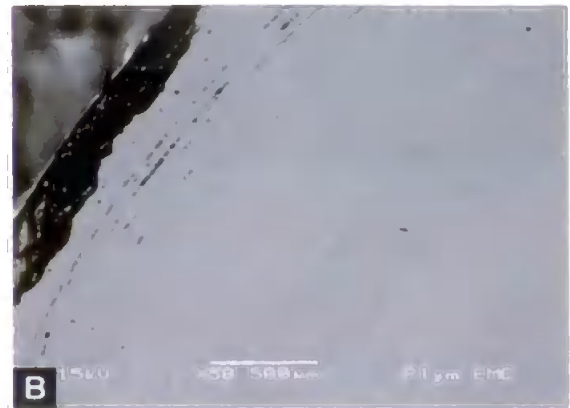


Plate 8. Backscattered SEM images showing the state of preservation of belemnite rostra from the Boyarka River, Siberia. All scale bars represent lengths stated on images. (A) Well preserved calcite with some slight alteration along growth lines at the rostrum margin. (B) Generally well preserved calcite but with some alteration along growth bands towards the rostrum margin. (C) Pyrite growth along growth line fractures at rostrum margin. (D) Fracture at rostrum margin showing little alteration. (E) Fracture running through apical canal. (F) Fracture running through apical canal. (G) Apical Canal. (H) Rostrum margin with fractures and displaying alteration along growth bands.

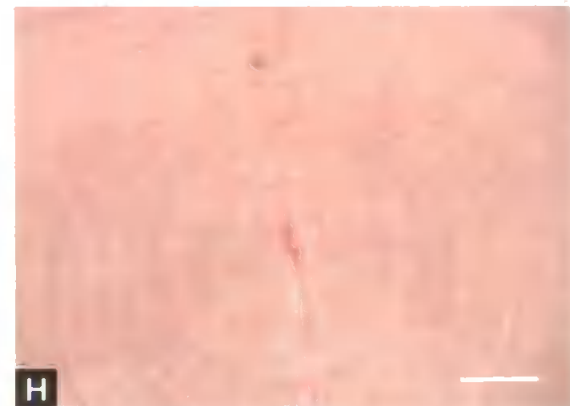
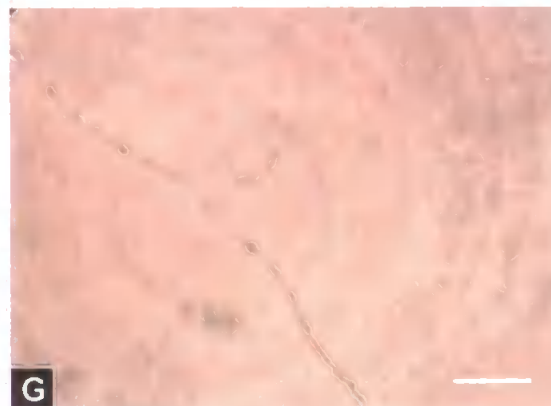
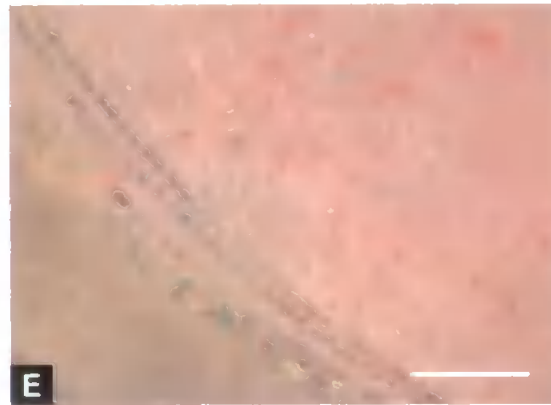
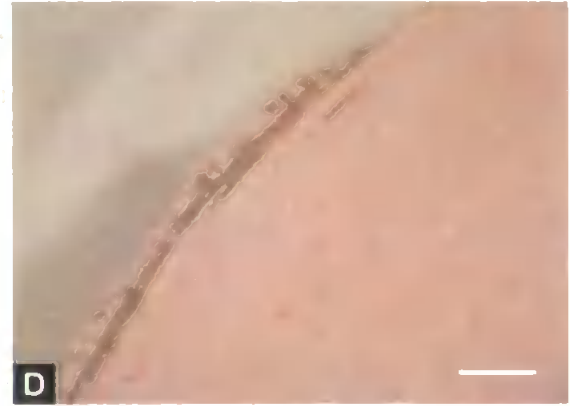
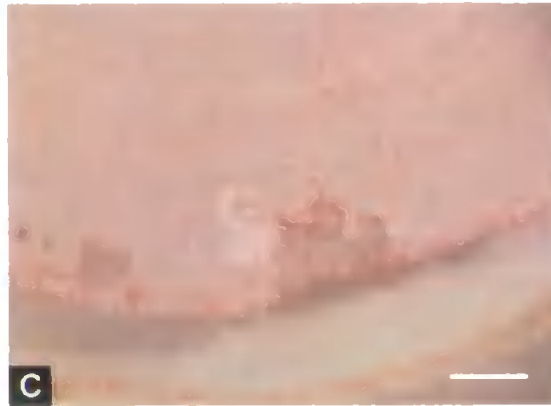
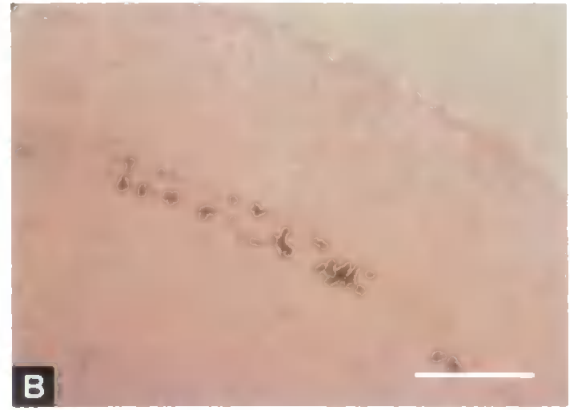


Plate 9. Carbonate stained images showing the state of preservation of belemnite rostra from the Boyarka River, Siberia. All scale bars represent 1 mm. (A) Very well preserved calcite at rostrum margin. (B) Generally well preserved calcite but with some pyrite growth along growth lines towards the rostrum margin. (C) Fractures and growth lines towards rostrum margin displaying alteration. (D) Generally well preserved calcite but with some alteration and pyrite growth at margin edge. (E) Rostrum margin showing alteration particularly along growth lines. (F) Rostrum margin showing alteration particularly along growth lines and around fractures. (G) Fracture running through apical canal. (H) Fracture running through apical canal.

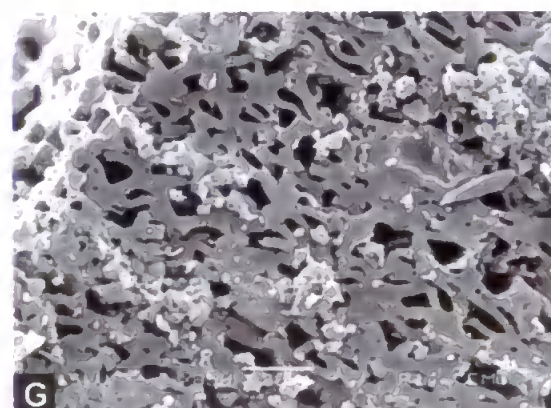
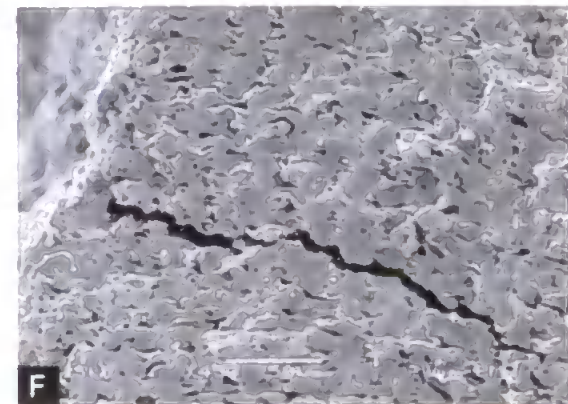
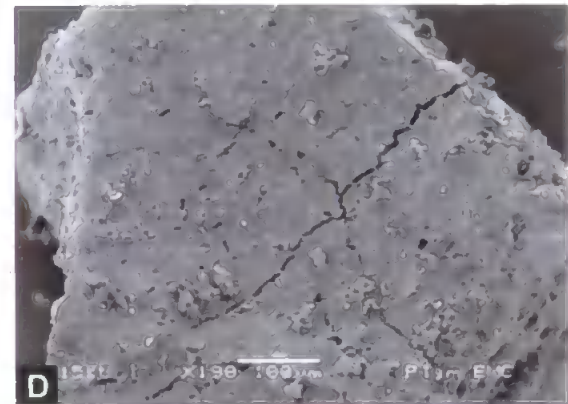
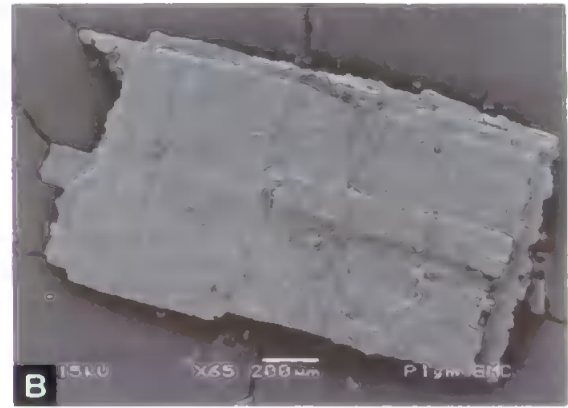
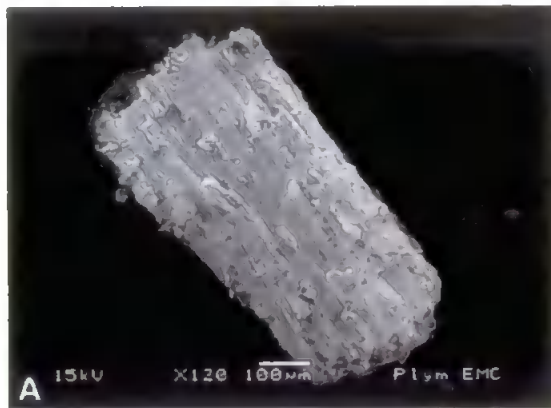


Plate 10. Scanning Electron Microscope images showing the state of preservation of fossil wood fragments from the Boyarka River, Siberia. All scale bars represent lengths stated on images. (A) Charcoal - woody structure preserved. (B) Charcoal - woody structure preserved. (C) Coal - blocky nature of fragment. (D) Charcoal-coal - mostly homogenised internal structure. (E) Coal - completely homogenised internal structure. (F) Charcoal-coal - homogenised and compacted internal structure. (G) Charcoal-coal - homogenised and compacted internal structure. (H) Charcoal - internal cellular structure preserved.

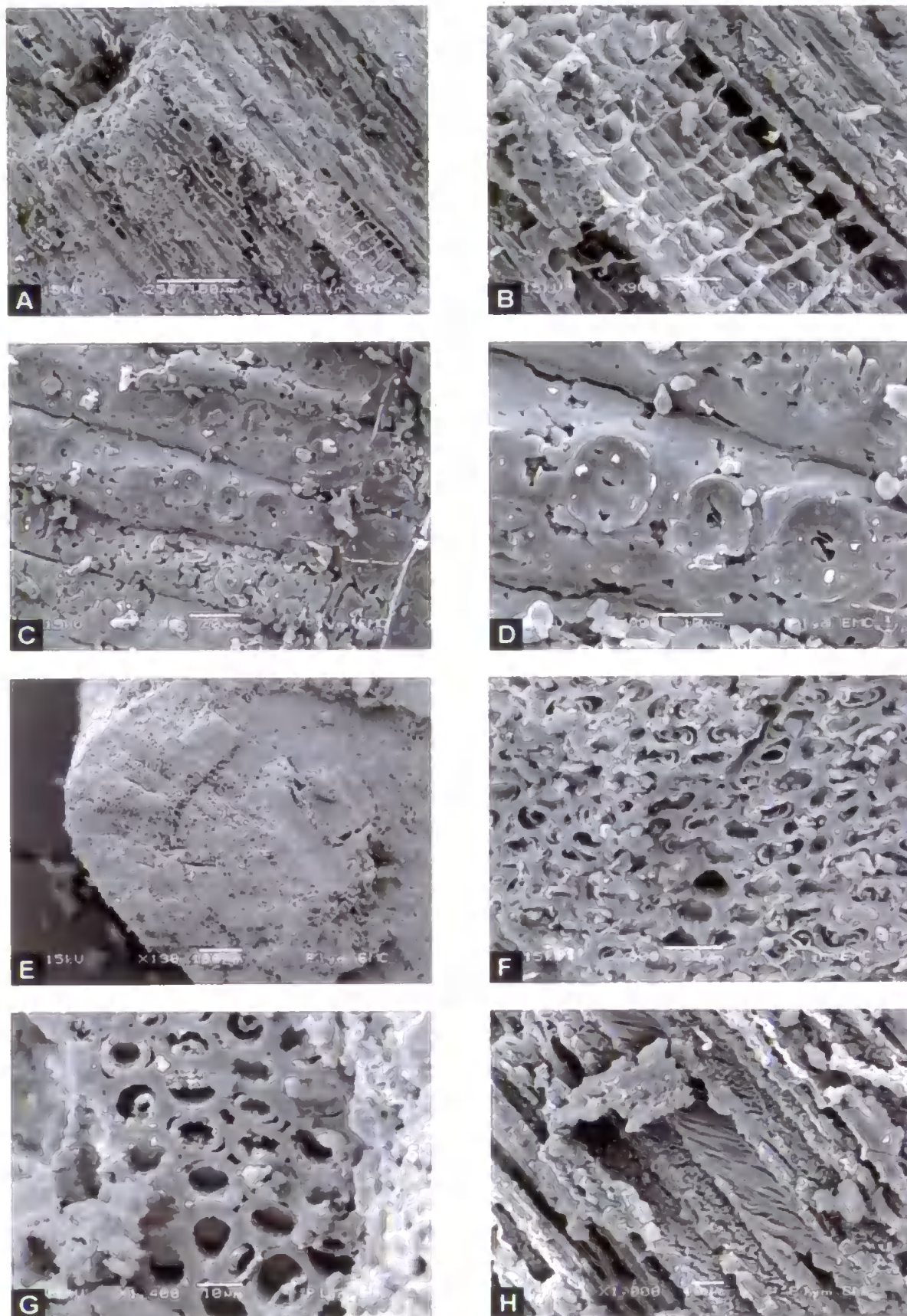


Plate 11. Scanning Electron Microscope images showing the state of preservation of fossil wood fragments from the Boyarka River, Siberia. All scale bars represent lengths stated on images. (A) Charcoal - internal cellular structure preserved. (B) Charcoal - internal cellular structure preserved (close-up of A). (C) Charcoal - internal cellular structure preserved. (D) Charcoal - internal cellular structure preserved (close-up of C). (E) Charcoal - internal cellular structure preserved. (F) Charcoal - internal cellular structure preserved (close-up of E). (G) Charcoal-coal - internal cellular structure displaying some signs of homogenisation. (H) Charcoal-coal - internal cellular structure displaying some signs of homogenisation.

8. IZHMA RIVER, TIMAN-PECHORA BASIN, RUSSIA

8.1. Location & Site Description

The Izhma River is a tributary of the Pechora River, both of which are situated within the Timan-Pechora Basin of north-eastern European Russia (Fig. 8.1). The Izhma River lies just west of the sub-Arctic Ural Mountains at a present-day latitude of $\sim 64^{\circ}\text{N}$. The sections exposed on the banks of the Izhma River begin north of the towns of Ukhta and Sosnogorsk, which are approximately 200 km south of the confluence of the Izhma and Pechora Rivers.

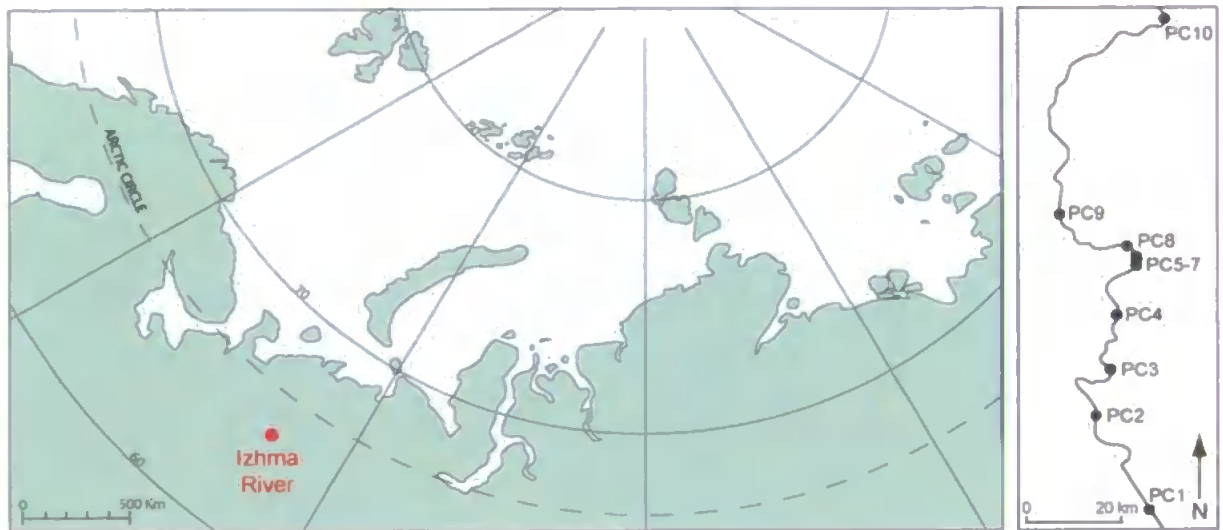


Figure 8.1 Location map of the Izhma River, Russia. The location of the Izhma River is shown (left) together with the relative positions of each of the sites examined (right).

Ten key locations were examined along the course of the Izhma River, ranging from Early Callovian (*Elatmae* ammonite Zone) to Early Hauterivian (*Bojarkensis* ammonite Zone) in age. The outcrops were in the form of low, river cuttings (containing belemnites) (Fig. 8.2) and pebbly river foreshores, with belemnites particularly common elements of the foreshore scree.



Figure 8.2 River-side cliff, exposure typical of the Izhma River, Russia.

8.2. Geological Setting

The Timan-Pechora Basin covers an area of $\sim 440,000 \text{ km}^2$ (O'Leary *et al.*, 2004). It is a passive margin basin that extends from northern Russia and into the Barents Sea, where it merges with the South Barents Sea Basin (Requejo *et al.*, 1995; O'Leary *et al.*, 2004) (Fig. 8.3). On the western margin of the basin is the Timan Ridge, a major linear basement elevation (striking NW-SE) thought to represent the collision of one or more small continental blocks with the East European Platform during the Ediacaran (Zonenshain *et al.*, 1990; Ismail-Zadeh *et al.*, 1997; O'Leary *et al.*, 2004). The eastern and northeastern margins of the basin are formed by the Urals fold-and-thrust belt, which developed during the collision of the East European and Siberian blocks during the Late Carboniferous-Permian (O'Leary *et al.*, 2004). A series of deep depressions on the east margin of the basin are known as the Pre-Urals Depression and were formed above a zone of Palaeozoic peri-craton subsidence during the Uralian Orogeny (Ismail-Zadeh *et al.*,

1997). The Timan-Pechora Basin tapers southwards towards the convergence of the Timan Ridge and the Ural Mountains and broadens northwards where it extends offshore (O'Leary *et al.*, 2004). Zonenshain *et al.* (1990) divided the basin into two broad, stable, basement highs each with relatively thin sedimentary cover (the Izhma-Pechorskaya (within which the studied section of the Izhma River is situated) and Khoreyverskaya depressions) (Fig. 8.3). These highs are divided by fault-defined, linear mobile belts containing relatively thick sedimentary successions (O'Leary *et al.*, 2004).

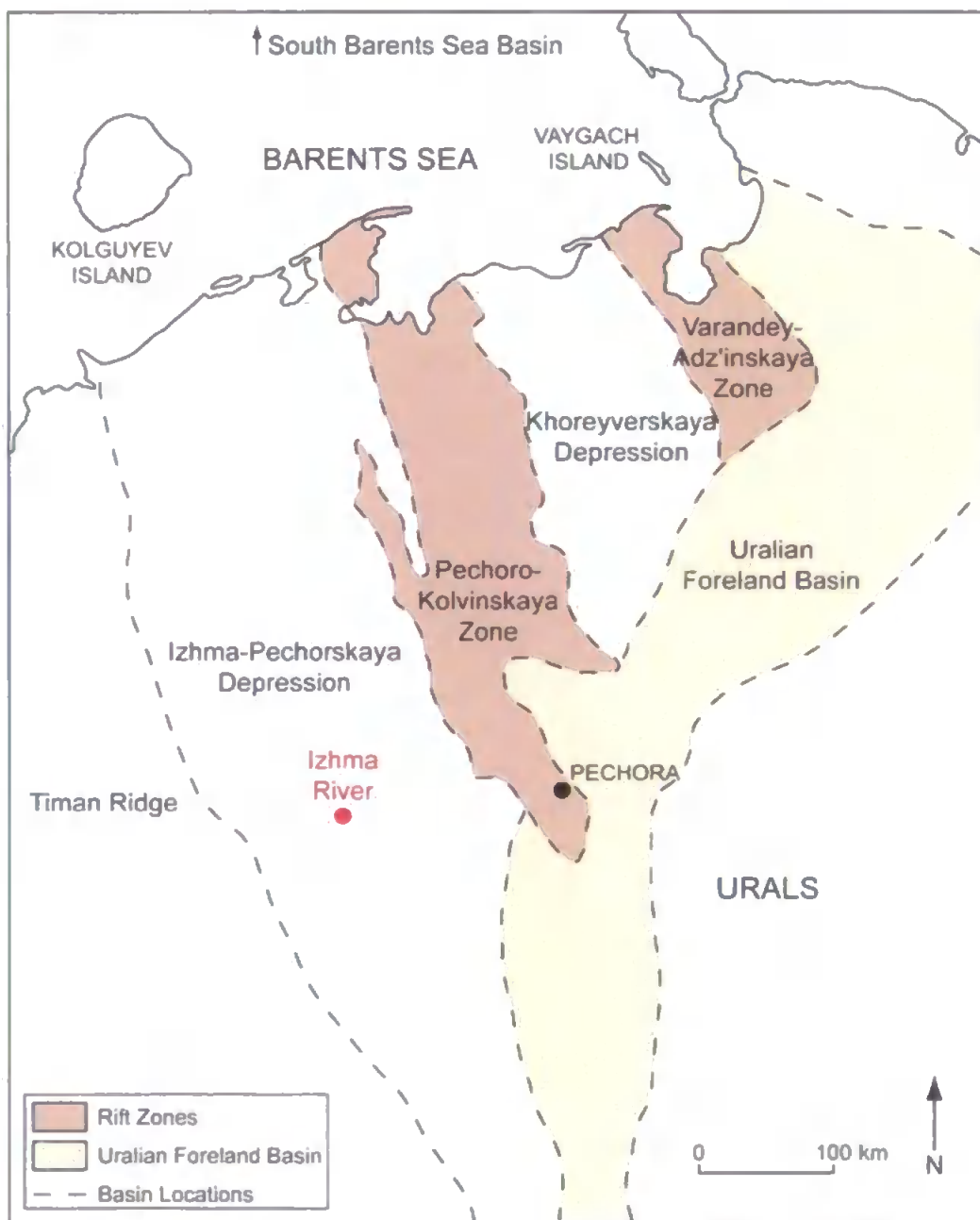


Figure 8.3 Simplified map of the Timan-Pechora Basin and surrounding areas. The principal structural zones are shown. Adapted after O'Leary *et al.* (2004).

During the Palaeozoic the Timan-Pechora Basin was a major extensional basin comprising a series of narrow grabens mainly orientated NNW-SSE (Banks *et al.*, 1997). Early Palaeozoic extension was particularly intense in the Middle-Late Devonian when the basin experienced rapid subsidence (Banks *et al.*, 1997; Ismail-Zadeh *et al.*, 1997). During the Early Permian another period of relatively rapid subsidence occurred in the Timan-Pechora Basin (Ismail-Zadeh *et al.*, 2004). This subsidence was the result of collision between the Baltic and Kazakstan plates at the time of the Uralian Orogeny, which was initiated in the Late Carboniferous/Permian (Banks *et al.*, 1997; Ismail-Zadeh *et al.*, 1997). Uralian activity was terminated in the Middle Triassic to Early Jurassic and a series of structural highs were formed, which now host over 250 known hydrocarbon accumulations in the region (Requejo *et al.*, 1995; Banks *et al.*, 1997).

The Timan-Pechora basement is exposed along the Timan Ridge and consists of metamorphosed sedimentary and volcanic rocks that have been intruded by granites (O'Leary *et al.*, 2004; Kuznetsov *et al.*, 2005). Overlying this thick metamorphosed basement are the Palaeozoic successions, which accumulated mainly in the western and central parts of the basin and are dominated by carbonate deposition, with episodes of siliciclastic sedimentation (Requejo *et al.*, 1995; O'Leary *et al.*, 2004). Finally, the continental to shallow marine siliciclastic Mesozoic sequence forms the dominant surface geology in the Timan-Pechora Basin (O'Leary *et al.*, 2004).

The Jurassic to Cretaceous Izhma River sequence is dominated by sandstones, siltstones and clays (Fig. 8.4), although, these are regularly affected by landslips and glacio-tectonic activity. The Lower Callovian (*Elatmae* Zone) outcrops ~2 km upstream of Porozhsk village and is represented by a poorly exposed, condensed sequence of clays containing abundant belemnites and phosphatic remains. A thin (15 cm) limestone horizon is also present. After a break in outcrop, Middle-Late Volgian sediments are exposed (*Panderi* to *Subditus* zones) ~1.8 km north of Kedvavom village. At the base, the sequence is dominated by calcareous grey claystones interbedded with black shales

containing belemnites. Belemnites become more abundant up sequence into the *Maximus* Zone, which is dominated by relatively well-bedded calcareous clays (layers of black shale are rare). Small carbonate concretions are scattered throughout and shells (mainly *Buchia*) are also common. The upper part of the *Maximus* Zone is composed of a relatively massive dark claystone. The Upper Volgian *Subditus* Zone is composed of phosphatic-rich silty claystone (similar to that of the *Panderi* Zone), with abundant shelly material and some belemnites.

The Basal Ryazanian *Pseudocraspedites/Surites* Zone (Fig. 8.4) outcrops ~6 km north of Kedvavom village, although, the exposure is generally poor. Silty sandstones at the base containing occasional small phosphatic nodules are overlain by dark grey/green sands containing rare *Surites* ammonites (~4 m thick). Above this sandy unit is a ~2 m thick band of heavily weathered, dark grey claystones with a pebble layer at the base. Belemnites occur throughout the succession, but are particularly common in a thin phosphatic horizon towards the top of the sand unit. Poorly preserved wood fragments also occur in this unit, but are quite rare.

The Upper Ryazanian *Tzikwinianus* Zone sediments (Fig. 8.4) are sandy at the base, but become increasingly clayey up sequence. The basal sands are grey, with abundant phosphatic concretions and belemnites. Abundant *Buchia* shells commonly occur in discrete horizons that are often associated with calcareous sands or phosphatic concretions. The sands become more iron rich towards the top of the sequence until the Ryazanian-Valanginian boundary, which is marked by an iron rich, red claystone bed of ~30 cm thickness.

Above the iron rich bed is a unit of light grey claystones that are silty at the base and contain *Polyptychities* sp. ammonites. These lowermost Valanginian deposits also contain dark grey claystones, grey/green sandstones and phosphatic claystones. Belemnites are common, particularly within layers of light grey/green claystones.

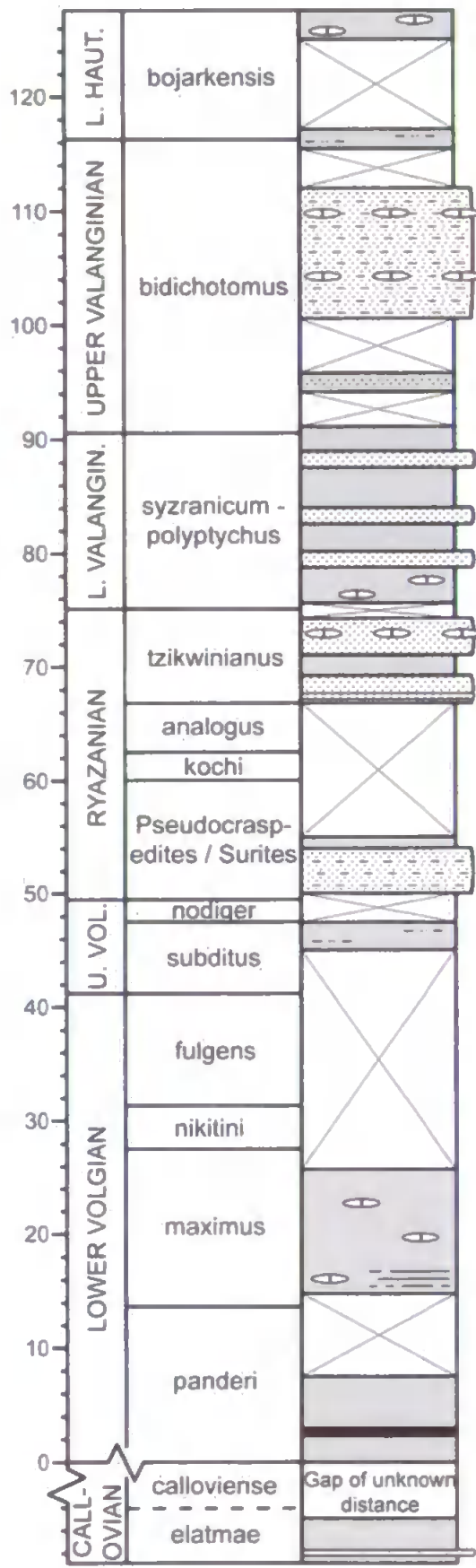


Figure 8.4 Sedimentary log and photographs of the Izhma River succession, Russia. Boreal (Russian) ammonite zones illustrated. See Figure 4.2 for key to log symbols. Scale is in metres.

The Upper Valanginian (*Bidichotomus* Zone) (Fig. 8.4) is composed of poorly exposed fine, clayey to silty, dark grey/green sandstones. Large carbonate concretions containing abundant *Buchia* and some ammonites (*Dichotomites* sp.) occur in horizons <50 cm thick near the base of the unit. Smaller concretions however, occur towards the top of the unit. Belemnites are not common in Upper Valanginian strata and when present are extensively weathered. The Lower Hauterivian (*Bojarkensis* Zone) outcrop is reasonably well exposed, although, it has been subjected to a degree of glacio-tectonic activity. Dark grey clays with concretions that contain *Buchia* and belemnites are the dominant lithology.

8.3. Sampling & Methodology

The ten major sites visited along the Izhma River provided samples from the Early Callovian (*Elatmae* Zone) and from the Middle Volgian (*Panderi* Zone) to Early Hauterivian (*Bojarkensis* Zone). Belemnites were collected from 67 different horizons. Wherever possible multiple specimens were collected from the belemnite horizons. In addition, 86 sediment horizons and 13 fossilised wood horizons were sampled, although, these samples have not been analysed here. All samples were collected in the summer of 2003 by Dr Gregory Price, University of Plymouth.

The preservation of belemnite rostra was evaluated through trace element and stable isotopic analysis, backscattered scanning electron microscopy (BSEM), cathodoluminescence (CL) and carbonate staining. The areas most susceptible to diagenesis were removed prior to isotopic and geochemical analysis.

Stable isotope data were generated on an Isoprime isotope ratio mass spectrometer (GV Instruments, UK), at the University of Plymouth, UK and on a VG Optima mass spectrometer at the NERC Isotope Geosciences Laboratory (NIGL), Keyworth, UK. Replicate analyses were run at both institutions to ensure reproducibility. Trace element data were analysed by Inductively Coupled Plasma-Atomic Emission Spectrometer (ICP-AES) using a Perkin Elmer Optima 3300RL ICP-AES system (with autosampler) at the

NERC ICP facility, Department of Geology at Royal Holloway, University of London. For a full description of the methodology used see Chapter 4.

8.4. Results

The Izhma River belemnites (Fig. 8.5) collected were of the Boreal Realm genera *Cylindroteuthis*, *Acroteuthis*, *Pachyteuthis* and *Lagonibelus*. Most of the belemnite rostra were composed of translucent calcite and displayed concentric banding. BSEM, CL and carbonate staining analysis (Plates 12-14) were conducted on 16 out of 60 specimens in order to assess the typical preservation. These techniques identified Fe-rich areas and some pyrite replacement particularly around the rostrum margins and apical canal as well as along fractures and strong growth bands. The areas shown to be especially prone to alteration were either avoided or removed prior to subsampling.



Figure 8.5 Photographs of belemnites from the Izhma River succession, Russia. Age and Formation unknown. (A) Belemnite with serpulid worm trace. (B) Belemnites in foreshore scree.

Trace element analysis of Fe and Mn concentrations was carried out on every belemnite sample in order to provide detailed information about the level of preservation. The concentrations of Fe and Mn range from 7-312 ppm, mean 25 ppm and 2-105 ppm, mean 10 ppm respectively. Plots of Fe and Mn against $\delta^{18}\text{O}$ (Fig. 8.6) were used to constrain diagenetic alteration. A cross-plot of Fe and Mn is also provided to show the range of these trace element values (Fig. 8.7) as stable isotope analysis was not conducted on the most diagenetically altered specimens from this site. Belemnites with high

concentrations of Fe (>150 ppm) and Mn (>100ppm) were considered post-depositionally altered and were excluded from further analysis.

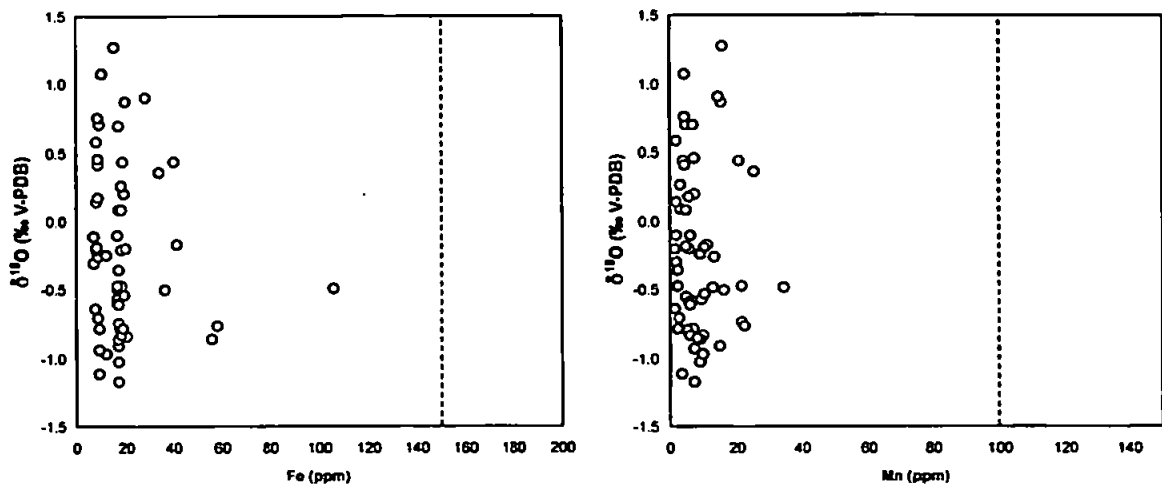


Figure 8.6 Cross-plots of $\delta^{18}\text{O}$ against Fe (left) and Mn (right). The dashed lines indicate the cut off values for well preserved samples.

Additional element abundances are as follows: Sr 719-1504 ppm, mean 1192 ppm, Mg 281-1374 ppm, mean 621 ppm and Ca, 23% - 33 %, mean 31 %. Stable isotope analyses were conducted on 60 of the well-preserved belemnite samples. The carbon and oxygen isotope values of the Callovian to Early Hauterivian Izhma River belemnites were -0.98 to 2.67 ‰ and -1.32 to 1.27 ‰ respectively. The most negative carbon isotope values (-0.98 ‰) are observed in the Lower Volgian *Panderi* Zone and values remain relatively low to (between -0.98 and 0.83 ‰) until the Lower Valanginian *Syzranicum-Polyptychus* zones, where the initiation of a positive carbon isotope excursion is observed. The $\delta^{13}\text{C}$ maxima (2.67 ‰) occur in the Upper Valanginian *Bidichotomus* Zone and are followed by a return towards pre-excursion values in the Early Hauterivian *Bojarkensis* Zone. A similar long-term trend is recorded in the $\delta^{18}\text{O}$ data. Relatively low oxygen isotope values persist throughout the Volgian and Early Ryazanian (-1.32 to -0.11 ‰) until a shift towards more positive values occurs from the Upper Ryazanian and into the Lower Hauterivian. Maximum $\delta^{18}\text{O}$ values (1.27 ‰) occur during the Upper Valanginian *Bidichotomus* Zone. A cross-plot of the $\delta^{18}\text{O}$ and $\delta^{13}\text{C}$ data (Fig. 8.8) shows a significant positive correlation (at the 99% confidence level).

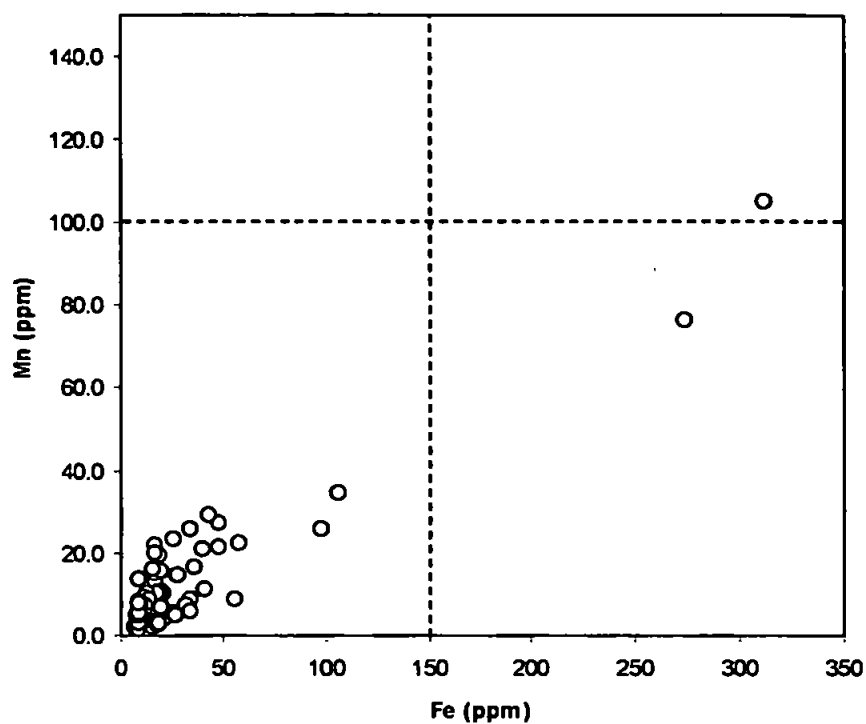


Figure 8.7 Cross-plot of Mn and Fe. The dashed lines indicate the cut off values for well preserved samples.

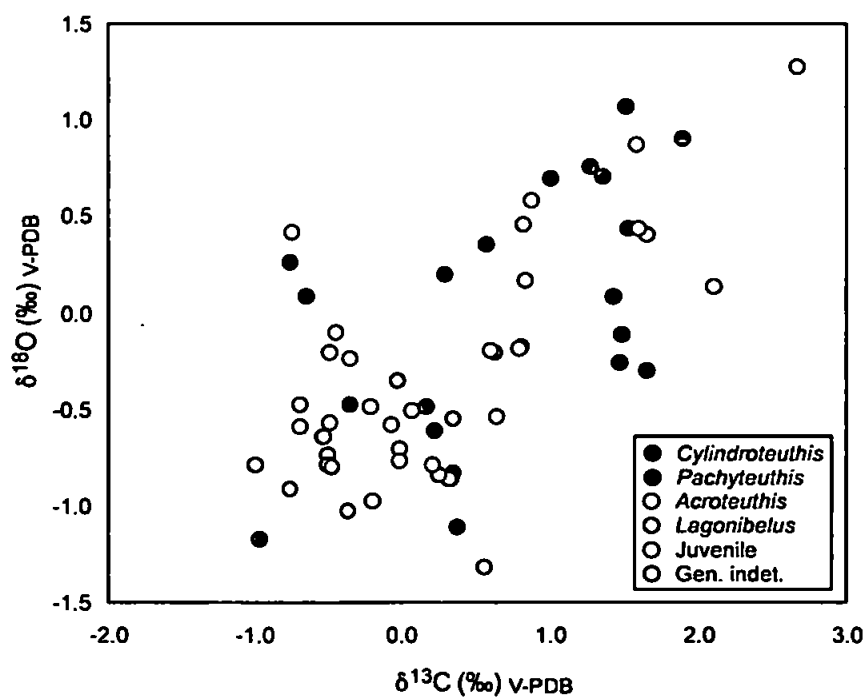


Figure 8.8 Cross-plot of $\delta^{18}\text{O}$ and $\delta^{13}\text{C}$ values derived from belemnites from the Izhma River succession, Russia.

8.5. Discussion

8.5.1. Stable Isotope, Geochemical & Taxonomic Records

The stable isotope and trace element records from the Callovian-Hauterivian Izhma River succession have been presented here together with data pertaining to the generic classification of the belemnite specimens (Figs 8.9 & 8.10). The purpose of this was to assess the impact (if any) of genus-specific differences in isotope or trace element fractionation.

In neither the stable isotope nor El/Ca records does one genus appear to be consistently more positive or negative than the others. In addition, each genus displays a similar degree of scatter within the records presented (e.g., ~2.0 ‰ for isotopes). At Staffin Bay and the Boyarka River, the belemnite genus *Cylindroteuthis* displayed more scatter than any other genus in both the stable isotope and El/Ca records. It was hypothesised that this was in part due to the predominance of this genera compared with the others present. Interestingly, the number of specimens measured from each of the three dominant genera at the Izhma River section was very similar, for example 19 *Pachyteuthis*, 14 *Acroteuthis* and 13 *Lagonibelus* specimens were analysed. This provides some support for the idea that particularly dominant genera will display the most scatter. It should be noted however, that the genus *Cylindroteuthis* is especially rare in this succession (only 2 specimens analysed) so an enhanced degree of scatter in this genus cannot be ruled out. If taxonomic differences in fractionation do exist here, these data suggest that they are likely to have only a minor effect on the stable isotope and geochemical records. It is therefore highly unlikely that the trends observed here are caused solely by genus-specific effects. The trends are therefore interpreted as the result of environmental fluctuations.

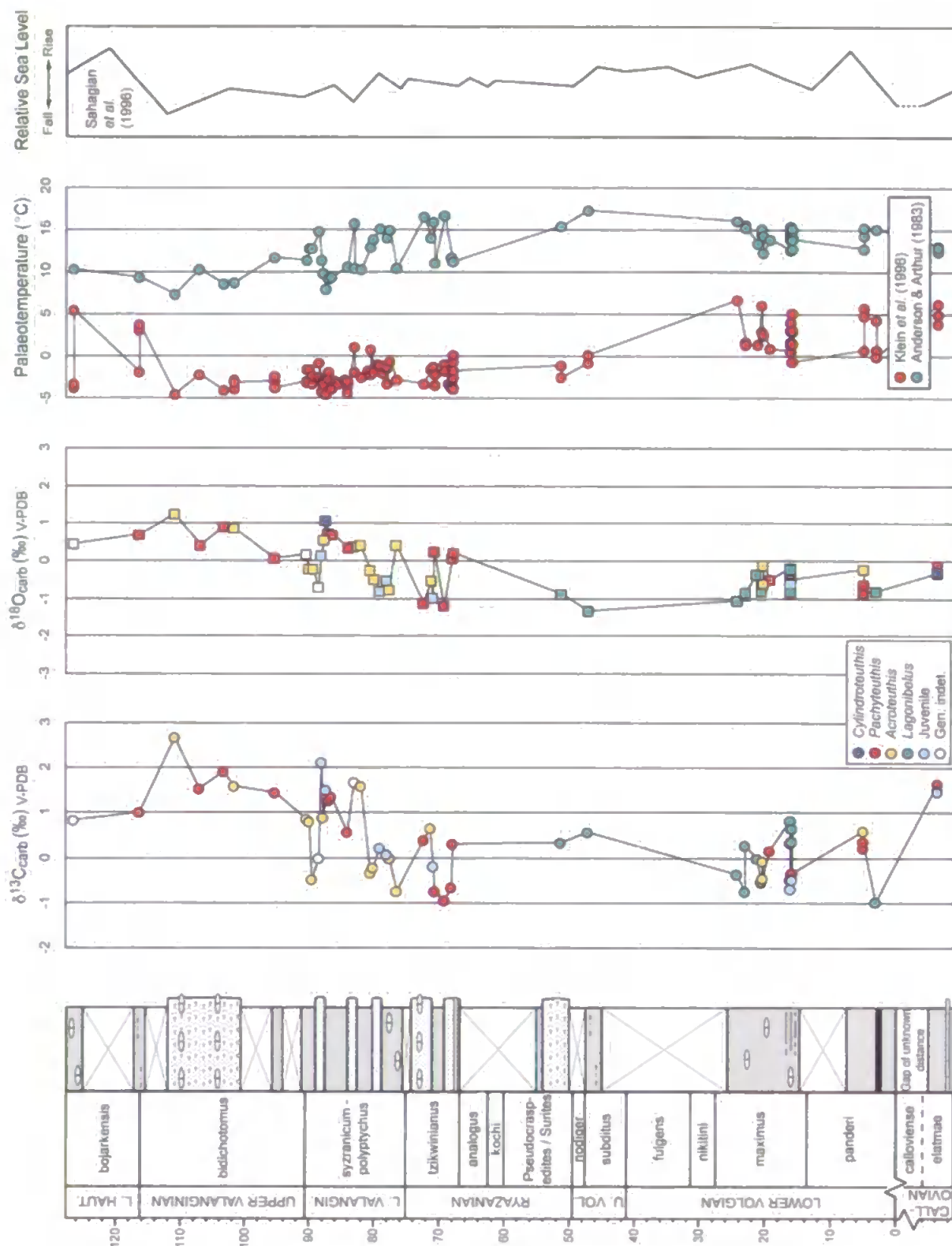


Figure 8.9 $\delta^{13}\text{C}$ and $\delta^{18}\text{O}_{\text{carb}}$ records from the Callovian-Lower Hauterivian Izhma River succession, Russia. Calculated palaeotemperatures and sea level are also shown. Boreal (Russian) ammonite zones illustrated. See Figure 4.2 for key to log symbols. Scale is in metres.

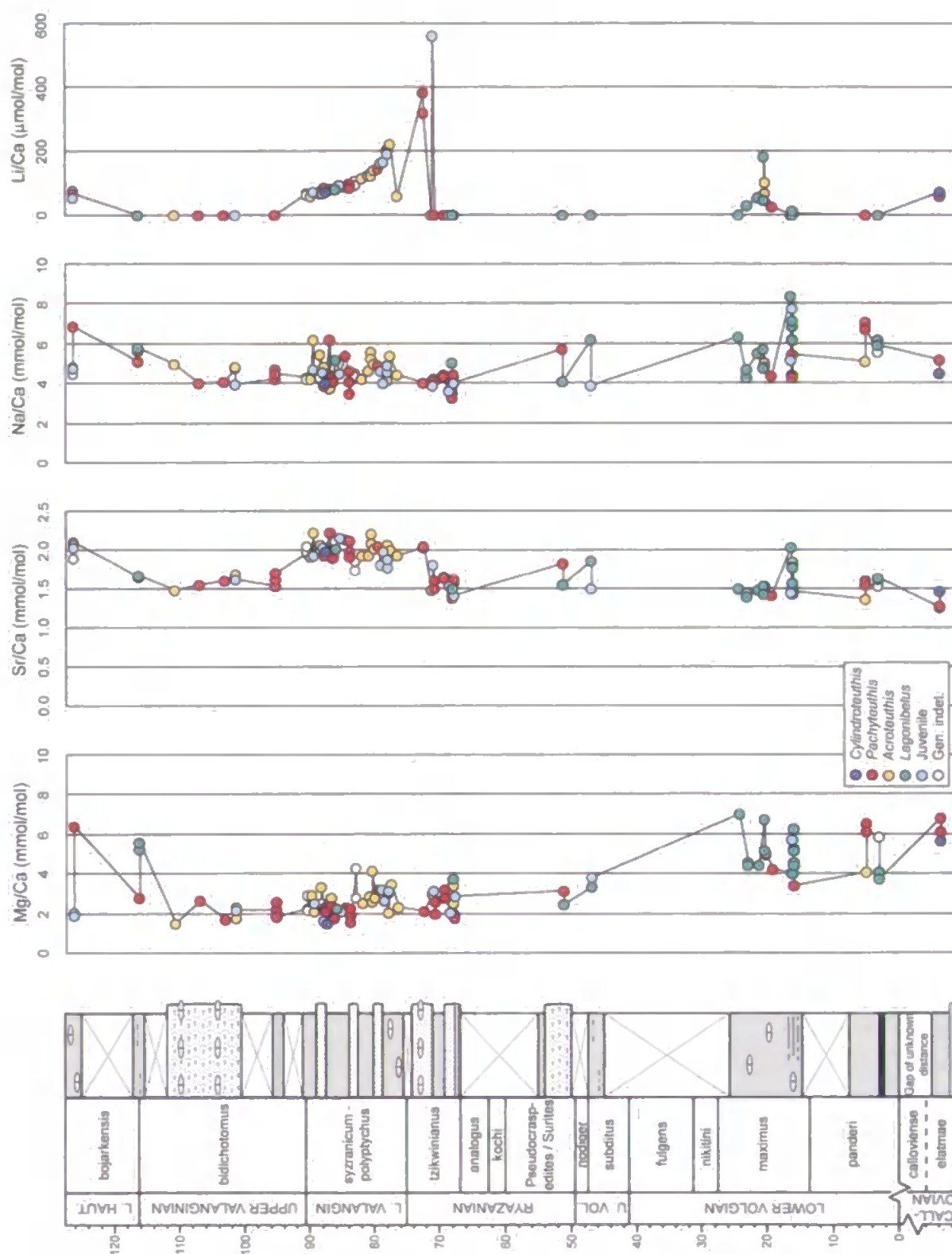


Figure 8.10 El/Ca records from the Callovian-Lower Hauterivian Izhma River succession, Russia. Boreal (Russian) ammonite zones illustrated. See Figure 4.2 for key to log symbols. Scale is in metres.

8.5.2. The Oxygen Isotope Record & Palaeotemperature Implications

The oxygen isotope record (Fig. 8.9) shows a long-term trend of relatively stable values from the Volgian to Ryazanian (fluctuating between approximately -1.0 and 0.0 ‰) and then a shift to more positive values (1.27 ‰) from the Upper Ryazanian and into the Upper Valanginian. The oxygen isotope values presented here display approximately 1-2 ‰ scatter, which is consistent with published belemnite records (e.g., van de Schootbrugge *et al.*, 2000; Wierzbowski, 2002; Price & Mutterlose, 2004). Considerably less scatter is observed in the Izhma River succession than in the Boyarka River succession (see Chapter 7) which covers a similar time interval (Ryazanian-Hauterivian) and is approximately 10° further north in terms of palaeolatitude.

The scatter observed in the Izhma River data could be the result of taxonomic variability (as discussed previously), diagenetic alteration or salinity fluctuations. The presence of major diagenetic alteration has been ruled out by the extensive screening described earlier, although it is possible that subtle alteration may have escaped detection. The data are therefore considered to primarily reflect environmental fluctuations.

As discussed previously, belemnites are commonly believed to secrete their calcite very close to isotopic equilibrium with the surrounding seawater (e.g., Taylor & Ward, 1983; Morrison & Brand, 1986; Rosales *et al.*, 2004a; Rexfort & Mutterlose, 2006). It is therefore possible to estimate palaeotemperatures using the oxygen isotope composition of belemnite calcite, although calculations of absolute values are unlikely since belemnites are an extinct group of organisms. The palaeotemperatures calculated here should therefore be considered as a guide to the potential palaeotemperatures for the region.

The palaeotemperature estimates from the Izhma River succession (Fig. 8.9) were calculated using the equation of Anderson & Arthur (1983). The range of temperatures observed here is from 7.3 to 17.3°C, with an average value for the whole succession of 13.0°C. These values were calculated using a value of -1 ‰ SMOW, which is consistent with previously published literature on the Jurassic and Cretaceous periods (e.g., Pirrie &

Marshall, 1990; Marshall, 1992; Sælen *et al.*, 1996; Price & Sellwood, 1997; Podlaha *et al.*, 1998; Price & Mutterlose, 2004; Rosales *et al.*, 2004a, b). The palaeotemperatures decrease up succession with the highest values in the Upper Volgian *Subditus* Zone and the lowest values in the Upper Valanginian *Bidichotomus* Zone.

8.5.3. The Elemental Records & Palaeotemperature Implications

The rationale and implications of considering *El/Ca* ratios together with $\delta^{18}\text{O}$ data were discussed in Chapter 5. Long term trends are observed in the elemental ratios presented here (Fig. 8.10). The Mg/Ca ratios show a decrease in values from the Callovian and into the Upper Valanginian, with a brief fluctuation to higher values in the Lower Hauterivian. The Sr/Ca curve shows a slight increase in values until the Upper Valanginian, where a return to lower values occurs. The Na/Ca ratios reveal a slight shift towards lower values through the succession and the Li/Ca ratios show generally low values with occasional rapid fluctuations to very high values, most notably in the Upper Ryazanian *Tzikvinianus* Zone. The reason for these spikes is unclear.

Cross-plots of *El/Ca* against $\delta^{18}\text{O}$ (Fig. 8.11) show no correlation between Sr/Ca and $\delta^{18}\text{O}$, Na/Ca and $\delta^{18}\text{O}$, and Li/Ca and $\delta^{18}\text{O}$. The correlation between Mg/Ca and $\delta^{18}\text{O}$ however revealed a statistically significant negative correlation (at the 99% confidence level). This is the first instance where a significant correlation has been observed between Mg/Ca and $\delta^{18}\text{O}$ in this study. The negative relationship is consistent with the published belemnite data (e.g., McArthur *et al.*, 2000; Bailey *et al.*, 2003; Rosales *et al.*, 2004a, b) and the work of Steuber & Rauch (2005) on modern skeletal calcite. The Mg/Ca ratio is commonly considered to be one of the most accurate palaeotemperature proxies available, primarily because unlike $\delta^{18}\text{O}$ it is not thought to be significantly influenced by salinity fluctuations (e.g., Klein *et al.*, 1996; Lear *et al.*, 2000; Bailey *et al.*, 2003; Rosales *et al.*, 2004a, b; Immenhauser *et al.*, 2005). The correlation between Mg/Ca and $\delta^{18}\text{O}$ as observed here suggests that temperature is the major control of both proxies for the

Callovian-Upper Valanginian interval at the Izhma River. This assumes that belemnites have a similar temperature sensitivity to modern biogenic calcites.

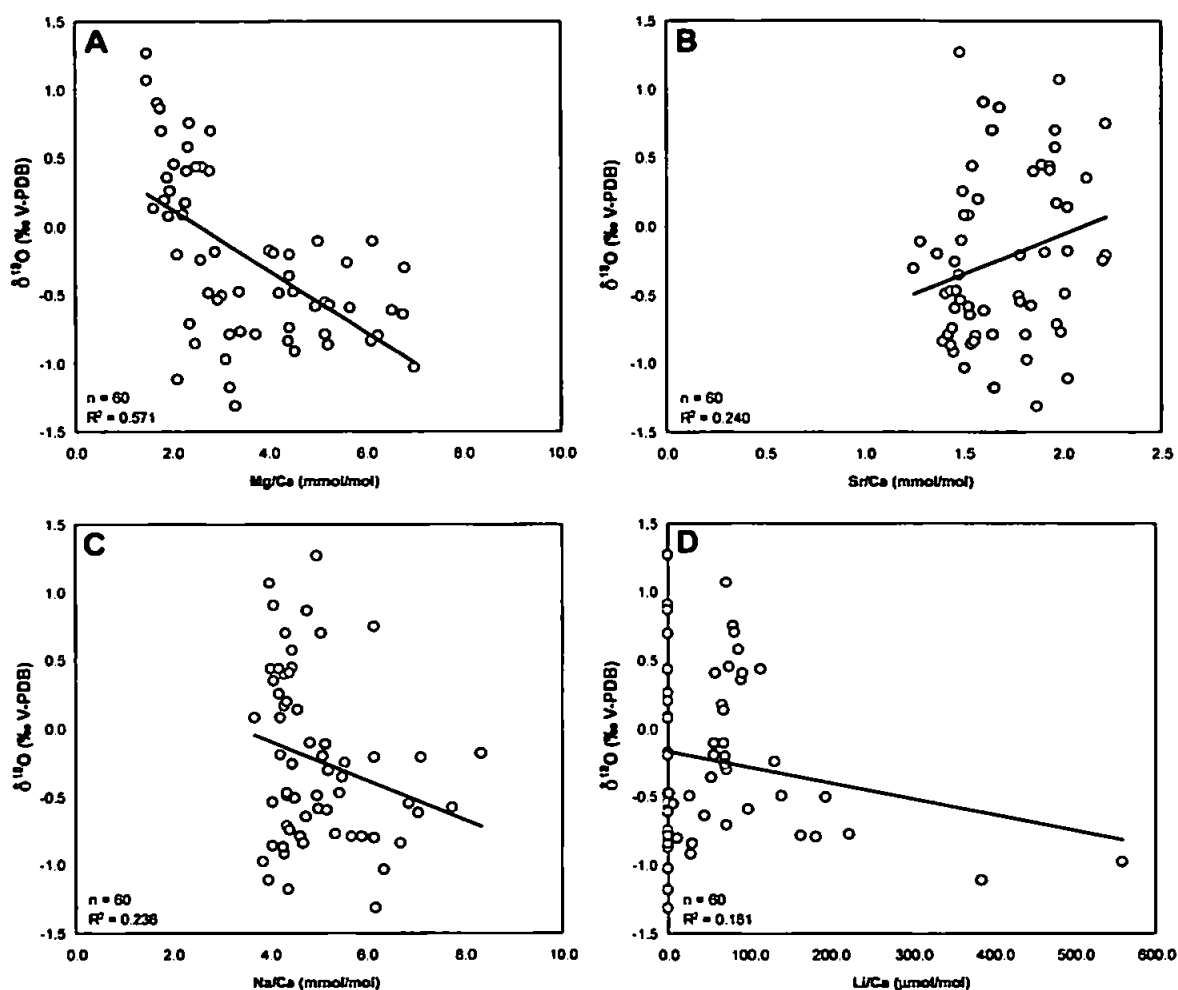


Figure 8.11 Cross-plots of $\delta^{18}\text{O}$ against (A) Mg/Ca, (B) Sr/Ca, (C) Na/Ca and (D) Li/Ca for the Izhma River belemnites.

Palaeotemperatures were calculated from the Mg/Ca ratios using the equation of Klein *et al.* (1996) (Fig. 8.9). The calculated values ranged from -4.5 to 6.7°C , with an average temperature for the whole succession of -0.9°C . The average offset between the palaeotemperature calculations for the succession is 13.9°C . This value is extremely high, especially given the significance of the correlation and the obvious inverse relationship (observed using a linear regression line) between Mg/Ca and $\delta^{18}\text{O}$. The significance of the correlation suggests that both variables are influenced by one prevailing factor (presumable temperature). The observed offset between the calculated palaeotemperature averages, however, suggests that salinity must have had a highly significant and consistent impact on

$\delta^{18}\text{O}$, which seems unlikely. If the observed temperature difference was attributed solely to influence from salinity, a change in salinity of 13.8 ‰ is required, which seems impossible. Even if the $\delta^{18}\text{O}_{\text{seawater}}$ value of Roche *et al.* (2006) for the high latitudes (-1.5 ‰ SMOW) is used to replace the standard estimate of -1 ‰ SMOW (which would give a $\delta^{18}\text{O}$ palaeotemperature average of 11.0°C) a change in salinity of 12 ‰ would still be required. Episodes of freshening in the high latitudes can be caused by input from riverine runoff (which is particularly likely on the Russian platform) and seasonal ice melt. These factors are likely to have had an affect on the Izhma River $\delta^{18}\text{O}$ data, however, such factors alone are unlikely to account for the required magnitude of salinity change. The Mg/Ca data must therefore be viewed with caution. As discussed previously, sub-freezing temperature values could not possibly be recorded by belemnites as they would not have been able to survive in such conditions. Immenhauser *et al.*, (2005) suggest that it may only be appropriate to apply the Klein *et al.*, (1996) equation to temperatures in the range of 5-23°C where the temperature-Mg relationship is linear. In addition, the data presented here suggest that the use of Mg/Ca palaeotemperature equations may be inappropriate for belemnites and that any subsequent calculation of salinity influence is probably not reliable, especially at relatively low temperatures.

8.5.4. The Carbon Isotope Record

The marine carbonate $\delta^{13}\text{C}$ record (Fig. 8.9) shows a shift to more negative values between the Callovian and Lower Volgian. Values remain fairly consistent (between -1.0 and 1.0 ‰) until the Lower Valanginian which witnesses the initiation of a positive carbon isotope excursion with the maximum (2.67 ‰) occurring in the Upper Valanginian *Bidichotomus* Zone. A return towards pre-excursion values is observed in the Lower Hauterivian. The positive carbon isotope excursion occurs at the same time as a shift towards more positive values in the $\delta^{18}\text{O}$ record (which is consistent with a fall in palaeotemperature). Using data from Sahagian *et al.* (1996) the initiation of the positive

carbon isotope excursion in the Izhma River succession occurs during a period of sea level fall. This is contrary the relationship observed in the Boyarka River succession, where the initiation of the positive excursion was coincident with a sea level rise. It should be noted, however, that the shift towards more positive values in the Izhma River succession occurs slightly earlier than that in the Boyarka River succession assuming that the correlation is correct. It is likely that these excursions did actually occur simultaneously and the differences observed in this study are the result of limitations in sampling resolution and biostratigraphy. The Upper Valanginian positive carbon isotope excursion occurs during a time of frequently fluctuating sea level on the Russian Platform and in Siberia. Given the limitations mentioned above, it is therefore impossible to determine whether the initiation of the $\delta^{13}\text{C}$ excursion occurred during a period of relative sea level rise or fall, although if considered in terms of eustatic sea level change throughout the Jurassic and Cretaceous the excursion does occur during a period of relatively low sea level.

8.5.5. Volgian-Hauterivian Stable Isotope Records

As discussed in Chapter 7, published marine carbonate stable isotope records for the Early Cretaceous have been constructed primarily from successions in the Tethyan region. In terms of the $\delta^{13}\text{C}$ record, the overall pattern described from such research is one of decreasing $\delta^{13}\text{C}$ values across the Jurassic-Cretaceous boundary, relatively stable $\delta^{13}\text{C}$ values in the earliest Cretaceous, then a rapid mid- to Late Valanginian positive carbon-isotope excursion (occurring in the Tethyan *Campylotoxus* ammonite zone) and a subsequent return to pre-excursion values in the Upper Valanginian and Lower Hauterivian (Price & Mutterlose, 2004). The nature of the $\delta^{18}\text{O}$ record is obviously more variable, depending to a large degree on palaeolatitude.

Price & Mutterlose (2004) record palaeotemperature estimates of 7 to 21°C for the Volgian-Valanginian interval from the Yatria River, Siberia. This is compatible with the data presented here for the Izhma River succession, where a palaeotemperature range of

7.3 to 17.3°C is predicted for the same interval. These two locations are situated on the same landmass and at approximately the same palaeolatitude so similar values are to be expected and the reproducibility of such palaeotemperatures provides considerable confidence in these values. The lower end of these temperature ranges provides substantial evidence for the existence of cold conditions in the northern high latitudes at this time. Polyak *et al.* (2003) estimated modern temperatures for the region of -1 to 12°C based on benthic foraminiferal isotope studies in the Kara and Pechora Seas. By comparison, it would be reasonable to consider that a palaeotemperature range of 7-21°C could be consistent with the existence of a seasonal ice cover at the Arctic pole during the Late Jurassic and Early Cretaceous. If the Boyarka River $\delta^{18}\text{O}$ data are considered in addition to those of the Izhma and Yatria Rivers (which is again from the same landmass but approximately 10° further north in terms of palaeolatitude) the evidence for cold conditions is even more convincing. The calculated palaeotemperature range from the Boyarka River is from 2-19°C for the Ryazanian-Hauterivian interval based on oxygen isotopes.

The Izhma River data record a fall in palaeotemperature during the Valanginian period. This is consistent with a number of published studies that record evidence for a Valanginian cooling event (e.g., Mutterlose *et al.*, 2003; Pucéat *et al.*, 2003; Erba *et al.*, 2004; Weissert & Erba, 2004; Kessels *et al.*, 2006) (this evidence is discussed in Chapter 7). Ultimately, the studies presented here lend very strong support to the idea that the Late Jurassic and Early Cretaceous greenhouse climate was at times punctuated by sub-freezing conditions at the poles.

The Izhma River positive carbon isotope excursion observed here begins during the Lower Valanginian *Syzranicum*-*Polyptychus* zones (the *Polyptychus* Zone is correlatable with the Tethyan *Campylotoxus* Zone). The peak of the positive $\delta^{13}\text{C}$ excursion occurs in the *Bidichotomus* Zone which corresponds well biostratigraphically with the timing of the Tethyan excursion in the *Trinodosum* and *Callidiscus* ammonite zones (e.g., van de Schootbrugge *et al.*, 2000; Weissert & Erba, 2004). The excursion observed here also

correlates well with the positive carbon isotope excursion observed in the Boyarka River succession (Fig. 8.12). As discussed in the previous chapter, this excursion has been attributed to the first episode of greenhouse conditions during the Cretaceous period (Lini *et al.*, 1992) and episodes of platform drowning in the Tethys (e.g., Lini *et al.*, 1992; Föllmi *et al.*, 1994; Weissert *et al.*, 1998; Wortmann & Weissert, 2000). Van de Schootbrugge *et al.* (2000) however, recognised that during the Hauterivian at least two phases of platform drowning were not associated with positive carbon-isotope excursions and Wortmann & Weissert (2000) instead suggested that the sea-level rise and drowning of platform carbonates corresponded to the initiation of more positive carbon-isotope values.

The $\delta^{13}\text{C}$ excursion recorded here in the Izhma and Boyarka rivers however, occurs during a period of relatively low eustatic sea level according to the sea level curve of Sahagian *et al.* (1996) constructed for the Russian Platform. A period of sea-level lowstand would have resulted in the partial separation of the Boreal and Tethyan Realms (as confirmed by belemnite provinciality) and could have restricted ocean circulation and enhanced stratification to promote organic carbon burial in these high latitude locations, although the evidence for widespread Late Valanginian global marine black shales is limited (Price & Mutterlose, 2004). In addition, an increased input of nutrients resulting from the exposure and erosion of lowland areas (Brenchley *et al.*, 1994; Gröcke *et al.*, 1999; Price & Mutterlose, 2004) could have contributed to the positive carbon isotope excursion at this time.

Interestingly, the most positive carbon isotope values coincide with the most positive $\delta^{18}\text{O}$ values (and therefore the lowest palaeotemperatures). This could be explained by a fall in atmospheric CO_2 concentration and a subsequent drop in temperature as the result of a significant burial of sediments rich in organic carbon. Vincent & Berger (1985) termed this the 'Monterey Hypothesis'. Such a relationship was also observed by Price & Mutterlose (2004) for the Late Valanginian positive carbon isotope excursion

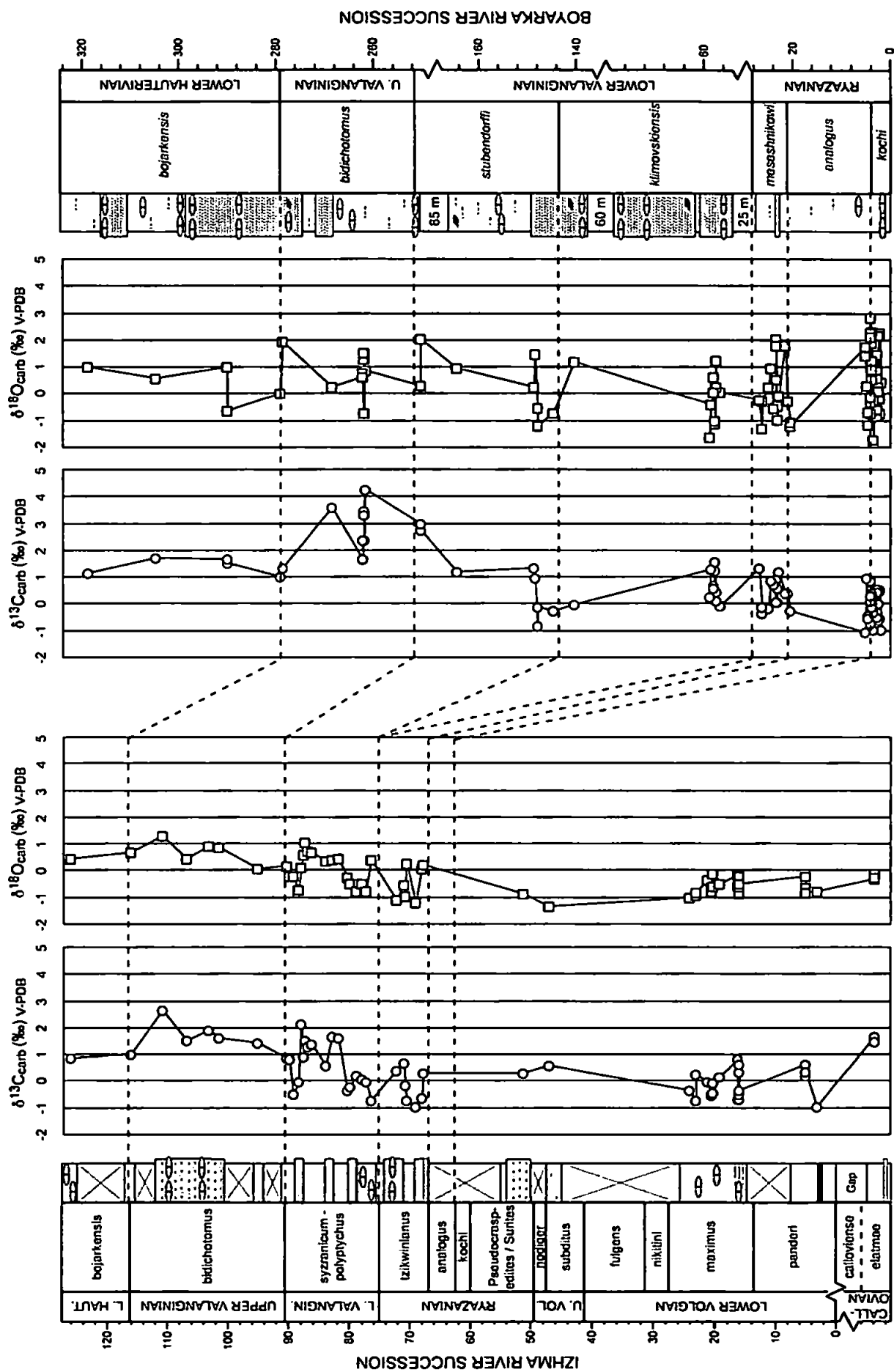


Figure 8.12 Ryazanian-Hauterivian $\delta^{13}\text{C}$ and $\delta^{18}\text{O}$ correlation between the Izhma River succession and the Boyarka River succession. See Figure 4.2 for key to log symbols.

from the Yatria River. This is not observed in the Boyarka River succession however, although this could in part, be due to the large degree of scatter present in the data.

8.6. Conclusions

- The data presented here comprise the first relatively high-resolution isotope investigation of marine biogenic carbonate (belemnites) $\delta^{13}\text{C}$ and $\delta^{18}\text{O}$ from the Izhma River, Russia.
- The average palaeotemperature derived from the Izhma River succession $\delta^{18}\text{O}$ record (using the Anderson & Arthur (1983) equation) was 13.0°C and the palaeotemperature range was 7.3°C to 17.3°C for the Callovian-Hauterivian interval. This suggests that contrary to popular opinion there was the potential for the existence of cold conditions during the Late Jurassic and Early Cretaceous greenhouse period.
- A fall in palaeotemperature is observed during the Valanginian. This is consistent with previously published evidence for a cooling event during the Valanginian period.
- The palaeotemperatures calculated from Mg/Ca ratios ranged from -4.5 to 6.7°C , with a average value of -0.9°C . The calculation of such low values casts doubt on the validity of using the Klein *et al.*, (1996) equation when applied to belemnites living in relatively low temperatures.
- The Late Valanginian positive carbon isotope excursion is recorded here in the Izhma River $\delta^{13}\text{C}$ curve. The timing and duration of this excursion is consistent with that observed in previously published Tethyan records and with that observed from the Boyarka River succession. This suggests that the $\delta^{13}\text{C}$ event influenced the total exchangeable carbon reservoir. The positive $\delta^{13}\text{C}$ excursion occurs at a time of relatively low sea level in Russia and Siberia. The exposure and erosion of lowland areas and restricted ocean circulation (and therefore enhanced stratification) associated with a period of sea-level lowstand may account for increased rates of organic carbon burial.

- The most positive carbon isotope values coincide with the most positive oxygen isotope values (and therefore the lowest palaeotemperatures). This could be explained by a fall in atmospheric CO₂ concentration and a subsequent drop in temperature as the result of a significant burial of sediments rich in organic carbon.

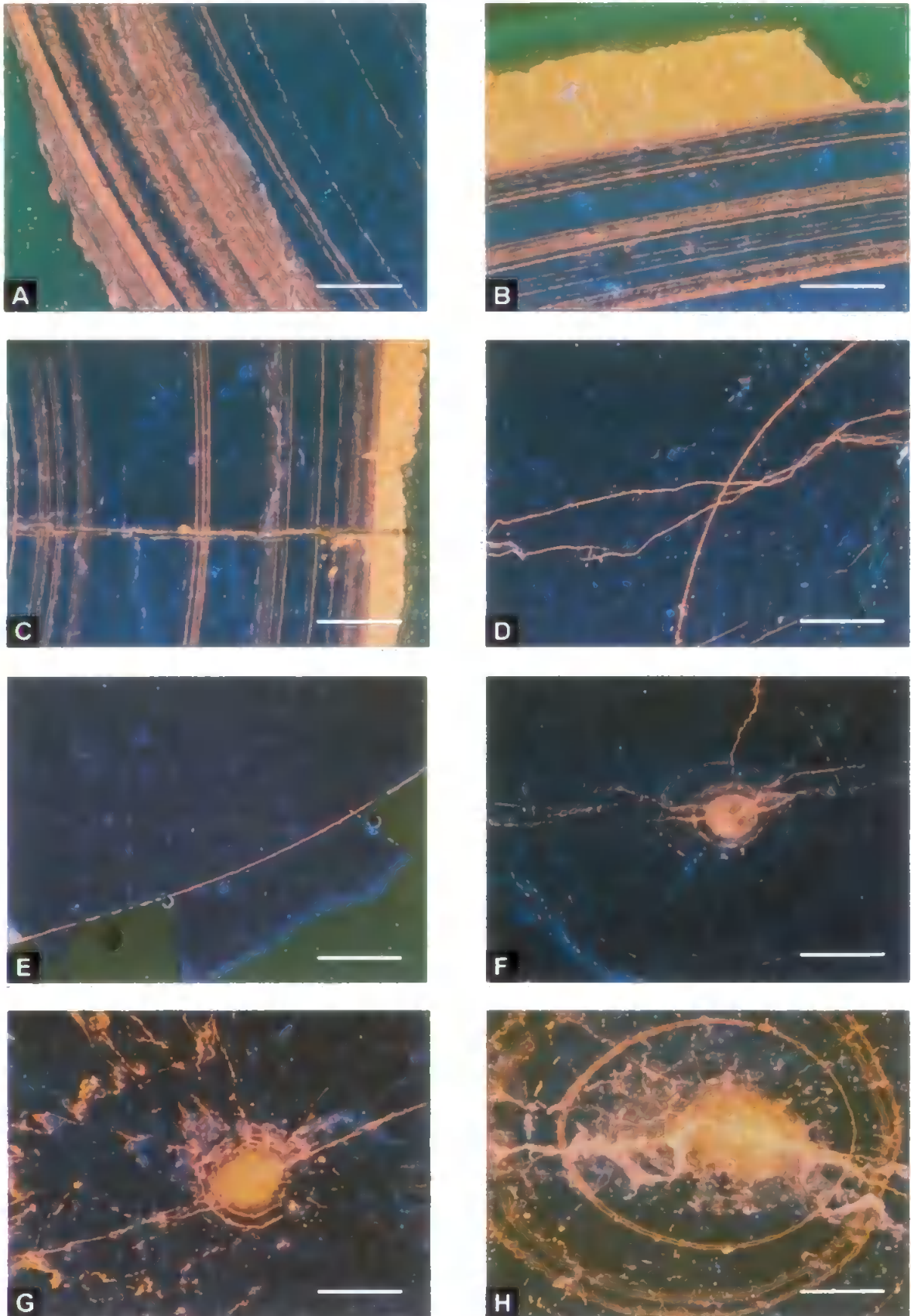


Plate 12. Cathodoluminescence images showing the state of preservation of belemnite rostra from the Izhma River, Russia. All scale bars represent 1 mm. (A) Growth bands towards rostrum margin displaying alteration. (B) Growth bands towards rostrum margin displaying alteration. (C) Fracture and growth lines displaying alteration. (D) Fractures and growth lines displaying alteration. (E) Generally very well preserved calcite. (F) Faint fractures emanating from apical canal and showing some alteration. (G) Apical canal with and some fractures displaying alteration. (H) Heavily altered growth bands and fractures surrounding the apical canal.

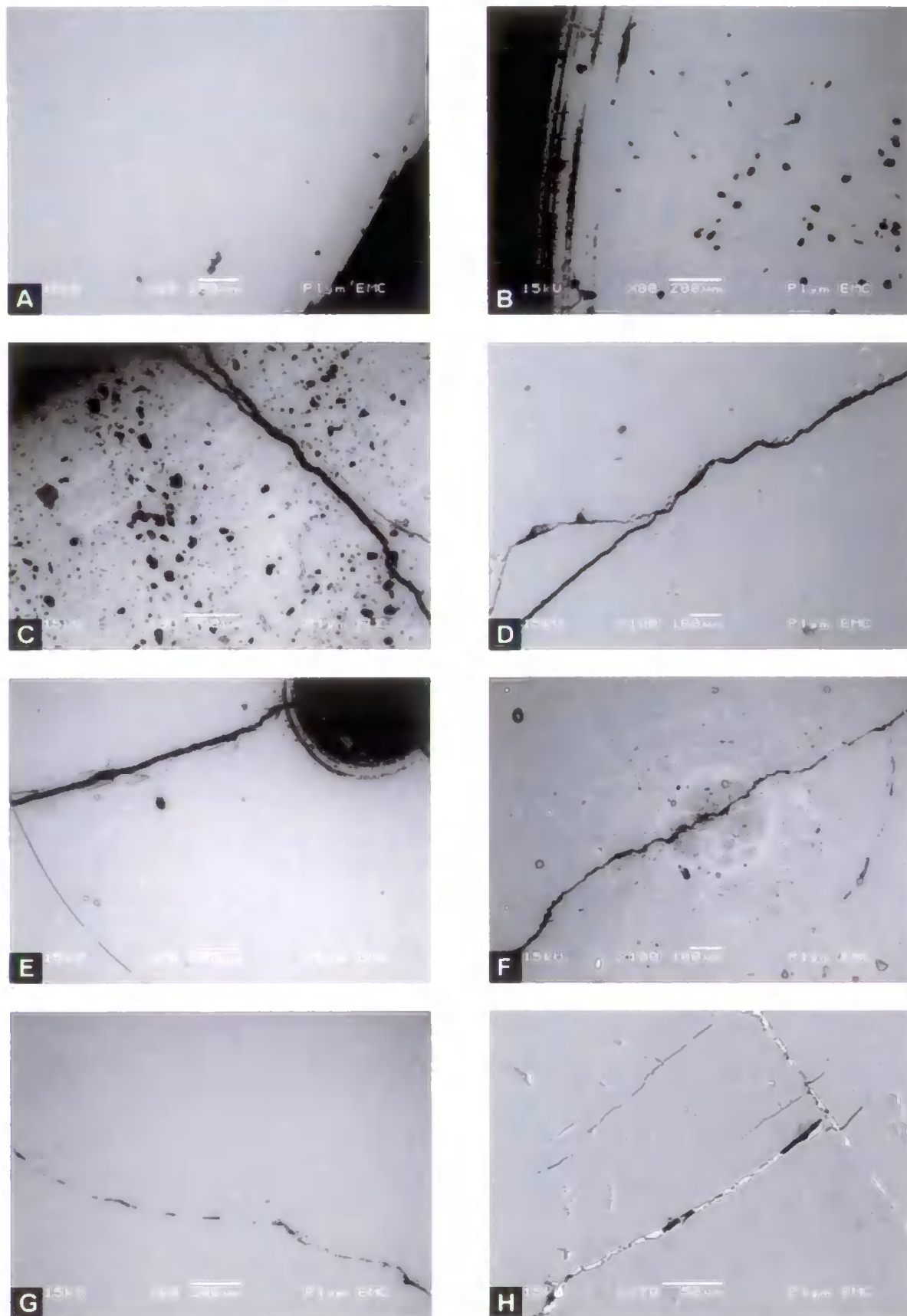


Plate 13. Backscattered SEM images showing the state of preservation of belemnite rostra from Staffin Bay, Isle of Skye. All scale bars represent lengths stated on images. (A) Very well preserved calcite. (B) Borings and growth line fractures at rostrum margin. (C) Fracture, borings and areas of alteration in rostrum. (D) Fracture running through apical canal. (E) Fracture emanating from apical canal. (F) Fracture running through diagenetically altered apical canal. (G) Generally well preserved calcite. (H) Fractures infilled with diagenetic cement.

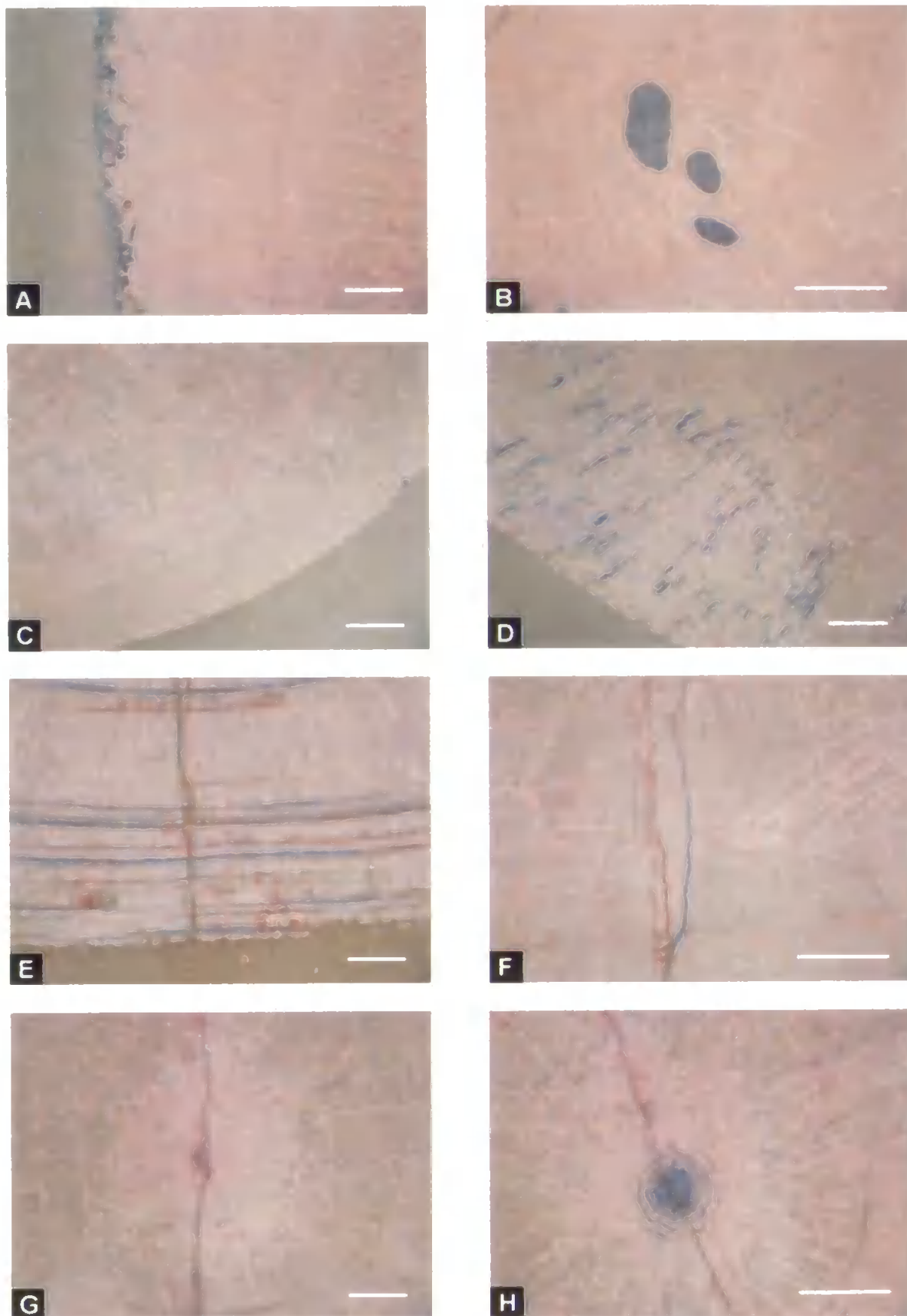


Plate 14. Carbonate stained images showing the state of preservation of belemnite rostra from the Izhma River, Russia. All scale bars represent 1 μm . (A) Rostrum margin displaying borings and alteration. (B) Borings infilled with diagenetic cement. (C) Very well preserved calcite. (D) Area near rostrum margin displaying alteration. (E) Fracture and growth lines displaying alteration. (F) Fractures displaying alteration in otherwise well preserved calcite. (G) Fracture running through apical canal. (H) Apical canal and surrounding growth lines displaying alteration.

9. FESTNINGEN & JANUSFJELLET, SVALBARD

9.1. Location & Site Description

Svalbard is an archipelago situated north of Norway on the edge of the Arctic Ocean. The islands have a latitudinal range of 74°N to 81°N and all are well within the present-day Arctic Circle. Festningen and Janusfjellet are both situated south of Isfjorden, on the principal island, Spitsbergen, at approximately 78°N (Fig. 9.1).

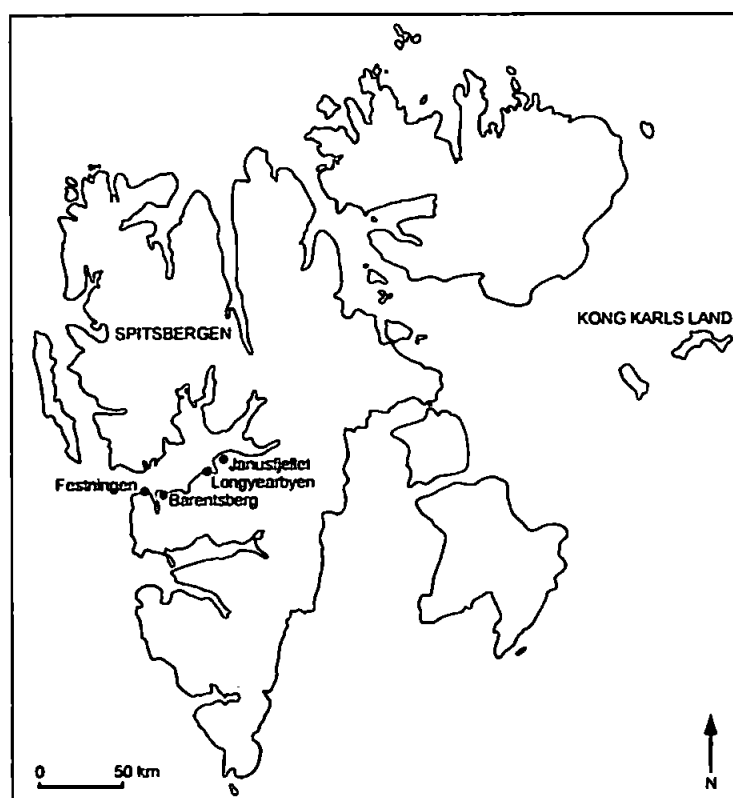


Figure 9.1 Location map of Svalbard. The field sites examined (Festningen and Janusfjellet) are shown.

Festningen is situated approximately 40 km southwest of the main town of Longyearbyen and near to the Russian mining town of Barentsburg. The outcrop at Festningen (Fig. 9.2) is in the form of a continuous low coastal cliff extending for approximately 7 km along the northern Nordenskiöld coast. Janusfjellet (Fig. 9.3) is situated inland, approximately 10 km north of Longyearbyen. The peak of Janusfjellet is approximately 800 m above sea level.



Figure 9.2 Low coastal cliff typical of the Festningen exposure. This photograph shows the Lower Valanginian Rurikfjellet Formation.



Figure 9.3 Typical exposure at Janusfjellet. This photograph shows the Volgian Argardhfjellet Formation.

9.2. Geological Setting

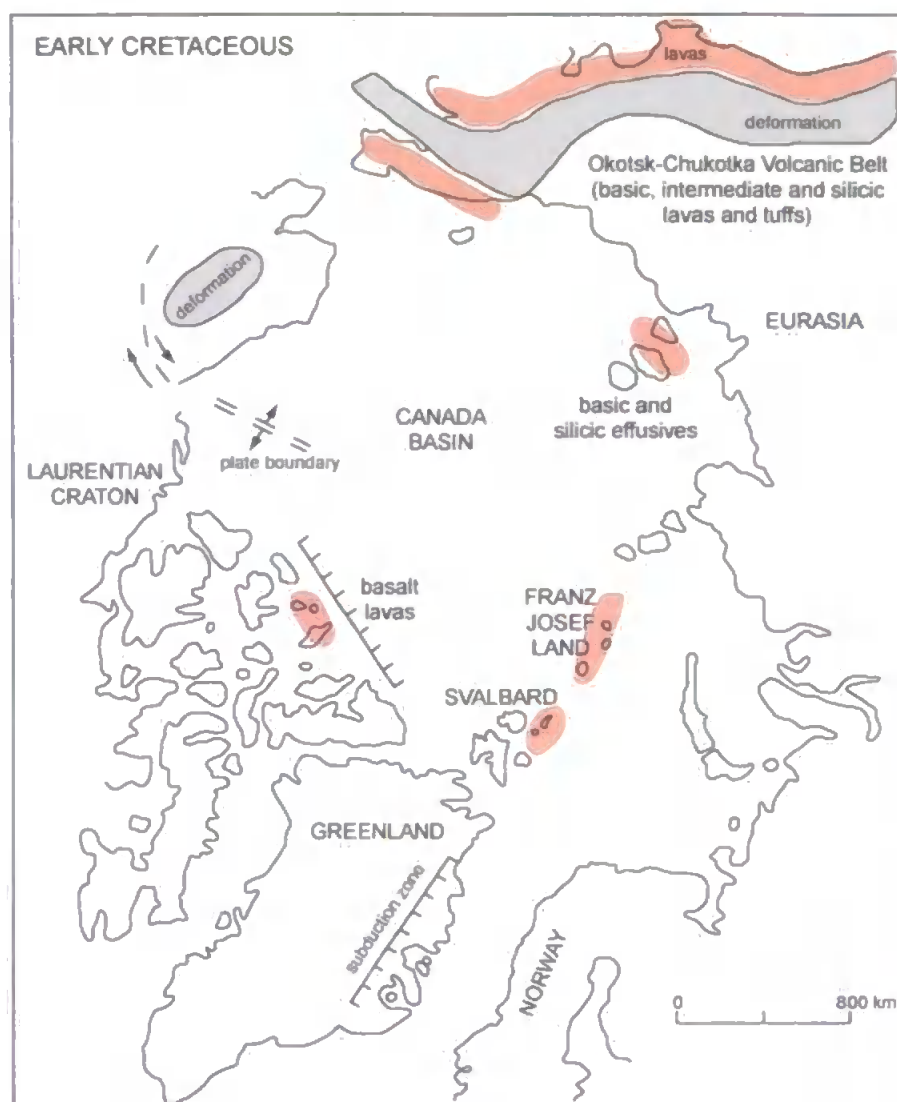


Figure 9.4 Simplified palaeogeographic map of the Arctic region. Structural and tectonic events are summarised. Adapted after Harland (1997)

During the Jurassic and Cretaceous, Svalbard was situated at a palaeolatitude of 60-70°N (Rowley & Lottes, 1988; Smith *et al.*, 1994; Ditchfield, 1997), just north of Greenland (Harland, 1969; McWhae, 1986) (Fig. 9.4). Throughout the Mesozoic, a stable platform regime prevailed on Svalbard, although, there is evidence for considerable igneous activity in the high Arctic region (north of Svalbard) during the Late Jurassic and Early Cretaceous (Worsley, 1986; Kelly, 1988; Bailey & Rasmussen, 1997; Maher, 2001). The magmatic activity on Svalbard was accompanied by significant vertical movements along major lineaments (Worsley, 1986; Bailey & Rasmussen, 1997). Magmatic material

includes sills, dikes and basalt flows that reveal increasingly intense activity eastwards (Harland, 1973, 1997; Worsley, 1986; Maher, 2001).

During the Early Jurassic, the Eastern Platform subsided (following a phase of uplift in the Triassic) whilst the main Spitsbergen Basin remained relatively stationary (Harland, 1997). This was caused by movement along the major Billefjorden lineament, the result of which was the existence of equivalent units of the Kapp Toscana Group immediately west and east of the lineament measuring 18 and 60-70 m respectively (Worsley, 1986).

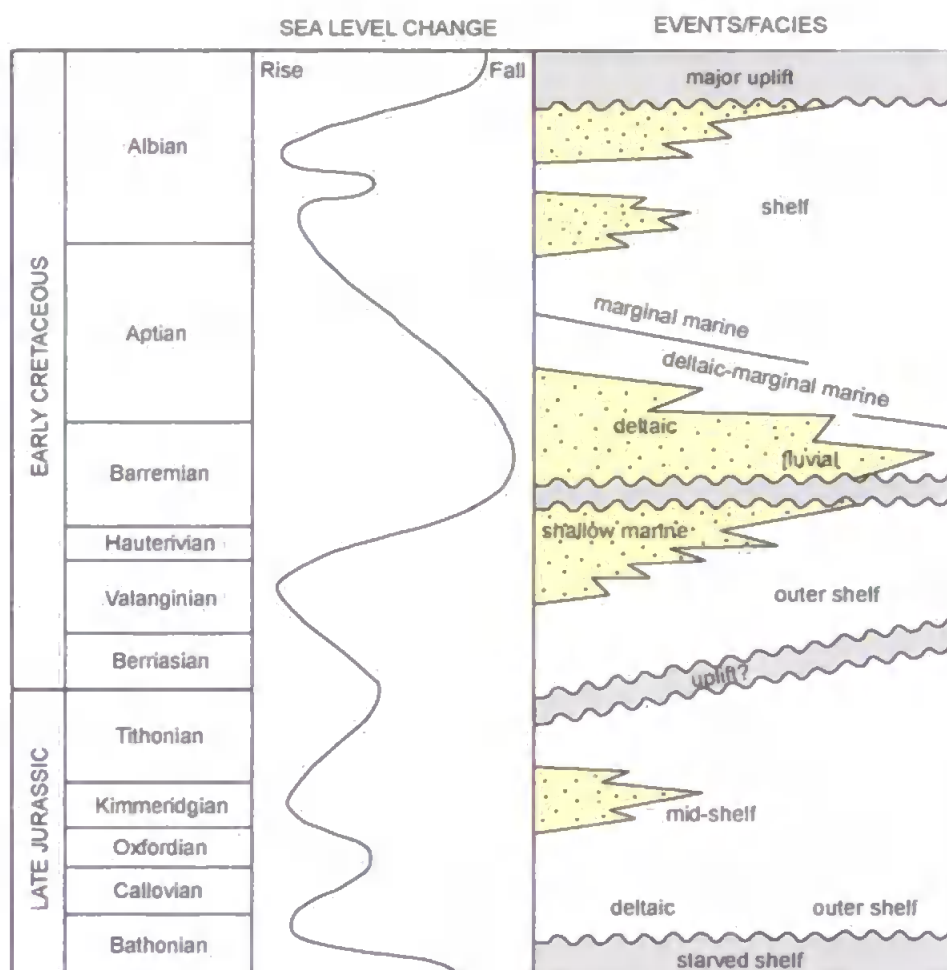


Figure 9.5 Summary of events and facies in the Late Jurassic and Early Cretaceous history of Svalbard. Adapted after Harland (1997).

A significant marine transgression commenced in the Late Bathonian and inundated both east and west Svalbard, whilst subsidence also became more pronounced in the west (Harland, 1997). This event led to the widespread deposition of the predominantly marine Adventdalen Group (Worsley, 1986; Harland, 1997; Dypvik *et al.*, 2002) (Fig. 9.5).

During the Callovian, subsidence in the Pechora region created open marine conditions from the Barents Shelf, across the Russian Platform and into the Tethys for the first time during the Jurassic (Harland, 1997). The Late Bathonian transgression was followed by a mid-Callovian regression and a subsequent Late Callovian to Oxfordian renewed transgression (Dypvik *et al.*, 2002), which reached a maximum in the Early Volgian (Harland, 1997). A further marine regression initiated in the mid-Volgian continued into the Early Cretaceous (Harland, 1997; Dypvik *et al.*, 2002). By the Late Volgian, access from the Barents Shelf to the Tethys across the Russian Platform was closed south of the Volga region, however this route had re-opened by the Middle Berriasian (Harland, 1997).

A period of major uplift in the north affected the whole Mesozoic platform from the Late Jurassic and was probably linked to the opening of the Canada Basin (Worsley, 1986; Bailey & Rasmussen, 1997). Such uplift initiated basinal closure to the north and finally resulted in a break of deposition and subsequent extensive erosion throughout the Late Cretaceous (Worsley, 1986; Dypvik *et al.*, 2002). As a result of this uplift, Lower Cretaceous sequences tend to become thicker and more complete to the south (Worsley, 1986) and Upper Cretaceous deposits appear to be absent on Spitsbergen altogether as the result of major tectonic uplift (Dypvik *et al.*, 2002) (Fig. 9.5). Following a major regression in the Barremian (Harland, 1997; Dypvik *et al.*, 2002), a long-term transgression continued into the Albian, at which time globally high sea-levels prevailed (Harland, 1997).

Jurassic and Cretaceous sedimentation on Svalbard was dominated by marine shelf deposition. The Bathonian to Albian Adventdalen Group (Fig. 9.6) comprises a ~2 km thick sequence of black marine shales, deltaic sandstones and delta front clastics (Parker, 1967; Worsley, 1986; Harland, 1997). The Adventdalen Group lies (with varying degrees of minor unconformity) on top of the Triassic Kapp Toscana Group (Kelly, 1997).

The Adventdalen Group forms an asymmetric syncline plunging gently to the SSE, which is exposed most extensively in southern Spitsbergen, with the major exposure south

of Isfjorden (Kelley, 1997). The group has been divided into the Janusfjellet Subgroup (which is divided into the Agardhfjellet and Rurikfjellet formations), the Helvetiafjellet Formation and the Carolinefjellet Formation (Parker, 1967; Harland, 1973, 1997; Dypvik, 1992; Dypvik *et al.*, 2002).

EARLY CRETACEOUS		ADVENTDALEN GROUP		CAROLINEFJELLET FORMATION		215 - 850m	Schönrockfjellet Mbr.	Shallow marine
							Zillerberget Mbr.	
							Langstakken Mbr.	
							Innkjegla Mbr.	
							Dalkjegla Mbr.	
				HELVETIAFJELLET FORMATION		50 - 100m	Glitrefjellet Mbr.	Marginal marine to fluvial
							Festningen Mbr.	
MIDDLE - LATE JURASSIC				JANUSFJELLET SUBGROUP	RURIKFJELLET FORMATION	300 - 800m	Ullaberget Mbr.	Distal marine to deep shelf
							Wimanfjellet Mbr.	
							Myklegardfjellet Bed	
		AGARDFJELLET FORMATION			Sløttsmoya Mbr.			
					Oppdalsåta Mbr.			
					Lardyfjellet Mbr.			
					Oppdalen Mbr.			

Figure 9.6 Stratigraphic chart for principal lithostratigraphic units of the Middle Jurassic to Early Cretaceous of Svalbard. Data from Harland (1997).

The Janusfjellet Subgroup (Fig. 9.6) (Bathonian to Barremian) was formed under marine shelf conditions and dominated by clay sedimentation, although silt and sand accumulation was also significant (Parker, 1967; Dypvik, 1985; Dypvik *et al.*, 1991a; Harland, 1997). The subgroup is ~300-800 m thick, has TOC values <10 % (although 1-4 % is more typical) and is dominated by Type III (with some Type II) kerogen (Hvoslef *et al.*, 1986; Harland, 1997). Belemnite and ammonite fossils are present throughout the Janusfjellet Subgroup (Parker, 1967; Harland, 1997).

The Agardhfjellet Formation (Fig. 9.6) (Bathonian to Volgian) has been divided into 4 different members (Dypvik *et al.*, 1991a, b). The formation is 243 m thick at the type locality and composed of dark grey-black shales exhibiting a fissile, papery appearance, with interbedded bioturbated siltstones, sandstones and thin carbonate bands

(Parker, 1967; Dypvik, 1985; Hvoslef *et al.*, 1986; Dypvik *et al.*, 1991b; Harland, 1997; Kelly, 1997). The Agardhfjellet Formation was deposited during a transgressive phase on an open marine shelf, where stagnant conditions were relatively common (Dypvik, 1985). Dypvik *et al.* (1992) suggest that the Agardhfjellet Formation was deposited in mid- to outer shelf regions. The exposure at Festningen is heavily weathered and iron and sulphur staining are particularly common throughout the shales. At Janusfjellet, the exposure is mostly in the form of laterally continuous concretionary horizons that are also heavily weathered.

The Oppdalen Member is a fining-upwards transgressive sequence from a well-cemented conglomeratic unit at the base (formed by erosion and reworking of the underlying Wilhelmøya Formation), through glauconitic sands, to marine clays and silts at the top (Dypvik *et al.*, 1991a, b; Harland, 1997; Kelly, 1997). The Lardyfjellet Member is dominated by organic rich dark grey to black shales that are finely laminated and devoid of bioturbation (Dypvik *et al.*, 1991a, b; Harland, 1997; Kelly, 1997). The Oppdalsåta Member is composed of highly bioturbated silts and fine sands throughout which several coarsening upwards sequences can be identified (Dypvik *et al.*, 1991a, b; Harland, 1997; Kelly, 1997). Finally, the Slottsmøya Member consists of dark grey to black shales and paper shales similar to those of the Lardyfjellet Member (Dypvik *et al.*, 1991a, b; Harland, 1997; Kelly, 1997).

The Berriasian to Barremian Rurikfjellet Formation (Fig. 9.6) was deposited during regressive shelf sedimentation, with deposition occurring on the outer to inner shelf and in prodeltaic depositional conditions (Dypvik *et al.*, 1992), and is relatively enriched in volcanogenic components compared with the Agardhfjellet Formation (Dypvik, 1985). The formation is 176 m thick at the type location and consists of dark grey shales, siltstones and sandstones, frequently interbedded with reddish carbonate horizons (Parker, 1967; Dypvik, 1985; Dypvik *et al.*, 1991b; Kelly, 1997). It has been divided into 3 distinct

units: the Myklegardfjellet Bed (oldest), the Wimanfjellet Member and the Ullaberget Member (Dypvik *et al.*, 1991a, b).

The Myklegardfjellet Bed was originally named by Birkenmajer (1980). It is a distinctive marker horizon that signals the transition between the Agardhfjellet and Rurikfjellet Formations across central and eastern Spitsbergen (Dypvik *et al.*, 1992). This bed varies in thickness from 0.5 to 10 m and consists of distinctive layers of white to yellow/green soft, plastic, weathered clays (Dypvik *et al.*, 1991b, 1992; Harland, 1997; Kelly, 1997). The bed was deposited by marine shelf processes at the culmination of a shallowing period in the depositional region (Dypvik *et al.*, 1992; Harland, 1997). The bed marks a change in depositional control, from global sea-level controlled shelf sedimentation to locally controlled, shallow shelf to prodeltaic/deltaic deposition (Dypvik *et al.*, 1992).

The Wimanfjellet Member comprises dark grey, silty, bioturbated shales containing irregular to cannon-ball shaped, reddish sideritic concretions (Dypvik *et al.*, 1991b; Harland, 1997). These are particularly common in the Festningen section. The Ullaberget Member consists of upwards-coarsening sequences of fine sands, silts and shales, with often well developed hummocky cross-stratification, planar cross-bedding and bioturbation (Dypvik *et al.*, 1991b; Harland, 1997; Kelly, 1997). Concretions similar to those of the Wimanfjellet Member are present in the lowermost beds of the Ullaberget Member (Dypvik *et al.*, 1991b). Harland (1997) attributes the deposition of the Ullaberget Member to progradation of the Festningen delta system.

The Barremian Helvetiafjellet Formation (Fig. 9.6) consists of a sequence of sandstones, shales and coals deposited in a continental environment (Parker, 1967; Steel *et al.*, 1977; Harland, 1997; Maher *et al.*, 2004). The unit varies from 50 to 100 m in thickness and contains coals of Type III and IV kerogen (Harland, 1997). The formation is divided into the Festningen and Glitrefjellet Members (Parker, 1967; Harland, 1997). The Festningen Member is a prominent, massive, hard light grey sandstone, weathering

yellow/orange (Parker, 1967). The Glitrefjellet Member is composed of coal measure-type facies, with abundant plant remains and poor quality coal (Parker, 1967; Harland, 1997). Steel *et al.* (1977) interpret this formation as a deltaic facies, with channel and crevasse splay sandstones, and interdistributary bay fines.

The Carlinefjellet Formation (Aptian to Albian) (Fig. 9.6) is divided into five members on the basis of sandstone-shale proportion. The formation is over 1200 m thick in places (Kelly, 1997) and signals a return to marine shelf deposition (Parker, 1967; Harland, 1997; Maher *et al.*, 2004). The succession is dominated by sandstones and shales, with some well developed ripple laminations, glendonites and rare fossils (Parker, 1967; Harland, 1997; Maher *et al.*, 2004). The top of the Carlinefjellet Formation is truncated by the Tertiary unconformity, the result of which is that post-Albian deposits have not been identified on Svalbard (Parker, 1967).

9.3. Sampling & Methodology

The Festningen samples ranged from Upper Oxfordian to Valanginian in age (although, it is worth noting that the Festningen section provides a complete succession from the Upper Carboniferous to Lower Cretaceous (Hoel & Orvin, 1937)). Belemnites were sampled from 25 well dispersed horizons from throughout the succession and glendonites were recorded from several horizons in the Valanginian. At Janusfjellet, belemnites were collected from 17 horizons and glendonites sampled from one major horizon only (again Valanginian in age). An attempt was made to collect multiple specimens from each horizon, however, the scarcity of belemnites at both Festningen and Janusfjellet meant that this was rarely possible. Sediment samples (~50) were collected from the Festningen section for nannofossil analysis by Dr Jörg Mutterlose, at the Ruhr-Universität, Bochum, Germany. All samples were collected in August 2005.

The preservation of belemnite rostra was assessed through trace element and stable isotope analysis in addition to BSEM, CL and carbonate staining. The areas of the rostrum

most susceptible to diagenesis were removed prior to stable isotope and trace element analysis.

Stable isotope analysis was conducted on a VG Optima mass spectrometer at the NERC Isotope Geosciences Laboratory (NIGL), Keyworth, UK. Trace element data were generated by Inductively Coupled Plasma-Atomic Emission Spectrometer (ICP-AES) using a Perkin Elmer Optima 3300RL ICP-AES system (with autosampler) at the NERC ICP facility, Department of Geology at Royal Holloway, University of London. For a full description of the methodology used see Chapter 4.

9.4. Results



Figure 9.7 Typical preservation of Svalbard belemnites. (A) Highly ferroan and fractured belemnite from the Volgian Argardhfjellet Formation (Janusfjellet). (B) Recrystallised belemnite rostrum from the Callovian Argardhfjellet Formation (Janusfjellet).

The belemnite rostra collected from both Festningen and Janusfjellet were generally very poorly preserved and fragmented (Fig. 9.7) making generic identification difficult, if not impossible (although the belemnites were known to be of Boreal affinities from the work of Doyle & Kelly (1988) conducted on belemnites from Kong Karls Land). In total, 18 out of 38 specimens were subjected to BSEM, CL and carbonate staining (Plates 15-17) in order to assess which areas of the belemnite rostra were commonly affected by diagenesis. The majority of the specimens were severely altered, with some exhibiting an exclusively blue colouration after carbonate staining, indicating that the

specimens were composed entirely of ferroan calcite (Plate 17). The CL technique, however, was much less effective at assessing the preservation of such specimens because the Fe levels were so high that they greatly exceeded the concentration of Mn (which is the catalyst for the CL reaction) and therefore, prevented luminescence. The BSEM analysis showed an abundance of sparry calcite and pyrite replacement, (which far exceeded any diagenetic alteration apparent in specimens from the other field locations considered here) particularly around the apical canal, the margins of the rostrum, on strong growth bands and along fractures (Plate 16). Also identified by these optical techniques was an infilling of quartz around the apical canal that was present in several specimens and the occurrence of deformation of the internal structure in some of the rostra. The areas prone to diagenetic alteration were either avoided or removed prior to subsampling.

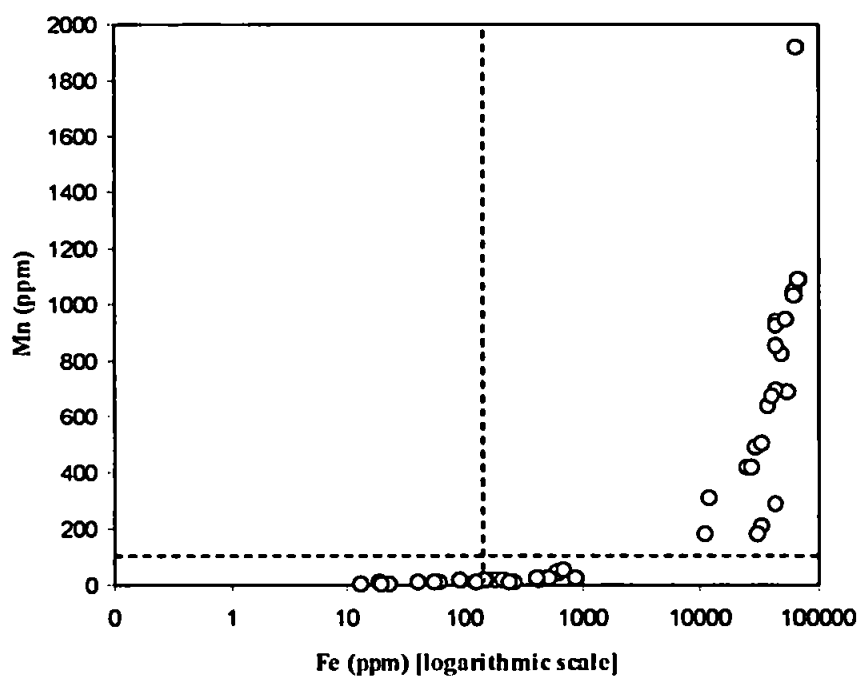


Figure 9.8 Cross-plot of Fe and Mn for belemnites from Svalbard. The dashed lines illustrate the cut off values from well preserved samples. Note the use of a logarithmic scale on the Fe axis.

Digenesis was further assessed using trace elements analysis, which was conducted on all 38 specimens in order to either confirm the presence of diagenetic alteration or to rule it out. The concentrations of Fe and Mn from the Festningen and Janusfjellet samples were as follows: Fe 12-68855 ppm, mean 19845 ppm; Mn 2-1911 ppm, mean 331ppm. A cross-plot of Mn and Fe was produced in order to constrain any diagenetic alteration (Fig.

9.8). Samples with concentrations of Fe and Mn exceeding 150 ppm and 100 ppm respectively were excluded from further analysis as they were considered likely to have undergone post-depositional alteration. In total 28 samples were rejected from further study on the basis of poor preservation.

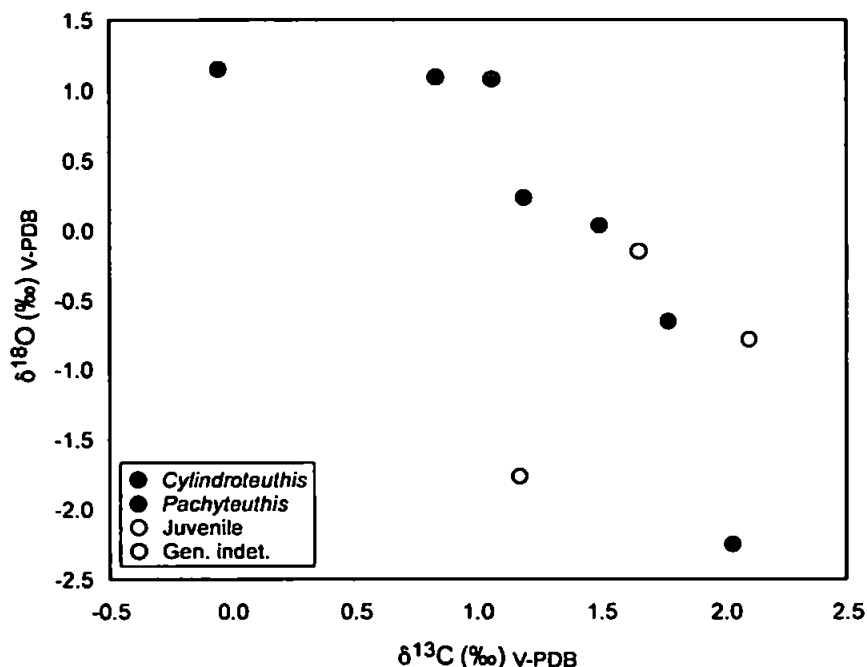


Figure 9.9 Cross-plot of $\delta^{18}\text{O}$ and $\delta^{13}\text{C}$ values derived from well preserved belemnites from Svalbard.

Additional trace element values were as follows: Sr 249-2857 ppm, mean 1117ppm; Mg 548-86290 ppm, mean 26404 ppm; Ca 7 % - 31 %, mean 22 %. Where diagenesis could be excluded oxygen and carbon isotope values ranged from -2.26 ‰ to 1.14 ‰ and -0.06 ‰ to 2.10 ‰ respectively. A cross-plot of $\delta^{18}\text{O}$ and $\delta^{13}\text{C}$ reveals a statistically significant negative correlation (at the 95 % confidence level) (Fig. 9.9). The well-preserved isotope data presented here comes from the Ryazanian-Upper Valanginian interval of the Svalbard succession, despite belemnite specimens also being collected from the Callovian-Volgian. In total, 9 separate belemnite horizons yielded potentially primary isotope values.

9.5. Discussion

9.5.1. Sedimentary Indicators of Palaeoclimate - Glendonites

Abundant stellate crystal aggregates were identified from the Upper Valanginian of the Rurikfjellet Formation at both the Festningen and Janusfjellet sections on Svalbard (Fig. 9.10). These mineral accumulations were yellow/orange/brown in colour, up to approximately 5 cm in size and composed of distinct crystals with pyramidal or flat terminations radiating out from a central nucleus. They were occasionally identified in Fe-rich concretions but were more commonly situated within dark mudstones or siltstones. These stellate aggregates are interpreted here as glendonites.

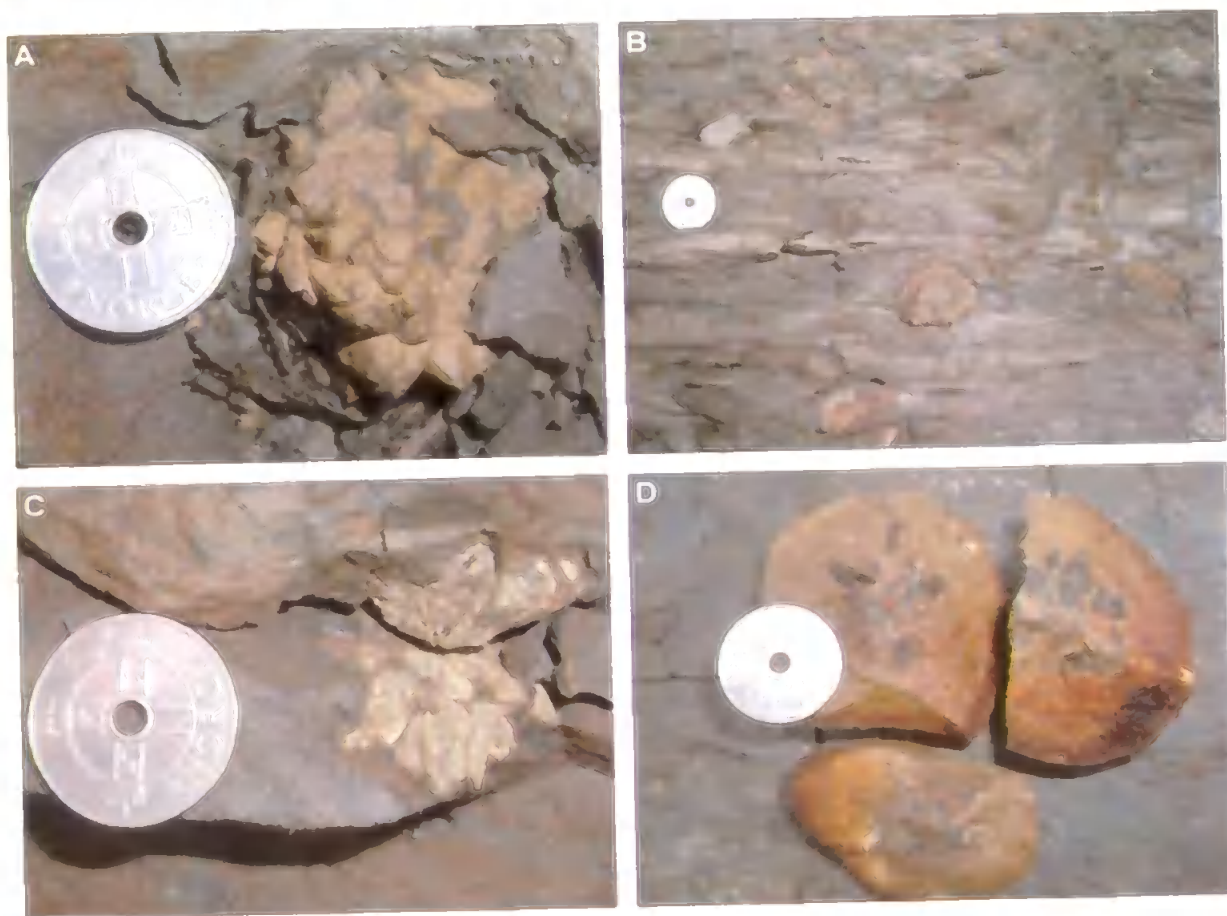


Figure 9.10 Glendonites from the Rurikfjellet Formation at Janusfjellet and Festningen. (A) Glendonite. (B) Abundance of glendonites. (C) Glendonite. (D) Glendonite in concretion.

Glendonites are calcite pseudomorphs after the metastable mineral ikaite ($\text{CaCO}_3 \cdot 6\text{H}_2\text{O}$) (DeLurio & Frakes, 1999). Sellwood & Price (1994) describe these pseudomorphs

as comprising of “obliquely striated and stepped crystals with a characteristic curved and tapered form”. Glendonites are most commonly associated with fine-grained dark mudstones and shales indicating reducing conditions and often interpreted as offshore to offshore-transition facies (Kemper, 1975; Kemper & Schmitz, 1975; England, 1976; DeLurio & Frakes, 1999; Jones *et al.*, 2006).

Glendonites are generally considered to represent cold depositional conditions (Shearman & Smith, 1985; Sellwood & Price, 1994; DeLurio & Frakes, 1999; Swainson & Hammond, 2001; Jones *et al.*, 2006) due to the environmental conditions required for ikaite precipitation. Ikaite forms at low temperatures in carbonate and calcium rich waters (Lennie *et al.*, 2004) and has only been observed naturally at temperatures between -1.9 and 7°C (Larson, 1994; Johnston, 1995; DeLurio & Frakes, 1999; Jones *et al.*, 2006). The exposure of ikaite to higher temperatures results in the mineral becoming unstable after which it is transformed can be calcite (Jones *et al.*, 2006). Modern day occurrences of ikaite have been identified at Ikka, Greenland (Pauly, 1963), where a carbonatite intrusion flows into a marine fjord (Buchardt *et al.*, 1997), in Antarctic marine sediments (Suess *et al.*, 1982), the Nankai trough, Japan (Stein & Smith, 1985) and on the Alaskan coast (Kennedy *et al.*, 1987).

The unstable nature of ikaite prevents long-term preservation in the geological record. However, the transformation of ikaite to calcite provides an opportunity for preservation in the form of glendonites. Glendonites have been identified and described from many locations worldwide, including, in the Neoproterozoic Twitya Formation, Canada (James *et al.*, 2005), the Permian of eastern Australia (Jones *et al.*, 2006), the Dwyka Group in the Great Karoo Basin, South Africa (McLachlan *et al.*, 2001), the Aptian Bulldog Shale, Australia (DeLurio & Frakes, 1999), the Valanginian & Aptian of Spitsbergen (Kemper, 1983) and in the present day Sea of Okhotsk, Eastern Siberia (Greinert & Derkachev, 2004).

Limited stable isotope studies have been conducted on glendonites, with attempts made to estimate the seawater temperature at which they formed (e.g., DeLurio & Frakes, 1999; Greinert & Derkachev, 2004). The major problems associated with such investigations however, are firstly that the oxygen-isotope composition of the source water is unknown and secondly, that equilibrium crystallisation cannot be guaranteed. Presumably the recorded oxygen-isotope composition represents the transition from ikaite to calcite. This transition is observed to occur when temperatures exceed a given range (probably near 8°C (Stein & Smith, 1985; DeLurio & Frakes, 1999)), however, the rate of temperature rise influences the level of preservation (only a gradual rise in temperature will preserve the ikaite morphology) and the exact temperature at which transition occurs is dependent on water chemistry (DeLurio & Frakes, 1999). Oxygen-isotope ratios derived from the Bulldog Shale glendonites yield palaeotemperature estimates of 12-18°C, which seems peculiarly high and could be the result of several factors, for example, the majority of the calcite may represent later infilling or the estimate of $\delta^{18}\text{O}_{\text{seawater}}$ may have been incorrect (DeLurio & Frakes, 1999).

Despite the problems associated with glendonite isotope studies it is probably reasonable to assume that the presence of glendonites in a geological succession represents cold conditions. The formation of the precursor mineral ikaite almost certainly took place in temperatures below 7°C and in marine successions at temperatures below 4°C, since marine ikaite has never been reported at temperatures exceeding this value (Bischoff *et al.*, 1993; Buchardt *et al.*, 1997). The presence of abundant glendonites in both the Festningen and Janusfjellet successions, therefore, confirms the presence of cold depositional conditions during the Late Valanginian in the region of Svalbard.

9.5.2. Sedimentary Indicators of Palaeoclimate - Outsized Clasts

Outsized clasts are fairly common in the Valanginian part of the Janusfjellet Subgroup at Festningen (Fig. 9.11). The clasts are small, dark, sub-rounded and often sub-

spherical, polished pebbles ($< \sim 2\text{cm}$) and are preserved either as individual stones or small clusters of stones within fine-grained facies, such as mudstone or fine-grained sandstone. The presence of relatively large clasts within a fine host sediment present a potential “hydrodynamic paradox” between the low energy depositional requirements of the host rock and higher energy conditions required to transport relatively large clasts (Bennett *et al.*, 1996). Clasts of this nature are often described as dropstones, a name derived from the likely method of deposition. Dropstones are introduced vertically or obliquely into the host sediment usually from some form of raft (Bennet & Doyle, 1996; Bennet *et al.*, 1996). The most common mechanism invoked to account for the presence of dropstones in a succession is deposition from icebergs or sea-ice (e.g., Frakes, 1979; Hambrey & Harland, 1981; Gilbert, 1990).



Figure 9.11 Outsized clast. Upper Valanginian Rurikfjellet Formation, Festningen.

Dropstones have been identified from Cretaceous sediments in Australia (Frakes & Francis, 1988; Francis & Frakes, 1993), from Late Jurassic and Early Cretaceous deposits

in Siberia (collated in Hambrey & Harland, 1981) and from Cretaceous and Paleogene sediments in Svalbard (Pickton, 1981). These deposits (and many others like them) have been attributed to ice-rafting and are therefore considered representative of cold climatic conditions, although, Bennett & Doyle (1996) question the reliability of dropstone evidence in demonstrating the presence of ice.

Dropstones may be transported and deposited in many ways. They could be either volcanic or meteoric projectiles (Bennett *et al.*, 1996) or they could be rafted by something other than ice. Bennett & Doyle (1996) describe several biological and physical processes that could deposit dropstones, for example, they could be rafted from vegetation such as seaweed, kelp and driftwood (e.g., Woodborne *et al.*, 1989; Bennett *et al.*, 1994; Doublet & Garcia, 2004), they could be gastroliths (e.g., Stokes, 1987; Clarkson, 1988) or indigestible stomach contents (e.g., Emery, 1965) or they could be floating stones. Gastroliths and indigestible stomach contents would be expected to form a small cluster of stones (Bennett *et al.*, 1996) and therefore cannot account for at least some of the deposits identified at Festningen. In addition, the stones at Festningen are never associated with skeletal remains. Floating stones are usually flat and are very limited in occurrence (Bennett *et al.*, 1996) and are therefore also unlikely to account for the outsized clasts identified. Perhaps the most likely alternative is rafting from vegetation, since this mechanism could deposit both individual stones and small clusters (Bennett *et al.*, 1994).

Polishing on at least one side of a pebble would be expected if it had been entrained in ice. In addition, the presence of striations on outsized clasts could be used to confirm deposition from ice-rafting. The pebbles observed here were often highly polished but no striations were observed, although this does not rule out deposition by ice. Other features often displayed by dropstones include evidence of sediment depression or deformation around the clasts, which would have been formed during impact and the draping of overlying sediments (Thomas & Connell, 1985; Jones *et al.*, 2006). Again, neither of these

features was observed at Festningen, although this is most likely due to the small size of the pebbles and consequently a low velocity of impact.

Although, ice-rafting cannot be confirmed as the mechanism of deposition for the outsized clasts observed at Festningen, the presence of such deposits lends some support to the idea that deposition could have occurred during cold conditions. Some of the pebbles identified were located within a few metres, stratigraphically, of glendonite deposits. The occurrence of both of these sedimentological features in the same succession is significant and goes some way to proving that cold conditions did occur in Svalbard during the Early Cretaceous.

9.5.3. Stable Isotope, Geochemical & Taxonomic Records

As discussed previously, taxonomic identification of belemnite rostra was very difficult with specimens from the Svalbard region due to generally poor preservation. The affect of taxonomic differences on stable isotope and geochemical records is therefore almost impossible to assess from this location. This problem is exacerbated by the limited nature of the isotope record as recorded here. Whilst the data available does not indicate a taxonomic influence on the isotope and elemental records, the limited nature of the data means that such an influence cannot be ruled out.

9.5.4. The Oxygen Isotope Record & Palaeotemperature Implications

Palaeotemperatures (Figs 9.12 & 9.13) were again calculated using the equation of Anderson & Arthur (1983) and assuming an isotopic composition for the water of non-glacial seawater at -1 ‰ SMOW and a typical marine salinity of ~ 34 ‰. The palaeotemperature range for the Ryazanian-Upper Hauterivian succession at Janusfjellet was 7.7 to 8°C, compared to a palaeotemperature range of 11.1 to 21.4°C for the Upper Valanginian interval of the Festningen succession. Combined, these two records provide a palaeotemperature range of 7.7 to 21.4°C for the Ryazanian-Upper Valanginian of

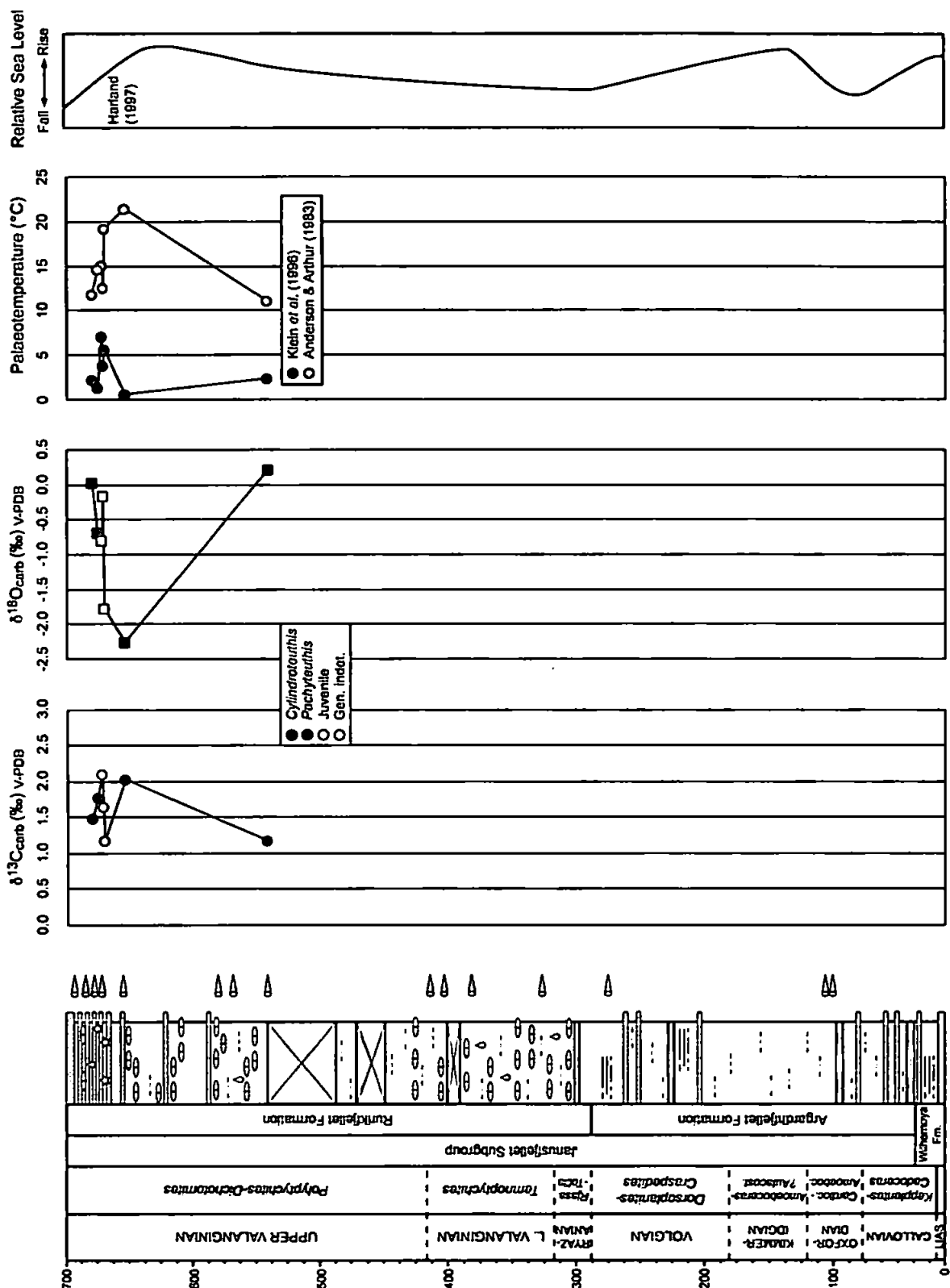


Figure 9.12 $\delta^{13}\text{C}$ and $\delta^{18}\text{O}$ records from the Upper Valanginian succession at Festningen, Svalbard. Calculated palaeotemperatures and a sea level curve are also shown. Svalbard/Barents Sea ammonite zonation is illustrated (see references within Harland (1997)). Indicated to the right of the sedimentological log (with a belemnite symbol) are the horizons from which belemnites were collected. See Figure 4.2 for key to log symbols. Scale is in metres.

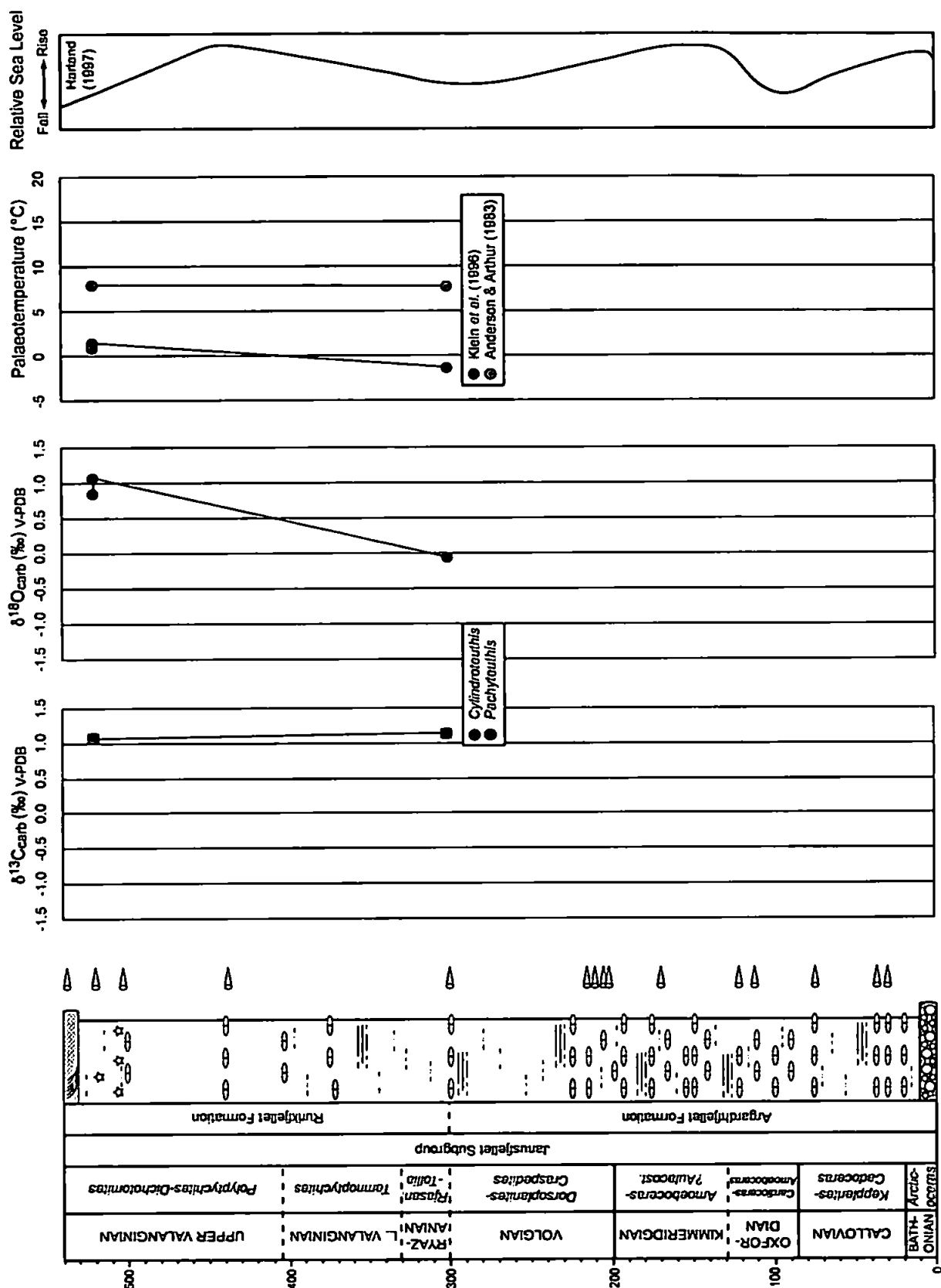


Figure 9.13 $\delta^{13}\text{C}$ and $\delta^{18}\text{O}$ records from the Ryazanian-Upper Valanginian succession at Janusfjellet, Svalbard. Calculated palaeotemperatures and a sea level curve are also shown. Svalbard/Barents Sea ammonite zonation is illustrated (see references within Harland (1997)). Indicated to the right of the sedimentological log (with a belemnite symbol) are the horizons from which belemnites were collected. Figure 4.2 for key to log symbols.

Svalbard and an average temperature of 13.0°C. The lowest values occur in the Ryazanian and the highest values in the Upper Valanginian *Dichotomites ammonite* zone. Surprisingly, the highest palaeotemperature estimates occur just prior to (~10 m below) the glendonite occurrences in the Festningen section, although the temperatures do drop significantly (from 21.4 to 11.1°C) where glendonites are most abundant. At Janusfjellet, belemnites and glendonites also co-occur during the Upper Valanginian. Here $\delta^{18}\text{O}$ derived palaeotemperatures give values of ~8.0°C. Interestingly, this is the estimated basal transition temperature for the change from ikaite to calcite in glendonites (e.g., Stein & Smith, 1985; DeLurio & Frakes, 1999).

9.5.5. The Elemental Records & Palaeotemperature Implications

Mg/Ca, Sr/Ca, Na/Ca and Li/Ca ratios were calculated here (as in the previous chapters) together with Mn/Ca in order to assess preservation. Those samples with Mn/Ca values exceeding 100 $\mu\text{mol/mol}$ were excluded from further analysis. Cross-plots of *EI/Ca* against $\delta^{18}\text{O}$ for the Ryazanian-Upper Valanginian Svalbard belemnites (Fig. 9.14) show statistically significant correlations (at the 99% confidence level) for Na/Ca with $\delta^{18}\text{O}$ and Li/Ca with $\delta^{18}\text{O}$ but not for Mg/Ca or Sr/Ca. The R^2 values for the correlations are as follows, 0.447 (Mg/Ca), 0.062 (Sr/Ca) 0.899 (Na/Ca) and 0.799 (Li/Ca). The strength of the correlations between Na/Ca and $\delta^{18}\text{O}$ and between Li/Ca and $\delta^{18}\text{O}$ is surprising as such correlations have not been observed in published belemnite studies (e.g., McArthur *et al.*, 2000; Bailey *et al.*, 2003; Rosales *et al.*, 2004a, b) nor have they been observed in the previous chapters (although Li/Ca and $\delta^{18}\text{O}$ did show a statistically significant correlation in the Boyarka River dataset). The reason for the significance of these correlations is unclear.

Long-term trends cannot be observed from the Janusfjellet succession (Fig. 9.15) because the succession contains only three data points (one in the Ryazanian and two in the Valanginian), however, there appears to be little change in the *EI/Ca* values recorded at

Janusfjellet. The long-term trends recorded from the Festningen succession (Fig. 9.16) are also difficult to interpret due to the sparsity of data. As is expected from the correlations observed in the El/Ca and $\delta^{18}O$ cross-plots (Fig. 9.14) Na/Ca and Li/Ca show a distinct shift to more negative values, which is followed by a return towards more positive values at the top of the succession (as is observed in the $\delta^{18}O$ record).

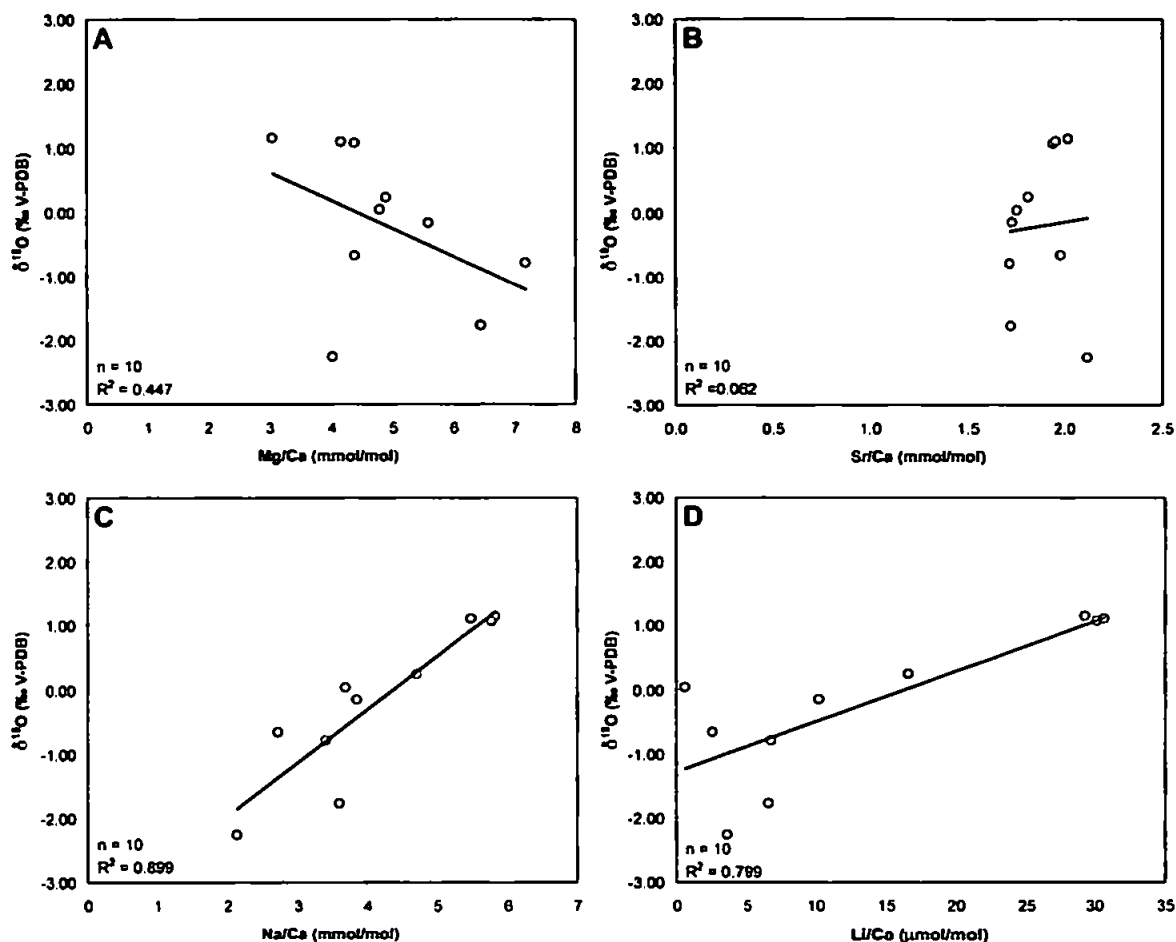


Figure 9.14 Cross-plots of $\delta^{18}O$ and (A) Mg/Ca, (B) Sr/Ca, (C) Na/Ca and (D) Li/Ca.

Mg/Ca ratios were used to calculate palaeotemperatures (Figs 9.12 & 9.13) for the Ryazanian-Upper Valanginian interval using the equation of Klein *et al.* (1996) (as in the previous chapters). The average palaeotemperature (for the Janusfjellet and Festningen sections combined) is 2.4°C and the range is -1.3 to 5.6°C. The average offset between the $\delta^{18}O$ derived values and Mg/Ca derived values for the combined Svalbard successions is 10.6°C. This temperature difference is linked to a distinct freshening of ~10 ‰, which equates to a change from a 'normal' marine salinity of 34 ‰ to a value of 24 ‰.

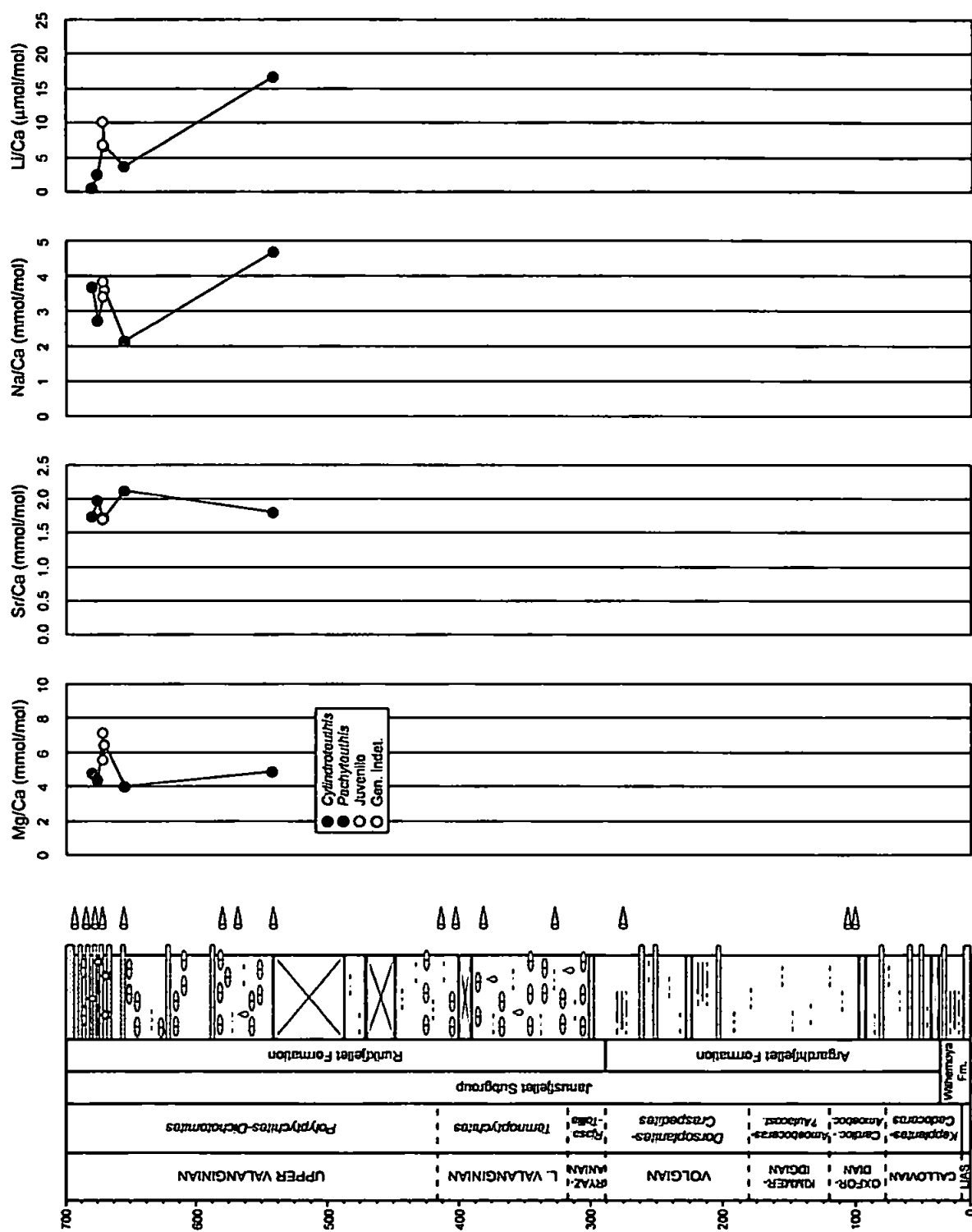


Figure 9.15 El/Ca ratios from the Upper Valanginian succession at Festningen, Svalbard. Svalbard/Barents Sea ammonite zonation is illustrated (see references within Harland (1997)). Indicated to the right of the sedimentological log (with a belemnite symbol) are the horizons from which belemnites were collected. See Figure 4.2 for key to log symbols. Scale is in metres.

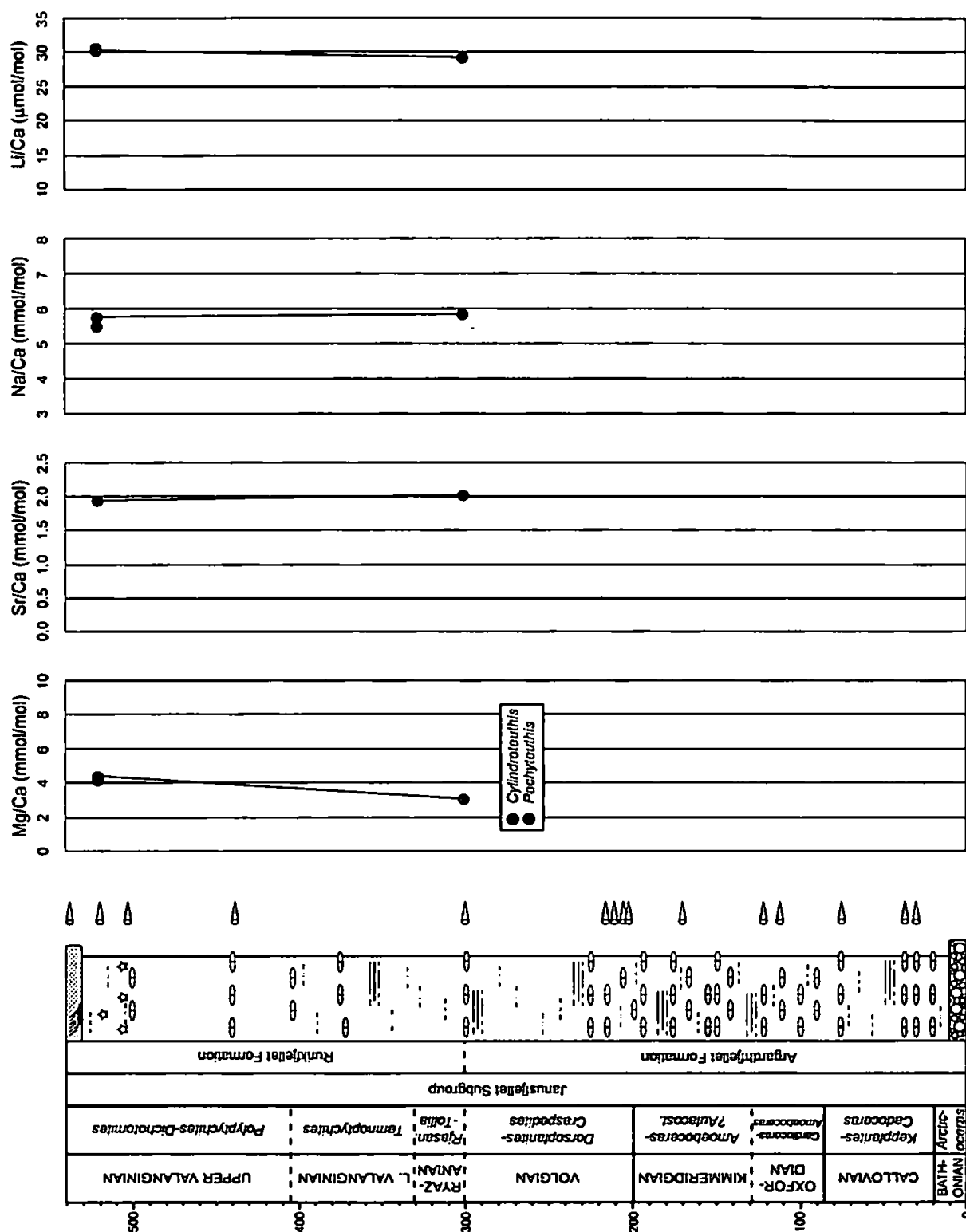


Figure 9.16 El/Ca ratios from the Ryazanian-Upper Valanginian succession at Janusfjellet, Svalbard. Svalbard/Barents Sea ammonite zonation is illustrated (see references within Harland (1997)). Indicated to the right of the sedimentological log (with a belemnite symbol) are the horizons from which belemnites were collected. See Figure 4.2 for key to log symbols.

This amount of freshening seems unlikely since belemnites are always associated with other marine organisms and are therefore unlikely to have survived in seawater with a salinity that low. If the oxygen isotope composition of seawater is assumed to be -1.5 ‰ (the value predicted by Roche *et al.* (2006) for the high latitudes) the average $\delta^{18}\text{O}$ derived palaeotemperature is 11.0°C (instead of 13.0°C). A change in temperature of 8.6°C can be interpreted as the result of an 8.4 ‰ change in salinity. This value still seems high, which suggests that Mg/Ca derived palaeotemperature estimates must be viewed with caution, particularly as the Mg/Ca calculations used here produce sub-freezing values for parts of the succession and such temperatures could not possibly be recorded by belemnite calcite.

9.5.6. The Carbon Isotope Record

Carbon isotope values from the Festningen and Janusfjellet successions range from -0.06 ‰ in the Ryazanian to 2.1 ‰ in the Upper Valanginian. Once again, the sparsity of data makes it difficult to interpret a long-term trend here. In spite of these difficulties however, a shift to more positive values in the Upper Valanginian is observed. This is consistent with the timing of the global carbon isotope positive excursion that occurs during this interval (and has been identified from carbonate and organic records presented in this study - see Chapters 7 & 8). The shift towards more positive carbon isotope values observed here is coincident with a relative sea level rise, although the maximum values occur during the onset of a sea level fall. This relationship observed between carbon isotope values and sea level is very similar to that observed from the Boyarka River succession, where the initiation of the positive carbon isotope excursion coincides with a sea level rise but the excursion maximum coincides with a sea level fall. As discussed previously, positive carbon-isotope excursions may be related to regressive conditions due to an increased input of nutrients resulting from exposure and erosion of lowland areas (Brenchley *et al.*, 1994; Gröcke *et al.*, 1999; Price & Mutterlose, 2004). In addition, the partial separation of the Boreal and Tethyan Realms during periods of sea-level lowstand

could have restricted ocean circulation and enhanced stratification to promote organic carbon burial in these high latitude locations (Price & Mutterlose, 2004).

9.5.7. Ryazanian-Valanginian Stable Isotope Records

The Ryazanian-Upper Valanginian temperatures calculated here (7.7 to 21.4°C, average 13.0°C) are consistent with palaeotemperatures calculated from published belemnite-derived oxygen-isotope data. Ditchfield (1997) calculated palaeotemperatures of 5.3 to 10.9°C for the Tithonian-Valanginian interval from Kong Karls Land, Svalbard. Other palaeotemperature estimates include those of Price *et al.* (2000) at 10-15°C for Yorkshire, England, McArthur *et al.* (2004) at 9-14°C also for Yorkshire, England, van de Schootbrugge *et al.* (2000) at 12-16°C for southeastern France and Price & Mutterlose (2004) at 7-21°C for the Yatria River, Siberia (Fig. 9.17). The palaeotemperature data presented here is consistent with the lowest values previously recorded for Ryazanian-Valanginian interval but also presents some surprisingly high temperature values.

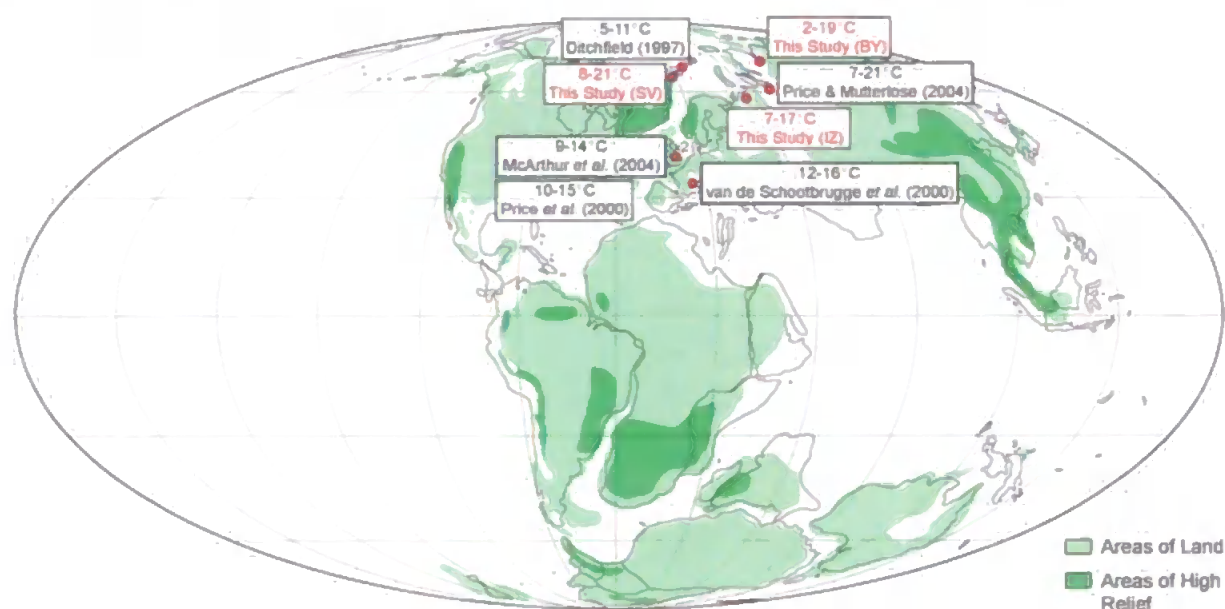


Figure 9.17. Valanginian palaeogeography map showing published belemnite derived palaeotemperatures for this time period. (SV = Svalbard; BY = Boyarka River; IZ = Izhma River).

The palaeotemperature estimates from the Ryazanian-Valanginian northern high latitudes (calculated from this study and by Price & Mutterlose (2004)) are more variable

than the estimates derived from the mid-latitudes (e.g., Price *et al.*, 2000; van de Schootbrugge *et al.*, 2000; McArthur *et al.*, 2004). This could be the consequence of several factors, firstly, increased seasonal temperature differences in the high latitudes compared with those in the mid- to low latitudes, secondly, the proximity of these sites (and in particular those in Russia and Siberia, which show the greatest variability) to a substantial landmass and hence the likely influence of riverine runoff and thirdly, the potential influence of seasonal ice-melt to these high latitude sites. An additional factor that could account for the observed high latitude variability is that Boreal Realm belemnite taxa could have a greater tolerance to changing environmental conditions than their Tethyan counterparts.

As discussed in previous chapters an Upper Valanginian positive carbon isotope excursion has been identified from the Tethyan region (e.g., Lini *et al.*, 1992; Channell *et al.*, 1993) and from the high latitudes (e.g., Price & Mutterlose, 2004; Boyarka River and Izhma River (this study)) and from both carbonate (e.g., Lini *et al.*, 1992; Channell *et al.*, 1993) and organic carbon records (e.g., Gröcke *et al.*, 2005; Boyarka River (this study)). The $\delta^{13}\text{C}$ shift to more positive values observed in the Svalbard successions is consistent with the timing of this seemingly global excursion.

9.6. Conclusions

- The data presented here comprise the first belemnite stable isotope study to be conducted from the Ryazanian-Upper Valanginian interval at Festningen and Janusfjellet, Svalbard.
- The preservation of belemnites at this site was very poor, although stable isotope analyses were possible from ~25% of the collected specimens.
- Glendonites and outsized clasts (interpreted here as glacial dropstones) were identified from the Svalbard successions. The presence of such deposits occurring in close

stratigraphic proximity lends definite support to the idea that cold conditions occurred in the northern high latitudes during the Early Cretaceous.

- The palaeotemperature range calculated from the belemnite $\delta^{18}\text{O}$ data is 7.7 to 21.4°C, with an average temperature of 13.0°C. This is consistent with previously published data for this time interval. Despite the variability observed, the existence of cold conditions is further supported by these data.
- The Mg/Ca derived palaeotemperature estimates range from -1.3 to 5.6°C, with an average temperature of 2.4°C. As noted in previous chapters, it would be impossible for belemnites to record sub-freezing temperatures, which casts doubt on the use of Mg/Ca palaeotemperature equations when applied to belemnite calcite.
- The $\delta^{13}\text{C}$ data display a shift to more positive values from the Ryazanian and into the Upper Valanginian (of ~2 ‰). This shift is consistent with the timing of the Upper Valanginian positive carbon isotope excursion, which has been recorded from the Tethyan region, from the high latitudes, from carbonate and from organic carbon records.

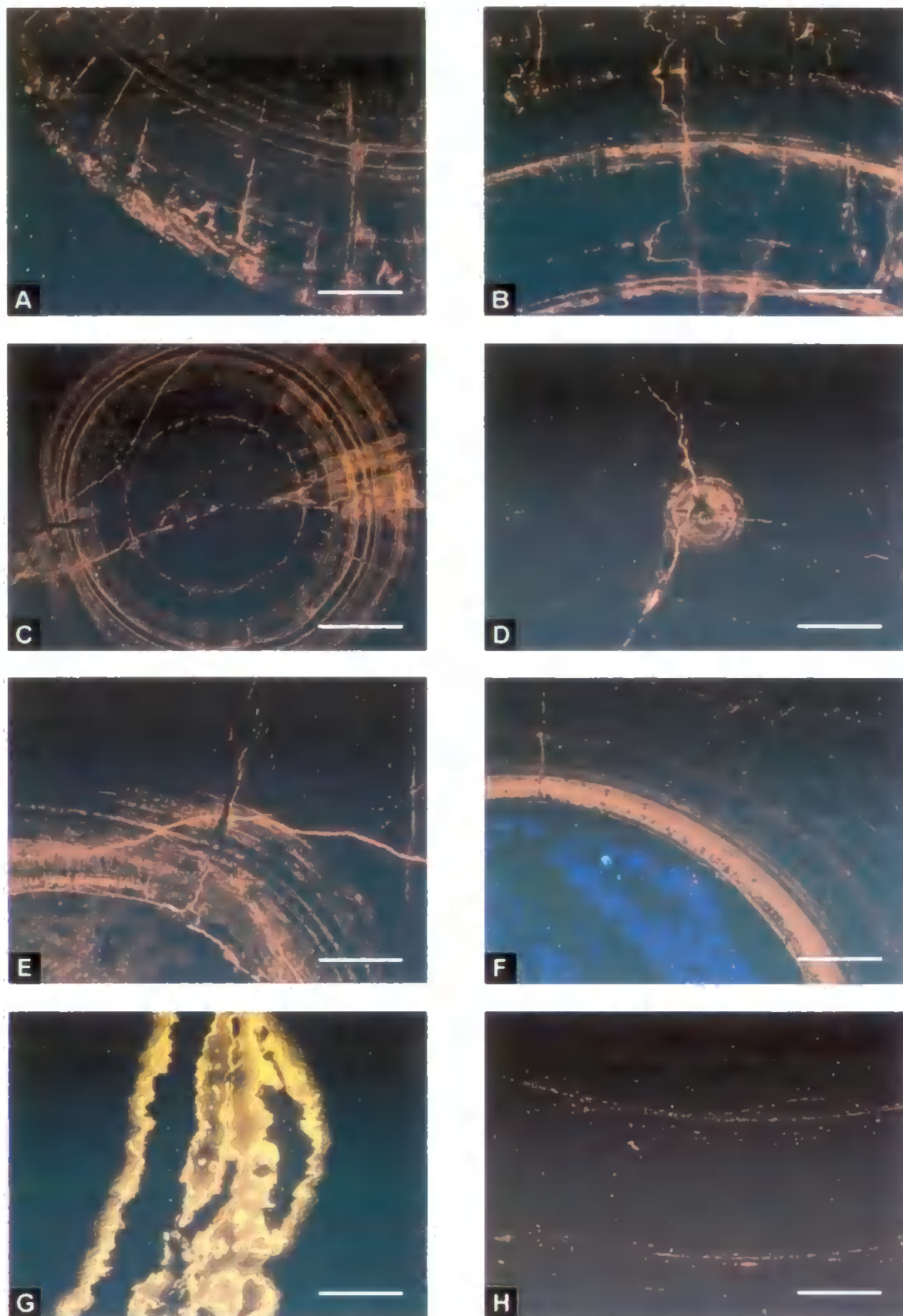


Plate 15. Cathodoluminescence images showing the state of preservation of belemnite rostra from Festningen and Janusfjellet, Svalbard. All scale bars represent 1 mm. (A) Rostrum margin, growth bands and fractures displaying alteration. (B) Growth bands and fractures displaying alteration. (C) Apical canal surrounded by growth bands displaying alteration. (D) Fractures emanating from apical canal. (E) Fractures and growth bands near apical canal displaying alteration. (F) Apical canal with sediment infilling. (G) Distinct cracks partially infilled with diagenetic cement. (H) Generally well preserved calcite.

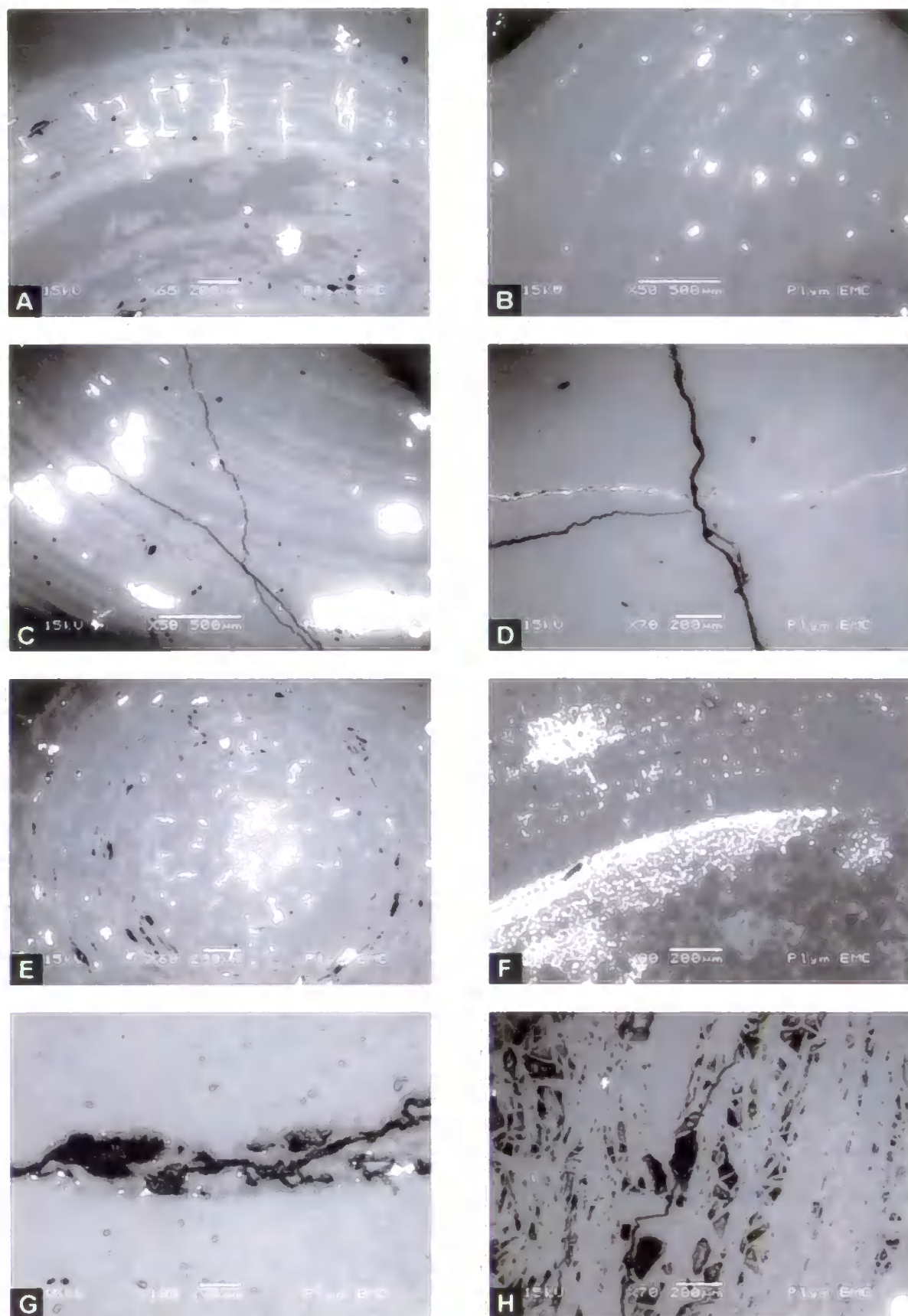


Plate 16. Backscattered SEM images showing the state of preservation of belemnite rostra from Festningen and Janusfjellet, Svalbard. All scale bars represent lengths stated on images. (A) Growth lines displaying strong alteration and some pyrite growth. (B) Growth lines displaying alteration. (C) Growth lines displaying strong alteration and the presence of pyrite. (D) Fractures running through apical canal, one infilled with pyrite. (E) Apical canal and surrounding growth lines displaying alteration and the presence of pyrite. (F) Edge of apical canal with presence of pyrite. (G) Fractures surrounded by alteration and with some pyrite infilling. (H) Deformed internal structure and areas of altered calcite around deformation.

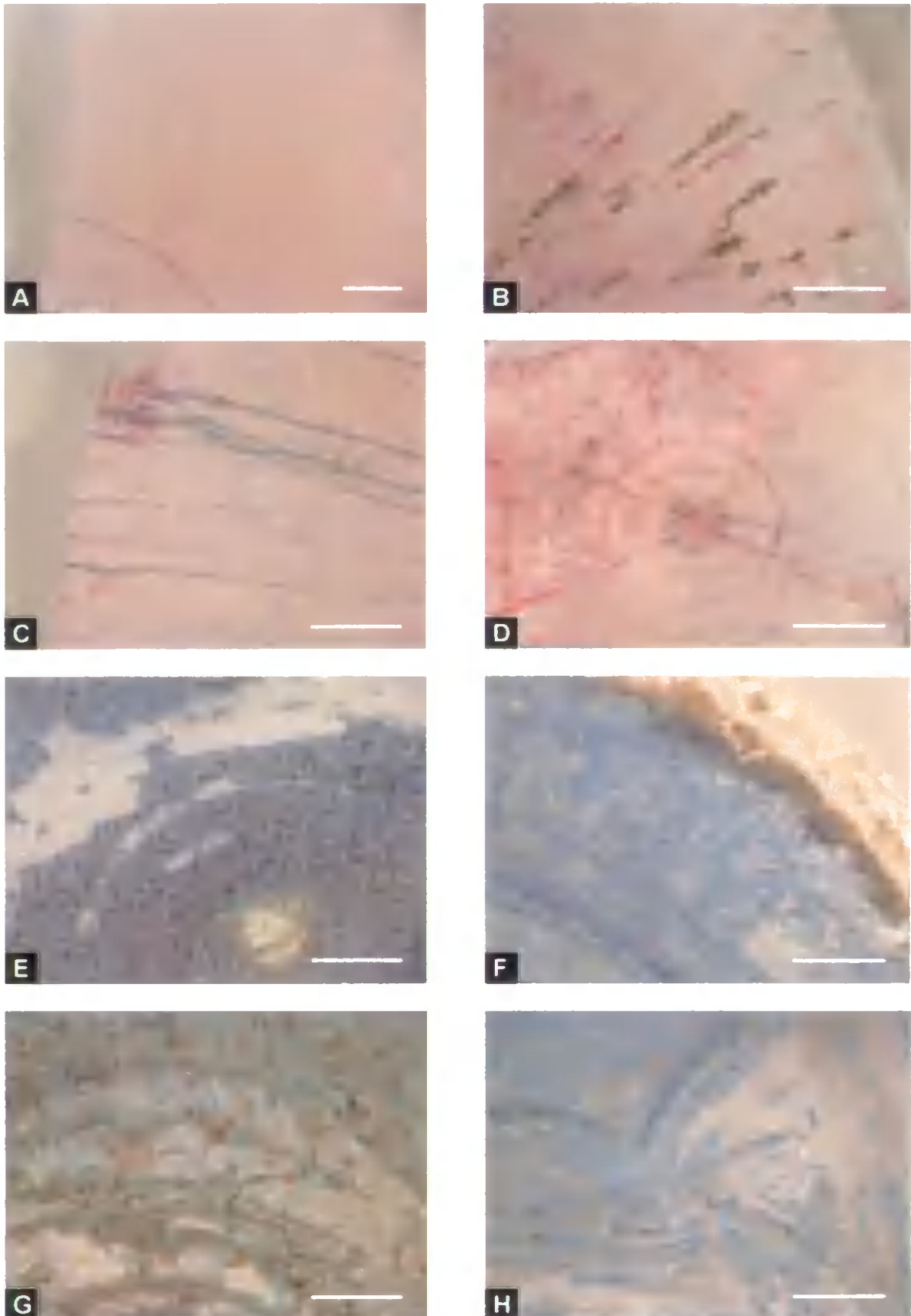


Plate 17. Carbonate stained images showing the state of preservation of belemnite rostra from Festningen and Janusfjellet, Svalbard. All scale bars represent 1 mm. (A) Very well preserved calcite. (B) Pyrite growth along fractures at rostrum margin. (C) Fractures emanating from rostrum margin displaying alteration. (D) Apical canal, fractures and growth lines displaying alteration. (E) Ferruginous calcite with some quartz replacement. (F) Ferruginous calcite. (G) Ferruginous calcite with some quartz replacement and pyrite growth. (H) Ferruginous calcite with some quartz replacement and deformation of internal structure.

10. DISCUSSION

This chapter will discuss two major themes in relation to the data presented in this study. Firstly, it will evaluate the use of belemnites as palaeoenvironmental indicators. This is of particular importance for appreciating both the limitations and the potential of the data investigated here. Secondly, the contribution of this study to the understanding of Late Jurassic and Early Cretaceous global palaeoenvironment will be examined.

10.1. Evaluating Belemnites as Palaeoenvironmental Indicators

10.1.1. Preservation

The belemnite specimens analysed in this research are considered to be generally well preserved and, therefore, represent the original isotopic and geochemical composition of the belemnite calcite. A range of methods were used in this study in order to assess the preservation of belemnite rostra. These methods were: CL, BSEM, carbonate staining and trace element analysis. In addition to these techniques, a preliminary visual inspection of each belemnite rostrum was conducted and opaque or cloudy specimens were rejected.

Each of the aforementioned techniques is extremely useful for assessing preservation, although, there are a number of limitations associated with their use. CL microscopy, for example, is not effective where the concentration of Fe greatly exceeds that of Mn, which is the catalyst for the luminescence reaction. Ferroan calcite highly enriched in Fe, therefore, does not show luminescence despite being severely diagenetically altered. This problem was encountered with several of the belemnite specimens analysed from Svalbard in the present study.

The major limitation associated with Backscattered Scanning Electron Microscopy is the ambiguity present in the generated image. Areas of alteration are highlighted by a change in tone on the greyscale image (i.e., lighter and darker greys) and subtle alteration

is therefore often difficult to distinguish. The BSEM technique however, provides a higher level of magnification than is available from any of the other screening methods, which allows more minor areas of alteration to be identified, although, such resolution is often unnecessary since those areas of minor alteration will often be confined to the segment of the rostrum being analysed and will not be present in the subsample from which subsequent isotope and geochemical analysis will be conducted.

Carbonate staining of belemnite rostra produces a very clear visual representation of preservation and is probably the most illustrative of the optical screening techniques applied here. The carbonate staining technique responds to the occurrence of Fe, unlike the CL technique, which utilises the presence of Mn. Well preserved calcite displays a pale pink colouration after staining, whilst Fe-rich areas appear as dark pink-mauve-purple-blue colours, depending on the abundance of Fe (blue represents highly ferroan calcite). This technique, therefore, shows not only the presence of diagenetic products but also the degree of alteration present. CL microscopy is also capable of this because a greater amount of Mn will create stronger luminescence. The problem with interpreting the CL reaction in this sense however, is that the strength of luminescence can be altered manually by modifying the gun current and gun voltage and a change in luminescence strength is not as visually striking as a change in colour (as demonstrated in the carbonate stained specimens).

Trace element analysis is perhaps the most useful of the tests for diagenesis as it provides a quantitative rather than qualitative assessment of alteration. High concentrations of Fe and Mn more or less guarantee that diagenetic calcite is present, although it should be noted that alteration can take place in the absence of Fe and Mn, for example under oxidising conditions (Marshall, 1992; Jones *et al.*, 1994).

In conclusion, it is important to assess belemnites for diagenetic alteration using a combined approach that incorporates both geochemical and optical techniques. Firstly, belemnite rostra must be examined using the naked eye. Only those specimens that display

a predominantly honey coloured and translucent appearance should be considered for further analysis. In addition, care should be taken where obvious signs of bioerosion are present on the rostrum margin. Optical screening techniques should then be performed on a representative range of samples, or where possible (with small datasets for example) such analyses should be carried out all specimens. Finally, trace element analysis (for Fe and Mn) should be conducted on every specimen. If this process is followed, all specimens affected by modest to severe post-depositional alteration, as well as many of those affected by very slight alteration should be recognised and removed. The remaining specimens can then be analysed for stable isotopes and trace element concentrations with the confidence that any trends recorded will not be the result of preservational factors.

10.1.2. Natural Variability in Belemnite Records

For each of the belemnite isotope or elemental records presented here a significant degree of scatter is present. This variability is not considered to be the result of diagenetic alteration as an extensive screening process was employed in order to eliminate altered specimens (as outlined above). The variability is therefore likely to be the result of real environmental change (e.g., temperature, salinity, ice volume), genus- or species-specific, ontogenetic or gender related differences in fractionation.

McArthur *et al.* (2004) observed a small (<0.4 ‰) offset in the $\delta^{18}\text{O}$ ratios recorded from co-occurring belemnites of the genera *Hibolites* (typically a Tethyan Realm genus) and *Acroteuthis* (typically a Boreal Realm genus) from the Early Cretaceous at Speeton, Yorkshire. This led them to allude to the possibility of genus related differences in the fractionation of biogenic calcite. Such differences could be caused by a difference in habitat (e.g., one genus inhabited the shallow shelf, whilst the other inhabited deeper waters), differences in migratory habits (possibly related to mating and feeding differences) or a slight offset from equilibrium fractionation in one or both of the genera. The major problem with assessing whether or not different genera record slightly different

stable isotope or geochemical signatures is that co-occurring belemnites consisting of a variety of genera are not common in the geological record. In the successions investigated here, only 10 belemnite horizons out of approximately 375 contained more than one genus (where taxonomic identification could be undertaken with confidence) and even then only one or two specimens from each genus were suitable for collection and analysis. Furthermore, if only one or two specimens from each genus is analysed, it is difficult to determine whether an observed difference in composition is attributable to generic factors or whether it is instead the result of changing environmental conditions between the deposition of each individual. Belemnites probably only lived for a few years (based on analogy with modern cephalopods) (Rexfort & Mutterlose, 2006), whilst deposition of a sedimentary horizon containing belemnites could require a considerably greater period of time to form. Doyle & Macdonald (1993) suggest that belemnite assemblages on a single bedding plane could require several thousand years to form. This, therefore, provides the opportunity to preserve a number of belemnites in a sedimentary horizon that would have lived at slightly different times and consequently would also have recorded slightly different geochemical compositions.

The analysis of co-occurring belemnites in this study (Table. 10.1) is inconclusive with regards to the influence of generic differences upon fractionation. In total, 23 belemnite horizons containing either co-occurring belemnites of the same genus (only 13 horizons out of ~375) or co-occurring belemnites of different genera (10 horizons) were identified. The offset observed in both the oxygen and carbon isotope values is highly variable, with offsets ranging between 0.04 and 2.39 ‰ for oxygen and between 0.02 and 1.96 ‰ for carbon (Fig. 10.1). The maximum offset in oxygen isotope values is observed between belemnites of the same genus (*Cylindroteuthis*), whilst the maximum offset in carbon isotope values is observed between different genera (*Cylindroteuthis* and *Pachyteuthis*). There appears to be no consistency in the amount of offset observed between co-occurring belemnites of the same genus and co-occurring belemnites of

different genera. In addition, there is no consistency between the nature of the offset observed where different genera are considered, for instance, where *Cylindroteuthis* and *Pachyteuthis* co-occur, neither genus records consistently heavier nor lighter isotope

Horizon No.	Age	Am. Zone	Genus	$\delta^{18}\text{O}$	$\delta^{18}\text{O}$ Offset	$\delta^{13}\text{C}$	$\delta^{13}\text{C}$ Offset	Mg/Ca	Na/Ca	Li/Ca	Sr/Ca
KH1-4; 32.30	Val.-Haut.	D.bid.-H.boy.	Cylindro.	-0.64	1.64	1.52	0.13	4.45	5.21	22.93	1.82
	Val.-Haut.	D.bid.-H.boy.	Cylindro.	1.00		1.65		5.08	5.86	34.47	1.88
KH1-4b; -20.00	L. Val.	D.bidichot.	Arcto.	2.05	1.73	2.73	0.23	2.60	5.50	7.24	2.19
	L. Val.	D.bidichot.	Arcto.	0.32		2.96		2.95	4.85	5.16	2.00
KH16; 2.80	E. Ryaz.	H.koc.-S.an.	Cylindro.	1.92	0.68	0.41	0.13	3.84	4.99	18.56	1.62
	E. Ryaz.	H.koc.-S.an.	Cylindro.	1.24		0.28		4.86	5.18	17.93	1.70
KH16; 2.95	E. Ryaz.	H.koc.-S.an.	Cylindro.	2.27	2.39	0.31	0.03	2.71	6.54	19.90	1.94
	E. Ryaz.	H.koc.-S.an.	Cylindro.	-0.12		0.28		5.27	5.39	29.18	1.54
PC1	E. Callov.	C.elatmae	Pachy.	-0.31	0.04	1.66	0.18	6.79	5.20	72.62	1.25
	E. Callov.	C.elatmae	Cylindro.	-0.26		1.48		5.62	4.49	71.82	1.46
PC2.1	Volg	D.max	Lagonib.	-0.64	0.15	-0.53	0.03	6.76	4.76	45.17	1.54
	Volg	D.max	Lagonib.	-0.79		-0.50		5.17	5.69	183.27	1.42
PC2.9	Volg	D.max	Lagonib.	-0.92	0.08	-0.75	1.02	4.55	4.32	28.60	1.45
	Volg	D.max	Lagonib.	-0.84		0.27		4.42	4.70	30.19	1.40
PC2.11	Volg	D.max	Lagonib.	-0.56	0.08	0.36	0.70	5.16	6.86	6.84	1.79
	Volg	D.max	Pachy.	-0.48		-0.34		3.41	5.44	2.47	1.47
SK1; 4.50	E. Oxf.	Mar-Cor	Cylindro.	1.24	0.34	2.14	0.89	7.53	6.14	38.03	1.45
	E. Oxf.	Mar-Cor	Cylindro.	0.90		3.03		8.41	6.44	50.12	1.28
SK1; 5.90	E. Oxf.	Mar-Cor	Cylindro.	1.43	0.17	2.13	0.02	6.54	5.17	29.56	1.30
	E. Oxf.	Mar-Cor	Cylindro.	1.26		2.11		8.00	6.97	31.11	1.59
SK2; 1.05	M. Oxf.	Den-Ten	Cylindro.	0.75	0.34	2.64	0.51	5.44	5.67	41.66	1.39
	M. Oxf.	Den-Ten	Cylindro.	1.09		3.15		4.88	5.78	42.58	1.38
SK2; 1.30	M. Oxf.	Den-Ten	Cylindro.	-0.61	0.88	4.02	1.77	4.75	4.91	32.15	1.36
	M. Oxf.	Den-Ten	Cylindro.	0.27		2.25		7.39	5.99	62.95	1.22
SK3; 6.40	E-M. Oxf.	Cor-Den	Cylindro.	0.66	0.64	2.87	1.13	5.09	4.81	57.01	1.24
	E-M. Oxf.	Cor-Den	Pachy.	1.30		1.74		4.54	5.01	47.06	1.35
SK4; 0.20	E-L. Call.	Koe-Lam	Cylindro.	0.27	1.01	2.74	0.82	5.35	5.84	43.50	1.55
	E-L. Call.	Koe-Lam	Pachy.	-0.74		1.92		7.83	6.17	55.07	1.49
SK4; 1.80	E-L. Call.	Koe-Lam	Cylindro.	-0.31	0.27	2.71	0.16	5.73	4.58	41.24	1.31
	E-L. Call.	Koe-Lam	Cylindro.	-0.03		2.87		4.63	5.64	30.66	1.52
SK4; 6.80	E-L. Call.	Koe-Lam	Cylindro.	0.27	0.24	2.57	0.23	6.73	4.42	33.84	1.30
	E-L. Call.	Koe-Lam	Belemn.	0.03		2.79		6.45	5.89	59.40	1.21
SK5; 4.15	E. Kimm.	Bay-Cym	Cylindro.	-0.58	0.23	2.17	0.11	3.70	4.09	32.92	1.45
	E. Kimm.	Bay-Cym	Pachy.	-0.35		2.28		3.74	4.95	36.37	1.54
SK5; 5.70	E. Kimm.	Bay-Cym	Cylindro.	-1.70	1.79	3.57	0.26	4.44	4.49	31.54	1.72
	E. Kimm.	Bay-Cym	Pachy.	0.09		3.31		3.26	4.44	39.77	1.50
SK5; 7.40	E. Kimm.	Bay-Cym	Pachy.	0.62	2.01	0.80	1.96	6.47	6.93	113.24	1.49
	E. Kimm.	Bay-Cym	Cylindro.	-1.39		2.76		4.42	4.23	40.60	1.45
SK5; 8.10	E. Kimm.	Bay-Cym	Pachy.	-0.49	0.66	2.11	0.87	5.65	7.09	70.25	1.66
	E. Kimm.	Bay-Cym	Cylindro.	-1.15		2.98		3.78	3.94	35.56	1.47
SK6; 1.50	E. Kimm.	Cym	Cylindro.	-0.97	0.15	2.49	0.26	4.65	4.53	40.14	1.42
	E. Kimm.	Cym	Cylindro.	-1.12		2.24		8.00	5.45	51.56	1.52
SK6; 7.50	E. Kimm.	Cym	Cylindro.	-0.25	1.21	1.24	0.59	7.93	6.47	55.73	1.59
	E. Kimm.	Cym	Cylindro.	-1.46		1.83		4.50	5.27	42.17	1.69
SK7; 5.70	Oxf.-Kim.	Reg-Bay	Pachy.	0.41	0.17	1.30	0.18	4.13	4.87	45.47	1.55
	Oxf.-Kim.	Reg-Bay	Cylindro.	0.24		1.49		5.78	5.41	47.84	1.53

Table 10.1 Table showing genus-level differences in stable isotope and geochemical measurements from coeval belemnites. Coeval belemnites of different genera are highlighted. Key to notation: KH (Boyarka River); PC (Izhma River); SK (Staffin Bay).

Sample No.	Age	Am. Zone	Genus	$\delta^{18}\text{O}$	$\delta^{18}\text{O}$ Offset	$\delta^{13}\text{C}$	$\delta^{13}\text{C}$ Offset	Mg/Ca	Na/Ca	Li/Ca	Sr/Ca
EA1; 0.05	L. Kimm.	Mutabilis	Cylindro.	-0.63	0.69	1.10	0.53	9.66	8.09	54.06	1.83
EA1; 0.05 B	L. Kimm.	Mutabilis	juv.	-1.32		1.63		7.46	6.55	32.52	1.98
KH17b; 1.55	L. Ryaz.	B. meses.	Cylindro.	-0.47	0.50	0.58	0.52	5.40	6.06	37.97	1.56
KH17b; 1.55 B	L. Ryaz.	B. meses.	juv.	-0.97		0.06		5.02	4.81	32.90	1.54
PC2.11	Volg. (?)	D. max (?)	Lagonib.	-0.56	0.02	0.36	0.84	5.16	6.86	6.84	1.79
	Volg. (?)	D. max (?)	juv.	-0.58		-0.48		5.25	7.76	-1.92	1.84
PC2.13	Volg. (?)	D. max (?)	Lagonib.	-0.18	0.42	0.83	1.51	4.03	8.35	0.00	2.03
	Volg. (?)	D. max (?)	juv.	-0.60		-0.68		5.68	5.17	0.00	1.46
SK3; 3.00	E-M. Oxf.	Cor-Den	juv.	0.72	0.17	3.97	2.24	3.50	5.10	46.97	1.32
	E-M. Oxf.	Cor-Den	juv.	0.89		1.73		14.22	11.00	100.12	1.80
SK3; 5.20	E-M. Oxf.	Cor-Den	juv.	0.69	0.36	0.01	3.64	6.62	5.49	54.49	1.39
	E-M. Oxf.	Cor-Den	juv.	0.33		3.65		4.59	5.29	46.85	1.37
SK4; 1.80	E-L. Call.	Koe-Lam	Cylindro.	-0.03	0.09	2.87	0.85	4.63	5.64	30.66	1.52
	E-L. Call.	Koe-Lam	juv.	0.05		2.02		4.79	4.28	30.73	1.38
SK5; 6.25	E. Kimm.	Bay-Cym	Cylindro.	-1.48	1.29	2.32	0.26	4.74	4.70	46.30	1.51
	E. Kimm.	Bay-Cym	juv.	-0.19		2.05		4.35	4.48	49.77	1.41
SK5; 7.20	E. Kimm.	Bay-Cym	juv.	-1.11	0.12	2.94	0.11	3.61	4.41	41.65	1.47
	E. Kimm.	Bay-Cym	Cylindro.	-1.23		3.06		5.57	4.49	37.28	1.47
SK6; 0.00	E. Kimm.	Cym	juv.	0.09	1.62	1.29	0.40	7.92	6.26	72.04	1.52
	E. Kimm.	Cym	Cylindro.	-1.53		1.69		6.19	4.65	45.09	1.46
SK6; 5.90	E. Kimm.	Cym	juv.	-1.74	0.85	0.84	0.15	7.42	5.89	55.60	1.43
	E. Kimm.	Cym	Cylindro.	-0.89		0.69		6.85	5.89	47.13	1.67
SK6; 7.20	E. Kimm.	Cym	Cylindro.	-0.67	0.09	1.31	0.71	4.70	5.17	46.05	1.54
	E. Kimm.	Cym	juv.	-0.76		2.01		4.84	5.00	38.50	1.51
SK6; 7.80	E. Kimm.	Cym	juv.	-1.85	0.97	2.39	1.20	4.84	4.90	40.10	1.62
	E. Kimm.	Cym	juv.	-0.88		1.19		10.28	7.02	65.23	1.56
SK7; 1.20	Oxf.-Kim.	Reg-Bay	juv.	0.38	1.36	1.87	0.22	4.37	4.84	36.03	1.50
	Oxf.-Kim.	Reg-Bay	juv.	-0.98		1.65		4.97	5.28	54.39	1.40
SK7; 14.80	Oxf.-Kim.	Reg-Bay	juv.	0.05	0.20	1.56	1.25	5.67	5.14	46.12	1.43
	Oxf.-Kim.	Reg-Bay	juv.	0.25		0.31		6.05	5.27	28.28	1.39
SK7; 15.40	Oxf.-Kim.	Reg-Bay	juv.	0.13	0.19	1.90	0.45	5.40	5.54	33.02	1.45
	Oxf.-Kim.	Reg-Bay	Cylindro.	0.32		1.44		6.05	6.02	36.50	1.50
SK7; 17.80	Oxf.-Kim.	Reg-Bay	juv.	-0.79	1.34	1.02	0.33	5.67	4.83	34.07	1.52
	Oxf.-Kim.	Reg-Bay	juv.	0.55		1.34		4.17	4.15	23.41	1.39
SK7; 20.90	Oxf.-Kim.	Reg-Bay	juv.	-0.43	0.08	1.35	0.46	4.76	4.54	25.37	1.53
	Oxf.-Kim.	Reg-Bay	juv.	-0.35		1.81		4.36	4.67	20.48	1.62
SK8; 27.20	E. Oxf.	Cor	Cylindro.	0.60	0.57	2.76	0.57	3.49	5.41	32.14	1.32
	E. Oxf.	Cor	juv.	0.03		3.33		4.48	4.85	24.70	1.26
SK8; 27.40	E. Oxf.	Cor	juv.	0.50	0.12	2.30	0.68	4.78	4.80	21.96	1.38
	E. Oxf.	Cor	juv.	0.62		2.98		3.91	4.79	12.74	1.35
SK8; 35.80	E. Oxf.	Cor	juv.	-0.17	0.09	3.63	0.33	5.13	4.82	20.12	1.31
	E. Oxf.	Cor	juv.	-0.26		3.30		4.19	4.92	21.58	1.38
SK10; 0.40	L. Oxf.	Ser-Reg	juv.	0.68	0.46	0.73	0.29	5.33	4.39	24.07	1.41
	L. Oxf.	Ser-Reg	juv.	0.22		0.44		5.03	4.73	23.19	1.47
SK10; 14.30	L. Oxf.	Ser-Reg	juv.	0.09	0.04	1.72	0.51	5.67	5.37	28.78	1.42
	L. Oxf.	Ser-Reg	juv.	0.13		1.20		10.82	7.12	39.64	1.39

Table 10.2 Table showing ontogenetic differences in stable isotope and geochemical measurements from coeval belemnites. Coeval belemnites of different ontogenetic stages are highlighted (i.e., adult and juvenile). Key to notation: KH (Boyarka River); PC (Izhma River); SK (Staffin Bay).

values. Ultimately, the data presented here cannot be used to either confirm or refute the existence of genus-specific differences in fractionation, because despite obvious offsets

between different genera occurring in the same horizon, similar levels of offset are also observed between co-occurring belemnites of the same genus.

Also analysed during this study was the effect of ontogeny on fractionation. This is because it is possible that juvenile specimens may record different geochemical values to adults. For example, belemnites may have lived in a different part of the water column whilst young (as seen in modern cephalopods) or there may have been a slight difference in fractionation at this age, possibly in response to rapid growth during the juvenile stage. Rexfort & Mutterlose (2006) recognise the rarity of juvenile rostra in the geological record, which they suggest may indicate extremely rapid early growth. The general absence of such material in the fossil record however may be explained solely by its relative fragility.

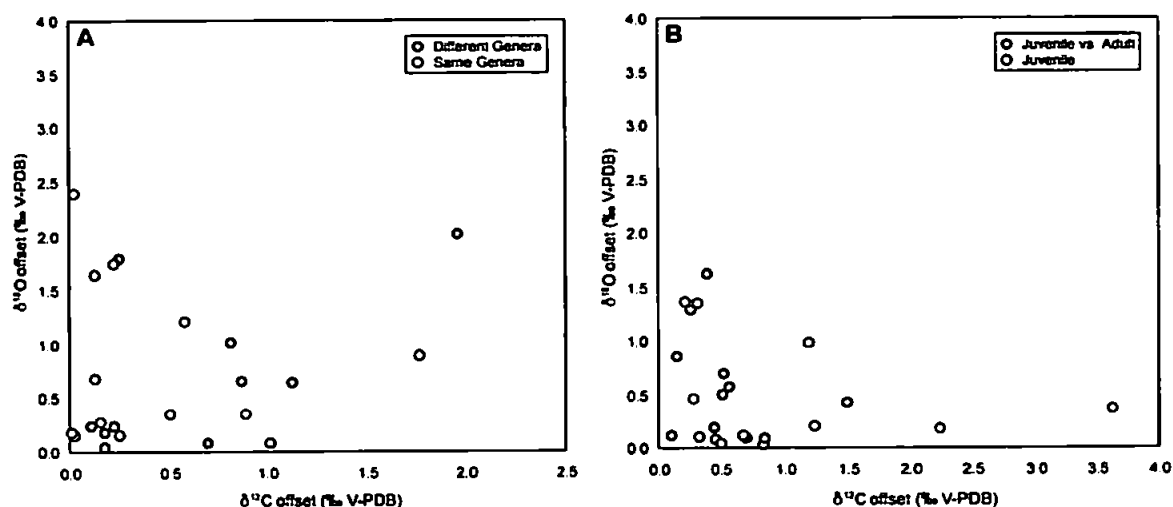


Figure 10.1 Cross plots of $\delta^{18}\text{O}$ and $\delta^{13}\text{C}$ offsets observed from coeval belemnites. (A) Genus-specific differences. (B) Ontogenetic differences.

Juvenile specimens were collected and analysed in this study (principally from Staffin Bay), with their stable isotope and geochemical composition recorded and subsequently compared with those of adult specimens (Table 10.2). The ontogenetic record displays great variability in the offset between isotope values, much like the generic record discussed above. High levels of offset were observed where juveniles were coeval with adult specimens as well as where different juvenile individuals were analysed from the same horizon (Fig. 10.1). Again, these data are inconclusive and cannot be used to

either confirm or refute the potential influence of ontogeny on the stable isotope and elemental records.

It seems likely that as the belemnite rostra studied here display significant variability even where taxonomic and ontogenetic effects can be ruled out, something else must be influencing that variability (either in conjunction with, or in isolation from, these factors). Recent analysis of extant specimens of *Sepia officinalis* (the common cuttlefish, which is commonly believed to be one of the closest living relatives of the belemnite) records significant variation in isotopic composition across the cuttlebone that has been attributed to changes in seasonal temperatures and migration (Rexfort & Mutterlose, 2006). It seems reasonable to assume that belemnites could also exhibit similar changes in isotopic composition across the rostrum. A preliminary investigation of this was conducted by Podlaha *et al.* (1998) where the internal variability of individual rostra was shown to be as much as 2 ‰ for both $\delta^{18}\text{O}$ and $\delta^{13}\text{C}$, suggesting that the variability observed in the belemnite record could be associated with this internal variability. It may, therefore, not be wise to drill small holes into the belemnite rostrum in order to collect a sample for isotopic analysis when a homogenised signal is preferred and instead to homogenise a larger segment of calcite (this approach was adopted here).

The scatter observed in the belemnite data presented here is generally consistent with that of published belemnite records from other successions (e.g., van de Schootbrugge *et al.*, 2000; Bailey *et al.*, 2003; McArthur *et al.*, 2004; Price & Mutterlose, 2004; Wierzbowski, 2004). Only the Boyarka River data displayed a greater amount of scatter than would have been expected. This is likely to be the result of the shallow nature of the Boyarka River succession, which presents a relatively dynamic depositional environment. By comparison, the Izhma River succession records significantly less variability over the same time period, probably as a consequence of the less variable nature of the deeper water succession.

Bulk rock records tend to produce much smoother curves than belemnites, which is the result of time averaging and the homogenisation of constituent particles. These processes dampen natural variability to produce less noisy curves than those generated from belemnites. For example, a 1 mm bulk sediment sample could represent anything in the range of 100-1000 years or more and could contain a number of different microscopic organisms, which may have inhabited a range of levels in the water column, whilst a 1 mm sample of belemnite calcite represents the environment of one individual and probably only for a period of months.

The scatter observed in belemnite data is, therefore, likely to be the result of real and natural variability. It is important to stress that in terms of palaeoenvironmental interpretation this natural variability is not a significant problem so long as long-term trends rather than small-scale fluctuations are interpreted.

10.1.3. Oxygen Isotopes

Oxygen isotope values in biogenic calcite reflect temperature as well as global (ice volume) and local (precipitation, runoff and evaporation) variations in $\delta^{18}\text{O}_{\text{seawater}}$. Only organisms which precipitate their calcite in equilibrium with their surroundings and remain unaltered after deposition will retain a pristine isotopic signal that reflects these factors. Belemnite rostra are believed to satisfy these criteria. It is commonly accepted that belemnites exhibited equilibrium fractionation for the oxygen isotope, although for the carbon isotope a slight offset from equilibrium precipitation may have been the norm. This is based on observations from modern cephalopods, which are known to secrete their shells very close to equilibrium with seawater (Taylor & Ward, 1983; Morrison & Brand, 1986; Rexfort & Mutterlose, 2006). In addition, belemnite rostra are composed of low-magnesium calcite, which is relatively resistant to post-depositional alteration. Belemnites therefore, frequently preserve a pristine isotopic signal that can be used to provide information about palaeoenvironments and palaeoenvironmental change.

Belemnites are relatively abundant in the fossil record, and can therefore be used to compare palaeotemperature estimates on considerable spatial and temporal scales. As mentioned previously, calculations of absolute palaeotemperature are highly problematic for an extinct group of organisms. This abundance of belemnites therefore provides the opportunity to compare relative values of temperature from successions worldwide, providing that the same temperature equation is utilised. Fortunately, the palaeotemperature equation of Anderson & Arthur (1983) for molluscan calcite is almost always used in belemnite studies together with an isotopic composition of -1 ‰ SMOW for an ice-free world (e.g., Price & Sellwood, 1994, 1997; Ditchfield, 1997; Price *et al.*, 2000; Price & Gröcke, 2002; Gröcke *et al.*, 2003; McArthur *et al.*, 2004; Price & Mutterlose, 2004). This equation and a $\delta^{18}\text{O}_{\text{seawater}}$ value of -1 ‰ SMOW were used throughout this study (despite evidence to suggest that a $\delta^{18}\text{O}_{\text{seawater}}$ value of -1.5 ‰ SMOW may be more appropriate for very high latitude locations – as discussed later). The belemnite derived palaeotemperatures can therefore be compared with each other (if not in terms of absolute values, then at least in terms of relative change) as well as with data generated from published studies.

The importance of being able to compare belemnites on a global scale is highlighted by the work of several authors that shows that different organisms can give different palaeotemperature results from the same locations, e.g., belemnites and ammonites (Tan *et al.*, 1970; Anderson *et al.*, 1994; Wierzbowski & Joachimski, 2006), belemnites and brachiopods (Voigt *et al.*, 2003) and belemnites and planktonic foraminifera (Huber *et al.*, 1995; Price *et al.*, 1996; Huber & Hodell, 1996). Tan *et al.* (1970), Anderson *et al.* (1994) and Wierzbowski & Joachimski (2006) record a lower range of palaeotemperatures for belemnites than for ammonites of the same succession, which the authors interpret as belemnites inhabiting colder, deeper waters than the ammonites that inhabited the warmer surface waters. It should also be noted that Voigt *et al.* (2003) recorded colder palaeotemperatures (by ~6°C) from belemnites than from co-

occurring brachiopods, although they interpreted this as the result of belemnite migration from higher latitudes during a cool event. Ultimately, belemnites appear to record cooler palaeotemperatures than known shallow water taxa (Lowenstam & Epstein, 1954; Pirrie & Marshall, 1990; Ditchfield *et al.*, 1994). At high latitudes, like those investigated in this study, belemnites are considered to represent minimum estimates of sea-surface temperatures at high latitudes as vertical ocean temperature gradients in relatively shallow, high latitude regions will be minimal (Barrera *et al.*, 1987; Price *et al.*, 1996). The results presented here are consistent with this theory, for example the calculated palaeotemperature range from the Boyarka River succession (of 2 to 19°C) is compatible with the modern temperature estimate for bottom waters in the region (of -1 to 12°C) as calculated by Polyak *et al.* (2003) from benthic foraminifera.

As mentioned previously a $\delta^{18}\text{O}_{\text{seawater}}$ value of -1 ‰ SMOW is commonly used for palaeotemperature calculations for the Jurassic and Cretaceous periods. As discussed in the previous chapters however, a spatially invariant estimate of $\delta^{18}\text{O}_{\text{seawater}}$ may not be appropriate. The uncertainty encountered with regards to the isotopic composition of Jurassic/Cretaceous seawater is one of the major problems associated with the calculation of absolute palaeotemperatures for this time. Roche *et al.* (2006) suggested that palaeolatitudinal differences in $\delta^{18}\text{O}_{\text{seawater}}$ composition would have significant implications for palaeotemperature calculations, namely that, for the late Mesozoic, existing low-latitude calculations have underestimated palaeotemperatures, whilst high latitude calculations have overestimated palaeotemperatures. Such a situation has further implications in terms of reconstructing latitudinal temperature gradients and ocean circulation patterns. Despite these new data, the traditional view of $\delta^{18}\text{O}_{\text{seawater}}$ composition (using a value of -1 ‰ SMOW for the Jurassic and Cretaceous) has been adopted here. This provides the potential for a more direct comparison of the data generated from this study with that from previously published studies, although, the affect

of using the Roche *et al.* (2006) $\delta^{18}\text{O}_{\text{seawater}}$ compositions is discussed later (see section 10.2.2).

10.1.4. Elemental/Ca Ratios

In many modern calcifying groups, the Mg/Ca, Sr/Ca, Na/Ca and Li/Ca ratios reflect calcification temperature, although each to a varying degree. As mentioned previously, $\delta^{18}\text{O}$ reflects temperature, salinity and ice-volume. Comparison of the two proxies should, therefore, provide an indication of the influence that such factors have had on the $\delta^{18}\text{O}$ ratio. Where strong correlations between $\delta^{18}\text{O}$ and *El/Ca* exist, temperature should be the dominant controlling factor. Conversely, where correlations are not observed, changes in salinity or ice-volume, interspecies or ontogenetic offset, metabolic activity or diagenesis may have had an influence.

Statistically significant correlations between $\delta^{18}\text{O}$ and *El/Ca* from this study were observed in the following cases: between $\delta^{18}\text{O}$ and Mg/Ca (Izhma River), $\delta^{18}\text{O}$ and Sr/Ca (Staffin Bay), $\delta^{18}\text{O}$ and Na/Ca (Svalbard) and $\delta^{18}\text{O}$ and Li/Ca (Boyarka River; Svalbard). An absence of correlation between $\delta^{18}\text{O}$ and *El/Ca* is therefore the norm for this study. This can be interpreted in one of two ways, either as the result of environmental factors (salinity and ice-volume) influencing the $\delta^{18}\text{O}$ record and therefore degrading the correlation, or as the result of physiological factors (metabolic activity and growth rate) influencing the *El/Ca* ratios. A significant impact from interspecies or ontogenetic offset or from diagenesis is unlikely as discussed previously (see sections 10.1.1 and 10.1.2), although these factors may account for some degree of scatter within the data.

If the absence of correlation is interpreted as being solely the result of environmental factors, significant salinity and ice-volume fluctuations are required throughout the northern high latitudes during the Late Jurassic and Early Cretaceous. Alternatively, if the absence of correlation is attributed primarily to physiological factors then the use of *El/Ca* ratios as belemnite palaeotemperature proxies becomes highly

questionable. Unfortunately, it is impossible to confirm which of these two mechanisms is controlling the general lack of correlation. It may be that environmental factors dominate certain relationships, whilst physiological factors dominate others. Previously published studies on *El/Ca* ratios have tended to suggest that for Li/Ca, Na/Ca and, in some circumstances, Sr/Ca physiological factors have controlled fractionation (e.g., Delaney *et al.*, 1985; Klein *et al.*, 1996; McArthur *et al.*, 2000; Bailey *et al.*, 2003), whilst for Mg/Ca fractionation is controlled by temperature (e.g., McArthur *et al.*, 2000; Bailey *et al.*, 2003; Rosales *et al.*, 2004a, b). A physiological effect on Li/Ca, Na/Ca and Sr/Ca would certainly be consistent with the data presented here, since in most cases no correlation is observed with $\delta^{18}\text{O}$. This is equally true for the Mg/Ca ratios, however, and if, as is supposed by most authors, Mg/Ca is controlled by temperature rather than physiological effects, the lack of correlation observed here would be the result of environmental influences (temperature and variation in $\delta^{18}\text{O}_{\text{seawater}}$) on the $\delta^{18}\text{O}$ record. In this case, the absence of correlation between the other *El/Ca* ratios would also be consistent with environmental influences on the $\delta^{18}\text{O}$ records rather than physiological influences on the *El/Ca* records. Ultimately, the *El/Ca* data generated from this study are inconclusive with regards to the nature of the factors influencing the *El/Ca* and $\delta^{18}\text{O}$ correlations. This has particular implications for estimates of the effects of salinity and ice volume on $\delta^{18}\text{O}$ records, which is the most common use an *El/Ca* ratio in belemnites. Such estimates must be made with care and trends rather than absolute values must be interpreted.

As discussed in the previous chapters the use of Mg/Ca palaeotemperature calculations for belemnites may not be appropriate. The Klein *et al.* (1996) equation was calibrated using the extant marine mussel *Mytilus trossulus* and was therefore considered here to be the most suitable equation for use on belemnites, since other palaeotemperature equations (e.g., those of Dwyer *et al.* (1995), Elderfield & Ganssen (2000) and Lear *et al.* (2002)) were calibrated using foraminifera and ostracods. It is acknowledged however, that McArthur *et al.* (2000) and Bailey *et al.* (2003) both used Mg/Ca palaeotemperature

equations derived from the above foraminifera and ostracod calibrations, even though, the justification for doing this is unclear. In fact, in neither study do the authors satisfactorily explain why such systematically distant taxa to the coleoid order Belemnitida are utilised, when a much closer related, taxon calibration (derived from the bivalve *Mytilus*) is available.

If the Lear *et al.* (2002) palaeotemperature equation (based on foraminifera) is applied to the Mg/Ca data presented in this study, for example for the Izhma River succession, then a calculated palaeotemperature range of 4.9 to 19.2°C and an average value of 12.2°C is generated. This can be compared to the Anderson & Arthur (1983) $\delta^{18}\text{O}$ derived palaeotemperature range of 7.3 to 17.3°C (average 13.0°C) and the Klein *et al.* (1996) range of -4.5 to 6.7°C (average -0.9°C) for the same succession. Based on this data, it is clear that the Lear *et al.* (2002) calibration presents Mg/Ca derived palaeotemperatures closest to those of the $\delta^{18}\text{O}$ calibration. It seems likely, that this is the reason that McArthur *et al.* (2000) and Bailey *et al.* (2003) selected this calibration rather than that of Klein *et al.* (1996) for their research since no other justification is given. Whether or not this is sufficient reason to select a calibration, especially given the taxonomic arguments against such a selection, is clearly debateable. In this study, the decision was taken that the use of foraminiferal or ostracod calibrations was not appropriate given the lack of taxonomic or ecological comparability with belemnites. In order to consider these calibrations as appropriate, a much more convincing argument than seemingly suitable palaeotemperatures must be presented.

The Mg/Ca calculated palaeotemperatures generated here using the Klein *et al.* (1996) equation, commonly record sub-freezing values that could not have been recorded by belemnites (as they almost certainly would not have survived in such conditions). In addition, the $\delta^{18}\text{O}$ composition of belemnite calcite is not expected to yield absolute values of palaeotemperature for two key reasons, firstly the $\delta^{18}\text{O}_{\text{seawater}}$ composition (on which the $\delta^{18}\text{O}_{\text{carbonate}}$ composition is dependent) can only be estimated and secondly, the $\delta^{18}\text{O}$

fractionation capacity of belemnites cannot be measured since the group is extinct. Despite belemnite Mg/Ca ratios being possibly independent of seawater composition, there is still an element of uncertainty with regards to the fractionation of Mg/Ca. Mg/Ca calculated palaeotemperatures must, therefore, not be considered as absolute values but as being descriptive of a trend, particularly where relatively low values are concerned. Immenhauser *et al.* (2005) questioned the validity of applying the Klein *et al.* (1996) temperature equation to fossilised skeletal calcites. They suggested that it may only be appropriate for temperatures in the range of 5-23°C where the temperature-Mg relationship is linear. In addition, they go on to suggest that the utility of Mg/Ca ratios may be limited by the ion regulating capability of the animals being considered.

If, as is commonly accepted, Mg/Ca ratios in biogenic calcite did reflect calcification temperature alone, (e.g., whilst $\delta^{18}\text{O}$ reflects temperature plus a salinity and/or ice volume effect), then where both proxies are measured it should be possible to calculate relative changes in $\delta^{18}\text{O}_{\text{seawater}}$. This has very recently been attempted using Early Cretaceous (Berriasian-Hauterivian) belemnites from France and Spain (McArthur *et al.*, in press). Such a calculation however, requires equilibrium fractionation of Mg/Ca, which for belemnites at least is highly questionable (see above). Nevertheless, if we assume here that equilibrium fractionation has occurred, it is possible to consider the effects of fluctuations in $\delta^{18}\text{O}_{\text{seawater}}$ on the $\delta^{18}\text{O}_{\text{carb}}$ composition. Figure 10.2 shows calculated $\delta^{18}\text{O}_{\text{seawater}}$ values for the Callovian-Hauterivian Izhma River succession. The average $\delta^{18}\text{O}_{\text{seawater}}$ value of -4.9 ‰ is indicated so that relative fluctuations about that mean can be considered, rather than considering absolute values of $\delta^{18}\text{O}_{\text{seawater}}$, which are probably unrealistic given the sub-freezing palaeotemperatures generated from the Mg/Ca ratios.

At the base of the Izhma River succession where palaeotemperature estimates are relatively high, the $\delta^{18}\text{O}_{\text{seawater}}$ values are relatively positive. Conversely, where a shift towards cooler temperatures is observed (in the Mg/Ca record) relative $\delta^{18}\text{O}_{\text{seawater}}$ values switch to being relatively negative. The presence of more negative $\delta^{18}\text{O}_{\text{seawater}}$ values

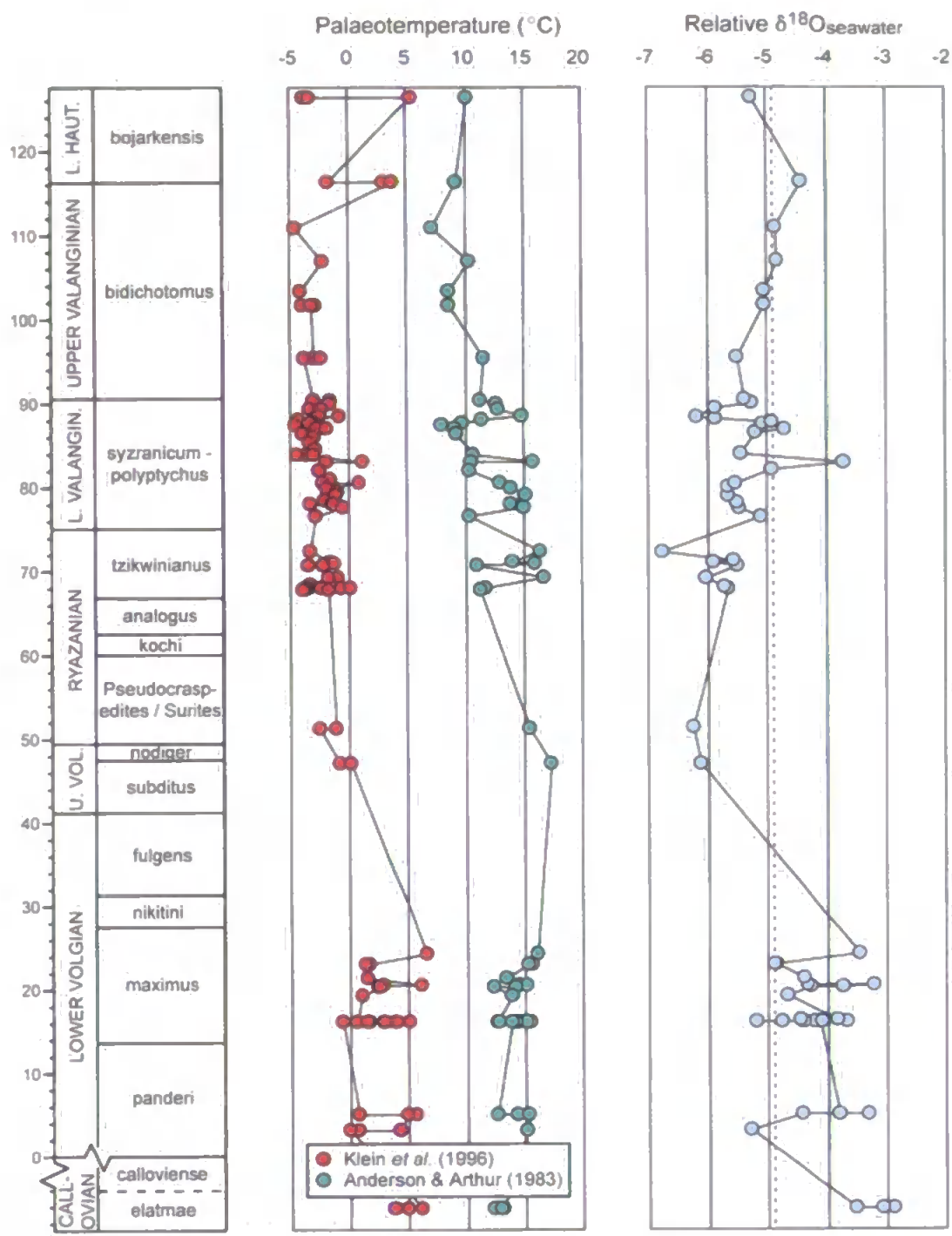


Figure 10.2 Calculated palaeotemperatures and relative $\delta^{18}\text{O}_{\text{seawater}}$ values for the Callovian-Hauterivian Izhma River succession, Russia. Boreal (Russian) ammonite zones are illustrated. Scale is in metres.

would be consistent with either a period of freshening or of ice melt, both of which would introduce isotopically depleted water into the system. The problem with this is that an average 2 ‰ fall in $\delta^{18}\text{O}_{\text{seawater}}$ composition would require a 4 ‰ freshening (according to the modified Railsback *et al.* (1989) and Woo *et al.* (1992) temperature-salinity model), which may be difficult to account for from freshwater input alone. The waning of ice-

sheets however, if of significant magnitude, may help to account for the $\delta^{18}\text{O}_{\text{seawater}}$ change. The issue here is that the shift towards more negative $\delta^{18}\text{O}_{\text{seawater}}$ values coincides with very cold palaeotemperatures if the Mg/Ca estimates are accepted. Even if the absolute palaeotemperature values are ignored and just the trend considered, the shift still coincides with a drop in temperature. Cold temperature values could be consistent with ice-melt if the melt was occurring locally but if it was occurring on a global scale such cold values are impossible. In addition, given the correlation between falling temperature and falling $\delta^{18}\text{O}_{\text{seawater}}$ values it seems inconceivable that the relative shift in $\delta^{18}\text{O}_{\text{seawater}}$ could be attributed to ice melt. In light of the problems associated with this model, it seems most unlikely that Mg/Ca ratios are faithfully recording temperature trends in belemnites.

Despite the quantity of elemental data presented in this study, which was generated from a number of locations as well as from a range of time periods, the usefulness of *El/Ca* data as a palaeoclimate proxy remains in doubt. In addition, no definite conclusions can be drawn with regards to the relative effects of environmental and physiological factors on the elemental ratios, nor can the observed Mg/Ca trends be convincingly related to palaeotemperature. Whilst this data does not rule out the use of *El/Ca* ratios as palaeotemperature proxies in certain circumstances, it does suggest that any interpretation of such data conducted in the future must be done with great care, at least until further research is conducted.

10.1.5. Carbon Isotopes

As discussed above, modern cephalopods are known to secrete their shells very close to isotopic equilibrium with seawater, although for the carbon isotope, a slight offset from equilibrium fractionation is not uncommon, with shells being slightly less enriched in $\delta^{13}\text{C}$ than might be predicted (Wefer and Berger, 1991; Klein *et al.*, 1996; Bettencourt & Guerra, 1999; Geist *et al.*, 2005). Assuming that this offset is also present in belemnites and that the offset is consistent, it should not present a problem for the interpretation of

carbon isotope values or trends, since most carbon isotope values are presented relative to a belemnite standard (V-PDB).

Where belemnite derived $\delta^{13}\text{C}$ records have been compared with temporally similar $\delta^{13}\text{C}$ records generated from other marine carbonate material (e.g., bulk rock, foraminifera, other macrofossils etc.) similar trends have been observed (e.g., van de Schootbrugge, 2000; Gröcke *et al.*, 2005). This confirms that belemnites faithfully record a $\delta^{13}\text{C}$ signal. Unlike oxygen isotope records, which are strongly influenced by temperature and therefore often by local conditions, carbon isotope curves record more global signals. The global $\delta^{13}\text{C}_{\text{seawater}}$ composition primarily reflects the distribution of global carbon between oxidised (carbonate, bicarbonate, carbon dioxide) and reduced (organic carbon) reservoirs (Jenkyns *et al.*, 2002). Distinctive excursions within the $\delta^{13}\text{C}$ record can therefore be correlated to provide a high resolution carbon isotope stratigraphy.

This approach of matching curves with a distinctive shape has been carried out on pelagic carbonates (e.g., Lini *et al.*, 1992; Padden *et al.*, 2002) other marine carbonates (e.g., belemnites - Podlaha *et al.*, 1998) and between marine carbonates and terrestrial organic matter (e.g., Gröcke *et al.*, 2005). The major problems with such correlations however, are that biostratigraphic control on the correlated successions is often weak and that small, isolated successions with different stratigraphic zonal schemes and/or sedimentological features (e.g., condensed sections and hiatuses) are common subjects for correlation. Such splicing together of small, isolated records only introduces more noise and inaccuracy into an already noisy system. The initiation of the Valanginian positive carbon isotope excursion, for example, was described by Channell *et al.* (1993) as occurring in the *Pachydicranus* Zone (now the uppermost Valanginian *Furcillata* Zone or the lowermost Hauterivian *Radiatas* Zone (McArthur *et al.*, in press)). By comparison, however, the initiation of the same excursion was assigned by Hennig *et al.* (1999) to the *Campylotoxus* Zone, the uppermost ammonite zone of the Lower Valanginian. In addition, Gröcke *et al.* (2005) record the initiation of the Valanginian positive carbon isotope

excursion from plant material in the Crimean *Submartini* Zone, which they correlate with the *Verrucosum* Zone of Europe. McArthur *et al.* (in press) however, note that Crimean excursion occurs over just 1.2 m of sediment and immediately above a sandstone unit where ammonites are unusually uncommon. They, therefore, suggest that condensation or a hiatus is present in the Gröcke *et al.* (2005) succession and that the strata recording the real onset of the excursion may not even be present making further carbon isotope correlation difficult.

The problem of correlation is particularly prevalent where marine carbonate and terrestrial organic carbon records are correlated. The comparison of marine with terrestrial carbon isotope curves is essential to confirm that isotopic patterns are of a global origin rather than the result of local or diagenetic factors. To date, such correlations have only been carried out from geographically different successions. This study is the first to investigate marine carbonate and terrestrial organic $\delta^{13}\text{C}$ records from the same succession and with samples collected simultaneously. This new approach eliminates any uncertainty associated with the correlation and allows conclusions about the relationship between the ocean and atmosphere systems to be drawn with confidence. The coeval marine and terrestrial $\delta^{13}\text{C}$ records investigated here were synchronous throughout the Ryazanian-Hauterivian Boyarka River succession and much of the Callovian-Kimmeridgian Staffin Bay succession. This demonstrates for the first time without any correlation related uncertainty that the ocean-atmosphere system was strongly linked at these times. The Staffin Bay record also provides information about a potential decoupling of the ocean-atmosphere system during the Callovian period. Presumably, either the marine or the terrestrial realm was being influenced by local factors at this time, although the nature of this influence needs further investigation.

10.2. Late Jurassic - Early Cretaceous Global Palaeoenvironment

10.2.1 Boreal Realm Data

The stable isotope and geochemical data presented in this study comprise the first high resolution investigation of the Late Jurassic-Early Cretaceous Boreal Realm (as defined by belemnites). A Callovian-Hauterivian compilation of the $\delta^{13}\text{C}$ and $\delta^{18}\text{O}$ data was generated in order to assess whether any long-term trends could be identified across the northern high latitude region (Fig. 10.3). In order to produce this compilation, the numerical age of each sample was estimated using the Gradstein *et al.* (2004) timescale.

The oxygen isotope compilation displays a considerable degree of natural variability, making the identification of long-term trends difficult but by no means impossible. The most negative $\delta^{18}\text{O}$ values (-2.8 ‰) occur in the Lower Kimmeridgian, whilst the most positive $\delta^{18}\text{O}$ values (2.8 ‰) occur in the Lower-Upper Ryazanian. In terms of global palaeotemperature, this equates to the highest palaeotemperatures (24°C) occurring in the Lower Kimmeridgian and the lowest palaeotemperatures in the Lower-Upper Ryazanian (2°C). Care must be taken with this approach however, because the warmest palaeotemperatures are recorded from the Helmsdale succession (at a palaeolatitude of ~45°N), whilst the coldest values are recorded from the Boyarka River succession (at a palaeolatitude of ~70°N), which may indicate that local environmental conditions have had some impact on the $\delta^{18}\text{O}$ record.

Despite this limitation, the $\delta^{18}\text{O}$ compilation provides significant evidence of predominantly warm conditions punctuated by cold episodes in the Late Jurassic and Early Cretaceous Arctic region. Oxygen isotope values exceeding 1 ‰ (which equates to ~ 8°C) are common in the Lower-Middle Oxfordian and in the Ryazanian-Lower Hauterivian intervals. For the Oxfordian, these values are almost certainly not an artefact of palaeolatitudinal differences because these positive values come from one of the lowest palaeolatitude sites (Staffin Bay). For the Ryazanian-Hauterivian interval, the observed

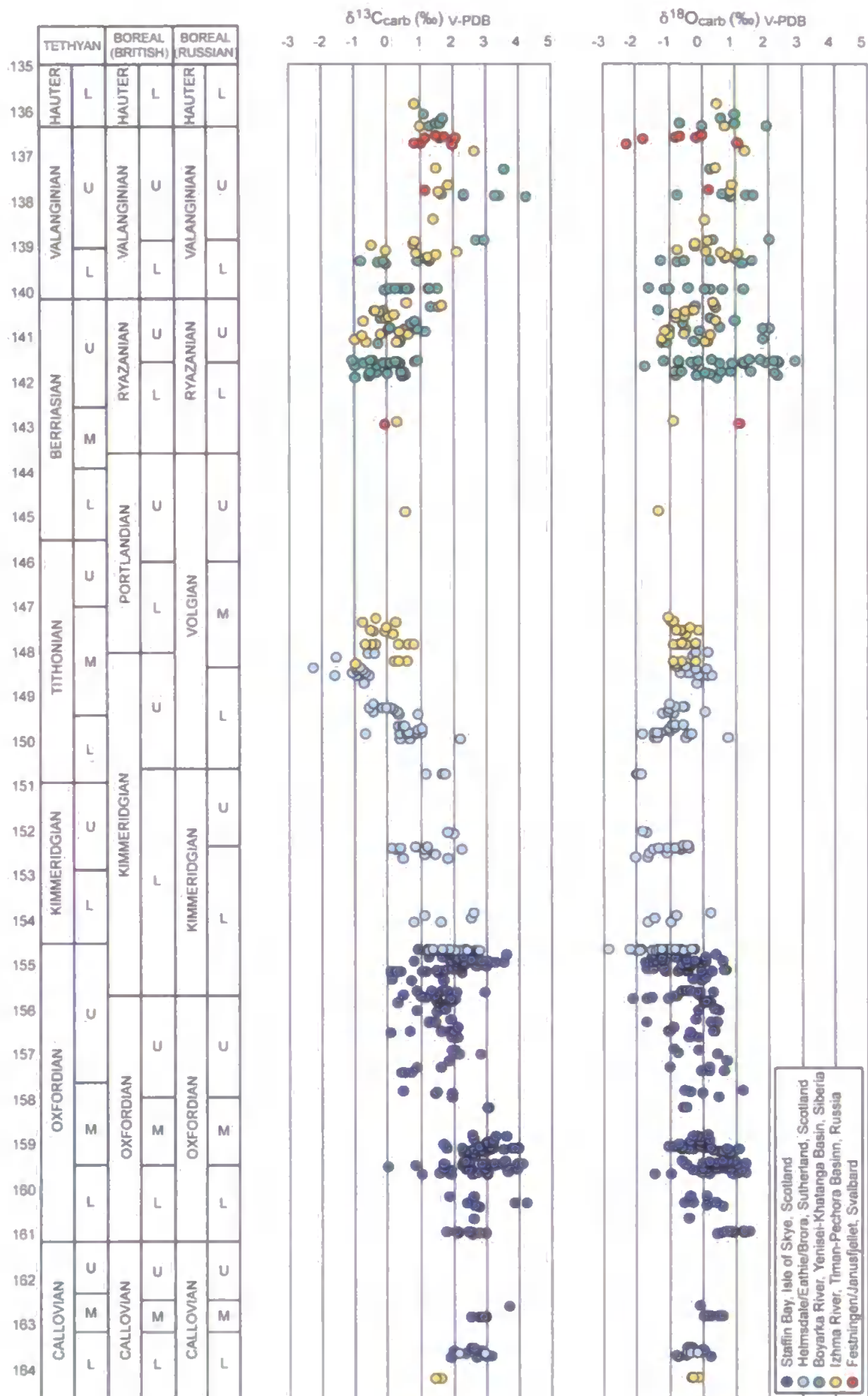


Figure 10.3 Callovian-Hauterivian compilation of $\delta^{13}\text{C}_{\text{carb}}$ and $\delta^{18}\text{O}_{\text{carb}}$ data derived from this study. Compilation was produced by estimating the numerical age of each sample. Scale is in Ma (after Gradstien *et al.* (2004)) and Tethyan, Boreal (British) and Boreal (Russian) timescales are illustrated.

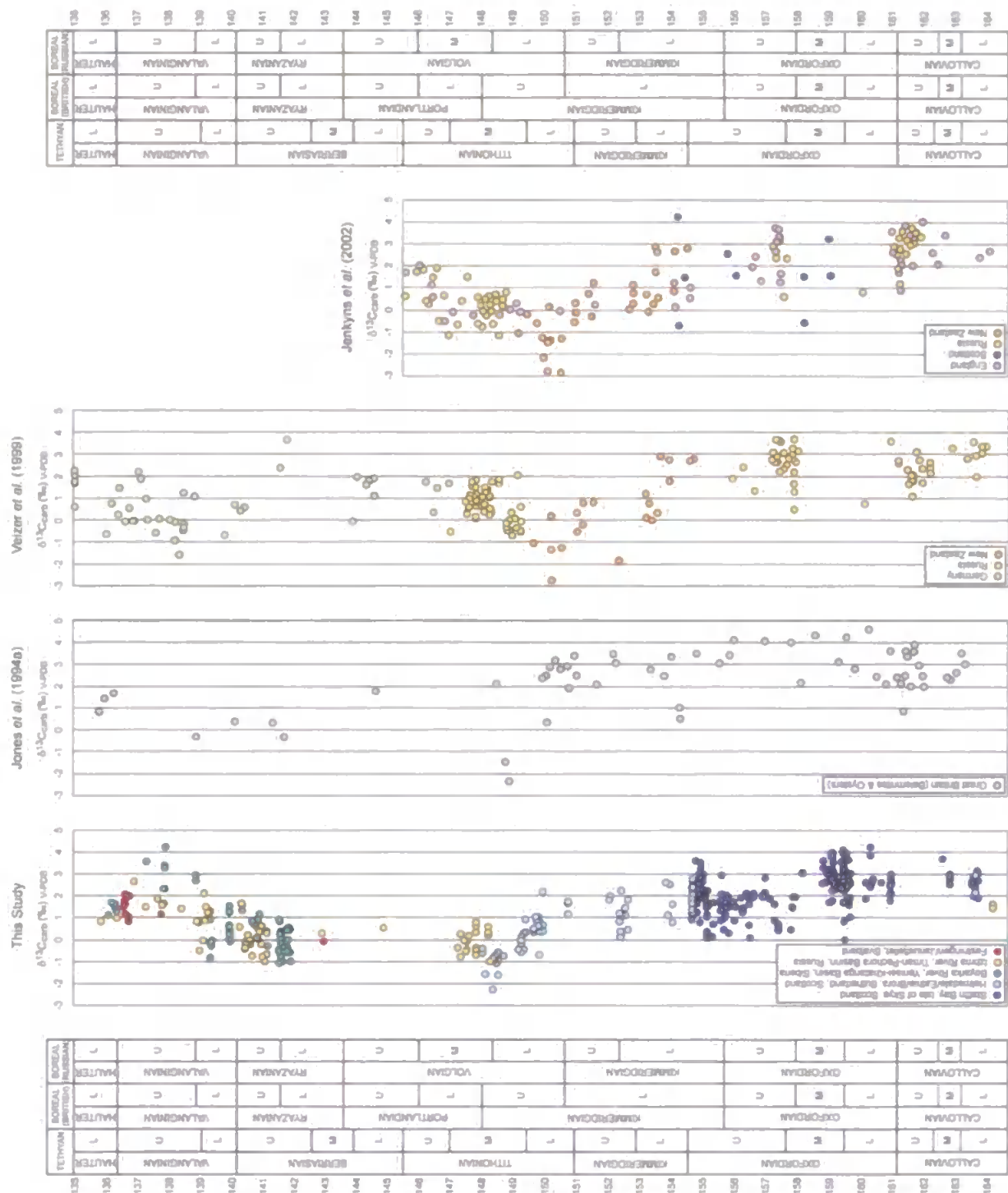
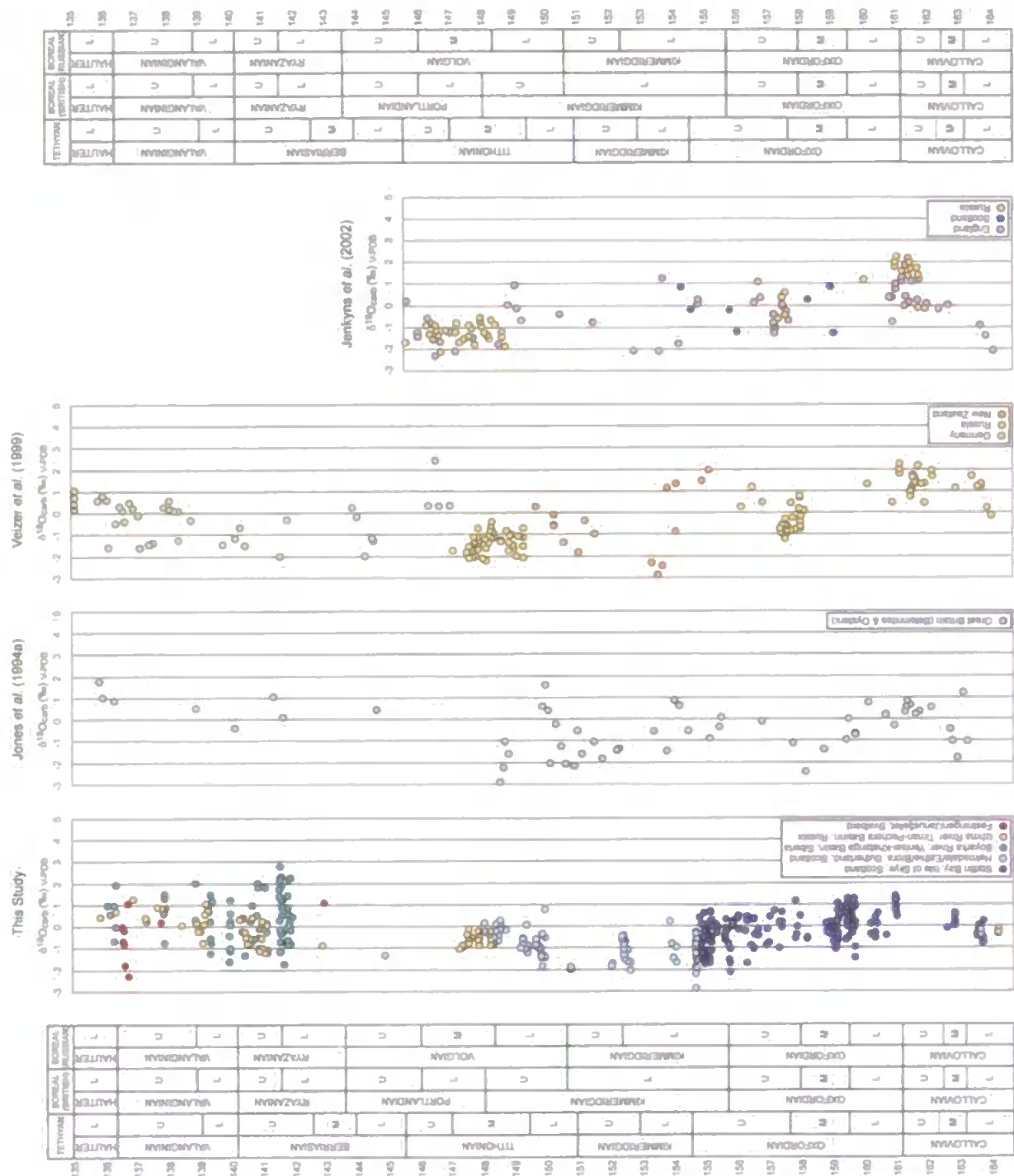


Figure 10.4a Callovian-Hauterivian compilation of $\delta^{13}\text{C}_{\text{carb}}$ data derived from this study and compared with published data. Isotope curves are correlated by age based on conversion to the Gradstein *et al.* (2004) timescale. Stable isotope data is derived from well-preserved belemnites unless otherwise stated. Scale is in Ma (after Gradstien *et al.* (2004)) and Tethyan, Boreal (British) and Boreal (Russian) timescales are illustrated:



$\delta^{18}\text{O}$ ratios are significantly higher than those observed from any of the other sites indicating that these values reflect genuinely lower palaeotemperatures (as low as 2°C). Despite the scatter present in the Boyarka River data for this interval a faint trend towards less negative $\delta^{18}\text{O}$ values from the Ryazanian and into the Hauterivian can be observed. This is consistent with the more distinct cooling trend observed in the Izhma River data for the same time interval. Interestingly, the occurrence of potential dropstones in Svalbard coincides with the latter part of this cooling trend (in the Upper Valanginian) and the coldest palaeotemperatures recorded from the Izhma River ($\sim 7^{\circ}\text{C}$) are also coincident with the occurrence of glendonites on Svalbard, lending strong support to the concept of a high latitude cooling episode at this time.

The presence of cold conditions as observed from the record presented here is consistent with published works that have also identified cold episodes during the Callovian-Oxfordian, which is coincident with a eustatic sea level fall (e.g., Dromart *et al.*, 2003a, b; Lecuyer *et al.*, 2003) and the Valanginian (e.g., Price, 1999; Puc  at *et al.*, 2003; Kessels *et al.*, 2006). A cold episode during the Tithonian/Volgian (e.g., Price, 1999; Schudack, 1999) has also been postulated, although evidence for this event is not observed here. This, however, may be due to the sparsity of data from this time interval.

Distinctive long-term trends can also be identified in the Callovian-Hauterivian carbon isotope compilation (Fig. 10.3). The Callovian-Volgian interval witnesses a gradual shift from relatively positive $\delta^{13}\text{C}$ values (exceeding 4 ‰ in the Oxfordian) to more negative values (-2.2 ‰). This is followed by a rapid excursion to more positive values (4.2 ‰) during the Valanginian and a return towards pre-excursion values in the Hauterivian. This pattern has also been identified in other Jurassic-Cretaceous global compilations (e.g., Jones *et al.*, 1994a; Podlaha *et al.*, 1998; Veizer *et al.*, 1999; Jenkyns *et al.*, 2002) (Fig. 10.4). In addition, elements of the overall pattern (e.g., the Oxfordian-Volgian/Tithonian fall in $\delta^{13}\text{C}$ values and the Valanginian positive $\delta^{13}\text{C}$ excursion) have also been observed in smaller scale studies and studies of isolated successions, both from

marine carbonate and terrestrial organic carbon records (e.g., Lini *et al.*, 1992; Weissert & Mohr, 1996; Weissert *et al.*, 1998; Bartolini *et al.*, 1999; Price *et al.*, 2000; van de Schootbrugge *et al.*, 2000; Cecca *et al.*, 2001; Padden *et al.*, 2002; Price & Gröcke, 2002; Gröcke *et al.*, 2003; Price & Mutterlose, 2004; Weissert & Erba, 2004; Gröcke *et al.*, 2005).

A comparison of the $\delta^{13}\text{C}$ and $\delta^{18}\text{O}$ data shows no consistent relationship between the two variables. The strongest relationship observed is that of the Valanginian Izhma River data, which reveal a positive correlation between $\delta^{13}\text{C}$ and $\delta^{18}\text{O}$ that can be explained by the 'Monterey Hypothesis,' where the significant burial of organic carbon rich sediments results in a fall in the concentration of atmospheric CO_2 and a subsequent drop in temperature.

The compilation of $\delta^{18}\text{O}$ Boreal Realm data presented here confirms that cold episodes occurred in the Arctic region during the Late Jurassic and Early Cretaceous, most strikingly during the mid-Ryazanian *Kochi-Analogus* zones and the Late Valanginian *Bidochotomus* Zone but also during the Lower Oxfordian *Cordatum* Zone. The $\delta^{13}\text{C}$ data confirm that the Arctic region faithfully records the same $\delta^{13}\text{C}$ signature as observed in the Tethyan regions. These findings are significant in terms of understanding the Late Jurassic-Early Cretaceous Arctic region as well as global palaeoenvironments.

10.2.2. Global Palaeoenvironmental Studies

Published palaeoenvironmental studies on the Late Jurassic and Early Cretaceous have tended to focus on the mid- to low latitudes or on the southern high latitudes, whilst studies focusing on the northern high latitudes are relatively fewer. The new data presented here address this knowledge gap and provide significant information with which to assess global palaeoclimate.

The data presented here are compared with those of similar published studies (i.e., those that concentrate on the stable isotope analysis of macroscopic (or large microscopic)

Age	Region (Estimated Palaeolatitude)	Organism	$\delta^{18}\text{O}$ values	Temperature ($^{\circ}\text{C}$)	Reference
Valanginian - Barremian	Speeton, Yorkshire, England (40°N)	Belemnites	-2.12 to +0.79	9-21	McArthur <i>et al.</i> (2004)
Valanginian - Hauterivian	Vocantian Basin, SE France (40°N)	Belemnites	-1.36 to +0.59	9-18 (12.7)	van de Schootbrugge <i>et al.</i> (2000)
Berriasian - (Hauterivian)	Western Tethyan Platform (35°N)	Fish Teeth/Bone	+19.2 to +22.0 (PO_4)	13-25 (19)	Pucéat <i>et al.</i> 2003
Ryazanian - Hauterivian	Boyarka River, Siberia (70°N)	Belemnites	-1.71 to +2.83	2-19 (10.6)	This study
Ryazanian - Upper Valanginian	Festningen/Janusfjellet, Svalbard (62°N)	Belemnites	-2.26 to +1.14	8-21 (13.0)	This study
Upper Ryazanian - Middle Hauterivian	Speeton, Yorkshire, England (40°N)	Belemnites	-0.88 to +1.11	8-15 (11.4)	Price <i>et al.</i> (2000)
Volgian - Hauterivian	Izhma River, Russia (60°N)	Belemnites	-1.32 to +1.27	7-17 (13.0)	This study
Volgian - Valanginian	Yatrla River, Siberia (62°N)	Belemnites	-2.26 to +1.34	7-21	Price & Mutterlose (2004)
Tithonian	Volga Basin, Russia (45°N)	Belemnites	-2.11 to -0.58	14-21 (17.3)	Gröcke <i>et al.</i> (2003)
Tithonian - Hauterivian	Germany (38°N)	Belemnites	-3.10 to +2.30	4-25	Velzer <i>et al.</i> (1999)
Tithonian?	Santa Cruz, Argentina (40°S)	Belemnites	-2.00 to -1.60	19-20 (19.8)	Bowen (1961)
Kimmeridgian - (Berriasian)	James Ross Island, Antarctica (84°S)	Belemnites	-1.02 to -0.26	13-16 (14.6)	Ditchfield <i>et al.</i> (1994)
Kimmeridgian - Tithonian	Mallorca, Spain (30°N)	Belemnites	-1.00 to +0.04	12-16 (13.8)	Price & Sellwood (1994)
Kimmeridgian	Cutch, India (33°N)	Belemnites	-0.59 to -0.40	13-15 (13.8)	Bowen (1966)
Kimmeridgian	Subpolar Urals (55°N)	Belemnites		(20)	Zakharov <i>et al.</i> (2005)
Kimmeridgian	Helmsdale, Sutherland, Scotland (45°N)	Belemnites	-2.84 to +0.78	9-24 (15.8)	This study
Middle Kimmeridgian - Tithonian	Milne Land, East Greenland (50°N)	Belemnites	-1.91 to -1.13	17-20 (18)	Bowen (1966)
Early Kimmeridgian	Hüdsruck, Germany (38°N)	Belemnites	-1.18 to -0.91	16-17 (16.1)	Bowen (1961)
Upper Oxfordian - Middle Tithonian	Kawhia Harbour, New Zealand (80°S)	Belemnites	-3.10 to +0.36	11-25 (17.8)	Gröcke <i>et al.</i> (2003)
Oxfordian - Volgian	Russian Platform (55°N)	Belemnites		7-18	Riboulleau <i>et al.</i> (1998)
Oxfordian - Tithonian	New Zealand (80°S)	Belemnites	-4.40 to +1.90	5-32	Velzer <i>et al.</i> (1999)
Oxfordian - Tithonian	Falkland Plateau, South Atlantic (55°S)	Belemnites	-1.88 to -0.85	16-20 (17.6)	Price & Sellwood (1997)
Oxfordian - Early Kimmeridgian	Scotland; Poland; Germany (40°N)	Belemnites	-1.88 to +0.81	9-20	Wierzbowski (2004)
Oxfordian	Polish Jura Chain, Central Poland (40°N)	Brachiopods	-2.5 to +0.4	11-23	Wierzbowski (2002)
Oxfordian	Polish Jura Chain, Central Poland (40°N)	Belemnites	-1.5 to +0.5	10-16	Wierzbowski (2002)
Callovian - Barremian	Falkland Plateau, South Atlantic (55°S)	Belemnites	-2.22 to +0.08	12-21 (17.4)	Price & Gröcke (2002)
Callovian - Volgian	Russia (55°N)	Belemnites	-2.30 to +2.20	4-22	Velzer <i>et al.</i> (1999)
Callovian - Kimmeridgian	Staffin Bay, Isle of Skye, Scotland (45°N)	Belemnites	-2.07 to +1.43	7-21 (12.4)	This study
Callovian - Oxfordian	Kachchh Basin, W India (33°N)	Belemnites	-2.17 to +0.28	11-21	Fürsich <i>et al.</i> (2005)
Bathonian - early Kimmeridgian	E France; Switzerland (35°N)	Shark/Fish Teeth	+18.7 to +21.4 (PO_4)	15-28 (21.3)	Dromart <i>et al.</i> (2003b)
Bathonian - Callovian	Kachchh Basin, W India (33°N)	Brachiopods	-2.88 to -1.66	19-24	Fürsich <i>et al.</i> (2005)
Bajocian - Valanginian	Kong Karls Land, Svalbard (62°N)	Belemnites	-0.97 to +1.64	5-18 (9.5)	Ditchfield (1997)
Bajocian - Kimmeridgian	Poland; England (40°N)	Bivalves (aragonitic)		13-27	Malchus & Steuber (2002)
Aalenian - Portlandian	Anglo-Paris Basin, France (35°N)	Shark/Fish Teeth	+18.5 to +22.3 (PO_4)	21-29	Lecuyer <i>et al.</i> (2003)

Table 10.3 Compilation of published Late Jurassic-Early Cretaceous $\delta^{18}\text{O}$ and palaeotemperature data. All palaeotemperatures were calculated using the equation of Anderson & Arthur (1983) (except for PO_4 values - see respective references) and a $\delta^{18}\text{O}_{\text{seawater}}$ value of -1‰. Data is arranged according to age and data from this study is highlighted. (Please note where possible palaeotemperatures were recalculated using raw data.)

fossils). By considering such similar studies, direct comparisons can be drawn with regards to relative palaeoclimate. Table 10.3 shows the palaeotemperatures calculated from published literature as well as from the sites investigated here. Data from belemnites, bivalves, brachiopods and fish teeth/bone are included from a range of locations worldwide (including England, France, Germany, Switzerland, Poland, Spain, India, Russia, Greenland, Argentina, New Zealand and Antarctica). The majority of the published data are concentrated in the northern mid-latitudes between ~30 and 40°N. Calculated palaeotemperatures for this region are typically in the range of 15-25°C for the Late Jurassic and Early Cretaceous, although values as low as 8°C in the Lower Hauterivian (Price *et al.*, 2000) and as high as 29°C at the Bathonian-Callovian boundary (Lecuyer *et al.*, 2003) have also been recorded.

Palaeotemperatures calculated from southern high latitude locations (e.g., the Falkland Plateau, New Zealand and Antarctica) reveal a range from 11 to 25°C. The upper end of the range is certainly consistent with high latitude warmth, although, the lowest values may be consistent with the presence of occasional cold episodes. Even lower values are observed from the northern high latitudes, where palaeotemperatures between 2 and 24°C are recorded. Again, the higher palaeotemperature values are compatible with high latitude warmth, whilst the lowest values suggest that cold episodes may occur at times.

The lowest palaeotemperatures calculated from each of the sites investigated in this study varied from 2-9°C. Such values are consistent with the few northern high latitude studies that have been published, for example, Ditchfield (1997) recorded values as low as 5°C from the Tithonian-Valanginian of Svalbard, Price & Mutterlose (2004) recorded values down to 7°C from the Volgian-Valanginian of Siberia and Riboulleau *et al.* (1998) recorded temperatures as low 7°C from the Oxfordian-Volgian of the Russian platform. In terms of relative palaeotemperature, the evidence appears to be consistent with the northern high latitudes being on average ~7°C cooler than the mid-low latitudes during Late Jurassic and Early Cretaceous time.

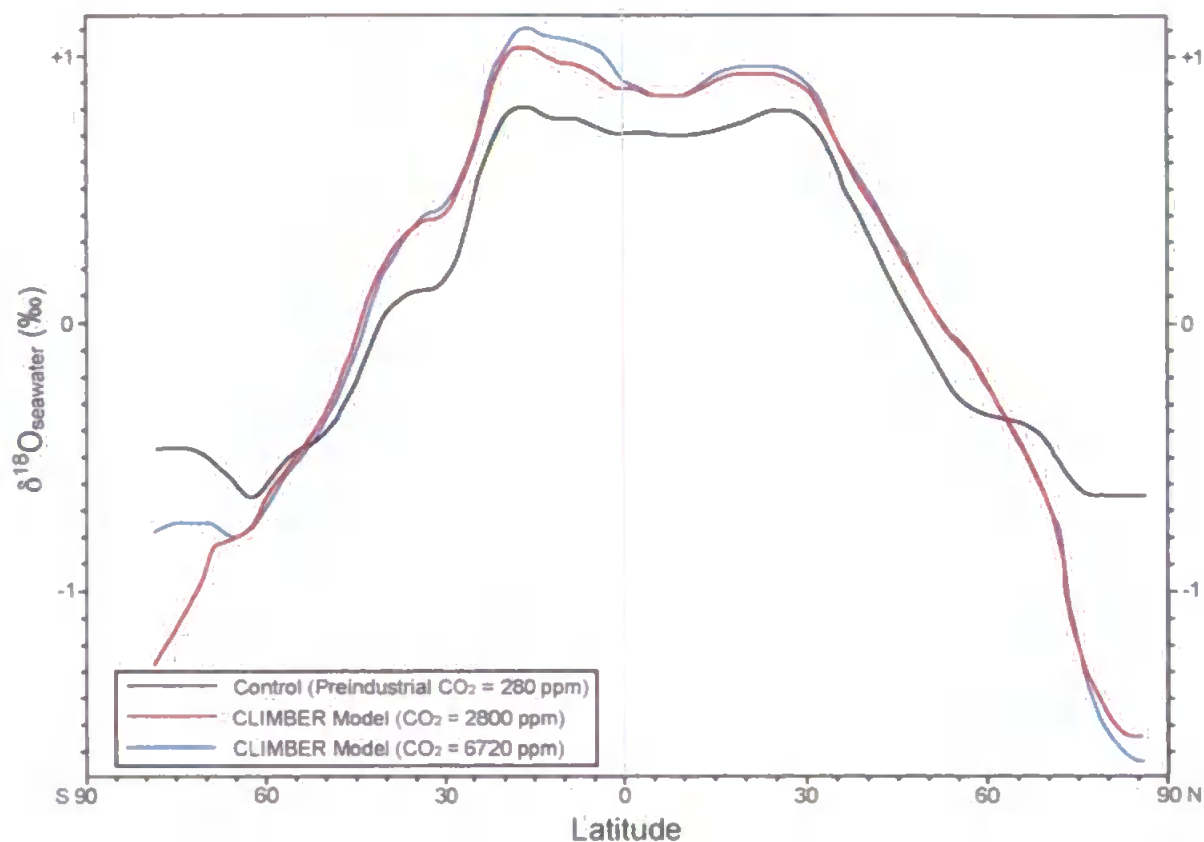


Figure 10.5 Latitudinal changes in $\delta^{18}\text{O}_{\text{seawater}}$ in warm climates. Adapted after Roche *et al.* (2006).

Roche *et al.* (2006) used a coupled climate model to investigate the distribution of surface water $\delta^{18}\text{O}$ composition under past warm climate conditions. One of the time periods considered in their research was the late Mesozoic greenhouse climate. Their results are shown in Figure 10.5. The latitudinal gradient produced by Roche *et al.* (2006) is broadly equivalent to that of the present day oceans for the mid- to low latitudes (e.g., Broecker, 1989; Zachos *et al.*, 1994), although for the high latitudes Roche *et al.* (2006) predict $\delta^{18}\text{O}_{\text{seawater}}$ values approximately 0.5 ‰ lower than those of the present day. If the Roche *et al.* (2006) model is correct, the palaeotemperature difference between the low and high latitudes is likely to be even greater, since $\delta^{18}\text{O}_{\text{seawater}}$ values in the mid-low latitudes are likely to be in the region of +0.5 to 1 ‰, whilst $\delta^{18}\text{O}_{\text{seawater}}$ values in the high latitudes ($>70^\circ$ palaeolatitude) are likely to be lower than -1 ‰ (Fig. 10.4), which would in effect raise low latitude temperature estimates and lower high latitude estimates. By substituting the standard $\delta^{18}\text{O}_{\text{seawater}}$ estimate of -1 ‰ with the Roche *et al.* (2006) range of values for $\delta^{18}\text{O}_{\text{seawater}}$ a change in latitudinal temperature gradient is observed when the data presented

in Table 10.3 for the Lower Kimmeridgian and Upper Valanginian is considered. These time intervals were chosen in order to illustrate the difference between a supposed warm period (the Lower Kimmeridgian) and cold period (the Upper Valanginian). Further subdivision of these time intervals (i.e., to ammonite zone level) was not possible due to a lack of published information.

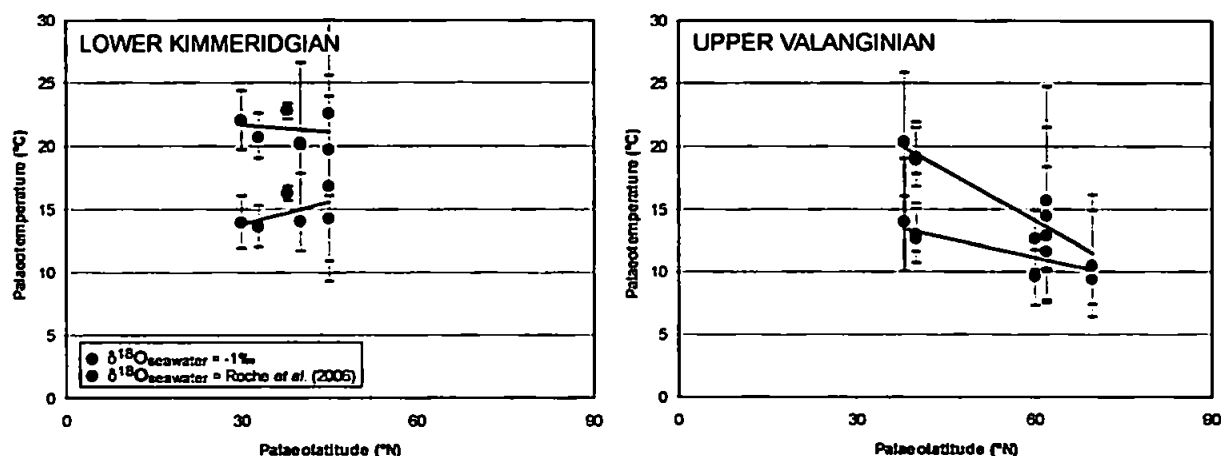


Figure 10.6 Calculated average palaeotemperatures for the Oxfordian and Valanginian periods. A $\delta^{18}\text{O}_{\text{seawater}}$ value of -1‰ and the Roche *et al.* (2006) $\delta^{18}\text{O}_{\text{seawater}}$ values are used. Only northern hemisphere locations and belemnite data were used.

Figure 10.6 provides an approximation of latitudinal differences in palaeotemperature for the northern hemisphere resulting from the different $\delta^{18}\text{O}_{\text{seawater}}$ estimates. This model assumes a homogenous Earth surface and does not take into account regional factors that may influence palaeotemperature. Allowing for this limitation, the Roche *et al.* (2006) values for $\delta^{18}\text{O}_{\text{seawater}}$ produce an increased temperature gradient for the Upper Valanginian data, with the offset between the calculated temperature values significantly smaller at higher latitudes. For the Kimmeridgian, the change in latitudinal gradient is less pronounced, although the relationship at this time is more difficult to assess owing to the limited latitudinal range of the data. The northern high latitude temperatures for the Upper Valanginian are on average approximately 10°C (at 70°N), although temperatures as low as $\sim 6^{\circ}\text{C}$ are recorded. During the Lower Kimmeridgian, the high latitude temperatures are estimated to be $\sim 20^{\circ}\text{C}$ (based on extrapolation of the trend line)

using the Roche *et al.* (2006) $\delta^{18}\text{O}_{\text{seawater}}$ latitudinal gradient. These significantly different high latitude palaeotemperature estimates suggest that both warm and cold conditions were present at the poles during different intervals of the Late Jurassic and Early Cretaceous.

The traditional view of continuously warm polar conditions during the Jurassic and Cretaceous greenhouse climate is still championed by many workers. For example, Jenkyns *et al.* (2004) recently extrapolated mid-Cretaceous temperatures in excess of 20°C for polar waters using the TEX₈₆ proxy. Such estimates of extreme polar warmth are also coincident with estimates for the tropics, only slightly warmer than those of the present day. This is especially true of the Late Cretaceous, where temperatures in excess of 15-20°C are commonly estimated for the poles (e.g., Huber *et al.*, 1995; Huber, 1998; Jenkyns *et al.*, 2004), whilst temperatures in the region of 33-37°C are postulated for the low latitudes (e.g., Clarke & Jenkyns, 1999; Norris *et al.*, 2002; Steuber *et al.*, 2005). The existence of such conditions however, poses a considerable problem, in that to date, the mechanism by which enhanced high latitude warming occurs without simultaneous warming in the tropics remains undefined. Sloan *et al.* (1995) summarised a number of mechanisms by which a low global temperature gradient might be achieved, including, an increase in the volume of warm deep/surface waters transported to the poles, increased high latitude albedo, increased cloud cover at high latitudes, cirrus cloud cover at low latitudes, or an expanded Hadley Cell. No definitive conclusion has yet been reached, although, the most commonly cited mechanism to account for such a situation is increased oceanic heat transport (e.g., Sloan *et al.*, 1995; Huber & Sloan, 1999; Bice & Norris, 2002). The problem with this model is that increased poleward heat transport produces more active circulation in the oceans, which may be incompatible with the formation of black shales during Oceanic Anoxic Events (OAEs) as are recorded in the Cretaceous period. Black shale formation is commonly attributed to oceanic stagnation, caused by slow oceanic circulation and consequent anoxia (Wilson & Norris, 2001) and may therefore contradict the model of increasingly active ocean circulation. The distinctive

provinciality of marine faunas at this time may also indicate that particularly active circulation would be unlikely. It is probable that marine provinciality was controlled to some degree by temperature or salinity gradients and, therefore, may not be compatible with enhanced circulation.

If, as this study suggests, an enhanced global temperature gradient relative to that traditionally envisaged (e.g., Barron, 1983) is present during intervals of the Late Jurassic and Early Cretaceous, for example when cold conditions are present at the poles, then the need to invoke complicated and often poorly understood mechanisms is removed at these times. Present day summer sea surface temperatures range from approximately 0°C at the poles to 28°C at the equator, with the present day average global temperature gradient therefore being in the region of 0.31°C per degree of latitude. The palaeotemperature gradient calculated using the Roche *et al.* (2006) $\delta^{18}\text{O}_{\text{seawater}}$ value and the data from this study was 0.26 for the Upper Valanginian, compared with a gradient of 0.10 for temperatures calculated using a $\delta^{18}\text{O}_{\text{seawater}}$ value of -1 ‰. The data presented here is, therefore, consistent with a moderate global temperature gradient during cold episodes of the Late Jurassic and Early Cretaceous. In this situation, oceanic heat transport would not need to be significantly increased, which would be compatible with belemnite provinciality and the deposition of black shales. The global rise in temperatures therefore, could probably be accounted for primarily by increased atmospheric CO₂ levels, although differences in palaeogeography may have also had an influence. When warm conditions exist at the poles however (for example, in the Lower Kimmeridgian), a relatively reduced global temperature gradient may still exist.

If this model is applied to the Late Cretaceous, for which tropical palaeotemperature estimates in the region of 35°C are relatively common, then the newly calculated palaeotemperatures would be approximately 45°C (using a $\delta^{18}\text{O}_{\text{seawater}}$ value of ~+1 ‰). This would also be consistent with a moderate global temperature gradient if polar temperatures in the region of 15-20°C are correct. Such high tropical values

however, may raise questions about the ability of calcifying organisms to live in these conditions and therefore also about the validity of the model. The Roche *et al.* (2006) data must therefore be utilised with care until further investigations can be carried out.

General Circulation Models (GCMs) have frequently been used in order to assess Cretaceous palaeoclimate (e.g., Moore *et al.*, 1992; Barron *et al.*, 1995; Price *et al.*, 1997; Poulsen *et al.*, 1999) and have often encountered difficulties modelling the extreme warmth at the poles and concomitant tropical temperatures in the region of 30-37°C. Barron *et al.* (1995) estimated that atmospheric carbon dioxide concentrations of approximately four times present day levels were required, together with a 1.2×10^{15} W increase in oceanic heat flux in order to best account for the greenhouse scenario. The model of Poulsen *et al.* (1999) however, produced temperatures that agreed well with the low latitude $\delta^{18}\text{O}$ palaeotemperature estimates for the mid-Cretaceous but not the warm polar estimates. Perhaps the existence of an increased global temperature gradient for parts of the Late Jurassic and Early Cretaceous could help resolve some of the discrepancies encountered in the GCMs by removing the need to invoke such a substantially increased poleward transport of oceanic heat to warm the poles and to prevent the tropics from overheating.

Evidence for genuinely cold conditions during the Late Jurassic and Early Cretaceous is limited to several discrete intervals such as the Lower Oxfordian *Cordatum* Zone, the mid-Ryazanian *Kochi-Analogus* zones and the Upper Valanginian *Bidichotomus* Zone. At these times it is perhaps possible that the Late Jurassic-Early Cretaceous Earth system functioned in much the same way as it does today, with the formation of polar ice increasing the salinity and density of polar waters and therefore dense cold bottom waters originating in the Arctic Ocean region and influencing thermohaline circulation to drive global climate (assuming that the required depth was available in the Arctic Ocean to generate circulation). This is something that will need to be considered and investigated in future palaeoceanographic models. In addition, the presence of at least seasonal ice cover

may have had an influence on the Earth's albedo as well as the distribution of fresh water. If this scenario is correct, the investigation of these cold intervals as a potential analogue with which to model future climate change is a very interesting prospect.

This research provides a significant compilation of northern high latitude Late Jurassic and Early Cretaceous data, which show that high latitude warmth was almost certainly the norm for this time. This warmth however, would have been punctuated by cold conditions during which limited polar ice may have formed. Perhaps the key characteristic of the Late Jurassic-Early Cretaceous high latitudes is climatic instability, which contrasts markedly with the low latitudes that are commonly believed to be much more stable. Previous research has provided snapshots of these conditions but this research for the first time provides a more comprehensive overview of this greenhouse climate. Strong evidence for both very warm and cold polar conditions is presented here suggesting that in the future, proponents of either warm or cold conditions will need to accept that both are likely to be a reality.

11. CONCLUSIONS

The principal aim of this research was to investigate the nature of Late Jurassic and Early Cretaceous northern high latitude climates, principally via stable isotope and geochemical proxies as derived from belemnites and fossilised wood. This has been achieved and a considerable contribution to the understanding of Late Jurassic and Early Cretaceous climate has been made.

11.1. Summary of Site Specific Investigations

The major palaeoenvironmental findings for each of the sites investigated in this study are summarised below.

11.1.1. Staffin Bay, Isle of Skye, Scotland

- Callovian-Kimmeridgian palaeotemperatures derived from the belemnite $\delta^{18}\text{O}$ record (using the Anderson & Arthur (1983) equation) were 6.7°C to 20.6°C (average 12.4°C). The highest palaeotemperatures were recorded in the Upper Oxfordian *Rozenkrantzi* Zone and the lowest palaeotemperatures in the Lower Oxfordian *Mariae-Cordatum* Zones.
- The $\delta^{13}\text{C}_{\text{org}}$ data record a broad Lower-Middle Oxfordian positive carbon isotope excursion of ~5 ‰. This trend is also observed in the $\delta^{13}\text{C}_{\text{carb}}$ data. This correlation indicates a strong coupling of the ocean-atmosphere system at this time and suggests that the total exchangeable carbon reservoir was affected. Such a relationship has never before been observed from a coeval marine and terrestrial record.
- The mid-Oxfordian negative carbon isotope excursions previously identified in the Tethyan regions are not recorded in the Staffin Bay data. These new data indicate that the Tethyan excursions may not represent fluctuations in the total exchangeable carbon

reservoir and, therefore, the fidelity of the methane hypothesis to account for this trend should be re-evaluated.

11.1.2. Helmsdale, Sutherland, Scotland

- Kimmeridgian palaeotemperatures derived from the belemnite $\delta^{18}\text{O}$ record (using the Anderson & Arthur (1983) equation) were 9.1 to 24.0°C (average 15.8°C). The highest palaeotemperatures were recorded in the Lower Kimmeridgian *Cymodoce* Zone and the lowest palaeotemperatures in the Upper Kimmeridgian *Elgans* Zone.
- The $\delta^{13}\text{C}_{\text{carb}}$ record shows a distinctive long-term trend towards more negative values throughout the Kimmeridgian. This is likely to be associated with a sea-level fall during which ^{12}C would be released by the weathering, erosion and oxidation of organic-rich sediments.
- The shift to low $\delta^{13}\text{C}$ values during the Kimmeridgian is also recorded from the Tethyan region and the northern and southern hemispheres. The widespread occurrence of this event suggests that the total global carbon reservoir was affected.

11.1.3. Boyarka River, Yenisei-Khatanga Basin, Siberia

- Ryazanian-Hauterivian palaeotemperatures derived from the belemnite $\delta^{18}\text{O}$ record (using the Anderson & Arthur (1983) equation) were 2.1 to 19.0°C (average 10.6°C). Both the highest and lowest palaeotemperatures were recorded in the mid-Ryazanian *Kochi-Analogus* zones.
- An Upper Valanginian positive carbon-isotope excursion is identified in both the $\delta^{13}\text{C}_{\text{org}}$ and $\delta^{13}\text{C}_{\text{carb}}$ records. This trend is consistent with that observed in Tethyan carbonate successions and therefore indicates a strong coupling of the ocean-atmosphere system at this time and suggests that the total exchangeable carbon reservoir was affected.
- The Boyarka River $\Delta\delta$ values may indicate a drop in atmospheric ρCO_2 . This is likely to be the result of enhanced organic carbon burial, which could lead to a drawdown of

ρCO_2 and a period of cooling in the late Valanginian. The palaeotemperature record is consistent with a slight cooling event.

11.1.4. Izhma River, Timan-Pechora Basin, Russia

- Callovian-Hauterivian palaeotemperatures derived from the belemnite $\delta^{18}\text{O}$ record (using the Anderson & Arthur (1983) equation) were 7.3°C to 17.3°C (average 13.0°C). A distinct fall in palaeotemperature is observed throughout the Valanginian period. This is consistent with previously published evidence for a cooling event during the Valanginian.
- The Late Valanginian positive $\delta^{13}\text{C}$ excursion is also recorded here. The timing and duration of this excursion is consistent with that observed in the Boyarka River succession. The positive $\delta^{13}\text{C}$ excursion occurs at a time of relatively low sea level in Russia and Siberia. The exposure and erosion of lowland areas and restricted ocean circulation (and therefore enhanced stratification) associated with a period of sea-level lowstand may account for increased rates of organic carbon burial.
- The most positive carbon isotope values coincide with the lowest palaeotemperatures. This could be explained by a fall in atmospheric CO_2 concentration and a subsequent drop in temperature as the result of a significant burial of organic carbon-rich sediments.

11.1.5. Festningen & Janusfjellet, Svalbard

- The preservation of belemnites at this site is generally very poor.
- Ryazanian-Upper Valanginian palaeotemperatures derived from the belemnite $\delta^{18}\text{O}$ record (using the Anderson & Arthur (1983) equation) were 7.7 to 21.4°C (average 13.0°C).
- Glendonites and outsized clasts were identified, lending support to the idea that cold conditions occurred in the northern high latitudes during the Early Cretaceous.

- The $\delta^{13}\text{C}$ data display a shift to more positive values from the Ryazanian and into the Upper Valanginian (of $\sim 2\text{‰}$). This shift is consistent with the timing of the Upper Valanginian positive carbon isotope excursion.

11.2. Wider Implications of Research

In addition to the findings outlined in the previous section, this research presented the opportunity to evaluate the use of belemnites as palaeoclimate indicators as well as to investigate Late Jurassic and Early Cretaceous global palaeoenvironmental conditions. The major conclusions drawn from this research are summarised below.

11.2.1. Belemnites as Palaeoenvironmental Indicators

- Belemnite preservation must be assessed using a combined approach incorporating both geochemical and optical techniques.
- Significant natural variability is present in belemnite data, although the reason for this is unclear. It is likely to be the combined result of a number of factors including genus-specific differences in fractionation (this could neither be confirmed nor refuted here), ontogenetic differences in fractionation (again this could be neither confirmed nor refuted), seasonal temperature variability, migration and comparison with homogenised bulk rock records. Providing long term trends are interpreted rather than small scale fluctuations, natural variability is not a significant problem.
- Oxygen isotope data are assumed to reflect fractionation temperature together with a salinity/ice-volume effect. This is, however, assumed to be the most appropriate belemnite palaeotemperature proxy.
- It is not possible to determine whether the elemental/Ca data generated in this study were influenced primarily by environmental factors (e.g., temperature) or physiological factors (e.g., metabolic activity and growth rate).

- Mg/Ca ratios regularly generated sub-freezing palaeotemperatures. This suggests that the use of the Klein *et al.* (1996) equation may not be suitable for belemnites, especially at relatively low temperatures.
- Calculations of relative $\delta^{18}\text{O}_{\text{seawater}}$ indicate that the Mg/Ca composition of belemnite calcite does not faithfully record temperature. This is based on the observation of a shift towards relatively negative $\delta^{18}\text{O}_{\text{seawater}}$ values coincident with a fall in palaeotemperature.
- The problems associated with correlating $\delta^{13}\text{C}$ records are eliminated here where a direct correlation between coeval marine carbonate and terrestrial organic carbon records from a given succession is possible. This confirms that the Jurassic-Cretaceous ocean-atmosphere system was strongly linked at times.

11.2.2. Late Jurassic - Early Cretaceous Global Palaeoenvironment

- A Callovian-Hauterivian compilation of $\delta^{13}\text{C}$ data for the Boreal Realm reveals relatively positive values in the Oxfordian, followed by a gradual shift to more negative values until the end-Volgian and a distinct positive carbon isotope excursion in the Valanginian. This confirms that the Arctic region records the same $\delta^{13}\text{C}$ signature as is observed in the Tethyan regions.
- A Callovian-Hauterivian compilation of $\delta^{18}\text{O}$ data for the Boreal Realm reveals evidence for warm polar conditions, punctuated by cold episodes during the Lower Oxfordian *Cordatum* Zone, the mid-Ryazanian *Kochi-Analogus* zones and the Upper Valanginian *Bidichotomus* Zone. This is consistent with published research. No Tithonian/Volgian cold episode was identified, although data were sparse through this interval.
- A comparison with published Late Jurassic-Early Cretaceous palaeotemperatures reveals a moderate global temperature gradient for the Upper Valanginian interval if

the standard estimate for $\delta^{18}\text{O}_{\text{seawater}}$ of -1 ‰ is substituted with the $\delta^{18}\text{O}_{\text{seawater}}$ estimates of Roche *et al.* (2006).

- The existence of a moderate global temperature gradient during cold episodes is contrary to the traditional view of greenhouse conditions, where extreme polar warmth is concomitant with temperatures similar to those of present day at the equator. No mechanism to account for such a scenario has ever been satisfactorily determined.
- The most commonly cited mechanism to account for a reduced thermal gradient is increased oceanic heat transport, although this may be incompatible with the formation of black shales and marine faunal provinciality.
- Throughout the Late Jurassic and Early Cretaceous high latitude warmth was almost certainly the norm. This warmth however, would have been punctuated by cold conditions during which limited polar ice may have formed. The key characteristic of the Late Jurassic-Early Cretaceous high latitudes is likely to be climatic instability, which contrasts markedly with the low latitudes that are commonly believed to be much more stable.
- During the cold episodes it is possible that the Earth's climate system functioned in much the same way as it does today. If this is the case, the Late Jurassic-Early Cretaceous interval represents an ideal analogue through which to investigate the nature of future climatic change.

11.3. Future Work

This study presents a significant amount of data with which to investigate the nature of Late Jurassic and Early Cretaceous northern high latitude palaeoclimates. It also highlights the areas where our current knowledge is limited and hence the areas that need to be addressed in order to resolve some of the uncertainties present here. The future work recommended as a result of this research falls into two key categories; firstly our

understanding of belemnite palaeoecology needs to be expanded and secondly additional high latitude data need to be examined.

Perhaps the most important element of future work is to further our understanding of belemnite palaeoecology by conducting high resolution investigations of modern analogues, namely *Sepia officinalis* and *Spirula spirula*. Preliminary work of this nature has been conducted by Rexfort & Mutterlose (2006), although significantly more data are needed. In particular, the extensive investigation of aquaria specimens is required. Analysis of genus-specific and ontogenetic differences in stable isotope and trace element fractionation must be focused on, in order to have any hope of truly understanding the limitations of belemnite data. Additional analyses of this nature must also be conducted on belemnite specimens so that comparisons can be drawn between the taxa. This requires the identification of belemnite rich horizons containing individuals belonging to either different genera or being of different ages. Work is currently being undertaken by John McArthur (University College London) to investigate genus-specific differences in belemnite fractionation using a deposit (of what is most likely fossilised Ichthyosaur vomit) containing abundant belemnite remains. The results of this research may provide information vital to furthering our understanding of belemnite fractionation.

In order to fully understand belemnite data it is also important to undertake further investigation into the nature of relative stable isotope and geochemical compositions of belemnites and other co-occurring organisms (e.g., brachiopods, benthic bivalves and ammonites). Preliminary work of this kind has been undertaken by several authors (e.g., Anderson *et al.*, 1994; Voigt *et al.*, 2003; Wierzbowski & Joachimski, 2006), although the results of such research have been very limited and desperately need expanding.

In addition to the required work on belemnite palaeoecology it is important to collect high resolution data from further high latitude sites (in both the northern and southern hemisphere). In particular, data should be sought from Greenland and Alaska

where very few studies have been conducted to date. If possible, attempts should also be made to investigate stratigraphically more extensive successions.

REFERENCES

- Abbink, O., Targarona, J., Brinkhuis, H. & Visscher, H. (2001). Late Jurassic to earliest Cretaceous paleoclimatic evolution of the southern North Sea. *Global and Planetary Change* **30**, 231-256.
- Abel, O. (1916). Palaobiologie der Cephalopoden aus der gruppe der Dibranchiaten. Fischer, Jena, 281 pp (in German).
- Ager, D. V. (1988). Mesozoic orgies? *Geology Today* **4**, 42.
- Alley, N. F. & Frakes, L. A. (2003). First known cretaceous glaciation: Livingston Tillite Member of the Cadna-owie Formation, South Australia. *Australian Journal of Earth Sciences* **50**, 139-144.
- Allman, M. & Lawrence, D. F. (1972). Geological Laboratory Techniques. Blandford Press, London, 335 pp.
- Anderson, F. M. (1945). Lower Cretaceous deposits in California and Oregon. *Special Papers of the Geological Society of America* **16**, 1-139.
- Anderson, F. W. & Cox, L. R. (1948). The 'Loch Staffin beds' of Skye: With notes on the molluscan fauna of the great Estuarine Series. *Proceedings of the Royal Physical Society of Edinburgh* **23**, 103-122.
- Anderson, F. W. & Dunham, K. C. (1966). The Geology of Northern Skye. Her Majesty's Stationary Office, Edinburgh.

Anderson, T. F. & Arthur, M. A. (1983). Stable isotopes of oxygen and carbon and their application to sedimentologic and environmental problems. *In* Arthur, M. A., Anderson, T. F., Kaplan, I. R., Veizer, J. & Land, L. S. (eds) *Stable Isotopes in Sedimentary Geology*. Society of Economic Paleontologists and Mineralogists Short course notes, 1.1-1.151.

Anderson, T. F., Popp, B. N., Williams, A. C., Ho, L. -Z. & Hudson, J. D. (1994). The stable isotopic records of fossils from the Peterborough Member, Oxford Clay Formation (Jurassic), UK: Palaeoenvironmental implications. *Journal of the Geological Society, London* **151**, 125-138.

Ando, A., Kakegawa, T., Takashima, R. & Saito, T. (2002). New perspective on Aptian carbon isotope stratigraphy: Data from $\delta^{13}\text{C}$ records of terrestrial organic matter. *Geology* **30**, 227-230.

Ando, A., Kakegawa, T., Takashima, R. & Saito, T. (2003). Stratigraphic carbon isotope fluctuations of detrital woody materials during the Aptian stage in Hokkaido, Japan: Comprehensive delta C-13 data from four sections of the Ashibetsu area. *Journal of Asian Earth Sciences* **21**, 835-847.

Aplonov, S. V. (1995). The tectonic evolution of West Siberia: An attempt at a geophysical analysis. *Tectonophysics* **245**, 61-84.

Arkell, W. J. (1933). *The Jurassic System in Great Britain*. Clarendon Press, Oxford, 681 pp.

Arkell, W. J. (1956). *Jurassic Geology of the World*. Oliver & Boyd, Edinburgh, 806 pp.

Backman, J., Bogdanov, N., Coakley, B., Edwards, M., Forsberg, R., Jackson, R., Jakobsson, M., Jokat, W., Kristoffersen, Y., Mayer, L. & Moran, K. (2002). Paleooceanographic and tectonic evolution of the Central Arctic Ocean. *Integrated Ocean Drilling Program Proposal 533*, 1-18.

Bailey, J. C. & Rasmussen, M. H. (1997). Petrochemistry of Jurassic and Cretaceous tholeiites from Kong Karls Land, Svalbard, and their relation to Mesozoic magmatism in the Arctic. *Polar Research* **16**, 37-62.

Bailey, T. R., Rosenthal, Y., McArthur, J. M., van de Schootbrugge, B. & Thirwall, M. F. (2003). Paleooceanographic changes of the Late Pliensbachian - Early Toarcian interval: A possible link to the genesis of an Oceanic Anoxic Event. *Earth and Planetary Science Letters* **212**, 307-320.

Bandel, K. & Kulicki, C. (1988). *Belemniteuthis polonica*: A belemnite with an aragonitic rostrum. In Wiedmann, J. & Kullmann, J. (eds) *Cephalopods - Present and Past*. Schweizerbart'sche Verlagsbuchhandlung, Stuttgart, 303-316.

Bandel, K. & Spaeth, C. (1988). Structural differences in the ontogeny of some belemnite rostra. In Wiedmann, J. & Kullmann, J. (eds) *Cephalopods - Present and Past*. Schweizerbart'sche Verlagsbuchhandlung, Stuttgart, 247-271.

Banks, N. L., de Boer, E. T., Scott, J. M. & Sheptunov, A. (1997). The South Kyrtael Oilfield, Timan-Pechora basin: Geological history and preliminary development plan. *Petroleum Geoscience* **3**, 371-378.

Baraboshkin, E. J. (1999). Berriasian-Valanginian (Early Cretaceous) seaways of the Russian Platform Basin and the problem of Boreal/Tethyan correlation. *Geologica Carpathica* **50**, 5-20.

Baraboshkin, E. J. (2002). Early Cretaceous seaways of the Russian Platform and the problem of Boreal/Tethyan correlation. *In* Michalik, J. (ed.) Tethyan/Boreal Cretaceous Correlation. Mediterranean and Boreal Cretaceous paleobiogeographic areas in Central and Eastern Europe. Publishing House of Slovak Academy, Bratislava, 39-78.

Baraboshkin, E. J. (2004). Boreal-Tethyan correlation of Lower Cretaceous ammonite scales. *Moscow University Geology Bulletin* **59**, 9-20.

Barrera, E., Huber, B. T., Savin, S. M. & Webb, P. -N. (1987). Antarctic marine temperatures: Late Campanian through early Paleocene. *Paleoceanography* **2**, 21-47.

Barron, E. J. (1983). A warm, equable Cretaceous: The nature of the problem. *Earth Science Reviews* **19**, 305-338.

Barron, E. J. & Washington, W. M. (1982). Atmospheric circulation during warm geologic periods: Is the equator-to-pole surface-temperature gradient the controlling factor? *Geology* **10**, 633-636.

Barron, E. J., Fawcett, P. J., Peterson, W. H., Pollard, D. & Thompson, S. L. (1995). A "simulation" of mid-Cretaceous climate. *Paleoceanography* **10**, 953-962.

Barron, E. J., Fawcett, P. J., Pollard, D. & Thompson, S. L. (1993). Model simulations of Cretaceous climates: The role of geography and carbon dioxide. *Philosophical Transactions of the Royal Society of London, Series B* **341**, 307-316.

Bartolini, A., Baumgartner, P. O. & Guex, J. (1999). Middle and Late Jurassic radiolarian palaeoecology versus carbon-isotope stratigraphy. *Palaeogeography, Palaeoclimatology, Palaeoecology* **145**, 43-60.

Bather, F. A. (1888). Shell-growth in Cephalopoda (Siphonopoda). *Annals and Magazine of Natural History* **6**, 298-310.

Bayle, E. & Zeiller, C. R. (1878). Explication de la carte géologique de la France. Fossiles principaux des terrains. Dufrenoy and Elie de Beaumont, Paris (in French).

Bennett, M. R. & Doyle, P. (1996). Global cooling inferred from dropstones in the Cretaceous: Fact or wishful thinking? *Terra Nova* **8**, 182-185.

Bennett, M. R., Doyle, P. & Mather, A. E. (1996). Dropstones: Their origin and significance. *Palaeogeography, Palaeoclimatology, Palaeoecology* **121**, 331-339.

Berner, R. A. (1994). 3GEOCARB II: A revised model of atmospheric CO₂ over Phanerozoic time. *American Journal of Science* **294**, 56-91.

Berner, R. A. & Kothavala, Z. (2001). GEOCARB III: A revised model of atmospheric CO₂ over Phanerozoic time. *American Journal of Science* **301**, 182-204.

Bersezio, R., Erba, E., Gorza, M. & Riva, A. (2002). Berriasian-Aptian black shales of the Maiolica Formation (Lombardian Basin, Southern Alps, northern Italy): Local to global events. *Palaeogeography, Palaeoclimatology, Palaeoecology* **180**, 253-275.

Bettencourt, V. & Guerra, A. (1999). Carbon- and oxygen-isotope composition of the cuttlebone of *Sepia officinalis*: a tool for predicting ecological information? *Marine Biology* **133**, 651-657.

Beutel, E. K., Nomade, S., Fronabarger, A. K. & Renne, P. R. (2005). Pangea's complex breakup: A new rapidly changing stress field model. *Earth and Planetary Science Letters* **236**, 471-485.

BGS. (1998). Helmsdale. Scotland Sheet 103E. Solid and Drift Geology. 1:50 000 Provisional Series. British Geological Survey, Keyworth, Nottingham.

Bice, K. L. & Norris, R. D. (2002). Possible atmospheric CO₂ extremes of the Middle Cretaceous (late Albian-Turonian). *Paleoceanography* **17**, 22.1-22.17.

Billups, K. & Schrag, D. P. (2003). Application of benthic foraminiferal Mg/Ca ratios to questions of Cenozoic climate change. *Earth & Planetary Science Letters* **209**, 181-195.

Birkenmajer, K. (1980). Jurassic-Lower Cretaceous succession at Agardhbukta, East Spitsbergen. *Studia Geologica Polonica* **66**, 35-52.

Bischoff, J. L., Fitzpatrick, J. A. & Rosenbauer, R. J. (1993). The solubility and stabilization of ikaite (CaCO₃.6H₂O) from 0°C to 25°C: Environmental and paleoclimatic implications for thynolite tufa. *Journal of Geology* **101**, 21-33.

Bishop, A. N. & Abbott, G. D. (1995). Vitrinite reflectance and molecular geochemistry of Jurassic sediments: the influence of heating by Tertiary dykes (northwest Scotland). *Organic Geochemistry* **22**, 165-177.

Bjerrum, C. J., Surlyk, F., Callomon, J. H. & Slingerland, R. L. (2001). Numerical Paleooceanographic study of the Early Jurassic transcontinental Lurasian Seaway. *Paleoceanography* **16**, 390-404.

Blüthgen, J. (1936). Die fauna und stratigraphie des Oberjura und UnterKreide von König Karl Land. Grimmer Kreis-Zeitung, Pommern, 91 pp (in German).

Bocherens, H., Friss, E. M., Mariotti, A. & Pedersen, K. R. (1993). Carbon isotopic abundances in Mesozoic and Cenozoic fossil plants: Palaeoecological implications. *Lethaia* **26**, 347-358.

Bodylevsky, V. I. (1960). Callovian ammonites from the northern Siberia. *Zap Leningradskogo Gornogo Institut* **37**, 49-82 (in Russian).

Bøggild, O. B. (1930). The shell structure of the mollusks. *Danske Videnskabernes Selska, Naturvidenskabe Mathematiske Avdelningen, 9. Raekke Kopenhagen* **2**, 258-325.

Boomer, I. (1994). Ostracod biostratigraphy of 2 borehole sections across the Toarcian Aalenian (Lias-Dogger) boundary, southern Germany. *Newsletters on Stratigraphy* **31**, 143-150.

- Bowen, G. J., Beerling, D. J., Koch, P. L., Zachos, J. C. & Quattlebaum. (2004). A humid climate state during the Palaeocene/Eocene thermal maximum. *Nature* **432**, 495-499.
- Bowen, G. J., Bralower, T. J., Delaney, M. L., Dickens, G. R., Kelley, D. C., Koch, P. L., Kump, L. R., Meng, J., Sloan, L. C., Thomas, E., Wing, S. L. & Zachos, J. C. (2006). Eocene hyperthermal event offers insight into greenhouse warming. *Eos* **87**(17), 165-169.
- Bowen, R. (1961a). Paleotemperature analyses of Mesozoic Belemnoida from Germany and Poland. *Journal of Geology* **69**, 75-83.
- Bowen, R. (1961b). Paleotemperature analyses of Belemnoida and Jurassic paleoclimatology. *Journal of Geology* **69**, 309-320.
- Bowen, R. (1966). Paleotemperature Analysis. Elsevier, Amsterdam, 265 pp.
- Bralower, T. J., Premoli Silva, I. & Malone, M. J. (2002). Proceedings of the Ocean Drilling Program, Initial Reports. Ocean Drilling Program, College Station, Texas. **198**, 1-148
- Brand, U. (1989). Biogeochemistry of Paleozoic North American brachiopods and secular variation of seawater composition. *Biogeochemistry* **7**, 159-193.
- Brand, U. & Veizer, J. (1980). Chemical diagenesis of a multicomponent carbonate system. 1: Trace elements. *Journal of Sedimentary Petrology* **50**, 1219-1236.

Brenchley, P. J., Marshall, J. D., Carden, G. A. F., Robertson, D. B. R., Long, D. G. F., Meidla, T., Hints, L. & Anderson, T. F. (1994). Bathymetric and isotopic evidence for a short-lived Late Ordovician glaciation in a greenhouse period. *Geology* **22**, 295-298.

Brentnall, S. J., Beerling, D. J., Osborne, C. P., Harland, M., Francis, J. E., Valdes, P. J. & Wittig, V. E. (2005). Climatic and ecological determinants of leaf lifespan in polar forests of the high CO₂ Cretaceous 'greenhouse' world. *Global Change Biology* **11**, 2177-2195.

Brewer, J. A. & Smythe, D. K. (1984). MOIST and the continuity of crustal reflector geometry along the Caledonian-Appalachian orogen. *Journal of the Geological Society, London* **141**, 105-120.

Broecker, W. S. (1989). The salinity contrast between the Atlantic and Pacific Oceans during glacial time. *Paleoceanography* **4**, 207-212.

Brookfield, M. E. (1976). The age of the Allt na Cuile Sandstones (Upper Jurassic, Sutherland). *Scottish Journal of Geology* **12**, 181-186.

Buchardt, B., Seaman, P. G., Düwel, L., Kristiansen, R. M., Kristiansen, A., Pedersen, G. H., Stockmann, G., Thorbjørn, L., Voss, M., Whiticar, M. J. & Wilken, U. (1997). Submarine columns of ikaite tufa. *Nature* **390**, 129-130.

Buffetaut, E. (2004). Polar dinosaurs and the question of dinosaur extinction: A brief review. *Palaeogeography, Palaeoclimatology, Palaeoecology* **214**, 225-231.

Callomon, J. H. (1963). Sexual dimorphism in Jurassic ammonites. *Transactions of the Leicester Literary and Philosophical Society* **57**, 21-51.

Cantrill, D. J., & Nichols, G. J. (1996). Taxonomy and palaeoecology of Early Cretaceous (Late Albian) angiosperm leaves from Alexander Island, Antarctica. *Review of Palaeobotany and Palynology* **92**, 1-28.

Casey, R. (1971). Facies, faunas and tectonics in Late Jurassic - Early Cretaceous Britain. In Middlemiss, F. A., Rawson, P. F., & Newall, G., (eds) *Faunal Provinces in Space and Time*. Geological Journal Special Issues. Seal House Press, Liverpool, 153-168.

Cecca, F., Savary, B., Bartolini, A., Remane, J. & Cordey, F. (2001). The Middle Jurassic-Lower Cretaceous Rosso Ammonitico succession of Monte Inici (Trapanese domain, western Sicily): Sedimentology, biostratigraphy and isotope stratigraphy. *Bulletin de la Societe Geologique de France* **172**, 647-659.

Chaloner, W. G. & Creber, G. T. (1990). Do fossil plants give a climatic signal? *Journal of the Geological Society, London* **147**, 343-350.

Channell, J. E. T., Erba, E. & Lini, A. (1993). Magnetostratigraphic calibration of the Late Valanginian carbon isotope event in pelagic limestones from Northern Italy and Switzerland. *Earth and Planetary Science Letters* **118**, 145-166.

Chesher, J. A. & Lawson, D. (1983). The Geology of the Moray Firth. *Institute of Geological Sciences Report* **83(5)**, pp. 32.

Christensen, W. K. (1976). Palaeobiogeography of Late Cretaceous belemnites of Europe. *Paläontologische Zeitschrift* **50**, 113-129.

Chumakov, N. M. (1981a). Mesozoic tilloids of the middle Volga, U.S.S.R. *In* Hambrey, M. J. & Harland, W. B. (eds) *Earth's pre-Pleistocene Glacial Record*. Cambridge University Press, Cambridge, 570.

Chumakov, N. M. (1981b). Scattered stones in Mesozoic deposits of North Siberia, U.S.S.R. *In* Hambrey, M. J. & Harland, W. B. (eds) *Earth's pre-Pleistocene Glacial Record*. Cambridge University Press, Cambridge, 264-265.

Clarke, L. J. & Jenkyns, H. C. (1999). New oxygen isotope evidence for long-term Cretaceous climatic change in the southern hemisphere. *Geology* **27**, 699-702.

Clarkson, E. N. K. (1998). *Invertebrate Palaeontology and Evolution*. Blackwell Science Ltd., Oxford, 452 pp.

Clarkson, P. D. (1988). Glacial erratics from the Brunt ice shelf, Coats Land, Antarctica. *British Antarctic Survey Bulletin* **81**, 1-10.

Cochran, J. K., Rye, D. M. & Landman, N. H. (1981). Growth rate and habitat of *Nautilus pompilius* inferred from radioactive and stable isotope studies. *Paleobiology* **7**, 469-480.

Coimbra, J. C., Arai, M. & Carreno, A. L. (2002). Biostratigraphy of Lower Cretaceous microfossils from the Araripe Basin, northeastern Brazil. *Geobios* **35**, 687-698.

Cope, J. C. W., Duff, K. L., Parsons, C. F., Torrens, H. S., Wimbledon, W. A. & Wright, J. K. (1980a). A correlation of Jurassic rocks in the British Isles. Part 2 - Middle and Upper Jurassic. *Geological Society of London Special Report* **15**, 1-109.

Cope, J. C. W., Getty, T. A., Howarth, M. K., Morton, N. & Torrens, H. S. (1980b). A correlation of Jurassic rocks in the British Isles. Part 1 - Introduction and Lower Jurassic. *Geological Society of London Special Report* **14**, 1-73.

Cox, B. & Doyle, P. (1996). Fossil focus: Belemnites. British Geological Survey, Nottingham, 2 pp.

Cox, B. M. (2001a). General introduction to Oxfordian and Kimmeridgian stratigraphy. *In* Wright, J. K. & Cox, B. M. (eds) British Upper Jurassic Stratigraphy (Oxfordian to Kimmeridgian). Geological Conservation Review Series No. 21. Joint Nature Conservation Committee, Peterborough, 1-10.

Cox, B. M. (2001b). Helmsdale. *In* Wright, J. K. & Cox, B. M. (eds) British Upper Jurassic Stratigraphy (Oxfordian to Kimmeridgian). Geological Conservation Review Series No. 21. Joint Nature Conservation Committee, Peterborough, 194-201.

Crame, J. A., McArthur, J. M., Pirrie, D. & Riding, J. B. (1999). Strontium isotope correlation of the basal Maastrichtian stage in Antarctica to the European and US biostratigraphic schemes. *Journal of the Geological Society, London* **156**, 957-964.

Cravo, A., Foster, P. & Bebianno, M. J. (2002). Minor and trace elements in the shell of *Patella aspera* (Röding 1798). *Environment International* **28**, 295-302.

Creber, G. T. & Chaloner, W. G. (1985). Tree growth in the Mesozoic and early Tertiary and the reconstruction of palaeoclimates. *Palaeogeography, Palaeoclimatology, Palaeoecology* **52**, 35-60.

Cresta, S., Goy, A., Ureta, S., Arias, C., Barron, E., Bernad, J., Canales, M. L., Garcia-Joral, F., Garcia-Romer, E., Gialanella, P. R., Gomez, J. J., Gonzalez, J. A., Herrero, C., Martinez, G., Osete, M. L., Perilli, N. & Villalain, J. J. (2001). The Global Boundary Stratotype Section and Point (GSSP) of the Toarcian-Aalenian boundary (Lower-Middle Jurassic). *Epsisodes* **24**, 166-175.

Czerniakowski, L. A., Lohmann, K. C. & Wilson, J. L. (1984). Closed system marine diagenesis: Isotopic data from the Austin Chalk and its components. *Sedimentology* **31**, 863-877.

Dave, A. & Chatterjee, T. K. (1996). Integrated foraminiferal and ammonoid biostratigraphy of Jurassic sediments in Jaisalmer Basin, Rajasthan. *Journal of the Geological Society of India* **47**, 477-490.

De Lurio, J. L. & Frakes, L. A. (1999). Glendonites as a paleoenvironmental tool: implications for Early Cretaceous high latitude climates in Australia. *Geochimica et Cosmochimica Acta* **63**, 1039-1048.

Delaney, M. L., Be, A., W. H. & Boyle, E. A. (1985). Li, Sr, Mg, and Na in foraminiferal calcite shells from laboratory culture, sediment traps, and sediment cores. *Geochimica et Cosmochimica Acta* **49**, 1327-1341.

Delattre, M. (1956). Faune de l'Aalénien de Mamers (Sarthe): Bélemnites. *Centre d'études et de documentation paléontologiques* **16**, 35-44 (in French).

Demaison, G. J. & Moore, G. T. (1980). Anoxic environments and oil source bed genesis. *Organic Geochemistry* **2**, 9-31.

Dettman, M. E., Molnar, R. E., Douglas, J. G., Burger, D., Fielding, C., Clifford, H. T., Francis, J. E., Jell, P., Rich, T., Wade, W., Rich, P. V., Pledge, N., Kemp, A. & Rozefelds, A. (1992). Australian Cretaceous terrestrial faunas and floras: Biostratigraphic and biogeographic implications. *Cretaceous Research* **13**, 207-262.

Dickens, G. R., O'Neil, J. R., Rea, D. K. & Owen, R. M. (1995). Dissociation of oceanic methane hydrate as a cause of the carbon isotope excursion at the end of the Paleocene. *Paleoceanography* **10**, 965-971.

Dickson, J. A. D. (1965). A modified staining technique for carbonates in thin section. *Nature* **205**, 587.

Dickson, J. A. D. (1966). Carbonate identification and genesis as revealed by staining. *Journal of Sedimentary Petrology* **36**, 491-505.

Ditchfield, P. W. (1997). High northern palaeolatitude Jurassic-Cretaceous palaeotemperature variation: new data from Kong Karls Land, Svalbard. *Palaeogeography, Palaeoclimatology, Palaeoecology* **130**, 163-175.

Ditchfield, P. W., Marshall, J. D. & Pirrie, D. (1994). High latitude palaeotemperature variation: New data from the Tithonian to Eocene of James Ross Island, Antarctica. *Palaeogeography, Palaeoclimatology, Palaeoecology* **107**, 79-101.

Donovan, D. T. & Toll, R. B. (1988). The gladius in coleoid (Cephalopoda) evolution. In Clarke, M. R. & Trueman, E. R. (eds) *The Mollusca. Volume 12. Paleontology and Neontology of Cephalopods*. Academic Press Incorporated, San Diego, 89-101.

d'Orbigny, A. (1842). Paléontologie Française. Terrain Jurassiques. I. (Céphalopodes). Victor Masson, Paris, 119 pp (in French).

d'Orbigny, A. (1842-1851). Description zoologique et géologique de tous les animaux mollusques et rayonnés fossiles de France comprenant leur application à la reconnaissance des couches. Victor Masson, Paris, 642 pp (in French).

d'Orbigny, A. (1845). Paléontologie universelle des coquilles et des mollusques. Victor Masson, Paris (in French).

d'Orbigny, A. (1850). Prodrôme de paléontologie stratigraphique universelle des animaux mollusques et rayonnés. Victor Masson, Paris (in French).

Doré, A. G. (1991). The structural foundation and evolution of Mesozoic seaways between Europe and the Arctic. *Palaeogeography, Palaeoclimatology, Palaeoecology* **87**, 441-492.

Doublet, S. & Garcia, J.-P. (2004). The significance of dropstones in a tropical lacustrine setting, eastern Cameros Basin (Late Jurassic-Early Cretaceous, Spain). *Sedimentary Geology* **163**, 293-309.

Doyle, P. (1985). Sexual dimorphism in the belemnite *Youngibelus* from the Lower Jurassic of Yorkshire. *Palaeontology* **28**, 133-146.

Doyle, P. (1987). Lower Jurassic - Lower Cretaceous belemnite biogeography and the development of the Mesozoic Boreal Realm. *Palaeogeography, Palaeoclimatology, Palaeoecology* **61**, 237-254.

Doyle, P. (1990a). The Biogeography of the Aulacocerida (Coleoidea). *In* Pallini, G., Cecca, F., Cresta, S. & Santantonio, M. (eds) *Atti del Secondo Convegno Internazionale, Fossili, Evoluzione, Ambiente, Pergola*. Editore Comitato Centenario Raffaele Piccinini, Pergola, 263-271.

Doyle, P. (1990b). The British Toarcian (Lower Jurassic) belemnites, Part 1. *Monograph of the Palaeontographical Society*, 1-49.

Doyle, P. (1992a). The British Toarcian (Lower Jurassic belemnites), Part 2. *Monograph of the Palaeontographical Society*, 1-41.

Doyle, P. (1992b). A review of the biogeography of Cretaceous belemnites. *Palaeogeography, Palaeoclimatology, Palaeoecology* **92**, 207-216.

Doyle, P. (2002). Oldest fossilised vomit pile uncovered. *Science* **295**, 1459.

Doyle, P. & Bennett, M. R. (1995). Belemnites in biostratigraphy. *Palaeontology* **38**, 815-829.

Doyle, P. & Kelly, S. R. A. (1988). The Jurassic and Cretaceous belemnites of Kong Karls Land, Svalbard. *Norsk Polarinstitutt Skrifter* **189**, 1-76.

Doyle, P. & Macdonald, D. I. M. (1993). Belemnite battlefields. *Lethaia* **26**, 65-80.

Doyle, P. & Shakides, E. V. (2004). The Jurassic Belemnite Suborder Belemnitheutina. *Palaeontology* **47**, 983-998.

Doyle, P., Donovan, D. T. & Nixon, M. (1994). Phylogeny and Systematics of the Coleoidea. *University of Kansas Paleontological Contributions, New Series* **5**, 1-15.

Doyle, P., Kelly, S. R. A., Pirrie, D. & Riccardi, A. C. (1997). Jurassic belemnite distribution patterns: Implications of new data from Antarctica and Argentina. *Alcheringa* **21**, 219-228.

Dromart, G., Garcia, J. -P., Picard, S., Atrops, F., Lécuyer, C. & Sheppard, S. M. F. (2003a). Ice age at the Middle - Late Jurassic transition? *Earth and Planetary Science Letters* **213**, 205-220.

Dromart, G., Garcia, J.-P., Gaumet, F., Picard, S., Rousseau, M., Atrops, F., Lecuyer, C. & Sheppard, S. M. F. (2003b). Perturbation of the carbon cycle at the Middle/Late Jurassic transition: Geological and geochemical evidence. *American Journal of Science* **303**, 667-707.

Dumitrescu, M., Brassell, S. C., Schouten, S., Hopmans, E. C. & Damste, J. S. S. (2006). Insatbility in the tropical Pacific sea-surface temperatures during the early Aptian. *Geology* **34**(10), 833-836.

Dwyer, G. S., Cronin, T. M., Baker, P. A., Raymo, M. E., Buzas, J. S. & Corregge, T. (1995). North Atlantic deepwater temperature change during late Pliocene and late Quaternary climatic cycles. *Science* **270**, 1347-1351.

Dypvik, H. (1985). Jurassic and Cretaceous black shales of the Janusfjellet Formation, Svalbard, Norway. *Sedimentary Geology* **41**, 235-248.

Dypvik, H. (1992). Sedimentary rhythms in the Jurassic and Cretaceous of Svalbard. *Geological Magazine* **129**, 93-99.

Dypvik, H., Håkansson, E. & Heinberg, C. (2002). Jurassic and Cretaceous palaeogeography and stratigraphic comparisons in the North Greenland-Svalbard region. *Polar Research* **21**, 91-108.

Dypvik, H., Nagy, J. & Krinsley, D. H. (1992). Origin of the Myklegardfjellet Bed, a basal Cretaceous marker on Spitsbergen. *Polar Research* **11**, 21-31.

Dypvik, H., Nagy, J., Eikeland, T. A., Backer-Owe, K. & Johansen, H. (1991b). Depositional conditions of the Bathonian to Hauterivian Janusfjellet Subgroup, Spitsbergen. *Sedimentary Geology* **72**.

Dypvik, H., Nagy, J., Eikeland, T. A., Backer-Owe, K., Andresen, A., Haremo, P., Bjærke, T., Johansen, H. & Strand, K. (1991a). The Janusfjellet Subgroup (Bathonian to Hauterivian) on Central Spitsbergen: A revised lithostratigraphy. *Polar Research* **9**, 21-43.

Dzyuba, O. S. (2004). Belemnites (Cylindroteuthidae) and biostratigraphy of the Middle and Upper Jurassic of Siberia. Publishing House of the Russian Academy of Sciences, Siberian Branch, Novosibirsk, 103 pp. (in Russian).

Dzyuba, O. S. (2005). Systematics and phylogeny of the boreal family Cylindroteuthidae: Problems solved and unsolved. In Košťák, M. & Marek, J. (eds) 2nd International Symposium. Coleoid cephalopods through time. Prague 2005. Short Papers/Abstracts Volume, Prague, 64-67.

Eichler, R. & Ristedt, H. (1966). Isotopic evidence on the early life history of *Nautilus pompilius* (Linné). *Science* **153**, 734-736.

Elderfield, H. & Ganssen, G. (2000). Past temperature and $\delta^{18}\text{O}$ of surface ocean waters inferred from foraminiferal Mg/Ca ratios. *Nature* **405**, 442-445.

Emery, K. O. (1965). Organic transportation of marine sediments. In Hill, N. M. (ed.) *The Sea*. Wiley, New York, 776-793.

Engeser, T. (1990). Major Events in Cephalopod Evolution. In Taylor, P. D. & Larwood, G. P. (eds) *Major Evolutionary Radiations*. Clarendon Press, Oxford, 119-138.

Engeser, T. & Bandel, K. (1988). Phylogenetic Classification of Coleoid Cephalopods. In Wiedmann, J. & Kullmann, J. (eds) *Cephalopods - Present and Past*. Schweizerbart'sche Verlagsbuchhandlung, Stuttgart, 105-115.

Engeser, T. S. & Clarke, M. R. (1988). Cephalopod hooks, both recent and fossil. In Clarke, M. R. & Trueman, E. R. (eds) *The Mollusca*. Volume 12. Paleontology and Neontology of Cephalopods. Academic Press Incorporated, San Diego, 133-151.

England, B. M. (1976). Glendonites: Their origin and description. *The Mineralogical Record* **7**, 60-68.

Epshteyn, O. G. (1978). Mesozoic - Cenozoic climates of northern Asia and glacial-marine deposits. *International Geology Review* **20**, 49-58.

Epstein, S., Buchsbaum, R., Lowenstam, H. A. & Urey, H. C. (1953). Revised carbonate-water isotopic temperature scale. *Bulletin of the Geological Society of America* **64**, 1315-1326.

Erba, E., Bartolini, A. & Larson, R. L. (2004). Valanginian Weissert oceanic anoxic event. *Geology* **32**, 149-152.

Espitalié, J., Deroo, G. & Marquis, F. (1985). La pyrolyse Rock-Eval et ses applications. *Revue de l'Institut Français du Pétrologie* **40**, 563-579 and 755-784 (in French).

Eyden, P. (2003). Belemnites: A quick look. *Tonmo.Com The Octopus News Magazine Online*, <http://www.tonmo.com/science/public/belemnites.php> (accessed on 14/08/06).

Falcon-Lang, H. J., & Cantrill, D. J. (2001). Leaf phenology of some mid-Cretaceous polar forests, Alexander Island, Antarctica. *Geological Magazine* **138**, 39-52.

Falcon-Lang, H. J., Cantrill, D. J. & Nichols, G. J. (2001). Biodiversity and terrestrial ecology of a mid-Cretaceous, high-latitude floodplain, Alexander Island, Antarctica. *Journal of the Geological Society, London* **158**, 709-724.

Feist, M., Lake, R. D. & Wood, C. J. (1995). Charophyte biostratigraphy of the Purbeck and Wealden of southern England. *Palaeontology* **38**, 407-442.

Fields, W. G. (1965). The structure, development, food relations, reproduction and life history of the squid *Loligo opalescens* Berry. *California Department of Fish and Game, Fish Bulletin* **131**, 1-108.

Fisher, I. S. J. & Hudson, J. D. (1987). Pyrite formation in Jurassic shales of contrasting biofacies. *In* Brooks, J. & Fleet, A. J. (eds) *Marine Petroleum Source Rocks*. Geological Society for London Special Publications, London, 69-78.

Föllmi, K. B., Weissert, H., Bisping, M. & Funk, H. (1994). Phosphogenesis, carbon-isotope stratigraphy, and platform evolution along the Lower Cretaceous northern Tethyan margin. *Geological Society of America Bulletin* **106**, 729-746.

Foster, C. B., Logan, G. A., Summons, R. E., Gorter, J. D. & Edwards, D. S. (1997). Carbon isotopes, kerogen types and the Permian-Triassic boundary in Australia: Implications for exploration. *Australian Petroleum Production and Exploration Association Journal* **37**, 472-488.

Frakes, L. A. (1979). *Climates through geologic time*. Elsevier, Amsterdam, 310 pp.

Frakes, L. A. & Francis, J. E. (1988). A guide to Phanerozoic cold polar climates from high-latitude ice rafting in the Cretaceous. *Nature* **333**, 547-549.

Frakes, L. A. & Krassay, A. A. (1992). Discovery of probable ice-rafting in the late Mesozoic of the Northern Territory and Queensland. *Australian Journal of Earth Sciences* **39**, 115-119.

Francis, J. E. & Frakes, L. A. (1993). Cretaceous climates. *In* Wright, V. P. (ed.) *Sedimentology Review 1*. Blackwell Scientific Publications, Oxford, 17-30.

Francis, J. E. & Poole, I. (2002). Cretaceous and early Tertiary climates of Antarctica: Evidence from fossil wood. *Palaeogeography, Palaeoclimatology, Palaeoecology* **182**, 47-64.

Frebold, H. (1957). The Jurassic Fernie Group in the Canadian Rocky Mountains and foothills. *Geological Survey of Canada Memoir* **287**, 197.

Fürsich, F. T. & Sykes, R. M. (1977). Palaeobiogeography of the European Boreal Realm during Oxfordian (Upper Jurassic) times: A quantitative approach. *Neues Jahrbuch für Geologie und Paläontologie. Abhandlungen* **155**, 137-161.

Fürsich, F. T., Singh, I. B., Joachimski, M., Krumm, S., Schlirf, M. & Schlirf, S. (2005). Palaeoclimate reconstructions of the Middle Jurassic of Kachchh (western India): An integrated approach based on palaeoecological, oxygen isotopic, and clay mineralogical data. *Palaeogeography, Palaeoclimatology, Palaeoecology* **217**, 289-309.

Fyfe, J. A., Long, D. & Evans, D. (1993). United Kingdom Offshore Report: The Geology of the Malin-Hebrides Sea area. Her Majesty's Stationary Office for the British Geological Survey, London, 91 pp.

Gale, A. S., Hardenbol, J., Hathway, B., Kennedy, W. J., Young, J. R. & Phansalker, V. (2002). Global correlation of Cenomanian (Upper Cretaceous) sequences: Evidence for Milankovitch control on sea level. *Geology* **30**, 291-294.

Garcia, J. P., & Dromart, G. (1997). The validity of two biostratigraphic approaches in sequence stratigraphic correlations: Brachiopod zones and marker-beds in the Jurassic. *Sedimentary Geology* **114**, 55-79.

Geist, J., Auerswald, K. & Boom, A. (2005). Stable carbon isotopes in freshwater mussel shells: Environmental record or marker for metabolic activity? *Geochimica et Cosmochimica Acta* **69**, 3345-3554.

Gilbert, R. (1990). Rafting in glacimarine environments. In Dowdeswell, J. A. & Scourse, J. D. (eds) *Glacimarine Environments: Processes and sediments*. Geological Society Special Publication No. 53. Geological Society, London, 105-120.

Golonka, J. & Bocharova, N. Y. (2000). Hot spot activity and the break-up of Pangea. *Palaeogeography, Palaeoclimatology, Palaeoecology* **161**, 49-69.

Gordon, W. A. (1973). Marine life and ocean surface currents in the Cretaceous. *Journal of Geology* **81**, 269-284.

Grabowski, J. & Pszczolkowski, A. (2006). Magneto- and biostratigraphy of the Tithonian-Berriasian pelagic sediments in the Tatra Mountains (central Western Carpathians, Poland): sedimentary and rock magnetic changes at the Jurassic/Cretaceous boundary. *Cretaceous Research* **27**, 398-417.

Gradstein, F., Ogg, J. & Smith, A. (2004). *A Geologic Timescale 2004*. Cambridge University Press, Cambridge, 589 pp.

Gradstein, F. M., Kaminski, M. A. & Agterberg, F. P. (1999). Biostratigraphy and paleoceanography of the Cretaceous seaway between Norway and Greenland. *Earth Science Reviews* **46**, 27-98.

Greinert, J. & Derkachev, A. (2004). Glendonites and methane-derived Mg-calcites in the Sea of Okhotsk, Eastern Siberia: Implications of a venting-related ikaite/glendonite formation. *Marine Geology* **204**, 129-144.

Gröcke, D. R. (1998). Carbon-isotope analysis of fossil plants as a chemostratigraphic and palaeoenvironmental tool. *Lethaia* **31**, 1-13.

Gröcke, D. R., Hesselbo, S. P. & Jenkyns, H. C. (1999). Carbon-isotope composition of Lower Cretaceous fossil wood: Ocean-atmosphere chemistry and relation to sea-level change. *Geology* **27**, 155-158.

Gröcke, D. R., Price, G. D., Robinson, S. A., Baraboshkin, E. Y., Mutterlose, J. & Ruffell, A. H. (2005). The Upper Valanginian (Early Cretaceous) positive carbon-isotope event recorded in terrestrial plants. *Earth and Planetary Science Letters* **240**, 495-509.

Gröcke, D. R., Price, G. D., Ruffell, A. H., Mutterlose, J. & Baraboshkin, E. (2003). Isotopic evidence for Late Jurassic - Early Cretaceous climate change. *Palaeogeography, Palaeoclimatology, Palaeoecology* **202**, 97-118.

Gustomesov, V. A. (1958). New Upper Jurassic belemnites from the Russian Platform. *Biulleten' Moskovskogo Obshchestva Ispytatelei Prirody Otdel geologique* **33**, 158-159 (in Russian).

Gustomesov, V. A. (1960). New Callovian belemnites from Timan. In Markovsky, B. P. (ed.) New species of fossil plants and invertebrates of the USSR 1(2). VSEGEI, Moscow, 190-192 (in Russian).

Gustomesov, V. A. (1964). Boreal Late Jurassic belemnites (Cylindroteuthidinae) of the Russian Platform. In Mikhailov, N. P. & Gustomesov, V. A. (eds) Boreal Late Jurassic cephalopods. Nauka Press, Moscow, 89-216 (in Russian).

Gustomesov, V. A. (1977). To the revision of Jurassic belemnites. *Biulleten' Moskovskogo Obshchestva Ispytatelei Prirody Otdel Geologique* **52**, 103-117 (in Russian).

Gustomesov, V. A. (1989). Phylogenetic relationships and stratigraphic significance of Cylindroteuthidae (Belemnitida) with rostra possessing ventral furrows. The revision of the genus *Lagonibelus*. *Biulleten' Moskovskogo Obshchestva Ispytatelei Prirody Otdel Geologique* **64**, 65-75 (in Russian).

Habicht, J. K. A. (1979). Paleoclimate, paleomagnetism, and continental drift. American Association of Petroleum Geologists Studies in Geology, Tulsa, Oklahoma, 31 pp.

Halasova, E. (1999). Calcareous nannofossil biostratigraphy of Lower Cretaceous pelagic carbonate sequences in Western Carpathians. *Geologica Carpathica* **50**, 30-31.

Hall, J. M. & Chan, L. H. (2001). Li/Ca in multiple species of benthic and planktonic foraminifera: Thermocline and glacial-interglacial changes. *American Geophysical Union, Fall Meeting Abstract*, #PP12A-0474.

Hallam, A. (1971). Provinciality in Jurassic faunas in relation to facies and palaeogeography. In Middlemiss, F. A., Rawson, P. F. & Newall, G. (eds) Faunal Provinces in Space and Time. Geological Journal Special Issues. Seal House Press, Liverpool, 129-152.

Hallam, A. (1975). *Jurassic Environments*. Cambridge University Press, Cambridge, 269 pp.

Hallam, A. (1981). *Facies Interpretation and the Stratigraphic Record*. W.H. Freeman, Oxford, 291 pp.

Hallam, A. (1985). A review of Mesozoic climates. *Journal of the Geological Society, London* **142**, 433-445.

Hallam, A. (1992). *Phanerozoic Sea Level Changes*. Columbia University Press, New York, 266 pp.

Hallam, A. (1993). Jurassic climates as inferred from the sedimentary and fossil record. *Philosophical Transactions of the Royal Society of London, Series B* **341**, 287-296.

Hambrey, M. J. & Harland, W. B. (1981). *Earth's pre-Pleistocene glacial record*. Cambridge University Press, Cambridge, 1004 pp.

Haq, B. U., Hardenbol, J. & Vail, P. R. (1987). Chronology of fluctuating sea levels since the Triassic. *Science* **235**, 1156-1167.

Harland, W. B. (1969). Contribution of Spitsbergen to understanding of tectonic evolution of North Atlantic region. *In* Harland, W. B. (ed.) *North Atlantic-geology and continental drift*. American Association of Petroleum Geologists Memoir, 817-851.

Harland, W. B. (1973). Mesozoic geology of Svalbard. *In* Pitcher, M. G. (ed.) Arctic Geology. Proceedings of the second international symposium on Arctic geology. American Association of Petroleum Geologists, Tulsa, 135-148.

Harland, W. B. (1997). Jurassic - Cretaceous history. *In* Harland, W. B. (ed.) The Geology of Svalbard. The Geological Society, London, 363-387.

Harland, W. B., Armstrong, R. L., Cox, A. V., Craig, L. E., Smith, A. G. & Smith, D. G. (1990). A Geological Timescale 1989. Cambridge University Press, Cambridge, 263 pp.

Hasegawa, T., Pratt, L. M., Maeda, H., Shigeta, Y., Okamoto, T., Kase, T. & Uemura, K. (2003). Upper Cretaceous stable carbon isotope stratigraphy of terrestrial organic matter from Sakhalin, Russia Far East: A proxy for the isotopic composition of paleoatmospheric CO₂. *Palaeogeography, Palaeoclimatology, Palaeoecology* **189**, 97-115.

Hay, W. W., DeConto, R. M., Wold, C. N., Wilson, K. M., Voigt, S., Schulz, M., Wold, A. R., Dullo, W. C., Ronov, A. B., Balukhovsky, A. N. & Söding, E. (1999). Alternative global Cretaceous paleogeography. *In* Barrera, E., & Johnson, C. C., (ed.) Evolution of the Cretaceous Ocean-Climate System. Special papers (Geological Society of America), 332. Geological Society of America, Boulder, Colorado, 1-48.

Hedges, J. I., Cowie, G. L., Ertel, J. R., Barbour, R. J. & Hatcher, P.L. (1985). Degradation of carbohydrates and lignins in buried wood. *Geochimica et Cosmochimica Acta* **46**, 701-711.

Heimhofer, U., Hochuli, P. A., Burla, S., Anderson, N. & Weissert, H. (2003). Terrestrial carbon-isotope records from coastal deposits (Algarve, Portugal): A tool for chemostratigraphic correlation on an intrabasinal and global scale. *Terra Nova* **15**, 8-13.

Henning, S., Weissert, H. & Bulot, L. (1999). C-isotope stratigraphy, a calibration tool between ammonite- and magnetostratigraphy: The Valanginian-Hauterivian transition. *Geologica Carpathica* **50**, 91-96.

Herman, A. B. & Spicer, R. A. (1996). Palaeobotanical evidence for a warm Cretaceous Arctic Ocean. *Nature* **380**, 330-333.

Herman, A. B. & Spicer, R. A. (1997). New quantitative palaeoclimate data for the Late Cretaceous Arctic: Evidence for a warm polar ocean. *Palaeogeography, Palaeoclimatology, Palaeoecology* **128**, 227-251.

Hesketh, R. A. P. & Underhill, J. R. (2002). The biostratigraphic calibration of the Scottish and Outer Moray Firth Upper Jurassic successions: a new basis for the correlation of Late Oxfordian - Early Kimmeridgian Humber Group reservoirs in the North Sea Basin. *Marine and Petroleum Geology* **19**, 541-562.

Hesselbo, S. P. & Coe, A. L. (2000). Jurassic sequences of the Hebrides Basin, Isle of Skye, Scotland. In Graham, J. R. & Ryan, A. (eds) Field Trip Guide Book, International Sedimentologists Association Meeting, Dublin. University of Dublin, Dublin, 41-58.

Hesselbo, S. P., Meister, C. & Gröcke, D. R. (2000). A potential global stratotype for the Sinemurian-Pliensbachian boundary (Lower Jurassic), Robin Hood's Bay, UK: Ammonite faunas and isotope stratigraphy. *Geological Magazine* **137**, 601-607.

Hesselbo, S. P., Morgans-Bell, H. S., McElwain, C., McAllister Rees, P., Robinson, S. A. & Ross, C. E. (2003). Carbon-cycle perturbation in the Middle Jurassic and accompanying changes in the terrestrial paleoenvironment. *The Journal of Geology* **111**, 259-276.

Hesselbo, S. P., Robinson, S. A., Surlyk, F. & Piasecki, S. (2002). Terrestrial and marine extinction at the Triassic-Jurassic boundary synchronized with major carbon-cycle perturbation: A link to initiation of massive volcanism? *Geology* **30**, 251-254.

Hewitt, R. A. (1980). Quantitative studies of some Jurassic belemnite assemblages. *Geobios* **13**, 173-197.

Hewitt, R. A., Westermann, G. E. G. & Judd, R. L. (1999). Buoyancy calculations and ecology of Callovian (Jurassic) Cylindroteuthid belemnites. *Neues Jahrbuch für Geologie und Paläontologie. Abhandlungen* **211**, 89-112.

Hoedemaeker, P. J. (1987). Correlation possibilities around the Jurassic/Cretaceous boundary. *Scripta Geologica* **84**, 1-55.

Hoedemaeker, P. J. & Herngreen, G. F. W. (2003). Correlation of Tethyan and Boreal Berriasian - Barremian strata with emphasis on strata in the subsurface of the Netherlands. *Cretaceous Research* **24**, 253-275.

Hoel, A. & Orvin, A. K. (1937). Das Festungsprofil auf Spitzbergen. Karbon - Kreide. I. Vermessungsergebnisse. *Skrifter om Svalbard og Ishavet* **18**, 1-59 (in German).

Hölder, H. (1973). *Miscellanea cephalopodica. Münstersche Forschungen zur Geologie und Paläontologie* **29**, 39-76 (in German).

Hounslow, M. W., Posen, P. E. & Warrington, G. (2004). Magnetostratigraphy and biostratigraphy of the Upper Triassic and lowermost Jurassic succession, St. Audrie's Bay, UK. *Palaeogeography, Palaeoclimatology, Palaeoecology* **213**, 331-358.

Housa, V., Krs, M., Man, O., Pruner, P. & Venhodova, D. (1999). Correlation of magnetostratigraphy and calpionellid biostratigraphy of the Jurassic Cretaceous boundary strata in the Western Carpathians. *Geologica Carpathica* **50**, 125-144.

House, M. R. (1988). Major Features of Cephalopod Evolution. In Wiedmann, J. & Kullmann, J. (eds) *Cephalopods - Present and Past*. Schweizerbart'sche Verlagsbuchhandlung, Stuttgart, 1-16.

Howarth, M. K. (1973). Lower Jurassic (Pliensbachian) ammonites. In Hallam, A. (ed.) *Atlas of Palaeobiogeography*. Elsevier, Amsterdam, 275-282.

Huber, B. T. (1998). Tropical paradise at the Cretaceous Poles? *Science* **282**, 2199-2200.

Huber, B. T. & Hodell, D. A. (1996). Middle-Late Cretaceous climate of the southern high latitudes: Stable isotopic evidence for minimal equator-to-pole thermal gradients; reply. *Geological Society of America Bulletin*. **108**, 1193-1196.

Huber, B. T., Hodell, D. A. & Hamilton, C. P. (1995). Middle-Late Cretaceous climate of the southern high latitudes: Stable isotopic evidence for minimal equator-to-pole thermal gradients. *Geological Society of America Bulletin*. **107**, 1164-1191.

Huber, H., Koeberl, C., McDonald, I. & Reimold, W. U. (2001). Geochemistry and petrology of Witwatersrand and Dwyka diamictites from South Africa: Search for an extraterrestrial component. *Geochimica et Cosmochimica Acta* **65**, 2007-2016.

Huber, M. & Sloan, L. C. (1999). Warm climate transitions: A general circulation modelling study of the late Paleocene thermal maximum (~56 Ma). *Journal of Geophysical Research* **104**, 16633-16656.

Hudson, J. D. (1962). The stratigraphy of the Great Estuarine Series (Middle Jurassic) of the Inner Hebrides. *Transactions of the Edinburgh Geological Society* **19**, 139-165.

Hudson, J. D. & Anderson, T. F. (1989). Ocean temperatures and isotopic compositions through time. *Transactions of the Royal Society of Edinburgh: Earth Sciences* **80**, 183-192.

Hudson, J. D. & Trewin, N. H. (2002). Jurassic. In Trewin, N. H. (ed.) *The Geology of Scotland*. 4th Edition. The Geological Society, London, 323-350.

Hurst, A. R. (1981). Mid Jurassic stratigraphy and facies at Brora, Sutherland. *Scottish Journal of Geology* **17**, 169-177.

Hvoslef, S., Dypvik, H. & Solli, H. (1986). A combined sedimentological and organic geochemical study of the Jurassic/Cretaceous Janusfjellet Formation (Svalbard), Norway. *Organic Geochemistry* **10**, 101-111.

Imlay, R. W. (1965). Jurassic marine faunal differentiation in North America. *Journal of Paleontology* **39**, 1023-1038.

Immenhauser, A., Nägler, T. F., Steuber, T. & Hippler, D. (2005). A critical assessment of mollusk $^{18}\text{O}/^{16}\text{O}$, Mg/Ca and $^{44}\text{Ca}/^{40}\text{Ca}$ ratios as proxies for Cretaceous seawater temperature seasonality. *Palaeogeography, Palaeoclimatology, Palaeoecology* **215**.

Irving, E. (1983). Fragmentation and assembly of the continents, mid-Carboniferous to present. *Geophysical Surveys* **5**, 299-333.

Ismail-Zadeh, A. T., Kostyuchenko, S. L. & Naimark, B. M. (1997). The Timan-Pechora Basin (northeastern European Russia): Tectonic subsidence analysis and a model of formation mechanism. *Tectonophysics* **283**, 205-218.

Jahren, A. H., Arens, N. C., Sarmiento, G., Guerrero, J. & Amundson, R. (2001). Terrestrial record of methane hydrate dissociation in the Early Cretaceous. *Geology* **29**, 159-162.

James, N. P., Narbonne, G. M., Dalrymple, R. W. & Kyser, T. K. (2005). Glendonites in Neoproterozoic low-latitude, interglacial, sedimentary rocks, northwest Canada: Insights into the Cryogenian Ocean and Precambrian cold-water carbonates. *Geology* **33**, 9-12.

Janney, P. E. & Castillo, P. R. (2001). Geochemistry of the oldest Atlantic oceanic crust suggests mantle plume involvement in the early history of the central Atlantic Ocean. *Earth and Planetary Science Letters* **192**, 291-302.

Jarvis, I. (1980). Palaeobiology of Upper Cretaceous belemnites from the phosphatic chalk of the Anglo-Paris Basin. *Palaeontology* **23**, 889-914.

Jeans, C. V., Long, D., Hall, M. A., Bland, D. J. & Cornford, C. (1991). The geochemistry of the Plenus Marls at Dover, England: Evidence of fluctuating oceanographic conditions and of glacial control during the development of the Cenomanian-Turonian $\delta^{13}\text{C}$ anomaly. *Geological Magazine* **128**, 603-632.

Jeletzky, J. A. (1965). Taxonomy and phylogeny of fossil Coleoidea (=Dibranchiata). *Papers of the Geological Survey of Canada* **65**, 72-76.

Jeletzky, J. A. (1966). Comparative Morphology, Phylogeny and Classification of Fossil Coleoidea. *University of Kansas Paleontological Contributions, Mollusca* **7**, 1-162.

Jeletzky, J. A. (1984). Jurassic-Cretaceous boundary beds of Western and Arctic Canada and the problem of the Tithonian-Berriasian stages in the Boreal Realm. *Geological Association of Canada Special Papers* **27**, 175-225.

Jenkyns, H. C. (1996). Relative sea-level change and carbon isotopes: Data from the Upper Jurassic (Oxfordian) of central and Southern Europe. *Terra Nova* **8**, 75-85.

Jenkyns, H. C., Forster, A., Schouten, S. & Sinninghe Damsté, J. S. (2004). High temperatures in the late cretaceous arctic ocean. *Nature* **432**, 888-892.

Jenkyns, H. C., Jones, C. E., Gröcke, D. R., Hesselbo, S. P. & Parkinson, D. N. (2002). Chemostratigraphy of the Jurassic system: applications, limitations and implications for palaeoceanography. *Journal of the Geological Society, London* **159**, 351-378.

Johnston, J. D. (1995). Pseudomorphs after ikaite in a glaciomarine sequence in the Dalradian of Donegal, Ireland. *Scottish Journal of Geology* **31**, 29-49.

Jones, A. T., Frank, T. D. & Fielding, C. R. (2006). Cold climate in the eastern Australian mid to Late Permian may reflect cold upwelling waters. *Palaeogeography, Palaeoclimatology, Palaeoecology* **237**, 370-377.

Jones, C. & Jenkyns, H. C. (2001). Seawater strontium isotopes, oceanic anoxic events, and seafloor hydrothermal activity in the Jurassic and Cretaceous. *American Journal of Science* **301**, 112-149.

Jones, C. E., Jenkyns, H. C., Coe, A. L. & Hesselbo, S. P. (1994a). Strontium isotopic variations in Jurassic and Cretaceous seawater. *Geochimica et Cosmochimica Acta* **58**, 3061-3074.

Jones, C. E., Jenkyns, H. C. & Hesselbo, S. P. (1994b). Strontium isotopes in Early Jurassic seawater. *Geochimica et Cosmochimica Acta* **58**, 1285-1301.

Kabal, Y. & Tasli, K. (2003). Biostratigraphy of the Lower Jurassic carbonates from the Aydıncık area (Central Taurides, S. Turkey) and morphological analysis of *Lituolipora termieri* (Hottinger, 1967). *Journal of Foraminiferal Research* **33**, 338-351.

Kauffman, E. G. (1973). Cretaceous bivalvia. In Hallam, A., (ed.) *Atlas of Paleobiogeography*. Elsevier, Amsterdam, Netherlands, 351-383.

Kear, A. J., Briggs, A. E. G. & Donovan, D. T. (1995). Decay and fossilization of non-mineralised tissue in coleoid cephalopods. *Palaeontology* **38**, 105-131.

- Kear, B. P. (2006). Marine reptiles from the Lower Cretaceous of south Australia: Elements of a high-latitude cold water assemblage. *Palaeontology* **49**, 837-856.
- Kelly, S. R. A. (1988). Jurassic through Cretaceous stratigraphy of the Barents Shelf. *In* Harland, W. B. & Dowdswell, E. K. (eds) *Geological Evolution of the Barents Shelf Region*. Graham & Trotman, London, 109-130.
- Kelly, S. R. A. (1997). The Adventdalen Group (Cretaceous - Jurassic). *In* Harland, W. B. (ed.) *The Geology of Svalbard*. The Geological Society, London, 52-59.
- Kemper, E. (1975). Upper Deer Bay Formation (Berriasian-Valanginian) of Sverdrop Basin and biostratigraphy of the Arctic Valanginian. *Geological Survey of Canada Paper* **75-1B**, 245-254.
- Kemper, E. (1983). Über kalt und warmzeiten der Unterkreide. *Zitteliana* **10**, 359-369 (in German).
- Kemper, E. (1987). Das klima der Kreide-zeit. *Geologisches Jahrbuch, A* **96**, 5-185 (in German).
- Kemper, E. & Schmitz, H. H. (1975). Stellate nodules from the Upper Deer Bay Formation (Valanginian) of Arctic Canada. *Geological Survey of Canada Paper* **75**, 109-119.
- Kemper, E. & Schmitz, H. H. (1981). Glendonite-indikatoren des polarmarinen abagerungsmilieus. *Geologische Rundschau* **70**, 759-773 (in German).

Kennedy, E. M., Spicer, R. A. & Rees, P. M. (2002). Quantitative palaeoclimate estimates from Late Cretaceous and Paleocene leaf floras in the northwest of the South Island, New Zealand. *Palaeogeography, Palaeoclimatology, Palaeoecology* **184**, 321-345.

Kennedy, G. L., Hopkins D. M. & Pickthorn W. J. (1987). Ikaite, the glendonite precursor, in estuarine sediments at Barrow, Arctic Alaska. *Geological Survey of Alaska Annual Meeting, Abstract, Programme 9*, 725.

Kessels, K., Mutterlose, J. & Michalzik, D. (2006). Early Cretaceous (Valanginian-Hauterivian) calcareous nannofossils and isotopes of the northern hemisphere: Proxies for the understanding of Cretaceous climate. *Lethaia* **39**, 157-172.

Khain, V. E., Sokolov, B. A., Kleshchev, K. A. & Shein, V. S. (1991). Tectonic and geodynamic setting of oil and gas basins of the Soviet Union. *American Association of Petroleum Geologists Bulletin* **75**, 313-325.

Klein, R. T., Lohmann, K. C. & Kennedy, G. L. (1997). Elemental and isotopic proxies of paleotemperature and paleosalinity: Climate reconstruction of the marginal northeast Pacific ca. 80 ka. *Geology* **25**, 363-366.

Klein, R. T., Lohmann, K. C. & Thayer, C. W. (1996). Bivalve skeletons record sea-surface temperature and $\delta^{18}\text{O}$ via Mg/Ca and $\delta^{18}\text{O}/^{16}\text{O}$ ratios. *Geology* **24**, 415-418.

Klein, R. T., Lohmann, K. C. & Thayer, C. W. (1996). Sr/Ca and $^{13}\text{C}/^{12}\text{C}$ ratios in skeletal calcite of *Mytilus trossulus*: Covariation with metabolic rate, salinity, and carbon isotopic composition of seawater. *Geochimica et Cosmochimica Acta* **60**, 4207-4221.

Koleva-Rekalova, E. & Metodiev, L. (2005). Preservational features of the Upper Pliensbachian - Lower Bajocian belemnite rostra from two clayey-limestone successions from the West Balkan Mtns (Bulgaria). Cathodoluminescence and geochemical tests. *Comptes rendus de l'Académie bulgare des Sciences* **58**, 789-794.

Körner, C., Farquhar, G. D. & Roksandic, Z. (1988). A global survey of carbon isotope discrimination in plants from high latitudes. *Oecologia* **74**, 623-632.

Kump, L. R. & Arthur, M. A. (1999). Interpreting carbon-isotope excursions: Carbonates and organic matter. *Chemical Geology* **161**, 181-198.

Küspert, W. (1982). Environmental changes during oil shale deposition as deduced from stable isotope ratios. In Einsele, G. & Seilacher, A. (eds) *Cyclic and Event Stratification*. Springer, Berlin, 482-501.

Kuznetsov, N., Udoratina, O. & Soboleva, A. (2005). Composition, structure and tectonic evolution of the Pre-Uralides and Timanides. *Mineralogical Society of Poland Special Papers* **26**, 52-56.

Lallier-Vergès, E., Bertrand, P., Huc, A. Y., Büchel, D. & Tremblay, P. (1993). Control of the preservation of organic matter by productivity and sulphate reduction in Kimmeridgian shales from Dorset, UK. *Marine and Petroleum Geology* **10**, 600-605.

Langford, F. F. & Blanc-Valleron, M. -M. (1990). Interpreting Rock-Eval pyrolysis data using graphs of pyrolyzable hydrocarbons vs. total organic carbon. *The American Association of Petroleum Geologists Bulletin* **74**, 799-804.

Langrock, U. & Stein, R. (2004). Origin of marine petroleum source rocks from the Late Jurassic to Early Cretaceous Norwegian Greenland Seaway - evidence for stagnation and upwelling. *Marine and Petroleum Geology* **21**, 157-176.

Langrock, U., Stein, R., Lipinski, M. & Brumsack, H. J. (2003). Late Jurassic and Early Cretaceous black shale formation and paleoenvironment in high northern latitudes: Examples from the Norwegian-Greenland Seaway. *Paleoceanography* **18**, Art. No. 1074.

Lapparent, A. F. (1960). Découverte de traces de pas de dinosauriens dans le Crétacé du Spitzberg. *Comptes Rendus de l'Académie des Sciences, Paris* **251**, 1399-1400 (in French).

Larsen, D. (1994). Origin and paleoenvironmental significance of calcite pseudomorphs after ikaite in the Oligocene Creede Formation, Colorado. *Journal of Sedimentary Research* **64**, 593-603.

Lea, D. W., Mashiotta, T. A. & Spero, H. J. (1999). Controls on magnesium and strontium uptake in planktonic foraminifera determined by live culturing. *Geochimica et Cosmochimica Acta* **63**, 2369-2379.

Lear, C. H., Elderfield, H. & Wilson, P. A. (2000). Cenozoic deep sea temperatures and global ice volumes from Mg/Ca in benthic foraminiferal calcite. *Science* **287**, 269-271.

Lear, C. H., Rosenthal, Y. & Slowey, N. (2002). Benthic foraminiferal Mg/Ca-paleothermometry: A revised core-top calibration. *Geochimica et Cosmochimica Acta* **66**, 3375-3387.

Leavitt, S. W. & Long, A. (1991). Seasonal stable carbon-isotope variability in tree rings: Possible palaeoenvironmental signals. *Chemical Geology (Isotope Geoscience Section)* **87**, 59-70.

Lecuyer, C., Picard, S., Garcia, J. P., Sheppard, S. M. F., Grandjean, P. & Dromart, G. (2003). Thermal evolution of Tethyan surface waters during the Middle-Late Jurassic: Evidence from delta O-18 values of marine fish teeth. *Paleoceanography* **18**, Article #1076.

Lee, G. W. (1925). Mesozoic rocks of East Sutherland & Ross. *In* Read, H. H., & Phemister, J., (eds) *The Geology of the Country around Golspie, Sutherlandshire*. Memoirs of the Geological Survey Scotland. His Majesty's Stationary Office, Edinburgh, 65-115.

Leitch, A. M., Davies, G. F., Wells, M. (1998). A plume head melting under a rifting margin. *Earth and Planetary Science Letters* **161**, 161-177.

Lennie, A. R., Tang, C. C. & Thompson, S. P. (2004). The structure and thermal expansion behaviour of ikaite, $\text{CaCO}_3 \cdot 6\text{H}_2\text{O}$, from $T = 114$ to $T = 293$ K. *Mineralogical Magazine* **68**, 135-146.

Lini, A., Weissert, H. & Erba, E. (1992). The Valanginian carbon isotope event: A first episode of greenhouse climate conditions during the Cretaceous. *Terra Nova* **4**, 374-384.

Lissajous, M. (1925). Répertoire alphabétique des bélemnites Jurassiques précédé d'un essai de classification. *Travaux Laboratoire de Géologie de la Faculté des Sciences, Lyon* **Mémoire 7**, 175 pp (in French).

Llanos, M. P. I. & Riccardi, A. C. (2000). The Neuquen composite section: magnetostratigraphy and biostratigraphy of the marine lower Jurassic from the Neuquen basin (Argentina). *Earth and Planetary Science Letters* **181**, 443-457.

Lloyd, C. R. (1982). The mid-Cretaceous earth: Paleogeography, ocean circulation and temperature, atmospheric circulation. *Journal of Geology* **90**, 393-443.

Loader, N. J., Switsur, V. R. & Field, E. M. (1995). High-resolution stable isotope analysis of tree rings: Implications of 'microdendroclimatology' for palaeoenvironmental research. *The Holocene* **5**, 457-460.

Longinelli, A. (1969). Oxygen-18 variations in belemnite guards. *Earth and Planetary Science Letters* **7**, 209-212.

Longinelli, A., Iacumin, P. & Ramigni, M. (2002). $\delta^{18}\text{O}$ of carbonate, quartz and phosphate from belemnite guards: Implications for the isotopic composition of ancient seawater. *Earth and Planetary Science Letters* **203**, 445-459.

Longinelli, A., Wierzbowski, H. & Matteo, A. D. (2003). $\delta^{18}\text{O}$ (PO_4^{3-}) and $\delta^{18}\text{O}$ (CO_3^{2-}) from belemnite guards from Eastern Europe: implications for palaeoceanographic reconstructions and for the preservation of pristine isotopic values. *Earth and Planetary Science Letters* **209**, 337-350.

Lowenstam, H. A. & Epstein, S. (1954). Paleotemperatures of the post-Aptian Cretaceous as determined by the oxygen isotope method. *Journal of Geology* **62**, 207-248.

MacLennan, A. M. & Trewin, N. H. (1989). Palaeoenvironments of the Late Bathonian - mid-Callovian in the Inner Moray Firth. *In* Batten, D. J. & Keen, M. C. (eds) Northwest European micropalaeontology and palynology. Ellis Horwood Limited, Chichester, 92-117.

MacLeod, N. (2005). Cretaceous. *In* Selley, R. C., Cocks, R. & Plimer, I. R. (eds) *Encyclopaedia of Geology*. Elsevier, London, 360-372.

MacQuaker, J. H. S. & Keller, M. A. (2005). Mudstone sedimentation at high latitudes: Ice as a transport medium for mud and supplier of nutrients. *Journal of Sedimentary Research* **75**, 696-709.

Maher, J. D. J. (2001). Manifestations of the Cretaceous High Arctic Large Igneous Province in Svalbard. *The Journal of Geology* **109**, 91-104.

Maher, J. D. J., Hays, T., Shuster, R. & Mutrux, J. (2004). Petrography of Lower Cretaceous sandstones on Spitsbergen. *Polar Research* **23**, 147-165.

Mahmoud, M. S., Omran, A. M. & Ataa, S. A. S. (1999). Stratigraphy of the Upper Jurassic Lower Cretaceous sequences from three boreholes, northern Egypt: Palynological evidence. *Newsletters on Stratigraphy* **37**, 141-161.

Makowski, H. (1963). Problem of sexual dimorphism in ammonites. *Palaeontologia Polonica* **12**, 1-92.

Malchus, N. & Steuber, T. (2002). Stable isotope records (O, C) of Jurassic aragonitic shells from England and NW Poland: Palaeoecological and environmental implications. *Geobios* **35**, 29-39.

Mangold, K. (1987). Reproduction. *In* Boyle, P. P. (ed.) *Cephalopod Life Cycles*. Volume 2. Comparative Reviews. Academic Press Plc. London, 157-200.

Marino, M. C., Andreini, G., Baldanza, A., D'Arpa, C., Mariotti, N., Pallini, G., Parisi, G. & Petti, F. M. (2004). Middle Jurassic - Early cretaceous integrated biostratigraphy (ammonites, calcareous nannofossils and calpionellids) of the Contrada Diesi section (South-Western Sicily, Italy). *Rivista Italiana di Paleontologia e Stratigrafia* **110**, 357-372.

Markwick, P. J. (1998). Fossil crocodilians as indicators of Late Cretaceous and Cenozoic climates: implications for using palaeontological data in reconstructing palaeoclimate. *Palaeogeography, Palaeoclimatology, Palaeoecology* **137**, 205-271.

Marshall, J. D. (1992). Climatic and oceanographic isotopic signals from the carbonate rock record and their preservation. *Geological Magazine* **129**, 143-160.

Martill, D. M. (1996). Fossils explained 17: Ichthyosaurs. *Geology Today* **12**, 194-196.

Martill, D. M., Taylor, M. A., Duff, K. L., Riding, J. B. & Bown, P. R. (1994). The trophic structure of the biota of the Peterborough Member, Oxford Clay Formation (Jurassic), UK. *Journal of the Geological Society, London* **151**, 173-194.

Matyja, B. A., Page, K. N., Wierzbowski, A. & Wright, J. K. (2004). Suboreal/Boreal ammonite succession at the Oxfordian/Kimmeridgian boundary in the Flodigarry section (Staffin Bay, Isle of Skye, UK). *Rivista Italiana di Paleontologia e Stratigrafia* **110**, 273-278.

McArthur, J. M. (1994). Recent trends in strontium isotope stratigraphy. *Terra Nova* **6**, 331-358.

McArthur, J. M., Donovan, D. T., Thirlwall, B. W., Fouke, B. W. & Matthey, D. (2000). Strontium isotope profile of the early Toarcian (Jurassic) oceanic anoxic event, the duration of ammonite biozones, and belemnite palaeotemperatures. *Earth and Planetary Science Letters* **179**, 269-285.

McArthur, J. M., Janssen, N. M. M., Reboulet, S., Leng, M. J., Thirwall, M. F. & van de Schootbrugge, B. (in press). Palaeo-temperatures, ice-volume, and isotope stratigraphy (Mg/Ca, $\delta^{18}\text{O}$, $\delta^{13}\text{C}$, $^{87}\text{Sr}/^{86}\text{Sr}$) for the Early Cretaceous (Berriasian, Valanginian, Hauterivian). *Earth and Planetary Science Letters*.

McArthur, J. M., Mutterlose, J., Price, G. D., Rawson, P. F., Ruffell, A. & Thirwall, M. F. (2004). Belemnites of Valanginian, Hauterivian and Barremian age: Sr-isotope stratigraphy, composition ($^{87}\text{Sr}/^{86}\text{Sr}$, $\delta^{13}\text{C}$, $\delta^{18}\text{O}$, Na, Sr, Mg), and palaeo-oceanography. *Palaeogeography, Palaeoclimatology, Palaeoecology* **202**, 253-272.

McHone, J. G. (2000). Non-plume magmatism and rifting during the opening of the central Atlantic Ocean. *Tectonophysics* **316**, 287-296.

McLachlan, I. R., Tsikos, H. & Cairncross, B. (2001). Glendonites (pseudomorphs after ikaite) in Late Carboniferous marine Dwyka beds in Southern Africa. *South African Journal of Geology* **104**, 265-272.

McWhae, J. R. (1986). Tectonic history of northern Alaska, Canadian Arctic, and Spitsbergen regions since Early Cretaceous. *American Association of Petroleum Geologists Bulletin* **70**, 430-450.

Meledina, S. V., Ilyina, V. I. & Nal'nyaeva, T. I. (1998). Parallel biostratigraphic scales of the Boreal Bathonian and Callovian in the North Pechora Region as a tool for interregional correlations. *Stratigraphy and Geological Correlation* **6**, 234-248.

Melinte, M. & Mutterlose, J. (2001). A Valanginian (Early Cretaceous) "boreal nanoplankton excursion" in sections from Romania. *Marine Micropaleontology* **43**, 1-25.

Meyers, P. A. (1997). Organic geochemical proxies of paleoceanographic, paleolimnologic and paleoclimatic processes. *Organic Geochemistry* **27**, 213-250.

Miller, J. (1988). Cathodoluminescence microscopy. In Tucker, M. (ed.) *Techniques in Sedimentology*. Blackwell Scientific Publications, Oxford, 174-190.

Miller, K. G., Sugarman, P. J., Browning, J. V., Kominz, M. A., Hernández, J. C., Olsson, R. K., Wright, J. D., Feigenson, M. D. & Van Sickle, W. (2003). Late Cretaceous chronology of large, rapid sea-level changes: Glacioeustasy during the greenhouse world. *Geology* **31**, 585-588.

- Miller, K. G., Wright, J. D. & Browning, J. V. (2005). Visions of ice sheets in a greenhouse world. *Marine Geology* **217**, 215-231.
- Milliman, J. D. (1974). *Marine Carbonates*. Springer-Verlag, New York, 375 pp.
- Miramand, P. & Bentley, D. (1992). Concentration and distribution of heavy metals in tissues of two cephalopods, *Eledone cirrhosa* and *Sepia officinalis*, from the French coast of the English Channel. *Marine Biology* **114**, 407-414.
- Miramand, P., Bustamante, P., Bentley, D. & Kouéta, N. (2006). Variation of heavy metal concentrations (Ag, Cd, Co, Cu, Fe, Pb, V, and Zn) during the life cycle of the common cuttlefish *Sepia officinalis*. *Science of the Total Environment* **361**, 132-143.
- Mitsuguchi, T., Matsumoto, E., Abe, O., Uchida, T. & Isdale, P. J. (1996). Mg/Ca thermometry on coral skeletons. *Science* **274**, 961-963.
- Monks, N. J., Hardwick, D. & Gale, A. S. (1996). The function of the belemnite guard. *Paläontologische Zeitschrift* **70**, 425-431.
- Moore, G. T., Hayashida, D. N., Ross, C. A. & Jacobson, S. R. (1992). Paleoclimate of the Kimmeridgian/Tithonian (Late Jurassic) world: I. Results using a general circulation model. *Palaeogeography, Palaeoclimatology, Palaeoecology* **93**, 113-150.
- Morgans-Bell, H. S., Coe, A. L., Hesselbo, S. P., Jenkyns, H. C., Weedon, G. P., Marshall, J. E. A., Tyson, R. V. & Williams, C. J. (2001). Integrated stratigraphy of the Kimmeridge Clay Formation (Upper Jurassic) based on exposures and boreholes in south Dorset. *Geological Magazine* **138**(5), 511-539.

Morrison, J. O. & Brand, U. (1986). Geochemistry of recent marine invertebrates. *Geoscience Canada* **13**, 237-254.

Morton, A. C. & Parson, L. M. (1988). Early Tertiary Volcanism and the Opening of the NE Atlantic. Blackwell Scientific Publications, London, 477 pp.

Morton, N. & Hudson, J. D. (1995). Field guide to the Jurassic of the Isles of Raasay and Skye, Inner Hebrides, NW Scotland. *In* Taylor, P. D. (ed.) *Field Geology of the British Jurassic*. Geological Society, London, 209-280.

Moss, S. J. & Finch, E. M. (1997). Geological implications of new biostratigraphic data from East and West Kalimantan, Indonesia. *Journal of Asian Earth Sciences* **15**, 489-506.

Müller-Stoll, H. (1936). Beiträge zur anatomie der Belemnnoidea. *Nova Acta Leopoldina Neue Serie* **4**, 159-226 (in German).

Mutterlose, J. (1988). Migration and Evolution Patterns in Upper Jurassic and Lower Cretaceous Belemnites. *In* Wiedmann, J. & Kullmann, J. (eds) *Cephalopods - Present and Past*. Schweizerbart'sche Verlagsbuchhandlung, Stuttgart, 525-537.

Mutterlose, J. (1998). The Barremian-Aptian turnover of biota in northwestern Europe: Evidence from belemnites. *Palaeogeography, Palaeoclimatology, Palaeoecology* **144**, 161-173.

Mutterlose, J., Brumsack, H., Flögel, S., Hay, W., Klein, C., Langrock, U., Lipinski, M., Ricken, W., Söding, E., Stein, R. & Swientek, O. (2003). The Greenland-Norwegian

- Seaway: A key area for understanding Late Jurassic to Early Cretaceous paleoenvironments. *Paleoceanography* **18**, Article #1010.
- Mutterlose, J., Schmid, F. & Spaeth, C. (1983). Zur Palaobiogeographie von Belemniten der Unterkreide in NW-Europa. *Zitteliana* **10**, 293-307 (in German).
- Naef, A. (1922). Die fossilen Tintenfische: Eine palaozoologische Monographie. Jena, 322 pp (in German).
- Nagy, J. & Seidenkrantz, M. S. (2003). New foraminiferal taxa and revised biostratigraphy of Jurassic marginal marine deposits on Anholt, Denmark. *Micropaleontology* **49**, 27-46.
- Naydin, D. P. & Teys, R. V. (1976). Oxygen isotope compositions of Eurasian Toarcian-Aalenian seas. *Geochemistry International* **13**, 163-173.
- Neumayr, M. (1883). Über klimatische Zonen während der Jura - und Kreidzeit. *Kaiserlichen Akademie der Wissenschaften in Wien, Mathematisch-Naturwissenschaftliche Klasse* **47**, 277-310 (in German).
- Neves, R. & Selley, R. C. (1975). A review of the Jurassic rocks of North-east Scotland. In Finstad, K. G., & Selley, R. C., (eds) Proceedings: Jurassic Northern North Sea Symposium. Norsk Petroleumsforening, Stavanger, JNNSS/5, 1-29.
- Norris, R. D., Bice, K. L., Magno, E. A. & Wilson, P. A. (2002). Jiggling the tropical thermostat in the Cretaceous hothouse. *Geology* **30**, 299-302.

- Oberbeck, V. R., Marshall, J. R. & Aggarwal, H. (1993). Impacts, tillites, and the breakup of Gondwanaland. *The Journal of Geology* **101**, 1-19.
- Ogg, J. G. (2004a). The Jurassic period. *In* Gradstein, F. M., Ogg, J. G. & Smith, A. G. (eds) A Geologic Time Scale 2004. Cambridge University Press, Cambridge, 307-343.
- Ogg, J. G. (2004b). Overview of Global Boundary Stratotype Sections and Points (GSSP's). *International Commission on Stratigraphy webpage*, <http://www.stratigraphy.org> (accessed on 14/08/06).
- Ogg, J. G., Agterberg, F. P. & Gradstein, F. M. (2004). The Cretaceous period. Gradstein, F. M., Ogg, J. G., & Smith, A. G., (eds) A Geologic Time Scale 2004. Cambridge University Press, Cambridge, 344-383.
- O'Leary, N., White, N., Tull, S., Bashilov, V., Kuprin, V., Natapov, L. & MacDonald, D. (2004). Evolution of the Timan-Pechora and South Barents Sea basins. *Geological Magazine* **141**, 141-160.
- O'Neill, B. R., Manger, W. L. & Hays, P. D. (2003). Growth and diagenesis of Middle Jurassic belemnite Rostra from northeastern Utah: Insights using cathodoluminescence. *In* Warnke, K., Keupp, H., & Boletzky, S., (eds) Coleoid cephalopods through time. Berliner paläobiologische Abhandlungen, Berlin, 241-251.
- Oppel, C. A. (1856-1858). Die Juraformation Englands, Frankreichs und des südwestlichen Deutschlands, Württemberger Naturforschende Jahreshefte. Ebner and Seubert, Stuttgart, 857 pp (in German).

O'Reilly, C., Wilson, T. & Sandring, J. (2005). The influence of tectonic activity on drainage networks and hydrocarbon prospectivity in Siberia. *American Association of Petroleum Geologists 2005 Conference Abstracts*, <http://aapg.confex.com/aapg/paris2005/techprogram/A99048.htm> (accessed on 10/08/2006).

Owen, R. (1844). A description of certain belemnites, preserved with a great proportion of their soft parts, in the Oxford Clay, at Christian-Malford, Wilts. *Royal Society of London, Philosophical Transactions* **134**, 65-85.

Padden, H., Weissert, H. & De Rafelis, M. (2001). Evidence for Late Jurassic release of methane from gas hydrate. *Geology* **29**, 223-226.

Padden, M., Weissert, H., Funk, H., Schneider, S. & Gansner, C. (2002). Late Jurassic lithological evolution and carbon-isotope stratigraphy of the western Tethys. *Eclogae Geologicae Helvetiae* **95**, 333-346.

Page, K. N. (1996). Mesozoic ammonoids in space and time. *In* Landman, N. H., Tanabe, K. & Davis, R. A. (eds) *Ammonoid Paleobiology. Topics in Geobiology*. Plenum Press, New York, 755-793.

Page, K. N. (2005). Jurassic. *In* Selley, R. C., Cocks, R. & Plimer, I. R. (eds) *Encyclopaedia of Geology*. Elsevier, London, 352-360.

Page, K. N. & Doyle, P. (1991). Other Cephalopods. *In* Martill, D. M. & Hudson, J. D. (eds) *Fossils of the Oxford Clay*. The Palaeontological Association, London, 144-162.

Palframan, P. F. B. (1966). Variation and ontogeny of some Oxfordian ammonites: *Tamarilliceras richei* (de Loriol) and *Creniceras reneggeri* (Oppel) from Woodham, Buckinghamshire. *Palaeontology* **9**, 290-311.

Parker, J. R. (1967). The Jurassic and Cretaceous sequence in Spitsbergen. *Geological Magazine* **104**, 487-505.

Pauly, H. (1963). "Ikaite", a new mineral from Greenland. *Arctic* **16**, 263-264.

Pavlow, A. P. (1892). Argiles de Speeten et leurs equivalents. *Biulleten' Moskovskogo Obshchestva Ispytatelei Prirody, n.s.* **5**, 181-267, 455-570 (in Russian).

Pavlow, A. P. (1914). Jurassic and Lower Cretaceous cephalopods of northern Siberia. *Imperatorskoi Akademii Nauka, St. Petersburg, Zapiski* **8**, **21(4)**, 1-68 (in Russian).

Pearce, C. R., Hesselbo, S. P. & Coe, A. L. (2005). The mid-Oxfordian (Late Jurassic) positive carbon-isotope excursion recognised from fossil wood in the British Isles. *Palaeogeography, Palaeoclimatology, Palaeoecology* **221**, 343-357.

Peters, K. E. (1986). Guidelines for evaluating petroleum source rock using programmed pyrolysis. *The American Association of Petroleum Geologists Bulletin* **70**, 318-329.

Phillips, J. (1835). Illustration of the geology of Yorkshire, or a description of the strata and organic remains of the Yorkshire coast. Printed for John Murray, London, 184 pp.

Phillips, J. (1865). A monograph of British Belemnitidae. Palaeontographical Society (Monograph), York, 128 pp.

Phillips, J. (1867). A monograph of British Belemnitidae. Palaeontographical Society (Monograph). York, 53-88.

Pickering, K. T. (1984). The Upper Jurassic 'Boulder Beds' and related deposits: A fault-controlled submarine slope, NE Scotland. *Journal of the Geological Society, London* **141**, 357-374.

Pickton, C. A. G. (1981). Palaeogene and Cretaceous dropstones in Spitsbergen. *In* Hambrey, M. J., & Harland, W. B., (eds) *Earth's pre-Pleistocene Glacial Record*. Cambridge University Press, Cambridge, 567-569.

Pirrie, D. & Marshall, J. D. (1990). High-paleolatitude Late Cretaceous paleotemperatures: New data from James Ross Island, Antarctica. *Geology* **18**, 31-34.

Pirrie, D., Doyle, P., Marshall, J. D. & Ellis, G. (1995). Cool Cretaceous climates: New data from the Albian of Western Australia. *Journal of the Geological Society, London* **152**, 739-742.

Podlaha, O. G., Mutterlose, J. & Veizer, J. (1998). Preservation of $\delta^{18}\text{O}$ and $\delta^{13}\text{C}$ in belemnite rostra from the Jurassic/Early Cretaceous successions. *American Journal of Science* **298**, 324-347.

Pollard, J. E. (1990). Evidence for diet. *In* Briggs, D. E. G., & Crowther, P. R., (eds) *Palaeobiology. A synthesis*. Blackwell, Oxford, 362-367.

Polyak, L., Stanovoy, V. & Lubinski, D. J. (2003). Stable isotopes in benthic foraminiferal calcite from a river-influenced Arctic marine environment, Kara and Pechora Seas. *Paleoceanography* **18**, 3/1-3/17.

Popp, B. N., Anderson, T. F. & Sandberg, P. A. (1986). Textural, elemental, and isotopic variations among constituents in Middle Devonian limestones, North America. *Journal of Sedimentary Petrology* **56**, 715-727.

Pörtner, H.-O. & Zielinski S. (1998). Environmental constraints and the physiology of performance in squids. *South African Journal of Marine Science*. **20**, 207-221.

Poulsen, C. J., Barron, E. J., Peterson, W. H. & Wilson, P. A. (1999). A reinterpretation of mid-Cretaceous shallow marine temperatures through model-data comparison. *Paleoceanography* **14**, 679-697.

Poulsen, N. E. (1992). Jurassic dinoflagellate cyst biostratigraphy of the Danish subbasin in relation to sequences in England and Poland - A preliminary review. *Review of Palaeobotany and Palynology* **75**, 33-52.

Price, G. D. (1999). The evidence and implications of polar ice during the Mesozoic. *Earth Science Reviews* **48**, 183-210.

Price, G. D. & Gröcke, D. R. (2002). Strontium-isotope stratigraphy and oxygen- and carbon-isotope variation during the Middle Jurassic-Early Cretaceous of the Falkland Plateau, South Atlantic. *Palaeogeography, Palaeoclimatology, Palaeoecology* **183**, 209-222.

Price, G. D. & Mutterlose, J. (2004). Isotopic signals from late Jurassic-early Cretaceous (Volgian-Valanginian) sub-Arctic belemnites, Yatria River, Western Siberia. *Journal of the Geological Society, London* **161**, 959-968.

Price, G. D. & Sellwood, B. W. (1994). Palaeotemperatures indicated by Upper Jurassic (Kimmeridgian-Tithonian) fossils from Mallorca determined by oxygen isotope composition. *Palaeogeography, Palaeoclimatology, Palaeoecology* **110**, 1-10.

Price, G. D. & Sellwood, B. W. (1997). Warm paleotemperatures from high Late Jurassic paleolatitudes (Falkland Plateau): Ecological, environmental or diagenetic controls? *Palaeogeography, Palaeoclimatology, Palaeoecology* **129**, 315-327.

Price, G. D., Ruffell, A. H., Jones, C. E., Kalin, R. M. & Mutterlose, J. (2000). Isotopic evidence for temperature variation during the Early Cretaceous (late Ryazanian - mid-Hauterivian). *Journal of the Geological Society, London* **157**, 335-343.

Price, G. D., Sellwood, B. W. & Pirrie, D. (1996). Middle-Late Cretaceous climate of the southern high latitudes: Stable isotopic evidence for minimal equator-to-pole thermal gradients: Discussion. *Geological Society of America Bulletin*. **108**, 1192-1196.

Price, G. D., Valdes, P. J. & Sellwood, B. W. (1997). Quantitative palaeoclimate GCM validation: Late Jurassic and mid-Cretaceous case studies. *Journal of the Geological Society, London* **154**, 769-772.

Price, G. D., Valdes, P. J. & Sellwood, B. W. (1998). A comparison of GCM simulated Cretaceous 'greenhouse' and 'icehouse' climates: Implications for the sedimentary record. *Palaeogeography, Palaeoclimatology, Palaeoecology* **142**, 123-138.

Prozorovskaya, E. L. (1993). Brachiopod subdivisions in the Jurassic of the southern ex-USSR. *Palaeogeography, Palaeoclimatology, Palaeoecology* **100**, 183-188.

Puc  at, E., L  cuyer, C., Sheppard, S. M. F., Dromart, G., Reboulet, S. & Grandjean, P. (2003). Thermal evolution of Cretaceous Tethyan marine waters inferred from oxygen isotope composition of fish tooth enamels. *Paleoceanography* **18**, 7/1-7/12.

Quenstedt, F. A. (1848). Petrefactenkunde Deutschlands. 1: Die Cephalopoden. Laupp'schen Buchhandlung, T  bingen, 581 pp (in German).

Quenstedt, F. A. (1856). Bemerkungen zum Geologischen Bilde Schwabens. In Sonst und Jetzt. Laupp'schen Buchhandlung, T  bingen, 48-57 (in German).

Railsback, L. B., Anderson, T. F., Ackerly, S. C. & Cisne, J. L. (1989). Paleoceanographic modelling of temperature-salinity profiles from stable isotope data. *Paleoceanography* **4**, 585-591.

Rampino, M. R. (1994). Tillites, diamictites, and ballistic ejecta of large impacts. *The Journal of Geology* **102**, 439-456.

Reitner, J. & Ulrichs, M. (1983). Echte weichteilbelemniten aus Untertorarcium (Posidonienschiefer) S  dwestdeutschlands. *Neues Jahrbuch f  r Geologie und Pal  ontologie. Abhandlungen* **165**, 450-465 (in German).

Requejo, A. G., Sassen, R., Kennicutt II, M. C., Kvedchuk, I., McDonald, T., Denoux, G., Comet, P. & Brooks, J. M. (1995). Geochemistry of oils from the northern Timan-Pechora Basin, Russia. *Organic Geochemistry* **23**, 205-222.

Rexfort, A. & Mutterlose, J. (2006). Stable isotope records from *Sepia officinalis* - a key to understanding the ecology of belemnites? *Earth and Planetary Science Letters* **247**, 212-221.

Rey, J. & Delgado, A. (2002). Carbon and oxygen isotopes: a tool for Jurassic and early Cretaceous pelagic correlation (southern Spain). *Geological Journal* **37**, 337-345.

Rey, J. & Delgado, A. (2005). Chemostratigraphic signals and sea-level changes from the Jurassic and Early Cretaceous in the Sierra de Quipar: Betic Cordilleras, southern Spain. *Geologiska Foreningens Forhandlingar* **127**, 25-32.

Riboulleau, A., Baudin, F., Daux, V., Hantzpergue, P., Renard, M. & Zakharov, V. (1998). Sea surface paleotemperature evolution of the Russian platform during the Upper Jurassic. *Comptes Rendus de la Academie des Sciences Serie II Fascicule A-Sciences de la Terre et des Planetes*. **326**, 239-246.

Rich, T. H., Vickers-Rich, P. & Gangloff, R. A. (2002). Polar dinosaurs. *Science* **295**, 979-980.

Riding, J. B. (2005). Middle and Upper Jurassic (Callovian to Kimmeridgian) palynology of the onshore Moray Firth Basin, northeast Scotland. *Palynology* **29**, 87-142.

Riding, J. B. & Thomas, J. E. (1997). Marine palynomorphs from the Staffin Bay and Staffin Shale formations (Middle-Upper Jurassic) of the Trotternish Peninsula, NW Skye. *Scottish Journal of Geology* **33**, 59-74.

Riegraf, W. & Hauff, R. (1983). Belemnitenfunde mit weichkörper, fangarmen und gladius aus dem Untertoarcium (Posidonienschiefer) und Unteraalenium (Opalinuston) Südwestdeutschlands. *Neues Jahrbuch für Geologie und Paläontologie. Abhandlungen* **165**, 466-483 (in German).

Roberts, A. (1989). Fold and thrust structures in the Kintradwell 'Boulder Beds' Moray Firth. *Scottish Journal of Geology* **25**, 173-186.

Robinson, S. A. & Hesselbo, S. P. (2004). Fossil-wood carbon-isotope stratigraphy of the non-marine Wealden Group (Lower Cretaceous, southern England). *Journal of the Geological Society, London* **161**, 133-145.

Robinson, S. A., Andrews, J. E., Hesselbo, S. P., Radley, J. D., Dennis, P. F., Harding, I. C. & Allen, P. (2002). Atmospheric $p\text{CO}_2$ and depositional environment from stable-isotope geochemistry of calcrete nodules (Barremian, Lower Cretaceous, Wealden Beds, England). *Journal of the Geological Society, London* **159**, 215-224.

Roche, D. M., Donnadieu, Y., Pucéat, E. & Paillard, D. (2006). Effect of changes in $\delta^{18}\text{O}$ content of the surface ocean on estimated sea surface temperatures in the past warm climate. *Paleoceanography* **21**, doi:10.1029/2005PA001220.

Roemer, F. A. (1836). Die Versteinerungen des norddeutschen Oolithen-Gebirges. Hahn'sche Hofbuchhandlung, Hannover, 218 pp (in German).

Roger, J. (1952). Sous-classe des Dibranchiata. *In* Piveteau, J. (ed.) *Traité de Paléontologie*. Victor Masson, Paris, 689-755.

Rosales, I., Quesada, S. & Robles, S. (2004b). Paleotemperature variations of Early Jurassic seawater recorded in geochemical trends of belemnites from the Basque-Cantabrian basin, northern Spain. *Palaeogeography, Palaeoclimatology, Palaeoecology* **20**, 253-275.

Rosales, I., Quesada, S. & Robles, S. (2006). Geochemical arguments for identifying second-order sea-level changes in hemipelagic carbonate ramp deposits. *Terra Nova* **18**, 233-240.

Rosales, I., Robles, S. & Quesada, S. (2004a). Elemental and oxygen isotope composition of Early Jurassic belemnites: Salinity vs. temperature signals. *Journal of Sedimentary Research* **74**, 342-354.

Rowley, D. B. & Lottes, A. L. (1988). Plate-kinematic reconstructions of the North Atlantic and Arctic: Late Jurassic to present. *Tectonophysics* **155**, 73-120.

Rowley, D. B. & Markwick, P. J. (1992). Haq *et al.* eustatic sea level curve: Implications for sequestered water volumes. *The Journal of Geology* **100**, 703-715.

Royer, D. L. (2006). CO₂-forced climate thresholds during the Phanerozoic. *Geochimica et Cosmochimica Acta* **70**, 5665-5675.

- Royer, D. L., Berner, R. A., Montañez, I. P., Tabor, N. J. & Beerling, D. J. (2004). CO₂ as a primary driver of Phanerozoic climate. *GSA Today* **14**, 4-10.
- Sælen, G. (1989). Diagenesis and construction of the belemnite rostrum. *Palaeontology* **32**, 765-798.
- Sælen, G. & Karstang, T. V. (1989). Chemical signatures of belemnites. *Neues Jahrbuch für Geologie und Paläontologie, Abhandlungen* **177**, 333-346.
- Sælen, G., Doyle, P. & Talbot, M. R. (1996). Stable-isotope analysis of belemnite rostra from the Whitby Mudstone Fm., England: Surface water conditions during deposition of a marine black shale. *Palaios* **11**, 97-117.
- Sahagian, D., Pinous, O., Olferiev, A. & Zakharov, V. (1996). Eustatic curve for the Middle Jurassic - Cretaceous based on Russian Platform and Siberian stratigraphy: Zonal Resolution. *American Association of Petroleum Geologists Bulletin* **80**, 1433-1458.
- Saks, V. N. & Nal'nyaeva, T. I. (1964). Upper Jurassic and Lower Cretaceous belemnites of the northern USSR. The genera *Cylindroteuthis* and *Lagonibelus*. Nauka Press, Leningrad, 168 pp (in Russian).
- Saks, V. N. & Nal'nyaeva, T. I. (1966). Upper Jurassic and Lower Cretaceous belemnites of the northern USSR. The genera *Pachyteuthis* and *Acroteuthis*. Nauka Press, Leningrad, 266 pp. (in Russian).
- Saks, V. N. & Nal'nyaeva, T. I. (1967). The systematics of Jurassic and Cretaceous belemnites. In Saks, V. N. & Nal'nyaeva, T. I (eds) *Problems of paleontological*

- substantiation of detailed Mesozoic stratigraphy of Siberia and the Far East of the USSR. Nauka Press, Leningrad, 6-27 (in Russian).
- Saks, V. N. & Nal'nyaeva, T. I. (1970). Early and middle Jurassic belemnites of northern USSR. Nannobelinae, Passaloteuthinae and Hastitidae. Nauka Press, Leningrad, 228 pp. (in Russian).
- Saks, V. N. & Nal'nyaeva, T. I. (1975). Early and middle Jurassic belemnites of northern USSR. Megateuthinae and Pseudodicoelitinae. Nauka Press, Leningrad, 191 pp. (in Russian).
- Schäfer, W. (1972). Ecology and Palaeoecology of Marine Environments. Oliver & Boyd, Edinburgh, 568 pp.
- Schleser, G. H. (1999). $^{13}\text{C}/^{12}\text{C}$ in growth rings and leaves: Carbon distribution in trees. *In* Jones, T. P. & Rowe, N. P. (eds) Fossil Plants and Spores: Modern Techniques. Geological Society, London, 306-309.
- Schouten, S., Hopmans, E. C., Schefuß, E. & Sinninghe Damsté, J. S. (2002). Distributional variations in marine crenarchaeotal membrane lipids: A new tool for reconstructing ancient sea water temperatures? *Earth and Planetary Science Letters* **204**, 265-274.
- Schrag, D. P., DePaolo, D. J. & Richter, F. M. (1992). Oxygen isotope exchange in a two-layer model of oceanic crust. *Earth and Planetary Science Letters* **111**, 305-317.

Schudack, M. E. (1999). Ostracoda (marine/nonmarine) and palaeoclimate history in the Upper Jurassic of Central Europe and North America. *Marine Micropaleontology* **37**, 273-288.

Scotese, C. R. (1991). Jurassic and Cretaceous plate tectonic reconstructions. *Palaeogeography, Palaeoclimatology, Palaeoecology* **87**, 493-501.

Sellwood, B. W. & Price, G. D. (1994). Sedimentary facies as indicators of Mesozoic palaeoclimate. In Allen, J. R. L., Hoskins, B. J., Sellwood, B. W., Spicer, R. A., & Valdez, P. J., (eds) *Palaeoclimates and their Modelling, with Special Reference to the Mesozoic Era*. Chapman & Hall, London, 17-25.

Sellwood, B. W., Price, G. D. & Valdes, P. J. (1994). Cooler estimates of Cretaceous temperatures. *Nature* **370**, 453-455.

Semenovich, V. N., Grambrg, I. S. & Nesterov, I. I. (1973). Oil and gas possibilities in the Soviet Arctic. In Pitcher, M. G. (ed.) *Arctic Geology*. The American Association of Petroleum Geologists, Tulsa, 194-203.

Sey, I. I. & Kalacheva, E. D. (1997). The Jurassic-Cretaceous boundary in the Boreal Realm (biostratigraphy and Boreal-Tethyan correlation). *Stratigraphy and Geological Correlation* **5**, 38-54.

Sey, I. I. & Kalacheva, E. D. (1999). Lower Berriasian of Southern Primorye (Far East Russia) and the problem of Boreal-Tethyan correlation. *Palaeogeography, Palaeoclimatology, Palaeoecology* **150**, 49-63.

Sha, J. G. & Frusich, F. T. (1993). Biostratigraphy of the Upper Jurassic-Lower Cretaceous bivalves *Buchia* and *Aucellina* of eastern Heilongjiang, northeast China. *Geological Magazine* **130**, 533-542.

Shaviv, N. J. & Veizer, J. (2003). Celestial driver of Phanerozoic climate? *GSA Today* **13**, 4-10.

Shearman, D. J. & Smith, A. J. (1985). Ikaite, the parent mineral of jarowite-type pseudomorphs. *Proceedings of the Geologists Association of London* **96**, 305-314.

Shulgina, N. I., Burdykina, M. D., Basov, V. A. & Århus, N. (1994). Distribution of ammonites, foraminifera and dinoflagellate cysts in the Lower Cretaceous reference sections of the Khatanga Basin, and Boreal Valanginian biogeography. *Cretaceous Research* **15**, 1-16.

Skelton, P. W. (2003). Introduction to the Cretaceous. In Skelton, P. W. (ed.) *The Cretaceous World*. Cambridge University Press, Cambridge, 9-41.

Sloan, L. C., Walker, J. C. G. & Moore, T. C. Jr. (1995). Possible role of oceanic heat transport in early Eocene climate. *Paleoceanography* **10**, 347-356.

Sluijs, A., Schouten, S., Pagani, M., Woltering, M., Brinkhuis, H., Damste, J. S. S., Dickens, G. R., Huber, M., Reichert, G. J., Stein, R., Matthiessen, J., Lourens, L. J., Pedentchouk, N., Backman, J. & Moran, K. (2006). Subtropical Arctic Ocean temperatures during the Palaeocene/Eocene thermal maximum. *Nature* **441**, 610-613.

- Smith, A. G., Hurley, A. M. & Briden, J. C. (1981). *Phanerozoic Palecontinental World Maps*. Cambridge University Press, Cambridge, 102 pp.
- Smith, A. G., Smith, D. G. & Funnell, B. M. (1994). *Atlas of Mesozoic and Cenozoic Coastlines*. Cambridge University Press, Cambridge, 99 pp.
- Smith, F. A., Wing, S. L. & Freeman, K. H. (2006). Plant biomarker signatures of floral change across the PETM. *Climate & Biota of the Early Paleogene. Volume of Abstracts. Bilbao* 121.
- Spaeth, C., Hoefs, J. & Vetter, U. (1971). Some aspects of isotopic composition of belemnites and related paleotemperatures. *Geological Society of America Bulletin* **82**, 3139-3150.
- Speranza, F., Satolli, S., Mattioli, E. & Calamita, F. (2005). Magnetic stratigraphy of Kimmeridgian-Aptian sections from Umbria-Marche (Italy): New details on the M polarity sequence. *Journal of Geophysical Research - Solid Earth* **110**, Art. No. B12109.
- Spero, H. J., Bijma, J., Lea, D. W. & Bemis, B. E. (1997). Effect of seawater carbonate concentration on foraminiferal carbon and oxygen isotopes. *Nature* **390**, 497-500.
- Spicer, R. A. & Corfield, R. M. (1992). A review of terrestrial and marine climates in the Cretaceous with implications for modelling the 'greenhouse earth'. *Geological Magazine* **129**, 169-180.
- Spicer, R. A. & Parrish, J. T. (1986). Paleobotanical evidence for cool north polar climates in middle Cretaceous (Albian - Cenomanian) time. *Geology* **14**, 703-706.

Spicer, R. A., Ahlberg, A., Herman, A. B., Kelley, S. P., Raikevich, M. I. & Rees, P. M. (2002). Palaeoenvironment and ecology of the middle Cretaceous Grenbenka flora of northeastern Asia. *Palaeogeography, Palaeoclimatology, Palaeoecology* **184**, 65-105.

Steel, R. J., Gjølberg, J. & Haarr, G. (1977). Helvetiafjellet Formation (Barremian) at Festningen, Spitsbergen - A field guide. *Norsk Polarinstitut Årbok 1977*, 111-128.

Stein, A. (1988). Basement controls upon basin development in the Caledonian foreland, NW Scotland. *Basin Research* **1**, 107-119.

Stein, C. L. & Smith, A. J. (1985). Authigenic carbonate nodules in the Nankai Trough, Site 583. *Initial reports of the Deep Sea Drilling Project* **87**, 659-668.

Stein, R., Rullkötter, J. & Welte, D. H. (1986). Accumulation of organic-carbon-rich sediments in the Late Jurassic and Early Cretaceous Atlantic Ocean - a synthesis. *Chemical Geology* **56**, 1-32.

Steuber, T. & Rauch, M. (2005). Evolution of the Mg/Ca ratio of Cretaceous seawater: Implications from the composition of biological low-Mg calcite. *Marine Geology* **217**, 199-213.

Steuber, T., Rauch, M., Masse, J.-P., Graaf, J. & Malkoč, M. (2005). Low-latitude seasonality of Cretaceous temperatures in warm and cold episodes. *Nature* **437**, 1341-1344.

- Stevens, G. R. (1963). Faunal Realms in Jurassic and Cretaceous belemnites. *Geological Magazine* **100**, 481-497.
- Stevens, G. R. (1965a). The Jurassic and Cretaceous belemnites of New Zealand and a review of the Jurassic and Cretaceous belemnites of the Indo-Pacific region. New Zealand Geological Survey, Wellington, 233 pp.
- Stevens, G. R. (1965b). Faunal Realms in Jurassic and Cretaceous belemnites. *Geological Magazine* **102**, 175-178.
- Stevens, G. R. (1967). Upper Jurassic fossils from Ellsworth Land, West Antarctica, and notes on Upper Jurassic biogeography of the South Pacific region. *New Zealand Journal of Geology and Geophysics*. **10**, 345-393.
- Stevens, G. R. (1971). Relationship of isotopic temperatures and faunal realms to Jurassic-Cretaceous palaeogeography, particularly of the S. W. Pacific. *Journal of the Royal Society of New Zealand* **1**, 145-158.
- Stevens, G. R. (1973a). Jurassic belemnites. In Hallam, A. (ed.) Atlas of palaeobiogeography. Elsevier, Amsterdam, 259-274.
- Stevens, G. R. (1973b). Cretaceous belemnites. In Hallam, A. (ed.) Atlas of palaeobiogeography. Elsevier, Amsterdam, 385-401.
- Stevens, G. R. & Clayton, R. N. (1971). Oxygen isotope studies on Jurassic and Cretaceous belemnites from New Zealand and their biogeographic significance. *Journal of Geology and Geophysics* **14**, 829-897.

Stewart, K. R., Embry A. F., Goodarzi, F. & Skibo, D. N. (1992). Evaluation of organic maturity and hydrocarbon source potential of the Ringnes Formation, Sverdrup Basin, Arctic Canada. *Organic Geochemistry* **18**, 317-332.

Stokes, W. L. (1987). Dinosaur gastroliths revisited. *Journal of Paleontology* **61**, 1242-1246.

Stoll, H. M. & Schrag, D. P. (1996). Evidence for glacial control of rapid sea level changes in the Early Cretaceous. *Science* **272**, 1771-1774.

Stoll, H. M. & Schrag, D. P. (2000). High-resolution stable isotope records from the Upper Cretaceous rocks of Italy and Spain: Glacial episodes in a greenhouse planet? *Geological Society of America Bulletin*. **112**, 308-319.

Stoll, H. M., Rosenthal, Y. & Falkowski, P. (2002). Climate proxies from Sr/Ca of coccolith calcite: Calibrations from continuous culture of *Emiliania huxleyi*. *Geochimica et Cosmochimica Acta* **66**, 927-936.

Stolley, E. (1911). Beitrage zur Kenntnie der Cephalopoden der Norddeutschen Unteren Kreide. 1: Die Belemniten der Norddeutschen Unteren Kreide. *Neues Jahrbuch fur Geologie und Palaontologie, Abhandlungen* **10**, 201-272 (in German).

Stolley, E. (1919). Die Systematik der Belemniten. *Jahresbericht des Niedersächsischen Geologischen Vereins* **11** 1-59, (in German).

Suess, E., Balzer, W., Hesse, K-F., Muller, P.J., Ungerer, C. A. & Wefer, G. (1982). Calcium Carbonate Hexahydrate from Organic-Rich Sediments of the Arctic Shelf: Precursors of Glendonites. *Science* **1216**, 1128-1131.

Swainson, I. P. & Hammond, R. P. (2001). Ikaite, $\text{CaCO}_3 \cdot 6\text{H}_2\text{O}$: Cold comfort for glendonites as paleothermometers. *American Mineralogist* **86**, 1530-1533.

Swinerton, H. H. (1936). A monograph of the British Lower Cretaceous belemnites. Palaeontographical Society (Monograph), 86 pp.

Sykes, R. M. (1975). The stratigraphy of the Callovian and Oxfordian stages (Middle-Upper Jurassic) in northern Scotland. *Scottish Journal of Geology* **11**, 51-78.

Sykes, R. M. & Callomon, J. H. (1979). The *Amoeboceras* zonation of the Boreal Upper Oxfordian. *Palaeontology* **22**, 839-903.

Tan, F. C., Hudson, J. D. & Keith, M. L. (1970). Jurassic (Callovian) paleotemperatures from Scotland. *Earth and Planetary Science Letters* **9**, 421-426.

Tanaka, N., Monaghan, M. C. & Rye, D. M. (1986). Contribution of metabolic carbon to mollusc and barnacle shell carbonate. *Nature* **320**, 520-523.

Tankard, A. J. & Balkwill, H. R. (eds). (1989). Extensional Tectonics and Stratigraphy of the North Atlantic Margins. American Association of Petroleum Geologists, Memoirs, 46 pp.

Tarduno, J. A., Brinkman, D. B., Renne, P. R., Cottrell, R. D., Scher, H. & Castillo, P. (1998). Evidence for extreme climatic warmth from Late Cretaceous Arctic vertebrates. *Science* **282**, 2241-2244.

Tarduno, J. A., Cottrell, R. D., Lippert, P. & Friedman, M. (2002). Extreme climates recorded in the Cretaceous High Arctic. *JOI/USSAC Workshop on Cretaceous Climate and Ocean Dynamics, Florissant, Colorado, Abstract Volume*, 76 pp.

Taylor, B. E. & Ward, P. D. (1983). Stable isotopic studies of *Nautilus macromphalus* Sowerby (New Caledonia) and *Nautilus pompilius* L. (Fiji). *Palaeogeography, Palaeoclimatology, Palaeoecology* **41**, 1-16.

Taylor, B. J., Thomson, M. R. A. & Willey, L. E. (1979). The geology of the Ablation Valley - Keystone Cliffs area, Alexander Island. *British Antarctic Survey Scientific Reports* **82**, 64 pp.

Thomas, G. S. P. & Connell, R. J. (1985). Iceberg drop, dump, and grounding structures from Pleistocene glacio-lacustrine sediments, Scotland. *Journal of Sedimentary Petrology* **55**, 243-249.

Thornton, P. R. (1968). Scanning Electron Microscopy. Chapman & Hall, London, 368 pp.

Thrasher, J. (1992). Thermal effect of the Tertiary Cuillins Intrusive Complex in the Jurassic of the Hebrides: an organic geochemical study. In Parnell, J. (ed.) Basins on the Atlantic Seaboard: Petroleum Geology, Sedimentology and Basin Evolution. Special Publication of the Geological Society London, London, 35-49.

Trewin, N. (1988). Use of the Scanning Electron Microscope in Sedimentology. *In* Tucker, M. (ed.) *Techniques in Sedimentology*. Blackwell Scientific Publications, Oxford, 229-273.

Trewin, N. H., Hurst, A., MacDonald, A. C. & Hamilton, R. F. M. (1990). Field Guide No. 8. Jurassic sedimentation and tectonics in the Brora-Helmsdale area, and Old Red Sandstone fluvial and lacustrine facies in N. Scotland. Department of Geology, Petroleum Geology, University of Aberdeen, 88 pp.

Tribovillard, N., Bialkowski, A., Tyson, R. V., Lallier-Vergès, E. & Deconinck, J. F. (2001). Organic facies variation in the Late Kimmeridgian of the Boulonnais area (northernmost France). *Marine and Petroleum Geology* **18**, 371-389.

Turner, J. (1966). The Oxford Clay of Skye, Scalpay and Eigg. *Scottish Journal of Geology* **2**, 243-252.

Tyson, R. V. (1989). Late Jurassic palynofacies trends, Piper and Kimmeridge Clay Formations, UK onshore and northern North Sea. *In* Batten, D. J., & Keen, M. C., (eds) *Northwest European micropalaeontology and palynology*. Ellis Horwood Limited, Chichester, 135-172.

Tyson, R. V. (2004). Variation in marine total organic carbon through the type Kimmeridge Clay Formation (Late Jurassic), Dorset, UK. *Journal of the Geological Society, London* **161**, 667-673.

Underhill, J. R. (1991). Implications of Mesozoic-Recent basin development in the Inner Moray Firth, UK. *Marine & Petroleum Geology* **8**, 359-369.

Urey, H. C. (1947). The thermodynamic properties of isotopic substances. *Journal of the Chemical Society*, 562-581.

Urey, H. C. (1948). Oxygen isotopes in nature and in the laboratory. *Science* **108**, 489-496.

Urey, H. C., Lowenstam, H. A., Epstein, S. & McKinney, C. R. (1951). Measurement of paleotemperatures of the Upper Cretaceous of England, Denmark and the south-eastern United States. *Geological Society of America Bulletin* **62**, 399-416.

Valdes, P. J., Sellwood, B. W. & Price, G. D. (1995). modelling Late Jurassic Milankovitch climate variations. *In* House, R., & Gale, A. S., (eds) *Orbital Forcing Timescales and Cyclostratigraphy*. Geological Society Special Publication, London, 115-132.

van de Schootbrugge, G., Föllmi, K. B., Bulot, L. G. & Burns, S. J. (2000). Paleooceanographic changes during the Early Cretaceous (Valanginian-Hauterivian): Evidence from oxygen and carbon stable isotopes. *Earth and Planetary Science Letters* **181**, 15-31.

van de Water, P. K., Leavitt, S. W. & Betancourt, J. L. (1988). Trends in stomatal density and $^{13}\text{C}/^{12}\text{C}$ ratios of *Pinus flexilis* needles during last glacial-interglacial cycle. *Science* **264**, 239-243.

van Kaam-Peters, H. M. S., Schouten, S., Köster, J. & Sinninghe Damsté, J. S. (1998). Controls on the molecular and carbon isotopic composition of organic matter deposited in

- a Kimmeridgian euxinic shelf sea: Evidence for carbohydrate preservation through sulphurisation. *Geochimica et Cosmochimica Acta* **62**, 3259-3283.
- Veevers, J. J. (2004). Gondwanaland from 650-500 Ma assembly through 320 Ma merger in Pangea to 185-100 Ma breakup: Supercontinental tectonics via stratigraphy and radiometric dating. *Earth Science Reviews* **68**, 1-132.
- Veevers, J. J., Tayton, J. W., Johnson, B. D. & Hansen, L. (1985). Magnetic expression of the continent-ocean boundary between the western margin of Australia and the eastern Indian Ocean. *Journal of Geophysics* **56**, 106-120.
- Veizer, J. (1983). Chemical diagenesis of carbonates: Theory and application of trace element technique. In Arthur, M. A., Anderson, T. F., Kaplan, I. R., Veizer, J. & Land, L. S. (eds) *Stable Isotopes in Sedimentary Geology*. Society of Economic Paleontologists and Mineralogists Short Course Notes, Dallas, 3.1-3.100.
- Veizer, J., Ala, D., Karam, A., Bruckschen, P., Buhl, D., Bruhn, F., Carden, G. A. F., Diener, A., Ebner, F., Godderis, Y., Jasper, T., Korte, C., Pawellek, F., Podlaha, O. G. & Strauss, H. (1999). $^{87}\text{Sr}/^{86}\text{Sr}$, $\delta^{13}\text{C}$ and $\delta^{18}\text{O}$ evolution of Phanerozoic seawater. *Chemical Geology* **161**, 59-88.
- Vincent, E. & Berger, W. H. (1985). Carbon dioxide and polar cooling in the Miocene: the Monterey Hypothesis. In Sundquist, E. T. & Broecker, W. S. (eds) *The Carbon Cycle and Atmospheric CO₂: Natural Variations Archean to Present*. Geophysical monograph. American Geophysical Union, Washington D. C., 455-469.

Vinogradov, V. A., Gramberg, I. S., Pogrebitsky, Y. E., Rabkin, M. I., Ravich, M. G., Sokolov, V. N. & Sorokov, D. S. (1973). Main features of geologic structure and history of North-Central Siberia. *In* Pitcher, M. G. (ed.) *Arctic Geology*. The American Association of Petroleum Geologists, Tulsa, 181-188.

Voigt, S. & Hilbrecht, H. (1997). Late Cretaceous carbon isotope stratigraphy in Europe: Correlation and relations with sea level and sediment stability. *Palaeogeography, Palaeoclimatology, Palaeoecology* **134**, 39-59.

Voigt, S., Wilmsen, M., Mortimore, R. N. & Voigt, T. (2003). Cenomanian palaeotemperatures derived from the oxygen isotope composition of brachiopods and belemnites: evaluation of Cretaceous palaeotemperature proxies. *International Journal of earth Sciences (Geologische Rundschau)* **92**, 285-299.

Vyssotski, A. V., Vyssotski, V. N. & Nezhdanov, A. A. (2006). Evolution of the West Siberian Basin. *Marine and Petroleum Geology* **23**, 93-126.

Wallmann, K. (2004). Impact of atmospheric CO₂ and galactic cosmic radiation on Phanerozoic climate change and the marine delta O-18 record. *Geochemistry, Geophysics, Geosystems* **5**, Article #Q06004.

Waltham, D. & Gröcke, D. R. (2006). Non-uniqueness and interpretation of the seawater ⁸⁷Sr/⁸⁶Sr curve. *Geochimica et Cosmochimica Acta* **70**, 384-394.

Waterston, C. D. (1952). The stratigraphy and palaeontology of the Jurassic rocks of Eathie (Cromarty). *Transactions of the Royal Society of Edinburgh* **62**, 33-51.

- Wefer, G. & Berger, W. H. (1991). Isotope paleontology: growth and composition of extant calcareous species. *Marine Geology* **100**, 207-248.
- Wei, G., Sun, M., Li, X. & Nie, B. (2000). Mg/Ca, Sr/Ca and U/Ca ratios of a porites coral from Sanya Bay, Hainan Island, South China Sea and their relationships to sea surface temperature. *Palaeogeography, Palaeoclimatology, Palaeoecology* **162**, 69-74.
- Weissert, H. (1989). C-isotope stratigraphy, a monitor of paleoenvironmental change: A case study from the Early Cretaceous. *Surveys in Geophysics* **10**, 1-61.
- Weissert, H. & Channell, J. E. T. (1989). Tethyan carbonate carbon isotope stratigraphy across the Jurassic-Cretaceous boundary: An indicator of decelerated global carbon cycling? *Paleoceanography* **4**(4), 483-494.
- Weissert, H. & Erba, E. (2004). Volcanism, CO₂ and palaeoclimate: A Late Jurassic-Early Cretaceous carbon and oxygen isotope record. *Journal of the Geological Society, London* **161**, 695-702.
- Weissert, H. & Lini, A. (1991). Ice age interludes during the time of Cretaceous greenhouse climate? In Müller, D. W., McKenzie, J. A. & Weissert, H. (eds) *Controversies in Modern Geology: Evolution of Geological Theories in Sedimentology, Earth History and Tectonics*. Academic Press Limited, London, 173-192.
- Weissert, H. & Mohr, H. (1996). Late Jurassic climate and its impact on carbon cycling. *Palaeogeography, Palaeoclimatology, Palaeoecology* **122**, 27-43.

Weissert, H., Lini, A., Föllmi, K. B. & Kuhn, O. (1998). Correlation of Early Cretaceous carbon isotope stratigraphy and platform drowning events: A possible link? *Palaeogeography, Palaeoclimatology, Palaeoecology* **137**, 189-203.

Westermann, G. E. G. (1969). Supplement: sexual dimorphism, migration, and segregation in living cephalopods. In Westermann, G. E. G. (ed.) Sexual dimorphism in fossil Metazoa and taxonomic implications. E. Schweizerbart'sche Verlagsbuchhandlung (Nägele u. Obermiller), Stuttgart, 250 pp.

Westermann, G. E. G. (1973). Strength of concave septa and depth limits of fossil cephalopods. *Lethaia* **6**, 383-403.

Whitehouse, F. W. (1924). Dimitobelidae - a new family of Cretaceous belemnites. *Geological Magazine* **61**, 410-416.

Wierzbowski, H. & Joachimski, M. (2006). The carbon and oxygen isotope records of Upper Bajocian-Bathonian calcareous fossils from the Polish Jura Chain. *Volumina Jurassica* **4**, 220-221.

Wierzbowski, A., Coe, A. L., Hounslow, M. W., Matyja, B. A., Ogg, J. G., Page, K. N., Wierzbowski, H. & Wright, J. K. (2006). A potential stratotype for the Oxfordian/Kimmeridgian boundary: Staffin Bay, Isle of Skye. *Volumina Jurassica* **4**.

Wierzbowski, H. (2002). Detailed oxygen and carbon isotope stratigraphy of the Oxfordian in Central Poland. *International Journal of Earth Sciences (Geologische Rundschau)* **91**, 304-314.

Wierzbowski, H. (2004). Carbon and oxygen isotope composition of Oxfordian - Early Kimmeridgian belemnite rostra: Palaeoenvironmental implications for Late Jurassic seas. *Palaeogeography, Palaeoclimatology, Palaeoecology* **203**, 153-168.

Wignall, P. B. & Hallam, A. (1991). Biofacies, stratigraphic distribution and depositional models of British onshore Jurassic black shales. In Tyson, R. V. & Pearson, T. H. (eds) *Modern and Ancient Continental Shelf Anoxia*. Geological Society Special Publications, London, 291-309.

Wignall, P. B. & Pickering, K. T. (1993). Palaeoecology and sedimentology across a Jurassic fault scarp, NE Scotland. *Journal of the Geological Society, London* **150**, 323-340.

Wilkinson, B. H. & Alego, T. J. (1989). Sedimentary carbonate record of calcium-magnesium cycling. *American Journal of Science* **289**, 1158-1194.

Wilson, P. A. & Norris, R. D. (2001). Warm tropical ocean surface and global anoxia during the mid-Cretaceous period. *Nature* **412**, 425-429.

Wilson, P. A., Norris, R. D. & Cooper, M. J. (2002). Testing the Cretaceous greenhouse hypothesis using glassy foraminiferal calcite from the core of the Turonian tropics on Demerara Rise. *Geology* **30**, 607-610.

Woo, K., -S., Anderson, T. F., Railsback, L. B. & Sandberg, P. A. (1992). Oxygen isotope evidence for high-salinity surface seawater in the Mid-Cretaceous Gulf of Mexico: Implications for warm, saline deepwater formation. *Paleoceanography* **7**, 673-685.

- Woodborne, M. W., Rogers, J. & Jarman, N. (1989). The geological significance of kelp-rafted rock along the west coast of South Africa. *Geo-marine Letters* **9**, 109-118.
- Woolfe, K. J. & Francis, J. E. (1991). An Early to Middle Jurassic glaciation - evidence from Allan Hills, Transantarctic mountains. *In* 6th International Symposium on Antarctic Earth Sciences, Japan, 652-653.
- Worsley, D. (1986). Evolution of an Arctic Archipelago. The Geological History of Svalbard. Den Norske Stats Oljeselskap a.s., Stavanger, 121 pp.
- Wortmann, U. G. & Weissert, H. (2000). Timing platform drowning to perturbations of the global carbon cycle with a $\delta^{13}\text{C}_{\text{org}}$ -curve from the Valanginian of DSDP Site 416. *Terra Nova* **12**, 289-294.
- Wright, J. K. (1989). The Early Kimmeridgian ammonite succession at Staffin, Isle of Skye. *Scottish Journal of Geology* **25**, 263-272.
- Wright, J. K. (2001). Staffin. *In* Wright, J. K. & Cox, B. M. (eds) British Upper Jurassic Stratigraphy (Oxfordian to Kimmeridgian). Geological Conservation Review Series No. 21. Joint Nature conservation Committee, Peterborough, 201-210.
- Yasamanov, N. A. (1981). Paleothermometry of Jurassic, Cretaceous, and Paleogene periods of some regions of the USSR. *International Geology Review* **23**, 700-706.
- Young, G. & Bird, J. (1822). A geological survey of the Yorkshire Coast. 1st edition. Whitby, 335 pp.

Young, R. E., Vecchione, M. & Donovan, D. T. (1998). The Evolution of Coleoid Cephalopods and their Present Biodiversity and Ecology. *South African Journal of Marine Science*. **20**, 393-420.

Zakharov, V. A., Baudin, F., Dzyuba, O. S., Daux, V., Zverev, V. V. & Renard, M. (2005). Isotopic and faunal record of high paleotemperatures in the Kinimeridgian of the Subpolar Urals. *Geologiya i Geofizika* **46**, 3-20.

Zakharov, V. A., Bogomolov, Y. I., Ilyina, V. I., Konstantinov, A. G., Kurushin, N. I., Lebedeva, N. K., Meledina, S. V., Nikitenko, B. L., Sobolev, E. S. & Shurygin, B. N. (1997). Boreal zonal standard and biostratigraphy of the Siberian Mesozoic. *Geology and Geophysics, Siberian Branch* **38**, 927-956. (in Russian).

Zeiss, A. (1986). Comments on a tentative correlation chart for the most important marine realms at the Jurassic/Cretaceous boundary. *Acta Geologica Hungarica* **29**, 27-30.

Ziegler, P. A. (1990). Geological Atlas of Western and Central Europe. Shell International Petroleum Maatschappij B. V., The Hague, 239 pp.

Zittel, K. (1895). Gröndzuge der Paläontologie (Palaeozoologie). Leipzig: Druck und Verlag von R. Oldenbourg, München, 971 pp (in German).

Zachos, J., Scott, L. D. & Lohmann, K. C. (1994). Evolution of early Cenozoic marine temperatures. *Paleoceanography* **9**, 3.53-387.

Zonenshain, L. P., Kuzmin, M. I. & Natapov, L. M. (1990). Geology of the USSR: A Plate Tectonic Synthesis. American Geophysical Union, Washington D.C., 242 pp.

APPENDIX 1
SYSTEMATIC PALAEOLOGY

APPENDIX 1. SYSTEMATIC PALAEOLOGY

A1.1. Introduction

The present understanding of Boreal belemnite systematics has been derived largely from the work of Saks & Nal'nyaeva (e.g., 1964, 1966, 1967) and Gustomesov (1964, 1977, 1989). Their interpretation is followed here, although it is worth noting that there has been some considerable disagreement regarding the validity of certain belemnite genera (Doyle & Kelly, 1988) and subgenera (Dzyuba, 2005), particularly within the family Cylindroteuthididae. For example, the position of *Pachyteuthis* and *Acroteuthis* (which have been considered synonymous by several authors) is discussed by Doyle & Kelly (1988) and the status of the genus/subgenus *Simobelus* is considered by Dzyuba (2005). Whilst such problems are acknowledged, the following system (based largely on the work of Saks & Nal'nyaeva (1964, 1966) Gustomesov (1960, 1964) and Doyle & Kelly (1988) has been adopted for the family Cylindroteuthididae:

- Genus: *Acroteuthis* Stolley, 1911

Subgenera: *Acroteuthis* Stolley, 1911; *Boreioteuthis* Saks & Nal'nyaeva, 1966; *Microbelus* Gustomesov, 1958

- Genus: *Cylindroteuthis* Bayle, 1878

Subgenera: *Cylindroteuthis* Bayle, 1878; *Arctoteuthis* Saks & Nal'nyaeva, 1964

- Genus: *Lagonibelus* Gustomesov, 1958

Subgenera: *Lagonibelus* Gustomesov, 1958; *Holcobeloides* Gustomesov, 1958

- Genus: *Pachyteuthis* Bayle, 1878

Subgenera: *Pachyteuthis* Bayle, 1878; *Simobelus* Gustomesov, 1958

The systematic descriptions given below use the terminology outlined by Doyle & Kelly (1988) and Doyle (1990b) (Fig A1.1). Approximate size ranges are indicated by the terms small (<60 mm), medium (60-80 mm) and large (>80 mm). All figures are natural size (x1) and specimens have been photographed in outline (venter forward), right profile (venter to the left) and where appropriate, transverse views (orientated with venter down). Recorded ranges and distributions are taken from Saks & Nal'nyaeva (1964, 1966), Doyle & Kelly (1988) and Mutterlose (1988).

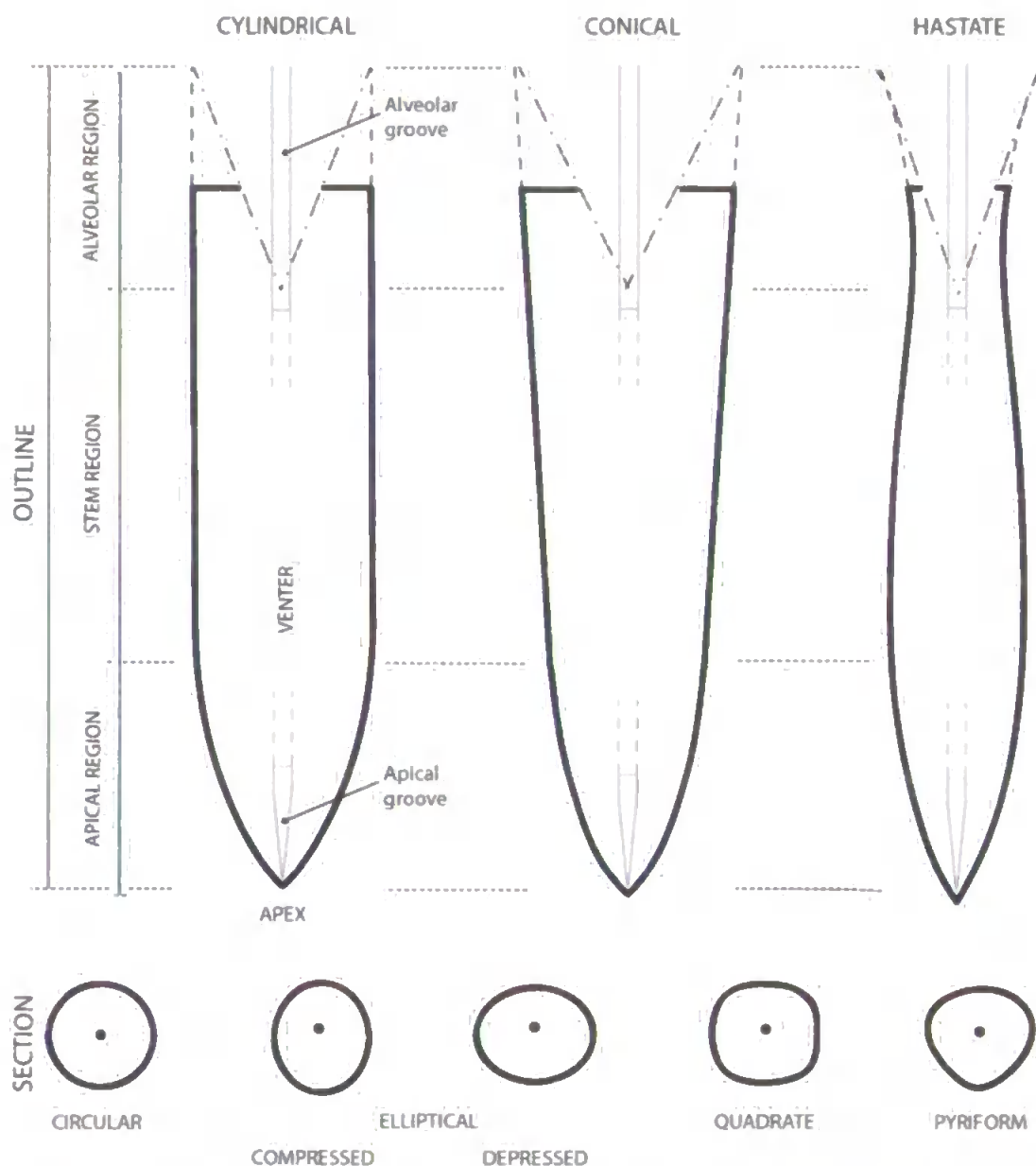


Figure A1.1 Morphological terms employed in the systematic descriptions of belemnite rostra. Adapted after Doyle & Kelly (1988) and Doyle (1990b).

A1.2. Systematic Descriptions

Class CEPHALOPODA Cuvier, 1794

Subclass COLEOIDEA Bather, 1888

Superorder BELEMNOIDEA Hyatt, 1884

Order BELEMNITIDA Zittel, 1895

Suborder BELEMNITINA Zittel, 1895

Family CYLINDROTEUTHIDIDAE Stolley, 1919

Genus *ACROTEUTHIS* Stolley, 1911

Type Species: *Belemnites subquadratus* Roemer, 1836

Diagnosis: (After Doyle & Kelly, 1988) Medium to large size. Robust. Symmetrical, conical to cylindriconeal outline. Profile asymmetrical with flat venter and often moderately inflated dorsum. Apex acute to moderately obtuse. Subquadrate and dorso-ventrally depressed in transverse section. Ventral apical groove short and indistinct, or long and well-defined. Phragmocone is ventrally displaced and penetrates one third to one half of the rostrum. Apical line is cyrtolineate.

Range: Recorded from Volgian to Barremian (Doyle & Kelly, 1988; Mutterlose, 1988).

Distribution: Widespread throughout the Boreal Realm (known from Northwest Europe, East Greenland, North Russia, Arctic Canada, North America, Siberia and Svalbard).

Remarks: There are three subgenera of *Acroteuthis*: *Acroteuthis* s. str., *A. (Boreioteuthis)* and *A. (Microbelus)*. The differences between these subgenera are discussed separately below. *Acroteuthis* differs from *Pachyteuthis* in possessing a generally less inflated

dorsum and a (dorso-ventrally) depressed rather than (laterally) compressed transverse section (Doyle & Kelly, 1988).

Subgenus ***ACROTEUTHIS*** Stolley, 1911

Type Species: *Belemnites subquadratus* Roemer, 1836

Diagnosis: (After Doyle & Kelly, 1988) Robust, cylindriconeal to conical *Acroteuthis*. Ventral apical groove short and indistinct. Subquadrate in transverse section.

Range: Recorded from Volgian to Barremian (Doyle & Kelly, 1988).

Distribution: Widespread throughout the Boreal Realm (known from Northwest Europe, East Greenland, North Russia, Arctic Canada, North America, Siberia and Svalbard).

Remarks: *Acroteuthis* s. str. is distinct from *A. (Boreioteuthis)*, which is more cylindrical with a long and distinct ventral apical groove, and from *A. (Microbelus)*, which is smaller, with weaker dorsal inflation and a more depressed transverse section (Doyle & Kelly, 1988).

***Acroteuthis (Acroteuthis) acrei* Swinnerton, 1936**

Plate 9, Figures 2-3; Plate 10, Figures 1-2.

1936 *Acroteuthis aceri* Swinnerton, p.14, pl. 4, figs 7-8; pl. 5, figs 9-13.

1966 *Acroteuthis (Acroteuthis) acrei* Saks & Nal'nyaeva, p. 119, pl. 29, figs 1-3; pl. 30, fig. 1.

Material: Boyarka River, Lower Valanginian (*Klimovskiensis* Zone) [KH13; Loose A, KH13; Loose B, KH13; 3.45] and Upper Valanginian to Lower Hauterivian (*Bidichotomus* to *Bojarkensis* zones) [KH6-7; Loose].

Description: Large and robust. Symmetrical outline, cylindrical to cylindriconeal. Asymmetrical in profile, with flattened venter, moderately inflated dorsum and some flattening of lateral flanks. Apex acute to moderately obtuse, with short and indistinct lateral groove. Subquadrate and depressed in transverse section. Phragmocone ventrally displaced and penetrates up to one half of the rostrum.

Range: Valanginian (Saks & Nal'nyaeva, 1966).

Remarks: Very similar morphology to *A. (A.) bojarke* Saks & Nal'nyaeva. However, the apex of *A. (A.) bojarke* is more mucronate than that of *A. (A.) acrei*. The specimen shown in Pl. 10, Fig. 2 shares all of the characteristics of *A. (A.) acrei* mentioned in the description above, although it is significantly shorter than the other specimens assigned to this species (97 mm compared with 124-138 mm). Nevertheless it has been identified here as *A. (A.) acrei* as no other species with comparable features and of an appropriate age could be identified.

***Acroteuthis (Acroteuthis) anabarensis* (Pavlow, 1914)**

Plate 8, Figures 2-4;

(*A. (A.)* cf. *anabarensis* - Plate 9, Figure 1.)

1914 *Belemnites (Piesetrobelus) anabarensis* Pavlow, p. 16, pl. 2, figs 1-3.

1966 *Acroteuthis (Acroteuthis) anabarensis* f. *curta* Saks & Nal'nyaeva, p. 103, pl. 24, fig. 4; pl. 25, figs 1-3.

1966 *Acroteuthis (Acroteuthis) anabarensis* f. *sulcatiformis* Saks & Nal'nyaeva, p. 103, pl. 24, figs 1-3; pl. 25, fig. 4.

1966 *Acroteuthis (Acroteuthis) anabarensis* f. *typica* Saks & Nal'nyaeva, p. 103, pl. 23, figs 1-4.

Material: Boyarka River, Lower Valanginian (*Stubendorffi* Zone) [KH18; 10.50]. Izhma River, Volgian (*Maximus* Zone) [PC2.6] and Upper Ryazanian to Valanginian

(*Tzikwinianus* to *Polyptychus* zones) [PC7.a2 B, PC7.c1].

Description: Large and robust. Symmetrical and conical to cylindriconeal in outline. Asymmetrical profile, with flattened venter and weakly inflated dorsum. Apex is obtuse. Apical line weak, but exaggerated by extensive weathering. Subquadrate in transverse section (with flat ventral edge due to flattening). Phragmocone is ventrally deflected and penetrates half-way down the rostrum.

Range: Late Berriasian to Valanginian (Saks & Nal'nyaeva, 1966).

Remarks: The specimen shown in Pl. 9, Fig. 1 (*A. (A.)* cf. *anabarensis*) is morphologically similar to those specimens described here as *A. (A.) anabarensis*, however it is cylindrical rather than conical in outline and is Middle Volgian in age, which is younger than recorded examples of *A. (A.) anabarensis*.

***Acroteuthis (Acroteuthis) arctica* Blüthgen, 1936**

Plate 7, Figure 5; Plate 8, Figure 1.

1936 *Acroteuthis arcticus* Blüthgen, p. 31, pl. 5, figs 4-5.

1966 *Acroteuthis (Acroteuthis) arctica* f. *elata* Saks & Nal'nyaeva, p. 95, pl. 20, figs 5-6; pl. 21, figs 1-3; pl. 22, figs 3-4.

1966 *Acroteuthis (Acroteuthis) arctica* f. *typica* Saks & Nal'nyaeva, p. 95, pl. 21, fig. 4; pl. 22, figs 1-2.

1988 *Acroteuthis (Acroteuthis) arctica* Doyle & Kelly, p. 25, pl. 9, figs 1-8.

Material: Boyarka River, Upper Ryazanian (*Meseshnikowi* Zone) and Lower Valanginian (*Klimovskiensis* Zone) [KH13; 4.35]. Izhma River, Upper Ryazanian to Valanginian (*Tzikwinianus* to *Polyptychus* zones) [PC7.a1].

Description: Large and moderately robust. Symmetrical and cylindric outline. Asymmetrical profile, with flattened venter and weakly inflated dorsum. Moderately acute apex, with indistinct apical groove. Transverse section elliptical and depressed. Phragmocone deflected towards venter and penetrates one third of rostrum.

Range: Late Volgian to Early Valanginian (Saks & Nal'nyaeva, 1966; Doyle & Kelly, 1988).

Acroteuthis (Acroteuthis) lateralis (Phillips, 1835)

Plate 10, Figure 3; Plate 11, Figures 1-3.

1835 *Belemnites lateralis* Phillips, edit. 3, p. 334, pl. 25, fig. 8.

1936 *Acroteuthis lateralis* Swinnerton, pp. 19, pl. 6, figs 3-9; pl. 7, figs 1-2; pl. 8, figs 1-2.

1966 *Acroteuthis (Acroteuthis) lateralis* Saks & Nal'nyaeva, p. 122, pl. 30, fig. 2; pl. 31, figs 1-3.

Material: Izhma River, Lower Valanginian (*Syzranicum* to *Michalskii* zones) [PC9a, PC9 GP22, PC9 GP24 A, PC9 GP24 B].

Description: Medium to large and very robust. Commonly broken between top of apical region and mid-stem. Symmetrical and cylindric to conical in outline. Distinctly asymmetrical in profile, with flattened venter and moderately to strongly inflated dorsum. Moderately acute apex, displaced ventrally. Short, generally indistinct ventral apical groove (although groove can be enhanced in poorly preserved specimens). Transverse section subcircular, except for ventral edge of section which is very straight, due to ventral flattening. Phragmocone strongly displaced towards venter, with deep penetration of the rostrum (up to one half of total length).

Range: Late Volgian to Berriasian of Russia (Saks & Nal'nyaeva, 1966). Valanginian of

the UK (Swinerton, 1936).

Remarks: The specimen shown in Pl. 11, Fig. 3 was assigned to this species despite the lack of apical region for identification. The transverse section (in the stem region) is the correct shape and the specimen is of the same age as the others identified here as *A. (A.) lateralis*. This specimen is the largest specimen collected during this research, and *A. (A.) lateralis* is the most massive of the species identified here.

Genus *CYLINDROTEUTHIS* Bayle, 1878

Type Species: *Belemnites puzosianus* d'Orbigny, 1842

Diagnosis: (After Doyle & Kelly, 1988) Large and elongate. Symmetrical, cylindrical to cylindriconeal outline. Profile, usually symmetrical with venter and dorsum equally inflated. Apex acute to very acute generally with short apical groove (mostly confined to the apex). Weakly to strongly compressed in transverse section. Some species have lateral lines. The phragmocone is moderately to strongly ventrally deflected and penetrates approximately one fifth of the rostrum. Apical line is cyrtolineate or goniolineate.

Range: Recorded from Bathonian to Hauterivian (Doyle & Kelly, 1988; Mutterlose, 1988).

Distribution: Widespread and common throughout the Boreal Realm (known from Northwest Europe, East Greenland, North Russia, Siberia, Svalbard, Arctic Canada, Alaska).

Remarks: There are two subgenera of *Cylindroteuthis*: *Cylindroteuthis* s. str. Bayle and *C. (Arctoteuthis)* Saks & Nal'nyaeva. The differences between these subgenera are discussed

separately below.

Subgenus ***CYLINDROTEUTHIS* Bayle, 1878**

Type Species: *Belemnites puzosianus* d'Orbigny, 1842

Diagnosis: (After Doyle & Kelly, 1988) Moderately elongate. Symmetrical and cylindrical in profile. Venter and dorsum weakly to moderately inflated. Apex acute, with well-developed ventral apical groove. Compressed and subquadrate in transverse section. Apical line cyrtolineate.

Range: Recorded from Bathonian to Valanginian (Doyle & Kelly, 1988).

Distribution: Widespread throughout the Boreal Realm in the Jurassic (Northwest Europe, East Greenland, North Russia, Siberia, Svalbard, Alaska) with numbers decreasing into the Cretaceous, when *C. (Cylindroteuthis)* became restricted to the Arctic Province (Stevens, 1973b; Doyle & Kelly, 1988).

***Cylindroteuthis (Cylindroteuthis) cuspidata* Saks & Nal'nyaeva, 1964**

Plate 4, Figure 8; Plate 5, Figures 1-3.

1964 *Cylindroteuthis (Cylindroteuthis) oweni cuspidata* Saks & Nal'nyaeva, p. 47, pl. 3, figs 1-8.

2004 *Cylindroteuthis (Cylindroteuthis) cuspidata* Dzyuba, p. 83, pl. 1, figs 1-2.

Material: Staffin Bay, Isle of Skye, Lower Callovian to Lower Kimmeridgian (*Koenigi* to *Cymodoce* zones) [SK4; 1.80, SK5; 4.70, SK6; 6.40, SK7; 20.25 A].

Description: Medium to large and elongate. Symmetrical and cylindriconeal to cylindrical in outline. Symmetrical profile. Moderately acute to acute apex, with a short

and weak ventral apical groove (although this groove may be exaggerated in poorly preserved specimens). Subcircular to subquadrate in transverse section.

Range: Middle Oxfordian to Kimmeridgian (Saks & Nal'nyaeva, 1964).

Remarks: Saks & Nal'nyaeva (1964) named a new subspecies of *C. (C.) oweni*, resulting in the designations *C. (C.) oweni oweni* and *C. (C.) oweni cuspidata*. These subspecies were later included within *C. (C.) puzosiana* (previously *C. (C.) oweni oweni*) and *C. (C.) cuspidata* (previously *C. (C.) oweni cuspidata*).

***Cylindroteuthis (Cylindroteuthis) lepida* Saks & Nal'nyaeva, 1964**

Plate 5, Figures 4-9.

1964 *Cylindroteuthis (Cylindroteuthis) lepida* Saks & Nal'nyaeva, p. 59, pl. 6, figs 1-6.

2004 *Cylindroteuthis (Cylindroteuthis) lepida* Dzyuba, p. 166, pl. 3, figs 3-4.

Material: Boyarka River, Lower to Upper Ryazanian (*Kochi* to *Meseshnikowi* zones) [KH17b; 1.35, KH17c; 1.50, KH17c; 2.55]. Staffin Bay, Isle of Skye, Lower Kimmeridgian (*Cymodoce* Zone) [SK6; 7.20, SK6; 7.40, SK6; 7.80].

Description: Medium to large and very elongate. Symmetrical and cylindrical in outline. Symmetrical profile. Some flattening of ventral flanks. Apex very acute, with long, but weak ventral groove (sometimes exaggerated by weathering, particularly in the Skye samples). Subcircular to subquadrate or elliptical (compressed) in transverse section. Shallow penetration of phragmocone.

Range: Volgian to Berriasian (Saks & Nal'nyaeva, 1964).

Remarks: *C. (C.) lepida* is very similar in appearance to *L. (H.) sitnikovi* Saks & Nal'nyaeva. *L. (H.) sitnikovi* is however, slightly less long and slender, with a more strongly developed ventral apical groove than *C. (C.) lepida*. Both species are present throughout the Volgian, although only *C. (C.) lepida* is known to continue into the Berriasian. For these reasons the specimens shown here were assigned to *C. (C.) lepida*.

Pl. 5, Figs 4, 6, 7 show specimens of *C. (C.) lepida* from the Isle of Skye. *C. (C.) lepida* has not been recorded from the Kimmeridgian, but these specimens have been assigned to this species as it is the closest match for the characteristics observed.

Pl. 5, Fig. 9 shows a juvenile specimen which has been tentatively assigned to this species. Although hastate in outline it is very elongate, with an acute apex and long, but faint apical groove. It occurs approximately 2 m below the other examples of *C. (C.) lepida* from the Boyarka River.

Cylindroteuthis (Cylindroteuthis) puzosiana (d'Orbigny, 1842)

Plate 4, Figures 1-7.

1842 *Belemnites puzosianus* d'Orbigny, pl. 16, figs 1-6.

1844 *Belemnites oweni* Pratt in Owen, p. 66, pl. 2, figs 3-4.

1964 *Cylindroteuthis (Cylindroteuthis) oweni oweni* Saks & Nal'nyaeva, pl. 1, figs 4-6; pl. 2, fig. 1.

1991 *Cylindroteuthis (Cylindroteuthis) puzosiana* Page & Doyle, p. 145, pl. 28, figs 1-4.

Material: Staffin Bay, Isle of Skye, Lower Callovian to Lower Kimmeridgian (*Koenigi* to *Cymodoce* zones) [SK3; 1.20, SK4; 11.50, SK5; 4.15, SK5; 4.35, SK6; 1.50, SK6; 6.55, SK8; 33.70].

Description: Large, elongate and slender. Symmetrical and cylindrical in outline. Symmetrical to subsymmetrical profile, with some flattening of venter. Moderately acute to acute apex that is slightly dorsally deflected (and particularly noticeable in juvenile

specimens), with a short and weak ventral apical groove (although this groove may be exaggerated by weathering). Subcircular to elliptical (compressed) in transverse section.

Range: Middle Callovian to Kimmeridgian (Saks & Nal'nyaeva, 1964).

Remarks: This species is very similar to *C. (C.) cuspidata*. *C. (C.) puzosiana*, however, tends to be more elongate and cylindrical rather than cylindriconeal.

The juvenile forms shown in Pl. 4, Figs 4-7 are here identified as *C. (C.)* cf. *puzosiana*. They share the known characteristics of the adult forms, however images of *C. (C.) puzosiana* juveniles are rarely available for comparison.

Subgenus *ARCTOTEUTHIS* Saks & Nal'nyaeva, 1964

Type Species: *Cylindroteuthis septentrionalis* Bodylevsky, 1960

Diagnosis: (After Doyle & Kelly, 1988) Elongate to very elongate. Cylindriconeal to cylindrical outline. Venter and dorsum very weakly inflated. Uncompressed and subcircular or weakly depressed and elliptical in transverse section. Apical grooves absent or weakly developed. Goniolineate apical line.

Range: Recorded from Oxfordian to Hauterivian (Doyle & Kelly, 1988).

Distribution: This species is largely restricted to the Arctic Basin (Siberia, North Russia, Alaska, Arctic Canada, Svalbard). *C. (Arctoteuthis)* developed many new species in the Arctic Province during the Late Volgian, although these were confined to the east of the Urals (Stevens, 1973).

Remarks: The major distinguishing feature of *C. (Arctoteuthis)*, compared with *C.*

(*Cylindroteuthis*), is the absence of a well-developed apical groove.

***Cylindroteuthis (Arctoteuthis) harabyensis* Saks & Nal'nyaeva, 1964**

Plate 3, Figures 2-3.

1964 *Cylindroteuthis (Arctoteuthis) harabyensis* Saks & Nal'nyaeva, p. 80, pl. 15, figs 1-3; pl. 16, figs 1-2.

Material: Boyarka River, Valanginian to Hauterivian (*Bidichotomus* to *Bojarkensis* zones) [KH1-4; 4.10, KH14; 4.30].

Description: Medium and elongate. Symmetrical and cylindriconeal in outline. Slightly to moderately flattened venter and slightly inflated dorsum. Acute apex with short apical groove (confined to apical region). Subcircular and weakly depressed in transverse section.

Range: Valanginian to Early Hauterivian (Saks & Nal'nyaeva, 1964).

***Cylindroteuthis (Arctoteuthis) pachsensis* Saks & Nal'nyaeva, 1964**

Plate 2, Figure 5; Plate 3, Figure 1.

1964 *Cylindroteuthis (Arctoteuthis) pachsensis* Saks & Nal'nyaeva, p. 76, pl. 11, fig. 1; pl. 12, fig. 4.

Material: Boyarka River, Upper Valanginian to Lower Hauterivian (*Bidichotomus* to *Bojarkensis* zones) [KH1-4; Loose, KH1-4; 21.40].

Description: Large and elongate (although relatively robust for *Cylindroteuthis*). Symmetrical and cylindrical to cylindriconeal in outline. Symmetrical profile, with slightly to moderately flattened venter. Acute apex with short apical groove that is often

exaggerated by weathering. Transverse section subcircular and weakly depressed.

Range: Early Hauterivian (Saks & Nal'nyaeva, 1964).

***Cylindroteuthis (Arctoteuthis) porrectiformis* Anderson, 1945**

Plate 1, Figures 1-3; Plate 2, Figures 1-2.

(*C. (A.) cf. porrectiformis* - Plate 2, Figure 3.)

1945 *Cylindroteuthis porrectiformis* Anderson, p. 988, pl. 9, fig. 3.

1964 *Cylindroteuthis (Arctoteuthis) porrectiformis* Saks & Nal'nyaeva, p. 77, pl. 12, figs 1-3; pl. 13, figs 1-2.

2004 *Cylindroteuthis (Arctoteuthis) porrectiformis* Dzyuba, p. 86, pl. 4, figs 1-5.

Material: Boyarka River, Lower to Upper Ryazanian (*Kochi* to *Meseshnikowi* zones) [KH16; 0.90, KH16; 2.45; KH16; 2.80, KH17b; 1.55, KH17c; 2.75]. Izhma River, Lower Valanginian (*Syzranicum* to *Michalskii* zones) [PC9; GP24 C].

Description: Large and very elongate. Symmetrical and cylindrical in outline. Symmetrical profile. Acute to moderately apex with a generally short apical groove, although this is sometimes extended by weathering. Transverse section compressed and elliptical.

Range: Middle Volgian to Early Berriasian (Saks & Nal'nyaeva, 1964).

Remarks: Pl. 2, Fig. 3 shows a specimen that is very like *C. (A.) porrectiformis* in appearance. However this specimen is Valanginian in age, and *C. (A.) porrectiformis* is not known from this time.

***Cylindroteuthis (Arctoteuthis) cf. subporrecta* Bodylevsky, 1960**

Plate 2, Figure 4.

1960 *Cylindroteuthis subporrecta* Bodylevsky, p. 194, pl. 47, fig. 5.

1964 *Cylindroteuthis (Arctoteuthis) subporrecta* Saks & Nal'nyaeva, p. 73, pl. 10, figs 4-5.

1966 *Cylindroteuthis (Arctoteuthis) subporrecta* Saks & Nal'nyaeva, p. 203, pl. 40, fig. 1.

Material: Boyarka River, Valanginian to Hauterivian (*Bidichotomus* to *Bojarkensis* zones)
[KH1-4; 13.00].

Description: Large and elongate. Symmetrical and conical to cylindriconeal in outline. Profile symmetrical. Very acute apex with a short apical groove that is extended by weathering. Subcircular and slightly depressed in transverse section.

Range: Early Hauterivian (Saks & Nal'nyaeva, 1964).

Remarks: This species is represented here by a single, poorly preserved specimen. It is very similar in appearance to *C. (A.) subporrecta* as illustrated in Saks & Nal'nyaeva (1966). However, the Saks & Nal'nyaeva (1966) specimen is very long and elongate (reaching ~225 mm in length). This specimen has been broken off in the stem region. It is, therefore, impossible to estimate how long this specimen would have been and whether it would have reached the length of *C. (A.) subporrecta*. It is also similar in appearance to *C. (A.) porrectiformis*, although the apex is perhaps too acute and the transverse section slightly the wrong shape (slightly depressed rather than elliptical and compressed) to assign this specimen to that species. It has therefore been assigned tentatively to *C. (A.) subporrecta*, which is known to occur in Russia at the appropriate time.

Genus **LAGONIBELUS** Gustomesov, 1958

Type Species: *Belemnites magnificus* d'Orbigny, 1845

Diagnosis: (After Doyle & Kelly, 1988) Medium to large and elongate. Symmetrical and cylindrical to cylindriconeal in outline. Symmetrical in profile and weakly inflated, with central, moderately acute apex. Some taxa have a flattened venter. Depressed and subquadrate to elliptical in transverse section. Moderate to strong ventral apical groove, may continue into stem region (where it broadens substantially). Phragmocone penetrates up to one quarter of the rostrum.

Range: Recorded from Callovian to Hauterivian (Doyle & Kelly, 1988; Mutterlose, 1988).

Distribution: This genus is common in the Boreal-Arctic Province (Siberia, North America, North Russia).

Remarks: There are two subgenera of *Lagonibelus*: *Lagonibelus* s. str. and *L. (Holcobeloides)*. The differences between these genera will be described separately below. *Lagonibelus* can be distinguished from *Cylindroteuthis* by a generally less slender form and more strongly developed apical groove.

Subgenus **LAGONIBELUS** Gustomesov, 1958

Type Species: *Belemnites magnificus* d'Orbigny, 1845

Diagnosis: (After Doyle & Kelly, 1988) Elongate and cylindrical to cylindriconeal outline. Symmetrical and weakly inflated profile, with flat venter. Depressed and quadrate in transverse section. Moderate apical groove.

Range: Recorded from Oxfordian to Hauterivian (Saks & Nal'nyaeva, 1964; Doyle & Kelly, 1988).

Distribution: This subgenus is common in the Boreal-Arctic Province (Siberia, North America, North Russia).

***Lagonibelus (Lagonibelus) gustomesovi* Saks & Nal'nyaeva, 1964**

Plate 7, Figure 4.

(*L. (L.)* cf. *gustomesovi* - Plate 7, Figure 3.)

1964 *Lagonibelus (Lagonibelus) gustomesovi* Saks & Nal'nyaeva, p. 99, pl. 18, figs 1-2; pl. 22, figs 1-4; pl. 23, fig. 1.

Material: Boyarka River, Lower Ryazanian (*Kochi* to *Analogus* zones) [KH16; Loose].
Izhma River, Upper Ryazanian to Valanginian (*Tzikwinianus* to *Polyptychus* zones) [PC7.a2 A].

Description: Large and elongate. Symmetrical and cylindrical outline. Symmetrical profile, with slightly flattened venter and weak dorsal inflation. Apex moderately obtuse, with a short, indistinct ventral groove. Transverse section subcircular.

Range: Late Volgian to Berriasian (Saks & Nal'nyaeva, 1964).

Remarks: The specimen shown in Pl. 7, Fig. 4 was broken off in the stem region. There is no evidence of the alveolus in transverse view and so this specimen must be a minimum of three quarters of the total specimen length.

Pl. 7, Fig. 3 shows a specimen of a very similar morphology to that shown in Pl. 7, Fig. 4, although this specimen is slightly shorter than might be expected for an example of

L. (L.) gustomesovi.

Subgenus **HOLCOBELOIDES** Gustomesov, 1958

Type Species: *Belemnites beaumontianus* d'Orbigny, 1842

Diagnosis: (After Doyle & Kelly, 1988) Medium to large and cylindrical outline. Symmetrical profile, weakly inflated. Depressed, elliptical to quadrate in transverse section. Strong, deep and long apical groove, extending into stem region.

Range: Callovian to Late Volgian (Saks & Nal'nyaeva, 1964; Doyle & Kelly, 1988).

Distribution: This subgenus is common in the Boreal-Arctic Province (Siberia, North America, North Russia).

Remarks: *L. (Holcobeloides)* and *L. (Lagonibelus)* are distinguished primarily by the strength of the apical groove. The groove of *L. (Holcobeloides)* is stronger, deeper and longer than that of *L. (Lagonibelus)*.

***Lagonibelus (Holcobeloides) memorabilis* (Gustomesov, 1964)**

Plate 6, Figure 1.

1964 *Cylindroteuthis (Lagonibelus) memorabilis* Gustomesov, p. 134, pl. 5, figs 4-5.

1964 *Lagonibelus (Holcobeloides) memorabilis* Saks & Nal'nyaeva, p. 120, pl. 27, figs 4-6; pl. 22.

Material: Izhma River, Middle Volgian (*Panderi* Zone) [PC3a B].

Description: Large and elongate. Symmetrical and cylindriconeal in outline. Symmetrical and cylindrical profile, with flattened venter. Very long and deep ventral

groove, extending through the stem and broadening and shallowing towards the alveolar region. Transverse section is elliptical (depressed) to subquadrate. Phragmocone penetrates approximately one fifth of rostrum.

Range: Late Kimmeridgian to Middle Volgian (Saks & Nal'nyaeva, 1964).

Remarks: The specimen shown here is missing the apical region of the rostrum.

***Lagonibelus (Holcobeloides) rosanovi* Gustomesov, 1960**

Plate 7, Figures 1-2.

1960 *Lagonibelus (Holcobeloides) rosanovi* Gustomesov, p. 195, pl. 45, figs 1-2.

1964 *Lagonibelus (Holcobeloides) rosanovi* Gustomesov, p. 130, pl. 5, figs 1-3.

1964 *Lagonibelus (Holcobeloides) rosanovi* Saks & Nal'nyaeva, p. 115, pl. 25, figs 4-5.

Material: Izhma River, Middle Volgian (*Maximus* Zone) [PC2.11 C, PC2.11 F].

Description: Large and elongate. Symmetrical and conical outline. Symmetrical profile, with slightly flattened venter. Very acute apex, with very strong, deep and long ventral groove extending through the stem region until the alveolus. Transverse section reniform in stem region (due to depth of groove) and subquadrate at alveolar region.

Range: Middle Volgian (Saks & Nal'nyaeva, 1964).

Remarks: *L. (H.) rosanovi* is very similar to the species *L. (H.) sitnikovi*, which is of a similar age; both species are recorded from the Volgian. The criteria used to separate the species here are as follows. *L. (H.) rosanovi* is generally longer, but less slender and more conical than *L. (H.) sitnikovi*.

***Lagonibelus (Holcobeloides) sitnikovi* Saks & Nal'nyaeva, 1964**

Plate 6, Figures 2, 4-7.

(*L. (H.)* cf. *sitnikovi* - Plate 6, Figure 3.)

1964 *Lagonibelus (Holcobeloides) sitnikovi* Saks & Nal'nyaeva, p. 122, pl. 28, figs 1-5.

Material: Izhma River, Middle to Upper Volgian (*Maximus* to *Pseudocraspedites* / *Surites* zones) [PC2.4, PC2.11 A, PC2.11 B, PC2.12 B, PC4a]. Boyarka River, Lower Ryazanian (*Kochi* to *Analogus* zones) [KH16; 1.15].

Description: Medium to large. Symmetrical and cylindrical to cylindriconeal outline (although juvenile forms are weakly hastate). Symmetrical profile, with slightly flattened venter. Very acute apex, with strong and deep ventral groove extending from apex to alveolus (groove is very faint or possibly absent at apex tip). Transverse section reniform in stem region (due to depth of groove) and subcircular at alveolar region.

Range: Volgian (Saks & Nal'nyaeva, 1964).

Remarks: The apparent absence of the ventral groove at the apex tip of some specimens might suggest that these specimens should belong to a different genus e.g., *Belemnopsis* rather than *Lagonibelus*. However, unlike *Belemnopsis* these specimens do not possess a reniform transverse section at the alveolar end and (apart from the juvenile forms) are not hastate.

Pl. 6, Fig. 3 shows a poorly preserved specimen, which has been identified as *L. (H.)* cf. *sitnikovi*. The specimen shares the same characteristics as the other *L. (H.) sitnikovi* specimens identified here. It is however, from the Lower Ryazanian, whilst *L. (H.) sitnikovi* has only been identified in the Volgian. The poor preservation prevents an accurate identification.

Genus ***PACHYTEUTHIS*** Bayle, 1878

Type Species: *Belemnites excentralis* Young & Bird, 1822

Diagnosis: (After Doyle & Kelly, 1988) Medium to large and robust. Outline symmetrical and conical to cylindriconeal. Profile is either symmetrical with a central apex, or asymmetrical with a flat venter and ventrally deflected or recurved apex. Ventral apical groove is short and sometimes difficult to distinguish. Moderately compressed and subquadrate or elliptical in transverse section. Phragmocone penetrates one half to two thirds of rostrum. Apical line cyrtolineate.

Range: Recorded from Aalenian to Hauterivian (Doyle & Kelly, 1988; Mutterlose, 1988).

Distribution: This genus is common throughout the Boreal Realm (Northwest Europe, East Greenland, North America, Siberia, North Russia, Svalbard).

Remarks: There are two subgenera of *Pachyteuthis*: *Pachyteuthis* s. str. and *P. (Simobelus)*. The differences between these subgenera will be discussed separately below. *Pachyteuthis* is easily distinguishable from *Cylindroteuthis* and *Lagonibelus*, which are both elongate with little or no inflation of the rostrum.

Subgenus ***PACHYTEUTHIS*** Bayle, 1878

Type Species: *Belemnites excentralis* Young & Bird, 1822

Diagnosis: (After Doyle & Kelly, 1988) Symmetrical and conical outline. Symmetrical or subsymmetrical profile with an acute central apex. Compressed and subquadrate or elliptical in transverse section.

Range: Recorded from Aalenian to Hauterivian (Doyle & Kelly, 1988).

Distribution: This subgenus is common throughout the Boreal Realm in the Jurassic (Northwest Europe, East Greenland, Siberia, North Russia, Svalbard). It is restricted to Siberia and Svalbard from the Early Cretaceous (Doyle & Kelly, 1988), with some endemic species known from Svalbard (Stevens, 1973b).

Remarks: The main identifying characteristic that distinguishes *P. (Pachyteuthis)* from *P. (Simobelus)* is a symmetrical profile. *P. (Pachyteuthis)* is symmetrical in profile, whilst *P. (Simobelus)* is asymmetrical with a flat venter and dorsal inflation.

***Pachyteuthis (Pachyteuthis) acuta* Saks & Nal'nyaeva 1966 (after Blüthgen, 1936)**

Plate 12, Figures 2-3.

(*P. (P.)* cf. *acuta* - Plate 12, Figure 4)

1936 *Acroteuthis johnseni* var. *acuta* Blüthgen, p. 32, pl. 5, figs 9-10.

1966 *Pachyteuthis (Pachyteuthis) acuta* Saks & Nal'nyaeva, p. 36, pl. 5, figs 3-5; pl. 6, fig. 1.

Material: Izhma River, Middle Volgian (*Maximus* Zone) [PC2.11 D, PC2.11 E, PC3 B].

Diagnosis: Large and robust. Outline, symmetrical and cylindriconeal. Subsymmetrical profile, with slightly flattened venter and some dorsal inflation. Central, moderately acute apex, with short, but distinct ventral groove. Transverse section subquadrate to elliptical (compressed).

Range: Late Volgian to Berriasian (Saks & Nal'nyaeva, 1966).

Remarks: *P. (P.) acuta* is morphologically very similar to *P. (P.) apiculata*. The species

have been divided here primarily on the robustness of the rostrum. *P. (P.) acuta* is slightly more robust than *P. (P.) apiculata* and has a slightly less acute apex.

Although this species has not been described in the Middle Volgian (it is only reported from the Upper Volgian onwards), specimens are here assigned to this species, as *P. (P.) acuta* is the closest match for the specimens.

The specimen shown in Pl. 12, Fig. 4 (*P. (P.)* cf. *acuta*) is slightly shorter and stouter than the other specimens of *P. (P.) acuta*.

***Pachyteuthis (Pachyteuthis) apiculata* Saks & Nal'nyaeva, 1966**

Plate 14, Figures 2-3.

1966 *Pachyteuthis (Pachyteuthis) apiculata* Saks & Nal'nyaeva, p. 33, pl. 6, fig. 2; pl. 8, figs 1-3.

2004 *Pachyteuthis (Pachyteuthis) apiculata* Dzyuba, p. 96, pl. 10, figs 4-5.

Material: Izhma River, Middle Volgian (*Maximus* Zone) [PC2.8, PC2.12 A].

Description: Large and robust (although quite slender for *Pachyteuthis*). Outline, symmetrical and cylindrical to cylindriconeal. Subsymmetrical profile, with slightly flattened venter and some dorsal inflation. Central, acute apex, with short, but distinct ventral groove. Transverse section subrounded to subquadrate.

Range: Volgian (Saks & Nal'nyaeva, 1966).

***Pachyteuthis (Pachyteuthis) excentralis* (Young & Bird, 1822)**

Plate 13, Figures 1-4.

(*P. (P.)* cf. *excentralis* - Plate 14, Figure 1.)

1822 *Belemnites excentralis* Young & Bird, edit. 2, p. 275, pl. 14, fig. 4; pl. 15, figs 2, 7.

1964 *Pachyteuthis (Pachyteuthis) excentrica* Gustomesov, p. 158, pl. 12, figs 1-3.

1966 *Pachyteuthis (Pachyteuthis) excentralis* Saks & Nal'nyavea, p. 45, pl. 10, figs 1-3; pl. 12, figs 1-2.

2004 *Pachyteuthis (Pachyteuthis) excentralis* Dzyuba, p. 90, pl. 10, figs 6-7; pl. 11, fig. 1.

Material: Staffin Bay, Isle of Skye, Lower Oxfordian to Lower Kimmeridgian (*Mariae* to *Cymodoce* zones) (SK1; 50.00, SK5, 2.70; SK5, 5.70, SK6; 4.50, SK7; 16.90].

Description: Large and robust rostrum. Symmetrical and cylindriconeal outline. Asymmetrical in profile, with flattened venter and weakly inflated dorsum. Some flattening of lateral flanks on several specimens. Moderately acute to acute central apex, with very short and weak apical groove (sometimes indistinguishable). Transverse section subquadrate to elliptical (compressed).

Range: Oxfordian to Kimmeridgian (Saks & Nal'nyaeva, 1966).

Remarks: *P. (P.) excentralis* has a very similar form to that of *P. (P.) explanata*. These species are both known from throughout the Oxfordian and Kimmeridgian of the Boreal Realm. *P. (P.) explanata* is generally slightly shorter and more robust than *P. (P.) excentralis* and has a more conical outline.

***Pachyteuthis (Pachyteuthis) cf. explanata* (Phillips, 1865)**

Plate 16, Figures 6-7, 9.

1865 *Belemnites explanatus* Phillips, p. 128, pl. 36, fig. 96.

1964 *Pachyteuthis (Pachyteuthis) explanata* Gustomesov, p. 163, pl. 14, figs 2-6.

1966 *Pachyteuthis (Pachyteuthis) explanata* Saks & Nal'nyaeva, p. 42, pl. 7, figs 1-5.

2004 *Pachyteuthis (Boreioteuthis) explanata* Dzyuba, p. 104, pl. 15, fig. 4; pl. 16, figs 1-3, 5, 6.

Material: Staffin Bay, Isle of Skye, Lower Oxfordian to Lower Kimmeridgian (*Cordatum*

to *Cymodoce* zones) [SK1; 60.20, SK3; 5.20, SK3; 5.80].

Description: Medium and robust (although relatively slender for *Pachyteuthis*). Outline symmetrical and cylindriconeal. Profile subsymmetrical with slightly flattened venter and some flattening of lateral flanks. Acute apex, deflected dorsally. Apical groove short and indistinct. Transverse section is elliptical (compressed).

Range: Oxfordian to Early Volgian (Saks & Nal'nyaeva, 1966).

Remarks: The specimens shown here are relatively young specimens and are, therefore, difficult to identify with confidence, as very few published images of comparable specimens exist.

***Pachyteuthis (Pachyteuthis) cf. ingens* Krimholz, 1929**

Plate 12, Figures 1.

1929 *Pachyteuthis ingens* Krimholz, p. 126, pl. 44, figs 1-3.

1966 *Pachyteuthis (Pachyteuthis) ingens* Saks & Nal'nyaeva, p. 59, pl. 11, fig. 1; pl. 12, fig. 3; pl. 13, figs 1-3.

2004 *Lagonibelus (Lagonibelus) ingens* Dzyuba, p. 129, pl. 7, figs 1-2; pl. 8, fig. 4.

Material: Izhma River, Upper Volgian (*Pseudocraspedites* / *Surites* Zone) [PC4].

Description: Large and robust. Symmetrical and cylindriconeal in outline. Subsymmetrical profile, with flattened venter. Apex missing, however short indistinct ventral groove identifiable towards base of stem region. Transverse section subcircular (but with flat ventral edge due to ventral flattening).

Range: Kimmeridgian to Early Volgian (Saks & Nal'nyaeva, 1966).

Remarks: This specimen (Pl. 12, Fig. 1) has been tentatively assigned to *P. (P.) ingens* due to the length and robustness of the stem region of the rostrum. *P. (P.) ingens* is one of very few belemnites to reach this size. *P. (P.) ingens* however is not known from the Upper Volgian. Positive identification is impossible without the apical region.

***Pachyteuthis (Pachyteuthis) panderiana* (d'Orbigny, 1845)**

Plate 14, Figure 4; Plate 15, Figures 1-3.

1845 *Belemnites panderianus* d'Orbigny, p. 423, pl. 30, figs 1-11.

1964 *Pachyteuthis (Pachyteuthis) panderi* Gustomesov, p. 159, pl. 11, figs 1-4.

1966 *Pachyteuthis (Pachyteuthis) panderiana* Saks & Nal'nyavea, p. 30, pl. 4, figs 2-4.

2004 *Pachyteuthis (Pachyteuthis) panderiana* Dzyuba, p. 92, pl. 10, figs 1-3; pl. 13, fig. 5.

Material: Staffin Bay, Isle of Skye, Lower Oxfordian to Lower Kimmeridgian (*Mariae* to *Cymodoce* zones) [SK1; 47.10, SK5; 3.90, SK5; 8.10, SK6; 2.40].

Description: Large and elongate. Symmetrical and conical to cylindriconeal outline. Profile asymmetrical, with slight ventral flattening and dorsal inflation. Apex moderately to very acute and either central or ventrally displaced. Short indistinct apical groove. Subrounded in transverse section.

Range: Oxfordian to Early Kimmeridgian (Saks & Nal'nyaeva, 1966).

Remarks: This species shows considerable morphological variation (as recorded by Gustomesov (1964) and Saks & Nal'nyaeva (1966)), from conical forms with a very acute apex to shorter, cylindrical forms with a less acute apex.

***Pachyteuthis (Pachyteuthis) subrectangulata* (Blüthgen, 1936)**

Plate 15, Figures 4-6; Plate 16, Figures 1-3.

(*P. (P.)* cf. *subrectangulata* - Plate 16, Figures 4-5)

1936 *Acroteuthis subrectangulatus* Blüthgen, p. 35, pl. 6, figs 10-11.

1966 *Pachyteuthis (Pachyteuthis) subrectangulata* Saks & Nal'nyaeva, p. 39, pl. 6, figs 3-6.

Material: Boyarka River, Lower Valanginian (*Klimovskiensis* to *Stubendorffi* zones) [KH13; 2.30, KH18; 7.10]. Izhma River, Upper Valanginian to Lower Hauterivian (*Bidichotomus* to *Bojarkensis* zones) [PC5 C, PC5 D, PC6.2, PC10a A, PC10a B].

Description: Medium to large rostrum. Symmetrical and cylindrical to cylindriconeal outline. Symmetrical in profile, but with a slightly flattened venter. Apex central and moderately acute, with a short and indistinct ventral groove. Subquadrate to elliptical and compressed in transverse section. Phragmocone deflected towards venter.

Range: Berriasian to Early Hauterivian (Saks & Nal'nyaeva, 1966).

Remarks: Several species have similar characteristics to *P. (P.) subrectangulata* e.g., relatively small specimens of *A. (A.) anabarensis*, *A. (A.) arctica* and *P. (P.) acuta*. However the specimens shown here were assigned to the species *P. (P.) subrectangulata* on the basis of robustness (*P. (P.) subrectangulata* is slightly less stout than the others) and their transverse sections, which, if slightly elliptical, are generally compressed rather than depressed (as in *A. (A.) anabarensis*, *A. (A.) arctica* and *P. (P.) acuta*).

***Pachyteuthis (Pachyteuthis) troslayana* (d'Orbigny, 1850)**

Plate 16, Figures 8, 10-11.

1850 *Belemnites troslayanus* d'Orbigny, p. 43.

1966 *Pachyteuthis (Pachyteuthis) troslayana* Saks & Nal'nyaeva, p. 50, pl. 9, figs 5-8.

2004 *Pachyteuthis (Boreioteuthis) troslayana* Dzyuba, p. 102, pl. 14, fig. 5; pl. 15, figs 1-3.

Material: Staffin Bay, Isle of Skye, Upper Oxfordian to Lower Kimmeridgian (*Regulare* to *Cymodoce* zones) [SK5; 5.70 B, SK6; 1.90, SK7; 1.10].

Description: Medium and relatively slender (for *Pachyteuthis*). Symmetrical and cylindrical to cylindriconeal outline. Profile subsymmetrical, with slight flattening of venter. Acute apex, with slight dorsal deflection. Short ventral apical groove. Subrounded in transverse section.

Range: Kimmeridgian (Saks & Nal'nyaeva, 1966).

Pachyteuthis (Pachyteuthis) sp. indet.

Plate 16, Figures 12.

Material: Lower Ryazanian of the Boyarka River (*Kochi* to *Analogus* zones) [KH16; 1.25].

Description: Medium rostrum. Symmetrical and cylindriconeal outline. Subsymmetrical profile. Apex moderately obtuse (although this could be the result of extremely poor preservation). Presence and extent of apical line uncertain. Transverse section subcircular.

Remarks: Although the specimen in Pl. 16, Fig. 12 is very poorly preserved it is possible

to ascertain that it is most probably a young specimen of *P. (Pachyteuthis)*. It is too short and robust to belong to either *Cylindroteuthis* or *Lagonibelus*, but appears to be less robust than *Acroteuthis*. It has little (if any) dorsal inflation so it has been assigned here to *P. (Pachyteuthis)* rather than *P. (Simobelus)*.

Pachyteuthis (Pachyteuthis) sp. indet. juv.

Plate 17, Figures 9-10.

Material: Izhma River, Upper Ryazanian to Upper Valanginian (*Tzikwinianus* to *Bidichotomus* zones) [PC5 A, PC7.c2].

Description: Short and robust. Symmetrical and subcylindrical to weakly hastate in outline. Profile symmetrical and cylindrical, with flattened venter. Apex acute and central, with a very short and indistinct ventral groove. Elliptical (depressed) in transverse section.

Genus *SIMOBELUS* Gustomesov, 1958

Type Species: *Belemnites breviaxis* Pavlow, 1892.

Diagnosis: (After Doyle & Kelly, 1988) Symmetrical and conical outline. Asymmetrical profile, with flat venter and ventrally displaced or recurved apex, often mucronate (with a sharp point). Subquadrate in transverse section.

Range: Recorded from Oxfordian to Hauterivian (Doyle & Kelly, 1988).

Distribution: This subgenus is common throughout the Boreal Realm (Northwest Europe, East Greenland, Arctic Canada, Siberia, North Russia, Svalbard). Some endemic species

are known from the Early Cretaceous of Svalbard (Stevens, 1973b; Doyle & Kelly, 1988).

***Pachyteuthis (Simobelus) cf. breviaxis* (Pavlow, 1892)**

Plate 17, Figure 3.

1892 *Belemnites breviaxis* Pavlow, p. 67, pl. 8, fig. 7.

1964 *Pachyteuthis (Simobelus) breviaxis* Gustomesov, p. 174, pl. 16, figs 2-4.

1966 *Pachyteuthis (Simobelus) breviaxis* Saks & Nal'nyaeva, p. 65, pl. 14, figs 5-6; pl. 15, fig. 1; pl. 19, fig. 4.

2004 *Simobelus (Simobelus) breviaxis* Dzyuba, p. 110, pl. 16, fig. 4; pl. 17, figs 1-3.

Material: Staffin Bay, Isle of Skye, Upper Oxfordian to Lower Kimmeridgian (*Regulare* to *Baylei* zones) [SK7; 20.25 B].

Description: Short and robust. Symmetrical and conical in outline. Asymmetrical profile, with flattened venter and some slight lateral compression. Acute apex, deflected dorsally and with a short and indistinct lateral groove. Elliptical (depressed) in transverse section. Phragmocone deflected ventrally.

Range: Middle Oxfordian to Kimmeridgian (Saks & Nal'nyaeva, 1966).

Remarks: Only one juvenile specimen of this species was recorded, making a positive identification difficult.

***Pachyteuthis (Simobelus) curvula* Saks & Nal'nyaeva, 1966**

Plate 17, Figures 1-2, 4.

1966 *Pachyteuthis (Simobelus) curvula* Saks & Nal'nyaeva, p. 84, pl. 7, fig. 6; pl. 8, figs 4-7.

1988 *Pachyteuthis (Simobelus) cf. curvula* Doyle & Kelly, p. 32, pl. 7, figs 10-12; pl. 8, figs 1-2.

Material: Boyarka River, Upper Ryazanian (*Meseshnikowi* Zone) [KH17b; Loose A, KH17b, Loose B, KH17c; 3.40].

Description: Medium and robust rostrum. Symmetrical and conical outline. Profile asymmetrical, with flattened venter (especially in apical region) and moderately to strongly inflated dorsum. Apex is ventrally displaced and mucronate. No distinguishable apical groove. Subrounded to subquadrate in transverse section. Phragmocone displaced towards venter.

Range: Berriasian (Saks & Nal'nyaeva, 1966).

***Pachyteuthis (Simobelus) insignis* Saks & Nal'nyaeva, 1966**

Plate 17, Figure 5.

1966 *Pachyteuthis (Simobelus) insignis* Saks & Nal'nyaeva, p. 73, pl. 17, figs 2-4; pl. 19, fig. 3.

2004 *Simobelus (Simobelus) insignis* Dzyuba, p. 121, pl. 18, fig. 1; pl. 21, figs 1-6.

Material: Izhma River, Middle Volgian (*Panderi* Zone) [PC3a A].

Description: Medium rostrum. Symmetrical and conical outline. Asymmetrical profile, with some flattening of venter. Strongly flattened laterally. Moderately acute apex with short and indistinct ventral groove. Subquadrate and compressed in transverse section.

Range: Volgian (Saks & Nal'nyaeva, 1966).

Suborder BELEMNOPSEINA Jeletzky, 1965

Family BELEMNOPSEIDAE Naef, 1922

Genus **BELEMNOPSIS** Bayle, 1878

Type Species: *Belemnites bessinus* d'Orbigny, 1942.

Diagnosis: (After Page & Doyle, 1991) Small to medium, slender and elongate. Outline symmetrical and hastate (sometimes weakly hastate). Cylindrical profile with acute apex. Depressed and reniform (kidney-shaped) in transverse section. Deep ventral groove, emanating in alveolar region and broadening towards apex. Very shallow penetration of phragmocone.

Range: Recorded from Toarcian to Valanginian (Mutterlose, 1988).

Distribution: This genus is widespread in the Indo-Pacific region from the Aalenian (Africa, India, Indonesia, New Zealand, Australia, Antarctica). Only recorded in the Boreal and Mediterranean regions until the Middle Oxfordian (Mutterlose 1988).

Remarks: Both *Belemnopsis* and *Lagonibelus* possess a long and deep ventral groove. They are easily distinguished, however, as the groove in *Belemnopsis* is present in the alveolar region and dies out towards the apex, whilst the reverse occurs in *Lagonibelus*.

***Belemnopsis* cf. *depressa* (Quenstedt, 1848)**

Plate 17, Figure 6.

1848 *Belemnites depressa* Quenstedt.

1991 *Belemnopsis depressa* Page & Doyle, p. 148, pl. 29, figs 3-4.

Material: Staffin Bay, Isle of Skye, Lower to Upper Callovian (*Koenigi* to *Lamberti* zones) [SK4; 10.50].

Description: Medium, elongate rostrum. Symmetrical and weakly hastate in outline. Cylindrical profile with acute apex. Strong and deep ventral alveolar groove, extending through stem region and shallowing towards the apex (where it disappears). Subquadrate and reniform in transverse section.

Range: Callovian (Page & Doyle, 1991).

Remarks: This specimen is very similar morphologically to *B. depressa*, although perhaps with a slightly more acute apex, and slightly weaker hastate form (however this may be within the variability of the species). *B. depressa* is common in the Middle Callovian of the Oxford Clay (e.g., Wiltshire and Cambridgeshire).

Genus *HIBOLITHES* Montford, 1808

Type Species: *Hibolithes hastata* Montford, 1808.

Diagnosis: (After Doyle & Kelly, 1988) Small to large, slender and elongate. Symmetrical and hastate in outline and profile. Maximum inflation in apical region, from which flanks converge towards the alveolus. Acute, obtuse or rounded apex. Normally circular in transverse section. Prominent ventral alveolar groove (does not reach apex). Phragmocone penetrates up to one fifth of the rostrum. Apical line is ortholineate.

Range: Recorded from Bajocian to Aptian (Doyle & Kelly, 1988; Mutterlose, 1988).

Distribution: This genus is common in the Tethyan Realm (South and Central Europe,

East Africa, Antarctica, South America, Australasia and India), with some Boreal Realm incursions (particularly in the Early Cretaceous) (Mutterlose, *et al.* 1983).

Remarks: The flanks of *Hibolithes* converge strongly towards the alveolus, whilst those of *Belemnopsis* do not. *Belemnopsis* also has a much stronger and deeper alveolar groove than *Hibolithes*. This strong groove gives *Belemnopsis* its reniform appearance in transverse section, compared with the generally circular transverse appearance of *Hibolithes*. *Belemnopsis* is therefore easily distinguished from *Hibolithes*, by shape and alveolar groove.

(?)*Hibolithes* sp. juv.

Plate 17, Figures 7-8.

Material: Staffin Bay, Isle of Skye, Lower to Middle Oxfordian (*Cordatum* to *Tenuiserratum* zones) [SK2; 2.80, SK8; 39.40].

Description: Small and slender rostrum. Symmetrical and hastate outline. Symmetrical and weakly hastate in profile, with a bulbous stem and apical region. Apex is central and acute. Faint alveolar groove present in the specimen shown in Pl. 17, Fig. 8 (does not extend past the middle of the stem region), but absent in the smaller specimen. Elliptical (depressed) in transverse section.

Remarks: These obviously juvenile forms have been assigned to the genus *Hibolithes* on the basis of their hastate form, and in the case of the specimen illustrated in Pl. 17, Fig. 8 evidence of a faint alveolar groove. It is impossible to confirm the identify of these specimens beyond genus level due to their small size (< 34 mm). However it is worth noting that *H. hastata* (Montford) is frequently recorded from the Upper Callovian and

Lower Oxfordian of the Oxford Clay (e.g., Cambridgeshire).

Belemnite gen. et sp. indet. juv. 1

Plate 17, Figure 11.

Material: Izhma River, Middle Volgian (*Maximus* Zone) [PC2.3].

Description: Small and robust. Symmetrical and cylindrical in both outline and profile. Flattened venter, plus some flattening of lateral flanks. Apex acute and slightly deflected ventrally. Short and indistinct ventral apical groove. Transverse section subquadrate to elliptical (compressed).

Remarks: This species is possibly a juvenile of *P. (Pachyteuthis)* based on the following features: The rostrum is robust and symmetrical in profile, with a short and indistinct apical groove and a slightly compressed transverse section.

Belemnite gen. et sp. indet. juv. 2

Plate 17, Figure 12.

Material: Izhma River, Upper Ryazanian to Valanginian (*Tzikwinianus* to *Polyptychus* zones) [PC7.c8].

Description: Small and robust rostrum. Outline symmetrical and cylindric conical to conical. Profile symmetrical and conical. Apex moderately obtuse (probably due to poor preservation). Transverse section subcircular with a flat ventral edge (due to flattening of the venter).

Remarks: The robust rostrum with flattened venter and depressed transverse section suggest that this specimen may be an *Acroteuthis* juvenile.

Belemnite gen. et sp. indet. juv. 3

Plate 17, Figure 13.

Material: Izhma River, Middle Volgian (*Panderi* Zone) [PC3 A].

Description: Small and moderately robust to elongate rostrum. Outline and profile both symmetrical and cylindrical. Flattened venter. Acute central apex with short and indistinct ventral apical groove. Lateral grooves present. Transverse section elliptical (depressed).

Remarks: This specimen is too slender to be *Acroteuthis*, although it may be *Pachyteuthis* or *Cylindroteuthis*. The presence of distinct lateral grooves may suggest that this is a *Cylindroteuthis* juvenile. This is possibly the same species as that shown in Pl. 17, Fig. 16 (Belemnite gen. et sp. indet. juv. 6).

Belemnite gen. et sp. indet. juv. 4

Plate 17, Figure 14.

Material: Izhma River, Upper Valanginian to Lower Hauterivian (*Bidichotomus* to *Bojarkensis* zones) [PC10].

Description: Small and robust. Symmetrical and hastate in outline. Profile asymmetrical and hastate. Maximum inflation at base of stem region. Apex strongly recurved. No ventral groove (apical or alveolar) identifiable. Faint lateral grooves present. Elliptical (depressed) in transverse section.

Remarks: This form is similar in appearance to the juvenile form of *Mesoteuthis tiungensis* (Saks). However, *M. tiungensis* has only been recorded from the Toarcian in Russia (Saks & Nal'nyaeva, 1975).

Belemnite gen. et sp. indet. juv. 5

Plate 17, Figure 15.

Material: Staffin Bay, Isle of Skye, Upper Oxfordian (*Serratum* to *Regulare* zones) [SK10; 12.70].

Description: Small and slender. Symmetrical and weakly hastate in both outline and profile. Maximum inflation at apical region. Acute central apex, with very short and faint ventral groove. Circular in transverse section.

Remarks: This specimen is too slender to be *Acroteuthis*, although it may be a *Pachyteuthis* or *Cylindroteuthis* juvenile. Due to the slenderness of the specimens *Cylindroteuthis* seems the more likely determination.

Belemnite gen. et sp. indet. juv. 6

Plate 17, Figure 16.

Material: Izhma River, Middle Volgian (*Maximus* Zone) [PC2.14].

Description: Very small rostrum. Outline, symmetrical and subcylindrical to very weakly hastate. Profile cylindrical. Acute apex. No ventral groove visible. Transverse section subcircular.

Remarks: This is possible the same species as the specimen shown in Pl. 17, Fig. 13.

Both specimens are from the Middle Volgian of the Izhma River.

CRETACEOUS										SPECIES				
LOWER														
Period	STAGE				STAGE									
	Stage	Ammonite Zone	Stage	Ammonite Zone	Stage	Ammonite Zone	Stage	Ammonite Zone						
LOWER	Hauterivian	Lower	regalis	Hauterivian	Lower	polyptichoides	Hauterivian	Lower		A. (A.) aceti Swin				
		Lower	nordicum		Hauterivian	Lower		bojarkensis	Hauterivian	Lower		A. (A.) embaerensis (Per.)		
		Lower	amblygonium			Hauterivian		Lower		iranovi	Hauterivian	Lower		A. (A.) cf. embaerensis (Per.)
		Lower	pithei					Hauterivian		Lower			Hauterivian	Lower
	Valanginian	Upper	Dichotomites	Valanginian			Upper			bidichotomus		Valanginian		Upper
		Upper	Polypylchites		Valanginian		Upper			Valanginian				Upper
		Lower	Paratella			Valanginian	Lower		polypt. + sub.		Valanginian			Lower
		Lower	astierphychus				Valanginian	Lower	quadrifidus				Valanginian	Lower
	Upper	albidum	Ryazanian	Upper				kimovskensis	Ryazanian			Upper		
	Upper	stenomphalus		Ryazanian	Upper			trikvirianus		Ryazanian		Upper		
	Lower	kozhi			Ryazanian	Lower		kozhi			Ryazanian	Lower		
	Lower	rundani				Ryazanian	Lower	Pseudoceras / Sudas				Ryazanian	Lower	
UPPER	Portlandian	Upper	lampughii				Portlandian	Upper	nodiger				Portlandian	Upper
		Upper	proplanorbatus	Portlandian				Upper	subditus	Portlandian				Upper
		Lower	primivus		Portlandian			Lower	fulgens		Portlandian			Lower
		Lower	oppressus			Portlandian		Lower	oppressus			Portlandian		Lower
	Kimmeridgian	Upper	herbertus				Kimmeridgian	Upper	nikitini				Kimmeridgian	Upper
		Upper	pluviosus	Kimmeridgian				Upper	virgatus +	Kimmeridgian				Upper
		Lower	clausenianus		Kimmeridgian			Lower	maximus		Kimmeridgian			Lower
		Lower	ebani			Kimmeridgian		Lower	panderi			Kimmeridgian		Lower
	Oxfordian	Upper	ebani - pers				Oxfordian	Upper	pseudocyclon				Oxfordian	Upper
		Upper	ebani - pers	Oxfordian				Upper	ebani - pers	Oxfordian				Upper
		Lower	ebani - pers		Oxfordian			Lower	ebani - pers		Oxfordian			Lower
		Lower	ebani - pers			Oxfordian		Lower	ebani - pers			Oxfordian		Lower
Kimmeridgian	Upper	eudorus	Kimmeridgian				Upper	eudorus	Kimmeridgian				Upper	
	Lower	mutabilis		Kimmeridgian			Lower	mutabilis		Kimmeridgian			Lower	
	Upper	cymodoce			Kimmeridgian		Upper	kitchini			Kimmeridgian		Upper	
	Lower	beylei				Kimmeridgian	Lower					Kimmeridgian	Lower	

Figure A1.2 Stratigraphical and geographical ranges of the belemnite species recorded in this study. Key to colours: Staffin Bay, Isle of Skye (blue); Boyarka River, Yenisei-Khatanga Basin, Siberia (red); Izhma River, Timan-Pechora Basin, Russia (green).

PLATES A1-17

All figures are natural size (x1) and specimens have been coated with ammonium chloride. Specimens have been photographed in outline (venter forward), right profile (venter to the left) and where appropriate, transverse views (orientated with venter down). Specimen numbers prefixed by the letters KH, PC and SK refer to specimens collected from the Boyarka River, Izhma River and Staffin Bay respectively. Specimens from Helmsdale (HL) and Svalbard (FS and JS) were not suitable for inclusion here.

PLATE A1.

1. *Cylindroteuthis (Arctoteuthis) porrectiformis* Anderson, 1945. (a) ventral outline, (b) right profile, (c) transverse section. Lower Ryazanian, *Kochi* to *Analogus* Zone material, Boyarka River, Siberia. (KH 16; 0.90)

2. *Cylindroteuthis (Arctoteuthis) porrectiformis* Anderson, 1945. (a) ventral outline, (b) right profile, (c) transverse section. Lower Ryazanian, *Kochi* to *Analogus* Zone material, Boyarka River, Siberia. (KH 16; 2.45)

3. *Cylindroteuthis (Arctoteuthis) porrectiformis* Anderson, 1945. (a) ventral outline, (b) right profile, (c) transverse section. Upper Ryazanian, *Meseshnikowi* Zone, Boyarka River, Siberia. (KH 17c; 2.75)



PLATE A2.

1. *Cylindroteuthis (Arctoteuthis) porrectiformis* Anderson, 1945. (a) ventral outline, (b) right profile. Upper Ryazanian, *Meseshnikowi* Zone, Boyarka River, Siberia. (KH 17b; 1.55)
2. *Cylindroteuthis (Arctoteuthis) (?)porrectiformis* Anderson, 1945. (a) ventral outline, (b) right profile. Lower Ryazanian, *Kochi* to *Analogus* Zone material, Boyarka River, Siberia. (KH 16; 2.80)
3. *Cylindroteuthis (Arctoteuthis) cf. porrectiformis* Anderson, 1945. (a) ventral outline, (b) right profile, (c) transverse section. Lower Valanginian, *Syzranicum* to *Michalskii* Zone material, Izhma River, Russia (PC9; GP24 C)
4. *Cylindroteuthis (Arctoteuthis) cf. subporrecta* Bodylevsky, 1960. (a) ventral outline, (b) right profile. Upper Valanginian or Lower Hauterivian, *Bidichotomus* to *Bojarkensis* Zone material, Boyarka River, Siberia. (KH1-4; 13.00)
5. *Cylindroteuthis (Arctoteuthis) pachsisensis* Saks & Nal'nyaeva, 1964. (a) ventral outline, (b) right profile, (c) transverse section. Upper Valanginian or Lower Hauterivian, *Bidichotomus* to *Bojarkensis* Zone material, Boyarka River, Siberia. (KH 1-4; 21.40)



PLATE A3.

1. *Cylindroteuthis (Arctoteuthis) pachsensis* Saks & Nal'nyaeva, 1964. (a) ventral outline, (b) right profile, (c) transverse section. Upper Valanginian or Lower Hauterivian, *Bidichotomus* to *Bojarkensis* Zone material, Boyarka River, Siberia. (KH 1-4; Loose)

2. *Cylindroteuthis (Arctoteuthis) harabyensis* Saks & Nal'nyaeva, 1964. (a) ventral outline, (b) right profile, (c) transverse section. Upper Valanginian or Lower Hauterivian, *Bidichotomus* to *Bojarkensis* Zone material, Boyarka River, Siberia. (KH 1-4; 4.30)

3. *Cylindroteuthis (Arctoteuthis) harabyensis* Saks & Nal'nyaeva, 1964. (a) ventral outline, (b) right profile, (c) transverse section. Upper Valanginian or Lower Hauterivian, *Bidichotomus* to *Bojarkensis* Zone material, Boyarka River, Siberia. (KH 1-4; 4.10)

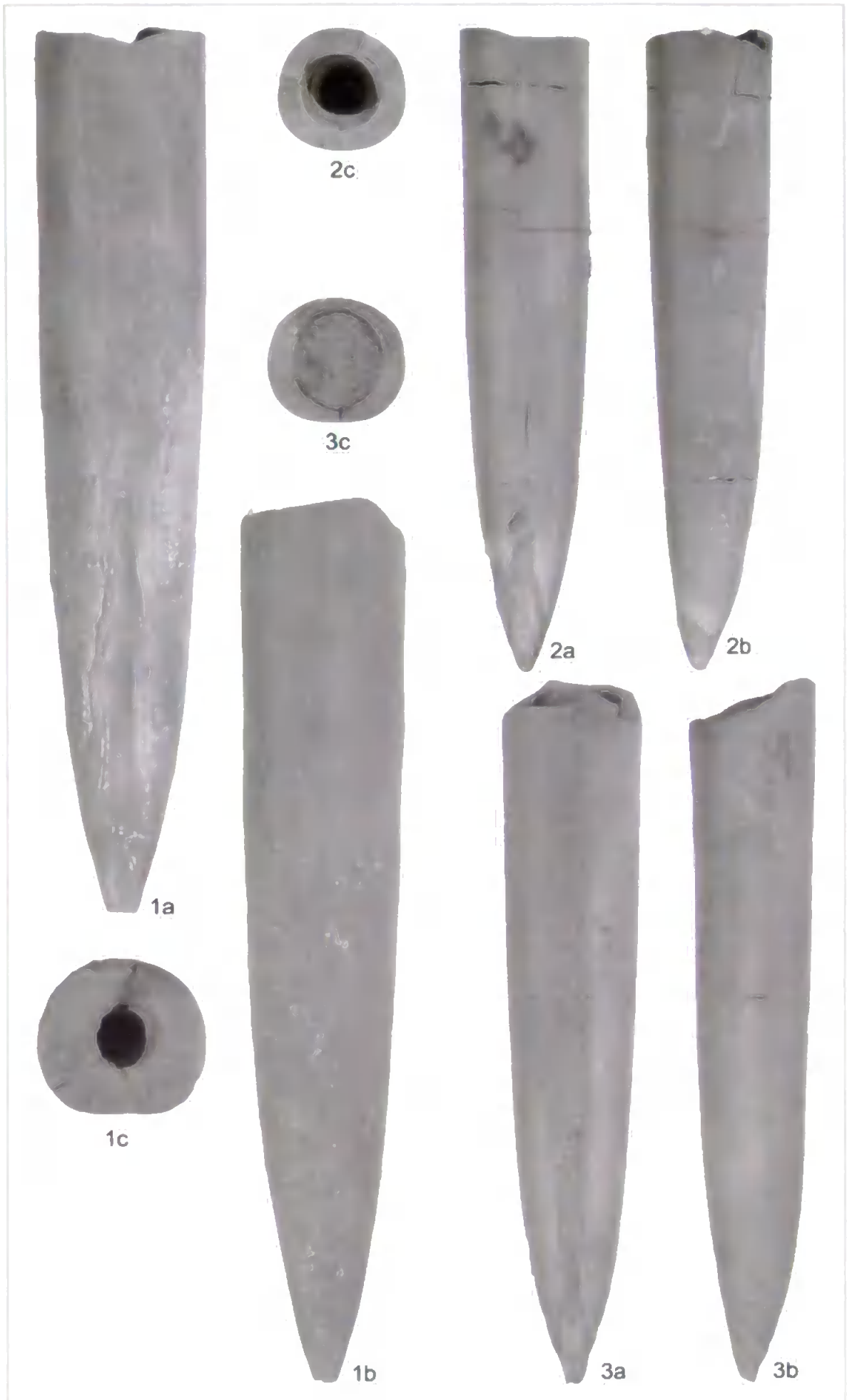


PLATE A4.

1. *Cylindroteuthis (Cylindroteuthis) puzosiana* (d'Orbigny, 1842). (a) ventral outline, (b) right profile. Lower Kimmeridgian, *Cymodoce* Zone, Staffin Bay, UK. (SK6; 6.55)
2. *Cylindroteuthis (Cylindroteuthis) puzosiana* (d'Orbigny, 1842). (a) ventral outline, (b) right profile, (c) transverse section. Callovian, *Koenigi* to *Lamberti* Zone material, Staffin Bay, UK. (SK4; 11.50)
3. *Cylindroteuthis (Cylindroteuthis) puzosiana* (d'Orbigny, 1842). (a) ventral outline, (b) right profile, (c) transverse section. Lower or Middle Oxfordian, *Cordatum* to *Densiplicatum* Zone material, Staffin Bay, UK. (SK3; 1.20)
4. *Cylindroteuthis (Cylindroteuthis) puzosiana* (d'Orbigny, 1842). (a) ventral outline, (b) right profile. Lower Kimmeridgian, *Baylei* to *Cymodoce* Zone material, Staffin Bay, UK. (SK5; 4.15)
5. *Cylindroteuthis (Cylindroteuthis) puzosiana* (d'Orbigny, 1842). (a) ventral outline, (b) right profile. Lower Oxfordian, *Cordatum* Zone, Staffin Bay, UK. (SK8; 33.70)
6. *Cylindroteuthis (Cylindroteuthis) puzosiana* (d'Orbigny, 1842). (a) ventral outline, (b) right profile. Lower Kimmeridgian, *Cymodoce* Zone, Staffin Bay, UK. (SK6; 1.50)
7. *Cylindroteuthis (Cylindroteuthis) puzosiana* (d'Orbigny, 1842). (a) ventral outline, (b) right profile, (c) transverse section. Lower Kimmeridgian, *Baylei* to *Cymodoce* Zone material, Staffin Bay, UK. (SK5; 4.35)

8. *Cylindroteuthis* (*Cylindroteuthis*) *cuspidata* Saks & Nal'nyaeva, 1964. (a) ventral outline, (b) right profile. Upper Oxfordian or Lower Kimmeridgian, *Regulare* to *Baylei* Zone material, Staffin Bay, UK. (SK7; 20.25 A)



PLATE A5.

1. *Cylindroteuthis (Cylindroteuthis) cuspidata* Saks & Nal'nyaeva, 1964. (a) ventral outline, (b) right profile, (c) transverse section. Lower Kimmeridgian, *Cymodoce* Zone, Staffin Bay, UK. (SK6; 6.40)
2. *Cylindroteuthis (Cylindroteuthis) cuspidata* Saks & Nal'nyaeva, 1964. (a) ventral outline, (b) right profile, (c) transverse section. Callovian, *Koenigi* to *Lamberti* Zone material, Staffin Bay, UK. (SK4; 1.80)
3. *Cylindroteuthis (Cylindroteuthis) cuspidata* Saks & Nal'nyaeva, 1964. (a) ventral outline, (b) right profile. Lower Kimmeridgian, *Baylei* to *Cymodoce* Zone material, Staffin Bay, UK. (SK5; 4.70)
4. *Cylindroteuthis (Cylindroteuthis) lepida* Saks & Nal'nyaeva, 1964. (a) ventral outline, (b) right profile, (c) transverse section. Lower Kimmeridgian, *Cymodoce* Zone, Staffin Bay, UK. (SK6; 7.40)
5. *Cylindroteuthis (Cylindroteuthis) lepida* Saks & Nal'nyaeva, 1964. (a) ventral outline, (b) right profile, (c) transverse section. Upper Ryazanian, *Meseshnikowi* Zone, Boyarka River, Siberia. (KH17c; 2.55)
6. *Cylindroteuthis (Cylindroteuthis) lepida* Saks & Nal'nyaeva, 1964. (a) ventral outline, (b) right profile. Lower Kimmeridgian, *Cymodoce* Zone, Staffin Bay, UK. (SK6; 7.80)
7. *Cylindroteuthis (Cylindroteuthis) lepida* Saks & Nal'nyaeva, 1964. (a) ventral outline, (b) right profile. Lower Kimmeridgian, *Cymodoce* Zone, Staffin Bay, UK. (SK6; 7.20)

8. *Cylindroteuthis (Cylindroteuthis) lepida* Saks & Nal'nyaeva, 1964. (a) ventral outline, (b) right profile. Upper Ryazanian, *Meseshnikowi* Zone, Boyarka River, Siberia. (KH17c; 1.50)

9. *Cylindroteuthis (Cylindroteuthis) (?)lepida* juv. Saks & Nal'nyaeva, 1964. (a) ventral outline, (b) right profile. Upper Ryazanian, *Meseshnikowi* Zone, Boyarka River, Siberia. (KH17b; 1.35)

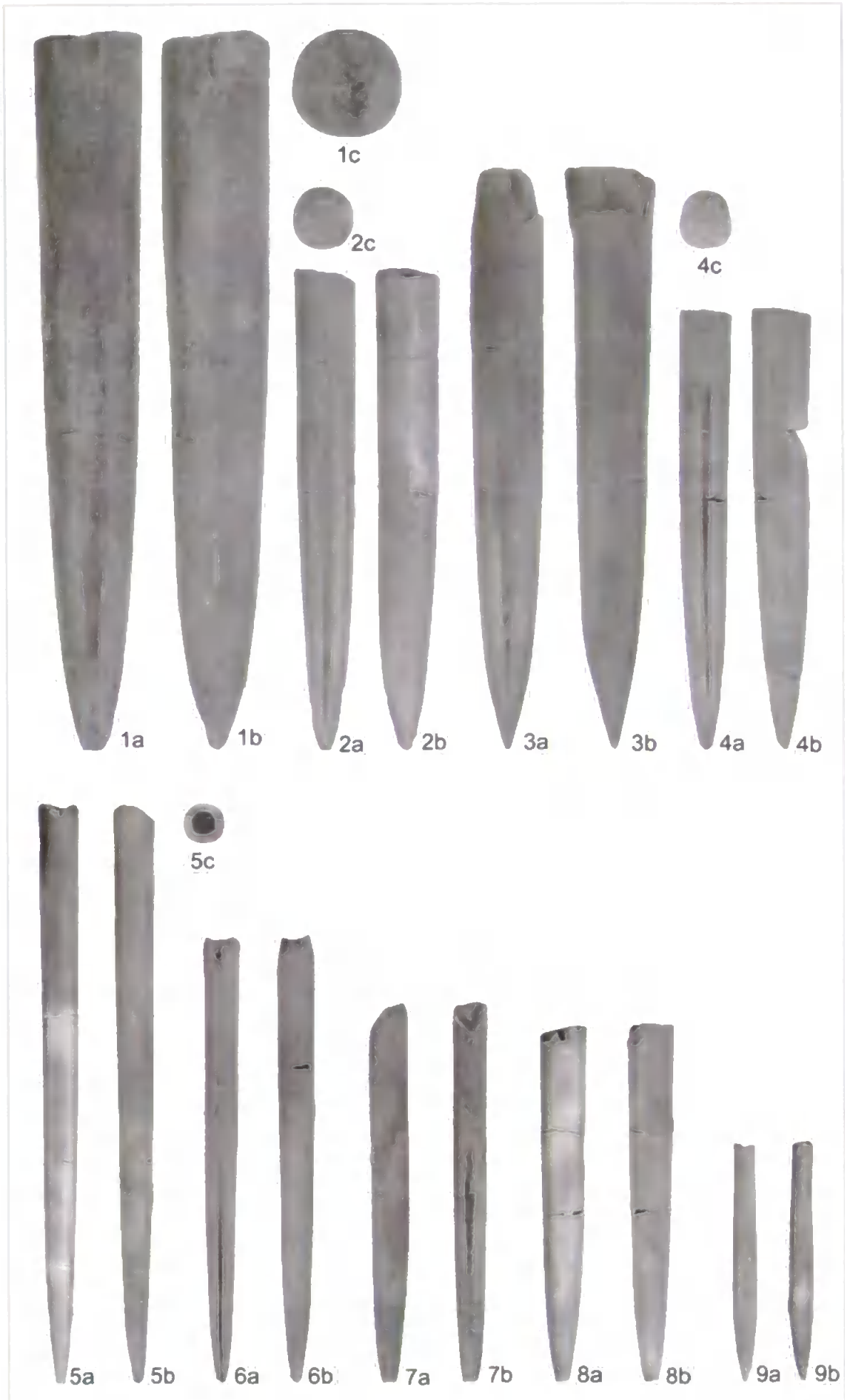


PLATE A6.

1. *Lagonibelus (Holcobeloides) memorabilis* (Gustomesov, 1964). (a) ventral outline, (b) right profile, (c) transverse section. Middle Volgian, *Panderi* Zone, Izhma River, Russia. (PC3a B)

2. *Lagonibelus (Holcobeloides) sitnikovi* Saks & Nal'nyaeva, 1964. (a) ventral outline, (b) right profile, (c) transverse section. Middle Volgian, *Maximus* Zone, Izhma River, Russia. (PC2.12 B)

3. *Lagonibelus (Holcobeloides)* cf. *sitnikovi* Saks & Nal'nyaeva, 1964. (a) ventral outline, (b) right profile. Lower Ryazanian, *Kochi* to *Analogus* Zone material, Boyarka River, Siberia. (KH16; 1.15)

4. *Lagonibelus (Holcobeloides) sitnikovi* Saks & Nal'nyaeva, 1964. (a) ventral outline, (b) right profile, (c) transverse section. Middle Volgian, *Maximus* Zone, Izhma River, Russia. (PC2.11 B)

5. *Lagonibelus (Holcobeloides) sitnikovi* Saks & Nal'nyaeva, 1964. (a) ventral outline, (b) right profile, (c) transverse section. Upper Volgian, *Subditus* Zone, Izhma River, Russia. (PC4a)

6. *Lagonibelus (Holcobeloides) sitnikovi* Saks & Nal'nyaeva, 1964. (a) ventral outline, (b) right profile. Middle Volgian, *Maximus* Zone, Izhma River, Russia. (PC2.11 A)

7. *Lagonibelus (Holcobeloides) sitnikovi* Saks & Nal'nyaeva, 1964. (a) ventral outline, (b) right profile, (c) transverse section. Middle Volgian, *Maximus* Zone, Izhma River, Russia. (PC2.4)

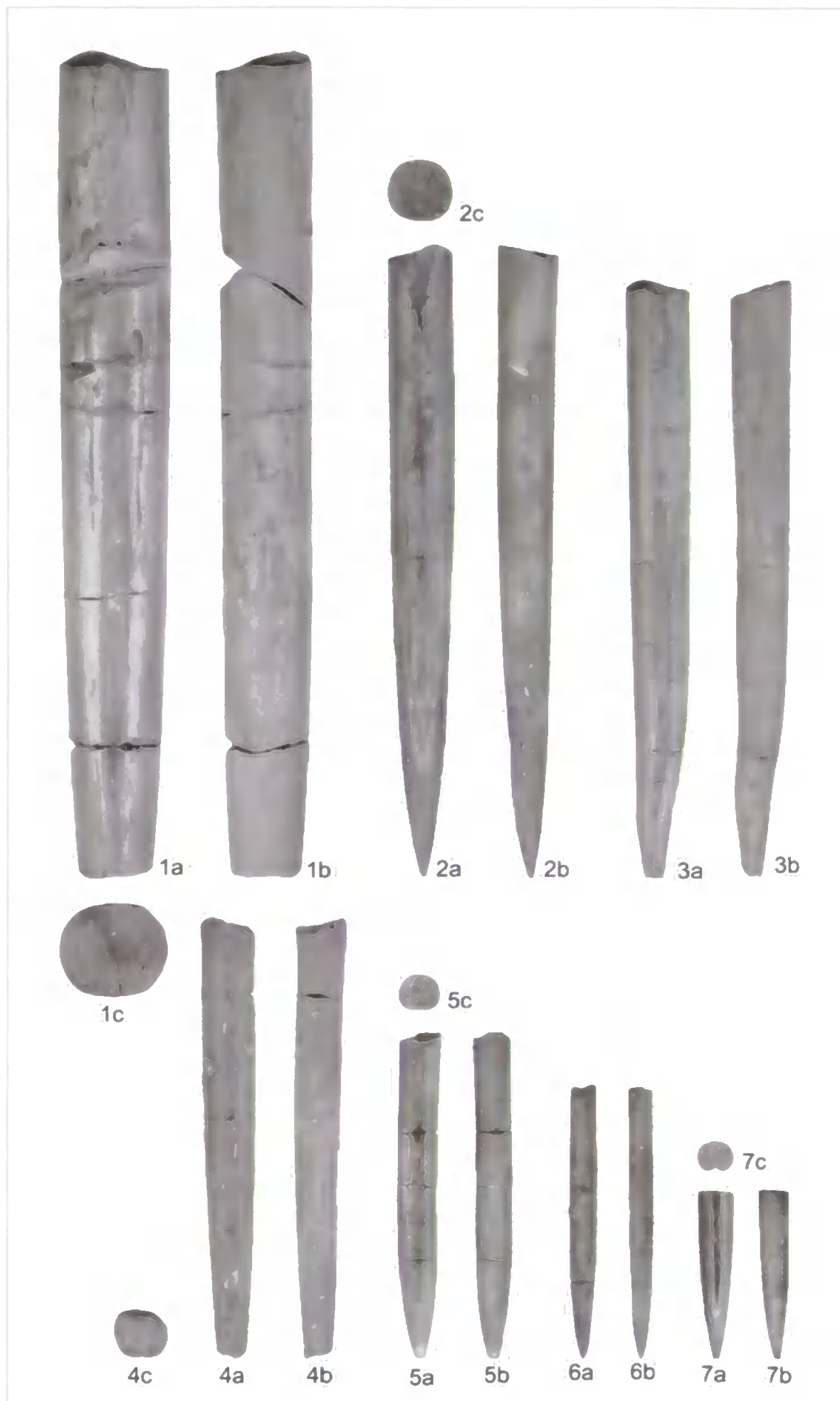


PLATE A7.

1. *Lagonibelus (Holcobeloides) rosanovi* Gustomesov, 1960. (a) ventral outline, (b) right profile, (c) transverse section. Middle Volgian, *Maximus* Zone, Izhma River, Russia. (PC2.11 F)

2. *Lagonibelus (Holcobeloides) rosanovi* Gustomesov, 1960. (a) ventral outline, (b) right profile, (c) transverse section. Middle Volgian, *Maximus* Zone, Izhma River, Russia. (PC2.11 C)

3. *Lagonibelus (Lagonibelus) cf. gustomesovi* Saks & Nal'nyaeva, 1964. (a) ventral outline, (b) right profile. Upper Ryazanian or Valanginian, *Tzikwinianus* to *Polyptychus* Zone material, Izhma River, Russia. (PC7.a2 A)

4. *Lagonibelus (Lagonibelus) gustomesovi* Saks & Nal'nyaeva, 1964. (a) ventral outline, (b) right profile, (c) transverse section. Lower Ryazanian, *Kochi* to *Analogus* Zone material, Boyarka River, Siberia. (KH 16; Loose)

5. *Acroteuthis (Acroteuthis) arctica* Blüthgen, 1936. (a) ventral outline, (b) right profile, (c) transverse section, (d) dorsal outline. Lower Valanginian, *Klimovskiensis* Zone, Boyarka River, Siberia. (KH13; 4.35)

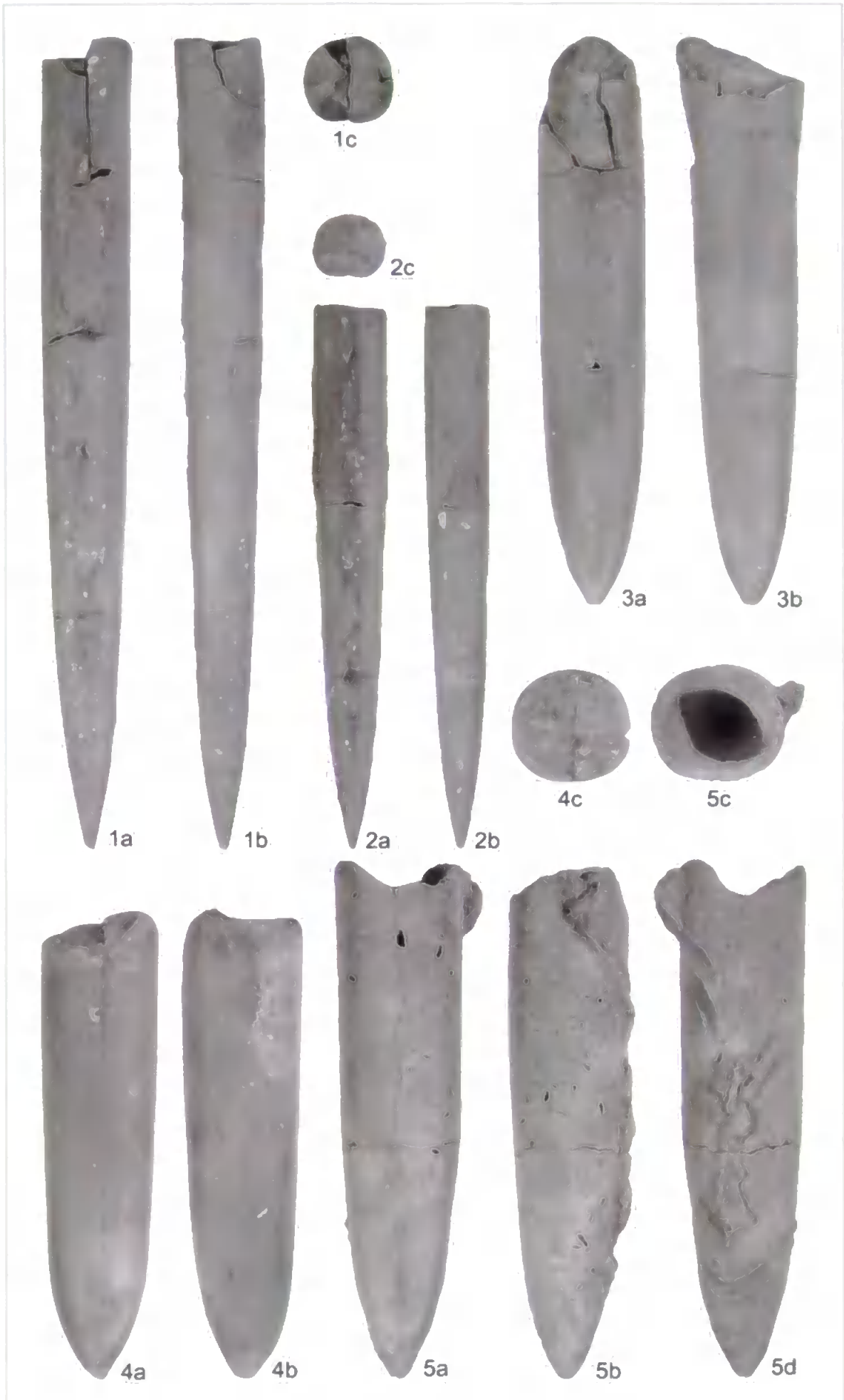


PLATE A8.

1. *Acroteuthis (Acroteuthis) arctica* Blüthgen, 1936. (a) ventral outline, (b) right profile, (c) transverse section. Upper Ryazanian or Valanginian, *Tzikwinianus* to *Polyptychus* Zone material, Izhma River, Russia. (PC7.a1)

2. *Acroteuthis (Acroteuthis) anabarensis* (Pavlow, 1914). (a) ventral outline, (b) right profile, (c) transverse section. Upper Ryazanian or Valanginian, *Tzikwinianus* to *Polyptychus* Zone material, Izhma River, Russia. (PC7.a2 B)

3. *Acroteuthis (Acroteuthis) anabarensis* (Pavlow, 1914). (a) ventral outline, (b) right profile, (c) transverse section. Upper Ryazanian or Valanginian, *Tzikwinianus* to *Polyptychus* Zone material, Izhma River, Russia. (PC7.c1)

4. *Acroteuthis (Acroteuthis) anabarensis* (Pavlow, 1914). (a) ventral outline, (b) right profile, (c) transverse section. Lower Valanginian, *Stubendorffi* Zone, Boyarka River, Siberia. (KH18; 10.50)

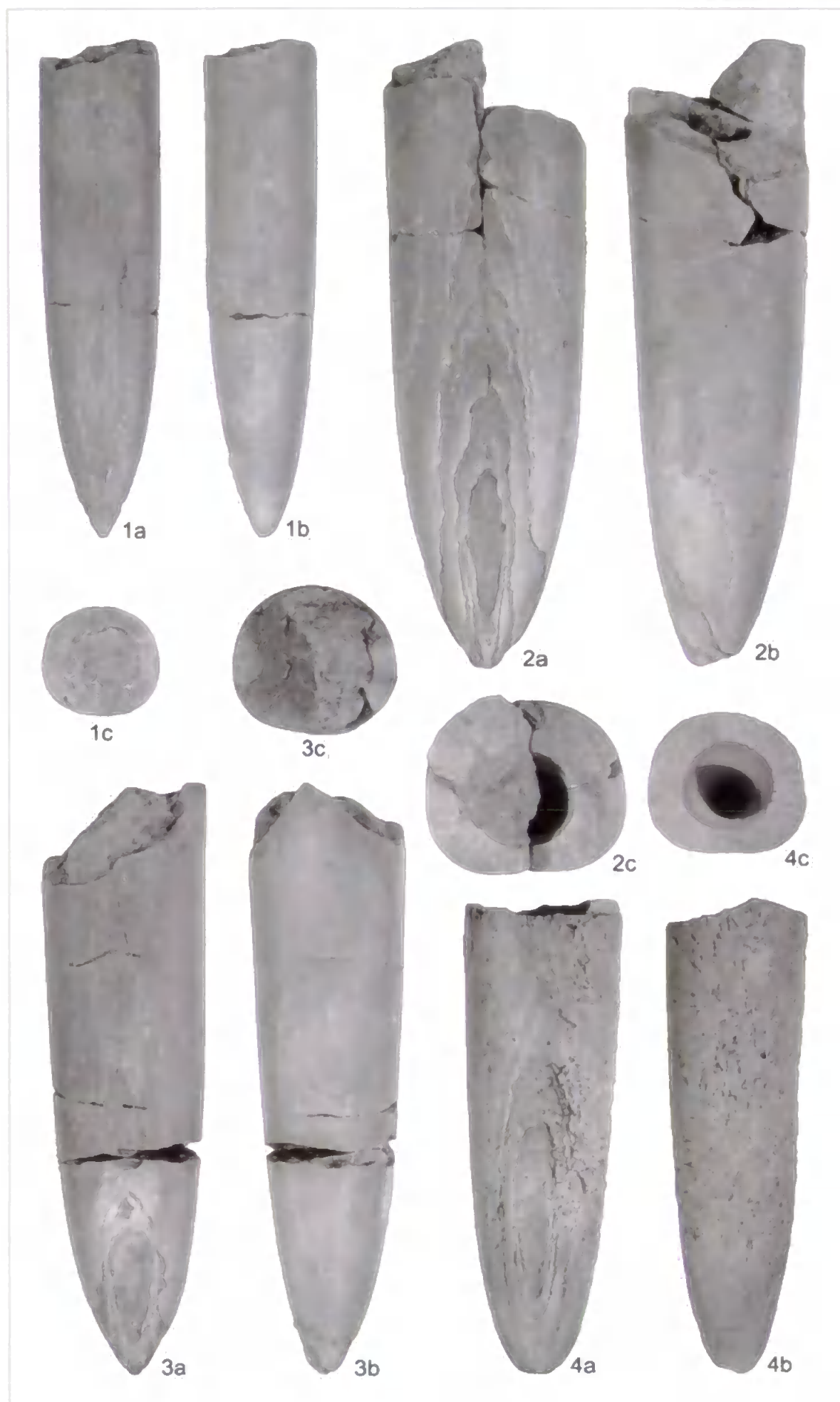


PLATE A9.

1. *Acroteuthis (Acroteuthis) cf. anabarensis* (Pavlow, 1914). (a) ventral outline, (b) right profile, (c) transverse section. Middle Volgian, *Maximus* Zone, Izhma River, Russia.
(PC2.6)

2. *Acroteuthis (Acroteuthis) acrei* Swinnerton, 1936. (a) ventral outline, (b) right profile, (c) transverse section. Lower Valanginian, *Klimovskiensis* Zone, Boyarka River, Siberia.
(KH13; Loose A)

3. *Acroteuthis (Acroteuthis) acrei* Swinnerton, 1936. (a) ventral outline, (b) right profile, (c) transverse section. Lower Valanginian, *Klimovskiensis* Zone, Boyarka River, Siberia.
(KH13; Loose B)

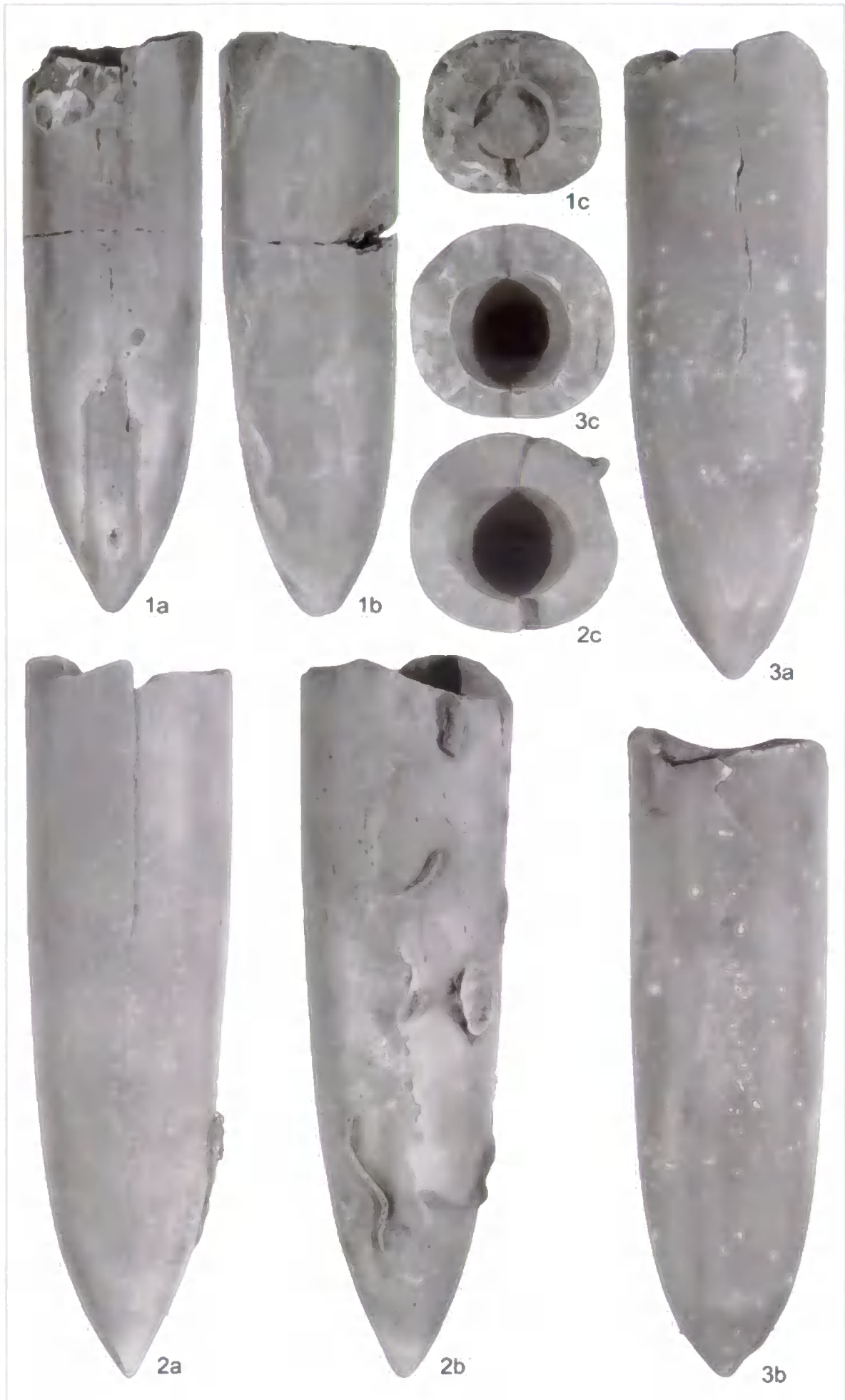


PLATE A10.

1. *Acroteuthis (Acroteuthis) acrei* Swinnerton, 1936. (a) ventral outline, (b) right profile, (c) transverse section. Lower Valanginian, *Klimovskiensis* Zone, Boyarka River, Siberia. (KH13; 3.45)

2. *Acroteuthis (Acroteuthis) acrei* Swinnerton, 1936. (a) ventral outline, (b) right profile, (c) transverse section. Upper Valanginian or Lower Hauterivian, *Bidichotomus* to *Bojarkensis* Zone material, Boyarka River, Siberia. (KH6-7; Loose)

3. *Acroteuthis (Acroteuthis) lateralis* (Phillips, 1835). (a) ventral outline, (b) right profile, (c) transverse section. Lower Valanginian, *Syzranicum* to *Michalskii* Zone material, Izhma River, Russia. (PC9 GP24 A)

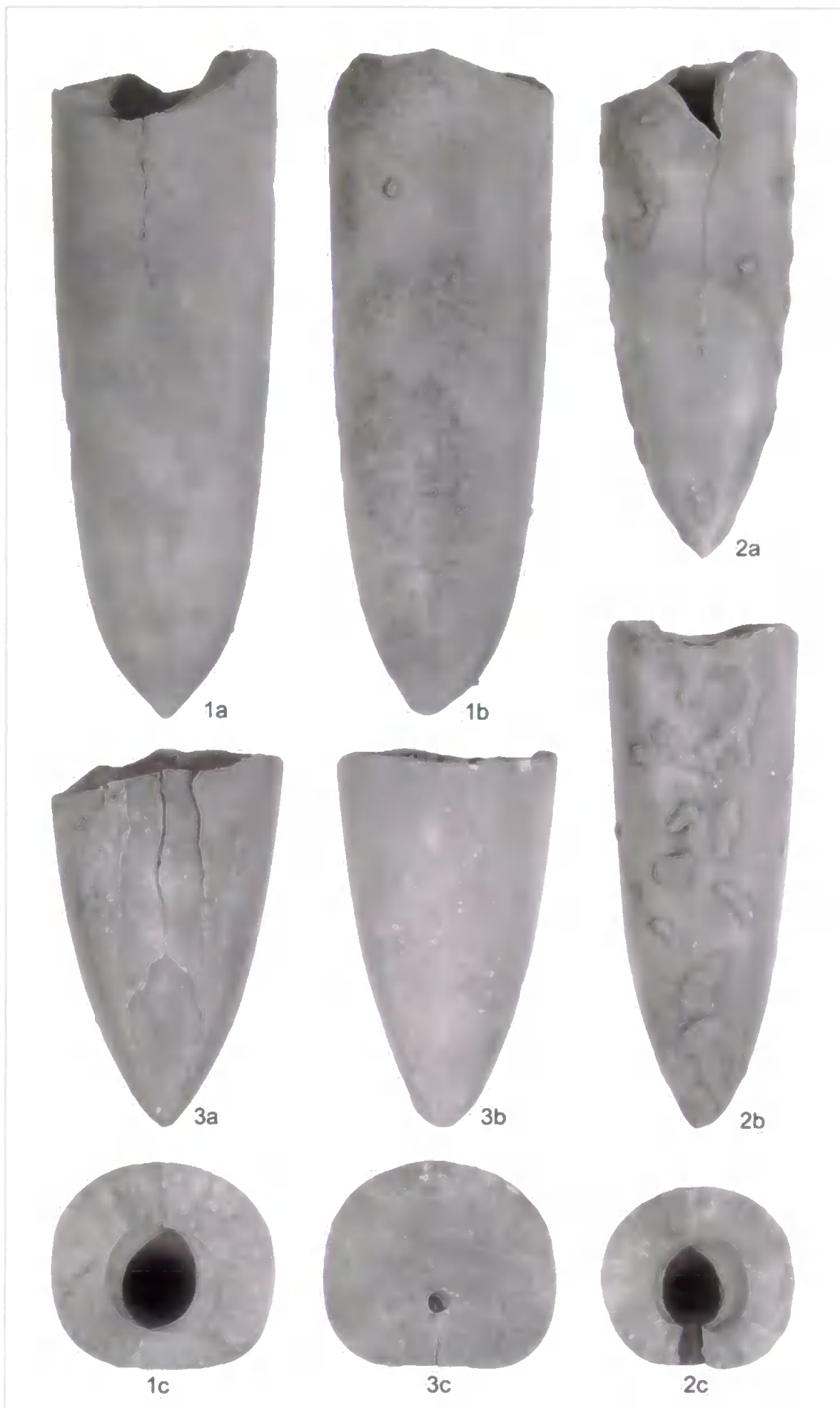


PLATE A11.

1. *Acroteuthis (Acroteuthis) lateralis* (Phillips, 1835). (a) ventral outline, (b) right profile, (c) transverse section. Lower Valanginian, *Syzranicum* to *Michalskii* Zone material, Izhma River, Russia. (PC9 GP24 B)

2. *Acroteuthis (Acroteuthis) lateralis* (Phillips, 1835). (a) ventral outline, (b) right profile, (c) transverse section. Lower Valanginian, *Syzranicum* to *Michalskii* Zone material, Izhma River, Russia. (PC9 GP22)

3. *Acroteuthis (Acroteuthis) lateralis* (Phillips, 1835). (a) ventral outline, (b) right profile, (c) alveolar transverse section, (d) stem transverse section. Lower Valanginian, *Syzranicum* to *Michalskii* Zone material, Izhma River, Russia. (PC9a)

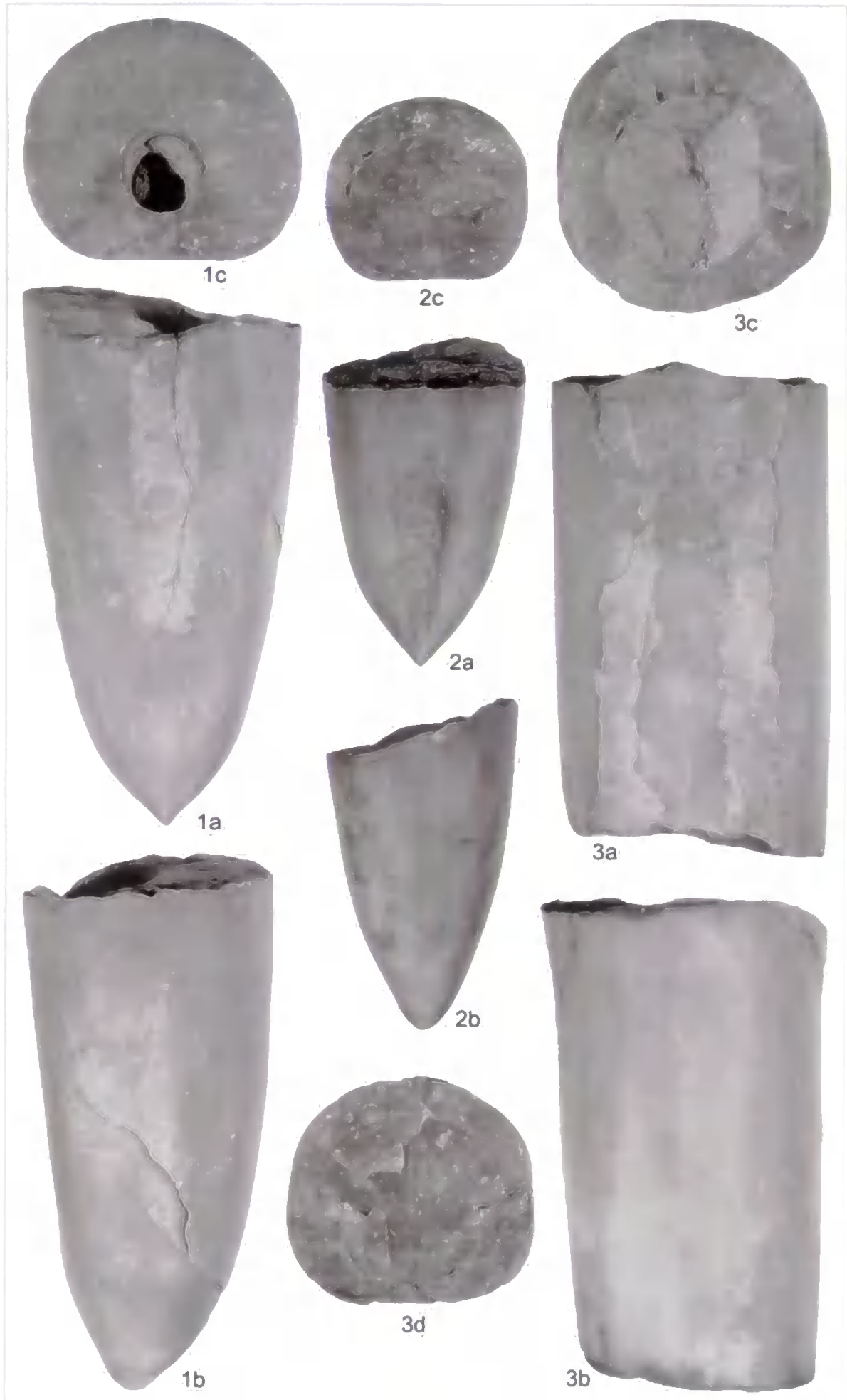


PLATE A12.

1. *Pachyteuthis (Pachyteuthis) cf. ingens* Krimholz, 1929. (a) ventral outline, (b) right profile, (c) stem transverse section. Upper Volgian, *Pseudocraspedites / Surites* Zone, Izhma River, Russia. (PC4)

2. *Pachyteuthis (Pachyteuthis) acuta* Saks & Nal'nyaeva 1966. (a) ventral outline, (b) right profile, (c) transverse section. Middle Volgian, *Maximus* Zone, Izhma River, Russia. (PC2.11 E)

3. *Pachyteuthis (Pachyteuthis) acuta* Saks & Nal'nyaeva 1966. (a) ventral outline, (b) right profile. Middle Volgian, *Maximus* Zone, Izhma River, Russia. (PC2.11 D)

4. *Pachyteuthis (Pachyteuthis) cf. acuta* Saks & Nal'nyaeva 1966. (a) ventral outline, (b) right profile, (c) transverse section. Middle Volgian, *Panderi* Zone, Izhma River, Russia. (PC3 B)

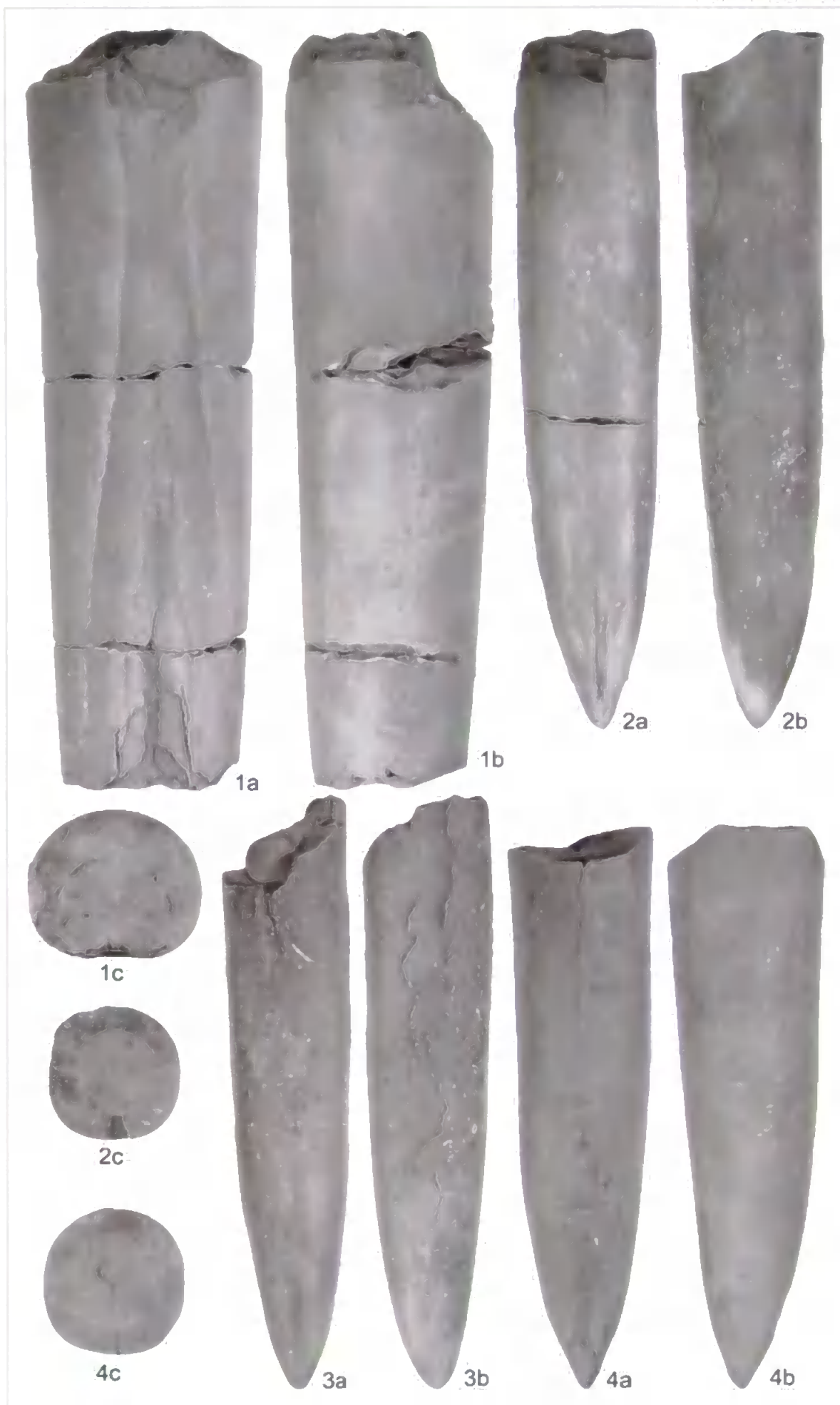


PLATE A13.

1. *Pachyteuthis (Pachyteuthis) excentralis* (Young & Bird, 1822). (a) ventral outline, (b) right profile. Upper Oxfordian or Lower Kimmeridgian, *Regulare* to *Baylei* Zone material, Staffin Bay, UK. (SK7; 16.90)

2. *Pachyteuthis (Pachyteuthis) excentralis* (Young & Bird, 1822). (a) ventral outline, (b) right profile. Lower Kimmeridgian, *Baylei* to *Cymodoce* Zone material, Staffin Bay, UK. (SK5; 5.70)

3. *Pachyteuthis (Pachyteuthis) excentralis* (Young & Bird, 1822). (a) ventral outline, (b) right profile. Lower Oxfordian, *Mariae* to *Cordatum* Zone material, Staffin Bay, UK. (SK1; 50.00)

4. *Pachyteuthis (Pachyteuthis) excentralis* (Young & Bird, 1822). (a) ventral outline, (b) right profile, (c) transverse section. Lower Kimmeridgian, *Baylei* to *Cymodoce* Zone material, Staffin Bay, UK. (SK5; 2.70)

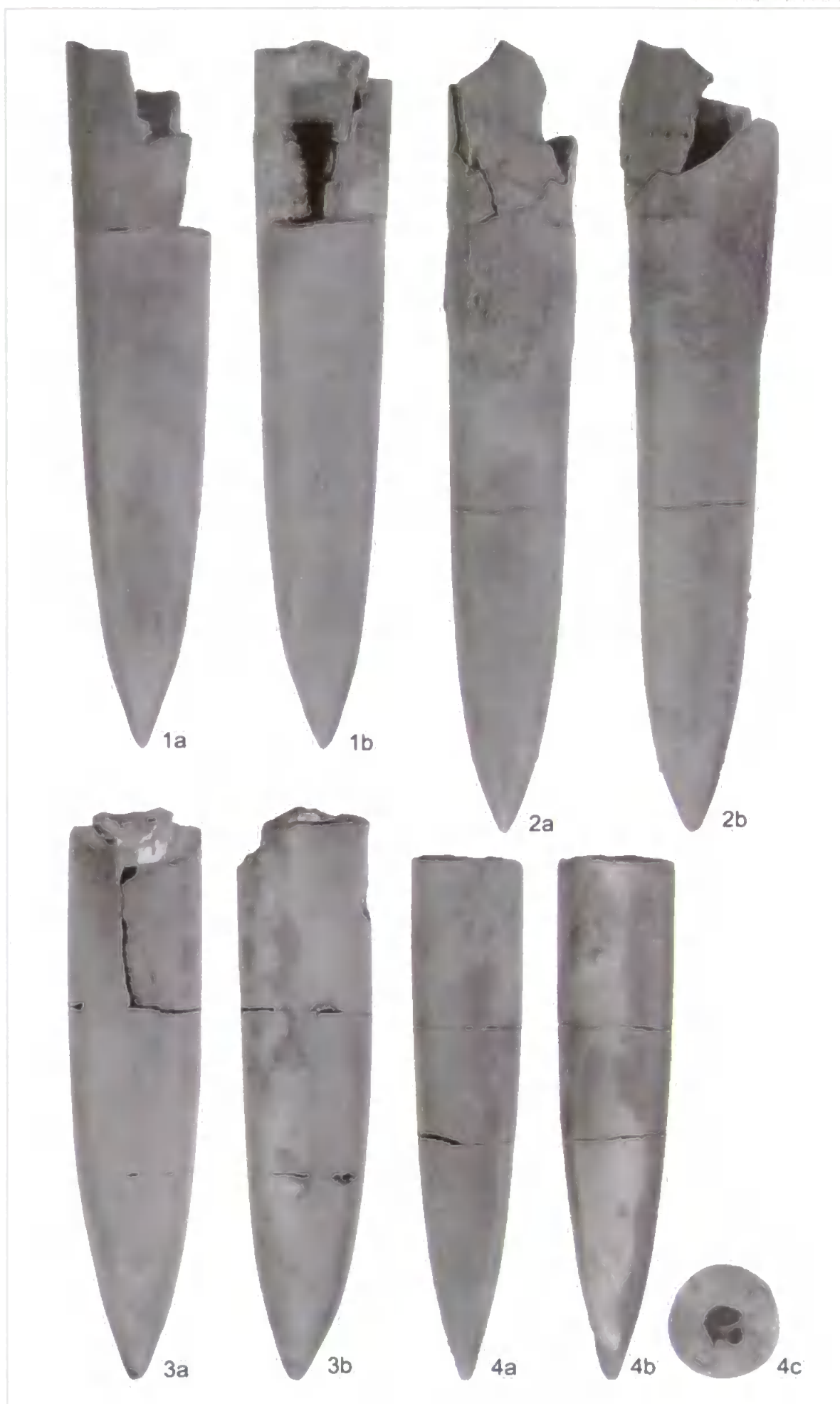


PLATE A14.

1. *Pachyteuthis (Pachyteuthis) cf. excentralis* (Young & Bird, 1822). (a) ventral outline, (b) right profile. Lower Kimmeridgian, *Cymodoce* Zone, Staffin Bay, UK. (SK6; 4.50)

2. *Pachyteuthis (Pachyteuthis) apiculata* Saks & Nal'nyaeva, 1966. (a) ventral outline, (b) right profile, (c) transverse section. Middle Volgian, *Maximus* Zone, Izhma River, Russia. (PC2.8)

3. *Pachyteuthis (Pachyteuthis) apiculata* Saks & Nal'nyaeva, 1966. (a) ventral outline, (b) right profile, (c) transverse section. Middle Volgian, *Maximus* Zone, Izhma River, Russia. (PC2.12 A)

4. *Pachyteuthis (Pachyteuthis) panderiana* (d'Orbingny, 1845). (a) ventral outline, (b) right profile, (c) transverse section. Lower Oxfordian, *Mariae* to *Cordatum* Zone material, Staffin Bay, UK. (SK1; 47.10)



PLATE A15.

1. *Pachyteuthis (Pachyteuthis) panderiana* (d'Orbingny, 1845). (a) ventral outline, (b) right profile, (c) transverse section. Lower Kimmeridgian, *Baylei* to *Cymodoce* Zone material, Staffin Bay, UK. (SK5; 8.10)

2. *Pachyteuthis (Pachyteuthis) panderiana* (d'Orbingny, 1845). (a) ventral outline, (b) right profile, (c) transverse section. Lower Kimmeridgian, *Baylei* to *Cymodoce* Zone material, Staffin Bay, UK. (SK5; 3.90)

3. *Pachyteuthis (Pachyteuthis) panderiana* (d'Orbingny, 1845). (a) ventral outline, (b) right profile. Lower Kimmeridgian, *Cymodoce* Zone, Staffin Bay, UK. (SK6; 2.40)

4. *Pachyteuthis (Pachyteuthis) subrectangulata* (Blüthgen, 1936). (a) ventral outline, (b) right profile, (c) transverse section. Lower Valanginian, *Klimovskiensis* Zone, Boyarka River, Siberia. (KH13; 2.30)

5. *Pachyteuthis (Pachyteuthis) subrectangulata* (Blüthgen, 1936). (a) ventral outline, (b) right profile, (c) transverse section. Upper Valanginian or Lower Hauterivian, *Bidichotomus* to *Bojarkensis* Zone material, Izhma River, Russia. (PC10a A)

6. *Pachyteuthis (Pachyteuthis) subrectangulata* (Blüthgen, 1936). (a) ventral outline, (b) right profile, (c) transverse section. Upper Valanginian or Lower Hauterivian, *Bidichotomus* to *Bojarkensis* Zone material, Izhma River, Russia. (PC10a B)

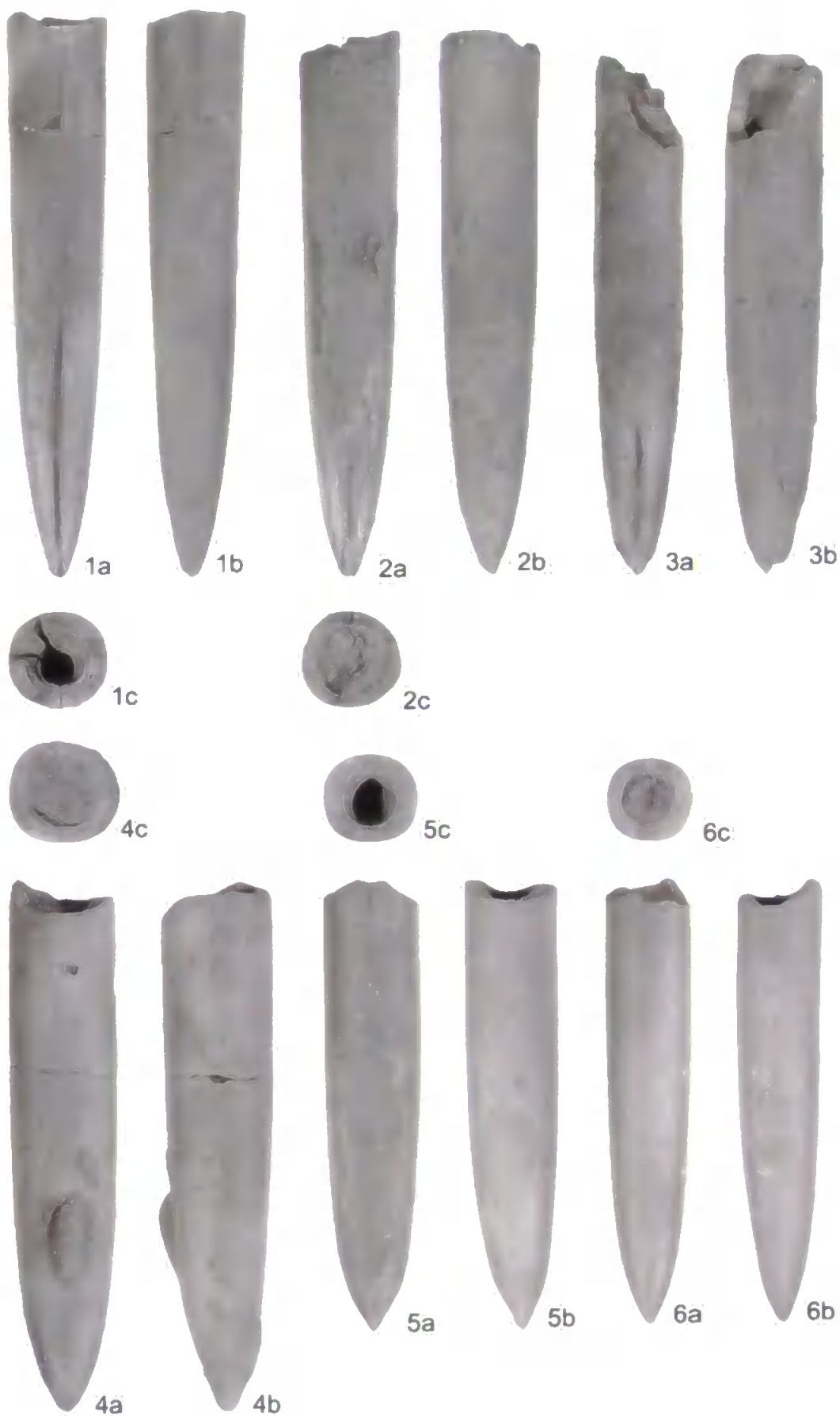


PLATE A16.

1. *Pachyteuthis (Pachyteuthis) subrectangulata* (Blüthgen, 1936). (a) ventral outline, (b) right profile, (c) transverse section. Upper Valanginian, *Bidichotomus* Zone, Izhma River, Russia. (PC5 D)
2. *Pachyteuthis (Pachyteuthis) subrectangulata* (Blüthgen, 1936). (a) ventral outline, (b) right profile, (c) transverse section. Upper Valanginian, *Bidichotomus* Zone, Izhma River, Russia. (PC5 C)
3. *Pachyteuthis (Pachyteuthis) subrectangulata* (Blüthgen, 1936). (a) ventral outline, (b) right profile, (c) transverse section. Lower Valanginian, *Stubendorffi* Zone, Boyarka River, Siberia. (KH18; 7.10)
4. *Pachyteuthis (Pachyteuthis) cf. subrectangulata* (Blüthgen, 1936). (a) ventral outline, (b) right profile, (c) transverse section. (?)Upper Valanginian, (?)*Bidichotomus* Zone, Izhma River, Russia. (PC6.2)
5. *Pachyteuthis (Pachyteuthis) cf. subrectangulata* (Blüthgen, 1936). (a) ventral outline, (b) right profile, (c) transverse section. Upper Valanginian, *Bidichotomus* Zone, Izhma River, Russia. (PC5 B)
6. *Pachyteuthis (Pachyteuthis) cf. explanata* (Phillips, 1865). (a) ventral outline, (b) right profile, (c) transverse section. Lower or Middle Oxfordian, *Cordatum* to *Densiplicatum* Zone material, Staffin Bay, UK. (SK3; 5.80)

7. *Pachyteuthis (Pachyteuthis) cf. explanata* (Phillips, 1865). (a) ventral outline, (b) right profile, (c) transverse section. Lower Oxfordian, *Mariae* to *Cordatum* Zone material, Staffin Bay, UK. (SK1; 60.20)
8. *Pachyteuthis (Pachyteuthis) troslayana* (d'Orbigny, 1850). (a) ventral outline, (b) right profile, (c) transverse section. Lower Kimmeridgian, *Baylei* to *Cymodoce* Zone material, Staffin Bay, UK. (SK5; 5.70 B)
9. *Pachyteuthis (Pachyteuthis) cf. explanata* (Phillips, 1865). (a) ventral outline, (b) right profile. Lower - Middle Oxfordian, *Cordatum* to *Densiplicatum* Zone material, Staffin Bay, UK. (SK3; 5.20)
10. *Pachyteuthis (Pachyteuthis) troslayana* (d'Orbigny, 1850). (a) ventral outline, (b) right profile. Lower Kimmeridgian, *Cymodoce* Zone, Staffin Bay, UK. (SK6; 1.90)
11. *Pachyteuthis (Pachyteuthis) troslayana* (d'Orbigny, 1850). (a) ventral outline, (b) right profile. Upper Oxfordian or Lower Kimmeridgian, *Regulare* to *Baylei* Zone material, Staffin Bay, UK. (SK7; 1.10)
12. *Pachyteuthis (Pachyteuthis) sp. indet.* (a) ventral outline, (b) right profile. Lower Ryazanian, *Kochi* to *Analogus* Zone material, Boyarka River, Siberia. (KH16; 1.25)

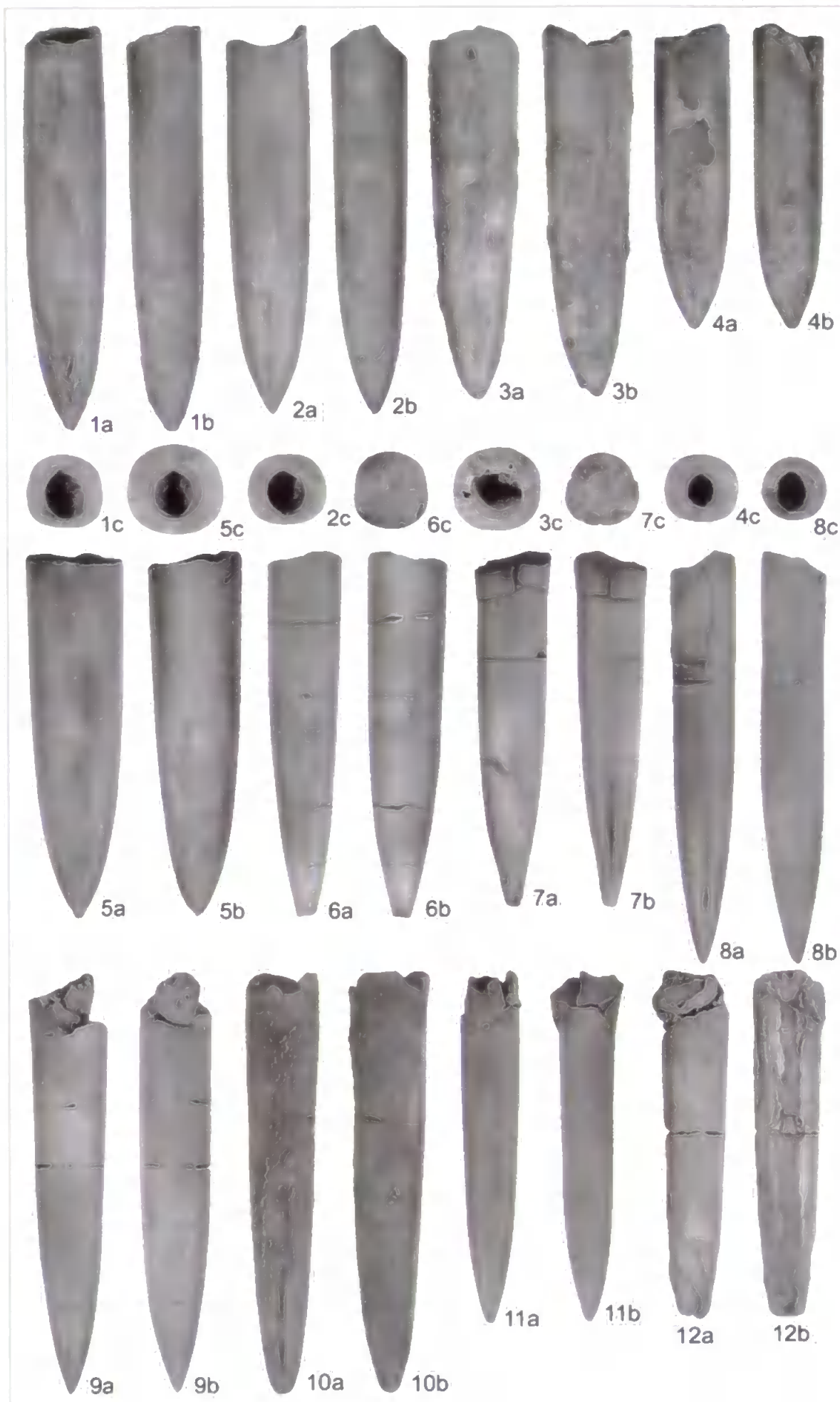


PLATE A17.

1. *Pachyteuthis (Simobelus) curvula* Saks & Nal'nyaeva, 1966. (a) ventral outline, (b) right profile, (c) transverse section. Upper Ryazanian, *Meseshnikowi* Zone, Boyarka River, Siberia. (KH17c; 3.40)

2. *Pachyteuthis (Simobelus) curvula* Saks & Nal'nyaeva, 1966. (a) ventral outline, (b) right profile, (c) transverse section. Upper Ryazanian, *Meseshnikowi* Zone, Boyarka River, Siberia. (KH17b; Loose A)

3. *Pachyteuthis (Simobelus) cf. breviaxis* (Pavlow, 1892). (a) ventral outline, (b) right profile. Upper Oxfordian or Lower Kimmeridgian, *Regulare* to *Baylei* Zone material, Staffin Bay, UK. (SK7; 20.25 B)

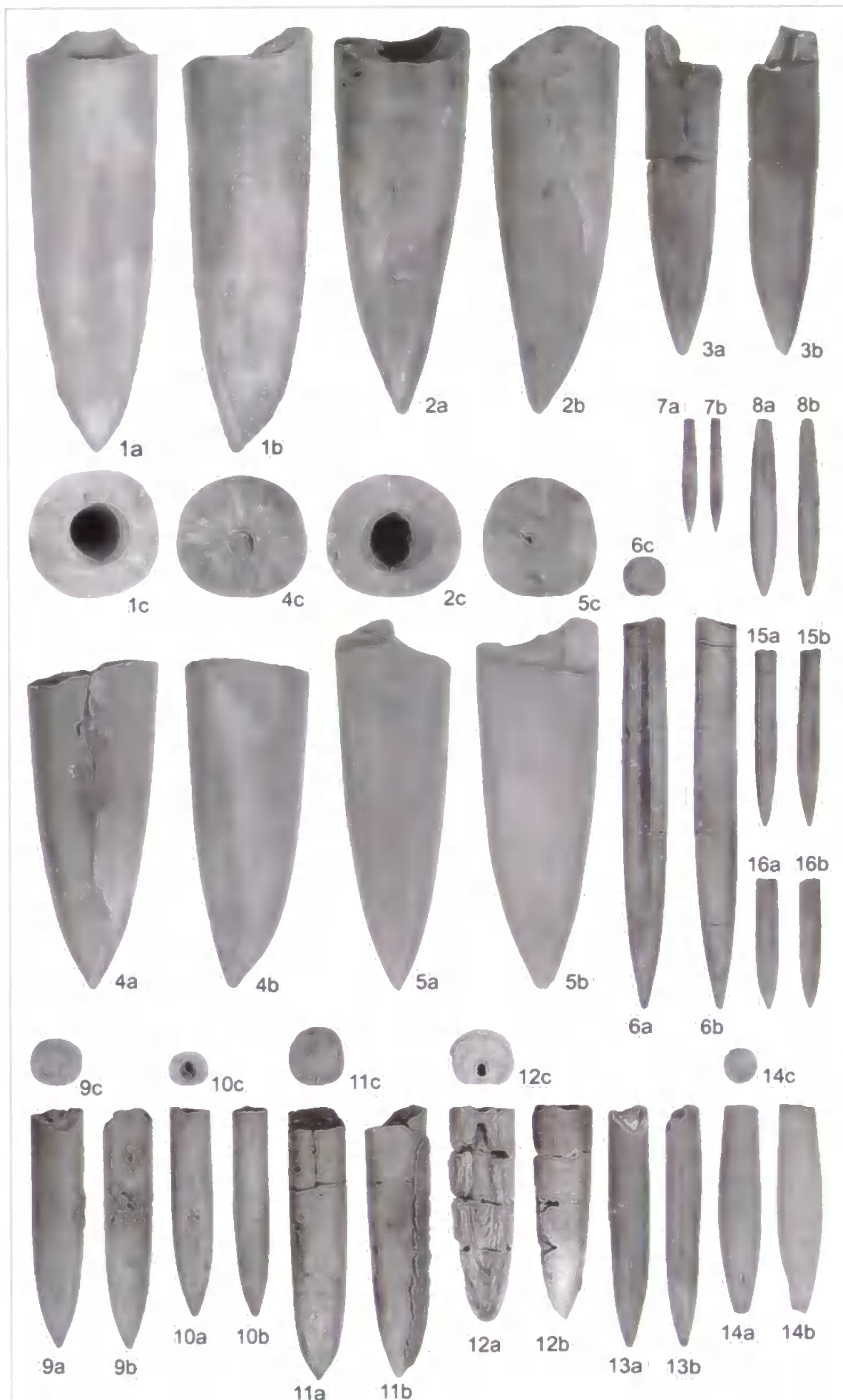
4. *Pachyteuthis (Simobelus) curvula* Saks & Nal'nyaeva, 1966. (a) ventral outline, (b) right profile, (c) transverse section. Upper Ryazanian, *Meseshnikowi* Zone, Boyarka River, Siberia. (KH17b; Loose B)

5. *Pachyteuthis (Simobelus) insignis* Saks & Nal'nyaeva, 1966. (a) ventral outline, (b) right profile, (c) transverse section. Middle Volgian, *Panderi* Zone, Izhma River, Russia. (PC3a A)

6. *Belemnopsis cf. depressa* (Quenstedt, 1848). (a) ventral outline, (b) right profile, (c) transverse section. Callovian, *Koenigi* to *Lamberti* Zone material, Staffin Bay, UK. (SK4; 10.50)

7. (?)*Hibolithes* sp. juv. (a) ventral outline, (b) right profile. Lower Oxfordian, *Cordatum* Zone, Staffin Bay, UK. (SK8; 39.40)
8. (?)*Hibolithes* sp. juv. (a) ventral outline, (b) right profile. Middle Oxfordian, *Densiplicatum* to *Tenuiserratum* Zone material, Staffin Bay, UK. (SK2; 2.80)
9. *Pachyteuthis* (*Pachyteuthis*) sp. indet. juv. (a) ventral outline, (b) right profile, (c) transverse section. Upper Ryazanian or Valanginian, *Tzikwinianus* to *Polyptychus* Zone material, Izhma River, Russia. (PC7.c2)
10. *Pachyteuthis* (*Pachyteuthis*) sp. indet. juv. (a) ventral outline, (b) right profile, (c) transverse section. Upper Valanginian, *Bidichotomus* Zone, Izhma River, Russia. (PC5 A)
11. Belemnite gen. et. sp. indet. juv. 1. (a) ventral outline, (b) right profile, (c) transverse section. Middle Volgian, *Maximus* Zone, Izhma River, Russia. (PC2.3)
12. Belemnite gen. et. sp. indet. juv. 2. (a) ventral outline, (b) right profile, (c) transverse section. Upper Ryazanian or Valanginian, *Tzikwinianus* to *Polyptychus* Zone material, Izhma River, Russia. (PC7.c8)
13. Belemnite gen. et. sp. indet. juv. 3. (a) ventral outline, (b) right profile. Middle Volgian, *Panderi* Zone, Izhma River, Russia. (PC3 A)
14. Belemnite gen. et. sp. indet. juv. 4. (a) ventral outline, (b) right profile, (c) transverse section. Upper Valanginian or Lower Hauterivian, *Bidichotomus* to *Bojarkensis* Zone material, Izhma River, Russia. (PC10)

15. Belemnite gen. et. sp. indet. juv. 5. (a) ventral outline, (b) right profile. Upper Oxfordian, *Serratum* to *Regulare* Zone material, Staffin Bay, UK. (SK10; 12.70)
16. Belemnite gen. et. sp. indet. juv. 6. (a) ventral outline, (b) right profile. Middle Volgian, *Maximus* Zone, Izhma River, Russia. (PC2.14)



APPENDIX 2
DATA TABLES : BELEMNITES

No.	Sample No.	Age	Am. Zone	Genus	Photo.	$\delta^{18}O$	$\delta^{13}C$	Ca	Na	Mg	K	Fe	Al	B	Ba	Li	Mn	Ni	Pb	Cr	Ti	Zn	CL	BCEM	Catb	Comments
1	HL1; 0.10 A	E. Klimm.	Cym	?		-1.32	1.26	30274.97	1095.62	1433.45	12.35	147.24	19.82	0.00	3.42	4.32	14.65		4.32	2.66	4.32	0.09	1070.32	2.19	22.67	
2	HL1; 0.10 B	E. Klimm.	Cym	?		-0.82	2.22	310294.41	801.63	20.55	30.23	20.55	0.00	0.00	8.28	4.32	14.65		4.32	6.15	0.00	0.00	1230.66	2.20	37.63	
3	HL1; 0.30 A	E. Klimm.	Cym	?		-0.58	1.83	300464.36	1108.66	1241.69	20.21	18.55	19.67	0.00	10.53	3.83	6.15		6.15	0.00	0.00	1121.61	2.08	17.24		
4	HL1; 0.30 B1	E. Klimm.	Cym	?		-1.13	1.99	305528.77	988.17	1225.70	10.45	14.78	20.08	0.00	9.38	3.65	3.31		3.31	0.00	0.00	1108.00	2.16	34.87		
5	HL1; 0.30 B1	E. Klimm.	Cym	?		-1.07	1.87	297873.37	1075.84	1504.16	40.08	30.49	19.72	0.00	13.24	3.82	8.13		8.13	0.00	0.20	1108.61	2.19	30.22		
6	HL1; 0.30 C	E. Klimm.	Cym	?		-1.96	1.63	318133.86	873.68	1479.40	12.64	37.48	20.71	0.00	8.62	4.08	6.84		6.84	0.00	0.00	1135.21	2.24	44.56		
7	HL1; 0.50 A1	E. Klimm.	Cym	?		-2.16	3.05	300944.84	1054.38	1168.66	15.21	251.23	19.84	0.00	8.73	3.37	39.65		39.65	0.00	0.00	1205.79	2.17	29.05		
8	HL1; 0.50 A1	E. Klimm.	Cym	?		-2.53	2.63	303372.06	908.62	1017.53	17.76	230.86	20.08	0.00	13.53	3.30	50.95		50.95	0.00	0.00	1204.54	2.13	28.14		
9	HL1; 0.50 B	E. Klimm.	Cym	?		-1.52	2.16	300966.20	899.39	820.62	13.45	32.45	19.60	0.00	5.38	3.00	14.50		14.50	0.00	0.00	1169.48	2.08	30.68		
10	HL1; 0.50 C	E. Klimm.	Cym	?		-1.80	2.82	289086.51	934.64	1035.36	12.42	12.10	19.26	0.00	3.19	3.31	5.02		5.02	0.00	0.00	1087.86	2.22	26.77		
11	HL1; 0.70 A	E. Klimm.	Cym	?		-1.50	2.04	302518.77	837.56	1120.46	15.08	39.25	20.73	0.00	14.81	3.01	5.31		5.31	0.00	0.00	1087.86	2.22	31.72		
12	HL1; 0.70 B	E. Klimm.	Cym	?		-1.30	1.80	289584.11	878.76	1169.39	19.65	29.87	18.80	0.00	7.30	2.86	5.08		5.08	0.00	0.00	1103.62	2.13	31.51		
13	HL1; 1.10	E. Klimm.	Cym	?		-1.38	2.46	283847.06	821.74	1052.06	15.45	31.88	20.21	0.00	4.07	2.16	40.07		40.07	0.00	0.00	1263.44	2.12	28.46		
14	HL1; 1.20	E. Klimm.	Cym	?		-2.84	1.47	313473.49	1163.46	1186.82	108.13	28.28	63.91	0.00	4.44	3.68	4.26		4.26	3.29	1169.17	2.68	40.71			
15	HL1; 1.80 A	E. Klimm.	Cym	?		-1.30	1.45	298177.00	960.53	1044.10	10.60	78.65	19.79	0.00	3.13	3.23	18.33		18.33	0.00	0.00	1270.67	2.08	18.62		
16	HL1; 1.80 B	E. Klimm.	Cym	?		-2.16	2.45	302736.15	830.51	988.07	13.36	36.41	18.52	0.00	6.31	2.17	21.15		21.15	0.00	0.00	1270.67	2.23	32.04		
17	HL1; 2.10 A	E. Klimm.	Cym	?		-0.87	1.28	287432.45	917.86	1026.24	23.86		43.61	18.80	0.00	3.81	3.24	11.04		3.24	0.00	0.00	1101.59	2.03	21.37	
18	HL1; 4.00 A1	E. Klimm.	Cym	?		-1.23	1.41	302171.75	1160.84	1318.73	18.87	11.74	18.86	0.00	1.83	3.75	5.77		5.77	0.00	0.00	1149.14	2.11	18.83		
20	HL1; 4.00 B	E. Klimm.	Cym	?		-0.82	1.80	306421.56	1089.84	1326.70	20.49	34.01	21.17	8.78	3.50	5.66	3.89		3.89	0.00	0.00	1180.43	2.11	18.01		
21	HL1; 4.70	E. Klimm.	Cym	?		-0.32	1.70	304878.89	1074.72	1047.83	14.56	45.69	21.36	0.00	9.16	3.79	22.61		22.61	0.00	0.00	1164.83	2.35	19.88		
22	HL1b; 3.10 A	E. Klimm.	Cym	?		-0.82	0.81	297570.57	1213.73	1949.51	19.26	45.16	20.15	0.00	4.78	2.80	4.62		4.62	0.00	0.00	1322.20	2.39	21.27		
23	HL1b; 3.10 B	E. Klimm.	Cym	?		-1.03	1.20	298719.97	1211.84	1517.12	43.89	119.23	20.78	0.00	14.36	3.51	29.74		29.74	0.00	0.00	1138.37	2.18	19.28		
24	HL1b; 3.10 C	E. Klimm.	Cym	?		-1.64	1.64	302178.52	923.85	1221.54	50.84	20.78	18.56	0.00	3.89	2.74	5.67		5.67	0.10	0.10	1127.70	2.28	39.57		
25	HL1b; 3.10 D1	E. Klimm.	Cym	?		-2.84	1.11	288171.81	1089.42	1920.02	26.47	209.71	18.75	0.00	36.82	3.01	23.64		23.64	0.00	0.00	817.46	2.07	19.53		
26	HL1b; 3.10 D1	E. Klimm.	Cym	?		-4.36	0.73	302315.63	781.54	1812.18	28.42	405.84	20.78	0.00	36.81	2.42	44.84		44.84	0.02	0.02	675.70	2.28	16.60		
27	HL1b; 13.60	E. Klimm.	Cym	?		-1.45	2.55	285304.82	902.88	727.11	17.56	42.57	20.14	0.00	7.66	1.85	21.31		21.31	0.00	0.00	1277.02	2.08	28.72		
28	HL1b; 20.80 A	E. Klimm.	Cym	?		-0.78	1.15	286517.66	1180.04	1722.80	39.27	11.86	23.16	0.00	13.58	2.89	3.10		3.10	2.13	1288.85	2.15	43.87			
29	HL1b; 27.80 A	E. Klimm.	Cym	?		0.28	2.65	286828.59	829.25	21.37	5.46	5.46	20.00	0.00	1.98	1.98	2.15		2.15	0.37	1129.04	2.04	27.05			
31	HL1b; 27.80 B	E. Klimm.	Cym	?		-3.64	-0.36	320831.83	1513.04	1784.06	59.76	54.58	21.63	5.46	12.19	4.16	19.87		19.87	0.00	0.00	1282.06	2.11	33.50		
32	HL1b; 3.2 A	E. Klimm.	Eudoxus	?		-1.78	1.87	285231.87	1220.84	1384.68	23.21	7.47	20.25	0.00	5.34	2.88	3.44		3.44	1.16	1462.57	1.84	34.64			
33	HL1; 1 A	E. Klimm.	Mutabilla	?		-2.00	1.83	287548.89	989.87	1074.35	19.66	36.20	19.04	0.00	7.05	2.89	5.88		5.88	1.62	1245.73	2.00	31.65			
34	HL1; 1 B	E. Klimm.	Mutabilla	?		-1.63	0.48	303513.51	884.78	1029.86	24.18	71.86	20.03	0.00	6.16	3.38	7.16		7.16	0.00	0.00	1144.88	2.10	30.80		
35	HL1; 3 A	E. Klimm.	Aulistod	?		-1.87	1.18	283642.36	879.53	1079.03	11.08	14.11	18.77	0.00	5.26	2.88	2.88		2.88	0.82	1343.43	1.85	31.73			
36	HL1; 3 B1	E. Klimm.	Aulistod	?		-1.80	1.70	310503.71	882.83	1119.37	15.20	16.75	20.76	0.00	1.47	5.76		5.76	0.00	0.00	1550.48	2.13	24.13			
37	HL1; 3 B1	E. Klimm.	Aulistod	?		-1.63	1.75	218781.30	888.88	1121.81	10.39	13.59	13.28	0.00	5.27	1.80	4.03		4.03	0.00	0.00	1101.85	1.50	24.81		
38	HL1; 4 A	E. Klimm.	Aulistod	?		-2.44	-0.30	416783.84	1820.81	3279.80	78.01	810.37	41.38	0.00	59.78	5.01	45.44		45.44	0.00	0.00	1917.87	2.82	47.06		
39	HL1; 4 A	E. Klimm.	Aulistod	?		-0.69	0.58	363002.00	1412.14	47.85	23.08	23.45	0.00	0.00	21.63	3.60	10.06		10.06	0.78	1328.38	1.84	31.78			
40	HL1; 6 B1	E. Klimm.	Winesleyen	?		-1.42	0.39	275214.42	1053.83	1080.22	18.84	28.58	19.51	0.00	21.63	3.60	10.06		10.06	0.00	0.00	1467.10	2.11	30.48		
41	HL1; 6 B1	E. Klimm.	Winesleyen	?		-0.48	0.69	363002.00	1412.14	47.85	23.08	23.45	0.00	0.00	21.63	3.60	10.06		10.06	0.00	0.00	1467.10	2.11	30.48		
42	HL1; 6 B1	E. Klimm.	Winesleyen	?		-1.34	0.41	302219.18	1119.36	1078.36	9.40	27.15	19.42	0.00	30.36	2.54	5.34		5.34	0.41	1467.10	2.11	30.48			
43	HL1; 6 B1	E. Klimm.	Winesleyen	?		-1.29	0.58	306513.68	1014.36	1187.36	11.87	129.61	21.44	0.00	18.37	1.74	7.66		7.66	0.00	0.00	1469.56	2.18	27.76		
44	HL1; 6 C	E. Klimm.	Winesleyen	?		-0.78	2.21	285288.71	1244.80	787.85	21.50	41.87	19.38	0.00	18.71	1.66	3.82		3.82	0.04	1542.28	1.98	23.61			
45	HL1; 6 D	E. Klimm.	Winesleyen	?		-1.28	0.58	306513.68	1014.36	1187.36	11.87	129.61	21.44	0.00	18.37	1.74	7.66		7.66	0.00	0.00	1469.56	2.18	27.76		
46	HL1; 7 A	E. Klimm.	Winesleyen	?		-0.28	0.28	287689.21	887.45	827.37	4.35	266.81	20.15	0.00	11.43	1.38	17.69		17.69	0.00	0.00	1390.21	2.18	30.36		
47	HL1; 7 B	E. Klimm.	Winesleyen	?		-2.51	-0.23	286878.84	1065.21	1432.55	48.24	413.67	20.15	0.00	23.91	2.87	28.04		28.04	0.00	0.00	1104.81	2.12	42.83		
48	HL1; 8 A1	E. Klimm.	Winesleyen	?		-0.38	0.42	302051.50	804.81	1412.14	8.17	45.34	18.86	0.00	7.71	1.65	8.88		8.88	0.49	1320.88	2.11	21.08			

[illegible]

98	EAT: 0.05 A I	L. Kimm.	Maraslis	Cylindro.		-0.63	1.10	266941.54	1392.63	1759.87	54.46	10.27	24.24	0.00	0.00	3.02	2.81	3.90			0.00	1201.18	2.41	28.94	*	*	*
100	EAT: 0.05 A II	L. Kimm.	Maraslis	Cylindro.		4.50	3.65	269777.53	1330.59	1763.12	38.06	9.09	23.59	0.00	0.00	2.73	3.35	3.05			0.76	1160.64	2.45	24.08			
101	EAT: 0.05 B	L. Kimm.	Maraslis	N.		-1.32	1.63	269153.49	1123.51	1354.01	30.20	15.77	24.00	0.00	0.00	4.07	1.98	8.35			0.82	1263.25	2.48	23.50			
102	EAT: 0.30	L. Kimm.	Maraslis	Cylindro.		-1.48	2.27	269770.35	883.82	740.37	30.56	15.12	23.28	0.00	0.00	2.28	1.20	2.38			0.00	1203.26	2.39	34.86	*	*	
103	EAT: 0.80 I	L. Kimm.	Maraslis	N.		-0.86	1.16	300011.07	1489.72	2971.53	70.53	37.14	23.88	0.00	0.00	3.36	2.63	5.75			0.00	1235.11	2.44	28.80			
104	EAT: 0.80 II	L. Kimm.	Maraslis	N.		-1.08	1.18	300012.53	1428.04	2771.69	52.04	41.14	24.75	0.00	0.00	3.28	2.45	5.53			0.00	1271.64	2.44	28.22			
105	EAT: 1.00	L. Kimm.	Maraslis	N.		-0.41	0.26	268804.04	1631.02	2231.63	61.40	12.86	23.25	0.00	0.00	4.75	2.36	3.80			0.00	1480.38	2.36	50.20	*	*	
106	EAT: 1.50	L. Kimm.	Maraslis	Cylindro.		-1.30	1.16	267763.69	1449.96	2171.03	53.72	20.61	22.91	0.00	0.00	3.76	2.99	2.69			0.26	1482.59	2.31	21.63			
107	EAT: 1.90 I	L. Kimm.	Maraslis	Cylindro.		-0.72	0.15	301589.84	1550.53	2241.70	45.32	30.09	23.31	0.00	0.00	3.57	3.28	3.34			0.00	1294.80	2.33	28.95			
108	EAT: 1.90 II	L. Kimm.	Maraslis	Cylindro.		-0.82	0.39	266780.12	1505.27	2256.19	38.02	33.39	22.98	0.00	0.00	3.79	2.93	3.33			0.00	1336.00	2.35	28.52	*	*	
111	EAT: 5.50 I	L. Kimm.	Maraslis	Cylindro.		-0.59	0.85	301427.53	949.60	629.59	28.23	78.59	23.72	0.00	0.00	36.18	1.01	3.05			0.52	1218.19	2.37	28.83	*	*	
112	EAT: 5.50 II	L. Kimm.	Maraslis	Cylindro.		-0.45	1.24	267794.91	1011.26	639.46	23.33	63.46	24.18	0.00	0.00	14.86	1.18	3.82			3.08	1222.61	2.37	28.16			
113	KH1: 4. 4.00 A	Val. Hout.	D bid. H. boy.	Cylindro?		0.88	4.24	264252.34	1100.61	727.21	8.15	14.94	19.84	0.00	0.00	1.60	1.24	3.45			0.82	1344.84	2.44	23.65			
114	KH1: 4. 4.40 I	Val. Hout.	D bid. H. boy.	Pecty.		0.78	2.36	306468.68	1091.56	689.63	-0.26	10.86	19.01	0.00	0.00	1.56	0.85	8.08			2.23	1339.47	2.48	18.72			
116	KH1: 4. 4.40 2	Val. Hout.	D bid. H. boy.	Pecty.		0.82	1.68	307768.28	1145.70	1074.80	6.81	16.88	18.77	0.00	0.00	1.60	0.85	7.71			-0.15	1363.50	2.35	21.54	*	*	
117	KH1: 4. 10.70	Val. Hout.	D bid. H. boy.	Pecty?		0.26	3.61	306469.55	1007.03	510.03	0.64	8.50	19.16	0.00	0.00	1.44	0.40	12.65			3.08	1429.28	2.17	21.57	*	*	
118	KH1: 4. 21.00	Val. Hout.	D bid. H. boy.	Acto.		1.84	1.33	306689.88	1189.71	941.05	9.88	10.38	19.94	0.00	0.00	1.11	1.59	38.62			3.35	1338.12	2.62	34.24			
119	KH1: 4. 32.30 A	Val. Hout.	D bid. H. boy.	Cylindro.		-0.94	1.52	306810.19	919.02	628.58	30.52	51.69	20.11	0.00	0.00	2.68	1.22	148.89			0.10	1214.34	3.14	28.51	*	*	
120	KH1: 4. 32.30 B	Val. Hout.	D bid. H. boy.	Cylindro.		1.00	1.65	312694.13	1051.17	963.88	35.12	6.39	20.03	0.00	0.00	1.35	1.87	10.47			0.05	1287.03	2.41	27.10			
121	KH1: 4. 47.10	Val. Hout.	D bid. H. boy.	Cylindro.		0.58	1.72	306864.79	1300.48	1209.42	54.65	7.41	20.47	0.00	0.00	1.65	0.80	12.39			2.97	1447.82	2.42	38.35			
122	KH1: 4. 61.10	Val. Hout.	D bid. H. boy.	Cylindro.		0.89	1.13	306872.46	1555.63	1816.50	30.06	13.29	19.66	0.00	0.00	1.88	0.90	10.10			3.33	1700.68	2.31	40.78			
123	KH1: 4b: 20.00 A	L. Val.	D bidichol.	Acto.		2.05	2.73	314824.26	694.24	488.05	0.00	13.39	18.31	0.00	0.00	2.18	0.39	7.86			3.06	1505.44	2.41	24.86			
126	KH1: 3. 3.05 I	E. Val.	N. Kimmov.	Acto.		0.28	0.11	306783.35	854.78	549.96	0.00	4.70	17.91	0.00	0.00	1.30	0.77	4.51			1.53	1342.30	2.27	23.42	*	*	
126	KH1: 3. 3.05 2	E. Val.	N. Kimmov.	Acto.		1.28	0.43	313539.52	1187.64	683.33	3.42	6.55	18.50	0.00	0.00	1.78	1.38	6.09			2.59	1308.69	2.39	21.38			
127	KH1: 3. 3.35 A I	E. Val.	N. Kimmov.	Pecty.		-1.12	1.75	304378.10	738.68	608.11	2.12	6.45	17.51	0.00	0.00	1.75	0.10	6.38			2.21	1323.83	2.64	30.17			
128	KH1: 3. 3.35 A II	E. Val.	N. Kimmov.	Pecty.		-0.89	1.56	311229.10	771.74	553.87	0.00	4.83	18.60	0.00	0.00	1.78	0.15	4.58			2.78	1361.63	2.25	28.07			
129	KH1: 3. 3.45 I	E. Val.	N. Kimmov.	Acto.		0.09	0.69	288321.39	1241.68	501.37	1.39	8.76	18.38	0.00	0.00	1.84	0.88	7.80			0.71	1468.31	2.31	19.85			
130	KH1: 3. 3.45 2	E. Val.	N. Kimmov.	Acto.		0.82	0.80	306580.30	1241.49	484.68	0.00	7.36	18.84	0.00	0.00	1.94	1.08	11.05			3.78	1481.59	2.36	21.13			
131	KH1: 3. Top 3.54	E. Val.	N. Kimmov.	Acto.		-0.40	1.30	306524.58	685.04	421.55	0.00	7.88	18.78	0.00	0.00	1.47	0.08	8.76			3.03	1217.81	2.44	24.49			
132	KH1: 1.10	E. Ryaz.	H. Koc. 5. an.	Cylindro.		2.28	0.50	306251.97	818.78	825.94	35.63	7.56	19.16	0.00	0.00	2.76	0.81	8.63			1.04	1362.48	2.47	40.38	*	*	
133	KH1: 1.30	E. Ryaz.	H. Koc. 5. an.	N. (C?)		0.28	0.49	307535.16	818.78	825.94	42.08	5.64	19.15	0.00	0.00	1.75	0.88	6.43			3.14	1141.80	2.35	29.51			
134	KH1: 1.50 A	E. Ryaz.	H. Koc. 5. an.	Cylindro?		0.11	-0.57	301840.78	1099.03	937.95	48.71	4.54	19.15	0.00	0.00	1.71	1.62	6.80			2.23	1122.11	2.37	31.69	*	*	
136	KH1: 1.50 B	E. Ryaz.	H. Koc. 5. an.	Cylindro?		2.28	0.03	306857.78	1042.15	1029.44	39.86	5.30	19.53	0.00	0.00	2.04	0.73	14.74			3.80	1282.36	2.40	31.73			
138	KH1: 1.60 I	E. Ryaz.	H. Koc. 5. an.	?		0.67	-0.30	297175.78	1320.88	1029.07	9.32	4.19	19.20	0.00	0.00	2.61	1.65	12.87			0.48	1248.45	2.35	23.91			
137	KH1: 1.60 2	E. Ryaz.	H. Koc. 5. an.	?		0.59	-0.32	306338.00	1327.13	1217.32	0.00	4.15	20.35	0.00	0.00	2.53	1.78	14.43			1.89	1171.69	2.55	20.89			
138	KH1: 1.65 I	E. Ryaz.	H. Koc. 5. an.	Cylindro?		-0.82	0.52	318890.84	864.87	819.48	12.42	3.63	21.57	0.00	0.00	2.02	1.77	4.83			2.74	1112.78	2.52	25.92			
139	KH1: 1.65 II	E. Ryaz.	H. Koc. 5. an.	Cylindro?		-0.61	0.45	318233.78	878.66	832.22	0.00	4.78	20.81	0.00	0.00	2.08	1.04	8.22			0.70	1143.86	2.52	28.86			
140	KH1: 1.70 A	E. Ryaz.	H. Koc. 5. an.	Cylindro?		-0.47	-0.51	318650.00	1013.31	721.43	0.00	3.12	21.63	0.00	0.00	2.22	1.26	18.40			2.37	1128.15	2.69	36.16			
141	KH1: 2.45 A	E. Ryaz.	H. Koc. 5. an.	Lapinh.		-0.21	-0.29	314041.14	1274.67	1440.41	22.17	5.58	20.58	0.00	0.00	1.82	1.65	12.60			4.72	1174.06	2.43	27.37			
142	KH1: 2.60 A	E. Ryaz.	H. Koc. 5. an.	Cylindro.		1.28	0.07	318994.38	1077.28	1010.42	19.48	3.73	20.05	0.00	0.00	4.24	2.48	9.86			1.80	1144.39	2.40	30.69			
143	KH1: 2.65 A	E. Ryaz.	H. Koc. 5. an.	Cylindro.		0.63	-0.03	314881.82	886.22	1077.12	14.02	6.08	20.62	0.00	0.00	4.56	2.73	1.18			2.45	1151.12	2.45	33.75			
144	KH1: 2.75	E. Ryaz.	H. Koc. 5. an.	N. (C)		0.54	-0.11	318804.89	1035.22	1058.69	28.12	3.33	21.08	0.00	0.00	1.87	1.03	8.28			2.94	1089.07	2.47	27.13			
146	KH1: 2.80 A I	E. Ryaz.	H. Koc. 5. an.	Cylindro.		1.82	0.41	320894.86	816.37	745.64	0.00	10.71	21.28	0.00	0.00	2.08	1.03	18.62			2.11	1132.67	2.62	28.45			
146	KH1: 2.80 A II	E. Ryaz.	H. Koc. 5. an.	Cylindro.		2.31	0.14	322853.61	889.69	889.72	0.00	8.67	21.38	0.00	0.00	1.91	1.01	19.65			3.47	1131.33	2.68	28.08			
147	KH1: 2.80 B	E. Ryaz.	H. Koc. 5. an.	Cylindro.		1.24	0.28	315840.07	838.31	829.78	14.12	8.12	21.17	0.00	0.00	1.88	0.88	5.87			3.52	1174.44	2.72	31.56			
148	KH1: 2.85 A	E. Ryaz.	H. Koc. 5. an.	Acto.		-0.32	-0.74	321087.48	1089.78	1057.63	19.88	9.33	20.74	0.00	0.00	4.31	2.42	3.92			4.65	1124.50	2.68	34.14			
149	KH1: 2.85 B	E. Ryaz.	H. Koc. 5. an.	Cylindro?		-0.71	0.11	315324.01	1148.24	1117.33	28.00	8.24	20.40	0.00	0.00	9.77	1.86	1.81			1.79	1052.00	2.65	34.81			
150	KH1: 2.85 A	E. Ryaz.	H. Koc. 5. an.	Cylindro.		2.27	0.31	314689.01	1180.21	517.67	0.00	14.44	20.64	0.00	0.00	4.69	2.48	30.73			2.49	1335.28	2.66	32.65			

[illegible]

[illegible]

[illegible]

384	SK5, 2.95	E. Kimm.	Bay-Cym	iv.		-1.68	1.50	295481.21	875.85	1153.89	44.11	0.00	24.26	0.00	1.80	2.82	6.05		0.38	910.63	1.75	27.04					
385	SK5, 3.10	E. Kimm.	Bay-Cym	?		-0.84	2.12	295877.62	910.04	865.06	41.89	34.38	23.51	0.00	1.60	2.89	5.01		4.18	908.34	3.09	19.82					
386	SK5, 3.40	E. Kimm.	Bay-Cym	Cylindro.		-1.13	2.21	297865.29	733.76	781.36	43.36	22.98	23.36	0.00	1.86	1.90	10.90		1.41	1018.40	1.73	21.37					
~	SK5, 3.90	E. Kimm.	Bay-Cym	-	x	-	-	-	-	-	-	-	-	-	-	-	-	-	-	-	-	-	-	-	-	-	-
387	SK5, 4.00	E. Kimm.	Bay-Cym	iv.		0.30	1.39	295457.60	768.95	958.69	46.28	259.78	22.34	0.00	2.48	2.22	83.06		1.58	875.31	1.69	24.62	x	x	x		
388	SK5, 4.15 A	E. Kimm.	Bay-Cym	Cylindro.	x	-0.58	2.17	293590.26	689.59	659.52	38.70	51.48	22.51	0.00	3.14	1.87	25.19		4.02	928.29	1.84	24.08					
389	SK5, 4.15 B	E. Kimm.	Bay-Cym	Pachy.		-0.35	2.28	295585.78	839.52	870.37	11.37	36.02	21.98	0.00	3.78	1.88	15.32		0.84	894.31	1.73	20.62	x	x	x		
390	SK5, 4.35	E. Kimm.	Bay-Cym	iv. (C.)	x	-0.53	1.38	292132.40	918.22	973.65	21.38	105.87	23.84	0.00	1.40	2.45	48.01		3.21	868.84	1.69	28.82					
391	SK5, 4.60	E. Kimm.	Bay-Cym	iv.		-0.47	2.73	298239.72	811.58	760.79	40.53	17.36	23.59	0.00	1.29	2.03	11.07		4.02	1017.95	1.75	20.74					
392	SK5, 4.70	E. Kimm.	Bay-Cym	Pachy?	x	-0.82	2.32	287816.70	747.48	791.75	23.01	41.33	22.70	0.00	2.03	1.88	11.16		2.18	922.84	2.21	27.86					
393	SK5, 5.25	E. Kimm.	Bay-Cym	Cylindro.		-0.44	2.37	294059.28	700.70	778.84	8.02	69.59	21.34	0.00	1.41	2.05	32.34		2.17	895.62	1.60	19.28					
394	SK5, 5.70 A	E. Kimm.	Bay-Cym	Cylindro.	2	-1.70	3.57	295126.28	759.81	795.27	12.87	55.16	23.21	0.00	2.56	1.81	17.18		4.44	1112.55	1.81	20.41					
395	SK5, 5.70 B	E. Kimm.	Bay-Cym	Pachy.		0.09	3.31	294232.38	749.65	580.65	12.21	0.00	21.86	0.00	1.23	2.03	1.88		2.46	988.39	1.62	26.76	x	x	x		
396	SK5, 5.90 A	E. Kimm.	Bay-Cym	Pachy?		0.45	1.87	295395.49	1015.37	778.69	14.12	168.87	22.09	7.50	2.89	2.43	82.08		4.41	1036.97	1.87	18.14					
397	SK5, 5.90 B	E. Kimm.	Bay-Cym	iv.		-0.22	1.63	298780.32	768.19	849.08	18.80	107.44	23.91	0.00	1.78	2.05	49.13		1.26	927.50	1.74	22.10					
398	SK5, 6.25 A	E. Kimm.	Bay-Cym	Cylindro.		-1.48	2.32	294898.02	794.87	848.86	13.38	0.00	24.22	0.00	1.50	2.38	2.62		1.89	975.58	1.68	28.60					
399	SK5, 6.25 B	E. Kimm.	Bay-Cym	iv. (C.)		-0.19	2.05	291091.86	748.58	767.45	18.07	77.73	22.80	6.89	2.56	2.51	35.31		1.48	899.36	1.87	21.47					
400	SK5, 7.20 A	E. Kimm.	Bay-Cym	iv. (C.)		-1.11	2.84	298334.51	724.43	826.70	14.89	4.12	22.87	9.81	1.38	2.07	8.65		2.78	917.13	1.68	19.40	x	x	x		
401	SK5, 7.20 B	E. Kimm.	Bay-Cym	Pachy?		-0.23	1.93	295888.39	890.85	1023.68	14.78	52.84	22.80	8.84	1.00	3.24	31.22		0.84	927.58	1.74	19.17					
402	SK5, 7.20 C	E. Kimm.	Bay-Cym	Cylindro.		-1.23	3.06	287823.03	740.74	971.84	19.63	97.83	22.28	7.10	2.29	1.86	44.57		3.29	922.84	2.09	27.72					
403	SK5, 7.40 A	E. Kimm.	Bay-Cym	Pachy.		0.02	0.80	294211.56	1130.34	1115.83	19.98	23.52	21.89	5.69	1.23	5.57	18.96		2.48	928.32	1.65	17.27	x	x	x		
404	SK5, 7.40 B	E. Kimm.	Bay-Cym	Cylindro.		-1.39	2.78	298998.42	725.83	800.85	8.36	30.55	22.55	8.47	1.69	2.10	6.31		2.47	949.20	1.67	25.48					
405	SK5, 7.70 A	E. Kimm.	Bay-Cym	Cylindro.		-1.23	2.89	292421.36	894.33	727.44	14.33	72.68	22.68	0.82	1.95	1.69	35.58		2.98	986.57	1.72	26.69					
406	SK5, 8.10 A	E. Kimm.	Bay-Cym	Pachy.	x	-0.49	2.11	296265.82	1205.48	1015.54	21.64	0.00	23.81	11.71	1.46	3.60	1.20		4.25	1075.19	1.67	15.57					
407	SK5, 8.10 B	E. Kimm.	Bay-Cym	Pachy.		0.09	2.55	289268.55	768.16	681.54	14.42	28.13	21.03	0.00	1.56	1.74	16.79		2.26	965.67	1.84	26.68					
408	SK5, 8.10 C	E. Kimm.	Bay-Cym	Cylindro.		-1.15	2.98	292781.28	681.08	670.94	12.92	185.34	23.07	0.00	2.72	1.80	34.39		2.12	942.23	1.70	20.00					
409	SK6, 0.30 A	E. Kimm.	Cym	iv? (C.)		-1.38	2.45	298404.09	688.62	740.22	14.50	147.27	21.90	0.00	2.30	1.67	53.78		1.83	971.75	1.84	25.42					
410	SK6, 0.00 A	E. Kimm.	Cym	iv.		0.09	1.29	295053.74	1027.59	1373.19	15.11	0.00	21.82	0.00	1.10	3.57	4.54		2.64	948.81	1.65	21.00	x	x	x		
411	SK6, 0.00 B	E. Kimm.	Cym	Cylindro.		-1.53	1.69	292040.20	779.00	1095.61	18.07	158.88	22.58	0.00	2.80	2.28	44.51		4.81	931.32	1.68	36.28					
412	SK6, 0.50 A	E. Kimm.	Cym	Cylindro.		-0.81	2.32	288508.98	751.15	538.69	0.00	0.00	22.15	8.69	2.61	1.30	5.95		2.18	971.41	2.03	29.41					
413	SK6, 1.50 A	E. Kimm.	Cym	Cylindro.	x	-0.97	2.49	298118.05	789.82	834.43	18.08	402.41	23.12	13.62	3.57	2.06	208.93		1.12	921.98	1.74	27.65	x	x	x		
414	SK6, 1.50 B	E. Kimm.	Cym	Cylindro.		-1.12	2.24	294902.37	922.20	1429.86	10.78	158.95	25.51	0.00	2.80	2.63	36.99		2.88	982.50	1.82	33.47					
~	SK6, 1.90	E. Kimm.	Cym	-	x	-	-	-	-	-	-	-	-	-	-	-	-	-	-	-	-	-	-	-	-	-	-
416	SK6, 2.30	E. Kimm.	Cym	iv.		0.04	1.69	295780.59	805.06	1117.33	26.44	131.01	23.93	0.00	3.43	2.87	71.81		1.88	929.01	1.74	19.25					
418	SK6, 2.40 A	E. Kimm.	Cym	iv.	x	0.31	1.77	295521.85	847.35	1090.85	15.46	173.83	22.90	0.00	1.88	2.75	91.74		2.21	888.99	1.62	20.15					
417	SK6, 2.40 B	E. Kimm.	Cym	?		-0.83	1.21	289482.69	1047.46	1737.15	54.24	2134.34	65.58	2.50	2.95	2.93	173.52		2.95	926.75	2.62	14.50					Borings
418	SK6, 2.50	E. Kimm.	Cym	iv.		-1.48	3.63	294089.48	951.25	880.58	18.89	0.00	21.14	7.71	1.90	1.78	2.03		1.78	1072.87	1.58	36.47	x	x	x		
419	SK6, 2.60 A	E. Kimm.	Cym	Cylindro?		0.44	1.88	292826.42	844.14	894.84	14.16	86.57	21.67	0.00	1.37	2.84	45.14		1.95	912.14	1.59	23.24					
420	SK6, 2.60 B	E. Kimm.	Cym	iv. (C?)		-0.35	1.77	289240.47	805.39	910.48	17.28	143.08	22.70	0.00	2.09	2.38	61.93		1.01	983.99	1.75	18.11					
421	SK6, 4.05	E. Kimm.	Cym	Cylindro.		-0.53	1.95	300128.02	937.82	899.21	13.00	53.07	22.88	0.00	2.58	2.81	26.53		2.74	1019.19	1.68	17.22					
~	SK6, 4.50	E. Kimm.	Cym	-	x	-	-	-	-	-	-	-	-	-	-	-	-	-	-	-	-	-	-	-	-	-	-
422	SK6, 5.30	E. Kimm.	Cym	Pachy?		-1.09	1.63	287405.72	1004.99	1267.58	17.86	374.10	23.50	0.00	4.83	2.81	59.84		2.58	1029.75	2.01	17.45	x	x	x		Decalc.
423	SK6, 5.55	E. Kimm.	Cym	Cylindro.		-0.33	0.39	287849.81	933.68	1218.80	14.12	151.55	21.92	0.00	1.91	2.36	78.13		2.49	986.91	1.58	18.69					
~	SK6, 5.80	E. Kimm.	Cym	-		-	-	-	-	-	-	-	-	-	-	-	-	-	-	-	-	-	-	-	-	-	-
424	SK6, 5.90 A	E. Kimm.	Cym	iv.		-1.74	0.84	304837.33	1029.81	1370.95	22.24	665.63	26.69	17.71	3.91	2.63	284.22		5.90	954.68	1.58	23.10					Decalc.
425	SK6, 5.90 B	E. Kimm.	Cym	Cylindro.		-0.89	0.89	285076.23	982.89	1183.55	9.40	723.78	23.49	7.66	4.47	2.33	305.05		0.00	1041.48	1.84	21.98					
~	SK6, 6.40	E. Kimm.	Cym	-	x	-	-	-	-	-	-	-	-	-	-	-	-	-	-	-	-	-	-	-	-	-	-
426	SK6, 6.55	E. Kimm.	Cym	Cylindro.	x	-0.45	1.48	293036.35	1118.16	1338.40	14.31	11.86	22.01	0.00	3.82	2.77	4.25		0.75	988.70	1.61	18.88					
427	SK6, 6.80	E. Kimm.	Cym	Cylindro.		-1.41	2.68	298328.06	838.61	715.19	8.02	92.10	23.44	0.00	3.84	1.65	40.30		2.38	1132.00	1.71	26.91					
428	SK6, 7.00	E. Kimm.	Cym	Cylindro.		-1.18	1.47	290504.25	775.59	897.81	10.73	68.93	23.68	0.00	3.14	1.87	41.71		3.70	1023.25	1.68	49.12					
429	SK6, 7.20 AJ	E. Kimm.	Cym	Cylindro.	x	-0.67	1.31	295128.77	878.08	841.25	12.95	3.21	23.20	0.00	2.05	2.35	9.24		4.05	994.77	1.73	18.24					Borings

[illegible]

APPENDIX 3
DATA TABLES : ORGANICS

[illegible]

[illegible]

[illegible]

[illegible]

248	SK3; 0.70	E-M. Oxf.	Cor-Den	M.W.D.											~
249	SK3; 0.85	E-M. Oxf.	Cor-Den	M.W.D.						2.79	1.25	37	39	431	-22.06
250	SK3; 1.20	E-M. Oxf.	Cor-Den	M.W.D.											-21.57
251	SK3; 1.50	E-M. Oxf.	Cor-Den	M.W.D.		4.50	5.31	4.76	4.86						-21.80
252	SK3; 2.00	E-M. Oxf.	Cor-Den	M.W.D.											-21.79
253	SK3; 2.20	E-M. Oxf.	Cor-Den	M.W.D.											-22.23
254	SK3; 3.00	E-M. Oxf.	Cor-Den	M.W.D.		4.63	4.60	4.66	4.63						-21.89
255	SK3; 3.50	E-M. Oxf.	Cor-Den	M.W.D.											-21.88
256	SK3; 5.20	E-M. Oxf.	Cor-Den	M.W.D.						3.36	1.10	23	37	425	-21.81
257	SK3; 5.55	E-M. Oxf.	Cor-Den	M.W.D.											-22.06
258	SK3; 5.65	E-M. Oxf.	Cor-Den	M.W.D.		2.10	2.44	2.05	2.20						~
259	SK3; 5.80	E-M. Oxf.	Cor-Den	M.W.D.											-21.86
260	SK3; 5.90	E-M. Oxf.	Cor-Den	M.W.D.											~
261	SK3; 6.15	E-M. Oxf.	Cor-Den	M.W.D.		6.24	6.23	6.30	6.26						-21.68
262	SK3; 6.40	E-M. Oxf.	Cor-Den	M.W.D.											-22.08
263	SK3; 7.35	E-M. Oxf.	Cor-Den	M.W.D.											-22.26
264	SK3; 7.55	E-M. Oxf.	Cor-Den	M.W.D.											-22.26
265	SK3; 7.90	E-M. Oxf.	Cor-Den	M.W.D.		1.41	1.86	1.28	1.52	1.98	1.42	82	43	426	-22.50
266	SK4; 0.20	E-L. Call.	Koe-Lam	M.W.D.		0.71	0.66	0.72	0.70	0.78	0.14	92	105	422	-24.90
267	SK4; 0.45	E-L. Call.	Koe-Lam	M.W.D.											-25.19
268	SK4; 1.05	E-L. Call.	Koe-Lam	M.W.D.						2.04	0.40	223	57	418	-26.28
269	SK4; 1.55	E-L. Call.	Koe-Lam	M.W.D.											-25.34
270	SK4; 1.80	E-L. Call.	Koe-Lam	M.W.D.						1.02	0.33	114	72	420	-24.96
271	SK4; 2.50	E-L. Call.	Koe-Lam	M.W.D.											-25.18
272	SK4; 3.20	E-L. Call.	Koe-Lam	M.W.D.											-25.10
273	SK4; 3.70	E-L. Call.	Koe-Lam	M.W.D.											-24.81
274	SK4; 6.80	E-L. Call.	Koe-Lam	M.W.D.		1.01	1.08		1.05						-23.05
275	SK4; 6.90	E-L. Call.	Koe-Lam	M.W.D.						0.50	1.87	49	317	421	-23.67
276	SK4; 8.95	E-L. Call.	Koe-Lam	M.W.D.											-23.04
277	SK4; 10.50	E-L. Call.	Koe-Lam	M.W.D.						1.88	1.27	44	97	426	-22.52
278	SK4; 11.50	E-L. Call.	Koe-Lam	M.W.D.		0.36	0.33	0.45	0.38						-22.92
279	SK5; -1.10	E. Kimm.	Bay-Cym	M.W.D.		2.89	2.85	2.88	2.87						-25.12
280	SK5; -0.60	E. Kimm.	Bay-Cym	M.W.D.											-24.46
281	SK5; 1.90	E. Kimm.	Bay-Cym	M.W.D.											-24.40
282	SK5; 2.10	E. Kimm.	Bay-Cym	M.W.D.											-24.39
283	SK5; 2.45	E. Kimm.	Bay-Cym	M.W.D.		1.93	2.38	2.12	2.14						-24.27

284	SK5; 2.70	E. Kimm.	Bay-Cym	M.W.D.											-24.40
285	SK5; 2.95	E. Kimm.	Bay-Cym	M.W.D.						1.68	0.48	111	73	428	-24.81
286	SK5; 3.10	E. Kimm.	Bay-Cym	M.W.D.		1.98	1.99	2.08	2.02						~
287	SK5; 3.40	E. Kimm.	Bay-Cym	M.W.D.											-24.74
288	SK5; 4.35	E. Kimm.	Bay-Cym	M.W.D.											-24.07
289	SK5; 4.60	E. Kimm.	Bay-Cym	M.W.D.		7.99	8.06	9.03	8.36						~
290	SK5; 4.70	E. Kimm.	Bay-Cym	M.W.D.						3.54	0.29	88	43	419	-23.84
291	SK5; 5.25	E. Kimm.	Bay-Cym	M.W.D.											-24.13
292	SK5; 5.70	E. Kimm.	Bay-Cym	M.W.D.		3.11	3.19	3.19	3.16						-24.05
293	SK5; 5.90	E. Kimm.	Bay-Cym	M.W.D.											-23.97
294	SK5; 6.25	E. Kimm.	Bay-Cym	M.W.D.		2.18	2.14	2.14	2.15						-23.91
295	SK5; 7.20	E. Kimm.	Bay-Cym	M.W.D.											-24.22
296	SK5; 7.40	E. Kimm.	Bay-Cym	M.W.D.		4.99	4.65	5.54	5.06						~
297	SK5; 7.70	E. Kimm.	Bay-Cym	M.W.D.											-24.67
298	SK5; 8.10	E. Kimm.	Bay-Cym	M.W.D.						3.19	0.40	197	47	420	-24.71
299	SK5; 8.95	E. Kimm.	Bay-Cym	M.W.D.		1.66	1.79	1.85	1.77						-24.00
300	SK6; -0.30	E. Kimm.	Cym	M.W.D.		1.39	1.34	1.37	1.37						-23.94
301	SK6; 0.00	E. Kimm.	Cym	M.W.D.											-24.07
302	SK6; 0.50	E. Kimm.	Cym	M.W.D.											-24.07
303	SK6; 1.50	E. Kimm.	Cym	M.W.D.						1.28	0.20	31	70	421	-23.54
304	SK6; 1.90	E. Kimm.	Cym	M.W.D.											-23.90
305	SK6; 2.30	E. Kimm.	Cym	M.W.D.											-23.89
306	SK6; 2.40	E. Kimm.	Cym	M.W.D.		1.95	1.86	1.60	1.80						~
307	SK6; 2.50	E. Kimm.	Cym	M.W.D.											-23.75
308	SK6; 2.60	E. Kimm.	Cym	M.W.D.											-23.85
309	SK6; 4.05	E. Kimm.	Cym	M.W.D.		3.57	3.29	3.33	3.40						-24.57
310	SK6; 4.50	E. Kimm.	Cym	M.W.D.											-24.47
311	SK6; 5.30	E. Kimm.	Cym	M.W.D.											-24.81
312	SK6; 5.55	E. Kimm.	Cym	M.W.D.											-25.28
313	SK6; 5.80	E. Kimm.	Cym	M.W.D.						2.76	0.26	165	45	416	-25.30
314	SK6; 5.90	E. Kimm.	Cym	M.W.D.		3.27	3.26	3.18	3.24						-25.06
315	SK6; 6.40	E. Kimm.	Cym	M.W.D.											-24.93
316	SK6; 6.55	E. Kimm.	Cym	M.W.D.											-24.99
317	SK6; 6.90	E. Kimm.	Cym	M.W.D.		3.58	3.77	3.75	3.70						-24.88
318	SK6; 7.00	E. Kimm.	Cym	M.W.D.											-24.95
319	SK6; 7.20	E. Kimm.	Cym	M.W.D.						2.18	0.31	82	56	415	-24.72

[illegible]

356	SK8; 31.80	E. Oxf.	Cor	M.W.D.		1.77	1.61	1.30	1.56						-21.86
357	SK8; 33.35	E. Oxf.	Cor	M.W.D.						5.44	1.68	44	28	427	-21.26
358	SK8; 33.70	E. Oxf.	Cor	M.W.D.											-21.66
359	SK8; 34.70	E. Oxf.	Cor	M.W.D.											-21.46
360	SK8; 35.80	E. Oxf.	Cor	M.W.D.											-21.50
361	SK8; 36.20	E. Oxf.	Cor	M.W.D.											-21.56
362	SK8; 39.40	E. Oxf.	Cor	M.W.D.		3.64	3.94	3.67	3.75						-21.95
363	SK9; -2.00	M-L. Oxf.	Ten-Glo	M.W.D.		2.24	2.79	2.23	2.42	5.23	1.72	64	28	424	-21.98
364	SK9; -1.70	M-L. Oxf.	Ten-Glo	M.W.D.											-22.59
365	SK9; -0.30	M-L. Oxf.	Ten-Glo	M.W.D.						1.04	3.28	59	94	424	-22.91
366	SK9; 0.40	M-L. Oxf.	Ten-Glo	M.W.D.											-22.30
367	SK9; 0.60	M-L. Oxf.	Ten-Glo	M.W.D.											~
368	SK9; 0.90	M-L. Oxf.	Ten-Glo	M.W.D.						3.31	1.73	61	34	428	-22.19
369	SK9; 1.00	M-L. Oxf.	Ten-Glo	M.W.D.											~
370	SK9; 1.20	M-L. Oxf.	Ten-Glo	M.W.D.		3.77	3.87	3.86	3.83						-22.29
371	SK9; 1.50	M-L. Oxf.	Ten-Glo	M.W.D.											-22.59
372	SK9; 2.00	M-L. Oxf.	Ten-Glo	M.W.D.											-21.77
373	SK9; 2.40	M-L. Oxf.	Ten-Glo	M.W.D.											-21.76
374	SK9; 2.70	M-L. Oxf.	Ten-Glo	M.W.D.											-21.70
375	SK9; 2.90	M-L. Oxf.	Ten-Glo	M.W.D.											-22.05
376	SK9; 3.40	M-L. Oxf.	Ten-Glo	M.W.D.		4.95	5.76	5.27	5.33						-22.10
377	SK9; 3.70	M-L. Oxf.	Ten-Glo	M.W.D.											-22.25
378	SK9; 3.90	M-L. Oxf.	Ten-Glo	M.W.D.											-22.25
379	SK9; 4.20	M-L. Oxf.	Ten-Glo	M.W.D.		2.61	2.53	2.53	2.56						-22.50
380	SK9; 4.70	M-L. Oxf.	Ten-Glo	M.W.D.						5.90	0.99	30	24	433	-21.69
381	SK9; 4.90	M-L. Oxf.	Ten-Glo	M.W.D.											~
382	SK9; 5.25	M-L. Oxf.	Ten-Glo	M.W.D.						1.81	2.56	45	49	426	-22.58
383	SK9; 5.65	M-L. Oxf.	Ten-Glo	M.W.D.											-22.53
384	SK9; 6.05	M-L. Oxf.	Ten-Glo	M.W.D.		2.05	2.15	2.01	2.07						-22.81
385	SK9; 6.70	M-L. Oxf.	Ten-Glo	M.W.D.											-22.75
386	SK9; 7.30	M-L. Oxf.	Ten-Glo	M.W.D.											-23.24
387	SK9; 7.55	M-L. Oxf.	Ten-Glo	M.W.D.											-23.11
388	SK9; 7.80	M-L. Oxf.	Ten-Glo	M.W.D.											~
389	SK9; 7.95	M-L. Oxf.	Ten-Glo	M.W.D.											-22.69
390	SK9; 8.55	M-L. Oxf.	Ten-Glo	M.W.D.		-1.08	-1.18	-1.50	-1.25	1.14	5.31	73	69	427	-23.27
391	SK9; 10.80	M-L. Oxf.	Ten-Glo	M.W.D.						4.43	0.19	29	28	422	-22.35

392	SK9; 12.50	M-L. Oxf.	Ten-Glo	M.W.D.											-23.19
393	SK9; 12.60	M-L. Oxf.	Ten-Glo	M.W.D.											~
394	SK9; 12.75	M-L. Oxf.	Ten-Glo	M.W.D.		3.84	3.83	4.13	3.93						~
395	SK9; 13.10	M-L. Oxf.	Ten-Glo	M.W.D.											-23.79
396	SK9; 13.40	M-L. Oxf.	Ten-Glo	M.W.D.		1.66	1.65	1.65	1.65	1.96	0.16	250	26	419	-24.26
397	SK10; 0.40	L. Oxf.	Ser-Reg	M.W.D.		1.59	1.58	1.59	1.59	1.78	0.19	123	26	427	-24.49
398	SK10; 0.90	L. Oxf.	Ser-Reg	M.W.D.											-24.43
399	SK10; 3.40	L. Oxf.	Ser-Reg	M.W.D.											-23.97
400	SK10; 4.60	L. Oxf.	Ser-Reg	M.W.D.						2.22	0.28	58	33	425	-23.15
401	SK10; 8.20	L. Oxf.	Ser-Reg	M.W.D.											-23.83
402	SK10; 12.20	L. Oxf.	Ser-Reg	M.W.D.		2.43	2.41	2.46	2.43						-24.34
403	SK10; 12.70	L. Oxf.	Ser-Reg	M.W.D.											~
404	SK10; 13.40	L. Oxf.	Ser-Reg	M.W.D.						1.63	0.24	91	30	425	-24.13
405	SK10; 14.30	L. Oxf.	Ser-Reg	M.W.D.		1.14	1.10	1.13	1.12						-24.28
406	SK10; 15.30	L. Oxf.	Ser-Reg	M.W.D.											~
407	SK10; 15.70	L. Oxf.	Ser-Reg	M.W.D.											-24.68
408	SK10; 21.90	L. Oxf.	Ser-Reg	M.W.D.		1.23	1.21	1.34	1.26	1.35	0.27	123	44	427	-25.18